NASA Conference Publication 3218

(2)

24th Annual Precise Time and Time Interval (PTTI) Applications and Planning Meeting

Proceedings of a meeting held at the Ritz-Carlton Hotel McLean, Virginia December 1–3, 1992

NASA Conference Publication 3218

24th Annual Precise Time and Time Interval (PTTI) Applications and Planning Meeting

Editorial Committee Chairman
Richard L. Sydnor
Jet Propulsion Laboratory
Pasadena, California

Proceedings of a meeting sponsored by the U.S. Naval Observatory, the NASA Goddard Space Flight Center, the Jet Propulsion Laboratory, the Space and Naval Warfare Systems Command, the Naval Research Laboratory, the Army Electronics Technology and Devices Laboratory, the Rome Laboratory, and the Air Force Office of Scientific Research and held at the Ritz–Carlton Hotel
McLean, Virginia
December 1–3, 1992

National Aeronautics
and Space Administration

Goddard Space Flight Center
Greenbelt, Maryland 20771

1993

PRECISE TIME AND TIME INTERVAL (PTTI) APPLICATIONS AND PLANNING MEETING

ORDER FORM FOR THE PROCEEDINGS

	Year	Cost	Available	Unavailable
1	1969			X
2	1970	$25.00	X	
3	1971	$25.00		X
4	1972	$25.00	X	
5	1973	$25.00	X	
6	1974	$25.00	X	
7	1975	$25.00	X	
8	1976			X
9	1977			X
10	1978	$25.00	X	
11	1979	$25.00	X	
12	1980	$25.00	X	
13	1981	$25.00	X	
14	1982	$25.00		X
15	1983			X
16	1984	$25.00	X	
17	1985	$25.00	X	
18	1986	$20.00	X	
19	1987	$25.00	X	
20	1988	$35.00	X	
21	1989	$65.00	X	
22	1990	$70.00	X	
23	1991	$85.00	X	
24	1992	$85.00	X	

Please circle copy(ies) requested and make the check payable to "Treasurer, PTTI". **Please do not add personal names or addresses to the pay line on the check. We cannot accept invoices.** Please return the check and the Order Form to:

Mrs. Sheila Faulkner
Chairman, PTTI Executive Committee
U. S. Naval Observatory
Time Service Department (TSS1)
3450 Massachusetts Avenue, N.W.
Washington, DC 20392-5420
(202) 653-1460 FAX: 202/653-0909

It is with great regret that we must announce we can no longer absorb the cost of air mailing to international addresses; therefore, the Proceedings will be shipped by Surface Mail. However, if you wish to pay the air mail postage, we will notify you of the cost before mailing.

When you register for the PTTI Meeting or order the Proceedings, your name is added to the PTTI Mailing list to automatically receive future meeting information.

EXECUTIVE COMMITTEE

Sheila C. Faulkner, Chairman
U.S. Naval Observatory

Ronald L. Beard
Naval Research Laboratory

Morton A. Dubinsky
Space and Naval Warfare Systems Command

Hugh S. Fosque
NASA Headquarters

Raymond L. Granata
NASA/Goddard Space Flight Center

Dr. Helmut Hellwig
Air Force Office of Scientific Research

Dr. William J. Klepczynski
U.S. Naval Observatory

Paul F. Kuhnle
NASA/Jet Propulsion Laboratory

Dr. Richard L. Sydnor
NASA/Jet Propulsion Laboratory

Dr. John H. Vig
Army Electronics Technology Laboratory

Dr. Joseph D. White
Naval Research Laboratory

Dr. Gernot M. R. Winkler
U.S. Naval Observatory

Dr. Nicholas F. Yannoni
Rome Laboratory

Nicolette Jardine
U.S. Naval Observatory

OFFICERS

GENERAL CHAIRMAN

MR. S. CLARK WARDRIP

AlliedSignal Technical Services Corporation

TECHNICAL PROGRAM COMMITTEE CHAIRMAN

MR. WILLIAM RILEY

EG&G

ASSISTANT TECHNICAL PROGRAM COMMITTEE CHAIRMAN

DR. SIGFRIDO LESCHIUTTA

Polytechnico Di Torino

TECHNICAL PROGRAM COMMITTEE MEMBERS

DR. LEONARD S. CUTLER

Hewlett-Packard

DR. HENRY F. FLIEGEL

The Aerospace Corporation

MR. PAUL F. KUHNLE

Jet Propulsion Laboratory

DR. SAMUEL R. STEIN

Timing Solutions Corporation

DR. RICHARD L. SYDNOR

Jet Propulsion Laboratory

MR. PHILIP E. TALLEY

The Aerospace Corporation

DR. JOHN R. VIG

Army Electronics Technology and Devices Laboratory

EDITORIAL COMMITTEE CHAIRMAN

DR. RICHARD L. SYDNOR

Jet Propulsion Laboratory
California Institute of Technology

EDITORIAL COMMITTEE MEMBERS

DR. LEONARD S. CUTLER

Hewlett-Packard Company

DR. G. JOHN DICK

Jet Propulsion Laboratory
California Institute of Technology

DR. RAYMOND FILLER

Army Electronics Technology and Devices Laboratory

MR. R. MICHAEL GARVEY

Frequency and Time Systems, Incorporated

MR. PAUL F. KUHNLE

Jet Propulsion Laboratory
California Institute of Technology

DR. DEREK MORRIS

National Research Council

MR. THOMAS K. TUCKER

Jet Propulsion Laboratory
California Institute of Technology

DR. JOSEPH D. WHITE

Naval Research Laboratory

PUBLICITY AND EXHIBITS CHAIRMAN

MR. FRANCIS MULLEN

Frequency and Time Systems, Incorporated

TECHNICAL ASSISTANCE

MR. PAUL KUSHMEIDER

AlliedSignal Technical Services Corporation

MR. JEFFREY S. INGOLD

AlliedSignal Technical Services Corporation

SESSION CHAIRMEN

SESSION I
Mr. Keith McDonald
Sat Tech Systems

SESSION IIA
Dr. Gernot M. R. Winkler
U.S. Naval Observatory

SESSION IIB
Dr. Henry F. Fliegel
The Aerospace Corporation

SESSION III
Mr. Philip E. Talley
The Aerospace Corporation

SESSION IVA
Dr. Leonard S. Cutler
Hewlett-Packard Company

SESSION IVB
Mr. Marc Weiss
National Institute of Standards and Technology

SESSION V
Dr. Samuel Stein
Timing Solutions Corporation

SESSION VIA
Mr. R. Brown
Bellcore

SESSION VIB
Mr. George Lutes
Jet Propulsion Laboratory

SESSION VII
Dr. James A. Barnes
Austron, Incorporated

ARRANGEMENTS

Sheila C. Faulkner
Paul F. Kuhnle
Dr. Richard L. Sydnor
Paul J. Kushmeider

FINANCE COMMITTEE

Dr. William J. Klepczynski
Sheila C. Faulkner

RECEPTIONISTS

The receptionists at the 24th Annual PTTI meeting were:

Ms. Brenda Hicks, U.S. Naval Research Laboratory
Ms. Nicolette Jardine, U.S. Naval Observatory
Mrs. Aline Kuhnle, Jet Propulsion Laboratory
Ms. Betty Jean McKnight, U.S. Naval Research Laboratory
Ms. Shirley Swann, U.S. Naval Research Laboratory
Mrs. Betty Wardrip, AlliedSignal Technical Services Corporation

PTTI ADVISORY BOARD COMMITTEES
1992

OFFICE	NAME	ORGANIZATION
Chairman	Mr. S. Clark Wardrip	BFEC
Vice Chairman	Mr. Martin B. Bloch	FEI
Finance Committee	Mr. Martin B. Bloch, Chairman	FEI
	Mr. S. Clark Wardrip	BFEC
	Mr. James L. Wright	CSR
	Mr. Gary Smith	KODE
Exhibits Committee	Mr. Francis Mullen, Chairman	FTS
	Dr. Martin W. Levine	SAO
	Mr. Ron C. Roloff	Austron
	Mr. Jack McNabb	TRAK
	Mr. William J. Riley	EG&G
	Dr. Robert F. C. Vessot	SAO
	Mr. Michael R. Tope	Truetime
Guest Speaker Committee	Mr. Robert H. Kern, Chairman	KERNCO
	Professor Carroll O. Alley	University of MD
	Dr. Leonard S. Cutler	HP
	Professor Bradford Parkinson	Stanford University
	Dr. Victor S. Reinhardt	Hughes
	Dr. Samuel R. Stein	Timing Solutions
	Dr. Richard L. Sydnor	JPL
Reports Committee	Mr. Terry N. Osterdock, Chairman	STI
	Mr. Paul F. Kuhnle	JPL
	Mr. Paul J. Kushmeider	BFEC
	Professor Harry Robinson	Duke University
	Mr. Philip E. Talley	Aerospace
	Dr. James A. Barnes	Austron
1991 PTTI Officers		
	General Chairman	
	Dr. Martin W. Levine	SAO
	Program Chairman	
	Mr. S. Clark Wardrip	BFEC
	PTTI Editorial Chairman	
	Dr. Richard L. Sydnor	JPL

NOTE: NON-GOVERNMENT OFFICERS OF THE PTTI ARE AUTOMATICALLY MEMBERS OF THE PTTI ADVISORY BOARD FOR THE YEAR(S) THAT THEY ARE IN OFFICE.

1992 ADVISORY BOARD MEMBERS
Mr. S. Clark Wardrip, Chairman
AlliedSignal Technical Services Corporation

Professor Carroll O. Alley
University of Maryland

Dr. James A. Barnes
Austron, Inc.

Mr. Martin B. Bloch
Frequency Electronics, Inc.

Mrs. Mary Chiu
Applied Physics Laboratory

Dr. Leonard S. Cutler
Hewlett-Packard Company

Dr. Henry F. Fliegel
The Aerospace Corporation

Mr. Robert H. Kern
Kernco, Inc.

Mr. Paul J. Kushmeider
AlliedSignal Technical
Services Corporation

Mr. Jack McNabb
TRAK Microwave

Mr. Donald Mitchell
TrueTime

Mr. Frank Mullen
Frequency and Time Systems, Inc.

Mr. Jerry Norton
Applied Physics Laboratory

Mr. Allen W. Osborne III
Allen Osborne Associates

Mr. Terry N. Osterdock
GPS Navigation, Inc.

Dr. Bradford W. Parkinson
Stanford University

Dr. Victor S. Reinhardt
Hughes Aircraft

Mr. William J. Riley
EG&G, Inc.

Dr. Harry Robinson
Duke University

Mr. Ronald C. Roloff
FTS/Austron

Dr. Samuel R. Stein
Timing Solutions Corporation

Mr. Philip E. Talley
The Aerospace Corporation

Mr. Michael R. Tope
TrueTime

Mr. James L. Wright
Computer Sciences/Raytheon

CONTENTS

OPENING ADDRESS

Captain Winfield Donat, III, USN
Supertendent, U.S. Naval Observatory

SESSION I

GPS Program Update

Chairman: Keith McDonald
SAT Tech Systems

SESSION IIA

Workshop on PTTI Applications

Moderator: Gernot M. R. Winkler
U.S. Naval Observatory

WORKSHOP A

Clock Performance and Its Measures: Stability and Accuracy

Moderator: Leonard Cutler
Hewlett-Packard Laboratories

WORKSHOP B

Clock User Interfaces

Moderator: Joseph D. White
U.S. Naval Research Laboratory

WORKSHOP C

Present and Future Needs: Is GPS the Only PTTI Source

Moderator: Raymond L. Filler
U.S. Army Research Laboratory

SESSION IIB

Pulsars and Relativity

Chairman: Henry F. Fliegel
The Aerospace Corporation

SESSION III

Program PTTI Requirements

Chairman: Philip E. Talley, Jr.
The Aerospace Corporation

SESSION IVA

Clock Devices

Chairman: Leonard S. Cutler
Hewlett-Packard

SESSION IVB

Time Transfer Modems

Chairman: Marc A. Weiss
National Institute of Standards and Technology

SESSION V

Evening Workshop
Measurement Techniques and Algorithms for Time Generation and Synchronization with High Reliability

Moderator: Samuel R. Stein
Timing Solutions Corporation

SESSION VIA

Telecommunications Synchronization

Chairman: R. Brown
Bellcore

SESSION VIB

Fiber Optic Frequency Distribution

Chairman: George F. Lutes
California Institute of Technology
Jet Propulsion Laboratory

SESSION VII

Clock Modeling

Chairman: James A. Barnes
Austron, Incorporated

CORRECTIONS AND ADDENDA

IN MEMORIAM—CECIL C. COSTAIN

Robert J. Douglas and Derek Morris
Institute of National Measurement Standards
National Research Council
Ottawa, Ontario, Canada KIA OR6

It is with sadness that we record the untimely passing of Dr. Cecil C. Costain on Decmber 18, 1991 in Ottawa, Canada. Cec was well known to many people in the field of time and frequency and he often attended the PTTI meetings. For many years he was the official Canadian delegate to the Consultative Committee for the Definition of the Second (CCDS) and took an active part in the committee work. He served on the CCDS Steering Committee for TAI. He was also an active participant in the work of Study Group 7 of the Consultative Committee on International Radio (CCIR). This Study Group deals with time and frequency services, and related topics. He also served as a member of Commission 31 of the International Astronomy Union (IAU). In addition to his work in the field of time and frequency, Cec played an important role in the development of science in Canada. His stature, his keen intellect and sense of humour, his cheerful optimism, and his forthright opinions will be sorely missed.

Cec grew up in farming country in Saskatchewan, and attended the University of Saskatchewan as an undergraduate, receiving his B.Sc. in 1941. During the Second World War, he was commissioned in the Royal Canadian Navy, then served with distinction on secondment to the Royal Navy as an officer handling the newly developed radar systems on board ship in the Pacific. At the age of 21, Cec was on top of the aircraft carrier HMS Victorious in full charge of radar with 40 men under him! With his skillful experimental touch, his radar had greater range than anyone else's, and he received a commendation from the Admiral for having the best record in the fleet. He was awarded the Distinguished Service Cross in 1944, and retired with the rank of Lieutenant-Commander in 1945. After the war, Cec returned to the University of Saskatchewan for M.Sc. work, then traveled to Britain on a scholarship to study for his Ph.D. at Cambridge with Sir George Sutherland. After returning back across the Atlantic with Prof. Sutherland to finish his Ph.D. at the University of Michigan, he was recruited in 1951 into the new Spectroscopy Section in the Division of Physics at the National Research Council in Ottawa, where he put his wartime radar experience to good use in setting up an important laboratory in microwave spectroscopy. This rapidly became one of the major world centers for microwave spectroscopy, and many of the notable international figures in the field worked with him as postdoctoral or visiting workers.

As a microwave spectroscopist, Cec was noted for his careful work, and insight into the problems of accurate molecular structural determination. He largely resolved the ambiguities then encountered among bond lengths and angles determined from different isotopic variants of a molecule in a seminal paper in 1953 which showed that the systematic isotopic substitution of each atom led to a consistent set of structural parameters. The "Costain r_s–structure" quickly became the standard technique in the field.

In 1972, Cec left the Spectroscopy Section and became head of the Time and Frequency Section of the Physics Division of NRC. There he oversaw the development, by Al Mungall, of the NRC cesium clocks used as Canada's primary standards of time and frequency with accuracies of $5x10^{-14}$. He improved the dissemination of accurate time throughout Canada by radio, telephone, and satellite. He put into operation talking clock systems and computer time systems which give accurate time by telephone. He was also pivotal in early international comparisons of time scales using the Hermes, Symphonie, and Anik geostationary satellite for two–way time transfer amongst NRC (Ottawa, Canada), NIST (Boulder, Colorado), USNO (Washington,D.C., USA), LPTF (Paris, France), and PTB (Braunschweig, West Germany), achieving a precision as good as 0.2 nanosecond.

Cec worked for many years trying to persuade governments to extend the period of daylight–saving time. He was pleased when his suggestions wee finally accepted by North America. He was elected as a Fellow of the Institute of Electrical and Electronics Engineers in 1981, "For leadership in the development of primary frequency standards and two–way time transfer techniques via geostationary satellites". He continued in charge of Canada's time standards until his retirement from NRC in 1986.

He served as President of the Canadian Association of Physicists 1980–1981 and in 1985 he was honoured with the presentation of their Medal for Achievement in Physics. He was elected as a Fellow of the Royal Society of Canada in 1974. These honours were richly deserved, and Cec continued to play an active role in support of science until his untimely death.

Cec was loved and respected by all who knew him for his integrity and his contagious enthusiasm. We are proud to have had him as a colleague and as a friend. He will be greatly missed in the years ahead.

IN MEMORIAM—FRANCIS H. MULLEN

Ron C. Roloff
Frequency and Time Systems
34 Tozer Road
Beverly, Massachusetts 01915

It is with deep regret that we announce the death of Francis H. Mullen of Reading, Massachusetts at his home on February 10, 1993. He was 62 years old.

Frank was born in Worcester, Massachusetts and attended St. Peter's High School, Worcester Junior College and the Wentworth Institute. He joined the U.S. Air Force and was a veteran of the Korean Conflict.

Frank is remembered for his extraordinary dedication to Cesium Standards over a period of more than thirty years. He was involved in the engineering, operations, and sales of Cesium Standards. While his main strength was always sales, he also had a world wide reputation for technical knowledge, integrity, and dedication.

It was once said that Frank had a miniature Cesium Standard implanted in his brain because he was always contemplating a better cesium and a better use for Cesium Standards.

Frank started selling Cesium Standards in the early 1960's for the National Company. His first sales were the vacuum tube Cesium Standards of the time. He was Sales Director at National Radio from 1971 through 1980. He started with Frequency and Time Systems, Inc. in January of 1980. During his years at FTS, he was Manager of Government Sales, Product Manager for Cesium Standards, and Sales Manager for Cesium Instruments. He received a merit reward for "Outstanding Salesmanship" in 1982.

Frank was a member of the PTTI for many years. He served in various roles in the organization. His most recent position was that of Exhibit Chairman.

He was also a member of the Old Crows Association.

He is survived by his wife, Jean M. (Butler) Mullen, 2 daughters, his mother, Vera (Hildreth) Mullen, a brother and 3 sisters.

His work for the PTTI and the community will be sorely missed. We have lost a good friend and an active participant in the Frequency and Time field.

Opening Address

Captain Winfield Donat, III, USN
Superintendent, U.S. Naval Observatory

It is, indeed, my pleasure to welcome you to the 24^{th} Annual PTTI Planning and Applications Meeting, and, at the same time have the opportunity to make a few comments at the outset.

Today, the field of Precise Time and Time Interval seems to be a real enigma, because it seems to violate one of the fundamental paradigms of good timekeeping. The ideal condition in timekeeping is usually described in terms of a well–defined, repetitive phenomenon, one that never varies, both in the short term and in the long term. Stability is the key! But when one looks at the field of PTTI these days, one sees change, innovation, and exciting technological advances. Because we did things a certain way yesterday in no way means that we will be doing it the same way tomorrow.

The fundamentals of PTTI change as new technological advances are incorporated into systems; and, now, change is truly commonplace in our field. With the new technology, current and potential users are closely reviewing the possible applications to do their jobs more accurately, more securely, faster, and more cheaply. Yes, the "C–word"...change...extends these days far beyond the political arena, and our historically quiet and constant area of interest is anything but quiet and constant today.

In one area, near and dear to my heart, we can see this most clearly. The nation's Master Clock at the USNO is a dynamic, evolving entity. If anyone here visited the USNO a year or more ago, then please visit again because you will see change. As you know, the USNO Master Clock is a very unique timing system. It is the heart of all DoD timed systems and is the national time reference. It is the real–time, physical realization of a mathematical time scale based on a large number of diverse clocks. Currently, all of these clocks are located on the grounds of the USNO. But that will not be the case in the near future.

Historically, the USNO has used a network of Precise Time Reference Stations (PTRSs) to distribute and monitor time in different geographical areas, but they have not served in the Master Clock system *per se*. As we reported in our Annual Summary of PTTI Requirements and Operations this year, the establishment of our Ultra–High Precision Time Reference Stations (UHPTRSs), to serve as a part of the Master Clock, will change the single–site Master Clock concept. We expect that this new type of timing facility will include some of the latest developments in clock systems technology and environmental stability currently achievable. It is an exciting, new concept in the way time will be kept, computed, and distributed in the future. It is the first step toward a distributed timekeeping infrastructure, a node with significant timing capability, in support of what is anticipated to be increasing requirements of PTTI systems in

the DoD and throughout our nation.

Over the past year, I have become more and more concerned over the need to increase the precision and interoperability of timed DoD systems. In order to derive the full measure and benefit of military systems within constrained resources, the need for standardization and automation is essential. While it may not be obvious to all end–system users, there are many systems in which timing is imbedded, even hidden, in the overall specifications, but is vital to the system achieving its specified performance.

In order for these systems to reach specifications, timing requirements must be addressed and clearly articulated in development. Such systems will—no doubt—take advantage of the rapid improvements being made. For example, through sophisticated mathematical techniques, a local timekeeping system in very remote areas can be maintained with impressive stability. Systems engineers are and will continue to incorporate into their projects other such advances in order to reduce and remove the traditional human interface with timed systems.

Historically, the fields of navigation and timing have been strongly linked. From the times when the Englishman John Harrison made his seagoing chronometer, to our modern satellite navigation systems, clocks have played a major role in navigation systems. In order to get a mile accuracy in his position, Harrison's clock only had to keep time to within 4 seconds. Today, our modern navigation systems—TRANSIT, LORAN, OMEGA, Global Positioning System—with their clocks can determine position very much better, GPS in fact to within meters, the latter corresponding to several tens of nanoseconds accuracy.

While time has played such an important role in navigation, it is appropriate to note that navigation systems have played an important role in PTTI, as well. Having knowledge of one's position by some means allows the PTTI user to derive time from all modern navigation systems with greater simplicity than actually deriving position. In the early sixties, the PTTI community was getting time from the Navy Navigational Satellite System (TRANSIT) to about 35 microseconds on a routine basis. LORAN–C allowed the timing community to get time to about 200 nanoseconds on a regular basis. Even Omega was used for a while for timing.

Of course, along came GPS. GPS now has 19 satellites in orbit providing not only the best navigational data available to DoD components, but also the best timing data that have ever been made available to the vast majority of PTTI users in the field. GPS PTTI performance over the last year, as in previous years, has improved. While the GPS system time is kept to within one microsecond of UTC(USNO), as a time transfer mechanism it provides precise time to users at an accuracy to within plus/minus one hundred nanoseconds of UTC(USNO).

Similar to the field of navigation, the atomic clocks used in our laboratories have seen significant progress over the last few decades. The workhorse of the industry, the cesium–beam clock, was introduced in the early sixties. It kept time to within several hundred nanoseconds from day to day. By the early seventies, the high performance cesium–beam tube was introduced. These clocks kept time to about 20–40 nanoseconds per day. Today, we have on the market an improved version that promises to minimize the effect of environmental conditions on clock performance. Preliminary data indicate that these new clocks are performing remarkably well in a variety of conditions. Another great stride forward.

New timing procedures are showing up everywhere. The evolution and transformation of one of our national communications systems into a state–of–the–art digital network using GPS as the precise time source, rather than an independently maintained clock system, shows the capabilities that are being integrated into many timed systems. Obviously, both efficiency and effectiveness were served in this upgrade. Other national communications networks rely on precise time from LORAN.

During the year, several other areas have made some new strides forward. Regularly scheduled two–way communications satellite time transfers between North America (USNO) and Europe (Technical University of Graz [TUG] & Observatoire de la Côte d'Azur [OCA]–were inaugurated utilizing an INTELSAT satellite. Envisioned international networks, such as this, will soon become a force in the improved development of the international time scale. I consider these to be important events for several reasons, including the Observatory's need to coordinate the DoD time reference standard with other international standards to ensure continuity of precision, and the strengthening of time coordination that supports our European allies.

In addition, the use of laser pulses to synchronize clocks between North America (McDonald Observatory) and Europe (OCA) was accomplished for the first time. This technique still holds the promise of being the most accurate time transfer method currently possible. Time transfer accuracy around 300 picoseconds was realized in this exercise.

Yes, everywhere we look today in the timing business, change is at hand. The magnificent work of so many has delivered to us great technological capabilities. Our challenge is to be smart in their use. PTTI is becoming such a important part of our everyday life that we cannot afford to ignore the necessary considerations regarding infrastructure support and compatibility.

Certainly in the DoD, precise time plays an ever–increasing role in effective employment of our assets, and in this age of sophisticated weaponry and very complex battle–group management and tactics, split second timing is far more than just a catch phrase. We must be always conscious of the need to address issues of precise time calibration and verification; interoperability of multiple systems; precise coordination of sensors and fire control systems, communications links and navigation systems; internal precise time distribution and local control; physical vulnerability and risks to critical timing sources; and overall data fusion.

Even the PTTI Meeting has innovation this year. Over the years, the PTTI meeting has attempted to bring together the users and the developers of PTTI. Sometimes there have been panels which discussed a topic relevant at the time. This year we are hoping to make you – the attendees – the panel. It is very important that we get you to share your experiences and learn about operating systems and those nearing operational status in regard to their timing capabilities. We also need to know what the future needs are for timing support. Clearly, realizing the extent of change today forces us to become very aggressive in planning for the timing support for tomorrow's systems.

This afternoon, we will have a set of three workshops. All attendees are strongly encouraged to voice their opinions, concerns, and requirements. Speakers are encouraged to join in, too. In order that the thoughts brought out during the workshop become more focused and more useful as background for the numerous discussions which take place during the meeting, Dr. Winkler will summarize the results of the workshop. His comments will surely be a catalyst in

fostering the exchange and sharing of ideas.

It is the purpose of this conference to stress the important role of PTTI to everybody concerned with timed systems, e.g., engineers, managers, planners, users, designers, etc. The role of this meeting cannot be underestimated. It is the ONE conference not edicated solely to the "technologists" of the industry. Its audience is broadband, and we have attempted to bring in people whose interests in the subject range across the constantly expanding PTTI field of today.

So, I wish you every success in this conference and am excited to join with you as we benchmark and assess the ever-changing world of precise time and time interval.

THE TIME KEEPING SYSTEM FOR GPS BLOCK IIR

H. C. RAWICZ[1], M. A. EPSTEIN and J. A. RAJAN
ITT Aerospace/Communications Division
100 Kingsland Road, Clifton, NJ

Abstract

The precision time keeping system (TKS) in the Global Positioning System (GPS), Block IIR satellites is designed to operate under severe natural and man made environmental conditions. The Block IIR TKS provides precise, autonomous time keeping for periods of up to seven months, without the intervention of the GPS Control Segment. The TKS is implemented using both linear and non–linear controls. The resulting TKS architecture uses a hybrid analog/digital phase locked loop (PLL). The paper provides details of the design and analysis of the TKS. The simulation techniques and the test bed activities used in performing the TKS design trade–offs are described. The effects of non–linear controls are analyzed using a TKS computer simulation of the PLL. The results from a hardware test bed are provided that verify desired TKS operation. The design criteria for the TKS computer simulation and the hardware test bed are indicated. The concepts for verification and testing of the TKS computer simulation and hardware test bed are presented.

GPS BLOCK IIR

Global Positioning System (GPS) is an all weather, worldwide, passive navigation system that is currently in use for a variety of land, water, air, and space navigation applications. ITT Aerospace/Communications Division(ITT A/CD) is a leader in the development of space payloads and has been involved in the design of various portions of the GPS space segment from the inception in mid '70s. ITT is currently developing the Total Navigation Payload (TNP) for the next generation (Block IIR) GPS satellites. Block IIR GPS satellites provide longer life, improved performance, crosslink ranging and enhanced crosslink communication capabilities. The Block IIR TNP also provides autonomous operation for up to 210 days without Control Segment intervention. Autonomous navigation is achieved using a two way ranging and data exchange process between the GPS satellites in the constellation. Further details of GPS Block IIR Autonomous Navigation (AutoNav) can be found in [1].

TIME KEEPING SYSTEM

The Time Keeping System (TKS) is the heart of the GPS TNP and provides an accurate time base for each satellite in the GPS system. TKS derived timings are used to provide accurate timing for

[1]Dr. H. C. Rawicz is also an assistant professor at Trenton State College, Trenton, NJ.

the other payloads in the GPS satellites and also constitutes the reference to the navigation ranging signals. GPS user receivers determine accurate time, 3D position and 3D velocity by measuring ranges and range rates to a set of four GPS satellites. The accuracy of the user's position, velocity and time determination depends on the accuracy of the data transmitted to the user, the geometry of the four satellites used and the precision of the TKS system.

TKS ARCHITECTURE

The TKS loop architecture is a Phase Lock Loop (PLL) based implementation that has enhanced single event upset and radiation performance. Figure 1 shows the block diagram of the TKS architecture. A detailed description of the TKS architecture can be found in [2]. The TKS system utilizes two frequency sources, one is a reference frequency source (derived from an atomic frequency standard) and the other is a system frequency source (derived from a VCXO). The system frequency source (10.23 MHz) is the output of the TKS system that provides precise timing to GPS satellites. The two frequency sources are coupled via a sampled data control loop, referred to as the TKS PLL. The 10.23 MHz TKS system clock has the excellent short term stability of the VCXO and the excellent long term stability of the atomic frequency standard (AFS). The exact value of the AFS's natural frequency is not critical. The TKS system can be used with either a Cesium AFS (CAFS) or a Rubidium AFS (RAFS). This paper will primarily concentrate on TKS performance when using RAFS. The AFSs natural frequency is approximately 13.4 MHz. The two frequency sources are independently divided to provide a 1.5 second reference epoch signal and a 1.5 second system epoch signal. The phase difference between these two signals are precisely measured by a hardware phase meter. The output of the phase meter is the driving signal for the TKS PLL which is implemented in software.

TKS LOOP

The TKS phase lock loop (PLL) combines: (1) the excellent short term stability of a voltage controlled crystal oscillator (VCXO) to enable superior short time interval TKS accuracy, and (2) the excellent long term stability of the AFS to enable superior long time interval TKS accuracy. The selection of the loop time constant enables proper selection of this crossover between VCXO and AFS stabilities. Varying the crossover time interval will have an impact on the TKS output Allan Variance. A shorter crossover interval increases the contribution of hardware component noise to the Allan variance. A longer crossover interval increases the contribution of VCXO drift to the Allan variance. Effects of this trade–off are discussed later using simulation results.

The software implementation of the control loop also allows clock corruptions to be easily added to limit the accuracy provided to unauthorized GPS users. To maintain full accuracy for the authorized users who have access to the clock corruptions, the gain of the VCXO has to be periodically estimated. The TKS performs an open loop gain characterization of the VCXO initially, and subsequently, when the loop is closed and tracking, the gain is periodically updated using a minimum mean square estimator. The estimated gain of the VCXO from its digital frequency command to its analog frequency output (the VCXO transfer function) is compensated for by the gain control so that the gain from the output of the PLL compensation filter to the VCXO output is kept at unity to within small fractions of a percent under all conditions. This compensation enables the

authorized users to achieve the full accuracy of the TKS system. Without the compensation, this gain could vary several percent causing noticeable TKS accuracy degradation.

The heart of the gain control is an equation which has as its input the digital frequency command from the PLL loop filter and as its output the digital control value that drives the VCXO input. The gain tracking uses a localized linear equation around the operating point of the VCXO. The gain control technique takes advantage of the small variations used for clock corruptions, as they are within the linear range of the VCXO at normal operating points. The gain tracking algorithm measures the changes in the VCXO transfer function during the period the clock corruptions are being applied. Any changes in gain are decoupled from the PLL output by modifying the frequency command at the same time the gain equation is changed so that the output will not exhibit any step changes. The performance improvements achieved using gain compensation are described in later sections.

TKS SIMULATION

The TKS simulation activity was undertaken: (1) to get insight into the performance prior to the availability of flight hardware and software, (2) to evaluate the algorithms for compliance to required performance, (3) to refine the algorithms and simplify them for ease of implementation, (4) to perform algorithm trade–offs and (5) to reduce development risk. The simulation also allowed the algorithms to be verified at an accelerated time compared to real-time, and used a higher order programming language, enabling faster performance evaluation.

The TKS simulation implements the difference equations that describe the Z transform of the TKS hardware, and the algorithms of the TKS software. The hardware error sources are also modeled. The block diagram of the TKS simulation is shown in Figure 2.

There are three major error sources in the TKS system, namely: the AFS, the VCXO, and the phase meter. The phase meter outputs the digital phase difference between the two oscillators and is the error detector for the PLL. In order to accurately simulate the PLL, the three error sources are modeled by noise generators that have the specified Allan Variance of each error source.

The AFS noise is simulated by combining two Allan Variance noise generators, an initial slope of $\tau^{-0.5}$ for small and moderate τ, and a final slope of τ^0 for large TAU. The actual AFS has a slope of τ^0 for very small τ. This can be ignored because the PLL bandwidth is such that the PLL dramatically attenuates the Allan Variance of the AFS input for TAUs almost an order of magnitude larger than the maximum τ of the ignored portion. The inherent drift of the AFS is also ignored because the GPS Control Segment measures and compensates for that drift as part of its normal procedures. The resulting Allan Variance of the RAFS is shown in Figure 3.

The phase meter noise is simulated using a uniform random number generator. The TKS phase meter has a 600 MHz oscillator which is used to measure the length of the phase interval. The random number represents the phase of the oscillator at the start of the phase error interval. The output of the simulated phase meter is the oscillator period multiplied by the number of counts in the phase error interval. The phase meter noise is the difference between the phase meter output and the actual phase error interval. Drift in the frequency of the phase meter oscillator can be neglected as it causes an insignificant change in the quantization interval. Random noise pickup

in the phase meter circuitry is also neglected due to its high frequency nature compared to the forward path bandwidth of the PLL. The resulting Allan Variance of the phase meter is shown in Figure 4.

The VCXO noise is simulated using an Allan Variance noise generator with an initial slope of τ^0 for small τs and an Allan Variance noise generator with a slope of $\tau^{0.5}$ for moderate and large TAUs to represent the drift in the VCXO. The resulting Allan Variance of the VCXO is shown in Figure 5.

The Allan Variance noise generator used for generating a τ^0 slope is a modified version of the one presented in [3]. The Allan Variance noise generator used for generating a $\tau^{-0.5}$ slope is obtained by integrating the output of a Gaussian random number generator. The Allan Variance noise generator used for generating a $\tau^{0.5}$ slope is obtained by double integrating the output of a Gaussian random number generator.

TKS HARDWARE TEST BED

The TKS hardware test bed, which consists of brassboard and engineering development model (EDM) hardware, was used to accelerate development of TKS algorithms on the real hardware, prior to the availability of flight hardware. The test bed provided an early, fast, low cost demonstration of the feasibility of the VCXO loop and validated the performance of the operational hardware, and the TKS algorithms. The test bed also provided confirmation of the correctness of the TKS simulation model. The use of off the shelf hardware and test software with only the functions needed to test the PLL has made the cost of the hardware test bed minimal. The test bed activities enabled improvements in hardware and software. The test bed was upgraded as more and more flight like hardware were available. The test bed activities provided considerable reduction in the development risk of the flight hardware meeting TKS performance needs. It also enabled a through testing of the TKS with specially designed test bed tests. The following paragraphs describe the test bed development.

The initial test bed had no EDM hardware. The AFS 13.4 Mhz signal was provided by a HP 3325B synthesizer driven by an off the shelf EG&G 10 MHz RFS-10 Rubidium oscillator. The reference and system epoch generators used existing counters which ITT A/CD had built as part of a demonstration unit for a precursor program to the present GPS Block IIR program. The software algorithms were programmed and executed using the C language on an IBM compatible AT 286 PC. The phase meter function was performed by an off the shelf GT–100 Universal Counter PC card with a precision of 0.1 nanoseconds. The test bed used a demonstration unit digital VCXO at 10.23 MHz (nominal center frequency) with a digital input that drove two precision digital to analog converters to control the output frequency.

The initial test bed demonstrated the feasibility of generating a precision GPS 10.23 MHz signal using a VCXO that was locked to an AFS at a different non harmonically related frequency. The output signal was phase locked to the AFS, with and without clock corruptions, to within a fraction of a nanosecond. This initial demonstration program used externally generated values for centering the VCXO and compensating for the VCXO transfer function.

In the past year, as EDM hardware became available, they were incorporated into the test bed and

checked out. First, the demonstration VCXO was replaced by a single thread VCXO with the same input controls as the EDM unit and then the single thread unit was replaced by a dual unit flight configuration EDM VCXO. Also a phase meter which has the same 600 MHz counting technique and the same 1.67 nanosecond quantizing noise as the flight phase meter was incorporated into the test bed. In addition, the software was upgraded to use the operational centering, VCXO gain control and gain tracking. The rest of the hardware was unchanged except that the PC was upgraded to a 386 machine. With the new software and hardware, the test bed TKS system could center, characterize, and track the AFS to a fraction of a nanosecond without any outside values or assistance.

The test bed performance was compared to the prediction of the TKS simulator and theoretical calculations. As shown below, there was agreement between the measured test bed performance and the predicted performance. The success of the cross check has provided confidence in the GPS TKS design in general, including the correctness of the hardware design, the software algorithms, and the TKS simulator.

CO–VERIFICATION OF TKS SIMULATION AND TEST BED

The first step to co–verification was to insert a step function into the error in the PLL hardware test bed. This was accomplished by adding a constant to the digitized error in the test bed control computer and monitoring the digitized error after the step function insertion point for a period of time. Exactly the same step function was inserted at exactly the same point in the simulation and exactly the same monitoring was performed. Figure 6 shows an overlay of the two monitored points, one in the simulation and one in the test bed. Note that the two transients differed only by the noise pickup present at the test bed error point. This showed that the deterministic dynamics of the test bed and the simulation matched.

The next step was to record the digitized steady state error at the output of the phase meter of the hardware test bed and exactly the same point in the simulation. These errors were then used to compute the Allan Variance of the phase meter error for the hardware test bed and the simulation. The shape of the Allan Variance curves matched, however the amplitude was different. The difference was due to the smaller quantization of the purchased phased meter initially used in the test bed.

A brassboard phase meter was built which used the same design parameters as the production phase meter. This unit was placed in the test bed. There was initially a question as to whether the brassboard unit was working as designed. Open loop tests of the phase meter were performed, but inherent drifts in the test bed prevented statistically usable results. The solution was to sample the closed loop, steady state error at the output of the phase meter in the test bed and compute its Allan Variance for comparison to the equivalent Allan Variance from the simulation. Figure 7 shows the results with the PLL subject to pseudo clock corruptions and on line gain tracking. Note that at low TAU where the phase meter noise would dominate, there was less than 10% difference between the Allan Variance curves from the test bed and the simulation. This led us to the conclusion that the simulation of the phase meter was correct, that the brassboard phase meter was also operating as designed, and that the difference was attributable to the noise pickup in the system.

TKS PERFORMANCE TRADE–OFFS

The bandwidth of the PLL is chosen to achieve the best TKS Allan Variance (at the output of the PLL). This selected bandwidth is such that it attenuates the effects of the AFS and the phase meter for small TAU and the effect of the VCXO for large TAU. Figure 8 shows that if the PLL time constant is too small, the phase meter noise at the output get too large. It also shows that if the PLL loop time constant is too long, the drift of the VCXO gets too large. The result was a loop time constant which was a tradeoff between the two noise effects at the output of the PLL.

The bandwidth of the PLL also affects the transient responses to steps and ramps that might be caused by an undesired severe environmental disturbance. Figure 9 shows how the transient response changes as a function of the PLL time constant. It shows that the smaller the time constant, the faster the response and the smaller the peak. Therefore the smaller time constant is desirable from a transient point of view. The TKS design uses a dual time constant: a short time constant during transients and a long time constant during steady state. Figure 10 compares the initial lock–on transient using switched, dual time constants and using a single long time constant. The reduction in settling time and amplitude deviation is dramatic.

The PLL has to operate closed loop to make the VCXO output exactly follow the AFS phase plus the clock corruptions that have been introduced. The simulation was used to determine the effect of clock corruptions on the closed loop operation compared to a case with no corruption. Clearly the unauthorized users who do not have access to the clock corruptions will see their time, range, and range rate accuracies degrade. On the other hand, the authorized users who have access to the clock corruption values can remove the effects of the clock corruptions and achieve full accuracy of the TKS. Figure 11 shows that there is a very small increase in the Allan Variance at the output of the PLL when clock corruptions are in effect. This will be the TKS performance available to the authorized users.

The implementation of clock corruptions as an open loop perturbation requires VCXO gain tracking. The algorithm for gain tracking was implemented in both the simulation and the test bed. Figure 12 shows the computer simulation output Allan Variance with and without gain tracking. There was no significant difference between the two graphs. Note that Figure 7 is the Allan Variance for the test bed and the computer simulation of the phase meter output in the presence of clock corruptions and gain tracking. The results agree to within about 10-20%. This shows that the hardware and the simulation agree, validating the VCXO characterization and gain tracking approaches and algorithms in the presence of clock corruptions.

To insure that there was no interaction between the stability of the system and the non-linear characteristics of the VCXO gain tracking algorithms, a BODE plot was made of the simulation with gain tracking activated. Figure 13 is the results of this test and indicate that there is no detectable deviation in the BODE plot with and without gain tracking. Also, the BODE plot is what was expected based on the deterministic design of the PLL, and shows sufficient gain and phase margins, ensuring the stability of the design.

CONCLUSIONS

As expected, the simulation and test bed activities were valuable tools that enabled the TKS design and development, prior to the availability of the flight hardware, thereby mitigating the development risk. The resulting TKS design with dual time constant has excellent transient behavior and steady state stability, providing a near optimal TKS system.

ACKNOWLEDGEMENTS

The authors wish to acknowledge the contributions of R. Smid of ITT A/CD in leading the TKS design effort, J. Petzinger and A. Baker of ITT A/CD for their contribution to the design, P. Katsihtis for his test bed efforts, and T. Hazard, a summer student from Trenton State College, for his assistance in the simulation efforts.

REFERENCES

[1] Brower, S., Klein, D., Slonaker, P., Chen, G., and Doyle, L., *"GPS Block IIR Autonomous Navigation Emulator"*, presented at the Institute Of Navigation Conference in Sept. '91.

[2] Baker, A., *"GPS Block IIR Time Standard Assembly Architecture."*, presented at the 22nd Annual PTTI Meeting in Dec. '90, pp. 317–324.

[3] Barnes, J. A., and Greenhall, C. A., *"Large Sample Simulation Of Flicker Noise"*, presented at the 19th Annual PTTI Meeting in Dec. '87, pp. 203–217.

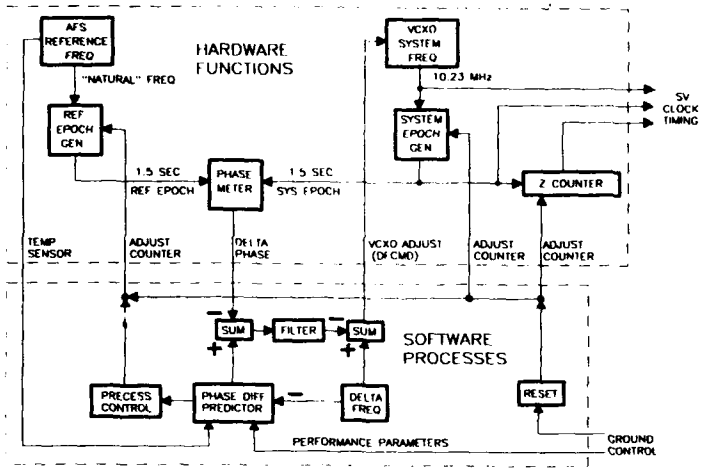

Figure 1: TKS Architecture

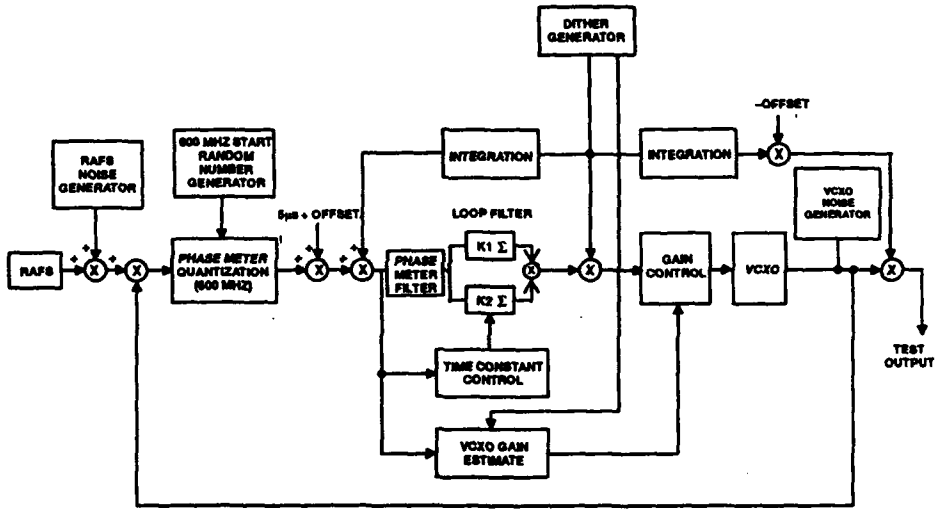

Figure 2: TKS Simulation Signal Flow

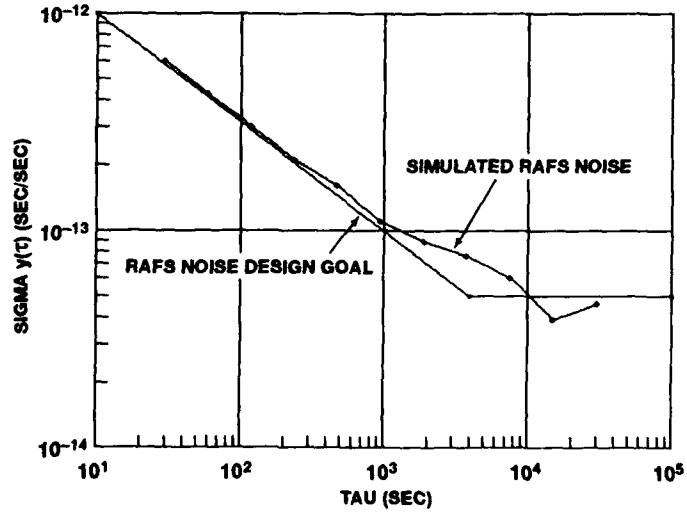

Figure 3: Simulated RAFS Allan Variance

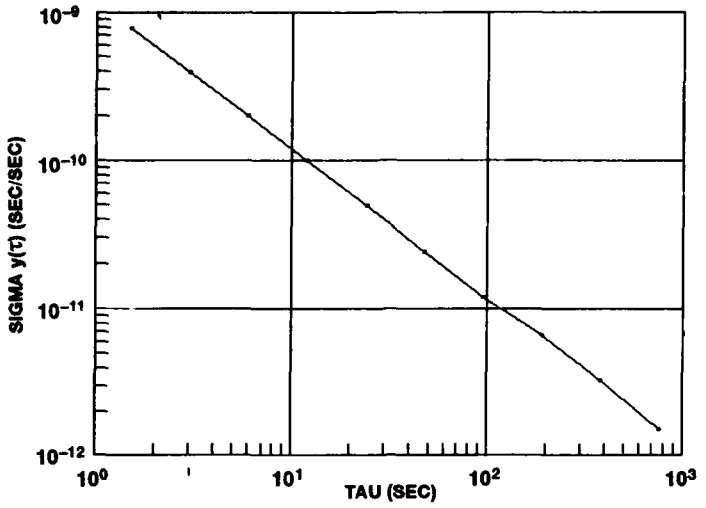

Figure 4: Simulated Phase Meter Allan Variance

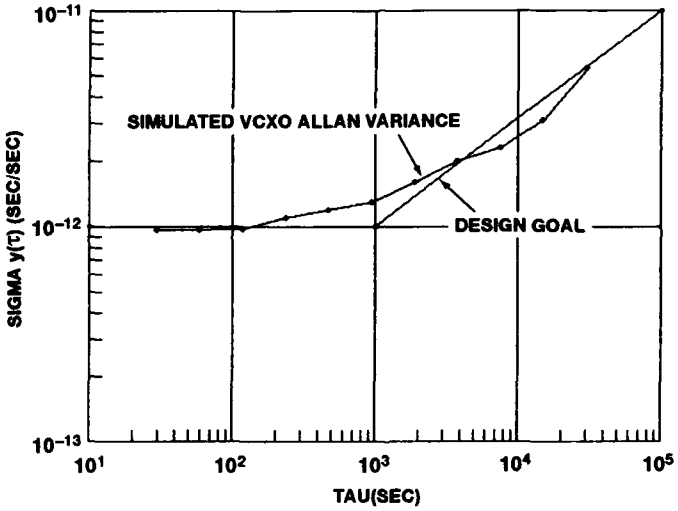

Figure 5: Simulated VCXO Allan Variance

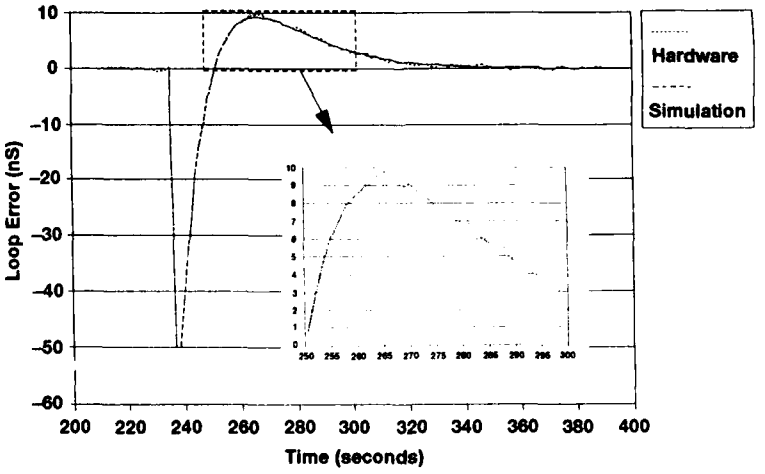

Figure 6: Phase Jump Response of TKS Test Bed and Simulation

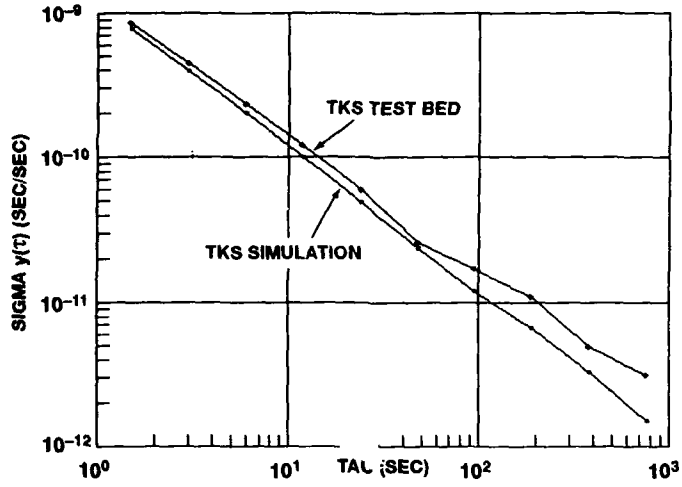

Figure 7: Loop Error Allan Variance of TKS Test Bed and Simulation

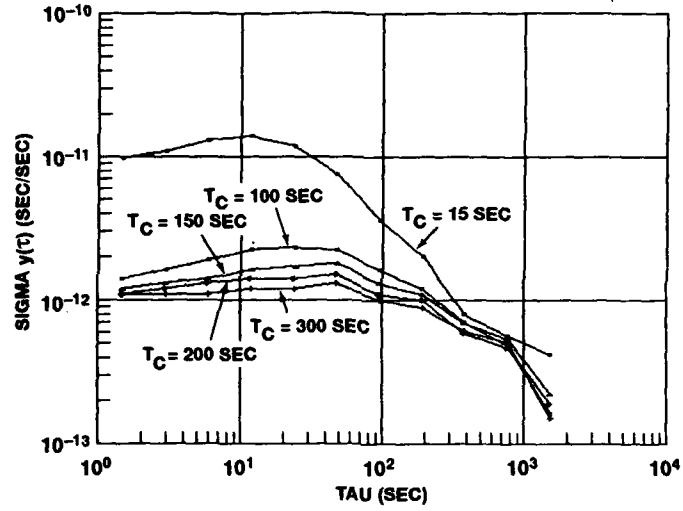

Figure 8: TKS Allan Variance When Using RAFS (Variation With Loop Time Constant)

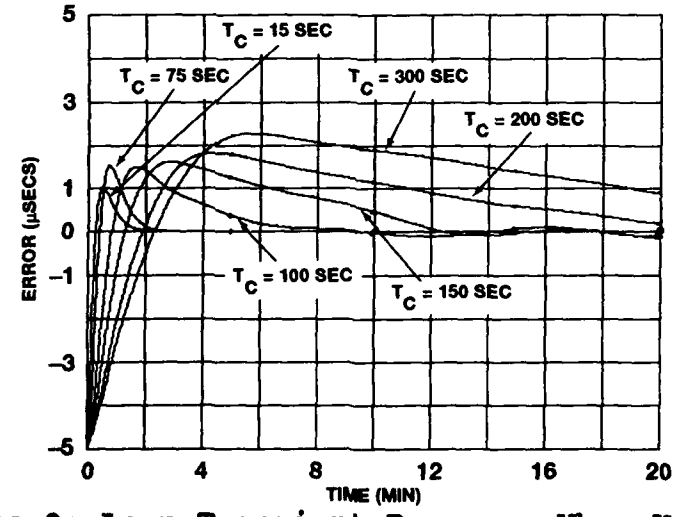

Figure 9: Loop Transient Response When Using RAFS (Variation With Loop Time Constant)

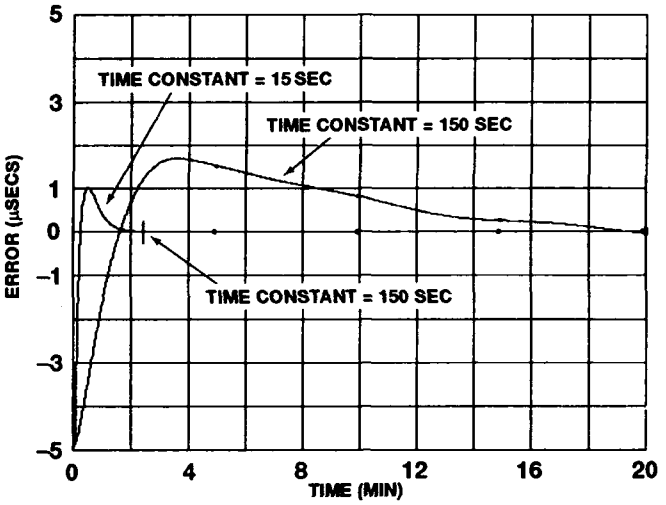

Figure 10: Loop Transient Response When Using RAFS (Single Vs Dual Loop Time Constants)

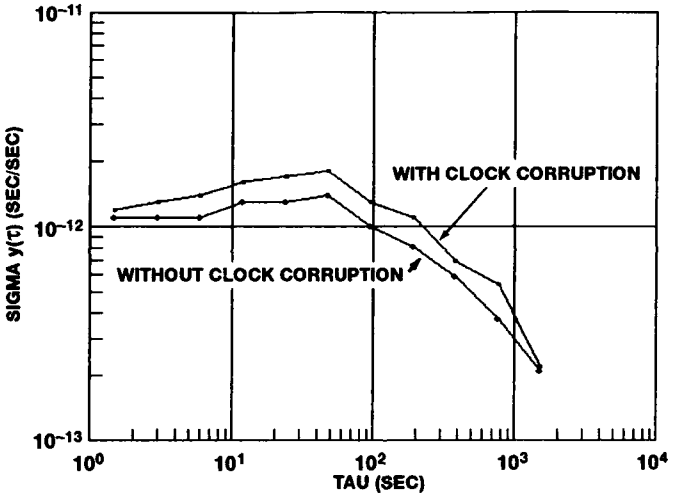

Figure 11: PLL Output Allan Variance When Using RAFS (With And Without Clock Corruptions)

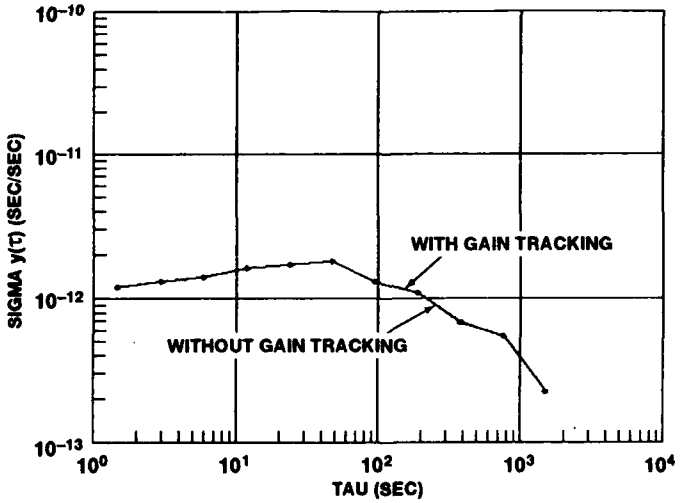

Figure 12: PLL Output Allan Variance When Using RAFS (With And Without Gain Tracking)

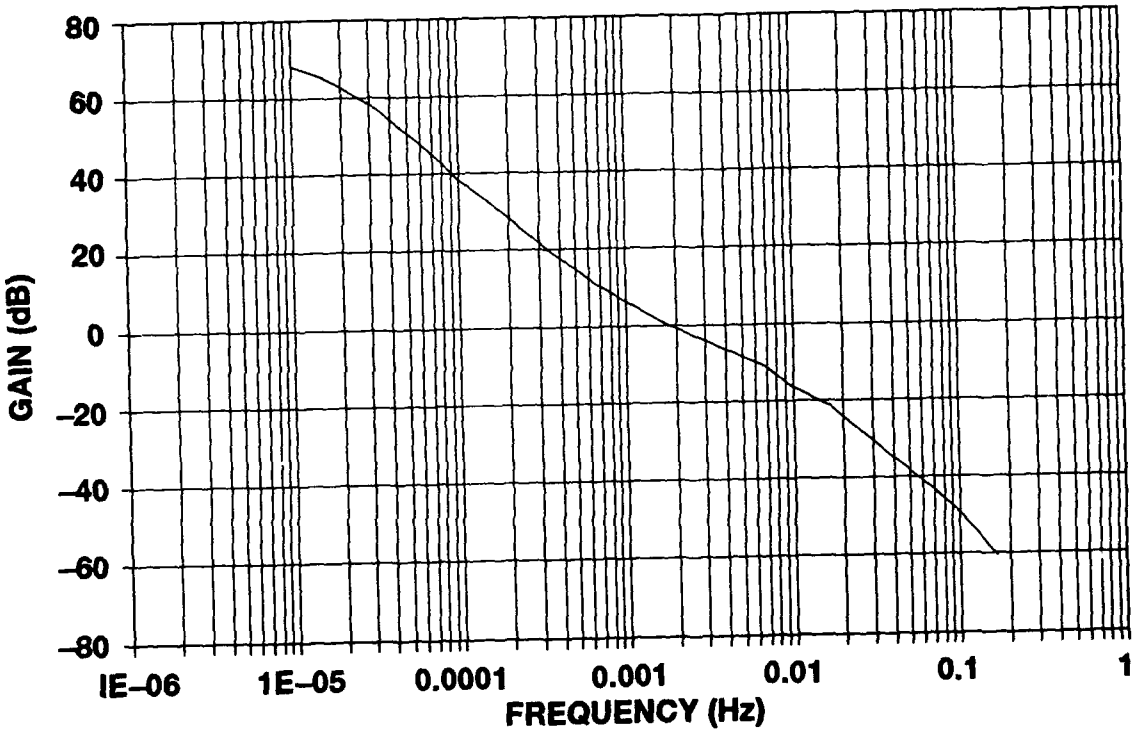

(a) Gain Plot

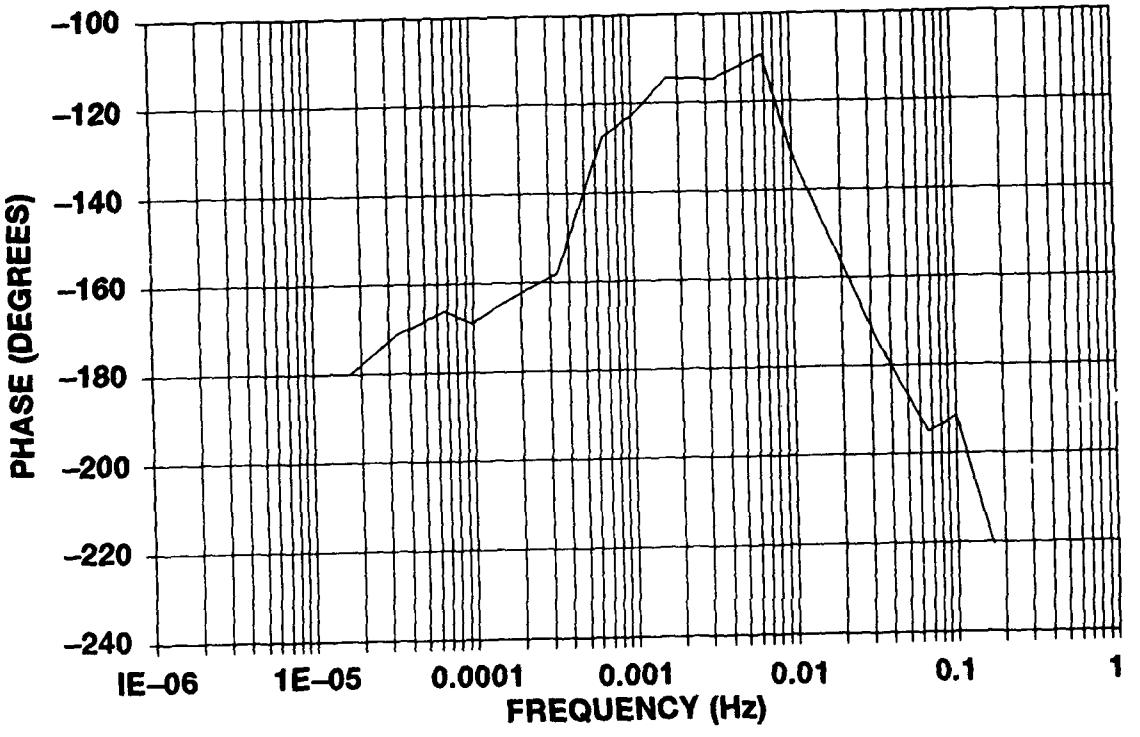

(b) Phase Plot

Figure 13: Bode Plot for the PLL
(With Clock Corruptions and Gain Tracking)

PROGRESS ON GPS STANDARDIZATION

C. Thomas
Secretary, CGGTTS
on behalf of the CGGTTS members

Bureau International des Poids et Mesures
Pavillon de Breteuil
92312 Sèvres Cedex, France

Abstract

It has been clear for some time that a desirable and necessary step for improvement of the accuracy of GPS time comparisons is to establish GPS standards which may be adopted by receiver designers and users. For this reason, a formal body, the CCDS Group on GPS Time Transfer Standards (CGGTTS), was created in 1991. It operates under the auspices of the permanent CCDS Working Group on TAI, with the objective of recommending procedures and models for operational time transfer by the GPS common–view method. It works in close cooperation with the Subcommittee on Time of the Civil GPS Service Interface Committee.

The members of the CGGTTS have met in December 1991 and in June 1992. Following these two formal meetings, a number of decisions have been taken for unifying the treatment of GPS short–term data and for standardizing the format of GPS data files. A formal CGGTTS Recommendation is now being written concerning these points. This paper relates on the work carried out by the CGGTTS.

INTRODUCTION

At present the accuracy of worldwide time transfer using GPS in common view can reach the level of a few nanoseconds provided that some precautions are taken (accurate GPS coordinates, measured ionospheric delays and precise ephemerides) [1]. But at such a level of accuracy other problems arise. These arise mainly from the lack of standardization in commercial GPS receiver software and hardware, and there is also a need to remove SA effects [2, 3].

A group of fifteen experts has been formed for drawing on user and manufacturer standards for GPS time receivers to be used for common–view time transfer. This group, the CCDS Group on GPS Time Transfer Standards (CGGTTS) operates under the auspices of the permanent Working Group on TAI of the Comité Consultatif pour la Définition de la Seconde.

The CGGTTS can undertake formal actions. These actions are considered by the CCDS, which in turn may choose to transmit some of them in the form of recommendations to the Comité

International des Poids et Mesures and then to the Conférence Générale des Poids et Mesures. The CGGTTS is complementary to the Subcommittee on Time of the CGSIC (Civil GPS Service Interface Committee) which is mainly a forum for the exchange of information between the US military operators of GPS and the civil timing community.

The CGGTTS organized an open forum on GPS standardization, which was immediately followed by the first formal meeting in Pasadena (California, USA) in December 1991. The minutes are available from the Secretary of the CGGTTS (BIPM). These minutes, sent in March 1992 to national timing centers and to GPS receiver manufacturers, include a proposed GPS data format and a letter calling for feedback. The discussion was then open and the members of the CGGTTS, taking the opportunity offered by the CPEM'92, decided to meet in Paris on 11 June 1992. The objective set for this 2nd formal meeting was to take a final decision about the GPS data format and to agree on its schedule of implementation. Formally, these decisions should be written in a CGGTTS Recommendation.

DECISIONS TAKEN DURING THE 2ND FORMAL MEETING

The detailed discussion held during the 2nd formal meeting in Paris can be found in 'The Report of the 2nd Meeting of the CCDS Group on GPS Time Transfer Standards'. This Report is available from the Secretary of the CGGTTS (BIPM). Here only a brief summary is given.

1. Implementation of new software in GPS time receivers

The National Institute of Standards and Technology (NIST, Boulder, Colorado, USA) is ready to prepare new EPROMs to incorporate in present GPS time receivers of the NIST type. The final version of these available by June 1993.

The NIST–type GPS time receivers are either prototypes, made by NIST, or commercially available devices made by Allen Osborne Associates (California, USA). NIST will send new EPROMs to laboratories equipped with NIST prototypes. Allen Osborne Associates should provide new EPROMs to laboratories equipped with commercial NIST type receivers. These EPROMs will be copies of NIST EPROMs. Other GPS time receiver manufacturers will have to prepare and distribute their own EPROMs.

2. Reference time scale, start–time and mid–point of a GPS track

The CGGTTS adopted the international time scale UTC as unique reference time scale to monitor GPS tracks. It follows that the BIPM must issue a new type of International GPS Tracking Schedule in which start–times of tracks, defined as the actual first UTC second of satellite observation, are explicitly given. Possibly Schedule n22 (December 1993) will be of this new type. In addition, the track–length is definitively chosen by the CGGTTS to be 13 minutes (780s).

The choice of UTC as the reference time scale, of the actual first second of observation as

the definition of the start–time of a track, and of 780s as the fixed track–length, allows the computation of strict common–views (i.e. synchronised to within the 1s) necessary to reduce on–board clock dither effects, brought about by SA, to less than a nanosecond.

The CGGTTS next decided that most of the quantities reported in the GPS data files should be reported at the actual mid–point of the track, defined as the mid–point of the actual observation.

3. Short–term data processing

The CGGTTS defined a standard for how short–term data should be processed in the receiver. This is explicitely given in Annex I of this paper.

The CGGTTS also insisted on the necessity of using standardized models, in particular for estimating ionospheric and tropospheric delays, when these models are already proposed in the Interface Control Document of the US Department of Defense or in the NATO Standardization Agreement (STANAG).

The observation results, i.e. the time differences [Local reference clock – GPS time] reported for each track, must include the estimation of ionospheric and tropospheric delays as obtained through these models. Room is available somewhere else in the GPS data file for reporting measured atmospheric delays.

4. Data format

The detailed data format chosen by the CGGTTS is given in Annex II of this paper. Only some specific remarks are given here:

- The Modified Julian Date (MJD) is not truncated, i.e. it is given in 5 columns.
- All quantities, including satellite elevation and azimuth, results of observations and estimates of modelled or measured tropospheric and ionospheric delays, are reported at the mid–point of the track, except the time of the track, given in hours, minutes and seconds, which is reported at the start–time of the track.
- A file header is created. It includes the name of the receiver maker, the receiver type, the receiver serial number, the software version number, the channel number, the description of the ionospheric measurement system, the name of the laboratory, the coordinates of the station and different delays entered in the receiver.
- The parameter Issue of Data Ephemeris, which identifies the broadcast ephemerides used by the receiver to compute pseudo–ranges during a given track is added to the format.
- Occasionaly missing data are represented by a series of successive 9s.

5. Other problems

The CGGTTS recalled that an additional step towards increased accuracy would be the use of a semi–empirical model for estimating tropospheric delays. It would be then necessary to record outside environmental parameters such as temperature, humidity and pressure.

The CGGTTS could take the opportunity of EPROMs change to ask makers for the implementation of an option allowing the output of short–term data and of all parameters and fundamental constants used by the receiver. The CGGTTS also suggested that GPS time receivers should be able to cover the 24 hours of a day with regular tracks.

CONCLUSIONS

A Draft Recommendation including the conclusions of the discussions held during the 2nd formal meeting of the CGGTTS has been prepared and is given below. A 3rd formal meeting of the CGGTTS will be necessary for reaching a definitive agreement about this Recommendation, which may be proposed at the CCDS during its next meeting (March 1993).

REFERENCES

[1] Lewandowski W., Petit G., Thomas C., *"Accuracy of GPS Time Transfer Verified by the Closure around the World,"* In Proc. 23rd PTTI, 1991, 331–339.

[2] Lewandowski W., Petit G., Thomas C., *"GPS Standardization for the Needs of Time Transfer,"* In Proc. 6th EFTF, 1992, 243–248.

[3] Lewandowski W., Petit G., Thomas C., *"The Need for GPS Standardization,"* In Proc. 23rd PTTI, 1991, 1–13.

DRAFT RECOMMENDATION

The CCDS Group on GPS Time Transfer Standards,

considering

- that the observation, using the common–view method, of satellites of the Global Positioning System, is one of the most precise and accurate methods for time comparison between remote clocks kept on the Earth or in its close vicinity,

- that this method has demonstrated capabilities for providing accuracy at the level of 1ns, when using accurate GPS antenna coordinates, post–processed precise satellite ephemerides, measured ionospheric delays and the results of campaigns of differential receiver calibration,

- the need for removing the effects of Selective Availability, currently implemented on Block II satellites,

- the lack of standardization in commercial GPS time receiver software, which threatens the sub–nanosecond level in the accuracy of GPS time transfer,

recommends,

- the use of UTC as the unique reference time scale for monitoring GPS satellite tracks,
- that the BIPM continues to prepare the regular International GPS Tracking Schedule, for observation of GPS satellites in common–view, in which the time of a track is characterized by the start of the first second of observation and in which the length of each track is fixed to 780s,
- that short–term data processing be performed according to a unique method detailed in Annex I,
- that all modelled procedures, parameters and constants, needed in short–term data processing be deduced from the information given in the Interface Control Document of the US Department of Defense or in the NATO Standardization Agreement (STANAG), and be updated at each new issue,
- that short–term data, parameters and constants used by GPS time receiver software be output according to the user's will, thanks to the implementation of an adequate option in the receiver operation,
- that GPS time receiver should be able to cover the twenty–four hours of a day with regular tracks,
- that GPS data be recorded and transmitted in data files arranged according to the data file format given in Annex II, including in particular a header with detailed information, and where most of the quantities are reported at the actual mid–time of tracks.
- that GPS time receiver manufacturers act towards the concrete implementation of these new dispositions.

ANNEX I

GPS short–term data processing

Short–term data processing is performed as follows:

i) Pseudo–range data measurements are taken every second, the first second corresponding to the nominal starting time of the track.

ii) A least–squares quadratic fit is applied to periods of 15s length, the quadratic fit result is estimated at the mid–point of the 15s period.

iii) Broadcast ephemeris and other broadcast and modelled parameters are evaluated at the time corresponding to the mid–point of the same 15s period; these corrections are applied to the results of ii).

iv) The nominal track length is 780s.

v) At the end of the track, a least–squares linear fit is performed to all the data resulting from iii). The result of this linear fit is made up of an estimate of the quantity to be measured, reported at the mid–point of the actual track, and of a slope and a rms given in the GPS data file.

ANNEX II

CCDS GPS Data Format Version 1

The CCDS GPS Data Format Version 1 is composed of:

i) a file header with detailed information on the GPS equipment (line 1 to 12),

ii) a blank line (line 13),

iii) a line header with the acronyms of the reported quantities (line 14),

iv) a unit header with the units used for the reported quantities (line 15),

v) a series of data lines, one line corresponding to one GPS track. The data lines are ordered in increasing chronological order (line 16, 17, 18, etc.).

Note: * stands for a blank and text to be written in the data file is indicated between ' '.

1. File header

Line 1: 'CCDS*GPS*DATA*FORMAT*VERSION*1'
Title to be written. Minimum 30 columns.

Line 2: MAKER*TYPE*SERIAL NUMBER*YEAR*SOFTWARE NUMBER
Name, type, serial number, first year of operation,
and eventually software number of the GPS time receiver.
As many columns as necessary.

Line 3: 'CH*=*'CHANNEL NUMBER
Number of the channel used to produce the data included in the file,
CH = 1 for a one-channel receiver. Minimum 5 columns.

Line 4: MAKER*TYPE*SERIAL NUMBER*YEAR (IONO CALIB)
Name, type, serial number, and first year of operation of the equipment used for ionospheric measurements. Blank if none.
Similar to line 2 if included in the time receiver.
As many columns as necessary.

Line 5: LABORATORY
Acronym of the laboratory where observations are performed.
As many columns as necessary.

Line 6: 'X*=*' X COORDINATE 'm'
X coordinate of the GPS antenna, in m and given with 2 decimals.
As many columns as necessary.

Line 7: 'Y*=*' Y COORDINATE 'm'
Y coordinate of the GPS antenna, in m and given with 2 decimals.
As many columns as necessary.

Line 8: 'Z*=*' Z COORDINATE 'm'
Z coordinate of the GPS antenna, in m and given with 2 decimals.
As many columns as necessary.

Line 9: 'INT*DLY*=*' INTERNAL DELAY 'ns'
Internal delay entered in the GPS time receiver,
in ns and given with 1 decimal. As many columns as necessary.

Line 10: 'CAB*DLY*=*' CABLE DELAY 'ns'
Delay coming from the cable length from the GPS antenna to the main unit, entered in the GPS time receiver,
in ns and given with 1 decimal. As many columns as necessary.

Line 11: 'REF*DLY*=*' REFERENCE DELAY 'ns'
Delay coming from the cable length from the reference output to the main unit, entered in the GPS time receiver,
in ns and given with 1 decimal. As many columns as necessary.

Line 12: REFERENCE
Identifier of the time reference entered in the GPS time receiver,
it can be for instance a clock number or a local UTC.
As many columns as necessary.

Line 13: blank line.

2. Line header

Line 14: 'PRN*CL**MJD**HHMMSS*TRKL*ELV*AZTH***REFSV*****
*SRSV*****REFGPS****SRGPS**DSG*IOE*MDTR*SMDT*MDIO*SMDI*'
Line to be written when no ionospheric measurement system is in operation. The acronyms are explained in 4. 101 columns.

or

Line 14: Line 14: 'PRN*CL**MJD**HHMMSS*TRKL*ELV*AZTH***REFSV*****
*SRSV*****REFGPS****SRGPS**DSG*IOE*MDTR*SMDT*MDIO*SMDI*
MSIO*SMSI*ISG*'
Line to be written when a ionospheric measurement system is in operation. The acronyms are explained in 4. 115 columns.

3. Unit header

Line 15: '**********UTC****s**.1dg*.1dg****.1ns*****
.1ps/s*****.1ns****.1ps/s*.1ns*****.1ns.1ps/s.1ns.1ps/s'
Line to be written when no ionospheric measurement system is in operation. 101 columns.

or

Line 15: '**********UTC****s**.1dg*.1dg****.1ns*****
.1ps/s*****.1ns****.1ps/s*.1ns*****.1ns.1ps/s.1ns.1ps/s
.1ns.1ps/s.1ns'
Line to be written when a ionospheric measurement system is in operation.
115 columns.

4. Data line

Line 16: column 1: blank.

Line 16: columns 2-3: '12' PRN
Satellite vehicle PRN number. No unit.

Line 16: column 4: blank.

Line 16: columns 5-6: '12' CL
Hexadecimal class byte. No unit.

Line 16: column 7: blank.

Line 16: columns 8-12: '12345' MJD
Modified Julian Day. No unit.

Line 16: Line 16, column 13: blank.

Line 16: Line 16, columns 14-19: '121212' HHMMSS
Hour, minute, second at the beginning of the track.
In hour, minute and second referenced to UTC.

Line 16: column 20: blank.

Line 16: columns 21-24: '1234' TRKL
Track length. In s.

Line 16: column 25: blank.

Line 16: columns 26-28: '123' ELV
Satellite elevation at the mid-point of the track. In 0.1 degree.

Line 16: column 29: blank.

Line 16: columns 30-33: '1234' AZTH
Satellite azimuth at the mid-point of the track. In 0.1 degree.

Line 16: column 34: blank.

Line 16 columns 35-45: '+1234567890' REFSV
Time difference resulting from the treatment of Annex I, applied on short-term measurements of [Reference Clock - Satellite Clock], reported at the mid-point of the track. In 0.1ns.

Line 16: column 46: blank.

Line 16: columns 47-52: '+12345' SRSV
Slope resulting from the treatment of Annex I, applied on short-term measurements of [Reference Clock - Satellite Clock]. In 0.1ps/s.

Line 16: column 53: blank.

Line 16: columns 54-64: '+1234567890' REFGPS
Time difference resulting from the treatment of Annex I, applied on short-term measurements of [Reference Clock - GPS time], reported at the mid-point of the track. In 0.1ns.

Line 16: column 65: blank.

Line 16: columns 66-71: '+12345' SRGPS
Slope resulting from the treatment of Annex I, applied on short-term measurements of [Reference Clock - GPS time]. In 0.1ps/s.

Line 16: column 72: blank

Line 16: columns 73-76: '1234' DSG
[Data Sigma] Root mean square of the linear fit performed on data measurements (see Annex I). In 0.1ns.

Line 16: column 77: blank.

Line 16: columns 78-80: '123' IOE
[Index of Ephemeris] Three digit decimal code (0-255) indicating the ephemeris used for this computation. No unit.

Line 16: column 81: blank.

Line 16: columns 82-85: '1234' MDTR
Modelled tropospheric delay at the mid-point of the track.
In 0.1ns.

Line 16: column 86: blank.

Line 16: columns 87-90: '+123' SMDT
Slope of the modelled tropospheric delay over all the track.
In 0.1ps/s.

Line 16: column 91: blank.

Line 16: columns 92-95: '1234' MDIO
Modelled ionospheric delay at the mid-point of the track.
In 0.1ns.

Line 16: column 96: blank.

Line 16: columns 97-100: '+123' SMDI
Slope of the modelled ionospheric delay over all the track.
In 0.1ps/s.

Line 16: column 101: blank.

Line 16: columns 102-105: '1234' MSIO
Measured ionospheric delay at the mid-point of the track.
In 0.1ns.

Line 16: column 106: blank.

Line 16: columns 107-110: '+123' SMSI
Slope of the measured ionospheric delay over all the track.
In 0.1ps/s.

Line 16: column 111: blank.

Line 16: columns 112-114: '123' ISG
[Ionospheric Sigma] Root mean square of the ionospheric measurement.
In 0.1ns.

Line 16: column 115: blank.

5. Conclusions

The format for one line of data can be represented as follows:

```
0000000000000000000000000000000000000000000000
0000000001111111111222222222233333333334444444
1234567890123456789012345678901234567890123456
PRN*CL**MJD**HHMMSS*TRKL*ELV*AZTH***REFSV*****
**************UTC****s**.1dg*.1dg****.1ns*****
*12*12*12345*121212*1234*123*1234*+1234567890*
```

```
000000000000000000000000000000000000000000000000000011
444555555555566666666667777777777888888888999999999900
789012345678901234567890123456789012345678901234567890
*SRSV*****REFGPS****SRGPS**DSG*IOE*MDTR*SMDT*MDIO*SMDI*
.1ps/s*****.1ns****.1ps/s*.1ns*****.1ns.1ps/s.1ns.1ps/s
+12345*+1234567890*+12345*1234*123*1234*+123*1234*+123*

11111111111111
00000000111111
23456789012345
MSIO*SMSI*ISG*
.1ns.1ps/s.1ns
1234*+123*123*
```

An example, made up with fictitious data is proposed in the formal Report of the 2nd Meeting of the CGGTTS, available from the BIPM.

QUESTIONS AND ANSWERS

Judah Levine, NIST, Boulder, Colorado: It would be very helpful if the new format maintained some form of error detection and error correction from the point of view of automatic receivers. We run a real time network of receivers in which all the data is acquired by machine in real time. It would be very helpful for us to have methods of detecting transmission errors. I think that it is particularly important in the header, since errors in the header field may result in interpreting the transmission differently. An error in the header field may result in the data becoming unreadable.

Mr. Petit: You are right. Actually, this format is the present status of the format, and is nearly the final form. If anything is to added, is is some kind of parity check, or a similar thing to make sure that, for example, each line is constituted correctly.

U.S. COAST GUARD GPS INFORMATION CENTER (GPSIC) AND ITS FUNCTION WITHIN THE CIVIL GPS SERVICE (CGS)

GPSIC staff
Updated November 3, 1992

Abstract

In 1987, the U.S. Department of Defense (DOD) formally requested that the U.S. Department of Transportation (DOT) take responsibility for providing an office that would respond to nonmilitary user needs for GPS information, data, and assistance. DOT accepted this responsibility and in February 1989, named the Coast Guard as their lead agency for the project. Since that time, the U.S. Coast Guard has worked with the U.S. Space Command to develop requirements and implement a plan for providing the requested interface with the civil GPS community.

The Civil GPS Service (CGS) consists of four main elements:

- ***GPS Information Center (GPSIC) - provides GPS status information to civilian users of the system***
- ***Civil GPS Service Interface Committee (CGSIC) - established to identify civil GPS user technical information needs in support of the CGS program***
- ***Differential GPS (DGPS) - Coast Guard Research and Development Project***
- ***PPS Program Office (PPSPO) - (Under development) will administer the program allowing qualified civil users to have access to the PPS signal***

This paper will provide details about the services these organizations provide.

OVERVIEW OF THE CIVIL GPS SERVICE

In 1987, the Department of Defense (DOD) formally requested the Department of Transportation (DOT) assume responsibility for establishing and providing an office that would respond to nonmilitary user needs for GPS information, data, and assistance. In February 1989, the Coast Guard assumed the responsibility as the lead agency within DOT for this project. Three areas requiring interaction were identified:

- Near real-time operational status reporting
- Distribution of the precise satellite ephemerides

- Civil use of the precise positioning service

In 1988, the U.S. Space Command (USSPACECOM) invited the U.S. Coast Guard to assist in the development of the DOD Operational Capability Reporting Management System (ORMS). Since that time, the U.S. Coast Guard Radionavigation Division has worked with USSPACECOM to develop requirements and implement a plan to provide the requested interface with the nonmilitary GPS community. Most of these civil GPS services are now in place; others are planned to be ready by the time GPS is fully operational.

ORGANIZATIONAL STRUCTURE OF THE CIVIL GPS SERVICE

As the Department of Transportation (DOT) operational agency, the U.S. Coast Guard is responsible for the oversight and management of the Civil GPS Service. The function is implemented by the organizational shown in Figure 1.

Chief, Office of Navigation Safety and Waterway Services (G-N) – located at Coast Guard Headquarters, provides top-level oversight and management of the CGS program. The primary responsibility is the provision of broad, high-level policy guidance. This direction is provided in support of:

- DOT positions
- Congressional mandates
- Federal Radionavigation policies

This office is the focal point for information feedback from the Civil GPS Service Interface Committee. Members of this staff interface with the heads of other Federal agencies with an interest in the Civil GPS Service program.

Chief, Radionavigation Division (G-NRN) – also located at Coast Guard Headquarters, is the program manager responsible for the activities of the PPSPO and the GPSIC operations. This office assists with the budgetary planning for these services.

The Civil GPS Service consists of four main elements:

The GPS Information Center (GPSIC) is the operational entity of the CGS which provides GPS status information to civilian users of the Global Positioning System based on input from the:

- GPS control segment
- Department of Defense (DOD)
- Other sources

The Civil GPS Service Interface Committee (CGSIC) was established to identify civil GPS user technical information needs in support of the Civil GPS Service program. Its purpose and goal is of an information exchange nature only.

The Coast Guard's Differential GPS (DGPS) Project was established to develop an extension of GPS to enhance the Standard Positioning Service (SPS) for civil users in the maritime regions of the United States.

The PPS Program Office (PPSPO) is responsible for administering the program which will allow qualified civil users to have access to the Precise Positioning Service (PPS) signal. This program office

is currently under development in the Radionavigation Division of the Office of Navigation Safety and Waterways Service (G-NRN-2) located at Coast Guard Headquarters in Washington, D.C.

The DOT Navigation Council and the DOT Radionavigation Working Group will continue in their traditional roles in the oversight of navigation including radionavigation.

Two other DOT agencies have Civil GPS Service functions:

The Federal Aviation Agency (FAA) handles aviation issues, including Notices to Airmen (NOTAM), the National Aviation Standard for GPS, and GPS integrity as it relates to aviation.

The Research and Special Programs Administration (RSPA) handles intermodal navigation issues and planning.

Although DOT has been given the principal oversight and management responsibilities for the Civil GPS Service, other federal agencies will play a role. The involvement of Federal agencies, other than those under DOT, will be particularly appropriate with regard to users outside of the navigation community.

THE GPS INFORMATION CENTER (GPSIC)

The Coast Guard's GPS Information Center (GPSIC) is a part of the Omega Navigation System Center (ONSCEN), located in Alexandria, Virginia. It has been providing information since March, 1990, on a test and evaluation basis.

The GPSIC is a public information service. At the present time, there is no charge for the information provided. A GPS Information Center Users Manual is available upon request. This publication covers the various GPSIC services and how to access them; it also goes into some detail on how to use the GPSIC electronic bulletin board system.

Since its inception, the GPSIC has experienced rapid growth. It now consists of a dozen people, and five more are expected in the next year. This growth has allowed an expansion of normal working hours to improve the timeliness of GPSIC information. Hours are now continuous: 24 hours a day, 7 days a week, including federal holidays.

THE GPSIC MISSION

The mission of the Global Positioning System Information Center (GPSIC) is to:

- gather,
- process, and
- disseminate

timely GPS status information to civil users of the global positioning satellite navigation system.

Specifically, the functions to be performed by the GPSIC include the following:

- Provide the Operational Advisory Broadcast Service (OAB)
- Answer questions by telephone or written correspondence
- Provide information to the public on the GPSIC services available
- Provide instruction on the access and use of the information services available
- Maintain tutorial, instructional and other relevant handbooks and material for distribution to users
- Maintain records of GPS broadcast information, GPS data bases or relevant data for reference purposes
- Maintain bibliography of GPS publications
- Maintain and augment the computer and communications equipment as required
- Develop new user services as required

GATHERING GPS INFORMATION

A Memorandum of Agreement (MOA) between the U.S. Space Command (USSPACECOM) and the Coast Guard establishes policies and procedures for the exchange of GPS status information. This agreement addresses relative roles and responsibilities of each organization. A similar MOA has been signed specifying form, format and frequency of GPS status information distributed from Air Force Space Command to the U.S. Coast Guard Omega Navigation System Center.

The U.S. Air Force Second Satellite Operations Squadron (2SOPS), which operates the GPS Master Control Station (MCS) in Colorado Springs, provides the following GPS information for the GPSIC:

Notice Advisory to NAVSTAR Users (NANU) are near real-time operational status capability reports. NANUS are issued to notify users of future, current, or past satellite outages, system adjustments, or any condition which might adversely affect users. NANUS are generated by 2SOPS as events occur.

GPS Status Messages contain general information that is downloaded daily from the 2SOPS's bulletin board. The message contains information about the satellite orbit (plane/slot), clocks, and current or recent NANUS. Status Messages are generated by 2SOPS once a day Monday thr[illegible] Friday.

Almanacs contain the orbital information and clock data of all the satellites. The almanac for all satellites can be obtained from downloading the continuously transmitted data stream from any satellite.

In addition to receiving information from the MCS, the GPSIC works with representatives of the National Geodetic Survey (NGS) to offer NGS computed precise GPS orbit data to the public via the GPSIC bulletin board. This data is called precise ephemeris data. NGS provides data products "SP3" (in ASCII format) and "EF18" (in binary format). In the past, NGS distributed this information on diskettes by mail to some users. Precise ephemeris data describes the orbit of each satellite as observed by numerous ground stations. It is useful in making a refined determination of where the satellites were at some time in the past. The time lag for this information is now about five weeks, but NGS plans to reduce it to two weeks eventually.

For more information about Precise Ephemeris Data, contact: National Geodetic Information Branch (NG174)
Charting and Geodetic Services, National Ocean Service
Nationa; Oceanic and Atmospheric Administration
Rockville, MD 20852 Telephone:(301)–443–863

Features of the GPSIC services are created and improved in response to suggestions from our users. The GPSIC will continue to work with GPS organizations to ensure the continuation and development of the best possible user services. Specifically, the GPSIC will:

- Maintain liaison with other U.S. Government agencies as necessary to sustain GPS system status, technical information exchange and resource availability
- Maintain liaison with the Civil GPS Interface Committee and international civil GPS organizations to establish the requirements for GPS information exchange

DISSEMINATING GPS INFORMATION

The GPSIC sends GPS status information to civil users through Operational Advisory Broadcasts (OAB). These broadcasts contain the following general categories of GPS performance data:

- Current constellation status
- Recent (past) outages
- Scheduled (future) outages
- Almanac data

The Operational Advisory Broadcast (OAB) consists of textual matter containing the GPS performance data listed above. Conditions that impair the GPS for navigational purposes receive special attention and wide distribution.

The Operational Advisory Broadcast is updated by the GPSIC staff at a minimum of once per day. OAB's are updated more frequently if information on changes in the constellation is received. The following table outlines the update schedule for sources of GPS information received by the GPSIC:

SOURCE	UPDATE SCHEDULE
NANU	The GPSIC staff processes NANUS as soon as possible
STATUS MESSAGE	The GPIS watch standers post a new message daily (ususally around 1 pm, Eastern time) Monday through Friday except Federal holidays
ALMANAC	The almanac is updated once a week, plus whenever changes that appreciably affect system coverage accur.
NGS	Precision ephemeris dat is updated weekly, since each data set covers one week, but some variations occur due to deifferences in processing time at at NGS.

The Operational Advisory Broadcast is disseminated through the following media:

- GPSIC Computer Bulletin Board System (BBS) *item GPSIC 24-Hour Status Recording*
- WWV/WWVH worldwide high-frequency radio broadcasts
- Coast Guard Marine Information Broadcasts (MIB)
- DMAHTC Broadcast Warnings
- DMAHTC Weekly Notice to Mariners
- DMA Navigation Information Network (NAVINFONET)
- NAVTEX Data Broadcast

Some of these services have limited time or space available for GPS information. The following paragraphs describe each service and the GPS information available.

GPSIC BULLETIN BOARD SYSTEM (BBS)

Any user who has access to a computer and a modem can call the GPSIC BBS for information. The BBS is free and open to all. However, users will have to pay their own connection charges (long distance telephone or public data network costs). First-time callers are asked to register on-line (provide their names, addresses, etc.) before proceeding to the BBS main menu.

Through the BBS, a wide range of information is available 24 hours a day. BBS information is updated whenever the other GPSIC sources are (see schedule).

Users may call the BBS via either telephone or SprintNet (a public data network). Ordinary telephone is the easiest for most people, but SprintNet offers a high speed error-free alternative for those (especially international callers) who may have difficulty in getting a good data connection over the voice phone lines.

To contact the BBS, call: (703)-866-38980

Modem speeds of 300 to 14,400 bps and most common U.S. or international protocols are supported. Communications parameters should be set to: 8 data bits, No parity, 1 stop bit (8N1), asynchronous comms, full duplex. We have eight phone lines at this number, and two auxiliary numbers to accommodate modems which may be incompatible with the ones on 866-3890.

The BBS SprintNet number is: 311020201328

(Or abbreviate to 202-1328 if accessing SprintNet via telephone to one of their modems.) For SprintNet access, users must set up their own accounts with Sprint or a similar public data network which has a "gateway" to SprintNet. For more information, call: (800)736-1130 (U.S.) or (913)541-6876 (international).

Users who need further information or assistance may call the GPSIC watchstander at: (703)-866-3806

GPS information on the BBS includes:

- NANUs
- Status Messages
- Almanacs
- Precise Ephemeris Data
- Coast Guard DGPS Project Updates
- CGSIC Meeting Announcements, etc.

The BBS also contains information about other radionavigation systems:

- Omega Status Messages
- Loran-C User Notification Messages

In addition, the BBS has areas set aside for general information about radionavigation and associated topics:

- The text of the Federal Radionavigation Plan
- U.S. Naval Observatory "series 4" timing messages
- USAF/NOAA Solar and Geophysical Activity reports
- The Coast Guard's Radionavigation Bulletin
- The GPSIC Users Manual (includes a BBS users manual)
- Other items which may be of interest to the GPS/radionavigation community

The BBS is menu-driven and has an extensive set of on-line help utilities. Users can page the system operator (/p Sysop) to request more personalized assistance.

GPSIC 24-HOUR GPS STATUS RECORDING

The 24-hour status recording provides information in voice format. The amount of information is strictly limited since the maximum tape length is 92 seconds long.

The reach the status recording, call: (703)-866-3826

The following information is available on the 24hour status recording depending on the space available. The information is prioritized as listed below:

- Cautionary Statement
- Current system status
- Forecast outages
- Historical outages
- Other changes in the GPS

OTHER DISTRIBUTION MEDIA

GPS information available from each of these additional sources is prepared and assembled at the GPSIC. These sources were chosen because they were already established to provide other types of information. Most of these service are already used by a portion of the GPS user community, primarily marine navigators. These services offer significant advantages in coverage and accessibility. The following section provides:

- Description of each information source
- Type of GPS information available
- How the user can obtain the GPS information

WWV/WWVH: Since 1923, the National Institute of Standards and Technology (NIST), formerly National Bureau of Standards, has provided a highly accurate time service to the national and international time and frequency community. NIST currently broadcasts continuous signals from its high frequency radio stations. Services provided by WWV/WWVH include:

- Time announcements
- Standard time intervals
- Standard frequencies
- Geophysical alerts
- Marine storm warnings
- Omega Navigation System status reports
- Universal Time Coordinated (UTC) time corrections
- BCD time code
- GPS information

GPS information is broadcast in voice on WWV/WWVH at the following times and frequencies:

STATION	LOCATION	FREQUENCY	TIME
WWV	FT. COLLINS COLORADO	2.5, 5, 10. 15, 20 MHz	Minutes 14 and 15
WWVH	KAUAI HAWAII	2.5, 5. 10, 15 MHz	Minutes 43 and 44

The time for the WWV/WWVH GPS broadcast is strictly limited. Depending on the space available the GPS information is prioritized as listed below:

- Cautionary Statement
- GPSIC operating hours and phone number
- Current system status

- Forecast outages
- Other changes in GPS Status

USCG AND DMA MIB: USCG Marine Information Broadcasts and DMA Broadcast Warnings are methods by which important maritime navigation information is disseminated in the most expedient manner. This system covers a variety of topics of interest to mariners including:

- Status of navigation aids
- Weather
- Search and Rescue (SAR) operations
- Military exercises
- Marine obstructions
- Ice reports
- Changes in channel conditions
- Important bridge information

Within the United States, the U.S. Coast Guard and the Defense Mapping Agency Hydrographic/Topographic Center (DMAHTC) are responsible for broadcasting navigation information described above.

The Coast Guard provides vital maritime information in voice format via an established system of VHF and HF radio broadcasts. These Marine Information Broadcasts (MIB) include the following types of messages:

Urgent Messages concern the safety of a person, ship, aircraft or other vehicle.

Safety Messages contain important navigational or meteorological warnings that cannot be delayed because of hazardous conditions.

Scheduled Broadcasts include:

- Notice to Mariners (NTM)
- Hydrographic information
- Storm warnings
- Advisories
- Other important marine information
- Safety and urgent messages which remain in effect

Cancellation Messages are sent by the originator to cancel previous broadcast when action is no longer necessary.

USCG Marine Information Broadcasts are issued via voice and continuous wave (CW) transmissions. The following table outlines the MIB frequencies:

VHF-FM, Cha 16, Cha 22A	Information that applies to inland waters seaward to 25 nautical miles.
Mf 2182 and 2670 kHz	Duplicates VHF-FM broadcasts and additional cover waters out to 200 nautical miles
HF-CW 500 kHz	Info that applies to waters from the coastline to 200 nautical miles off shore

Broadcasts are scheduled several times a day depending on the location of the broadcasting site. Stations designated to make regularly scheduled broadcasts are listed in the Coast Guard Radio Frequency Plan. The length of messages broadcast is kept to a minimum.

DMAHTC is responsible for broadcasting navigation information concerning the "high seas". Information is provided in message format via an established system of message dissemination. DMA broadcasts are known as NAVAREA, HYDROLANT, or HYDROPAC and are generally geared to the deep draft mariner.

DMAHTC also publishes a weekly Notice to Mariners (NTM) containing USCG Marine Information Broadcasts and DMA Broadcast Warnings for a seven day period.

GPS status information is found in Section III of the Notice to Mariners, which summarizes voice or data broadcast warnings.

Additional information on the DMA Notice to Mariners Information is available from:

Director: Defense Mapping Agency Hydrographic/Topographic Center
Attention: MCNM 6500 Brooks Lane Wahington, D.C. 20315-0030 (301)-227-3126

DMA NAVINFONET: In carrying out its mission to produce Notices to Mariners, DMA has developed a data base called Automated Notice to Mariners System (ANMS). This data base contains information dealing with navigational safety. It is a supplemental source of up-to-date maritime information for the user. The software developed for this data base provides remote query capabilities which DMA makes available to the entire maritime community through the Navigation Information Network (NAVINFONET). NAVINFONET provides information in data format via telephone modem. Information includes:

- Chart Corrections
- Broadcast Warnings
- MARAD Advisories
- DMA List of Lights
- Anti-Shipping Activities Messages
- Oil Drill Rig locations
- Corrections to DMA Hydrographic Product Catalogs
- U.S. Coast Guard Light Lists & GPS

The following GPS information is available from the DMA NAVINFONET under item 8 in the bulletin board menu:

- Cautionary Statement
- Current system status
- Forecast outages
- Historical outages
- Almanac data
- Civil GPS Service information

Users must register for the NAVINFONET bulletin board off-line before they will be granted access to the system. For a user ID and information book contact DMA at the address listed above:

Attention: MCN/NAVINFONET (301)-227-3296

NAVTEX: NAVTEX is a an internationally adopted radio telex system used to broadcast marine navigational warnings and other safety related information to ships. This system assures worldwide coverage by transmitting on an international frequency of 518 KHz. Vessels' NAVTEX receiver/teleprinters are permanently tuned to the worldwide frequency and remain on standby to receive and print out all the messages automatically. Navigation information broadcasted through NAVTEX includes:

- Notices to mariners
- Weather warnings and forecasts
- Ice warnings
- Other marine information

Coast Guard Atlantic and Pacific Area Commanders coordinate NAVTEX broadcasts transmitted by all Coast Guard Communications stations. NAVTEX messages are normally broadcasted four times a day which may be increased to six broadcasts with a maximum duration of 40 minutes.

NAVTEX messages are categorized by subject area. GPS status messages are in NAVTEX category "J". GPS information available from NAVTEX includes the following:

- Cautionary Statement
- Current system status
- Forecast outages
- Other changes in GPS Status

CONTINGENCY PLAN FOR LOSS OF GPSIC COMMUNICATIONS

If communications with the GPSIC were disrupted for an extended period of time (as might happen with a fire or similar casualty), we would announce the problem on the WWV/WWVH radio broadcasts, at the times normally set aside for GPS information. If GPSIC services were set up at an interim location, the new phone numbers would be announced on WWV/WWVH.

Users can hear WWV broadcasts by phone, as well as radio at 14 - 15 minutes past the hour: (303)-499-7111

PUBLICATIONS AVAILABLE FROM THE GPSIC

The GPSIC publishes documents which provide detailed information about GPS, other radionavigation systems, the GPS Information Center and how to obtain these services. The following table describes the GPSIC publications available:

PUBLICATION	DESCRIPTION
GPSIC USERS MANUAL	Provides detailed instructions on the access and use of the services available at the GPSIC
GPSIC BROCHURE	Describes information services provided by the GPSIC
GPS FACTS & FIGURES	Describes the system, its concept, accuracies and applications
DGPS BROCHURE	Describes the US Coast Guard's Differential GPS Project
OMEGA FACTS & FIGURES	Describes the OMEGA Radionaviagation system
LORAN C FACTS & FIGURES	Describes LORAN C
RADIOBEACON FACTS & FIGURES	Describes Radiobeacons

The GPSIC distributes documents provided by other GPS interested organizations. The following table describes other GPS publications available through the GPSIC:

PUBLICATION	PUBLISHER	DESCRIPTION
NAVSTAR GHPS USER EQUIPMENT	JPO	Describes the system, equipment, applications and capabilities
GPS NAVSTAR OVERVIEW	JPO	Provides general information about GPS
ICD 200	JPO	Technical information about the GPS signal–to–receiver interface

GPS ROAD SHOW

In an effort to make the public aware of the services offered by the GPSIC, the GPSIC sets up a GPS display at trade shows throughout the United States. The GPSIC staff distributes brochures and answers questions about GPS in order to educate users about the system.

GPSIC WATCHSTANDERS

In addition to updating the OAB, the GPSIC watchstander responds to individual user inquiries, comments, and concerns about civil access to, and use of, the GPS. The GPSIC now has watchstanders on duty 24 hours a day, 7 days a week, so this service is available anytime. Most inquiries can be answered immediately over the phone. Some technical questions or requests are referred to a more authoritative source.

If you would like to comment on any of these services or ask questions about present or future services write to: Commanding Officer (GPSIC), US Coast Guard Omega Navigatin System Center, 7323 Telegraph Road, Alexandria, Virgibia 22310-3998, Tel. (703)-866-3806, FAX (703)-866-3825.

CIVIL GPS SERVICE INTERFACE COMMITTEE (CGSIC)

The roles of the Civil GPS Service Interface Committee (CGSIC) are to:

- Provide a forum for exchanging technical information in the civil GPS user community regarding GPS information needs

- Identify types of information and methods of distribution to the civil GPS user community
- Identify any issues that may need resolution by the CGS program office

The CGSIC will work with the following organizations:

- U.S. Coast Guard Office of Navigation Safety and Waterway Services (Civil GPS Program Office)
- DOT Navigation Working Group
- Joint DOD/DOT Radionavigation Working Group

The Civil GPS Service Interface Committee is comprised of representatives from relevant private, government, and industry user groups, both U.S. and international.

The CGSIC consists of:

- General Committee
- Three Subcommittees

The Committee is jointly chaired by the U.S. Coast Guard and the DOT Research and Special Programs Administration (RSPA). The joint chair is based on the USCG being DOT's lead agency for the civil GPS service which includes the government's interface with civil GPS users, and RSPA's responsibility to coordinate intermodal navigation planning with DOD.

The Civil GPS Service Interface Committee may create subcommittees to identify specific areas of civil GPS user information needs and facilitate technical information exchange as required. Standing subcommittees have been established for:

- Timing Information
- International Information
- Reference Station, Technology, and Applications

The International Information Subcommittee (IISC) of the Civil GPS Service Interface Committee is investigating the feasibility of a regional international information media. The GPSIC would provide the OAB into an electronic mailbox designated, controlled, and financed by the IISC.

The Civil GPS Service Interface Committee meets as necessary to exchange technical information regarding civil GPS information needs.

For additional information on the CGSIC, contact the GPS Information Center.

DIFFERENTIAL GPS (DGPS)

Consistent with its role as the civil interface for GPS, the U.S. Coast Guard has a research and development project to develop an extension of GPS, known as differential GPS (DGPS). This is an enhancement to the Standard Positioning Service (SPS) which should achieve accuracies of 10 meters or better for civil users in the maritime regions of the United States.

Based on encouraging results of operational testing of a prototype reference station, a project has been initiated to implement DGPS in U.S. near-coastal areas to improve upon current harbor and harbor-approach navigation accuracy. Project plans are being formulated. Additional prototypes began operation during September/October 1991. If fully funded, an operational system is expected by 1996.

For additional information on DGPS, contact: Commandant (G-NRN), US Coast Guard, 2100 2nd Street, S.W., Washington, D.C., Tel. (202)-267-0283, FAX. (202)-267-4427.

PRECISE POSITIONING SERVICE PROGRAM OFFICE (PPSPO)

The Precise Positioning Service Program Office (PPSPO) will administer civil applications and collect fees for access to encoded Precise Positioning Service (PPS) capabilities.

The Government will publish detailed guidance for users interested in requesting access to PPS once policy is established for the following:

- Submitting applications
- Granting approval for user access
- Establishing operational procedures and compliance requirements for accessing data from the GPS PPS

The Federal Radionavigation Plan (FRP) contains general criteria for qualified civil use of PPS. Access determination will be made on a case by case basis. The following criteria may be refined as Government policy is developed:

- Access is in the U.S. national interest
- Security requirements can be met
- There are no other means reasonably available to the civil user to obtain a capability equivalent to that provided by the GPS PPS

For additional information on the PPSPO, contact Commandant (G-NRN) at the address listed above or telephone: Commandant (G–NRN), TEL. (202)-267-0298, FAX (202)-267-4427.

FEDERAL RADIONAVIGATION PLAN (FRP)

The Federal Radionavigation Plan (FRP) contains the official statement of government policy on civil use of GPS. This plan covers other government operated radionavigation systems in addition to GPS. The FRP is updated biennially. Information provided includes:

- Policy and plans for the future radionavigation systems mix
- GPS System description
- Table of SPS and PPS signal characteristics
- Various other topics

The text of the Federal Radionavigation Plan (minus tables and illustrations) is available on the GPSIC electronic bulletin board.

To order a copy of the FRP (stock number 008-047-00402-8), contact the U.S. Government Printing Office at: Superintendent of Documents, Order Section, U.S. Government Printing Office, Washington, D.C. 20402, Tel. (202)-783-3238.

THE GPSIC QUICK REFERENCE OAB DISTRIBUTION

The GPS Information Center provides the Operational Advisory Broadcasts through the following services:

Service	Availability	Info Type	Contact Number
GPSIC Watchstander	24 hours a day	User Inquiries	(703) 866–3806 FAX (703) 866–3825
GPSIC Computer Bulletin Board Sevice	24 Hours a day	Status, Fore/Hist, Outages, NGS Data, OMEGA/FRP, Misc. Info	(703) 866–3890 300 – 14,400 bps – or – SprintNet (X.25) 311020201328
GPSIC Voice Tape Recording hline WWV	24 hours a day Minutes 14 & 15	Status, Foecasts, Historic Status, Forecasts	(703 866–3826 2.5, 5, 10, 15, and 20MHz
WWVH	Minutes 43 & 44	Status, Forecasts	2.5, 5, 10 and 15 MHz
USCG MIB	When Broadcasted	Status, Forecasts	VHF Radio, Marine Band
DMA Broadcast Warnings	When Broadcasted	Status, Forecasts, Outages	
DMA Weekly Notice to Mariners	Published and Mailed Weekly	Status, Forecasts, Outages	(301) 227–3126
DMA Navinfonet Automated Notice to Mariners System	24 hours a day	Status, Forecasts, Historic, Almanacs For More Information Call	(301) 227–3351 300 BAUD (301) 227–5925 1200 BAUD (301) 227–4360 2400 BAUD (301) 227–3296
Navtex Data Broadcast	When Broadcasted 4 – 6 times a day	Status, Forecasts, Outages	518 kHz

QUESTIONS AND ANSWERS

Mr. R. Langley, University of New Brunswick: The United States Naval Observatory automated data service has a link to the Internet computer communications network. Those of us who are on that network would find it convenient to have that information on Internet. Are there any plans for you to interface with the network?

Lt. L. Barndt, USCG: We have looked at interfacing with Internet, or other public data network, and it is something we have budgeted for. We are experiencing budget problems, just like any other federal agency at this time. I expect that we will have another public data network connection. We are already connected to Sprintnet which has helped a lot of our overseas customers who are having integrity problems. Also, our phone numbers will change in January, 1993. They will be supplied in a press release.

Question: Is it possible to get access to NANU news in real time?

Lt. L. Barndt: I would defer that to someone from the master control station. We have been told that what we do is an advisory service and the way they send that through the auditing system it is not going to be available to civil users in real time. They are working on a warm system. I do not even think that is going to be close to real time. Could someone from the National Control Station maybe help me out?

Comment: That is true; that is the way we do business today. The NANU news is not real time. There is automation being looked at in development, but it is not on the near term horizon. People are finding ways to get that information, in terms of satellite help from the almanac data as broadcast. We recently tried to establish some rules in terms of things we know are going to happen. For instance we are going to do a Delta V this Friday. If anybody cared about which means the clocks will be off, by publishing the information two weeks in advance, we hope to minimize the unexpected outages. If we build in the ones that occur in one satellite at a time, they should be transparent with the number of satellites available, but there is a more real time system coming on line. We will continue to do a better job at forecasting and also at localizing those forecasts; so we are working at it.

COMPARISON OF GPS AND GLONASS COMMON–VIEW TIME TRANSFERS

W. Lewandowski, G. Petit, C. Thomas
Bureau International des Poids et Mesures
Pavillon de Breteuil
92312 Sèvres Cedex, France

G.T. Cherenkov, N.B. Koshelyaevsky, S.B. Pushkin
Institute of Metrology for Time and Space
Russian National Time & Frequency Service
Mendeleevo, Moscow region, 141570, Russia

Abstract

It has already been shown than even with a simple daily averaging of GLONASS data at each site, continental GLONASS time transfer can be achieved at a level of several tens of nanoseconds. A further step is to carry out observations of GLONASS satellites by the common–view method. This paper reports a comparison of GPS and GLONASS common–view time transfers between Russia and Western Europe. At each site, a GPS receiver and a GLONASS receiver are connected to the same atomic clock. Both GPS receivers are of NBS type and the GLONASS receivers are of type A–724. As GPS common–view time transfer between Sèvres and Mendeleevo is accomplished at a level of a few nanoseconds in precision, it gives an excellent reference with which to evaluate the performance of GLONASS common–view time transfer.

INTRODUCTION

Two global space navigation systems, the US GPS and the Russian GLONASS, are at the about same stage in the development of their space segments, but they are unequally used for international time comparisons. GPS, with a large range of time–specialized receivers, has for many years been exploited worldwide for accurate time transfer [1], while GLONASS is still used on an experimental basis by only a few laboratories [2,3]. Although at present GPS time transfer fully satisfies the needs of time metrology, it is the sole operationally effective method and the lack of redundancy is felt. There is also a growing concern about GPS degradation by Selective Availability and Anti–Spoofing. In this context GLONASS is of increasing interest as an excellent additional source.

For the past three years VNIIFTRI (Mendeleevo, Moscow Region, Russian Federation) and some other Russian time laboratories have used Russian–built GLONASS navigation receivers for time

comparisons. Since June 1991, VNIIFTRI has operated a commercial GPS time receiver on loan from the BIPM. Since February 1992, the BIPM has operated Russian GLONASS receiver on loan from the VNIIFTRI. This provides, for the first time, an opportunity for direct comparison of GLONASS common–view with GPS common–view time transfers.

THE EXPERIMENT

Two remote atomic clocks separated by about 2800 km have been compared by independent space links, GPS common–view and GLONASS common–view (Fig.1) in an experiment covering the period from April 2 to June 23, 1992.

On each site a GPS receiver and a GLONASS receiver are connected to a single clock, an Hydrogen–maser at Mendeleevo and a caesium standard at Sèvres. On both sites the receivers for each satellite system are of the same type, – AOA TTR6 at Mendeleevo and AOA TTR5 at Sèvres for GPS, and A-724 at both locations for GLONASS.

In common-view time transfer, two remote stations receive the signals from the same satellite at the same time and exchange the data to compare their clocks (Fig. 2). The main advantage of this method, introduced in 1980 for GPS [**4**], is that satellite clock error contributes nothing (satellite time disappears in the difference). Also over distances of up to a few thousands of kilometers the impact of other errors, such as poor estimation of ionospheric delay or broadcast ephemerides, is diminished. By using the same type of receiver, as in our case, the consistency of the comparison is improved as possible software errors are removed by the common-view approach.

GPS COMMON-VIEW LINK

The GPS time receivers correct observations for atmospheric refraction. Tropospheric delay is computed by a model which is a function of the elevation of the GPS satellite and of the altitude of the observation site. Ionospheric delay is estimated from a model using broadcast parameters.

The coordinates of the GPS antennas are expressed in the ITRF88 reference frame and were provided by the BIPM method of differential positioning [**5,6**] with respect to the closest ITRF sites. The estimated uncertainty of coordinates at Mendeleevo, obtained through a link with the ITRF laser site in Graz (Austria), is 70 cm, and that at Sèvres is 30 cm (link with the ITRF laser site in Grasse, France). The uncertainties of the GPS ground antenna coordinates can have an impact on the accuracy of this GPS common–view link of up to a few nanoseconds.

The GPS receivers used are not differentially calibrated, however, according to the available data, the uncertainty of the difference of their internal delays is 10 ns.

A standard GPS track for common-view observations has a duration of 13 minutes. The choice of this length is imposed by the 12.5 minute interval at which are broadcast the ionospheric parameters. A typical GPS track is shown by figure 3. The receiver processes short–term measurements, smoothing them over a period of 15 seconds through use of a second degree fit [**1,7**]. A linear fit of the 15 second points is used to deduce the time difference between the satellite and laboratory clocks for the mid–point of the 13 minute track. The slope of the linear fit for Block I satellites is usually no bigger than several ps/s and the corresponding standard deviation ranges from 3 to 20 ns depending on the multipath effects.

The GPS common–view time transfer was realized from the about 35 tracks of Block I and Block II satellites available daily (Fig.5). During this experiment the Block II satellites were subject to Selective Availability, so that strict common views were required [8]. A Vondrak smoothing [9], which acts as a low–pass filter with a cut–off period of about 0.5 day, is performed on the raw common-view values. For this experiment, the smoothed values are interpolated for the times of occurrence of GLONASS common views. The precision of this GPS link, estimated from the residuals of the smoothed values, is about 4 ns.

GLONASS COMMON–VIEW LINK

The organization of the GLONASS common–view link is determined by manual operation of the A–724 navigation receiver. This receiver does not have an interface to allow the connection of an external micro–computer for automatic control and data recording. Therefore two operators, one at Mendeleevo and one at Sèvres, have to read the receiver screens simultaneously and write the observations on a paper sheet. This limits the length of track to 3 minutes and the number of common–view observations to about 5 per day.

The choice of the 3 minutes track is also influenced by the 2.5 minute GLONASS navigation message length. The short–term manual observations are realized every 15 seconds. A typical GLONASS track is given in figure 4. A linear fit of the short–term data is used in post–processing to deduce the time difference between the satellite and laboratory clocks for the middle of the 3–minute track. The slopes of the linear fit do not usually exceed a few tens of ps/s and the corresponding standard deviations are of order a few ns. These particularly small standard deviations can possibly be explained by the fact that the observations displayed on the screen are not raw ones, but come from a smoothing done by the receiver. No information is available on the nature of this smoothing.

The A–724 GLONASS navigation receiver does not correct its observations for tropospheric delay. The ionospheric delay is estimated by a fixed model which does not depend on external parameters.

The coordinates of the GLONASS antennas are expressed in the SGS 85 reference frame with an estimated uncertainty of 5 m. They were obtained at each site by averaging a series of navigation solutions. The uncertainties of GLONASS ground antenna coordinates can have an impact on the accuracy of GLONASS common–view link of a few tens of nanoseconds.

The GLONASS receivers were compared side by side for several days before one was shipped to the BIPM. Their differential delays should be known to within a few nanoseconds.

The GLONASS common views are presented on figure 6. The numerous gaps in the data, due to interruption of observations during weekends and vacations, preclude any sophisticated statistical analysis and smoothing.

COMPARISON OF GLONASS AND GPS COMMON–VIEW TIME TRANSFERS

As the GPS common–view link between Mendeleevo and Sèvres is realized with a precision of a few nanoseconds it serves as an excellent reference for estimation of the precision of the GLONASS common–view link. GLONASS raw common–view values are compared to the GPS smoothed and

interpolated values in figure 7. Note that the GPS and GLONASS results differ by a fairly constant bias with peak–to–peak discrepancy of about 40 ns. The mean of these differences over the duration of the experiment is 43 ns. The root mean square of the residuals to the mean, which is taken as an estimation of the confidence of the mean, is equal to 13 ns.

The bias of 43 ns between the GLONASS common views and the GPS common–views is partially due to an approximate calibration of the GLONASS and GPS equipment and partially due to the large error in GLONASS ground antenna coordinates. The noise affecting the GLONASS common views is also partially due to coordinate error, to the absence of a tropospheric correction and to an imprecise estimate of ionospheric correction. Table I shows comparison of typical GLONASS raw data with GPS smoothed data. In the last column the 43 ns bias has been removed. If we compare the last column of Table I with the differences between GPS raw data and GPS smoothed data, given in Table II, we find that the noise affecting raw GLONASS common views is not much greater than that affecting raw GPS common views.

To illustrate this, consider figures 8 and 9 which present, respectively, comparisons of GPS smoothed common views with GPS raw common views, and GPS smoothed common views with GPS common views affected by a coordinate error of 14 m artificially introduced. A constant bias and noise similar to that affecting raw GLONASS common views can be seen.

CONCLUSION

This study demonstrates that even with GLONASS navigation receivers not designed specifically for timing purposes, the common–view time transfer can be realized with precision close to that found in the early stages of GPS common–view time comparisons.

More accurate determinations of GLONASS antenna coordinates in the SGS 85 reference frame would significantly improve GLONASS common–view time transfer.

Manual mode of operation of the GLONASS receivers was possible only during short period of this experiment. The development of automatic GLONASS receivers dedicated especially for time transfer is an urgent challenge.

REFERENCES

[1] W. Lewandowski, C. Thomas, *"GPS time transfer,"* in Proc. of the IEEE, Special Issue on Time and Frequency, pp. 991-1000, July 1991.

[2] P. Daly, G. T. Cherenkov, N. B. Koshelyaevsky, S. Pushkin, *"Satellite time transfer between UTC(USNO) and UTC(SU) using Navstar GPS and GLONASS,"* in Proc. 4th Institute of Navigation Technical Meeting, pp. 199–206, September 1991.

[3] P. Daly, N.B. Koshelyaevsky, W. Lewandowski, G. Petit and C. Thomas, *"Comparison of GLONASS and GPS time transfers between two West European time laboratories and VNIIFTRI,"* in Proc. 23rd PTTI meeting, pp. 341–350, 1991.

[4] D.W. Allan and M.A. Weiss, *"Accurate time and frequency transfer during common–view of a GPS satellite,"* in Proc. 34th Ann. Symp. on Frequency Control, pp. 334–346, May 1980.

[5] B. Guinot, W. Lewandowski, *"Improvement of the GPS Time Comparisons by Simulta-*

neous Relative Positioning of the Receiver Antennas," in Bulletin Géodésique, 63, pp. 371–386, 1989.

[6] W. Lewandowski, *"High Accuracy Ground–Antenna Coordinates for GPS Time Transfer,"* in Proc. IAG Symposium G2-Permanent Satellite Tracking Networks for Geodesy and Geodynamics, Vienna, August 1991, in press.

[7] W. Lewandowski, G. Petit, C. Thomas, *"The Need for GPS Standardization,"* in Proc. 23rd PTTI meeting, pp. 1–9, 1991.

[8] D.W. Allan, M. Granveaud, W.J. Klepczynski and W. Lewandowski, *"GPS time transfer with implementation of Selective Availability,"* in Proc. 22nd PTTI meeting, pp. 145–156, 1990.

[9] J. Vondrak, *"A Contribution to the Problem of Smoothing Observational Data,"* in Bull. Astron. Inst. Czechoslovakia, 20, pp. 349–355, 1969.

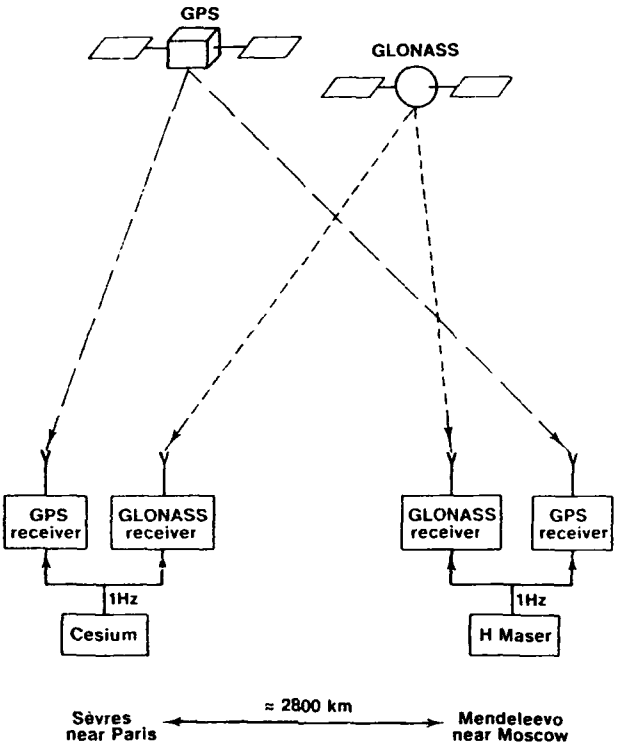

FIGURE 1. ***The experiment configuration.***

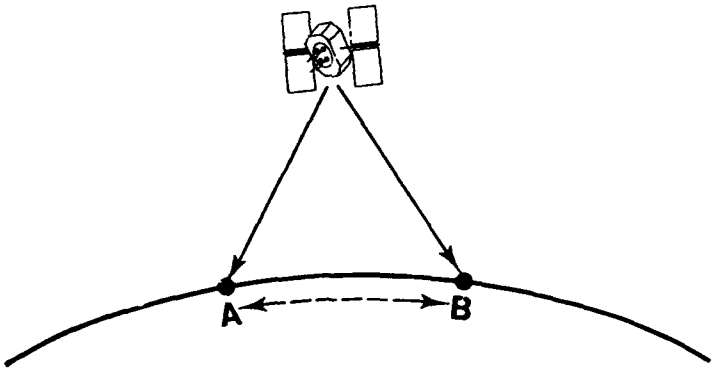

FIGURE 2. ***Common-view time transfer: Clock A - Clock B = [Clock A - satellite time] - [Clock B - satellite time].***

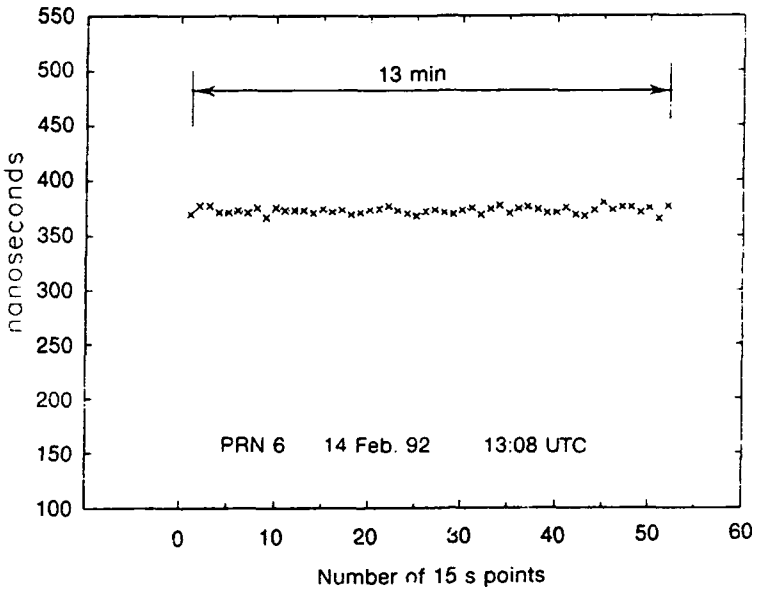

FIGURE 3. ***A typical GPS track of a Block I satellite. Short-term GPS data [Local Cs Clock - GPS time] taken every 15 seconds at the BIPM, for a 13-minute track of PRN 6 on 14 February 1992.***

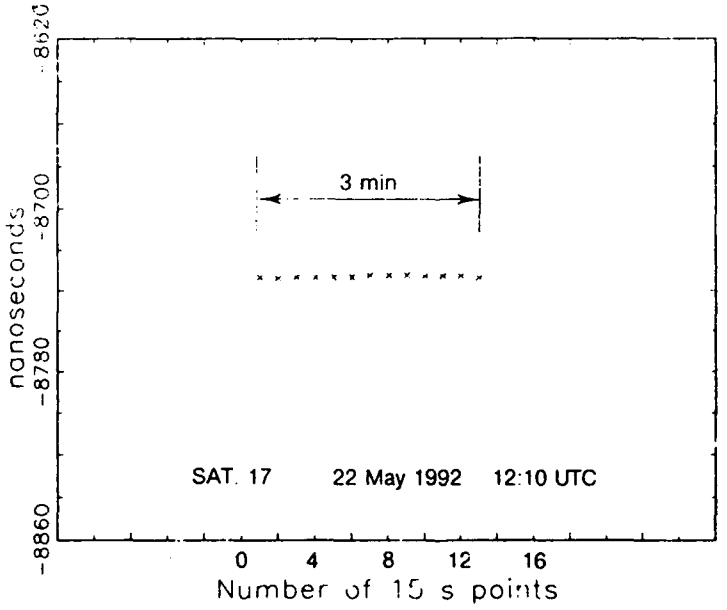

FIGURE 4. ***A typical GLONASS track. Short-term GLONASS observations [Local Cs Clock - GLONASS time] taken manually every 15 seconds at the BIPM, for a 3-minute track of Sat. 17 on 22 May 1992.***

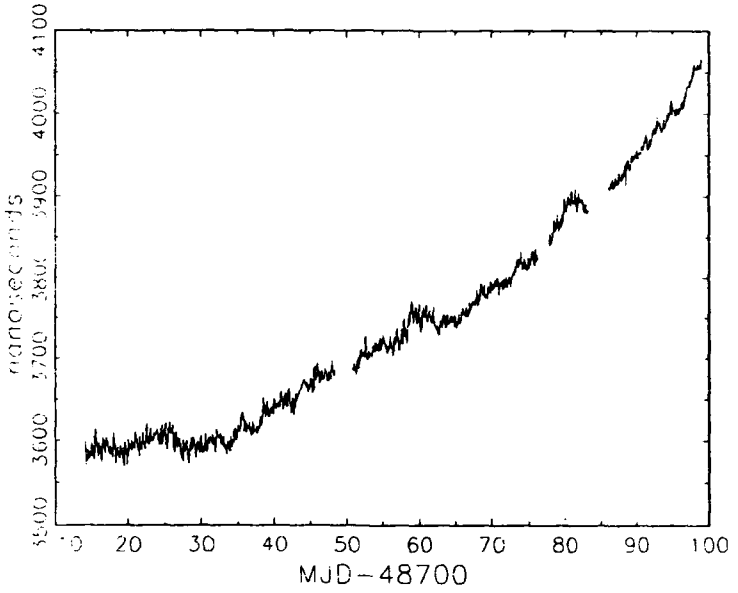

FIGURE 5. ***[BIPM Cs Clock - VNIIFTRI H-maser] by GPS common-view.***

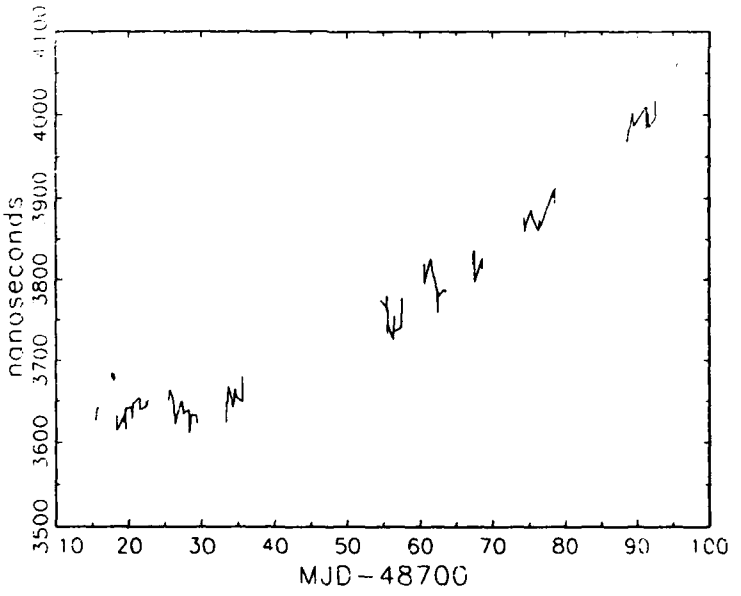

FIGURE 6. ***[BIPM Cs Clock - VNIIFTRI H-maser] by GLONASS common-view.***

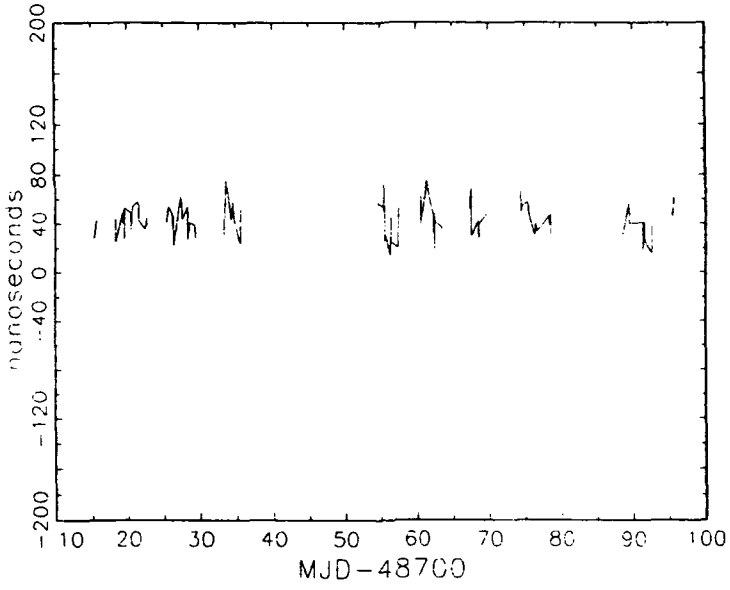

FIGURE 7. ***[BIPM Cs Clock - VNIIFTRI H-maser] by raw GLONASS minus [BIPM Cs Clock - VNIIFTRI H-maser] by smoothed GPS.***

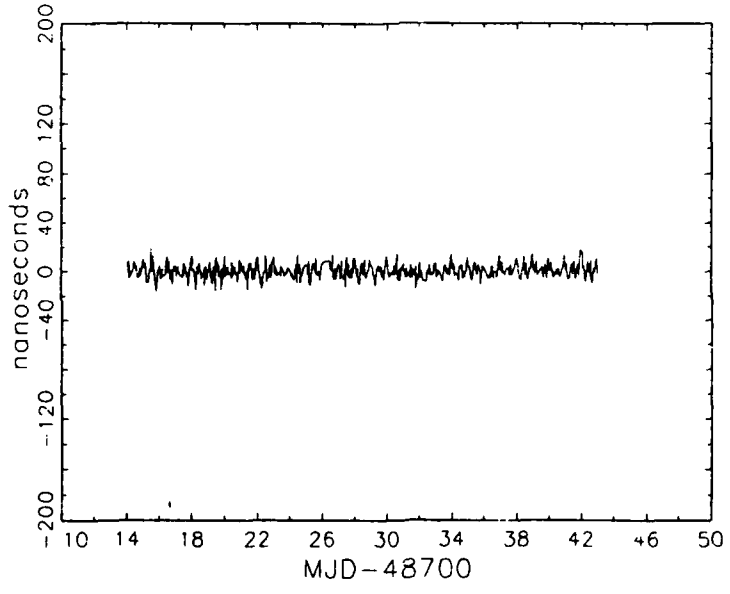

FIGURE 8. ***[BIPM Cs Clock - VNIIFTRI H-maser] by raw GPS minus [BIPM Cs Clock - VNIIFTRI H-maser] by smoothed GPS.***

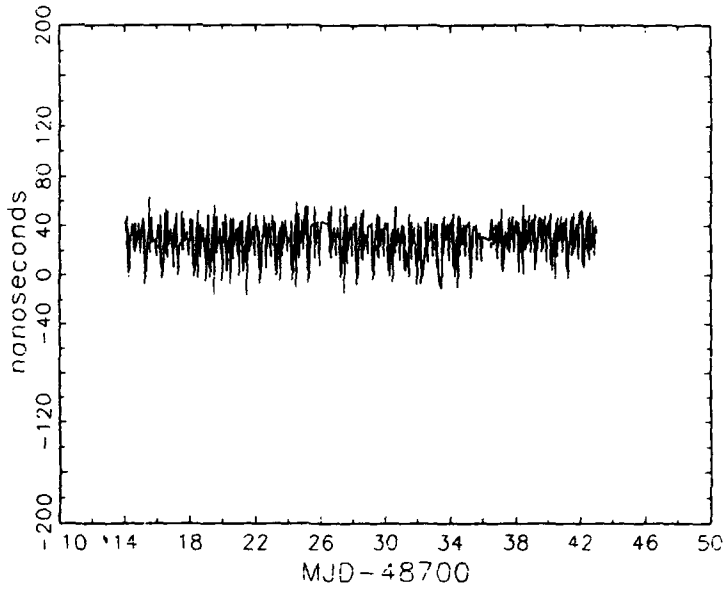

FIGURE 9. ***[BIPM Cs Clock - VNIIFTRI H-maser] by raw GLONASS affected by artificially introduced 14 m antenna coordinate error minus [BIPM Cs Clock - VNIIFTRI H-maser] by smoothed GPS.***

TABLE I. ***A sample of [BIPM Cs Clock - VNIIFTRI H-maser] by raw GLONASS minus [BIPM Cs Clock - VNIIFTRI H-maser] by smoothed GPS.***

Date April 1992	Start Time UTC h	m	SV GLO	GLO -GPS smoothed ns	GLO -GPS smoothed -43ns ns
3	7	40	7	28.0	-15
3	9	40	19	28.2	-14
3	14	20	22	43.0	0
6	6	48	2	44.7	4
6	7	40	3	24.8	-18
7	6	40	3	49.1	6
7	7	10	3	40.9	-2
7	11	10	17	51.4	8
7	13	15	15	27.8	-15
7	14	10	19	53.5	11
8	9	40	17	48.4	5
8	11	10	17	33.9	-9
8	13	10	19	44.8	2
8	14	10	20	53.9	11
9	6	40	5	58.0	15
9	11	10	19	55.0	12
9	12	10	19	43.1	0
9	14	10	20	41.8	-1
10	9	40	19	35.7	-7
10	13	40	22	45.0	2
10	14	10	22	39.7	-3
13	9	40	22	41.8	-1

TABLE II. ***A sample of [BIPM Cs Clock - VNIIFTRI H maser] by raw GPS minus [BIPM Cs Clock - VNIIFTRI H maser] by smoothed GPS.***

Date April 1992	Start Time UTC h	m	PRN	GPS raw - GPS smoothed ns
11	15	36	12	-2.8
11	16	4	3	-4.3
11	17	24	3	-2.2
11	19	32	3	0.1
11	20	4	23	-2.3
11	21	56	11	3.6
11	22	28	23	2.4
12	1	56	14	-0.1
12	3	16	15	-3.9
12	3	48	13	-1.9
12	4	36	14	-1.5
12	4	52	18	-1.9
12	5	24	24	-5.9
12	7	32	6	-7.2
12	9	24	6	5.5
12	11	0	12	-9.3
12	11	16	2	7.4
12	12	4	13	14.0
12	12	20	12	-1.7
12	13	40	12	3.2
12	13	56	13	-0.7
12	14	28	20	-0.9
12	15	0	24	6.1
12	15	32	12	0.9
12	16	0	3	-9.3

QUESTIONS AND ANSWERS

Professor Alley, University of Maryland: You were using the CA code in each instance, I gather. There is no SA or AS on the Soviet system at the present time. Do you have plans to use the P-code analog on the GLONASS?

Dr. Lewandowski: Of course, we would like to, but there are no receivers. Some are being developed, and as soon as they are ready, we will use them.

Questioner: I would like to point out that we do currently have a P-code, dual frequency GLONASS receiver that you can purchase any time you like.

PTTI WORKSHOP
SESSION A
"CLOCK PERFORMANCE AND ITS MEASURES: STABILITY AND ACCURACY"

Moderator: Leonard Cutler
Hewlett–Packard Laboratories

SHORT TERM STABILITY

- Short term stability—behavior(usually expressed in the time domain) where stochastic effects dominate–time range varies with type of standard
- Questions of drift *vs* flicker noise
- Often evidence of random walk of frequency
- Random frequency jumps leadto $\tau^{+1/2}$ behavior– sensitive to averaging time and possition of time windows
- Other measure usually used to look at environmental effects
- In telecomm often see "phase hits"–how to characterize? (Separate into "jitter" and "wander" with 20 Hz sample rate and 10 Hz boundary
- Noise should be related to physics whenever possible
- Air Force cares about 10^{-12} frequency steps
- Always need to characterize noise of measuring system

ENVIRONMENTAL EFFECTS

- Effects in space mainly temperature & radiation–Cs temperature coefficient small–Rb perhaps 100 times worse
- Telecomm concerned with temperature–often see $\pm 3 \rightarrow 10°C$ occurring rapidly–ned to worry about static and dynamic effects
- Rb response to magnetic field & radiation?
- Spaces Cs (Block I and Block II) show some drift–what is the cause?
- Space quartz looks good with respect to slow steady radiation
- Dual mixer scheme shows temperature coefficient
- Radiation effects on H maser wall coating (John's Hopkins applied Physics Laboratory)
- Need to worry about cross coupling of environmental parameters
- Environmental egffects often nonlinear–need to specify ranges
- Effects of shock and vibration
- Questions of mechanical stability

LONG TERM STABILITY

- Need more definitions–range of times, etc.

MOST IMPORTANT POINTS

- Communication, communication, communication...
- Better definitions
- Get involved with telecomm, etc. needs
- Telecomm and Frequency/Time communities need to communicate—Telecomm community is writing a document on frequency and time terms–should coordinate with CCIR, etc.–Helmut Hellwig chairs a committee (SCC 27) which is writing a standard on F&T matters–also IEEE document 1139

CLOCK USER INTERFACES

Joe White, Moderator
U.S. Naval Research Laboratory

The following features were discussed:

Autolock: Locking on the wrong peak manually is a common problem, particularly in field sites where the operators do not have to work the clocks frequently.

Lower Weight: Many users felt that clocks, primarily cesium clocks, are too heavy. They expressed a willingness to trade some internal battery capacity for lower weight.

Computer Control/Monitoring: Several users felt that direct connection between a clock and a computer would simplify their operations by automatic clock monitoring. There was also interest in using a compputer interface to control the clock.

Outputs: In addition to the usual 1, 5, and 10 Mhz outputs, there was also interest in 100 MHz and 16 MHz. Fiber optic output was considered to be desirable in future desighns although some concern about noise was expessed.

Digital (calibrated) Frequency Control: This was considered desirable to achieve repeatable frequency adjustments. Tuning *via* synthesizer adjustment rather than C-field was felt desirable. The range of the tuning should be broad enough to get beats for measurements. Fine resolution was also desirable.

Cavity Tuning: Maser cavity tuning should also be user controllable.

Time of Day Ouput: This was felt to be immportant because of the ambiguity of tick measurements. Leap second handling is also important.

Reliability/Maintainability: Fewer periodic adjusments should be necessary. Infant mortality is a concern. Field *vs.* factory maintenance was an important owner decision. Issues include the high turnover of personnel, speed of repair, modular repair, and knowing that it works when fixed.

Remote Diagnosis and BIT (built-in-test): These were considered to be very important. Users wanted to be able to determine that a clock had really failed and be able to take appropriate action.

Monitors: More is better was the consensus to provide the operator with as much information about the health as possible. Microwave power level monitors were desired for cesium clocks. RS-232/HPIB and remote ops were felt to be important to provide the best interface to the user as opposed to front panel displays.

Output Isolation: Clocks with multiple outputs should have high isolation between outputs to minimize upsets caused by someone connecting or disconnecting loads. The parallel 5 MHz outputs on the front and rear panels of cesium clocks were cited as an example of this problem.

The following items were discussed regarding operators:

There is a trade-off on training. Factory training on clock maintenance is desirable. The availability of clocks and tet equipment was cited. It was agreed that it was impractical from the standpoints of cost and time to have every person trained at or even by the manufacturer. Instead, training a "trainer" at a factory facility was a good compromise.

Operators should be able to send data back from the field to a higher level of support for help in solving clock problems.

As expressed in the section on features, clocks should be self-diagnosing and the operator should be able to take corrective action based on that information.

Operators need help in locating problems (e.g. GPS/Rb hybrid). Troubleshooting flowcharts and on-line diagnostics would be helpful.

PTTI WORKSHOP
SESSION C
"PRESENT & FUTURE NEEDS: IS GPS THE ONLY PTTI SOURCE?"

Moderator: R. L. Filler, US Army Research Laboratory

The session opened with the topic of reliance on GPS for precise time. The moderator read the following submission from John Vig, Army Research Laboratory:

> *"GPS is an outstanding navigation system, and it is also an accurate source of precise time due to the presence of high quality atomic clocks on the GPS satellites. It makes good sense for military systems to take advantage of the precise timing ability of GPS, however, although GPS is not at risk today, as more and more systems become dependent on this system, GPS becomes a more and more attractive target for future adversaries. (GPS has been designed for high survivability, but GPS satellites are not impossible to shoot down, GPS ground control stations are vulnerable to attack and sabotage, and GPS can be jammed.) Some system designers believe that, due to the availability of precise time from GPS, low quality clocks can be designed into systems that would otherwise require high accuracy clocks. Systems that rely on GPS without having clocks good enough to maintain autonomous synchronization will become unavailable whenever GPS is unavailable. GPS should be used to assist with clock synchronization and not as a substitute for good clocks. A DoD policy is needed on the conditions under which other DoD systems may rely on GPS."*

Comments (paraphrased from memory)

1. Lt. Col. Freer (USAF): There should NOT be a DoD policy. This is reminiscent of the DoD policy on Ada. Let "market pressures" decide on reliance on GPS.
2. Dr. G. Winkler: There should be a request to have a formal PTTI requirement placed on GPS. It now only has a navigation requirement.
3. Dr. S. Stein: There should be backups to GPS such as LORAN and/or comm. systems.

The second topic was the questionnaire borrowed from Frequency and Time Systems (FTS). It was suggested by Dr. Gernot Winkler, USNO, that a questionnaire of this sort might be useful for defining the requirements of the PTTI community.

Comments

1. The moderator asked several rhetorical questions:

   a. "Who are the right people to fill out such a questionnaire?"

   b. "Who are the right people to receive the data?"

2. Phil Talley, The Aerospace Corp., related a story about his trying to arrange a PTTI session on user requirements. Seven or eight prime contractors were interested initially but backed out in the end. The reason is unknown.

The third topic was "Poor coupling between system developers and government laboratories." The moderator read the following submission from John Vig:

> *"The frequency control technology area is different from most others in that the majority of experts in the field are at government or government related organizations, i.e., at NIST, ARL, NRL, USNO, AFOSR, Aerospace Corp., Jet Propulsion Laboratory, and Johns Hopkins Applied Physics Laboratory. The major system contractors have minimal expertise and no R&D capability in this field. Yet, when a problem arises that calls for R&D, not only do the contractors (and government program managers) have no incentive to make use of the expertise that resides in government, there is a disincentive for involving the government laboratories. The contractors usually look upon the government laboratories as competitors for the available R&D funds, and the program managers are usually reluctant to admit to the lack of a required component; obtaining the necessary components is 'the contractor's problem.' "*

Comments

The question of responsibility was raised. If a government entity makes a suggestion to a contractor, the contractor takes this as a requirement, and possibly a change of scope so the contractor can charge the government for added work.

Final Comment from Moderator

Workshops such as this one should be the main agenda for the PTTI meeting. We need more of them with preadvertised topics to get wider participation. The proceedings, should be published with action items and, in future years, follow-up reports on accomplishments.

Pulsar Astrometry by Using VLBI (PSR0329 between Kashima 26mø & Usuda 64mø)

S. Hama, H.Kiuchi, Y.Hanado, Y.Takahashi, M.Imae
Communications Research Laboratory
893 Hirai, Kashima, Ibaraki, 314 Japan

K.Fujisawa, H.Hirabayashi, H.Kobayashi
ISAS, 3-1 Yoshinodai, Sagamihara, Kanagawa, 229 Japan

Abstract

Communications Research Laboratory (CRL), carried out a VLBI (Very Long Baseline Interferometer) experiment of the pulsar 0329+54 on November in 1992 between Kashima 26mø and Usuda 64mø. We got a correlation for it by using K-3 VLBI correlator, which was developed by CRL. Though we observed a slow pulsar this time, we are going to make millisecond pulsar experiments by making good use of this result and by using K-4 correlator which is under developing in CRL. Its result will give us precise positions and proper motions of pulsars which are useful for obtaining precise pulsar timing.

Introduction

Many radio observatories are interested in measurement of precise pulsar timing. Its position and the proper motion are important parameters to estimate the pulsar timing. There are two major methods to get them --- deriving from the timing data itself, and VLBI. The problems of each method are as follows;

timing: precise and stable data over a long range is necessary
a good software for parameter estimation is necessary

VLBI: two large antennas are necessary
"gating" is necessary to throw away the data which doesn't contain the pulse itself

Pulsar VLBI was conducted several times so far. For example,
by VLA [1] --- short baselines
by VLBI [2] --- making use of gating function of Mk-IIIa correlator
by VLBI [3] --- gating by software
The pulsar gating function of K-3 correlator was used this time.

Correlation Amplitude of Pulsar VLBI

The condition required for pulsar VLBI is discussed here. In Japan, as Nobeyama 45mø antenna is dedicated for frequency over 10GHz, Usuda 64mø and Kashima 34mø are taken as the best couple of antenna. In practice Kashima 34mø has been in trouble since this August. Kashima 26mø antenna, therefore, is selected for this estimation. Let them have suffix "u" and "k". Then estimated correlated amplitude ρ is;

$$\rho = \frac{\pi D_k D_u S}{8k} \cdot \sqrt{\frac{\eta_k \eta_u}{T_k T_u}} \times 10^{-26} \qquad (1)$$

where D; antenna diameter [m]

η; antenna efficiency
T; system temperature [K]
s; flux density of the star [Jy]
k; Boltzmann constant [J/K]

Generally speaking data of pulsar strength and profile is not so sufficient. One of the reason is they are not stable over time and frequency. So, this is just a rough estimation. In the case of PSR0329, Downs et.al.[4] gives its peak amplitude in 2388MHz as 2.6Jy and Lyne et.al.[5] gives its profile as shown in Fig.1. Then we can adopt an average strength 0.5Jy over 50ms. By using the following parameters ;

D_k=26[m], D_u=64[m], η_k=0.5, η_u=0.7, T_k=100[K], T_u=30[K], k=1.38E-23

$$\rho = 1.79 \times 10^{-4} \quad (2)$$

is obtained. This is not easy to detect for 100-200 second integration time which is popular for geodetic VLBI.

So it is useful to gate out the data which doesn't contain pulse and to integrate only the pulse as shown in Fig.2. As it is generally hard to know the a priori position of the pulse in the period, the gating positions are set n different ways using n correlation units. Gating by software is also possible and is tried successfully by Petit et.al.[3]

How gating improves correlated amplitude and S/N ? Let's think about the case shown in Fig.2 where noise has average amplitude 1 and a rectangle pulse signal has amplitude A and duration 1/n of the pulse period.
In a normal correlation processing, S (signal) is A/n and N (noise) is 1, which makes S/N = A/n
In the case of gating the pulse, the integration time is 1/n which makes the average amplitude of the noise $\sqrt{n}$. As S is A, S/N becomes A/$\sqrt{n}$. Thus S/N is improved $\sqrt{n}$ times. In case n=8 and the antenna pair is the Kashima 26mø and the Usuda 64mø, the detection of the fringe is possible as follows;

$$\rho = 1.43 \times 10^{-3} \quad (3)$$

It is true that n times long observation also improves its S/N $\sqrt{n}$ times, but gating has the following merits;
1. Restrictions of the antenna machine time and slewing are less
2. Not sensitive to the long-term instability of the frequency standard
3. Tape consumption and restrictions of the tape length are less
4. Good for faint pulsars because the correlated amplitude itself is large

Correlation Processing System of CRL and its problems

The correlation processing system of CRL is shown in Fig.3. Both K-3 and K-4 tape are possible to be processed. The software NKROSS was modified for pulsar processing. It is written with HP Basic and run on a personal computer HP330 (the CPU is 68020). A priori parameter is given from the HP330 to the correlator and the correlation data is acquired by the host through GPIB every PP (parameter period; usually one through four seconds). The gating function of the K-3 correlation processor is only once per PP. So we selected PSR0329+54 which has long period as 714.5ms and is strong enough to get the fringe. The ideal PP should be the same as the pulse period. But, as PP is quantized by 5ms we set PP 1 second which is close to the pulse period. The timing of opening and closing of the gate can be set in the unit of bit (250ns) by the host.

The dispersion is always problem for pulsar observation. The pulse period is stretched out to Δt as[5];

$$\Delta t = 8.3E3*DM*RF^{-3}*BW \ [sec] \quad (4)$$

where, DM: Dispersion Measure [pc/cm^3]
RF: Observing Frequency [MHz]
BW: Bandwidth [MHz]

In this experiment PSR0329 gives
DM=27[pc/cm^3], RF=2300[MHz], BW=2[MHz] then,

$$\Delta t = 36.8\,\mu s \quad (5)$$

is obtained. This value is far smaller than 50ms which is estimated as the pulse duration in the last section. Moreover, when the bandwidth ranges over 100MHz for bandwidth synthesis, Δt is only 1.97ms which is still smaller than the 50ms. Of course this should be compensated in the case of bandwidth synthesis.

A small problem appeared in the actual processing. Fringe rotation (=RF*$d\tau$, $d\tau$ is delay rate) was very small because the baseline is short (200km), frequency is low (2.3GHz), the right ascension is high. Our K-3 correlator makes use of 3 level-quantized sinusoidal function (as Fig.4) to compensate fringe rotation. On the other hand the data to be integrated within a PP is small because of gating. Some PP's, therefore, have most data on the correlation-restricted area. It means that such PP is given heavy weighting even if its quality is bad. This is notable in the case of short period pulsars.

The Result of the Experiment

The parameters of the experiments are shown in Table 1. Strong radio source 3C84 is used for an initial clock search. The period P=714.5ms is divided by n so that each gating time is 1/n of the pulse period.

Fig.5 shows the result when the data is processed in normal geodetic mode. Fig.6 is processed with the gating of P/16 over the same integration time. Fig.6 has a clearer fringe than Fig.5 because the S/N is improved as mentioned before. Sometimes PP with a large correlation amplitude is seen in Fig.6. The reason is probably that mentioned in the last section.

Table 2 shows the correlation amplitude for both gated to period/16 and non-gated when the parameter is integration time. As there is only one gating (P/16 in this case) in a PP (= 1sec this time), the efficiency of the integration time is P/1. Gating, therefore, improved the amplitude by the factor 16*P/1(=11.4).
In Table 3 the amplitude is compared between pulse area and non-pulse area.
In Table 4 the parameter is n; the number the period is divided with. The integration time is 480sec. The amplitude increases almost in proportion to n.

Pulsar VLBI for Millisecond Pulsars

We plan to make VLBI experiment also for millisecond pulsar. In the case of 1937+21, let's confirm if we get its fringe by using Eq.1. Kashima 34mø is taken this time instead of the 26mø antenna. As shown in Table 5, average intensity[6] is so small that normal correlation gives the fringe which is under the limit of the detection. But after the gating of P/16(=97us), fringe can be detected. The dispersion of 1937+21, whose DM is 71[pc/cm^3], becomes;

Δt = 43.7ns for RF=1.5GHz, BW=250kHz
Δt = 349.2ns for RF=1.5GHz, BW=2MHz
Δt = 96.9ns for RF=2.2GHz, BW=2MHz

In the case of 1.5GHz, wide bandwidth as 2MHz makes wave wider than P/16. So wider gating and narrower bandwidth should be selected for lower frequency.

References

(1) Backer, Fomalont, Goss, Taylor, Weisberg, "Accurate timing and Interferometer Positions for the Millisecond Pulsar 1937+21 and the Binary Pulsar 1913+16", 1985 *A.J.* 90

(2) Bartel, Cappallo, Whitney, Chandler, Ratner, Shapiro, Tang, "Frame Tie *via* Millisecond Pulsar VLBI", Workshop on Impact of Pulsar Timing & Cosmology, 1990

(3) Petit, Fayard, Lestrade, "A Method to enhance the cross correlation of millisecond-pulsar VLBI data: observations of PSR1937+214", 1990 *A & A*.231

(4) Downs, Reichley, "JPL Pulsar Timing Observations II", 1983 *Ap.J.Suppl*.53

(5) Lyne, Graham-smith, "Pulsar astronomy" p157 Cambridge U. Press 1990

(6) Foster, Fairhead, Backer, "A Spectral Study of Four Millisecond Pulsars", *Ap.J.* 378, 1991

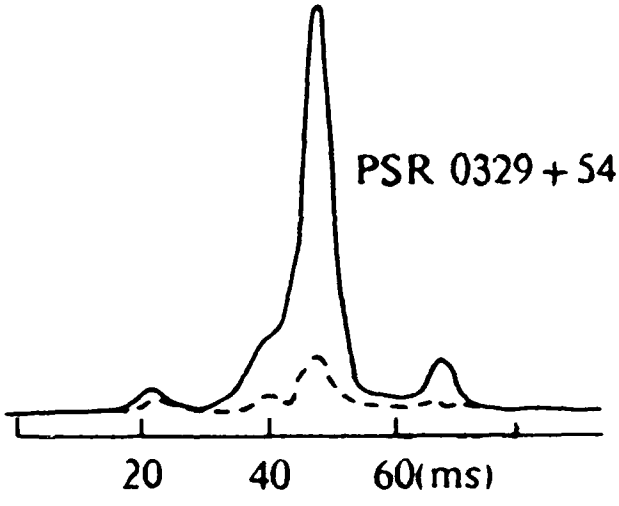

Fig.1 Profile of PSR0329+54

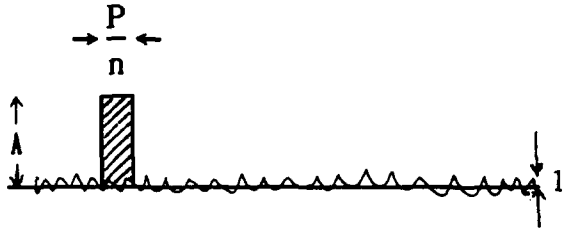

P : period of the pulse

Normal	S=A/n	N=1	S/N=A/n
Gated	S=A	N=$\sqrt{n}$	S/N=A/$\sqrt{n}$

Fig.2 Gating for Pulsar

Correlation & Integration
only within the shadowed area

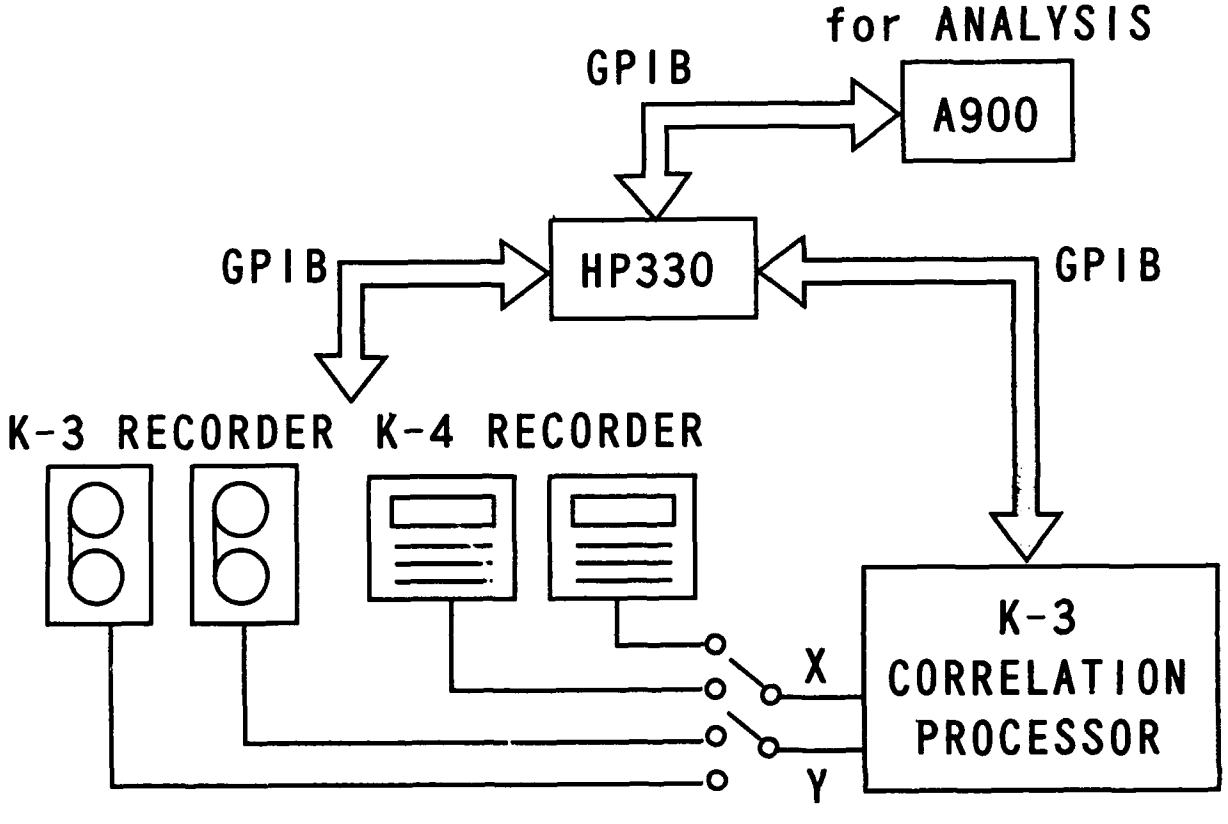

Fig.3 Correlation Processing System of CRL

Table 1 Parameter of the pulsar VLBI experiment

Baseline	Kashima26mø-Usuda64mø
Observed Star	PSR0329+54, 3C84
Frequency	2222.99MHz
Bandwidth	2MHz
Polarization	RHCP
Correlation	K-3 correlator at Kashima

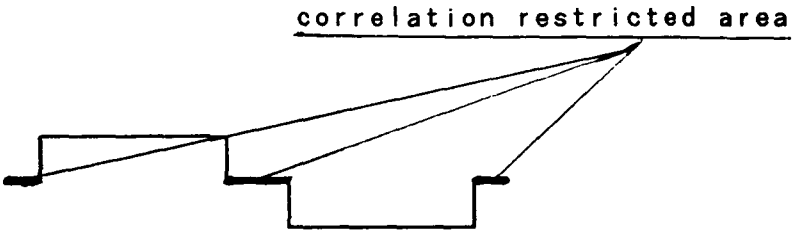

Fig.4

3-level sin function for compemsation of fringe rotation

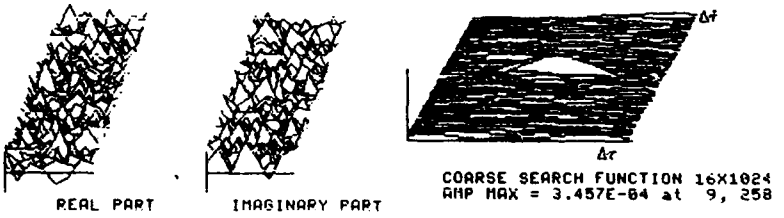

Fig.5 Normal correlation of PSR0329
(at 2.3GHz, BW=2MHz, Integration=480sec)

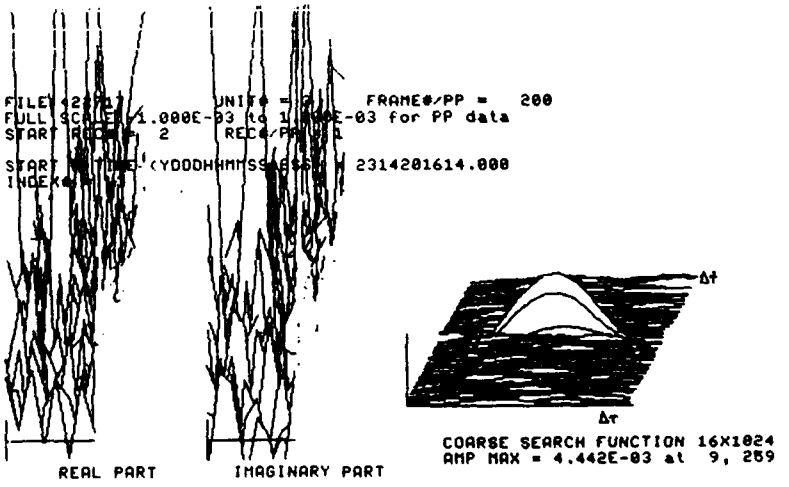

Fig.6 Gated correlation of PSR0329
(at 2.3GHz, BW=2MHz, Integration=480sec)

Table 2 Correlation Amplitude
(Gate time = period/16)

Gated	Non-gated	Integration time
4.44E-3	0.35E-3	490sec
4.77E-3	0.39E-3	250sec
4.47E-3	0.46E-3	125sec

Table 3 Correlation Amplitude
(Integration time = 250sec)

1.04E-3	(area A)
4.77E-3	(area B)
1.22E-3	(area C)

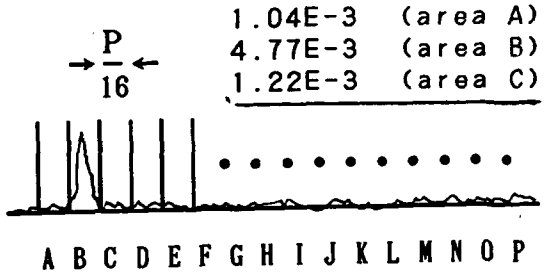

Table 4 Correlation Amplitude
(Integration time = 480sec)

0.35E-3	without gating
0.93E-3	(n=4)
2.01E-3	(n=8)
4.44E-3	(n=16)

Table 5 Correlation Amp. of millisecond pulsar 1937+21
(assumed gating covers 3/4 of the total flux)

	Average Intensity	Without gating	Gated (n=8)	Gated (n=16)
1.5GHz	9mJy	9.5E-5	5.7E-4	1.1E-3
2.2GHz	3.3mJy	2.9E-5	1.8E-4	3.5E-4

(gating time is period/n)

Dispersion $\Delta t =$ 43.7ns for RF=1.5GHz, BW=250kHz
$\Delta t =$ 349.2ns for RF=1.5GHz, BW=2MHz
$\Delta t =$ 96.9ns for RF=2.2GHz, BW=2MHz

QUESTIONS AND ANSWERS

D. Allan, Allan Time: Do you have any stability measurements against any reference clocks? eg: The arrival time stability against a reference clock.

S. Hama, CRL: Now we use a reference clock; a cesium. The Cesium is compared to UTC Japan by using GPS.

D. Allan: Do you have some results?

S. Hama: For timing measurement, I do not have the figure, but we are conducting timing measurement experiment. We have some results, so I can show you later.

D. Allan: Thank you.

AN ENSEMBLE PULSAR TIME

Gérard Petit and Claudine Thomas
Bureau International des Poids et Mesures
Pavillon de Breteuil
92312 Sèvres CEDEX, France
and
Patrizia Tavella
Istituto Elettrotecnico Nazionale G. Ferraris
Strada delle Cacce 91
10135 Torino, Italy

Abstract

Millisecond pulsars are galactic objects that exhibit a very stable spinning period. Several tens of these celestial clocks have now been discovered, which opens the possibility that an average time scale may be deduced through a long-term stability algorithm. Such an ensemble average makes it possible to reduce the level of the instabilities originating from the pulsars or from other sources of noise, which are unknown but independent.

We present the basis for such an algorithm and apply it to real pulsar data. It is shown that pulsar time could shortly become more stable than the present atomic time, for averaging times of a few years. Pulsar time can also be used as a flywheel to maintain the accuracy of atomic time in case of temporary failure of the primary standards, or to transfer the improved accuracy of future standards back to the present.

1. MILLISECOND PULSARS

Pulsars are neutron stars which spin rapidly and have a strong magnetic field. This generates a directional beam of electromagnetic radiation, which makes the pulsars detectable when the Earth happens to lie on the path of the beam. In 1982 the first element of a new class of pulsars, millisecond pulsars, was discovered, PSR1937+21 [1]. These millisecond pulsars not only spin much more rapidly, but have distinct physical properties that make them essential to an understanding of the evolution of pulsars.

It was quickly recognized that the period of rotation of PSR1937+21 is very stable. Since 1982, astronomers have carried out timing observations which measure the time of arrival (TOA) of the radio pulses relative to an atomic time scale. They have also discovered many more millisecond pulsars, which are now regularly observed at a number of observatories. The technique allows measurement of the TOAs with a precision of order 1 μs. Such a precision maintained over the whole period of observation (many years) makes it possible to reach a level of stability unequalled by any

other technique. This opens new paths in astronomy and astrophysics: detection of gravitational waves, probe of relativity in strong fields and high velocities, detection of planets orbiting pulsars, etc [2].

As the measurements are referred to atomic time (AT), pulsar analysis demands that this reference time scale be as stable as possible. Conversely it must be possible to transfer the stability of the rotation of pulsars to atomic time if the former appears to be better for certain averaging times.

2. PULSAR TIME

2.1. Astrometric analysis of pulsar data

The measurement system detects the TOA of pulses at the phase center of a radiotelescope. The TOAs are labelled in a local atomic time scale, and can later be referred to any time scale by the appropriate time transfer technique. It is possible to relate the TOAs to physical parameters like the position of the pulsar, that of the Earth, the spin rate of the pulsar etc. The goal of pulsar data analysis is to determine the set of physical parameters that best fits the observations.

To give a simple representation of the physical relation, we can consider the ideal case of a pulsar with a constant period, without motion relative to the solar system, and fictitiously observed at the geocentre. In this case the TOA observations would be regularly spaced except for an annual variation due to the orbital motion of the Earth. This one–year signature would determine the astrometric position of the pulsar, and the period would be determined as the average spacing between TOAs. The true situation is of course more complicated [3], but the general outline is similar.

2.2. Pulsar Time

The astrometric analysis provides a deterministic model to predict the arrival times of pulses. This is equivalent to defining an individual time scale PTi for pulsar i as follows: if A is the event "arrival of pulse n of pulsar i at a given observatory", $PTi(A)$ is the TOA computed from the model for this pulse. This way we define a time scale which is usable, although a bit cumbersome: with a radiotelescope and an adequate measurement system, any event can be compared to the arrival of a pulse, at least in theory, just as any event can be compared to the 1pps of an atomic clock.

For a given pulse, $PTi(A)$ is the predicted TOA and AT(A) is the observed TOA referred to the atomic time scale AT. The residuals of the timing data analysis, computed as observed minus predicted values, represent the difference of the two time scales AT minus PTi at the dates of the observations.

2.3. Relationship between AT and PT

In the present state of pulsar observations, the measurement uncertainty is as low as 0.2 μs in the best case [4], but more generally is at the level of 1 μs. It is clear that the instabilities of the present realizations of AT can be larger than 1 μs for averaging times of a few years. Indeed the fractional frequency instability of the present best realization of an uniform atomic time is estimated at about 2×10^{-14} [5] and statistical analysis of the timing residuals of PSR1937+21 over several years of

observation [2] indicates that the instability of AT–PT reaches similar values for averaging times larger than one year.

It is thus tempting to assume that the intrinsic stability of PT (ie. the stability of the rotation of the pulsar) is better than that of AT, and to use PT as a reference. In doing this, three problems arise.

First, it is not possible to define PT independently from AT. This is due to the variation of the rotation period of the pulsar, which cannot be described by a physical model. The variation of the period is assumed to be linear with time, but its rate can be determined only by reference to another time scale, that is to AT [6].

Second, AT–PT is the list of residuals to a fit which determines the physical parameters defining PT. All but three of the fitted parameters correspond to short term periods (maximum one year), and the remaining three correspond to a second–order polynomial of time. Thus such a fit filters from the residuals all terms with short periods (up to one year) and long periods (of order the time span T), so the instability of AT–PT can validly be estimated only for averaging times between about 2 years and T/2. From this, we can infer the instability of AT only for averaging times long enough to bring the measurement noise down to an instability level comparable with that of AT. These times may range from six months to several years depending on the measurement system and the pulsar.

Finally, several other sources of noise affect AT–PT, in addition to the intrinsic noise of AT and of the rotation of pulsars. Among them are interstellar propagation effects, uncertainties in the ephemeris of the solar system, and gravitational waves. All these contributions have identifiable signatures so that in theory it is possible to discriminate among them, as proposed with the concept of the pulsar timing array [7]. But for our purpose of finding a stable time scale with which to compare AT, it is much more convenient to assume that all sources of noise except AT are independent for different pulsars, and to average them by defining PT as a weighted average of the individual scales from several pulsars PTi. To do this we have to devise an appropriate stability algorithm, a procedure similar to that used for atomic clocks.

3. ALGORITHM FOR AN ENSEMBLE PULSAR TIME SCALE

The leading idea is to define a suitable algorithm that allows the computation of an ensemble pulsar time PT with the best long–term stability (integration times from 2 years up to T/2), as discussed in section 2. In pursuit of this aim, the following choices seem appropriate: PT is computed *a posteriori* with the largest possible data sets;

- PT is a weighted average of each pulsar contribution;
- weights are chosen according to the long–term stability, over some years, of each pulsar;
- precautions are taken to avoid the injection of unwanted noises by residual deterministic trends.

An algorithm corresponding to these characteristics has been devised and tested on simulated data, as reported in [8], and it is here adopted for the analysis of real observation data.

3.1. Preparation of data

As seen in section 2, the pulsar observation data are the results of an analysis in which the different parameters of a model have been estimated. To the aim of constructing an ensemble pulsar time, further analysis is necessary. It is desirable that the raw timing observations are made available and reduced with the same theoretical model to ensure the consistency of residuals. When the only available data are the residuals, it is desirable that the parameters of the models are provided to check that no important differences exist between the models used. In particular, if the residuals concern the same pulsar as observed by different observatories, the differential drift of one data set versus another, if any, has to be removed.

The residuals obtained are (AT–PTi) where AT is a chosen reference atomic time. They should contains only random components, apart from the residual deterministic trends due to uncertainties in the estimation of the parameters of the model.

In the computation of a time scale, equispaced data are convenient. Since we are interested in the long–term behavior of pulsar time, it is possible to construct a set of equispaced data with a suitable short–term average of the available residuals. We have chosen to use residual series with data spaced by 0.1 year. In order to prepare such series we process the available residuals with a moving average on a 0.2 y ar interval (containing at least three data points) centered on the date of interest. After such processing the resulting equispaced data are not really the residuals of observations, but an average of them, and their stability for integration times lower than 0.2 year is biased. Since we are interested in the stability for integration times larger than one year, this is not a restriction.

3.2. Ensemble algorithm

In analogy with what is done for atomic time scales, the definition of the ensemble pulsar time PT is the weighted average of the basic measurements (AT–PTi). It is defined in the form of the difference AT–PT, as

$$AT - PT = \sum_{i}^{8} w_i (AT - PT_i)$$

where w_i is the relative weight assigned to pulsar i. Weights are defined as inversely proportional to the instability of each pulsar for an integration time of a few years. This can be realized by taking for example the inverse of the Allan variance for 2.5 years, normalized to unity.

Since PT is computed *a posteriori*, when the complete set of data is available, each pulsar enters the ensemble with a fixed weight corresponding to the estimated level of instability.

To optimize the long–term stability, it appears important to have a good estimation of the drift of the pulsar period in order to avoid a residual drift occulting the long–term stability. This requires an observation time long enough to smooth the measurement noise (white phase noise) and to reach the long–term stability floor of the atomic reference time scale. At present, using TAI as reference atomic time, this level is estimated to be 2×10^{-14}. If the instability of TAI–PTi reaches this level, the residual drift will not degrade the stability for the integrating time of interest. If for any reason other sources of noise exceed this level and the long–term instability of TAI–PTi does not reach the above floor, the long–term behavior of pulsar i is treated as unstable and this pulsar enters the

ensemble with a lower weight.

In the present test the weights have been estimated by computing the Allan variance of TAI–PTi. If more data sets were available it might be worth estimating the instability by an N–cornered hat technique or by reference to an equal weight average, as discussed in [8].

The weight of each pulsar is fixed, but the number of observed pulsars can change as new pulsars are discovered or an observatory interrupts the pulsar timing. When the number or weight of clocks changes in an atomic time scale, suitable corrections are added[9] to avoid time or frequency jumps. In case of an average of pulsar residuals, all the deterministic trends have already been removed, and the only possible effect is a time jump resulting from computations with ensembles having a different number of residuals. So the removal or entry of a new pulsar is accompanied by a time correction that ensures the continuity of the pulsar ensemble scale. Such correction, a, is defined as

$$AT - PT = AT - (PT' + a),$$

where PT' is the new ensemble pulsar time computed with the data available after the change. It is easy to see that the correction, a, is just the difference in time between the new PT' and the old one.

4. APPLICATION TO REAL DATA

4.1. Available data

In this first experiment with real pulsar observations, the available data are the published residuals of the timing measurements performed at Arecibo Observatory [10]. They concern PSR1937+21 for the period 1984.9 to 1991.2, PSR1855+09 for the period 1986.2 to 1991.2 and PSR1957+20 for the period 1988.4 to 1991.2.

The residuals have been processed according to the procedure described above to obtain equispaced data with an interval of 0.1 year. Since all data come from the same observatory and have been analysed with similar models, the residuals have been used without further processing.

The residuals used TAI–PTi are reported in Figure 1 and their estimated Allan deviations in Figure 2. From the instability behavior it can be seen that pulsars 1937+21 and 1855+09 reach comparable instability levels for an integration time of about 2 years, while 1957+20 is ten times worse. For this reason the weights adopted for 1937+21 and 1855+09 are equal, while the weight of 1957+20 is 100 times lower (For the period in which all three pulsars were measured, the weights are respectively .497, .497, .006)

4.2. Results

The ensemble pulsar time PT, computed with the real data described above and compared with TAI, is shown in Figure 3. From the instability analysis (Figure 4) it can be verified that the ensemble PT is more stable than any single PTi for integration times in the range 1 to 2.5 years. In this region the Allan variance of TAI–PT is almost fixed at the level 2×10^{-14}. Assuming that, for the integration time of interest, the instability of TAI–PT is mostly due to that of TAI itself, it is interesting to examine the long–term behavior of TAI–PT. To do that, a Vondrak smoothing has been applied to smooth the noise due to Fourier components with periods lower than 1.5 year.

The result may be seen in Figure 3. It shows a cubic signature which is mostly due to the fact that a second order polynomial has been removed, nevertheless some information about the behavior of TAI can also be inferred. This is discussed in section 5.

5. DISCUSSION

5.1. Estimation of the stability of TAI and PT

For averaging times from 1 to 2.5 years, the measured fractional frequency instability of TAI–PT is about 2×10^{-14} (Figure 4). As this is also the estimated long term instability (and inaccuracy) of TAI [11], we have a good indication that PT and TAI can both be assigned an upper limit of 2×10^{-14} for 2–year stability. We have tried to confirm this indication by performing two simple tests on the present data set.

First we consider how the uncertainty in the determination of the time derivative of the pulsar period $\dot{P}$ (linked to a quadratic term of time in the residuals) can influence the estimated stability of each pulsar time, and consequently its attributed weight and the average PT. From the 1937+21 data, the uncertainty on $\dot{P}$ is estimated to 2×10^{-25} s/s [10]. This corresponds to a quadratic term of 6×10^{-23} s^{-1}, which has a theoretical 2–year Allan deviation of 0.7×10^{-14}. If we arbitrarily add such a quadratic term to the residuals, we observe that the 2–year frequency instability of this pulsar is not significantly changed, and the instability of the average is very similar.

Second we try to refer the pulsar data, and PT, to another atomic time scale. In the computation of TAI, the BIPM first generates a free–running time scale named EAL. TAI is then derived from EAL by steering its frequency to that of the primary frequency standards. As a test we have used EAL as a reference for pulsar data, and computed EAL–PT. It is interesting to note that the comparison with TAI–PT provides two hints which favor TAI, as might be expected. The difference between TAI and EAL over the period of reference arises mainly from a number of frequency steerings, after mid–89, that bend TAI "upwards" (to a net amount of 1 μs at the end of 1991). It can be seen in Figure 5 that this bending makes TAI–PT wander less than EAL–PT, a kind of visual indication that the steerings acted in the right direction. This is confirmed by the 2–year Allan deviation which is 10% higher for EAL–PT. Although this is not statistically very significant, it may provide the first evidence that the steering of TAI resulted in a time scale more stable in the long term, because it is more accurate.

This application to real data has limited value because only 3 pulsars were used, and for only 2 of them has TAI–PT reached a level of stability comparable with that of TAI. Furthermore the dataset with 2 pulsars or more covers a period of only 5 years. Nevertheless the outcome of this work looks promising because we have reached the level where we can infer some information about TAI, and the situation is one which will evolve rapidly. From the present programme of pulsar observations we anticipate that at the end of the century we shall have 10 to 16 years of observations on 6–8 pulsars, half of them yielding data comparable to PSR1937+21, ie. showing a 2–3 year Allan deviation of a few parts in 10^{14}, the remaining ones reaching this level after 5–10 years. This will considerably improve the stability of the ensemble average.

5.2. Transfer of the accuracy of atomic time

It is possible to take advantage of the long term stability of PT to transfer the accuracy of atomic time from one period of time to another, provided continuity in the pulsar observations is maintained. This is because, under the proposed scheme, the random part of the long term instability of PT can be decreased by averaging to a level much lower than that of the uncertainty in the present realization of the atomic second.

One application could be to use PT as a flywheel to maintain the accuracy of atomic time in the event of a temporary failure of the primary frequency standards. Similarly, when a future frequency standard with improved stability has been in continuous operation for years (and eventually provides a new definition of the second), PT will allow a backwards transfer, making it possible to evaluate the accuracy of our present atomic time scales. In this case, however, a limitation could arise from the random part of the instability of PT itself, which may be worse than that of the new standard for long averaging times. Such a situation is illustrated in Figure 6 where we show the result of a simulation. We have generated an atomic time scale which has an accuracy in the 10^{-14} range for 15 years and in the 10^{-16} range for the next 15 years, and a pulsar time PT which has random errors in the 10^{-15} range. When PT is referred to AT over the whole period, P and $\dot{P}$ can be determined so well that, over the first 15 years, AT–PT reveals the inaccuracies of AT (dashed line). In contrast when only the first 15 years are available, AT–PT only reveals the instabilities in AT (dotted line).

6. CONCLUSION

A millisecond pulsar can provide a time scale whose long term stability could be comparable with, or even better than, that of the present atomic time. Using data from many pulsars, it is possible to derive an average pulsar time scale that has a stability better than atomic time and better than the time derived from individual pulsar data. This improvement holds for averaging times from above one year up to about half the period of observation. A simple algorithm to realize this goal has been described.

A tentative application of the above procedure to real data yields limited results because very few pulsars have been observed, and the time span of the observations is only a few years. Nevertheless it seems that such a realization of pulsar time reaches the level of instability of atomic time. Current programme of observations make it possible to have enough data at the end of the century to estimate the instabilities of the present atomic time. If a more accurate atomic time scale is then available, it will also be possible to determine the present inaccuracies of atomic time.

REFERENCES

[1] D.C. Backer, S.R. Kulkarni, C. Heiles, M.M. Davis, W.M. Goss, *"A millisecond pulsar"*, Nature, 300, 615–618, 1982.

[2] J.H. Taylor, *"Millisecond pulsars: Nature's most stable clocks"*, Proc. IEEE, 79, 7, 1054–1062, 1991.

[3] R. Blandford, R. Narayan, R.W. Romani, *"Arrival–time analysis for a millisecond pulsar"*,

J. Astrophys. Astr., 5, 369–388, 1984.

[4] J.H. Taylor, *"Pulsar timing and relativistic gravity"*, Phil. Trans. Roy. Soc., 341, 117–134, 1992.

[5] A. Bauch, K. Dorenwendt, B. Fischer, T. Heindorff, E.K. Müller, R. Schröder, *"CS2: The PTB's new primary clock"*, IEEE Trans., IM–36, 613–616, 1987.

[6] B. Guinot, G. Petit, *"Atomic time and the rotation of pulsars"*, Astron. Astrophys., 248, 292–296, 1991.

[7] R.S. Foster, D.C. Backer, *"Constructing a pulsar timing array"*, Ap. J., 361, 300–308, 1990.

[8] G. Petit, P. Tavella, C. Thomas, *"How can millisecond pulsars improve the long term stability of atomic time scales"*, Proc. 6th European Frequency and Time Forum, 57–60, 1992.

[9] B. Guinot, *"Some properties of algorithms for atomic time scales"*, Metrologia, 24, 185–198, 1987.

[10] M.F. Ryba, *"High precision timing of millisecond pulsars"*, PhD dissertation, Princeton University, June 1991.

[11] Bureau International des Poids et Mesures, *"Annual report of the BIPM Time section"*, Vol. 4, 1991.

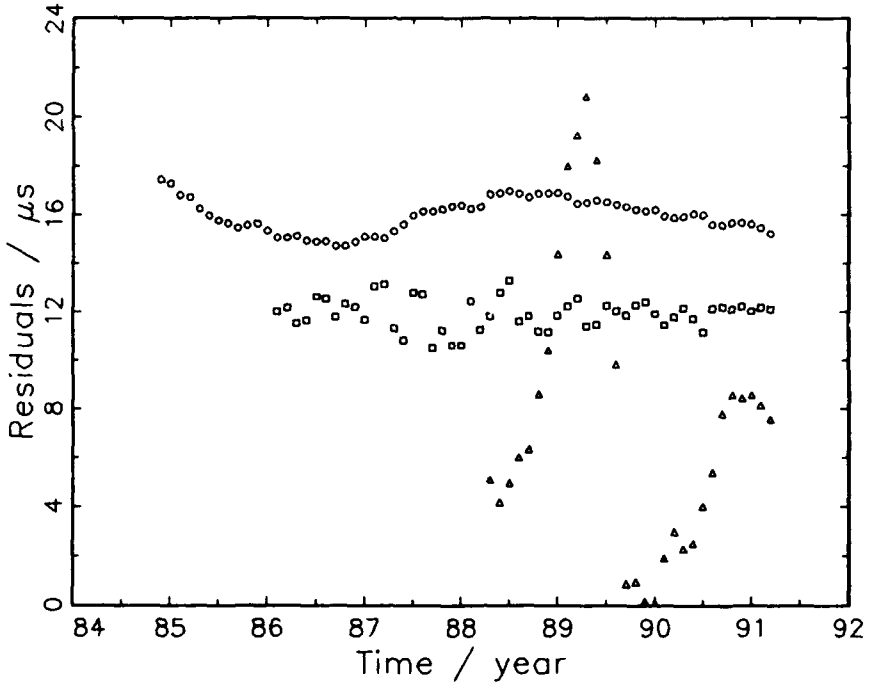

FIGURE 1: Timing residuals referred to TAI for 3 pulsars: 1937+21 (circles), 1855+09 (squares) and 1957+20 (triangles). The residuals have been averaged to equally-spaced data. For clarity, an arbitrary constant has been added to each data set.

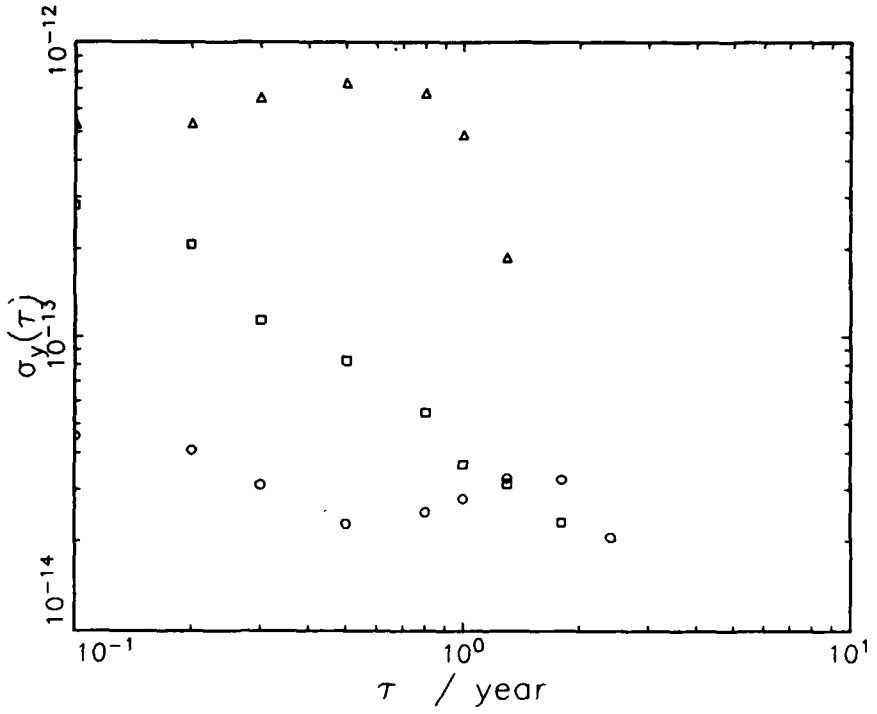

FIGURE 2: Square root of the two-sample Allan variance $\sigma_y(\tau)$ for the pulsar data of Figure 1 (The same symbols have been used).

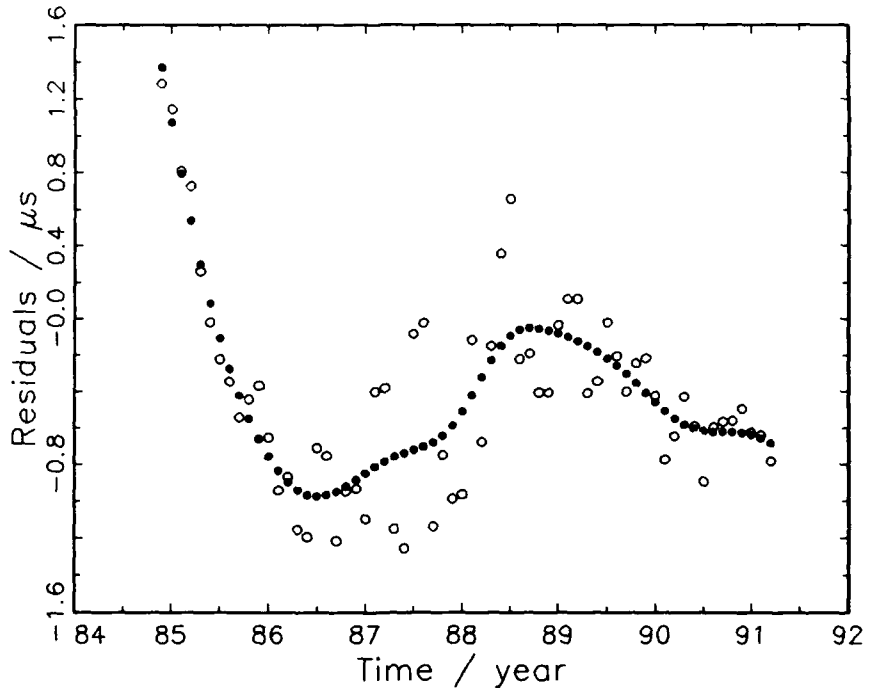

FIGURE 3: Difference TAI - PT, where PT is the ensemble pulsar time. Filled circles correspond to a Vondrak smoothing with a cut-off period of 1.5 year applied to the data.

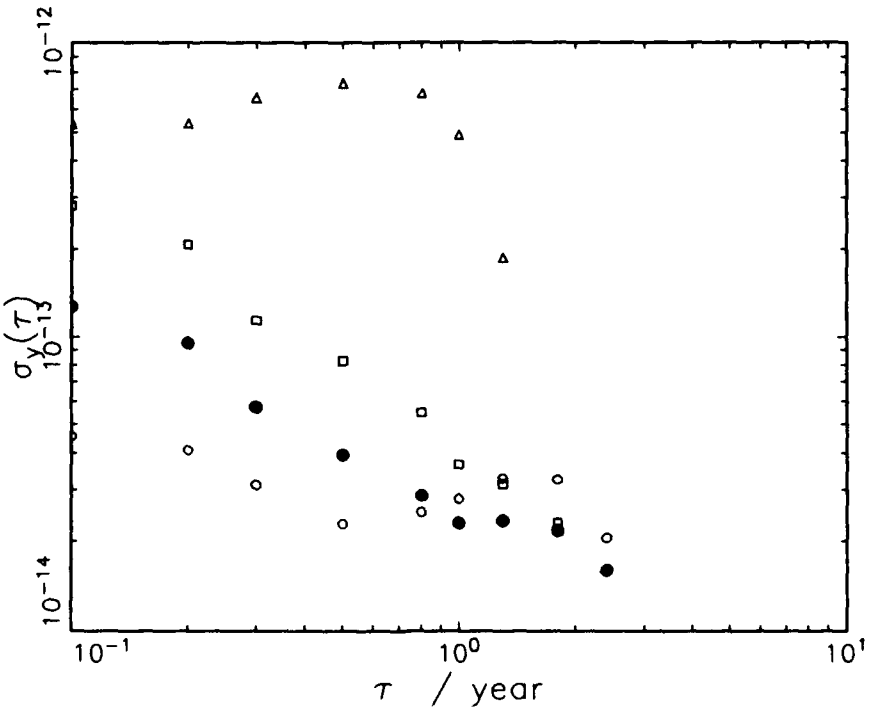

FIGURE 4: Square root of the two-sample Allan variance $\sigma_y(\tau)$ for TAI - PT (filled circles). Values for each pulsar from Figure 2 are also reported.

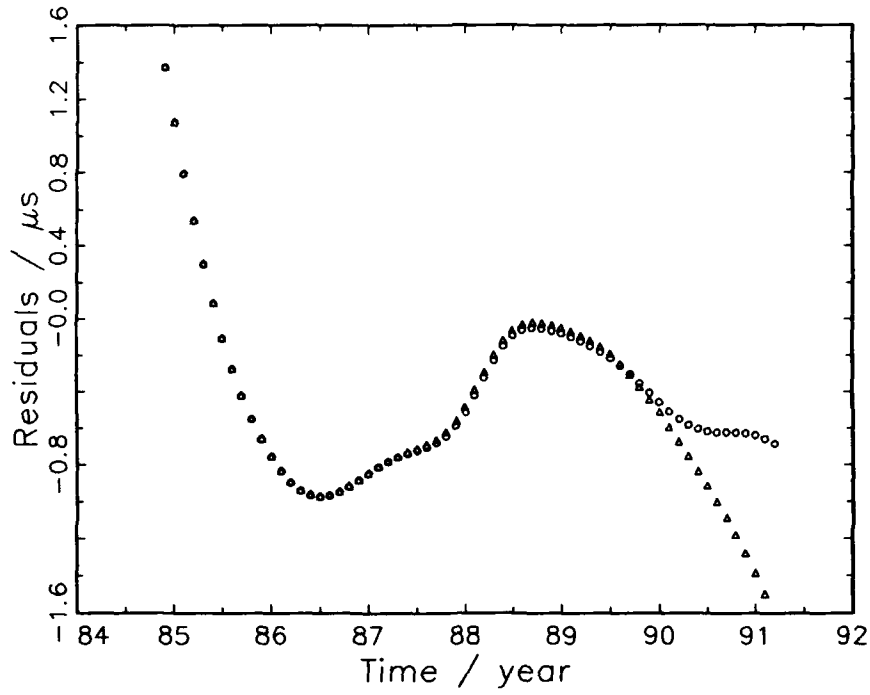

FIGURE 5: Differences TAI - PT (circles) and EAL - PT (triangles). A Vondrak smoothing with a cut-off period of 1.5 year has been applied to the data.

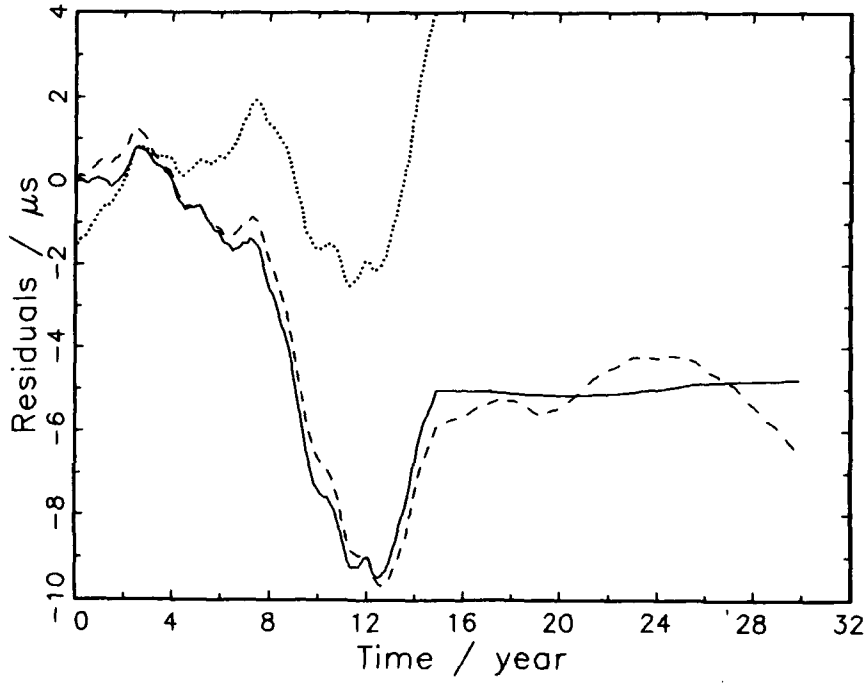

FIGURE 6: An atomic time AT with 10^{-14} accuracy for 15 years and 10^{-16} accuracy for 15 more years is simulated (solid line). A simulated pulsar time PT with 10^{-15} stability is referred to AT over the 30 years (dashed line). It allows to transfer the accuracy of AT from the last 15 years to the first 15 years to the 10^{-15} level. When PT is referred to AT over the first 15 years only (dotted line), it merely allows to estimate the instabilities of AT.

QUESTIONS AND ANSWERS

D. Matsakis, USNO: It seems like it doesn't meet the criterion of common sense, but here is my argument. You take the best pulsar and say that it's maybe 2 or 3 times worse than what you think the atomic clocks are. Then you average in another pulsar which you know is worse and you average it in with the same weight which might be the wrong way to average it and you say you're as good. That doesn't seem to be quite right.

G. Petit, BIPM: The ways we have chosen are representative of the stability of the pulsar for averaging times of say 2 years here.

D. Matsakis: I am not questioning the weight. I am just saying you will expect to maybe you do square root of two better or something like that; but now you're saying your direction here is good, and when you look at the two curves, the long term things, they don't really seem to agree with each other.

G. Petit: Which two curves?

D. Matsakis: No, the one you show with the three pulsars. The one that was very bad which seems to have a systematic problem to it, if I may comment there.

G. Petit: You mean the residuals themselves?

D. Matsakis: Yes. Well, all the stability on the first, where they showed all three pulsars together.

G. Petit: This one?

D. Matsakis: Yes, that one. It doesn't seem to me like those two pulsars, the two good pulsars agreed with each other more than they agreed with the atomic clocks. If I were to look at that I would say that the millisecond pulsar; the best pulsar is the deviant one of the three; the worst one, on the basis of the long term thing; long term residuals.

G. Petit: We cannot say the stability will obtain $2\times10^{-14}\pm0.001$. What we can say is the level of stability that is achieved by using two pulsars which have comparable stability of three years. This is a level of stability which is achieved is comparable to that of TAI. So that pulsar time itself is not lost in TAI. So it is at least as good.

G. Winkler, USNO: Is it possible to apply the three cornered hat method to resolve these four differences?

G. Petit: Yes, it's a way to estimate stability of which pulsar given the difference of atomic time minus pulsar time. You can in fact with the cross differences with pulsar time, 1 minus pulsar time and estimate that each stability of each pulsar time is squared. I've mentioned that we have not used this for this case because the case that two pulsars are the same weight and either one was (?) but clearly for several, or if you have many pulsars, it is a way to do it.

D. Allan, Allan Time: Another question which I think is very relevant here. If you look at the history of atomic time keeping frequency standards have improved about an order of magnitude every seven years. If you project the year 2000, we should be another order of magnitude better. We know of devices that should be at least that good if not better than 10^{-15} to 10^{-16} by that time and if you now look at the fundamental problem with pulsar metrology, it is the measurement noise. Even with the new upgrade at Arecibo, which is costing ten

million dollars, we anticipate the noise level to go down to 100 nanoseconds. If I do optimum statistical processing using modified $\sigma_y(\tau)$, I expect to see a clock projected into the future at that level of an integration time of about 200 years. I'm limited by the measurement noise in other words.

G. Petit: Yes, but if you consider that now it is expected to find one pulsar in every one hundred square degrees of the sky, you can anticipate to have several hundred pulsars to average. So pulsar time could gain a lot of stability just by statistical arranging.

D. Allan: So you're saying that by sheer numbers if I had 100 pulsars then I would have an improvement of the factor of 10 from statistical independence, is that what you're saying?

G. Petit: Yes.

D. Allan: Even with that if you drop that down to 20 years, the projected improvement in atomic clocks would out strip anything you can achieve from pulsars.

G. Petit: That is true but what I am also saying is that we can take advantage of the whole set of pulsar data and we can use the future improvement of atomic clocks to gain information at the present atomic time. That is also a use of millisecond pulsars.

D. Allan: I am happy to see the data. I am just projecting that by the year 2000, you may be left in the dust.

G. Petit: Well anyway, why do you assume I would be happy to have 10^{-15} time scales to get better data.

Question: *Question about whether you've taken relativity and inertial frame effects into account* for pulsar time?

G. Petit: That is taken into account in the last phase, which we have not developed because, with a simple model, it is actually much more complicated. That analyzes here to fit the model to the observation, takes into account everything which has to be taken into account; including relativity and whatever you want.

EXPERIMENTAL COMPARISON OF TIME SYNCHRONIZATION TECHNIQUES BY MEANS OF LIGHT SIGNALS AND CLOCK TRANSPORT ON THE ROTATING EARTH

R.A. Nelson,[a] C.O. Alley, J. D. Rayner, Y.H. Shih,[b]
C.A. Steggerda,[c] B.C. Wang, and B.W. Agnew

Department of Physics, University of Maryland, College Park, Maryland 20742

Abstract

An experiment was conducted to investigate the equivalence of two methods of time transfer in a noninertial reference frame: by means of an electromagnetic signal using laser light pulses and by means of the slow ground transport of a hydrogen maser atomic clock. The experiment may also be interpreted as an investigation of whether the one-way speeds of light in the east-west and west-east directions on the rotating earth are the same. The light pulses were sent from a laser coupled to a telescope at the NASA Goddard Optical Research Facility (GORF) in Greenbelt, Maryland to the U.S. Naval Observatory (USNO) in Washington, DC. The optical path was made possible by a 30-cm flat mirror on a water tower near GORF and a 25-cm flat mirror on top of the Washington National Cathedral near USNO. The path length was 26.0 km with an east-west component of 20.7 km. The pulses were reflected back over the same path by a portable array of corner cube reflectors. The transmission and return times were measured with a stationary Sigma Tau hydrogen maser and a University of Maryland event timer at GORF, while the times of reflection were measured with a similar maser and event timer combination carefully transported to USNO. Both timekeeping systems were housed in highly insulated enclosures and were maintained at constant temperatures to within $\pm 0.1^{\circ}C$ by microprocessor controllers. The portable system was also protected from shock and vibration by pneumatic supports. The difference ΔT between the directly measured time of reflection according to the portable clock and the time of reflection calculated from the light pulse signal times measured by the stationary clock was determined. For a typical trip $\Delta T < 100$ ps and the corresponding limit on an anisotropy of the one-way speed of light is $\Delta c/c < 1.5 \times 10^{-6}$. This is the only experiment to date in which two atomic clocks were calibrated at one location, one was slowly transported to the other end of a path, and the times of transmission, reflection, and return of short light pulses sent in different directions along the path were registered.

INTRODUCTION

The precision of time synchronization techniques made possible by hydrogen maser atomic clocks, event timers, and short pulse laser ranging systems implies that relativistic effects must be modelled

[a] Present address: W.L. Pritchard & Co., Inc., 7315 Wisconsin Avenue, Suite 520E, Bethesda, MD 20814.
[b] Present address: Department of Physics, University of Maryland Baltimore County, Catonsville, MD 21228.
[c] Present address: Bendix Field Engineering Corporation, Lanham, MD, 20706.

in the practical realization of a spatially distributed time scale. The prescription requires the adoption of an appropriate set of conventions and a coordinate reference frame so that a self-consistent scale of coordinate time can be established [1, 2]. There are two methods for the comparison of remote clocks: the propagation of an electromagnetic signal and the transport of an intermediate portable clock.

Experiments are required to test the assumptions and interpretation of the theoretical model. These experiments also provide a means to investigate the foundations of the metric theory of space, time, and gravitation, in which the behavior of clocks and light pulses plays a central role. In particular, the equivalence of the two methods of time synchronization in the noninertial reference frame of the rotating earth was recently tested at the University of Maryland [3]. This experiment may also be interpreted as a test of the isotropy of the one-way speed of light in the east-west and west-east directions.

In the experiment, short pulses of light were sent from a laser coupled to the 1.2-meter telescope at the NASA Goddard Optical Research Facility (GORF) in Greenbelt, Maryland, to the U.S. Naval Observatory in Washington, DC. The pulses were reflected back over the same path by a portable array of corner cube reflectors. The proper time of emission τ_1 and proper time of return τ_3 of each pulse were recorded by a hydrogen maser and event timer at GORF. The proper time of reflection τ_2 was recorded by a second hydrogen maser and event timer carefully transported to USNO. The two timekeeping systems were calibrated both before and after the portable clock trip. If the corresponding coordinate times of reflection calculated from the measurements by the portable clock and the electromagnetic signals are respectively t_2^{PC} and t_2^{ES}, the quantity

$$\Delta T \equiv t_2^{\mathrm{PC}} - t_2^{\mathrm{ES}} \tag{1}$$

should be zero in any self-consistent relativistic prescription. The object of the experiment was therefore to determine ΔT.

Research in preparation for this experiment has been reported in previous PTTI papers. In 1982 measurements of light pulse time comparisons were first performed over the optical link using cesium beam clocks to support the proposed LASSO experiment [4]. With the cooperation of the Johns Hopkins University Applied Physics Laboratory, several trips were made in 1987 to test the feasibility of using a hydrogen maser as a portable clock. In one trip a time transfer between APL and USNO was completed with a time closure of less than 200 ps [5]. A pilot experiment to measure ΔT was carried out during the spring and summer of 1988 using a Sigma Tau maser borrowed through the courtesy of APL and JPL as the portable clock and an APL NR-series maser on loan from the NASA Crustal Dynamics Project that was kept at GORF. Subsequently, the present experiment was carried out over the period from September 1988 through April 1989 using two Sigma Tau masers loaned by the National Radio Astronomy Observatory VLBI program. Preliminary results were described at the 1988 PTTI meeting [6].

This is the first experiment in which two atomic clocks were calibrated at one location, one was slowly transported to the other end of a path, and the times of transmission, reflection, and return of short light pulses sent in different directions along the path were registered. In contrast to experiments of the Michelson-Morley type [7], in which light is sent around a closed path, these measurements test the isotropy of the one-way speed of light. However, unlike other recent experimental tests, such as Mössbauer gamma ray absorption experiments on a rotating disk [8, 9] and atomic beam laser

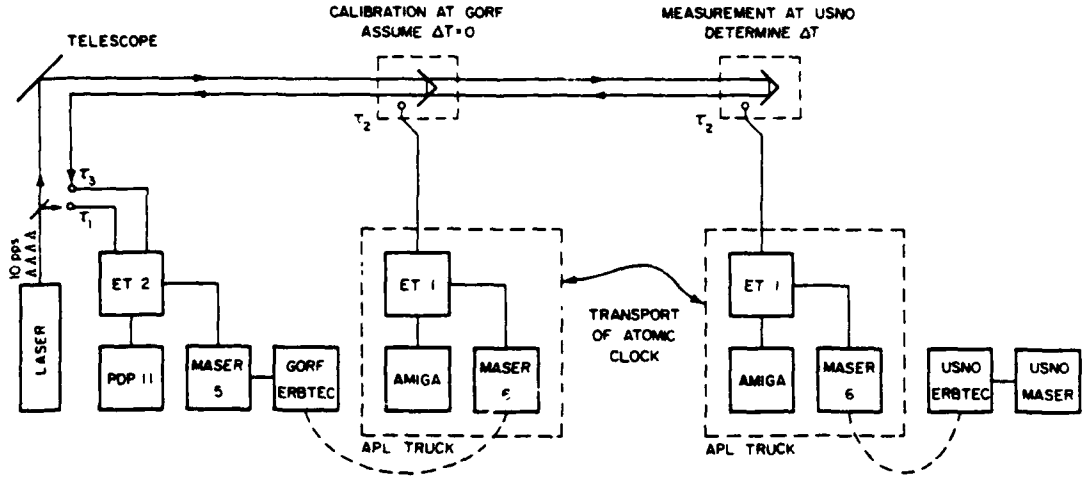

Figure 1. Schematic diagram of experiment.

spectroscopy measurements [10], this experiment uses short light pulses involving the group velocity and actual measurements of time rather than waves involving the phase velocity and measurements of phase difference or frequency. It complements two other experiments involving hydrogen masers at the opposite ends of a path: the JPL experiment of Krisher *et al.* [11, 12], in which a possible diurnal variation was monitored in a continuous laser signal sent along a fiber-optic link, and the Smithsonian Astrophysical Laboratory experiment of Vessot *et al.* [13], in which the rate of a rocket-borne hydrogen maser was measured as a function of height, speed, and direction.

EXPERIMENT DESIGN

A schematic diagram of the experiment is illustrated in *Figure 1.* The phase difference between the portable and stationary masers was monitored continously at GORF, interrupted only by the portable clock trips. Before and after a trip, a series of optical measurements with the laser pulses was also performed at GORF to calibrate the time measurement systems assuming $\Delta T = 0$ locally. Then the portable system was transported to USNO and the optical measurements were repeated to determine the value of ΔT at the other end of the path. The portable clock was compared with one of the USNO masers to verify its stability while at the remote site.

Assume that coordinate time is established by synchronization with the clock at GORF. Then the coordinate time of reflection of each light pulse according to the method of clock transport is

$$t_2^{\mathrm{PC}} = \tau_2 + \Delta t_{\mathrm{rel}}^{\mathrm{PC}} \tag{2}$$

where $\Delta t_{\mathrm{rel}}^{\mathrm{PC}}$ is a relativistic correction for clock transport. Similarly, the coordinate time of reflection obtained by using electromagnetic signals is

$$t_2^{\mathrm{ES}} = \tau_1 + \frac{1}{2}(\tau_3 - \tau_1) + \Delta t_{\mathrm{rel}}^{\mathrm{ES}} = \frac{1}{2}(\tau_1 + \tau_3) + \Delta t_{\mathrm{rel}}^{\mathrm{ES}} \tag{3}$$

where $\Delta t_{\mathrm{rel}}^{\mathrm{ES}}$ is a relativistic correction for electromagnetic signals. The value of ΔT is therefore

$$\Delta T = (\tau_2 + \Delta t_{\mathrm{rel}}^{\mathrm{PC}}) - \left[\frac{1}{2}(\tau_1 + \tau_3) + \Delta t_{\mathrm{rel}}^{\mathrm{ES}}\right] = \left[\tau_2 - \frac{1}{2}(\tau_1 + \tau_3)\right] + \Delta t_{\mathrm{rel}} \tag{4}$$

where $\Delta t_{\rm rel} \equiv \Delta t_{\rm rel}^{\rm PC} - \Delta t_{\rm rel}^{\rm ES}$. The individual relativity corrections $\Delta t_{\rm rel}^{\rm PC}$ and $\Delta t_{\rm rel}^{\rm ES}$ depend on the coordinate system but in any self-consistent relativistic prescription their difference $\Delta t_{\rm rel}$ is independent of the coordinate system. Physically, this is because the apparatus with which the measurements are performed cannot be affected by the choice of coordinate system in which the data are analyzed. For example, in a locally inertial system, $\Delta t_{\rm rel}^{\rm PC} = \int_{\rm path}(v^2/2c^2 - gh/c^2)\,d\tau$ and $\Delta t_{\rm rel}^{\rm ES} = 0$, where v is the portable clock velocity, g is the acceleration of gravity, and h is the height above the geoid. Alternatively, in an earth-centered rotating coordinate system, $\Delta t_{\rm rel}^{\rm PC} = \int_{\rm path}(v^2/2c^2 - gh/c^2)\,d\tau + 2\omega A/c^2$ and $\Delta t_{\rm rel}^{\rm ES} = 2\omega A'/c^2$, where ω is the angular rate of rotation of the earth and A or A' is the equatorial projection of the area bounded by the path and the earth's radii at each end of the path. Therefore, if the portable clock path coincides with the light path, so that $A = A'$, in either case

$$\Delta t_{\rm rel} = \frac{1}{c^2}\int_{\rm path}\left(\frac{1}{2}v^2 - gh\right)d\tau\,. \tag{5}$$

The portable clock correction has been tested experimentally in the neighborhood of the earth [14]. The isotropy of the one-way speed of light investigated by the present experiment requires that this difference in corrections should be frame-invariant.

The actual measurements are the clock "registration times" τ_1^*, τ_2^*, and τ_3^*. The corresponding proper times associated with the stationary clock are

$$\tau_1 = \tau_1^* - \Delta\tau_{\rm S} \tag{6a}$$

and

$$\tau_3 = \tau_3^* - \Delta\tau_{\rm S} \tag{6b}$$

while the proper time associated with the portable clock is

$$\tau_2 = \tau_2^* - \Delta\tau_{\rm P} - \Delta\tau_{\rm PS} \tag{7}$$

where $\Delta\tau_{\rm S}$ and $\Delta\tau_{\rm P}$ are the total systematic offsets due to cable delays and response times in the stationary and portable systems, respectively, and $\Delta\tau_{\rm PS}$ is the proper time offset due to the phase difference between the two systems. The net systematic delay is

$$\Delta\tau_{\rm del} \equiv \Delta\tau_{\rm P} - \Delta\tau_{\rm S}\,. \tag{8}$$

Due to inefficiencies in optical detection, only about 50 out of 1000 pulses yield measurements of all three times. Therefore, the measurements of τ_1^*, τ_2^*, and τ_3^* are merged on a computer for all of the laser pulses to identify the corresponding sets of values. The matching program produces distributions for the differences

$$\Delta T_{21}^* \equiv \tau_2^* - \tau_1^* \tag{9a}$$

and

$$\Delta T_{31}^* \equiv \tau_3^* - \tau_1^*\,. \tag{9b}$$

Therefore, we can express Eq. (4) in the form

$$\Delta T = \Delta T_{21}^* - \frac{1}{2}\Delta T_{31}^* - \Delta\tau_{\rm del} - \Delta\tau_{\rm PS} + \Delta t_{\rm rel} \tag{10}$$

where $\Delta t_{\rm rel}$ is given by Eq. (5). This is the primary working equation for the experiment. The delay $\Delta\tau_{\rm del}$ is eliminated by the calibration measurement at GORF, while the proper time offset $\Delta\tau_{\rm PS}$ between the portable and stationary masers at the time of the remote measurement is determined by interpolation.

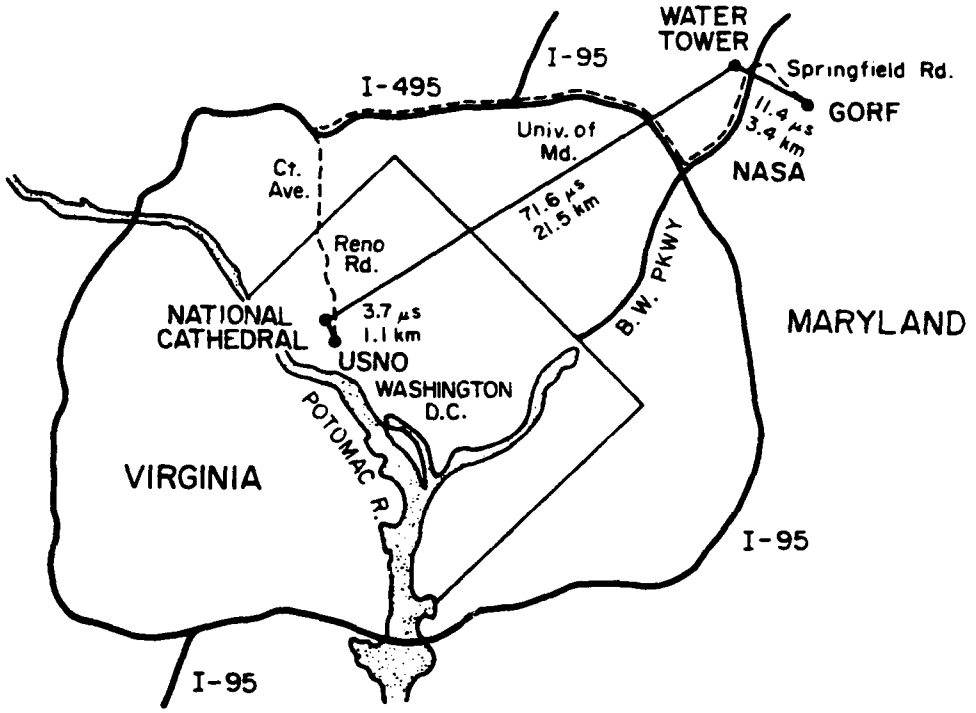

Figure 2. Optical path across Washington and portable clock route.

OPTICAL PATH AND CLOCK ROUTE

The optical path from GORF to USNO is illustrated in *Figure 2.* A truck equipped with an electrical power generator was provided by APL and was used to carry the portable maser. The 1.2–meter telescope at GORF is at longitude 76° 49.7′, latitude 39° 1.4′, and elevation 43 m. The site is shown in *Figure 3.* The retroreflector array was set up in front of Building 1 at USNO at longitude 77° 4.0′, latitude 38° 55.3′, and elevation 79 m. The truck is shown parked at this location in *Figure 4.* Due to local topography, there is no direct line of sight. However, the optical path was made possible by a 30–cm flat mirror on a water tower near GORF and a 25–cm flat mirror on top of the Washington National Cathedral near USNO. The path length was 26.0 km with an east–west component of 20.7 km. The 37.4 km route taken by the portable clock in the truck is indicated by a broken line.

During a calibration measurement, light pulses from the telescope were reflected off a small mirror mounted on the tower labeled "laser beacon system" in *Figure 3.* This system previously had been disassembled and the dome removed. The telescope is shown in the calibration position in *Figure 5.* The truck containing the portable maser can be seen (partially obscured by a trailer office) with the portable detector behind it. A closeup view of the detector package is illustrated in *Figure 6.*

A telephone was installed at each location. On the night of a measurement, the activities were coordinated by means of a telephone conference call. A minimum team consisted of three people at GORF to operate the laser and event timer and to coordinate activities; one person at the water tower and one person at the cathedral to adjust the mirrors; and three people at USNO to drive the truck, adjust the detector, and run the portable event timer. *Figure 7* shows the beam as seen from the cathedral. The green laser flashes from the water tower were brighter than all other lights visible and the signal arriving at USNO projected shadows of the detector against the side of the truck.

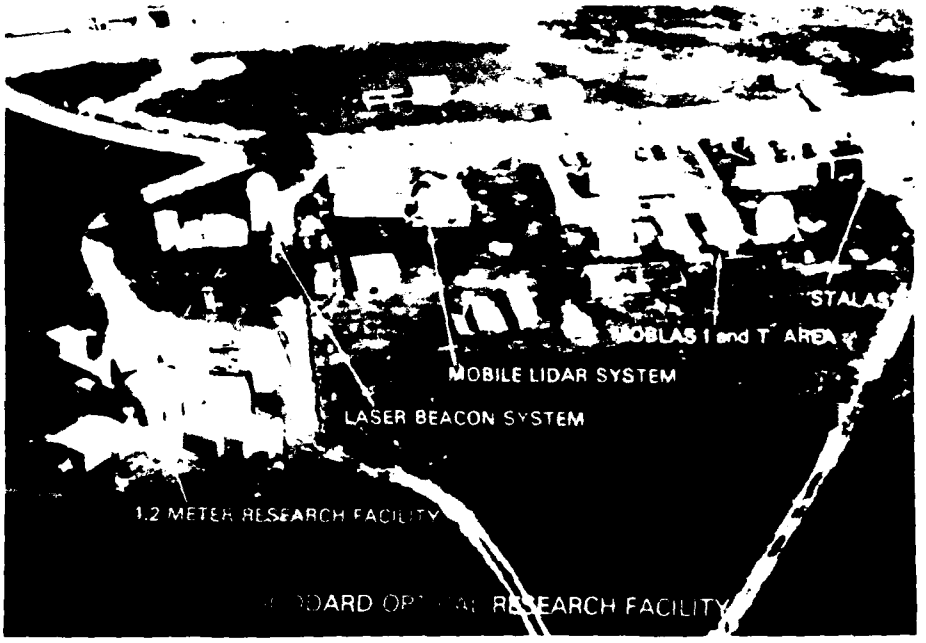

Figure 3. Overhead view of the NASA Goddard Optical Research Facility (GORF).

Figure 4. Truck parked in front of Building 1 at USNO where optical measurements are taken.

Figure 5. 1.2-meter telescope. The laser is in the structure beneath the telescope. The building at left contains the telescope tracking computer. The building in rear contains the stationary maser and event timer and electronic equipment. The water tower is visible on the horizon.

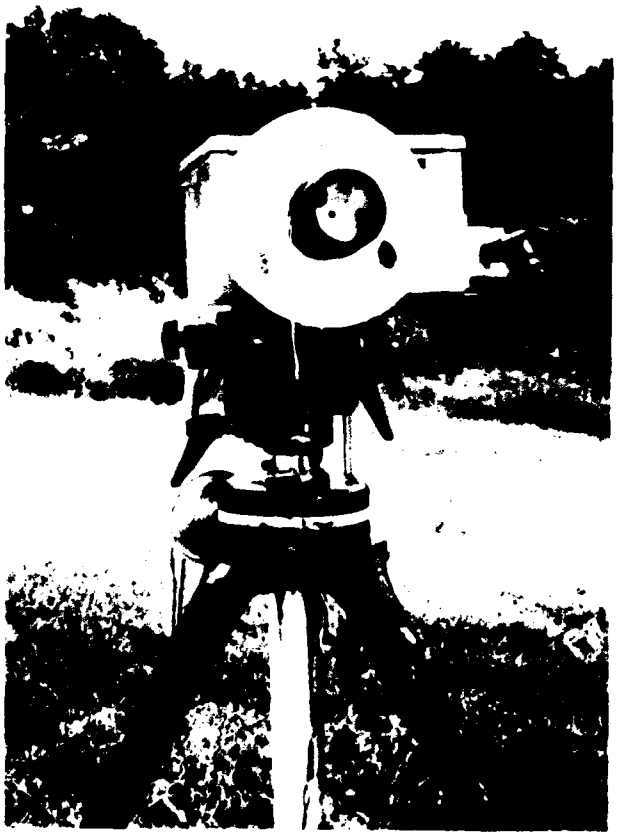

Figure 6. Portable corner cube reflectors and detector.

Figure 7. Laser beam from water tower as seen from the cathedral. The illuminated structure at left is a 215–m high television broadcast antenna.

MASERS AND EVENT TIMERS

The masers used in this experiment were Sigma Tau masers 5 and 6 that were loaned by the National Radio Astronomy Observatory near Soccoro, NM. Maser 5 was kept at GORF and maser 6 was kept in the truck. These masers were part of a group of ten that were constructed for NRAO by Harry Peters and his associates at the Sigma Tau Standards Corporation for use in the Very Long Baseline Interferometry program [15].

The two event timers used in this experiment were developed by the University of Maryland Quantum Electronics Group, as described in Reference [6]. Each event timer has two channels and can measure the epoch of an event to a precision of 20 ps. Data at GORF were recorded by a PDP–11 computer and data for the portable system were recorded by an Amiga PC carried in a van that accompanied the truck.

The portable maser and event timer were contained in a specially constructed, highly insultated enclosure mounted on pneumatic supports. The temperature of the interior of the enclosure was maintained constant to within $\pm 0.1°C$ by a Shimaden SR–22 PID microprocessor. The truck interior was also temperature controlled. The configuration of the portable maser and event timer is shown in *Figure 8*. Similarly, the stationary maser and event timer at GORF were maintained within temperature controlled enclosures with the same level of stability. All maser cabling used a temperature–stabilized foam–dielectric cable manufactured by Cablewave Systems (FLC 12-50J) with type "N" connectors. The temperature sensitivity of this cable is about 10 ppm/°C.

The phase difference between the portable and stationary masers was monitored at GORF continuously except during the portable clock trips with an Erbtec system [16]. This system utilizes a

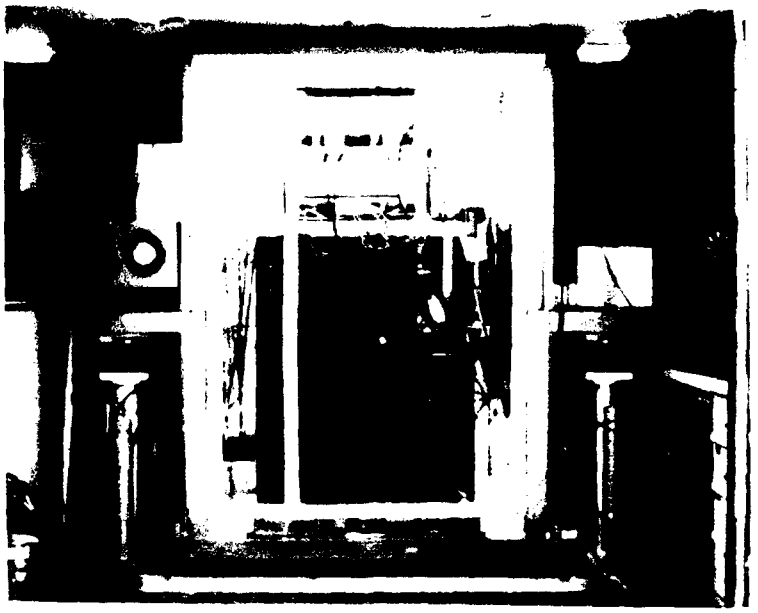

Figure 8. Portable maser and event timer within enclosure.

principle of mixing the 5–MHz frequency of each maser with a synthesized frequency of 4.999 990 MHz to generate two 10–Hz beat signals. The phase difference between these beat signals can be measured by standard methods and is equal to the phase difference between the 5–MHz signals themselves. The resolution is 0.2 ps with an ambiguity of 200 ns.

LASER AND DETECTORS

The laser is a Q–switched, mode–locked, cavity dumped neodymium–YAG (Nd: YAG) stable resonator with two amplifiers. The fundamental infrared wavelength of 1064 nm is converted to green at 532 nm by frequency doubling with a nonlinear crystal. The conversion efficiency is more than 40%. The output energy in the green is 10 mJ with a stability of 10%. The average pulse width was 70 ps and the repetition rate was 10 Hz.

A passive polarization switch coupled the laser to the telescope. The light was reflected by a thin film polarizer and entered the telescope through a zero–order quarter–wave plate, which changed the polarization from linear in the vertical direction to circular. The beam emerging from the telescope was about 30 cm in diameter and passed to one side of the secondary mirror. The returning pulses suffered some depolarization but were mostly circularly polarized in the opposite sense. The quarter–wave plate changed the polarization from circular back to linear in the horizontal direction. The light then passed through the thin film polarizer and was reflected by a dichroic mirror to the return pulse detector.

The τ_1–detector for the outgoing pulse was a Lasermetrics model 3117PD high–speed silicon PIN diode with a risetime of less than 150 ps and a jitter of less than 10 ps. The τ_3–detector was a Hamamatsu microchannel plate photomultiplier tube with a risetime of 150 ps and a time jitter on the order of 30 ps. The τ_2–detector in the portable timing electronics was an RCA C30902E avalanche photodiode

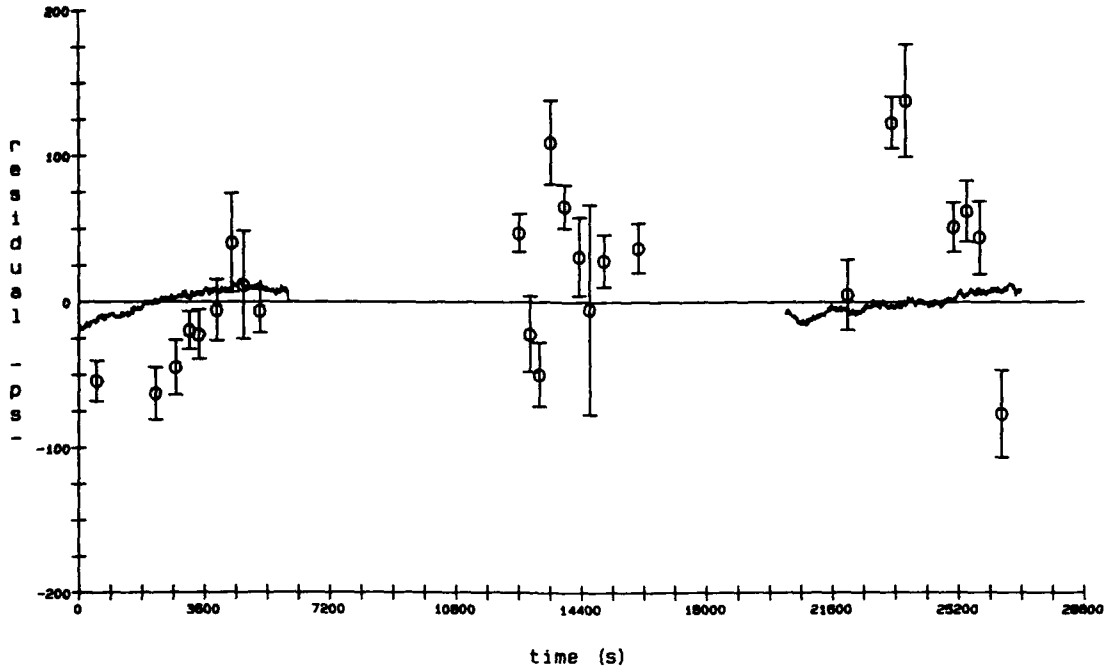

Figure 9. Measurement residuals for the trip of March 22, 1989. Data at left and right are calibration measurements performed at GORF. Data in center are ΔT measurements performed at USNO. Solid lines represent maser phase comparisons. Circles represent optical measurements, where error bars indicate standard deviations of the mean.

cooled with dry ice and operated in the avalanche mode. The risetime was approximately 500 ps with a jitter on the order of 150 ps. The measured energy sensitivity was approximately 10 ps/mV. The output level was held constant to within about 10% of 150 mV by adjusting the incident light with an iris on the detector package, as illustrated in *Figure 6.*

RESULTS

A parabola was fitted to the maser relative phase measurements obtained before and after each trip by the method of least squares. The pretrip and posttrip optical measurements were next fitted to this parabola to remove the constant systematic delays associated with the cables and electronics. The relative difference between the optical measurements performed at USNO and the interpolated maser phase measurements then determined ΔT. Measurement residuals for a typical trip are illustrated in *Figure 9.* The values for all nine trips in which a complete set of measurements were obtained are summarized in *Table 1.* Plots of measurement residuals for these trips and a composite plot of optical residuals are given in the Appendix.

For a typical trip $\Delta T < 100$ ps and the corresponding limit on the anisotropy of the one-way speed of light is $\Delta c/c < 1.5 \times 10^{-6}$. By comparison, if there had been a Galilean effect associated with the earth's motion around the sun at a velocity of 30 km/s, the result would have been $\Delta T = -6.9$ ns. However, the data are not sensitive to a hypothetical Galilean effect of 83.1 ps associated with the earth's rotational velocity of 360 m/s at latitude 39°.

The relativity correction Δt_{rel} of Eq. (5) was integrated numerically using Simpson's rule. The truck velocity was monitored with a Stewart-Warner "sender" unit attached to the speedometer cable. The

Table 1
Measured values of ΔT according to Eq. (10)

Trip	ΔT		*Maser rate change*
	mean	sd	posttrip − pretrip
	(ps)	(ps)	($\times 10^{-14}$)
March 10	65.2	27.1	+3.7
March 16	69.9	89.7	−2.7
March 21	82.6	48.0	−1.8
March 22	35.6	68.9	+0.6
March 25	−6.6	38.1	−1.9
March 28	123.2	73.4	−2.0
April 9	−14.4	36.6	+0.2
April 11	35.4	52.8	+1.4
April 13	−29.4	22.1	+0.3

sender generates a squarewave whose frequency is proportional to the velocity. A frequency–to–voltage converter circuit was used to record the velocity as a function of time on a strip chart recorder. The truck was driven at a maximum velocity of 50 km/h to minimize vibration. Elevations were determined from topographic maps. The resulting velocity correction is +2.6 ps and the elevation correction is −12.6 ps, yielding a net correction of − 10.0 ps. There is an additional correction of −14.3 ps per hour of dwell time at USNO due to higher elevation. A typical trip required about one hour to drive each way and two hours to perform the optical measurements. The total correction upon return to GORF was thus about −50 ps. The Sagnac correction $2\omega A/c^2$ due to the earth's rotation is 83.1 ps in an earth–centered coordinate system, but this correction was not included in the data reduction since it should apply equally to light propagation and clock transport for coincident paths.

The atmosphere affects the determination of range but not the transfer of time [4]. In the case of a range measurement by the radar technique, the delays caused by the atmosphere are additive. In contrast, in an optical time transfer the atmospheric delays are subtracted. The standard deviations of ΔT^*_{21} and ΔT^*_{31} were of the order of 100 ps and 200 ps, respectively, for a trial of about 1000 pulses over 100 seconds. The variation was approximately the same for calibration measurements at GORF (1 μs round trip time) and for optical time transfer measurements at USNO (174 μs round trip time). Thus the data support the assumption that atmospheric fluctuations over the round trip time of flight were neglible.

The principal limiting factor of the experiment was the poorly understood response of the detectors. For an improvement in the result, the time jitter due to light intensity fluctuations of the τ_2–detector, in particular, must be reduced. A second source of ambiguity was the change in rate of the portable maser, which was typically about 1 part in 10^{14} between the pretrip and posttrip calibration measurements. In several tests, it was found that rate changes were not induced during an uninterrupted trip; rather they took place during a pause in the trip. Changes in maser orientation also caused a rate change. Improvement in the enclosure suspension and use of one of a new generation of Sigma Tau masers having a varactor instead of a thermal mechanism in the autotune circuit would likely reduce these changes and permit a linear (rather than parabolic) fit of the maser phase difference.

Acknowledgments

We wish to thank Gernot Winkler and Gart Westerhout of USNO, Warner Miller of USAF, and Henry Fliegel of the Aerospace Corporation for financial support; Lauren Rueger and Al Bates of APL, Lute Maleki of JPL, Peter Dachel and Bob Price of Bendix, Robert Coates of NASA, and Peter Napier and Larry Beno of NRAO for the loan of masers; Harry Peters of Sigma Tau for technical advice; Ron Beard, Joe White, and Al Gifford of NRL and Paul Wheeler of USNO for additional equipment and invaluable assistance; Jim Wilcox of APL for assistance with the truck; Hüseyin Yilmaz of Hamamatsu for theoretical discussions and equipment; and Charles Misner of the University of Maryland for theoretical advice.

References

[1] International Radio Consultative Committee, "Relativistic Effects in a Terrestrial Coordinate Time System," Report 439-4, *Recommendations and Reports of the CCIR, 1986*, Vol. VII, pp. 134 – 138.

[2] G.M.R. Winkler, "Synchronization and Relativity," *Proc. IEEE* **79**, 1029 –1039 (1991).

[3] R.A. Nelson, "Experimental Comparison Between Two Methods for Synchronization of Remote Clocks on the Rotating Earth: The Propagation of an Electromagnetic Signal Using Laser Light Pulses and the Transport of a Hydrogen Maser Atomic Clock," Ph.D. dissertation, University of Maryland, 1990.

[4] C.O. Alley, J.D. Rayner, C.A. Steggerda, J.V. Mullendore, L. Small, and S. Wagner, "Time Transfer Between the Goddard Optical Research Facility and the United States Naval Observatory Using 100 Picosecond Laser Pulses," in *Proc. 14th PTTI Meeting*, 243 – 276 (1982).

[5] L.J. Rueger, M.C. Chiu, S.D. Deines, R.A. Nelson, J.T. Broomfield, and C.O. Alley, "Portable Hydrogen Maser Clock Time Transfer at the Subnanosecond Level," in *Proc. 19th PTTI Meeting*, 345 – 365 (1987).

[6] C.O. Alley, R.A. Nelson, Y.H. Shih, B.W. Agnew, R.E. Bartolo, J.T. Broomfield, J.A. Fogelman, J.C. Hunt, M.G. Li, M.A. Perry, J.D. Rayner, C.A. Steggerda, B.C. Wang, M.J. Chandler, L.J. Rueger, and J. Wilcox, "Differential Comparison of the One–Way Speed of Light in the East–West and West–East Directions on the Rotating Earth," in *Proc. 20th PTTI Meeting*, 261 – 285 (1988).

[7] A. Brillet and J. Hall, "Improved Laser Test of the Isotropy of Space," *Phys. Rev. Lett.* **42**, 549 – 552 (1979).

[8] K.C. Turner and H.A. Hill, "New Experimental Limit on Velocity–Dependent Interactions of Clocks and Distant Matter," *Phys. Rev.* **134**, B252 – B256 (1964).

[9] G.R. Isaak, "The Mössbauer Effect: Application to Relativity," *Phys. Bull.* **21**, 255 – 257 (1970).

[10] E. Riis, L.-U. Andersen, N. Bjerre, O. Poulsen, S.A. Lee, and J.L. Hall, "Test of the Isotropy of the Speed of Light Using Fast–Beam Laser Spectroscopy," *Phys. Rev. Lett.* **60**, 81 – 84 (1988).

[11] T.P. Krisher, L. Maleki, L.E. Primas, R.T. Logan, G.F. Lutes, J.D. Anderson, and C.M. Will, "Final Results of a New Test of Relativity," in *Proc. 21st PTTI Meeting*, 171 – 179 (1989).

[12] T.P. Krisher, L. Maleki, G.F. Lutes, L.E. Primas, R.T. Logan, J.D. Anderson, and C.M. Will, "Test of the Isotropy of the One–Way Speed of Light Using Hydrogen Maser Frequency Standards," *Phys. Rev. D* **42**, 731 – 734 (1990).

[13] R.F.C. Vessot and M.W. Levine, "A Test of the Principle of Equivalence Using a Space–Borne Clock," *Gen. Rel. Grav.* **10**, 181 – 204 (1979).

[14] C.O. Alley, "Proper Time Experiments in Gravitational Fields With Atomic Clocks, Aircraft, and Laser Light Pulses," in *Quantum Optics, Experimental Gravitation, and Measurement Theory*, edited by P. Meystre and M.O. Scully (Plenum, New York, 1983), pp. 363 – 427.

[15] H. Peters, B. Owings, T. Oakley, and L. Beno, "Hydrogen Masers for Radio Astronomy," in *Proc. 41st Symp. Frequency Control*, 75 – 81 (1987).

[16] S. Stein, D. Glaze, J. Levine, J. Gray, D. Hillard, D. Howe, and L. Erb, "Performance of an Automated High Accuracy Phase Measurement System," in *Proc. 36th Symp. Frequency Control*, 314 – 320 (1982).

APPENDIX

Plots of Measurement Residuals

Maser 6 (Truck) - Maser 5 (GORF); t2 - (t1 + t3)/2
Trip of March 10, 1989

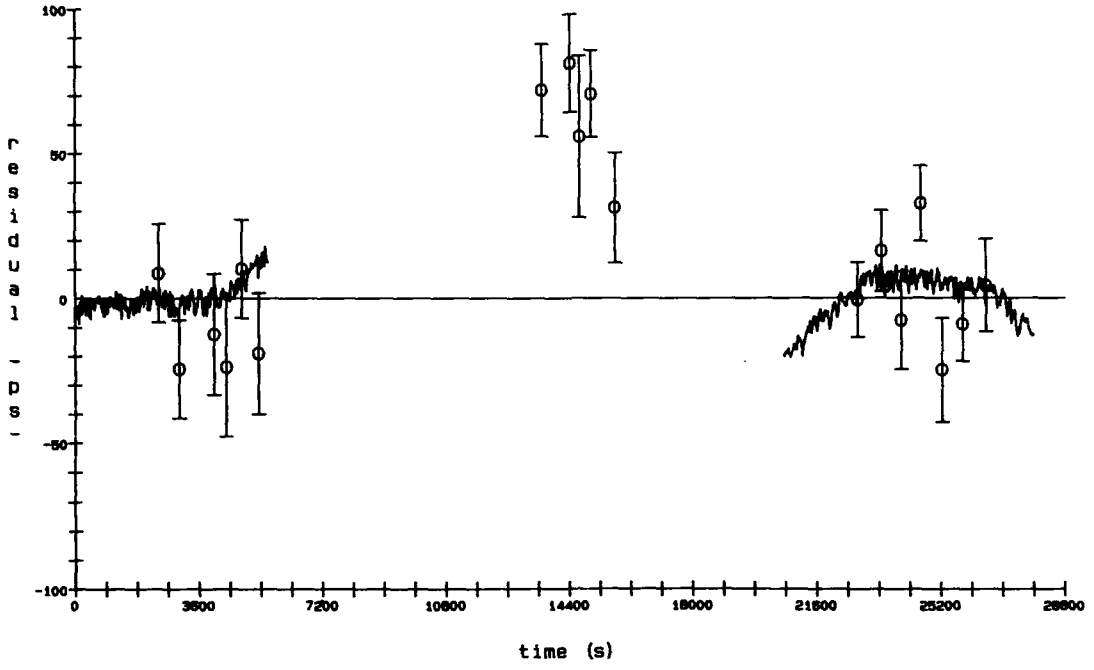

Maser 6 (Truck) - Maser 5 (GORF); t2 - (t1 + t3)/2
Trip of March 16, 1989

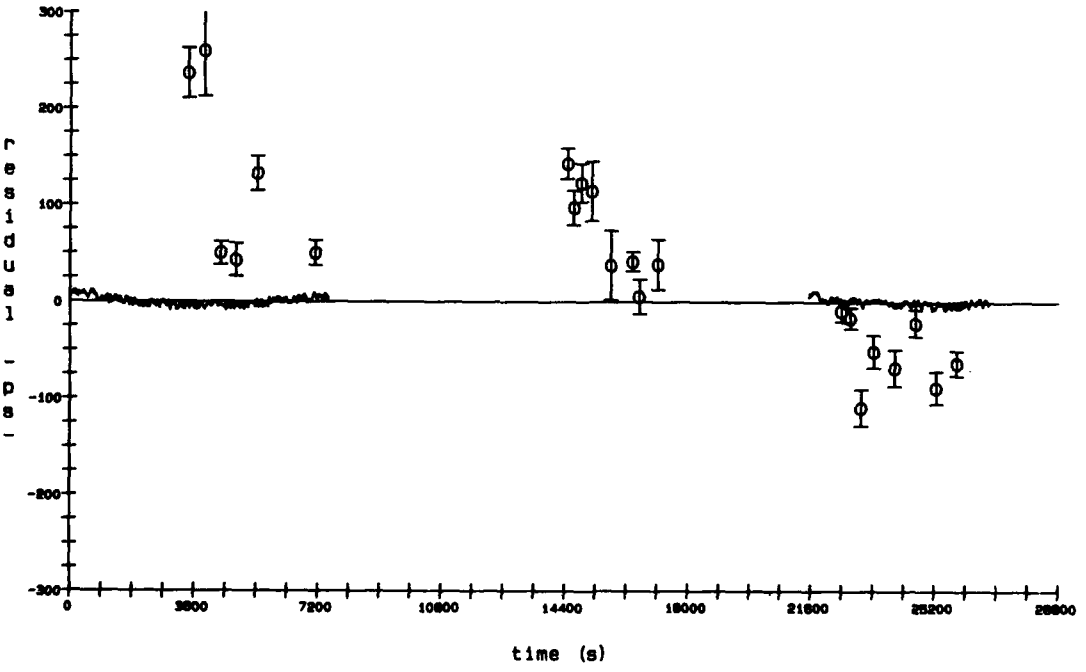

Maser 6 (Truck) - Maser 5 (GORF); t2 - (t1 + t3)/2
Trip of March 21, 1989

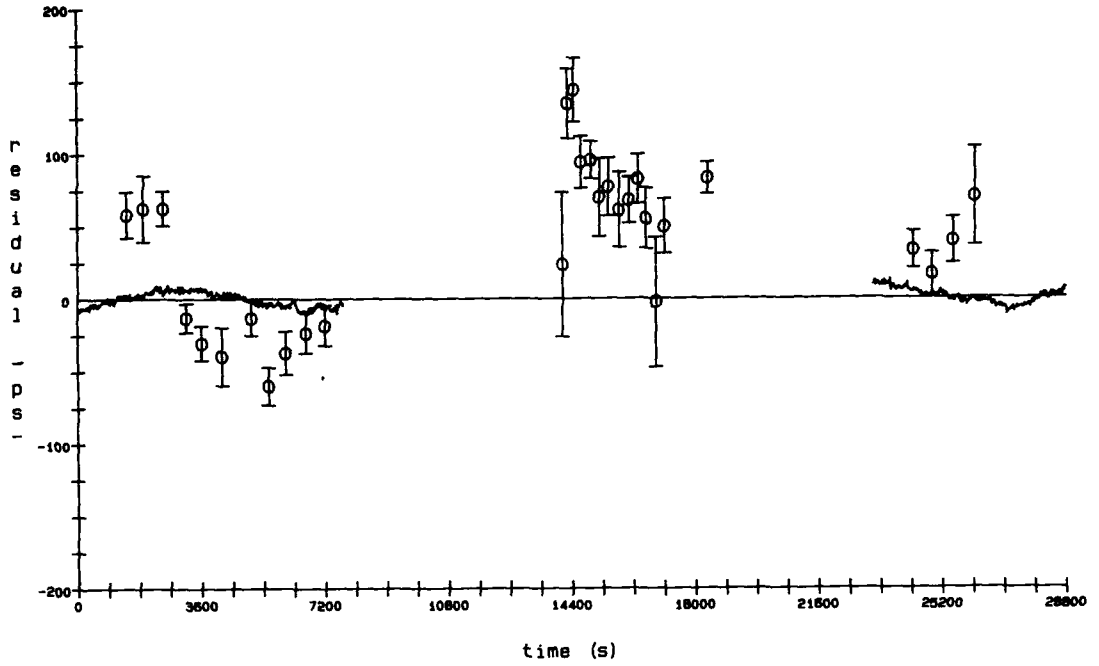

Maser 6 (Truck) - Maser 5 (GORF); t2 - (t1 + t3)/2
Trip of March 22, 1989

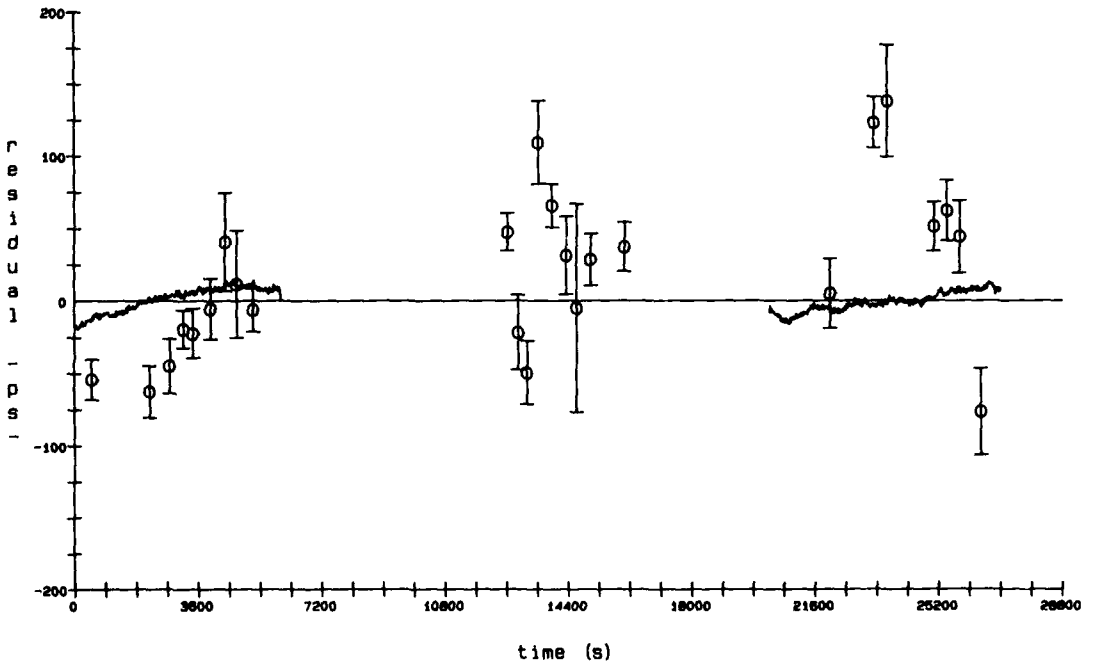

Maser 6 (Truck) - Maser 5 (GORF); t2 - (t1 + t3)/2
Trip of March 25, 1989

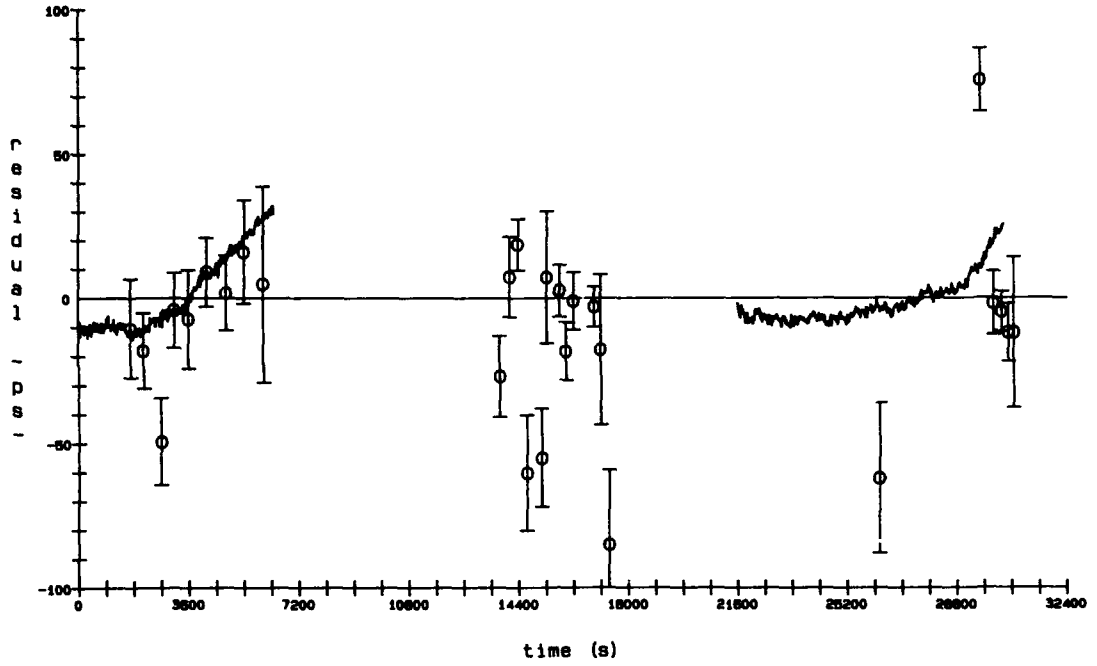

Maser 6 (Truck) - Maser 5 (GORF); t2 - (t1 + t3)/2
Trip of March 28, 1989

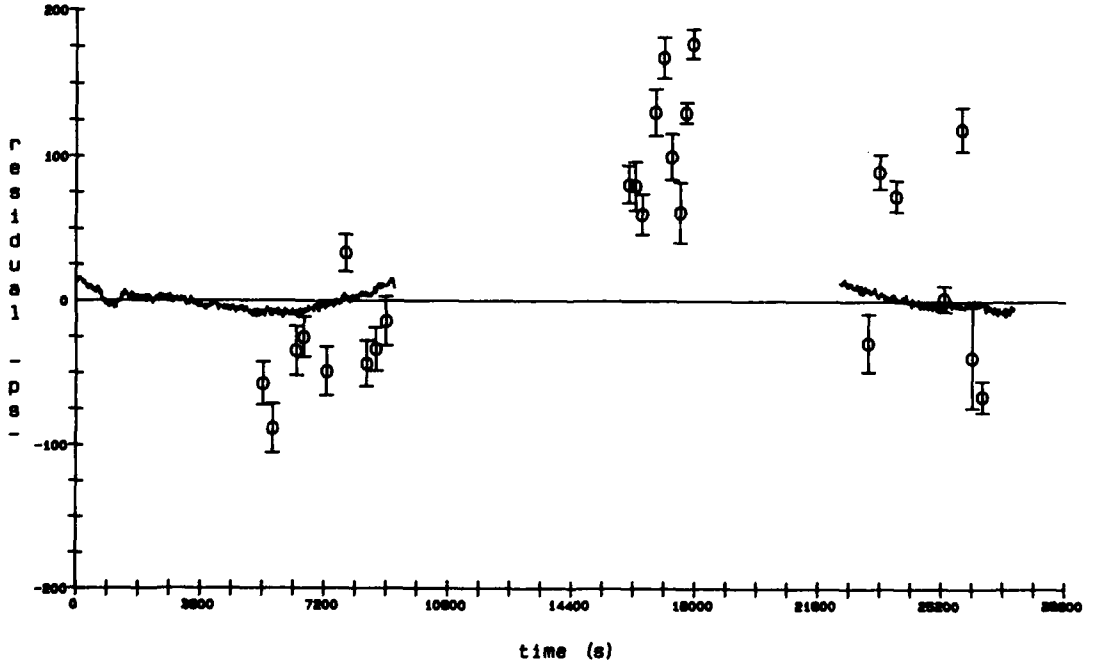

Maser 6 (Truck) - Maser 5 (GORF); t2 - (t1 + t3)/2
Trip of April 9, 1989

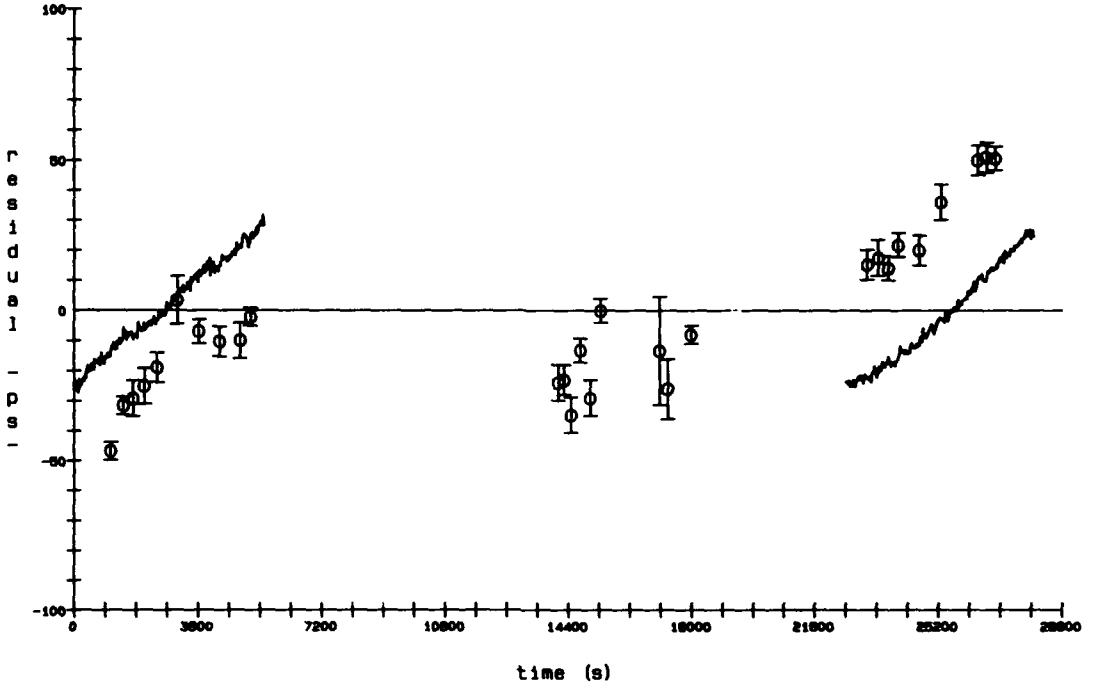

Maser 6 (Truck) - Maser 5 (GORF); t2 - (t1 + t3)/2
Trip of April 11, 1989

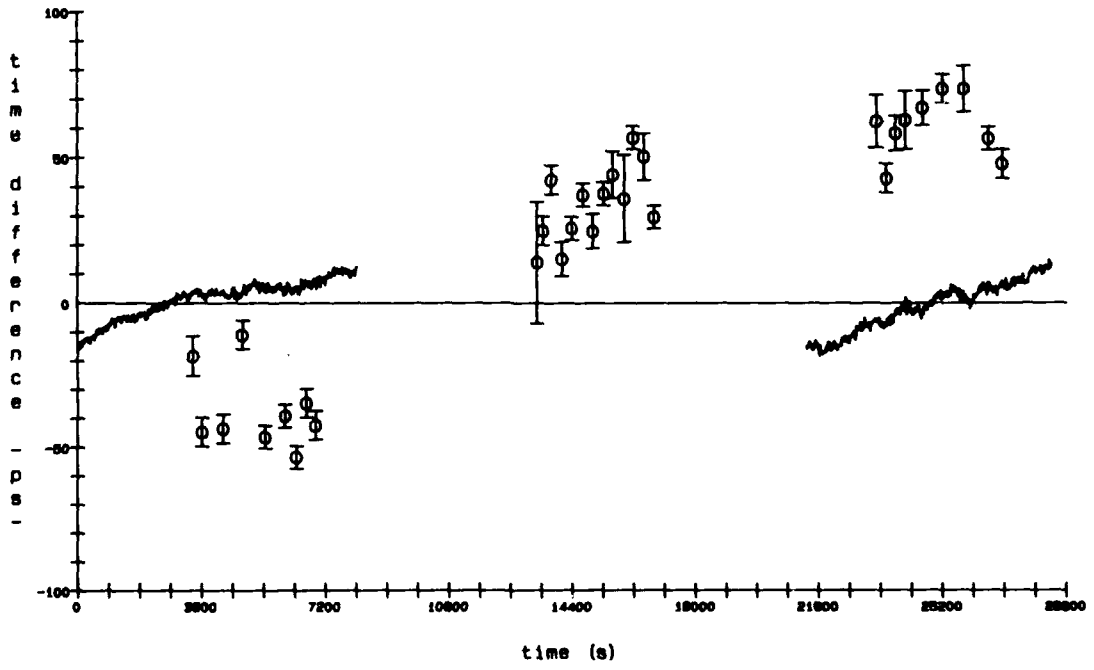

Maser 6 (Truck) - Maser 5 (GORF); t2 - (t1 + t3)/2
Trip of April 13, 1989

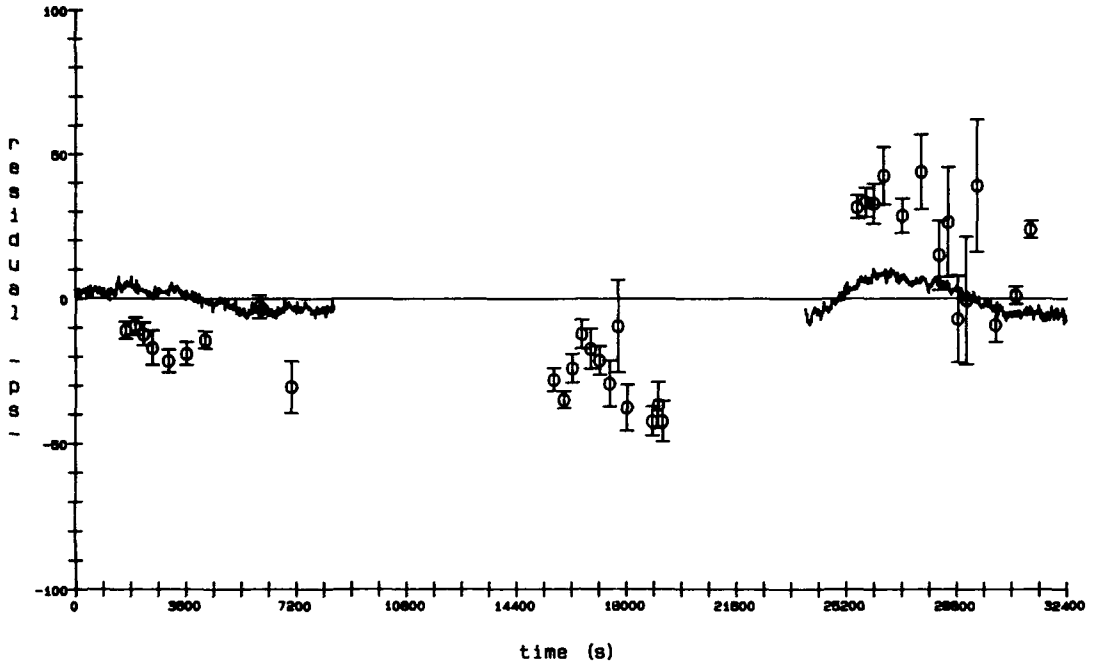

Maser 6 (Truck) - Maser 5 (GORF); t2 - (t1 + t3)/2
All Trips

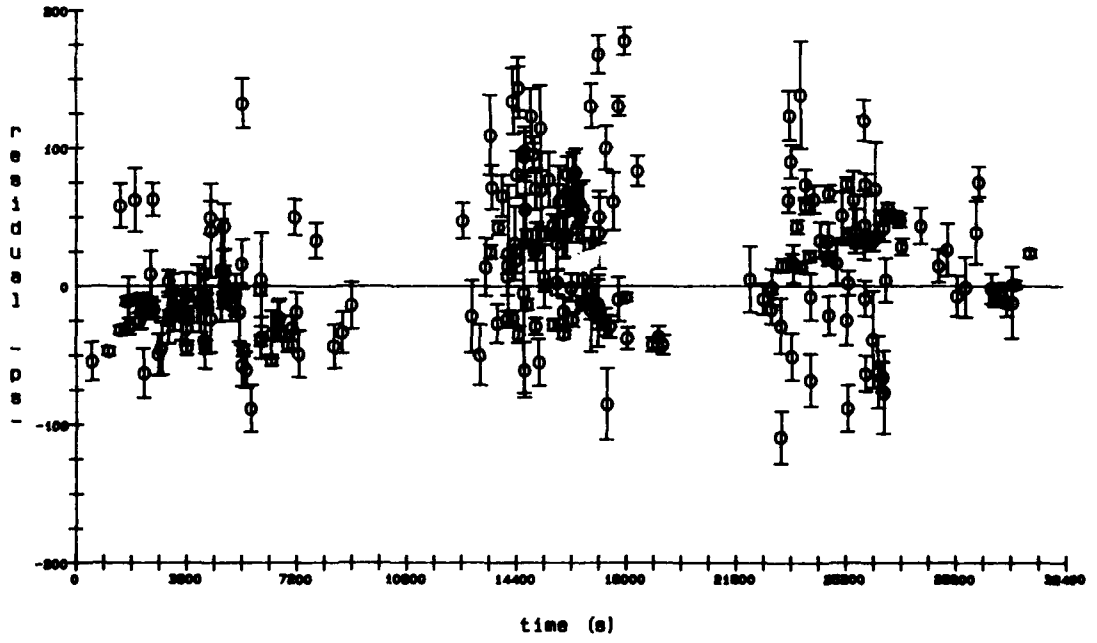

QUESTIONS AND ANSWERS

E. Mattison, SAO: To what do you ascribe the scatter in the measurements by light beams? What is the major contributor to the noise there? Also it seems as if the post trip calibration data had more scatter than the pretrip calibration. Was that always the case and to what to you ascribe that?

R. Nelson, University of Maryland: I am glad you asked the question because I wanted to point out what we consider to be our major source of error. Our major source of error, in our judgment, was the response of the T2 detector. Time jitter was approximately 150 picoseconds and it was primarily due to the sensitivity of the detector to the fluctuations in light intensity. It was energy sensitive. I do not think it is fair to say that the post trip calibration were anymore scattered that the pretrip. I chose one particular example but it was only considered to be representative and not definitive.

Plans to Improve The Experimental Limit in The Comparison of the East–West and West–East One–Way Light Propagation Times on The Rotating Earth

C.O. Alley, T.E. Kiess, R.A. Nelson,[1] A.V. Sergienko,[2] Y.H. Shih,[2]
B.C. Wang, and F.M. Yang[3]
Department of Physics, University of Maryland
College Park, Maryland 20742 (USA)

Abstract

The preceding paper describes the results so far (interrupted in the Spring of 1989 because of lack of funds) of an experiment comparing the one-way light propagation times on the surface of the rotating Earth. For the 20 Km path length component in the East-West direction the predicted difference between the opposite sense propagation times would be 160 ps, if the $\approx$ 360 Km/s surface speed of the Earth gives effective light speeds of $3x10^8$ m/s $\pm$ 360 m/s. This could lead to a prediction of the difference between the clock transport and the light pulse synchronization methods described in the preceding paper: ΔT = 0.5 (160) = 80 ps. The current upper bound of $\approx$100 ps for Δ T is limited by poorly understood systematic errors. The most important seems to be intensity–dependent time delays in the remote light pulse avalanche photo-diode detector. This will be replaced by a continuously operating circular scan streak camera having single photon sensitivity and a time resolution of $\approx$ 5 ps. (This camera has recently been developed by the Xian Institute of Optics and Precision Mechanics in the P.R.C.). Better isolation from shocks and vibration for the Sigma–Tau hydrogen maser during transport will be provided. It is hoped that ΔT < 20 ps can be achieved.

Introduction

The experimental results reported in the preceding paper[1] and in greater detail in the Maryland Ph.D. dissertation of R.A. Nelson[2] are, we believe, the most precise comparisons of remote clocks ever achieved, both for the clock transport method and for the laser light pulse method. The experiments are also the first ever to measure directly the difference in the one–way propagation times of light pulses for the East-West and West–East directions between two fixed points on the rotating Earth. Several experimental difficulties have limited the comparison to an uncertainty of $\approx$100 ps. These will be discussed briefly. Improved techniques which may overcome them and allow an uncertainty of only 10-20 ps will be described.

[1]Present address: W.L. Pritchard & Co., Inc. 7315 Wisconsin Ave., Suite 520E, Bethesda, MD 20814
[2]Also at Department of Physics, University of Maryland, Baltimore County Campus, Baltimore, MD 21228.
[3]Visiting from the Shanghai Astronomical Observatory, People's Republic of China.

Why the Measurements Need To Be Improved

It is important to achieve an uncertainty substantially less than 80ps in the quantity ΔT defined below. This is the predicted value *if* the local group velocity of the short light pulse is not isotropic but exhibits a vector composition with the local surface velocity of 360 m/s. Let t_1 be the epoch of the transmission of the light pulse, t_2 be the epoch of reflection and detection at the remote site, and t_3 be the epoch of reception back at the initial site. We analyze the measurements in terms of the difference ΔT between the direct reading on the transported clock t_2 and the Einstein special relativistic prediction for the reading of the remote clock in terms of the times t_2 and t_3

$$\Delta T = t_2 - \left[\frac{t_1 + t_3}{2}\right] = \frac{1}{2}[(t_2 - t_1) - (t_3 - t_2)]$$

This can also be expressed in terms of the local speeds of light *if* these are different, having the value $c \pm r\omega$, where r is the distance to the spin axis of the Earth and ω is the angular velocity of the rotation. Let L be the projected path in the East–West direction. Then

$$\Delta T = \frac{1}{2}\left[\frac{L}{c - r\omega} - \frac{L}{c + r\omega}\right] \simeq \frac{Lr\omega}{c^2}$$

[In the preceding paper[1], the product Lr is written as 2A where A is the area of the isosceles triangle with side lengths L, r and r.]

Some of the scientific reasons for performing these one-way light propagation experiment from the standpoint of fundamental physics were given in the PTTI report in 1988 [3]. Let us here *note only* that actual experiments with atomic clocks and laser light pulses can, and must, play a crucial role in securing our knowledge for the formation of appropriate concepts in a complete and correct field theory of space, time and gravitation. This could be analogous to the role played by experiments on electric and magnetic phenomena in the 19th century (e.g. Faraday's iron filings, induction, etc) which led to Maxwell's theory of the electromagnetic field.

On the practical side, the Global Positioning System will not perform at its full accuracy unless the correct relativistic physics is used in the interpretation of the measurements. Let it be noted that in 1976 a mistake in the planned implementations in the GPS of the effect of the gravitational potential difference between the clocks in the space vehicles and those on the Earth was identified by Leonard Cutler, Gernot Winkler and the first author of this paper. This mistake was revealed during discussion after the presentation of the results of our proper time experiments with atomic clocks in aircraft [4,5,6]. It was planned to correct twice for the effect: first, by reducing the rate of the orbiting clocks by a physical offset, and, second, by wrongly allowing for a violet shift even after the physical offset. It took several years for the mistake to be corrected. (Some details are given in references [5] and [6]).

The method of interpreting monitor station measurements currently used by the control-segment of the Global Positioning System may be assuming an anisotropy of the speed of electromagnetic wave for the local observers. If this is not the correct physics, it may be one of the sources of systematic error in the GPS/Navstar performance.

The concern about this matter is caused in part by paragraph 20.3.3.4.3.5 in the Interface Control Document 200:

Geometric Range: The user shall account for the effects due to Earth rotation rate (reference Table 20-IV) during the time of signal propagation so as to evaluate the path delay in an inertially stable coordinate system.

The actual measurements by monitor station or users are, of course, made on the surface of the rotating Earth, a non-inertial system. The quoted paragraph is not very clear. One interpretation could be that for such observers the effective speed of signal propagation is $c \pm r\omega$. The interpretation of the measurements by the GPS control segment and the transformation to the Earth Centered Inertial Frame where calculations are done, are being actively investigated.

Effects of the Atmosphere

The total horizontal one-way path is about 27 km which amounts to some 4 vertical scale heights of the atmosphere. The additional contribution of the index of refraction, n (n-1 $\approx 3\times10^4$), to the 87 μs one-way time is 26 ns. However for the difference in one-way times which we are measuring, this contribution cancels if there is no change in the optical path in the atmosphere during the 174 μs round-trip time. It is generally accepted from studies of atmospheric fluctuations related to astronomical "seeing" that vertical paths require more than 2 ms to change appreciably. The scatter in our optical time comparison is about the same for the calibration measurements, with a path length of only a few hundred meters as for the remote measurement (see plots in the Appendix to [1]). This gives some confidence that the outgoing and incoming atmospheric delays are the same. The optical path over the city of Washington is far from the ideal location for this experiment. A path over land not occupied by people, or, of course, in an evacuated pipe, would be much better.

Brief Discussion of Sources of Error

Examination of the plots of measurement residuals for the nine trials given in the Appendix to the preceding paper [1] shows that the scatter in the optical comparisons is much larger than the hydrogen maser phase comparison during the calibrations. The traveling maser was compared with other masers at the USNO during the dwell time there and always exhibited good phase stability, but there was no way of determine whether a rate change had occurred during the transport of sufficient size to produce a significant offset. The good parabolic fits suggest that clock performance during transport was not a major source of error.

We suspect that the large fluctuations in intensity of the detected laser pulses, produced by the different optical paths from pulse to pulse (10 Hz laser repetition rate), each with a different spatial mottling pattern, are the major source of error. The cooled avalanche photodiode used as the t_2 detector exhibited sufficiently large intensity dependent time delay for this explanation to be plausible. However these delays have not been adequately understood or characterized.

Attempts were made during the optical measurements to keep the average intensity on the detector constant by visually monitoring the pulse heights on an oscilloscope and adjusting an aperture before the focusing lens of the detector. Inspection of the plots in the Appendix to the previous paper [1] shows that this technique still allowed substantial variation in timing from one 1,000 transmission shot average to the next. The points are the average values and the error bars

represent the standard deviation of the mean for the completed triplets t_1 , t_2 , t_3 . Due to the fluctuations many t_2 and t_3 events were not recorded.

One can ask whether the two event timers were performing correctly, the epochs t_1 and t_3 being recorded by the stationary event timer, and the epoch t_2 by the traveling duplicate event timer. There is a known temperature dependence on delays in these instruments but each was kept in a temperature controlled enclosure whose temperature was continuously monitored and kept within sufficient limits [2].

Planned Improvements

The major change will be the replacement of the t_2 and t_3 detectors by circular scan streak tubes containing tandem microchannel plate amplifier structures giving them sensitivity to single photoelectrons and a large dynamic range. The circular scan driven from a hydrogen maser avoids the start jitter in linear scan streak tubes and will serve as a vernier with ≈5ps resolution for the associated event timer. The readout will be by a CCD camera. All photoelectrons produced by the detected pulse (subject of course to the quantum efficiency of the S20 cathode) will be recorded. The centroid can be measured and the problems associated with triggering on the leading edge of pulses undergoing large intensity fluctuation largely avoided. These tubes are made by the Xian Institute of Optics and Fine Mechanics in the People's Republic of China. The Director of this Institute is Professor Hou Xun and the principle streak tube scientists are Drs. Niu Hanben and Zhao Jilai. No other streak tube manufactures can match the combination of circular scan and single photoelectron sensitivity. A schematic diagram of the instrument and its specifications are given at the end of this paper. It is hoped that this technique will solve the problem of intensity dependent time delays. It will also improve the event timing resolution from the current value of 20 ps to 5 ps. A prototype tube is being tested now in our laboratory.

We are also pursuing an interim approach to this optical timing problem. This is to experiment with superior performance avalanche photodiodes and active quenching circuits [7]. The diodes have been kindly lent to us by Professor Sergio Cova of the Polytechnical University in Milan and the experimental studies are just beginning in our laboratory.

The laser pulse duration used in the experiments so far has been on the order of 75 ps when it was will adjusted. We plan to use known techniques to reduce this to 35 ps. It is possible to reduce it further to 10 ps but this may not be effective because of the dispersion of the atmosphere which will increase the pulse duration.

During the nearly four years since the experiments were interrupted, the performance of Sigma-Tau hydrogen masers has improved and we hope that one of the latest models for use as the traveling clock can be kindly lent to us again by the Time Services Department of the U.S. Naval Observatory. We also plan to add an air suspension to the van which transports the clock and to provide better temperature control and mechanical isolation for the clock box. These measurements may allow the relativistic effects on clock transport which we know to exist from our early aircraft flights [4, 5, 6].

$$\Delta t_{rel} = \int \left(\frac{\Delta \Phi}{c^2} - \frac{1}{2} \frac{v^2}{c^2} \right) dt \cong 50 \text{ ps}$$

to be definitely observed in the ground transport. To this end we shall consider adding a GLONASS or GPS receiver to the van to aid in performing this integral.

Acknowledgments

We thank again the many members and institutions within the PTTI community who have supported our investigations. These are detailed in the preceding companion paper [1]. Here we wish to acknowledge with gratitude the new support of the Federal Aviation Administration Satellite Program Office and the AirForce Space Command whose joint Grant (FAA 92-G-0025) is allowing renewal of these experiments.

References

1. R.A. Nelson, C.O.Alley, J.D. Rayner, Y.H. Shih, C.A. Steggerda, B.C. Wang, and B.W. Agnew, *"Experimental Comparison of Time Synchronization Techniques by Means of Light Signals and Clock Transport on the Rotating Earth,"* Preceding paper in this volume: Proceedings of the 24th PTTI Meeting, (1992).
2. R.A. Nelson, *"Experimental Comparison Between Two Methods for Synchronization of Remote Clocks on the Rotating Earth: The Propagation of an Electromagnetic Signal Using Laser Light Pulses and The Transport of a Hydrogen Maser Atomic Clock"*, Ph.D. dissertation, University of Maryland, 1990.
3. C.O. Alley, R.A. Nelson, Y.H. Shih, B.W. Agnew, R.E. Bartolo, J.T. Broomfield, J.A. Fogelman, J.C. Hunt, M.G. Li, M.A. Perry, J.D. Rayner, C.A. Steggerda, B.C. Wang, M.J. Chandler, L.J. Rueger, and J. Wilcox, *"Differential Comparison of the One-Way Speed of Light in the East-West and West-East Directions on the Rotation Earth"*, in Proc. 20th PTTI Meeting, 261-285, (1988).
4. C.O.Alley, *"Relativity and Clocks"*, in Proceedings of the 33rd Annual Symposium on Frequency Control, U.S. Army Electronics Research and Development Command, Fort Monmouth, N.J., 4-39A (1979).
5. C.O.Alley, *"Proper Time Experiments in Gravitational Fields with Atomic Clocks, Aircraft, and Laser Light Pulses"*, in Quantum Optics, Experimental Gravitation, and Measurement Theory, edited by P. Meystie and M.O. Scolly (Plenum, New York, 1983), 363-427.
6. C.O. Alley, *"Introduction to Some Fundamental Concepts of General Relativity and to Their Required Use in Some Modern Timekeeping Systems"*, Pro. 13th PTTI Meeting, 687-724 (1981).
7. S.Cova, A.Lacita, M.Ghioni, G.Ripamonti, and T.A. Louis, *"20 ps Timing Resolution with Single Photon Avalanche Diodes"*, Rev. Sci. Instrum., 60, 1104-1110 (1989).

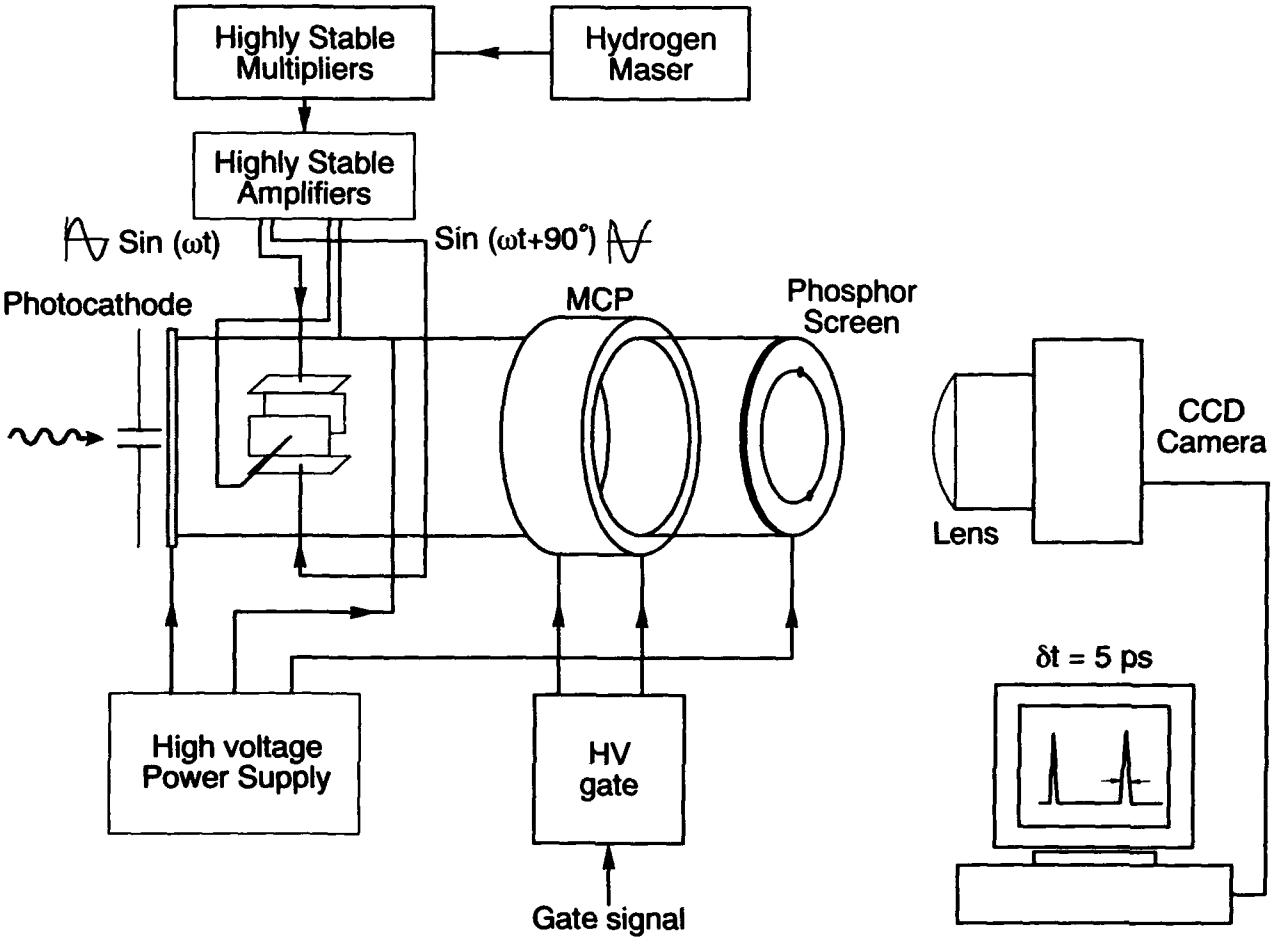

Schematic Diagram of Circular Scan Streak Camera

Specifications

24 mm diameter circular scan

2 watts rf at 300 MHz

2 MCP's in series: gain ≅ 10^6

Photocathode: S20

Photocathode sensitivity: 67 μA/lumen

Wavelength Range: 200-850 nm

Photocathode active area: 12 mm diameter

Phosphor: P20

Phosphor active area: 24 mm diameter

Deflection sensitivity: D_1 9.4 cm/kv, D_2 11.2 cm/kv

Space resolution: 24 line pairs/mm

Dynamic range: >390:1

Time resolution: 4.8 ps (test result)

Working frequency: 300 MHz

QUESTIONS AND ANSWERS

J. Levine, NIST: We have been in the Laser distance measurement business for a number of years. One of the problems that you may be facing is the anistropy in the index of a fraction in the two directions. It is an equivalent of multipath, and it does not quite cancel forward–backward because the air near the transmitter counts more than the end near the receiver. The problems are a lot worse on horizontal path than on a vertical path. Lunar ranging is not really subjected to the same kind of problems so that problem is a lot easier. My guess is at the end of the day it is going to cook you, because it varies quickly and it's not the same in both directions.

C. Alley: Yes, I appreciate your comments. I am well aware of the extra work you have done over the years and with welcome some further discussion. Do you find a change faster than 200 microseconds at the telescope? You find it does change appreciably in that time?

J. Levine: That is the order of the speed.

C. Alley: Our fundamental cycle time is 250 microseconds and that is just about fast enough. There were times when our data was changing faster than that and we have to drop the data out.

J. Levine: I think you are going across the city and that is much worse.

C. Alley: That is right; it makes it worse. We would be much better out west where you are, but we are trying to do something with what we have available.

J. Levine: I understand that, but at the end of the day, I think you are doing remarkably well but guess is you will not get a factor of five or ten times better.

C. Alley: I would hope you are wrong. We will find out, but you make a very relevant observation. Obviously, there is more that needs to be discussed.

H. Freer, Falcon AFB: Did you control your atmospheric temperature & humidity or try to control it and what kind of limits did you address in your varying measurements?

C. Alley: Controlling the atmospheric temperature where?

H. Freer: In other words did you take one reading at 6 AM when it was 50 degrees in Washington, another at 2 PM when it was 80 degrees, one when it was humid, and one when it was not humid?

C. Alley: There were very stringent conditions on when we could actually do these measurements. We had to have visibility of about 10 miles before we could even get enough signal coming back. We did record some of these meteorological variables. Unfortunately we can not control the weather, we have to wait until we get reasonably good conditions and these nine or so reasonably successful trips were out of maybe 15 actual all night sessions and out of many more of attempted and aborted measurements. So we probably should wait until the conditions are comparable and good and so on but we have not had that complete luxury. When we borrowed the clocks from the National Radio Astronomy Group we had them for a very limited period. They kindly extended that period twice but we had to make the measurements as we could and get them back. I hope in this next round we might have a somewhat more leisurely opportunity and can make some of the control that you have sensibly suggested.

LASSO observations at McDonald (Texas, USA) and OCA/CERGA (Grasse, France)

A preliminary analysis

Ch. Veillet, P. Fridelan..., D. Feraudy, Y. Boudon
OCA/CERGA Copernic F-06130 GRASSE

P.J. Shelus, R.L. Ricklefs, J.R. Wiant
McDonald Observatory/MLRS P.O. Box 1337 Fort Davis, Texas 79734

Abstract

The LASSO observations between USA and Europe have been made possible with the move of Meteosat 3/P2 toward 50°W. Two Lunar Laser Ranging stations participated into the observations : the MLRS at McDonald Observatory (Texas, USA) and OCA/CERGA (Grasse, France). Common sessions were performed since April 30, 1992, and will be continued up to the next Meteosat 3/P2 move further West (planed for January 1993). The preliminary analysis made with the data already collected by the end of November 1992 shows that the precision which can be obtained from LASSO is better than 100 ps, the accuracy depending on how well the stations maintain their time metrology, as well as on the quality of the calibration (still to be made.) For extracting such a precision from the data, the processing has been drastically changed compared to the initial LASSO data analysis. It takes into account all the measurements made, timings on board and echoes at each station. This complete use of the data increased dramatically the confidence into the synchronization results.

1. INTRODUCTION

The LASSO experiment has been described in a previous paper (Veillet et al, 1990) together with its first phase realized thanks to TUG satellite laser station (Graz, Austria), and OCA/CERGA lunar laser ranging facility (Grasse, France). Since that time, Meteosat 3/P2 (MP2), the satellite carrying LASSO on the geosynchronous belt, has been moved toward West, and is finally located at 50°W since December 1991.

In Europe, only the OCA/CERGA LLR station was able to range successfully to MP2 at such a low elevation (13°... from Grasse).

In the USA, two sites were suitable for LASSO observations :

- The 48" telescope at Goddard SFC (Greenbelt, Maryland), with a large aperture and a good longitude, is

unfortunately in a poor area for observing faint objects in the sky. It has been very busy with other important experiments, and, when available, had to face difficulties for acquiring visually the satellite.
- MLRS (McDonald Laser Ranging Station) has two important advantages. It is located at an good astronomical site, and it ranges successfully to the Moon. MP2 is then an easy target ...

A transatlantic phase of LASSO started at the beginning of 1992 with the following structure :
- MLRS and OCA/CERGA are the basic stations.
- GSFC 48" is willing to participate, but depending on the other programs to be pursued, and on the capabilty of seeing the satellite.
- OCA/CERGA prepares the schedule for the common observations.
- ESA/ESOC maintains the LASSO operations, providing on a weekly basis the raw data received from the satellite.
- OCA/CERGA receives the data from ESOC, the ranging measurements from the participating stations, and analyses them.

This organization worked all along 1992, and the observations together with their first (and preliminary) results will be presented below after a short description of the technical components of the experiment, i.e. LASSO and the two participating stations.

2. LASSO

The experiment has been described in various papers (i.e. Veillet et al, 1990). It is flying on board Meteosat 3/P2 and is made of two components :
- A laser pulse detector is linked to an event timer monitored by an oscillator. The arrival time of a pulse sent from a ground station is then recorded and the measurement sent back to the Earth together with the meteorological data.
- A retroreflector array sends back to the transmitting station part of the incoming light.

LASSO data are made of epochs recorded on different time scales :
- start time of a laser pulse from a participating station on its own time scale
- arrival time of a laser pulse at MP2 on the LASSO time scale
- return time of the reflected light on the same time scale as the start time

Every transmitted laser pulse gives a start time. If detected by LASSO, it gives an arrival time, and if echoes are received, a return time. A set of these three epochs for a same laser pulse is called **a triplet**. But a laser pulse can give only a start and arrival time, or a start and return time. At the beginning of LASSO, it was planned to make use of the triplets only. We will see later that, in the two other cases (two epochs only), there is still a valuable information.

3. The network

3.1 MLRS

The McDonald Laser Ranging Station (MLRS) is located at the McDonald Observatory (Ft Davis, Texas), an

excellent astronomical site. A 2.7-m telescope has been used for Lunar Laser Ranging (LLR) for two decades, and replaced by a smaller station devoted to LLR as well as Satellite Laser Ranging. MLRS entered the LASSO network because MP2 is quite far from the Earth (geosynchronous, at 36000 km ...) and its reflector array small. Compared to the current satellites used in SLR (Lageos, Ajisai, Starlette, Etalon, ...), it is a target which is not easy ! Attempts made from other SLR sites have shown this fact very clearly. But compared to the Moon, it is an easy target, in spite of a high magnitude which makes its visual acquisition difficult.

For the transatlantic phase of LASSO described here, MLRS has been the only site used within the USA. When organizing this phase, it was anticipated to work also with the 48" telescope at the NASA Goddard Space Flight Center (GSFC). Unfortunately, due to other experiments to be performed at the same time, and to the difficulty in acquiring MP2 visually, GSFC did not join the network.

3.2 OCA/CERGA LLR

The OCA/CERGA LLR station started observing LASSO soon after the launch of MP2 in 1988. Originally, the SLR station located nearby was supposed to be the LASSO site at the observatory. But MP2 had become a difficult target for the new generation SLR stations equipped with lasers delivering shorter pulses for a better range measurement, but then less powerful.

The previous phase of LASSO permitted to work with Graz (Austria) SLR station (Veillet et al, 1990). But with MP2 at its new 50° W location, only CERGA and San Fernando (Spain) were practical sites in Europe. San Fernando station, currently under refurbishment, was unable to join the network. Its location is more favourable than CERGA where MP2 is seen at only 14° elevation.

	Mc Donald	OCA/CERGA
Telescope diameter	75 cm	150 cm
Laser pulse length	200 ps	350 ps
Laser pulse energy	140 mJ	350 mJ
Laser repetition rate	10 Hz	10 Hz
MP2 elevation	26 °	14 °

The opposite table gives the main characteristics of the laser stations. The accuracy of the range measurement is directly related to the laser pulse length, as it is impossible to know if the detected photon comes from the beginning or the end of the laser pulse. The ability of the station to get echoes depends on the energy of the laser and the diameter of the telescope receiving the returning light.

4. The observations

At OCA, MP2 was continuously observed after its move (Oct 91), as it was before. The main difficulty is the clear weather needed in order to see the satellite at such a low elevation. At MLRS, the first echoes were obtained in April 92, and since then MLRS has been observing MP2 on a regular basis.

The scheduling was made from OCA, in accordance with both ESOC (where the payload is activated) and MLRS. The night at both sites was imperative, as it is impossible to range MP2 without seeing it. With the

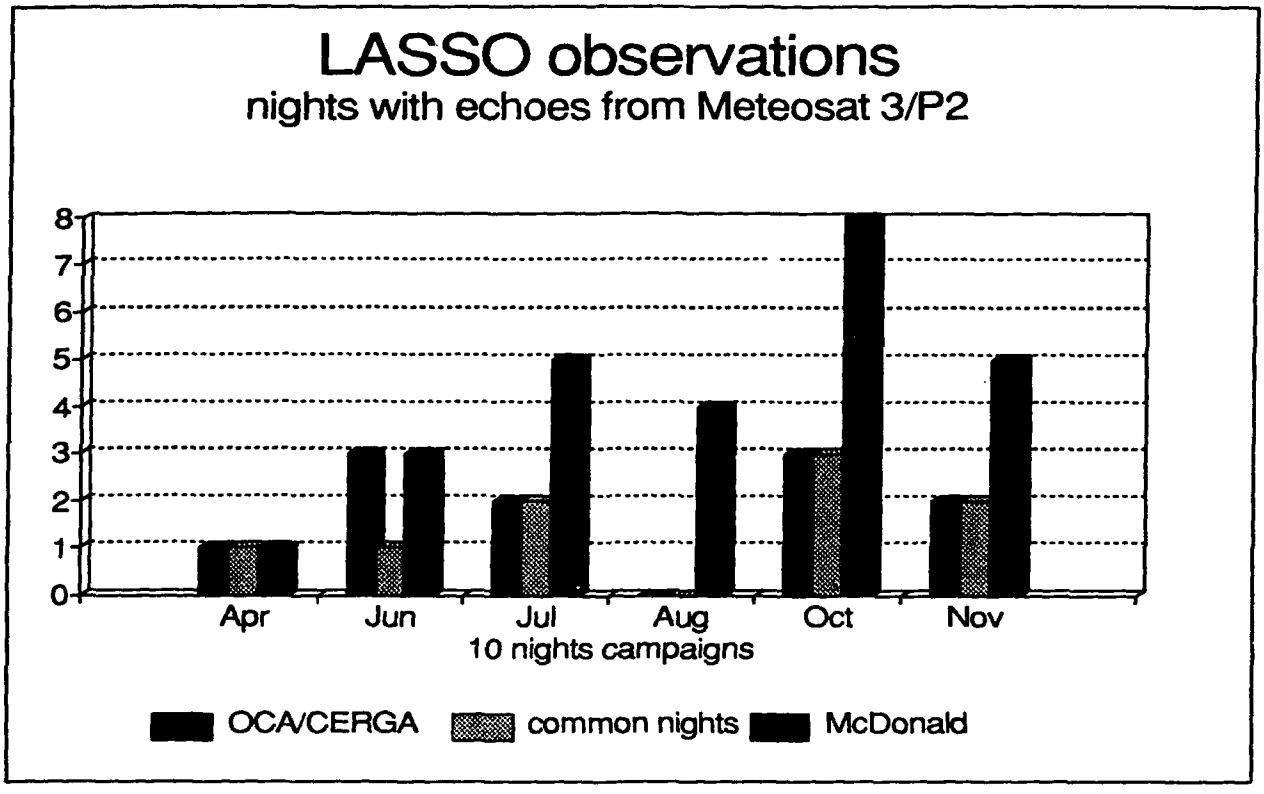

Moon too close to MP2 in the sky, it is impossible to distinguish MP2 against the illumated sky background. The period around new Moon was then chosen, and campaigns covering 10 nights every lunar month were organized. The figure above shows the amount of night where echoes were recorded at MLRS and OCA, together with the common nights, i.e. nights where LASSO data were acquired at both sites for a same LASSO session (1 hour duration).The data obtained in October are useless as MP2 was off during the sessions (Sun eclipses onboard).
A total of 7 nights over 9 months are up to now (end of November 1992) available for data processing.

Looking to the first echoes obtained at MLRS, it appeared that :
- the number of echoes from MLRS is generally small, yielding to few triplets for a session, and
- the sky is rarely clear enough at CERGA to get data from MP2 at 13°.

In order to extract the information with such poor conditions, we had to modify the data processing envisionned initially for LASSO.

5. The analysis

5.1 How to deal with so few data ?

The original data processing was as follows : The firing times of the laser at every participating station, here MLRS and OCA, are scheduled in such a way the pulses arrive on board a few milliseconds apart, for example from MLRS 4 ms before the pulse from OCA. As the onboard oscillator is designed to be stable enough, the direct difference between these arrival times is small enough to be interpreted as the difference on any of the station

time scales.The ground clocks can be linked with only a pair of such triplets, the LASSO oscillator vanishing. As MP2 is spinning at 100 rpm, the scheduling is uneasy as one needs to know the rate and phase of the satellite rotation for determining when the laser pulses should start from the ground to hit the LASSO detector. Rate and phase can be determined at OCA from laser observations prior to a LASSO session, but have to be sent to the other participating stations. The European phase demonstrated how ackward is this process. Even with a correct scheduling, the statistics is very poor, and it is extremely rare to have a pair of pulses providing a triplet. Another data handling has to be used for MLRS-OCA time transfer through LASSO.

For ten minutes, a station ranging at 10Hz (as MLRS and OCA) transmits to MP2 6000 laser pulses. As the satellite is rotating at 100 rpm, and the retroreflector array has an angle of view of 60°, one shot over six can be reflected and sent back to the station. It means that the maximal return rate is one per 600 ms. With a very clear sky, such a rate can be obtained at OCA. As the telescope is smaller and the laser less powerful at MLRS, the rate is lower. The angle of view of the LASSO laser detector is smaller than for the reflectors, and only one laser pulse over ten can be detected on MP2. As its sensitivity is not very large, the statistics is lower. As a result of these considerations, we observe that :

- the number of echoes is generally larger at OCA than at MLRS
- the number of LASSO detections is larger for OCA pulses than for MLRS ones.
- the number of triplets for ten minutes sessions is varying from nothing up to 100, depending on the station involved and on the meteorological conditions.

If we suppose that we have some triplets from a given station over ten minutes, we can assess the behavior of the onboard oscillator against the station clock. From observations made at OCA, the oscillator has been found performing well : the offset and rate of the LASSO clock can be determined accurately. The opposite figure below shows the LASSO clock versus OCA clock, an offset and rate being removed. The formal uncertainty on the offset is around 50 ps, and on the rate below 5.10^{-13}. Comparing the offset and rate versus OCA clock to the same parameters seen from MLRS provides a link between the station clocks. Again, the onboard oscillator vanishes, but now through a determination of its characteristics over a 10 mn time span.

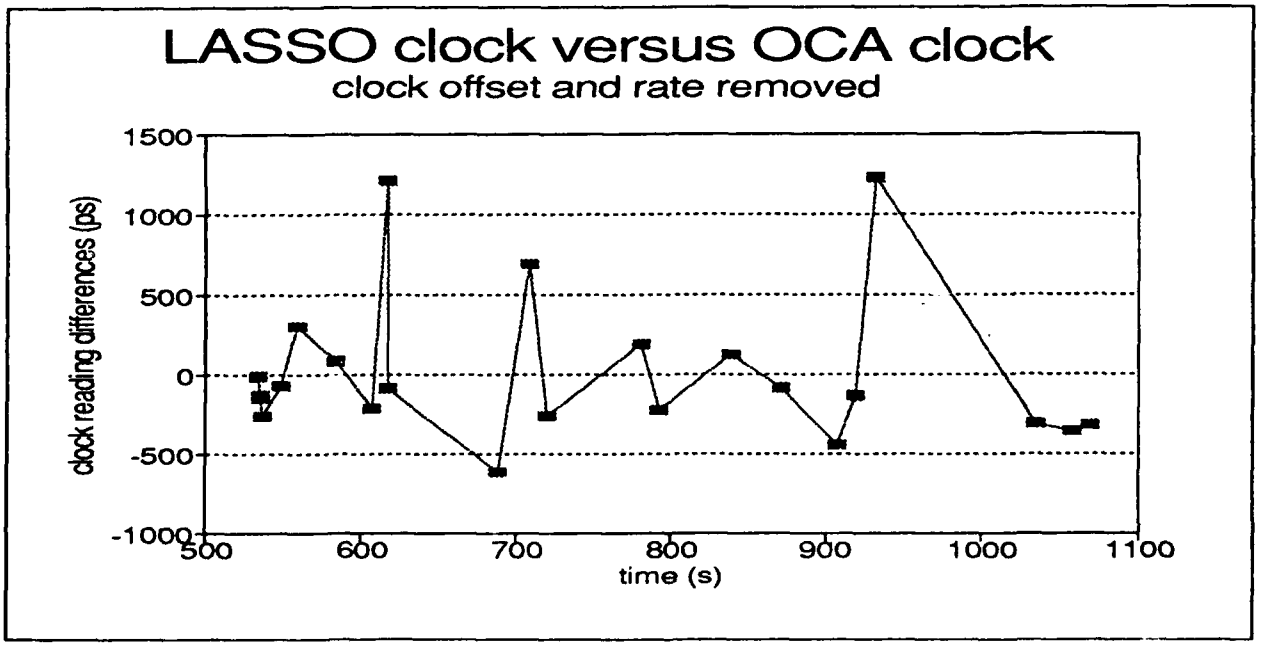

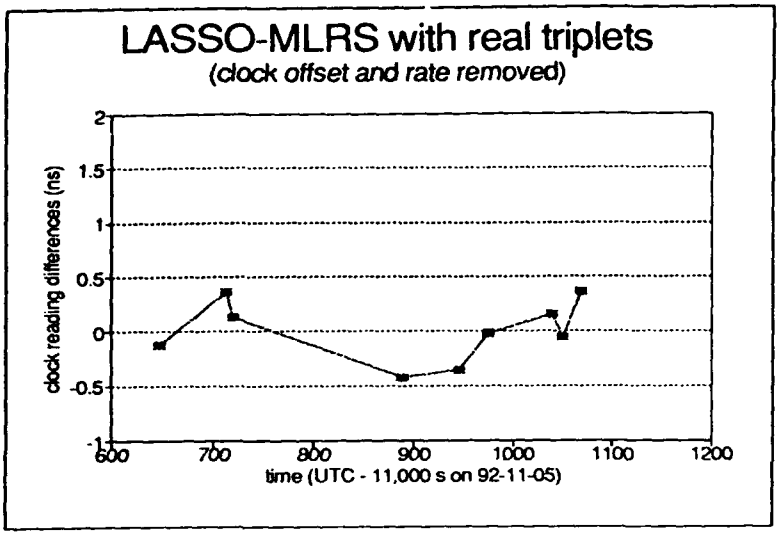

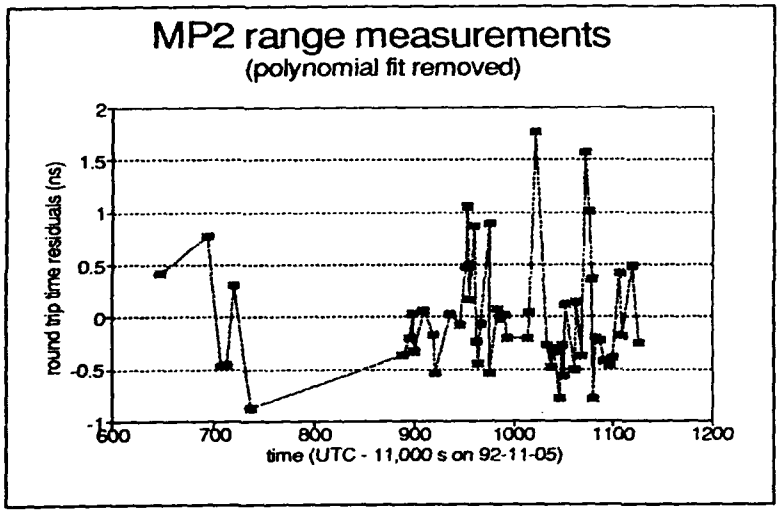

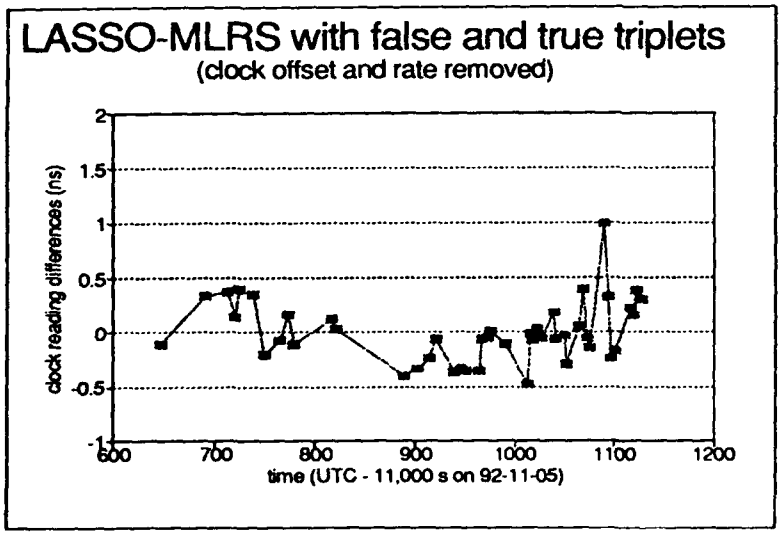

Unfortunately, many sessions give only a short number of triplets for a given station, and the observation of the LASSO clock is very poor. The opposite figure shows an example with 9 triplets determined for 300 seconds. It is sometimes worst, with only two or three triplets identified over the same time span! In such cases, the determination of the LASSO clock offset and rate is not precise enough for a good comparison of the station clocks. However, one can observe for such a session many echoes, and also many LASSO detection times, which can be used for improving the LASSO clock observation.

The opposite figure shows for the same session as before the range measurements. Each point corresponds to an observed return time. Most of the laser pulses did not provide any detection time on LASSO. Only nine of them did, as seen with the previous figure.The LASSO detections not associated to a return time come from a laser pulse for which it is possible to determine a return time by using the echoes obtained around. A polynomial fit is computed from all the returns for the considered session, and used for assessing the return time which could have been obtained for all the pulses without echo. The paires [start time - LASSO detection time] obtained through this process are now "false" triplets, using all the information from the echoes observed, and all the detection times onboard MP2.

The opposite figure shows the result of this process. It is a mixing of true triplets (already seen on the first plot above), and false triplets combining a real LASSO time and a recomputed echo time. All the data for common sessions have been treated using this *true-false* combination.

5.2 The results...

All the common sessions have been processed in a preliminary step. The echoes have been filtered, in order to eliminate the noise in the laser data. The LASSO epochs have been matched to laser pulses from one of the stations (the process is not easy, but details on it are beyond the scope of this paper). After the identification of the real triplets, false ones were obtained. The OCA and MLRS clocks have then been compared to the LASSO time scale. The opposite figures show the LASSO clock seen from the two sites for a given session. It covers 1200 seconds, and the behavior of the LASSO oscillator is clearly seen from both MLRS and OCA. A linear term has been removed independently for each station. Using only the data from one station could have been confusing, as the curve exhibits a non-linearity which can be interpreted as a frequency change of the LASSO oscillator, or as a problem in the laser ranging measurement (calibration change, ...). The agreement of the plots from both the stations allows us to assess that we really see the frequency changes of the onboard oscillator.

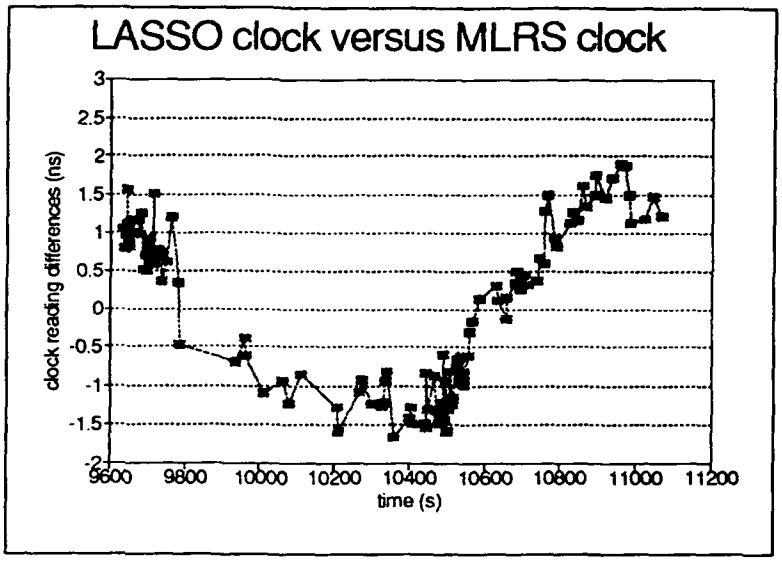

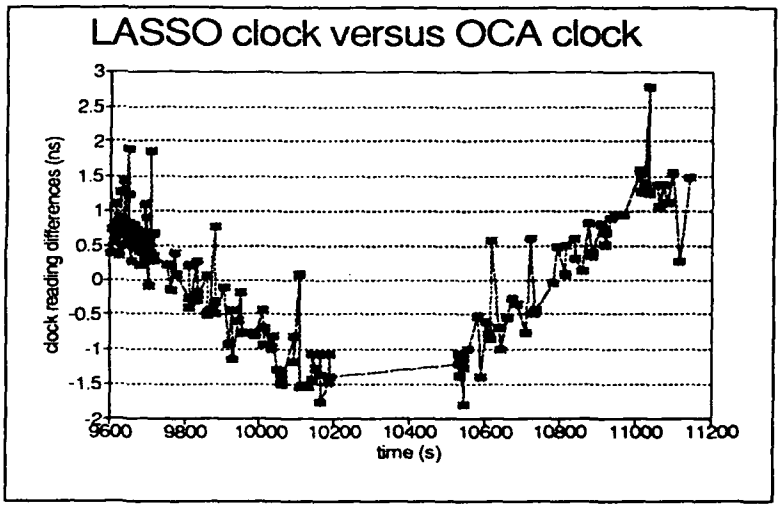

6. What about the precision ?

From the current analysis, the precision of LASSO time transfer is clearly better than 100ps. The number of data which can be acquired for 10 mn, using the concept of true and false triplets, is good enough to compensate the relatively long pulse length from OCA. The opposite figure shows the second linear part of the above figure. The formal uncertainty of the mean clock offset is 40 ps. The frequency drift (MLRS versus OCA) is determined with an uncertainty better than 2.10^{-13}.

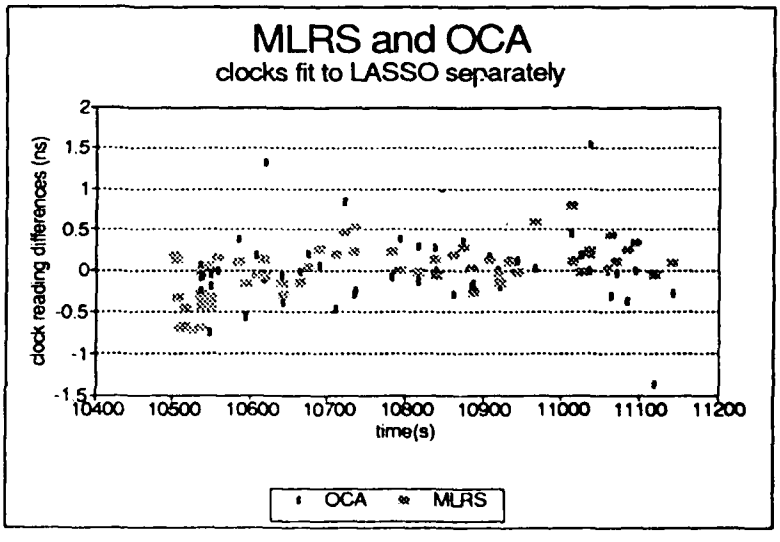

These uncertainties are much better than the anticipated ones. Two reasons for that : the laser pulses currently used are much shorter than those used at the time of the LASSO preparation, and the observation procedure as well as the data processing now used yield to much more data than originally planned. But uncertainty does not mean accuracy. For achieving an accuracy better than 100ps, we need to calibrate both the stations at the same level, and every station has to take care of the link between its own time scale and its ranging equipment, again at the 100ps level. This last point is not very easy to achieve. The beginning of 1992 should give an answer on how accurate can LASSO really be. But we can be sure right now that the LASSO equipment is suitable for time transfer at better than 100ps.

7. The future

After the calibration of MLRS and OCA stations, it will be possible to achieve one of the goals of LASSO: the comparison between two different time transfer techniques, GPS and LASSO, at the nanosecond level.

LASSO will move with its carrier Meteosat 3/P2 in Februray 1993 up to 75°W. The experiment will no longer be used from Europe (below the horizon !), but could be used by the US stations interested in LASSO, with the scheduling, data gathering and processing made from OCA. MLRS and GSFC laser stations could participate, in order to take benefit from this unique experiment still available for one or two years more.

The next step is to build a next generation LASSO, using the modern technology. To reach a 10ps precision seems easily feasable, looking back to what has been obtained from the existing LASSO. To keep the time metrology at a station at the same level is clearly not very easy, but it can be achieve through serious efforts. Such a new LASSO could fly for time transfer, and also other time-related experiments (relativistic tests, dynamics,...).

8. Conclusion

The preliminary analysis of common sessions of LASSO between MLRS and OCA shows that time transfer between remote sites through LASSO can be achieve with a precision better than 100ps. The only requirement for the station is to range to the satellite (10 shots per second) in the same 10mn time span. This result has been obtained thanks to a simplification of the observation scheduling and improvements of the data processing. A complete analysis of the LASSO data using the calibration results should provide a comparison between LASSO and GPS.

Acknoledgements : The authors wish to thank the observers at both stations for their help in observing Meteosat.

Reference

Veillet, C., D. Féraudy, J.M. Torre, J.F. Mangin, P. Grudler, F. Baumont, J. Gaignebet, J.L. Hatat, W. Hanson, A. Clements, J. Jespersen, M. Lombardi, D. Kirchner, G. Kirchner, H. Ressler, S. Fassi, W.J. Klepczynski, P.J. Wheeler, W. Powell, A. Davis, M. Granveaud, P. Uhrich. LASSO, two-way and GPS time comparisons, in *Proc. PTTI Conf. Dec 1990.*

QUESTIONS AND ANSWERS

H. Peters, Sigma Tau Standards: How much would the precision, accuracy and coordination improve if you could maintain one to two picoseconds stability in your standards at the station over periods up to 10,000 seconds?

C. Veillet: I am not sure I understood the question. It is clear that what we do in such a method is that we have over a few minutes an instantaneous comparison between two clocks; one is for example, our cesium and the other one is a cesium in Texas. That is what we have from the experiment. If you want to compare with GPS it means that GPS is not exactly at the time we hope for, but as you know with GPS you have time measurements, for example, for a few minutes, so you need to have some interpolation in a program. Their is also stress when you compare GPS and Two-Way Time Transfer. As long as that is a concern, the goal is to provide a clean time transfer to be compared with another technique. Therefore our goal for the next two months is to compare GPS with LASSO. For the rest if we want, for example, to compare LASSO with two way time transfer, it will be very difficult to have a time transfer session at exactly the same time we have a LASSO observation. For that we have a maser at our place, and it was planned to also have a maser moved in Texas along with a two way time transfer station. So that we can really compare the two techniques and to avoid this problem of instability of clocks. As long as we know there is no "two way" there, probably it is sufficient just to have the clock there and work compared to the GPS time schedule because of goal is to compare GPS and LASSO.

MIL–STDS and PTTI
What's Available and What Needs to be Done

James A. Murray
SFA, Inc.

Joseph D. White
U.S. Naval Research Laboratory
Washington, D.C. 20375

Abstract

The systems developer who needs PTTI capability has relatively little guidance in the form of military standards, particularly for systems using atomic clocks or other sources of very precise time and frequency. This paper will discuss the existing standards, including MIL–STD–188–115, MIL–F–2991(EC), and DOD–STD–1399. These documents were written several years ago and do not always reflect current practice or take advantage of more recent technology improvements. User needs have also changed over the years and some of those needs such as more detailed time codes are not being met. We will summarize what's available and what's good and bad about it.

The second part of the paper will make suggestions about what should be done in the future to promote and facilitate good PTTI design practice. Topics will include clock performance parameters, environmental considerations, time codes, signal isolation and time dissemination.

EXISTING STANDARDS AND THEIR ORIGINS

For years, the annual Frequency Control Symposium and the Precise Time and Time Interval Applications and Planning Meeting have tried to get up–to–date information on timing to the managers and designers. However, some of the key people don't know that they exist and some others don't know that they apply to their programs. Military standards written to alert responsible people to timing issues and to impart some standardization into timing systems have also had only moderate success — partly for the same reasons, but also because of their limited applicability or their inadequacy for some of the newer systems. One way to get the attention of potential precise time and frequency users is to place references to a DOD–STD or a MIL–STD in some of the more general standards, such as those for ships, aircraft, or installations, where integration of the systems should be addressed.

Standardization is not a new issue. The subject was addressed at the PTTI meeting in 1980 in a "Government Planners" session and an "Industry reviews session, in 1981 in a "PTTI Requirements and Specifications" forum, and in 1982 in a panel discussion on "Future Timing Requirements". In 1980, Martin Bloch of FEI reported to the PTTI Meeting that requiring small changes from an otherwise fairly standard product was costing the Government large amounts of money [1]. In 1981, James Bowser reported [2] that "...the planning process for PTTI support is less than a well defined, coordinated process".

About 10 years ago, Dr. Nicholas Yannoni of RADC called a meeting of Air Force PTTI users and found that precise timing devices were far from standardized; some cesium–beam standards, for example, produced only special, non–standard frequencies. The Navy found that each system requiring PTTI usually brought its own standards aboard, so that there was much duplication, but no means of coordination; there was some interest in the Navy for a standardized platform distribution system [3, 4]. In general, timing systems (even those aboard the same platform) had been developed completely independently. This is still a problem, but there has been some effort to resolve it.

MIL–STD–188–115 was developed as a standard for timing and synchronization of tactical and long–haul communications systems. It included some pet projects as well as some useful standardization. As in many committees, there were few specialists on the subject at hand, but it was not too difficult to accept the precedent of DOD–STD–1399–441, which had been drafted earlier by NAVELEX to help standardize Navy platform distribution systems. 1399 had little in the way of dogma, but did list some standard frequencies (100 kHz, 1 MHz and 5 MHz), precision time pulse rates of 1 pulse per second (1 PPS) and 1 pulse per minute (1PPM), and two time codes, each having an on–time feature. One was a 50 b/s, binary–coded–decimal (BCD), dc code giving units and tens of hours, minutes, and seconds once per second. (This time code and the other signals were provided by the Navy's cesium beam specification, MIL–F–28811(EC). The other was Time Code 2137, which gave the same information once per second, but used pulse–width modulation at a 25 PPS rate; the pulses could be either dc or an amplitude–modulated 1000 Hz carrier.

MIL–STD–188–115 adopted a preferred frequency of 5 Mhz (with 5 X 2n MHz acceptable) and a precision timing pulse rate of 1 PPS. It also required a clock either to display time of day (TOD) in hours, minutes, and seconds or to generate a time code with the same information. At first, the 1399 BCD code was considered. The goal for the standard was a minimum interface to allow collocated timing equipment to be shared or pooled. The purpose of the code was simply to resolve the ambiguity of the 1 PPS, although it could be used as a lower–precision, stand–alone time reference. However, there are other aspects of precise timing that might also be crammed into a time code, including the day of the year and a time figure of merit (TFOM). The BCD code was therefore allowed in three versions: the 6–digit (24–bit) TOD format, TOD plus a 3–digit (12–bit) day of year (DOY), and TOD plus DOY plus a 1–digit (4–bit) TFOM.

The TFOM was a new concept, at least to those in the 188–115 working group. It appeared that one normally knew the capabilities of the reference systems that were in use and therefore knew the time errors that could be expected. A clock ensemble might be able to estimate its own inaccuracy, and a GPS receiver might give a worthwhile assessment of accuracy based on signal–to–noise ratios, geometry of the satellites in use, and the consistency of the time solution with more than the minimum number of satellites. However, except for outright failures detected by built–in test equipment, a single clock generally does not know its own accuracy. An estimate might be made from the specified frequency stability, the accuracy of the last time and frequency updates, and the elapsed time since the updates, but inaccuracy can also come from undetected failures or environmental conditions. The TFOM, therefore, might be regarded as a warning, but not as a guarantee, unless there is a solid basis for verifying accuracy. Nevertheless, a TFOM definition was created for 188–115. Using the 1399–441 definition of precise time as 10 ms or better, the largest described error would be "greater than 10 ms or fault". The lower limit used in the TFOM was

1 ns, because technology was pushing such precision (if not accuracy), and the 188–115 TFOM ranked accuracies in decade steps from better than 1 ns to more than 10 ms.

When it was found out how the TFOMs were to be used, it was apparent that the 188–115 TFOM was not all that the users wanted. HAVEQUICK and others were seeking ways to use marginally capable clocks in what could be called a fluid timing hierarchy. The TFOM would be based on a sort of worst–case performance and the accuracy of the last update. Within some ranges of timing uncertainty, the TFOM would describe the uncertainty in increments as small as ten percent.

The interface control document for GPS military user equipment (ICD–GPS–060) was being developed at about the same time as MIL–STD–188–115 and made use of its timing interfaces. It provides for a time display, the full version of the BCD time code (Figure 1), and 1 PPS (Figure 2). It can also accept 1 PPS and the time code for quick acquisition of the GPS satellite signals. Because of its internal design, the user equipment (receiver) could not easily generate an accurate 5 MHz signal, so it does not supply one, but it did accept a 5 MHz input, which it terminated with a 50 Ohm resistor. Besides the 188–115 interface, the GPS user equipment has two other timing interfaces: a HAVEQUICK time code and a MIL–STD–1553 bus interface.

HAVEQUICK is a frequency–hopped communications system used by aircraft and other platforms. The HAVEQUICK time code is gaining in both popularity and content. The most recent version is the third. The MK–XV IFF was working towards a similar code before its development was discontinued, and it might have adopted the HAVEQUICK version. A working group of NATO is currently drafting a precise time and frequency standardization agreement (STANAG 4430) and appears to be leaning towards a HAVEQUICK–type code. The HAVEQUICK code has a nominal 10 μs resolution, although a shorter rise time could improve it.

The MIL–STD–1553 bus is basically a computer interface. GPS–ICD–060 shows it used in conjunction with the 1 PPS precision signal to distribute time.

STANDARDIZATION ISSUES

Standardization is more complex than it first seems. Part of the problem is the wide range of requirements vs. resources. A common standard of **performance**, for example, cannot simultaneously apply to a laboratory and a land–mobile unit. Standards based on current usage in the field could well stifle progress. Part of MIL–STD–188–115, in fact, prescribed performance standards specifically for the long–haul portion of the Defense Communications System. This performance could not be realized in many applications.

In choosing what to standardize, the full effect on all users must be taken into account. Simply selecting a common time scale can have major implications for PTTI: the versions of UTC maintained by different nations may differ by tens of microseconds. (The time scale used by the U.S. military is the version maintained by the U.S. Naval Observatory Master Clock). Within the expert PTTI community, such things can usually be handled rather easily, and they might be ignored by others who need only millisecond accuracy. For operational use at greater accuracies, they must be resolved beforehand, or means must be provided to the operators for dealing with them. Also, the UTC leap seconds can and often do lead to disorder within systems that need precise time only for synchronization. Some systems such as GPS and LORAN C do not observe them; International

Atomic Time might also be considered, but by going to any different time scale, a correction would have to be applied to the time given by the numerous UTC time–dissemination services.

Perhaps the best that can be done now is to standardize an interface that will not limit performance. Clock performance will, of course, continue to be platform–dependent, and each platform will require a clock that can satisfy its most demanding user system. However, a standardized interface that would **support** more demanding uses might still be realized if it does not intrude unnecessarily on system or platform design.

Assuming that the purposes of standardizing are to permit comparisons of clocks and to facilitate interoperation and time and frequency distribution, the elements specified in MIL–STD–188–115 (a precision timing pulse, a time code and a standard frequency) would seem appropriate, although the specifics of MIL–STD–188—115 might be subject to debate. For example, instead of the precision timing pulse, a precise timing mark might be some feature of the time code that describes when the mark occurred. For that matter, a standard frequency might also be recovered indirectly from the time code or the timing marks, but there is normally a need for clean, accurate standard frequencies in a precisely timed system.

It is a foregone conclusion that not all systems will be able to use the standardized signals and formats *per se*. An array of adapters or converters might be fielded to serve systems that cannot use the standardized interface directly, but the interface should be chosen to serve the great majority of current and future users without conversion.

In designing an interface, it must be considered how signals will be brought to and from it and possibly even what connectors or physical connections will constitute the interface. Because of the great amount of existing equipment and the local nature of most distribution systems, the interface should probably be electrical, even if fiber–optic lines are sometimes used. Since the standard frequency and precision timing signals are analog (as is the time code if its on–time feature is to be used as a time reference), small amounts of interference or noise can degrade them. For precise work, connectors should provide continuity of shielding used on the signal-bearing lines. Multi–pin connectors without individual line shielding should generally be avoided in order to reduce crosstalk and electromagnetic interference (EMI). There are, however, many uses of timing signals that are borderline according to the PTTI definition and for which multiple–conductor cables might suffice.

STANDARD FREQUENCY INTERFACES

Some performance attributes of interest at a standard frequency interface are the sometimes heavily overlapping qualities of frequency stability, spectral purity, single–sideband phase noise, harmonic content (for sine waves), spurious signal content, and jitter. Frequency accuracy is a performance function of the frequency reference, and the standard interface is intended only to preserve accuracy—not to establish it. It is assumed here that the phase of the standard frequency is of no interest to the user, but the constancy of the phase relationship with respect to the precision timing signal might well be consequential. It is probably too much to ask that an absolute phase relationship between the two signals be specified at the interface since they will most likely be distributed on separate lines, and the interpretation of the timing signal may also vary somewhat from user to user. An important relationship for many systems is that the standard frequency and the precision time signal be derived from the same clocking signal; thus, equipment using the standard

frequency would not have to be reset occasionally to maintain agreement with the precision time pulse.

The nominal frequency of the signal deserves some consideration. 5 MHz has been used by much military and civilian equipment and is a good compromise frequency for many purposes, although 10 MHz is gaining popularity. At 5 MHz, losses in common coaxial lines are low enough that it can be distributed more than 1000 feet with less than 6 dB loss. At higher frequencies, losses would increase, but at lower frequencies, small amounts of noise or interference would cause larger fractional frequency deviations or jitter. Conceptually, the MIL–STD–188–115 preferred frequency of 5 MHz, with options of 5 MHz X 2n may have some merit, although most existing 5 MHz equipment would require an active frequency divider (and perhaps a filter) if $n > 0$.

A standard frequency signal might be distributed as a sine wave or a pulse chain, such as a square wave. Narrow–band filtering can be used to recover the fundamental frequency of a square wave. However, a sine wave having the same fundamental power as a square wave would cause less EMI. A low–duty–cycle pulse train which could be generated with less power expenditure than a square wave would provide little power at the fundamental frequency, and triggering techniques would likely be employed to recover it; false triggering would be a threat in an impulse–noise environment and could produce very large instability in the recovered signal. The voltage and impedance of the standard frequency signal might be specified, although distribution amplifiers or attenuators can be used to adjust the voltage if the equipment can deliver a clean signal to the interface.

TIME CODE INTERFACES

While MIL–STD–188–115 permits either a time readout or a time code, a time code is more useful if timing information must be distributed around a platform or installation. Other situations that would be best served by a time code include initializing a precise time reference of an aircraft or land mobile platform whose power had been turned off. In these cases, if the mobile unit is then to maintain time autonomously, other information, such as the date and direction of an impending leap second, would be needed. For some automatic equipment, the day of the year and even the year of the century would also be required. For distribution around a platform or installation, a TFOM would not ordinarily be especially useful, except to declare failures detected by built–in test equipment or to warn a lower–level disciplined clock of substandard service being provided to it. If the platform might later use a time reference such as GPS, it may be more convenient for the externally loaded time code and the one provided by the GPS receiver to be in the same format, or at least a compatible format.

In the past, much information now being asked for in the various time codes was supplied manually. A "universal" time code might be developed, but before doing so, a wider search of time–code needs and practices should be made. Some thought might also be given to adapting an existing code. The 50–bit–per–second BCD code has insufficient room for expansion. The HAVEQUICK code does not give leap–second information, although there seems to be enough room for considerable expansion. The IRIG A, B, and G codes give a time of year at least once per second, but do not give the YOC, TFOM, or leap–second information. The "control" bits available in them might be designated to supply the other information. If the HAVEQUICK or an IRIG code is selected as the standard, any added bits or the use of existing control bits should be standardized; it would

be prudent also to leave sufficient room for additional information that might become standardized later. Even so, it would not be surprising if other functions were tacked onto the code just because it is convenient.

PRECISION TIMING SIGNAL INTERFACES

A precision timing signal might be part of a time code, or it could be a separate pulse rate. One pulse per second has been widely used in precise timing; the GPS user equipment ICD, MIL–STD–188–115, and much existing equipment specify a positive 20 us pulse with a rise time of less than 20 ns. This is a reasonable specification for much work, and it doesn't take too much coaxial cable to stretch a shorter rise time to 20 ns or more, anyway. Earlier equipment used a 10 V pulse, but some devices now use transistor–transistor–logic (TTL) output levels. (A TTL 50 Ohm line driver usually delivers about a 3 V pulse).

However, some laboratories and even operational systems are now dealing with single–nanosecond resolution. How different measuring instruments respond to a pulse rise of 20 ns (or more) is then pivotal. Given the difficulty of maintaining a shorter rise time, even if one were generated, a more practical approach may be to standardize on how a pulse is perceived by a user or measurement system. USNO has regularly used a specific voltage threshold in their portable clock measurements. (A 1 V threshold used earlier was later changed to 1.5 V to avoid noise that was present on some systems). But the difference in their practice and how a VSAT two–way time transfer modem or a GPS receiver used in simultaneous viewing would perceive the pulse might differ by a much as, say, 10 ns.

If a measurement standard were to be adopted, it might well include some other features that would improve reproducibility. In some of the current (10 V) pulse–generation specifications, the tolerances of the low and high levels of the pulse are one volt. These are simply undesirable by–products of pulse generation, but they limit flexibility in choosing a threshold. If the measurement system used capacitor coupling (e.g., the circuit of Figure 3), only the dynamic portion of the pulse would be of interest, and the tolerance of the low level would not be a concern. Furthermore, if the pulse rate is once per second, an input circuit time constant might be made small enough to reduce considerably the often experienced effects of ground loops at mains frequencies of 50 or 60 Hz.

A standard input circuit would not be needed by most users. However, if one is specified, it should be able to operate with both the 10 V and the TTL–level 1–pulse–per–second signals. The following specifications might be appropriate:

Input Impedance:

Nominal value: 50 Ohms
VSWR: <1.1 from 20 kHz to 200 MHz
<1.3 below 20 kHz
DC resistance: 50 Ohms ± 10 Ohms

Trigger circuit: Capacitor Input:

Time constant = 100 ± 20 μs
Trigger point: +1 V ± 0.1 V on dynamic rise

The VSWR specification is necessary both to avoid reflections and to set a standard impedance for measuring the pulse. A time constant of 100 μs is large enough to work with pulses of very large rise time (although accuracy would suffer) and small enough to discriminate against 60 Hz signals by almost 30 dB. A strict tolerance on the time constant is not needed unless the pulse rise time is more than 10 μs.

The length of the pulse is not especially critical if the leading edge is used as the reference feature. Only low–accuracy timing systems could use a long pulse to advantage; otherwise, a long pulse is just a waste of energy. A 10 or 20 μs pulse should be adequate for local distribution.

SUMMARY

A standard precise time and time interval interface could make it easier to serve and coordinate precisely timed military systems. Money could be saved; in some cases, by pooling or coordinating platform resources, performance and reliability could be improved. The degree of standardization will undoubtedly be a compromise because of the amount of existing equipment and the wide range of requirements and the technologies available to support them. Just standardizing the types of signals at a standard interface would be a step forward, even if amplifiers, hybrid connectors, or other crutches are sometimes needed.

Probably the most controversial element will be the time code. Several different time codes may be needed to serve different types of users. Modulated–carrier time codes, for example, are still needed for instrumentation recorders that cannot record DC signals and might also be used in voice–frequency circuits. DC codes are easier to generate and use in most other local applications. The MIL–STD–1553 code could be used to interface with computers, although for precise work, a precision timing pulse is also needed.

The content of a code would depend on where the basic information would be injected into the timing hierarchy. For example, will leap–second, day of year, or year of century information be injected manually? If so, where? If TFOMs are used, there should be a standard method of determining them or at least evaluating the confidence that should be placed on them. Used indiscriminately, TFOMs can cause large reliability problems. For the purpose of standardization, a coarse TFOM such as provided in MIL-STD–188–115, or even just a warning flag, might be adequate. The coarseness actually may be advantageous, because it would tend to discourage its

use for selecting a reference based on minor and meaningless TFOM differences. Space might be reserved in the code for user–defined TFOMs or other user–specific information; if it is, the type of user should also be identified so that other user types would not be confused by the information.

Finally, the question of applicability should be resolved. The interface could be required of each clock brought aboard by each platform system. (A clock for these purposes would contain its own oscillator and therefore be able to operate autonomously for some period of time). The whole picture changes if those responsible for platform design and integration also take responsibility for providing the precise time and frequency services needed by all precisely timed systems. (Such a philosophy was adopted from the start in the SSN–688 class of submarines and likely some other platforms). This approach is the one with the greatest potential for success.

REFERENCES:

[1] M. Bloch; *"Frequency and Time Generation and Control"*. 12th Annual PTTI Applications and Planning Meeting. Greenbelt, MD; December 1980.

[2] J. Bowser: *"Precise Time and Time Interval Users, Requirements and Specifications"*. 13th Annual PTTI Applications and Planning Meeting. Washington, DC; December 1981.

[3] R. Allen; *"The Navy's Stnadardized Precise Time and Time Interval Platform Distribution System"*. Proc. 36th Annual Symposium on Frequency Control; 1982.

[4] J. Murray; *"Platform Distribution System Specifications"*. Proc. 37th Annual Symposium on Frequency Control; 1983.

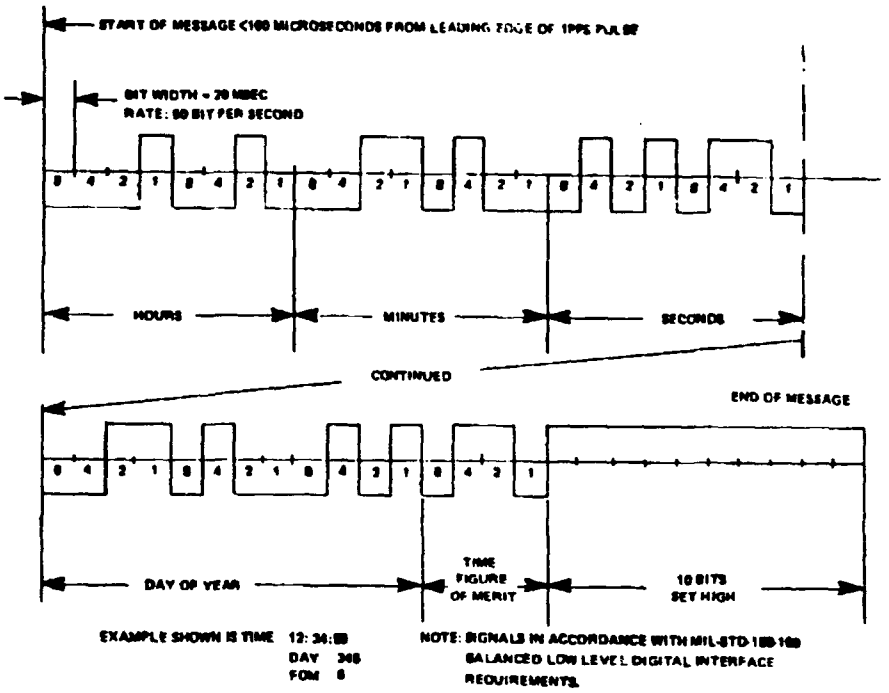

Figure 1. BCD Time Code

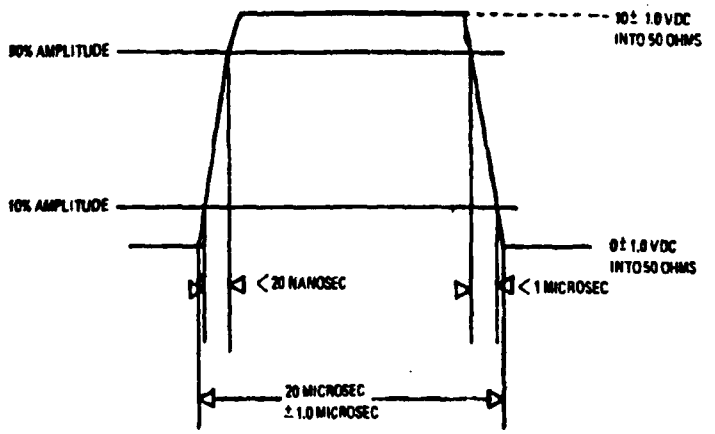

THE LEADING (POSITIVE GOING) EDGE OF THIS PULSE
INDICATES ONE SECOND ROLLOVER.

Figure 2 One Pulse per Second Output

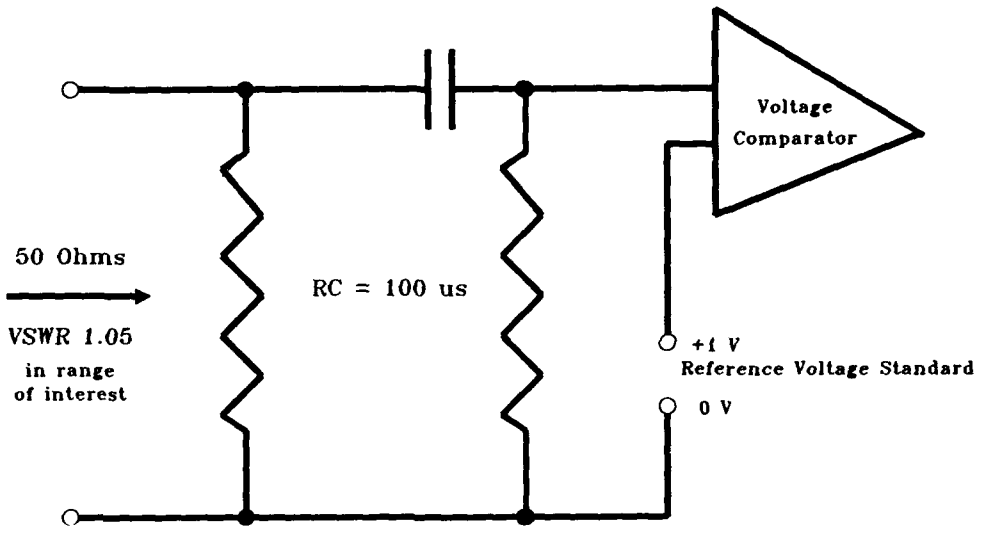

Example of Standard 1PPS Input Circuit
Figure 3.

QUESTIONS AND ANSWERS

G. Winkler, USNO: I think your excellent paper has raised several points. First the identification of the second and the problem of identification of the year. Many systems and our own operations with the observatory identify the second through the MJD plus six decimals. That is a very convenient way, strictly decimal and very easy to convert into any other format. After all, the calendar is well defined in advance and I think it avoids all these problems of the year change and the century and what have you. Second point, in the DSCS there is no reason what so ever why the DSCS came up without the same standards with the same procedures as LORAN and GPS and that is simply to ignore the leap second within the system. The problem is that we have difficulty in getting everybody together because DSCS is operated through the services with a more or less loose supervision by (?) and the problem is purely one of coordination, but my recommendation would be to do exactly the same thing as what we do in LORAN. That is have no interruption what so ever and a coherence in the electrical system, but do things through a table of coherence or a table of offset. After all OMEGA, LORAN, GPS and all of these systems do that and they avoid the problems of resetting modems and things like that. That would be my recommendation. The last point I wanted to make is to talk and clarify the situation with the UPC reference. That has come home very convincingly during the last meeting which in fact Dr. Beard has organized with the NATO representatives. That is really the only one way to do that and that is for GPS through the observatory reference. To produce as close a predicted value of UTC BIPM as we can make, because there is no better way to do it. The BIPM values; they come one or two months in arrears and we have to have a real time reference. The only way to avoid endless disputes and confusion is to adopt that policy and we have adopted that policy. There is only one difficulty and that is the annual terms, which exist in practically every operation when it goes to that kind of a precision to nanoseconds instead of long term time keeping. But I believe that problem will go away with the installation of a great number of the new cesium clocks into the system, the international system. They are much less sensitive to time, to temperature fluctuations and that will eliminate, I hope a great deal of that annual term. Until that happens the price that you pay are more frequent small frequency changes in the observatory time scale. These frequency changes are in the order of one or two parts in ten to the fourteen and they come practically every month. Whenever a new bulletin from the BIPM arrives we have to change our prediction. This, I think will go away as time goes on and we have a much better international system. Some discussion about what can be done, in that regard, by including better methods to make international time comparisons including some recommendations by the GPS Standardization Group, as we had yesterday. Considering a slight change maybe in the way (?) is implemented by BIPM. All of that will be discussed in a meeting next March. We will be very much interested to get some additional inputs concerning this questions.

J. Levine, NIST: I would like to endorse Dr. Winkler's recommendations very strongly; in particular two of his recommendations. (1). That time be given in terms of Modified Julian Day number in seconds which we use as well; it is a very useful system. I think that's an extremely good idea. (2) Endorse very strongly is the idea of using UTC BIPM. There is a difficulty of course as you pointed out with predicting it. We have the same difficulties and we have steering of a few parts in ten to the fourteenth every month as well. I think in the long run using UTC BIPM allows international coordination that allows for hand over among different standards laboratories. I think, I agree with you there are problems now and this is a goal we ought to move towards; because it will facilitate international coordination.

G. Winkler: The reaction to the first thing, and that, is for an electronic system such as the DSCS to avoid the leap second by simply continuing coherently and leave that change to the

interface between your electronic system and the clock on the wall. We do this with the table of coincidences as in the case of LORAN and through the GPS minus UTC correction which is another navigation message of GPS.

Comment: I am not clear when you say GPS has no leap second. I did an experiment in which the satellite message has knowledge ..

J. White, NRL: They broadcast the correction; there are multiple time scales broadcast by GPS.

G. Winkler: What we mean is the system, the electronics go on uninterrupted. There is no step, no resetting. Everything is done through the information change. What you do is you change the information in the navigation message, you change from 7 seconds to 8 during the next leap second. That is much easier to accomplish than to reset the whole system; reset clocks. In a case of the DSCS, what is being done and what has to be done right now is at some convenient time when the system, in other words, the star or whatever communication arrangement you have, when they have the calibration period that they can reset their modems to the new time 10 second period. I think this is a great inconvenience and should be avoided.

Question: What GPS documents also have the algorithms that tell you how GPS receivers should handle and ...

J. White: Yes, absolutely that is all in there. The GPS time itself does not have the leap seconds in it, they broadcast the leap second corrections to generate UTC.

Question: What is your recommendation on Figure of Merit?

J. White: I do not have a recommendation on Figure of Merit. I point out that Figure of Merit is something a lot of people want, that I do not think is handled well at the moment.

Comment: At the last ICD060, our agency was helpful in writing it up, and want everyone to know, if they have any recommendation on that ICD, there is a (?) process, a working group meeting and that has not occurred for that ICD for awhile. If you have recommendations for GPS changes, they should be submitted through JAPO and put in for future ICD meetings to determine whether or not these changes will be considered or approved; and that is rare.

G. Petit, BIPM: If the leap second is really a problem, why not think of removing this leap second, at least until we can introduce leap powers for example. Anyone who wants to know precisely the rotation of the earth, why not stop thinking of removing the leap second.

G. Winkler, USNO: I agree with you, in fact, when the leap second thing was brought up in 1967, the first proposal was to do it every leap day. However many seconds will be required at that moment, usually three or four, but that would require the tolerance limit to be extended from nine tenths or one second to more than ten seconds. There was a tremendous resistance to that and I do not know if that would be possible today. That is a subject that CCDS should address in the next March meeting.

J. Cecil, NUWC: I am the current chairman of the Range Commander Council Telecommunications Group Timing Committee. We are the ones that established these IRIG standards. I do not have a question, but I would just like to make the comment that when we go out and interrogate other DoD ranges to ask them, or inquire about upgrading these standards, we have a great deal of difficulty getting responses in a lot of cases. We would like to see that changed, so I can see your point in a lot of comments on what you would had to say.

Ron Beard, NRL: One comment on the leap second consideration in the NATO arena, which I am the U.S. representative on a working group. They are considering recommending adding a field for dissemination of leap second information through the standardized interface. So that is one approach around that. I think the significant point that has not been raised this morning through Joe's rather good paper is where is the interface? Is it between a clock and a local reference system? Is it in the field between system units? Exactly where is the interface that can be standardized. This is a problem we run into in the NATO arena. It is something that needs to be considered.

PTTI-Aided Ephemeris Calculation and Rapid Data Link Acquisition for Manned Space Flight

Alfred Anderman
Rockwell Space Systems Division
12214 Lakewood Blvd., Downey, CA 90241

Abstract

Complexity of future manned space flight mission control can be significantly reduced by integrating GPS, the PTTI source, into telemetry, tracking and command (TT&C). Future telecommunications, space tracking electronic intelligence, metrology, navigation, and data acquisition will thereby be served, including: 1) On-board ephemeris determination, 2) Reduced synchronization time for time division multiple access (TDMA) links, and 3) In-flight clock calibration, increasing on-board autonomy and reducing ground support costs.

Manned space transportation through the first quarter of the 21st century will probably depend on a mix of vehicles, including the Advanced Manned Launch System (AMLS), the Personnel Launch System (PLS), and continued use of the Shuttle Fleet. Precise Ephemeris is important on-board for mission success, status monitoring, also for rendezvous and docking. Use of GPS can eliminate ground based tracking/processing, enhancing autonomy and reducing communications bandwidth.

GPS time can simplify complicated functions used in bandwidth efficient time division multiple access (TDMA) communications, such as: 1) Precise and real-time synchronization of receive reference timing, 2) Transmit-timing and acquisition control, 3) Unique synchronization word (UW) detection, and 4) Elastic buffering. High clock accuracy provides increased signal-to-noise (S/N) ratio during acquisition, permitting narrower acquisition frequency and time windows.

Spaceborne systems requirements to provide capabilities such as: 1) Refinement of the GEM-72 gravity model based on satellite tracking observations from ATS-6 to GEOS-3, 2) Relativistic clock experiments, 3) NASA crustal dynamics program for developing space geodetic techniques to study the earth's crust, its gravity field, and earthquake mechanisms, and 4) Multi-disciplinary space geodetic tracking for studying global climatic changes are also reviewed.

A. INTRODUCTION

Future space vehicles will require a very precise time reference for communication and navigation functions, including: 1) Timing signals to maintain user synchronization within various digital spread spectrum communications networks, 2) Accurate clocking to encryption devices for military missions, to maintain security, and 3) Generation of a *"real time"*, time base to support integrated navigation functions, network acquisition, sensor data processing, correlation and fusion. Some speculation concerning potential additional PTTI-aided space applications is included at the end of this paper.

Independent redundancy, to assure reliability, also implies synchronization among the independent data sources, either 1) Loosely, involving buffering, comparing or voting, signaling consensus and/or marking completed intervals, or 2) Tightly, involving hardware comparison of voting, and a common time reference, whereas loose synchronization can employ separate time references.

B. SPACE SHUTTLE ORBITER (SSO) TIMING & CONTROL PROCESSING

1) MASTER TIMING UNIT

The Space Shuttle stable crystal-controlled master timing unit provides serial time reference signals to the on-board computers, pulse code modulation master units (PCMMUs), various time display panels, and synchronization to instrumentation and other subsystems, using separate GMT and Mission Elapsed Time (MET) time accumulators, as shown in Figure 1. Time outputs are a) Serial time code continually updated at 100 pps rate (IRIG-B), and b) Self-clocking Manchester II bi-phase demand outputs read out upon receipt of externally supplied enable signals.

Frequency stability is better than 1 part in 10^9 per day long term, and 1 part in 10^{10} standard deviation short term, using the Allan variance formula for averaging times of 0.5 1, 2, and 10 seconds, but requires 72 hour stabilization time after a power-off state at 35 deg.F. Master Timer derived time/clock/sync inputs to Shuttle operational instrumentation (OI) are shown in Fig. 2.

2) AVIONICS PERFORMANCE

The estimated three-sigma position and velocity errors at main engine cutoff (MECO) of about 4600 ft and 20 ft/sec could be updated in the post-MECO state to about 100 ft and 0.6 ft/sec in about 2 minutes, using GPS.

On-orbit TDRSS provides adequate state vectors using two-way range rate (Doppler) data through both satellites within one revolution, in about 60-90 minutes. With only one relay satellite available, the 1.5 pass minimum tracking interval is about 115 minutes. An integrated time line suggests that 120-195 minutes. are required from the start of tracking to maneuver execution. With a full GPS constellation the state could be determined within about 2 minutes, as for the post-MECO state. Updating and resetting externally requires use of the data processing system.

For ground entry navigation, using C-Band radar, the mission control center (MCC) updates on-board knowledge of position after blackout at about 150 kilofeet. altitude. GPS could provide accurate post-blackout navigation capability to about 200 ft and 1.2 ft/sec, or much better in differential mode. An orbiter GPS Development Flight Test (DFT) demonstration is planned for 1993 (Figure 3).

C. FUTURE MANNED SPACE VEHICLES AND THEIR AVIONICS ARCHITECTURES

Autonomy levels in future space avionics architectures will undoubtedly be increased, most likely with on-board health status processors as a first step, as shown in Figure 4, and on-board PTTI-

aided ephemeris determination and communication link synchronization not far behind.

Future manned space transportation will probably depend on a mix of vehicles, as indicated in Figure 5. On-going NASA studies have resulted in preliminary designs of Advanced Manned Launch Vehicle (AMLS) and Personnel Launch System (PSL), while anticipating continued use of the Shuttle Fleet through the first quarter of the 21st century [13]. A comparison of vehicle sizes is shown in Figure 6.

D. PRECISE TIME, FREQUENCY AND EPHEMERIS DETERMINATION

Of the various available systems, only Loran and GPS are capable of time synchronization to better than 100 nanoseconds, as shown in Figure 7, while differential GPS is capable of another order of magnitude improvement [12].

1) ON-BOARD TIME AND FREQUENCY

One nanosecond (ns) of time error is equivalent to 0.3 m range error. A spaceborne GPS system can provide precise time globally to an accuracy of 103 ns, as shown in the total RSS time transfer error budget of Table 1 [4, 6, & 11]. Accuracies to better than 10 ns, can be obtained by correcting for ionospheric delays with simultaneous view for coordinated users.

The Russian GLONASS, capable of similar accuracies relative to GLONASS UTC, has a known relationship to UTC (USNO) via the International UTC maintained by the Bureau International des Poids et Mesures (BIPM), Sevres, France, and could supplement GPS data to achieve reliability/availability levels demanded by the FAA and ICAO for commercial aviation.

GPS time is determined by the USNO Master Clock (MC) of the USNO Time Service Department (TS). GPS can provide UTC (USNO) time after correcting for the difference from UTC by an integral number of seconds. GPS system time is on a continuous time scale, referenced to midnight 5 Jan 1980, whereas UTC and Russian GLONASS time contain leap seconds that allow for the deceleration of the earth rotation. This number is provided as part of the navigation message, because it changes every time there is a leap second.

Upon network synchronization, the clock, timing signals, and real time base, derived from accurate crystal or rubidium frequency standards of performance summarized in Figure 8 and Table 2, will be slaved by software controlled by an assigned network controller, referenced using GPS, UTC or GMT [12].

Treating GPS as a Precise Time and Time Interval (PTTI) distribution system, semiconductor laser optical clock distribution can provide a virtually jitter-less timing source, if required. Accumulated dynamic clock jitter between ports of both correlated and uncorrelated sources is of the order of picoseconds [7].

2) PRECISE EPHEMERIS DETERMINATION

Precise ephemeris data is important on-board for mission success, status monitoring, also for rendezvous and docking. TDRS measures to better to better than 100m accuracy, but does not give instantaneous position fixes, as does GPS. Presently 60 to 195 minutes elapses between the start of tracking and the start of executing maneuvers. In low earth orbit, unpredictable atmospheric drag is the largest limit on prediction.

E. COMMUNICATIONS AND DATA SOURCE SYNCHRONIZATION

Using a GPS timing reference, communications with other GPS users can inter-operate immediately without first exchanging timing signals. Sub-microsecond accuracy timing derived from GPS brings new meaning to *"real time"*, in computer and communications synchronization.

1) END-TO-END LINK SYNCHRONIZATION

Carrier, clock, code, and network synchronization needs are summarized in Figure 9. A TDRS functional receiver block diagram, and a representative end-to-end communications block diagram, are provided in Figures 10 and 11 respectively [1, 2, & 14].

TDRSS provides short code PN lock acquisition with > 90% probability within 20 seconds at S/No values between 34 and 73 dB-Hz, and within 7 seconds for S/No >37 dB-Hz, and carrier within 10 seconds. TDRSS user transponders provide Doppler compensation within 1500 Hz of actual transponder center frequency, allowing for about 1% velocity uncertainty. GPS-derived velocity error is closer to 0.01%. Code acquisition strategies are matched to TDRSS-derived predicted position uncertainties.

With reduced GPS position and velocity uncertainties, acquisition windows could be considerably reduced in both time and frequency, leading to reduced sync times at increased S/No ratios. GPS time can also simplify the most complicated functions used in bandwidth efficient Time Division Multiple Access (TDMA) communications: precise and real-time synchronization of receive reference timing, transmit-timing control, acquisition control, unique synchronization word (UV) detection, and elastic buffering [7].

2) DATA SOURCE SYNCHRONIZATION

Independent redundancy requires some form of synchronization among the independent data sources. Soft, or loose, synchronization involves buffering, signaling consensus, and marking completed intervals, under program control over suitable inter module data links. Hard, or tight, synchronization requires hardware comparison or voting, and a common time reference. As used in the NASA Fault Tolerant Multi-processor (FTMP) and other high reliability concepts for manned aerospace vehicles, the timing reference must continuously remain within tolerances for time-correlated data transfer.

In the past, continuous timing references were maintained using fault-tolerant redundant clock distribution, based on majority logic voting algorithms. A set of GPS disciplined voltage-controlled

phase-locked crystal oscillators can ensure that failure of one of the oscillators does not destroy the phase lock of the survivors. Normally all clock receiver outputs are in phase lock with each other and with all the oscillators [12].

F. IN-FLIGHT CLOCK CALIBRATION FOR REDUCED REACQUISITION "TIME TO FIRST FIX"

Many aerospace vehicles carrying atomic clocks to provide precise time to their communications systems need to be calibrated before take-off. With a GPS receiver on-board they can be reset or calibrated in flight. The clock can then be used to reduce time to first fix (TTFF) if the receiver has to reacquire satellites, and enables it to perform direct P-Code acquisition.

G. ENVIRONMENTAL STUDY REQUIREMENTS

Although widespread need for highest PTTI accuracy may not be apparent, numerous applications for this accuracy will surface once the availability has been established. For instance, it may be of interest to review PTTI requirements of a PLS-type vehicle for supporting various environmental study programs.

1) GRAVITY MODEL REFINEMENT

Precise GPS techniques are making possible new kinds of large scale surveys of the earth and its resources using aerospace platforms. The use of GPS receivers in space vehicles for decimeter-level space navigation and geophysics - including gravity field determination - will map broad global features of the gravity field, while future aircraft equipped with GPS will chart fine, regional details of the same field.

Gravity Probe B (GP-B) used GPS as a sensor for a closed loop space guidance system, from its location after initial insertion to a very precise low earth orbit, to within 0.001 eccentricity, to within 0.001 degree inclination, and to alignment with the star Rigel to within 0.001 degree [3].

2) RELATIVISTIC CLOCK EXPERIMENTS

Gravity Probe-B was also part of a NASA project that tested two aspects of Einstein's relativity theory, to verify two gyroscope spin axis motions in earth orbit not predicted by Newtonian analysis. In a precisely polar orbit the two effects would be orthogonal, with magnitudes calculated to be 6600 and 42 milliarc-sec/year respectively [3]. The required long term clock stability is about 10^{-13}, or an accuracy of 10 ns, to successfully accomplish the relativistic clock experiment [5].

3) NASA CRUSTAL DYNAMICS PROGRAM FOR EARTHQUAKE MECHANISMS STUDY

Movements of the earth's crust include extremely slow centimeters per year movements of the continents relative to one another, and also their slow internal deformations. Measuring distances

between points up to thousands kilometers apart with accuracies exceeding a few parts in 100 million enables such movements to be detected.

Precision and accuracy of ground based GPS determined inter-station vectors for 50 - 450 km baselines were recently reported as better than 30 mm horizontally and 80 mm vertically, by comparing with very long baseline interferometry measurements. Such measurements provide details about strain across faults of plate boundaries [8].

4) SPACE GEODETIC TRACKING FOR GLOBAL CLIMATIC CHANGE STUDIES

The TOPEX/Poseidon oceanographic satellite will measure the topography of the open oceans using radar altimeters to a precision of a few cm. Measuring open ocean circulation and sea level as an indicator of global warning depends on detecting global sea level changes of about 1 mm/year [9].

Tide gauges presently used measure relative change between the land surface and sea levels. This relative change may be due to sea level rise or land subsidence or both. Satellite altimetry measurements will have to be related to a well defined terrestrial and space reference frame that must remain valid for decades, with respect to a network of earth fiducial points [9].

H. ENVIRONMENTAL STUDY SUPPORT

Reviewing the PTTI capabilities of a GPS-equipped PLS-type vehicle, potentially to support *"Mission to Planet Earth"*, environmental studies, the following presently appear unlikely: 1) Precision orbit injection to support GP-B-type gravity model refinement, or PTTI precision to support 2) GP-B-type relativistic clock experiments, 3) Monitoring earth crust movements,s or 4) Monitoring sea level changes for tracking climatic changes.

However years after dedicated environmental satellites have completed their missions, clearly a PLS-type vehicle will be able to measure long-term drifts, and to monitor relative movements of earth fiducial points.

I. SUMMARY AND CONCLUSIONS

GPS on-board time, synchronized to the GPS space segment, provides the extremely precise reference needed for navigation, positioning purposes, can serve as primary time transfer system, as well as for telecommunications, space tracking electronic intelligence, metrology, and data acquisition.

Discretionary use of the PLS vehicle, with GPS on board, as a flexible platform to perform environmental studies will depend on the PTTI availability, and - at the very lease could identify long-term relative movements of earth fiducial points established for various local or global reference frames.

Continuous on-board filtering and orbital element updating based on GPS can eliminate ground-based state vector updates, provide earlier payload deployment opportunities, save fuel due to reduced dispersion rendezvous, make up for loss of TACAN by the year 2000, also reducing communications bandwidth [10].

J. ACKNOWLEDGEMENTS

The author thanks Carl F. Ehrlich, AMLS/PLS Program Manager at the Rockwell Space Systems Division, and Howard Stone, of the AMLS/PLS Program Office at NASA Langley Research Center, for permission to include Figures 4 and 5, based on NASA Study Contract NAS1-18975 [14]. However the views expressed in this paper are for information only, and have not been endorsed by RIC or NASA.

K. REFERENCES

[1] Anderman A., *"Impact of AI, Fuzzy Logic, & GPS on Future Avionics,"*, RIC, Downey, CA

[2] Anon, *"Tracking and Data Relay Satellite System (TDRSS) Users Guide,"*, NASA/GSFC, Greenbelt, MD

[3] Axelrad P. & Parkinson B. W., *"Closed Loop Navigation and Guidance for Gravity Probe B Orbit Insertion,"*, Navigation, Vol. 36, No. 1, Spring 1989, P. 45-61

[4] Colombo O. L. & Peters M. F., *"Precision Long-Range DGPS for Airborne Surveys,"*, GPS World, April 1992, P. 44-50

[5] Green G. B. & Axelrad P., *"Space Applications of GPS,"*, Proc. ION National Technical Meeting, Jan. 1989, San Mateo, CA, P. 89-104

[6] GPS-86-12320-010, 11-30-85, NACSTAR GPS Phase III Interface Control Document ICD-GPS-060: *"GPS User Equipment - Precise Time and Time Interval (PTTI) Interface,"*, Space Division (AFSC) and Space and Naval Warfare Systems Command

[7] Kato S. et al, *"Application of Advanced Microelectronics to Large-Scale Communication Equipment - Compact and Maintenance Free TDMA Equipment,"*, IEEE Jour on Selected Areas in Comm., Vol. 8, No. 8, Oct 1990, P. 1551-1564

[8] Larson K.M. et al, *"GPS Application to Crustal Deformation Measurement: 1. Precision and Accuracy, and 2. Influence of Errors in Orbit Determination Networks,"*, Jour. Geophys. Res., Vol. 96, No. B10, 10 Sept 1991, P. 16547-16584

[9] McDoran P. F. & Born G. H., *"Time, Frequency, and Space Geodesy: Impact on the Study of Climate and Global Change,"*, Proc. IEEE, Vol. 79, No. 7, July 1991, P. 1063-1069

[10] Montez M. et al, *"Implementation of Shuttle GPS Capability,"*, 10-1-92, NASA/JSC, Houston, TX

[11] NATO-Team, *"Navstar GPS User Equipment, Public Release Version,"*, Feb. 1991, Navstar GPS Joint Program Office, LAAFS, CA

[12] RIC95-329, 3-28-85, *"Spacecraft Applications of Advanced GPS Technology Study,"*, a) Vol. 1, *"Time Synchronization Capabilities, and b) Draft Spec, "TDMA Spread Spectrum Time Frequency Reference System"*,

[13] *Rockwell SSD, "Advanced Manned Launch System/Personnel Launch System (AMLS/PLS) Study",: a) "AMLS Final Technical Review,", Aug., 1991, & b) "PLS Hardware/Software Design Description,", Aug. 1990*

[14] *Zillig D. J., "Performance and Design Requirements and Specification for the Second Generation TDRSS User Transponder,", 9-18-87, STDN No. 2203.9 NASA/GSFC. Greenbelt, MD*

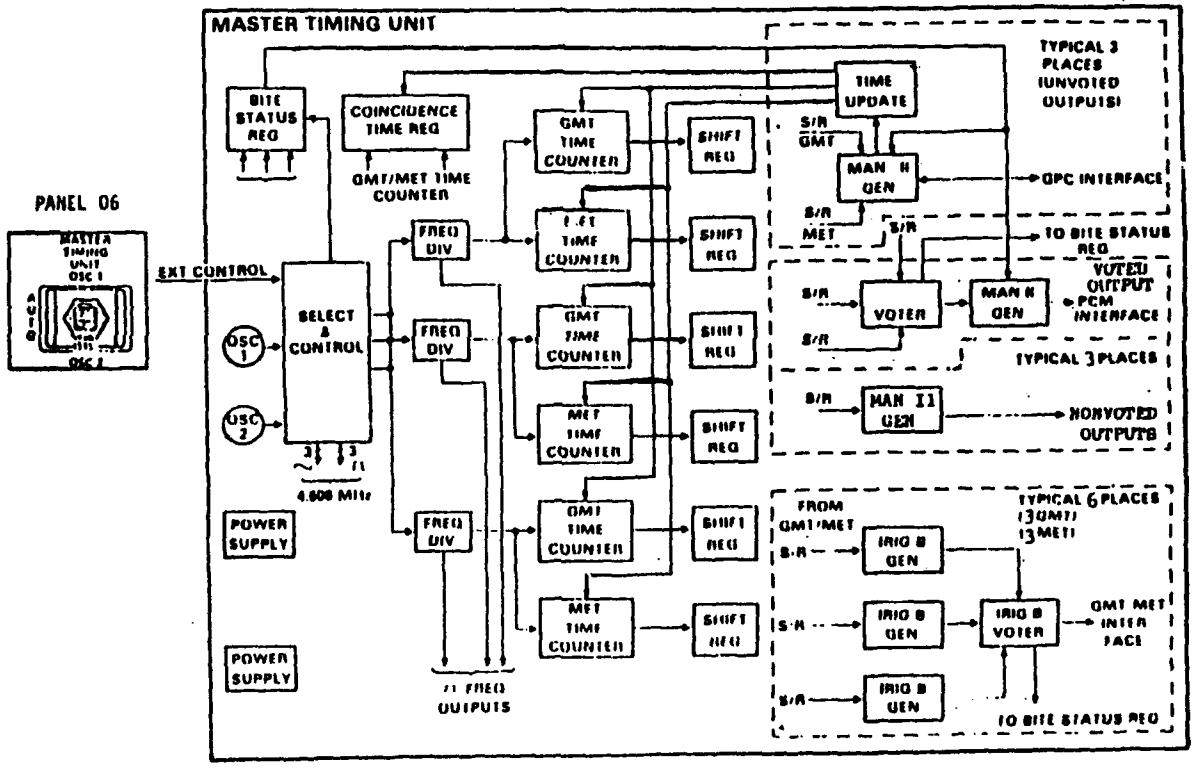

Figure 1. Space Shuttle Orbiter (SSO) Master Timing Unit (MTU)

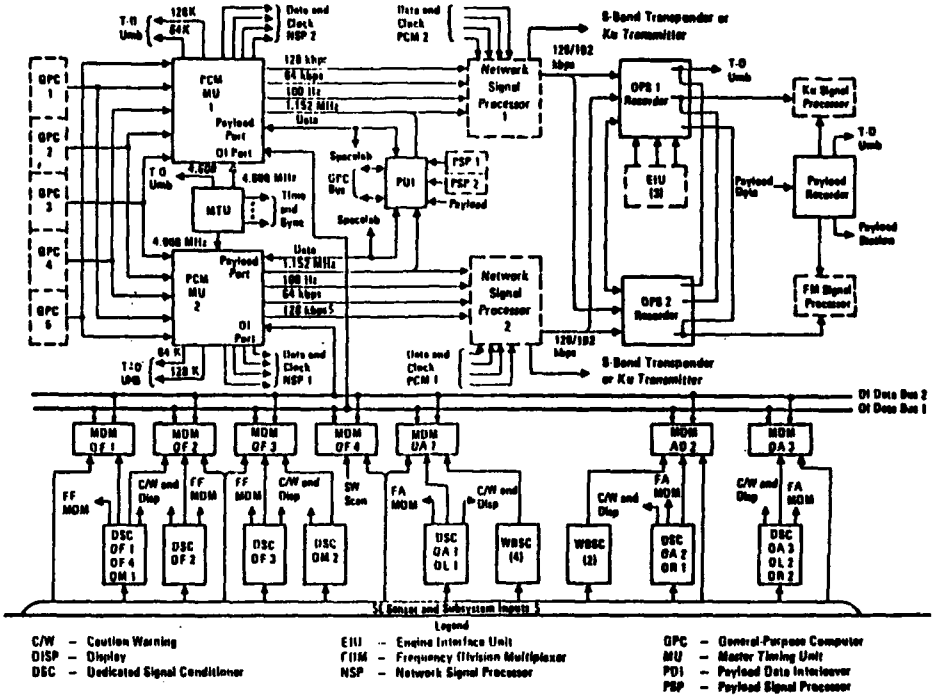

Figure 2. Time/Clock/Sync Inputs to Operational Instrumentation (OI)

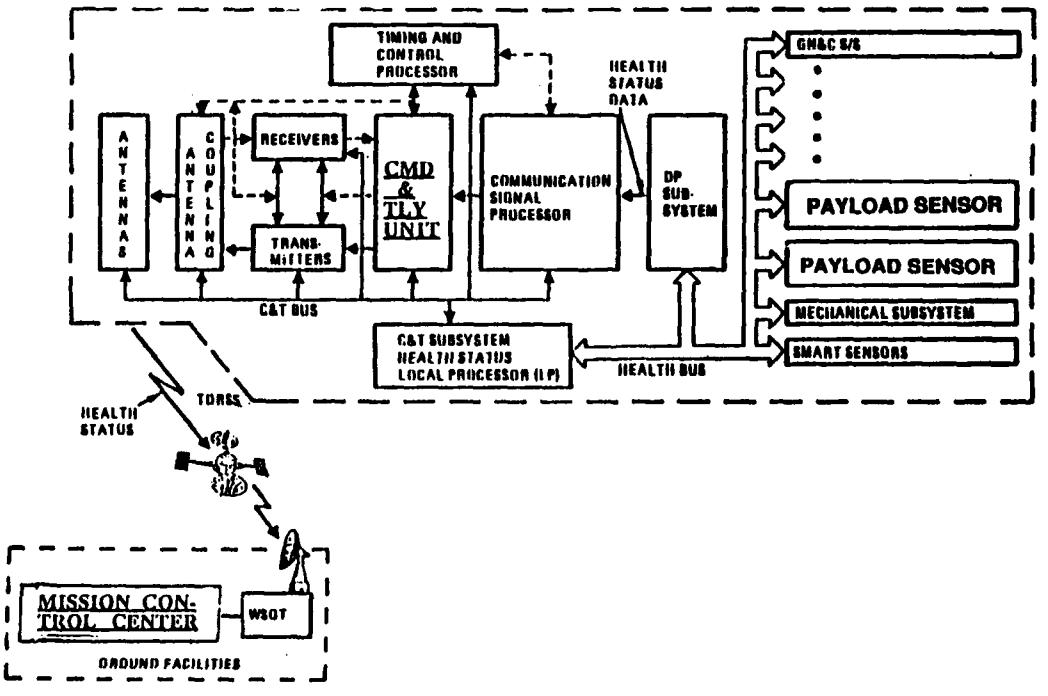

Figure 3. Timing and Control Processor Interface to Command & Telemetry Unit
(Partial Autonomy: Onboard Health Status Processor)

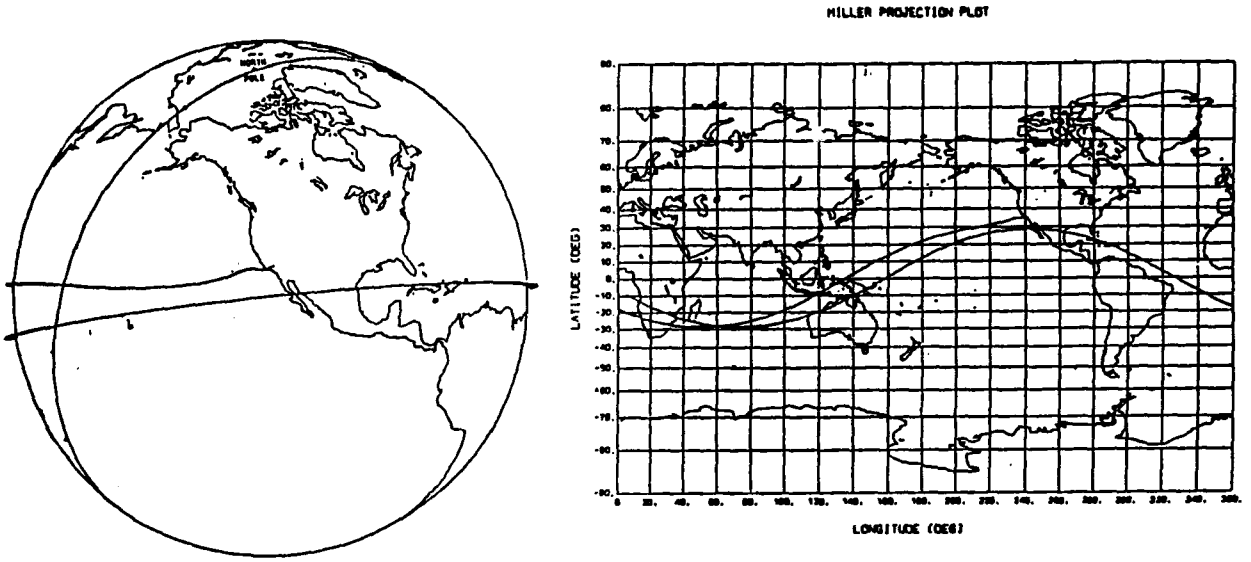

Figure 4. Space Shuttle GPS Developmental Flight Test (DFT) Profile: Orbit, Deorbit, and Entry

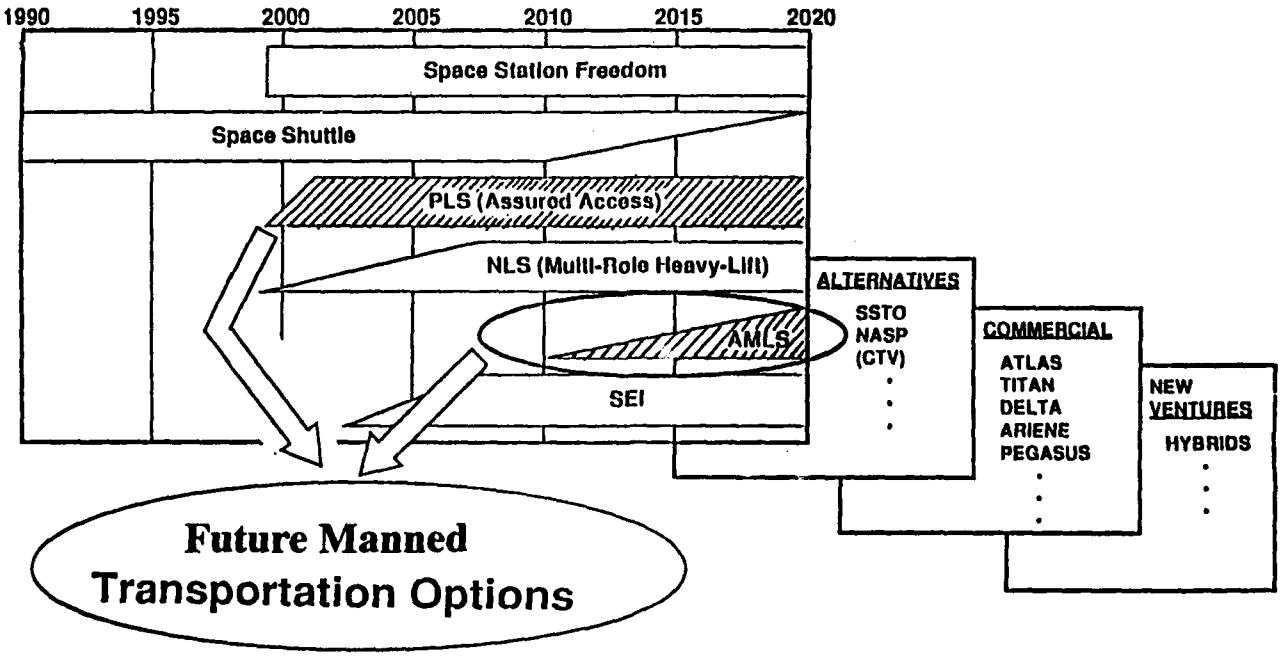

Figure 5. Role of AMLS & PLS in the Future Manned Space Transportation System

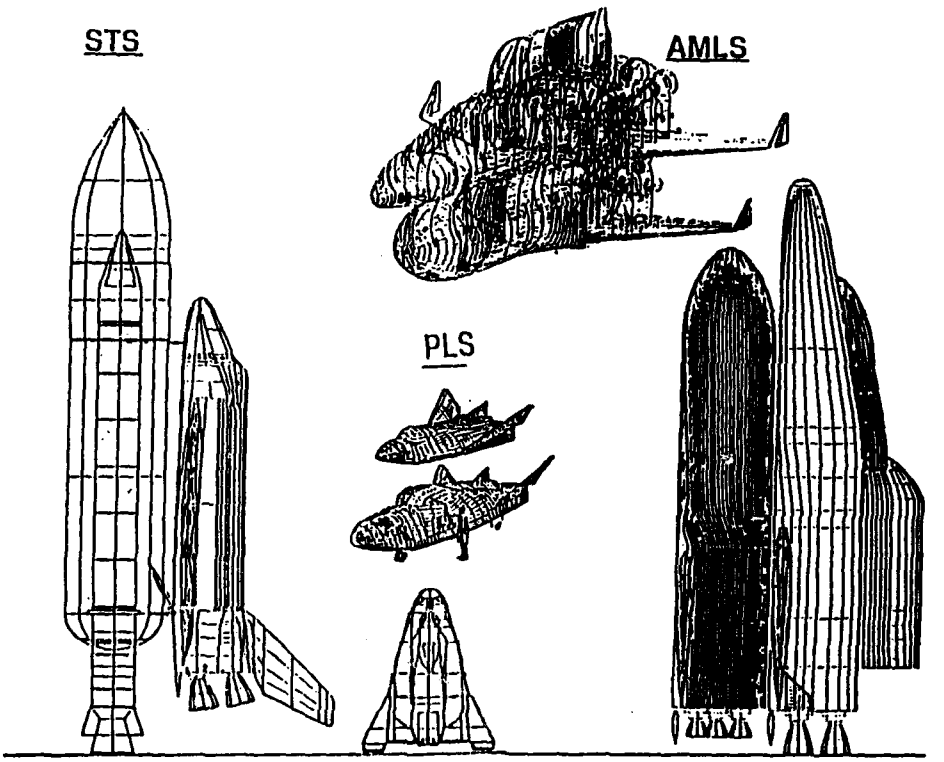

Figure 6. Relative Sizes of STS, AMLS, and PLS

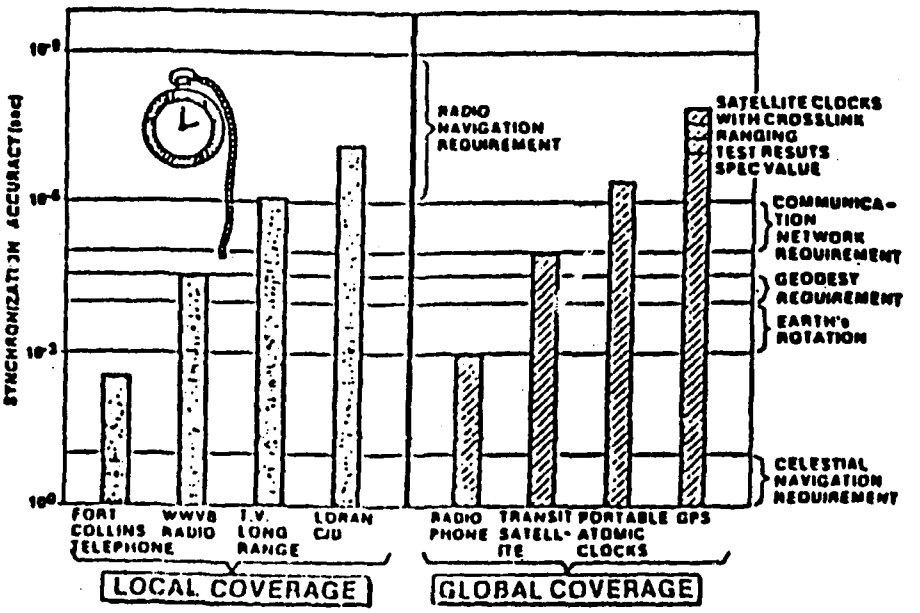

Figure 7. Time Synchronization Capabilities of Various Systems

	ERROR SOURCE	C/A CODE		P CODE	
		RAW MEASUREMENTS (ns)	SMOOTHED MEASUREMENTS (ns)	RAW MEASUREMENTS (ns)	SMOOTHED MEASUREMENTS (ns)
SPACE	CLOCK AND NAV SUB-SYSTEM STABILITY	0	0	0	0
	PREDICTABILITY OF SATELLITE PERTUBATIONS	0	0	0	0
	OTHER	0	0	0	0
CONTROL	EPHEMERIS PREDICTION MODEL IMPLEMENTATION	0	0	0	0
	OTHER	0	0	0	0
USER	IONOSPHERIC DELAY	0-30	0-30	0-7	0-7
	TROPOSPHERIC DELAY	0.6	0.6	0.6	0.6
	RCVR NOISE	32	5	6	1
	MULTIPATH	5	5	5	5
	OTHER	2	2	2	2
	POSITION ERROR	71	71	34	34
TOTAL ERROR	POSITION UNKNOWN	78.1-83.8	77.6-83.5	34.5-36.1	34.4-35.6
	POSITION KNOWN	32.4-44.6	7.3-31.5	8.1-12.2	5.5-10.7

COMPONENT	ERROR (ns) (1σ)
US NAVAL OBSERVATORY MEASUREMENT COMPONENT	70
CONTROL SEGMENT COMPONENT	30
GPS TIME PREDICTABILITY	47
NAVIGATION MESSAGE QUANTIZATION	3
SATELLITE ORBIT	11
SATELLITE CLOCK	32
SATELLITE GROUP DELAY	6
DOWNLINK AND USER EQUIPMENT	33
TOTAL (RSS) TIME TRANSFER ERROR BUDGET	103

Table 1b. GPS System Error Budget (Factor of 6, the Estimated Reduction of Receiver Noise Factor due to Smoothed Measurements was used)

Table 1. Coordinated Time Transfer Using GPS

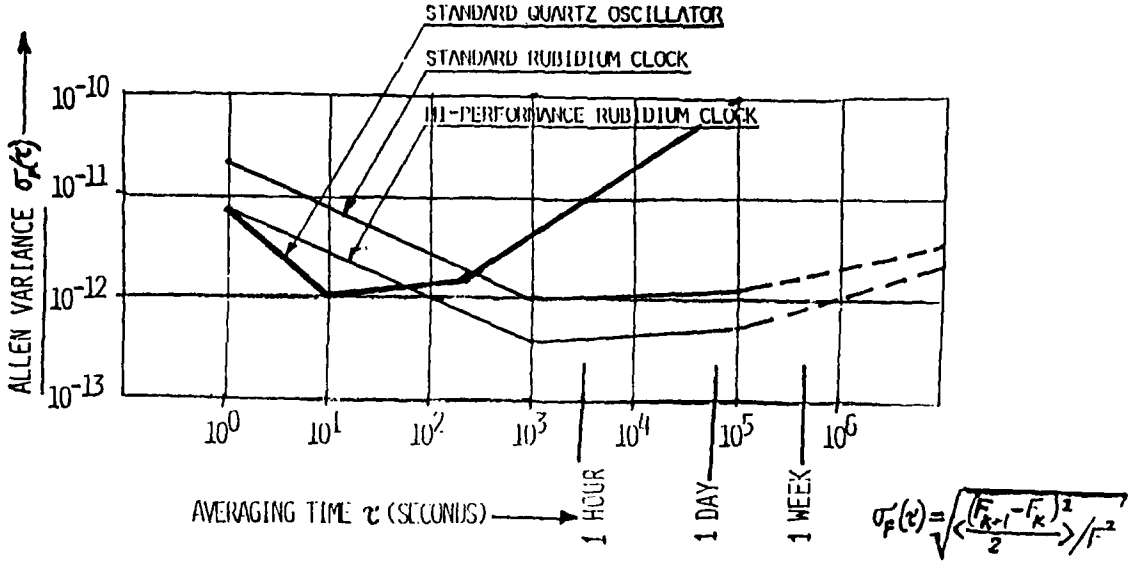

Figure 8. Comparison of Quartz Crystal Oscillator & Rubidium Clock Frequency Stability

DEFINITION: SYNCHRONIZATION IS THE PROCESS OF ALIGNING THE TIME SCALES BETWEEN TWO OR MORE PERIODIC PROCESSES THAT ARE OCCURRING AT SPATIALLY SEPARATED POINTS

1 CARRIER SYNC - REQUIRED FOR OPERATION OF PHASE-COHERENT DEMODULATOR. THE LOCAL CARRIER REFERENCE MUST AGREE CLOSELY IN FREQUENCY & PHASE WITH THE RECEIVED SIGNAL

2 CLOCK SYNC - EFFICIENT DATA DETECTION REQUIRES THAT THE RECEIVER KNOWS WHEN ONE DATA SYMBOL ENDS AND THE NEXT ONE BEGINS. A LOCAL CLOCK IS REQUIRED THAT IS ACCURATELY TIME-ALIGNED WITH RECEIVED PULSES

3 CODE SYNC - THE DECODER CANNOT OPERATE UNLESS THE RECOVERED SYMBOLS CAN BE SEPARATED INTO THE PROPER GROUPS. WITH CONVOLUTIONAL CODES, DECODER MUST ACHIEVE AND MAINTAIN NODE SYNC.

WITH BLOCK CODES, DECODER MUST ACHIEVE AND MAINTAIN WORD SYNC. WITH TIME DIVISION MUTIPLEX, THE DATA REGENERATOR MUST BE IN SYNC WITH DATA SAMPLES (FRAME SYNC).

4 NETWORK SYNC - REQUIRED IF DIGITAL DATA ARE RECEIVED FROM SEVERAL SOURCES, PROCESSED, AND RETRANSMITTED TO ONE OR MORE USERS THRU SWITCHES.

Figure 9. Types of Synchronization

SYSTEM PARAMETER	QUARTZ CRYSTAL OSCILLATOR	RUBIDIUM CLOCK
PRIMARY/SECONDARY STANDARD	NO	SECONDARY 6,834,682,613GHZ
FUNDAMENTAL WEAROUT MECHANISM	BASICALLY NONE	BASICALLY NONE
MAINTENANCE	BASICALLY NONE	BASICALLY NONE
PORTABILITY	VERY PORTABLE	VERY PORTABLE
APPLICATION	SPACE-AIR-GROUND	SPACE-AIR-GROUND
APPROXIMATE SIZE WEIGHT POWER COST	3" x 3" x 3" 1-2 LBS 2-5 WATTS $1.5K-4K	3" x 3" x 4.5" 2-4 LBS 10-18 WATTS $4K-$8K
SHORT TERM STABILITY TAU (τ) = 1 SECOND	$\sim 1 \times 10^{-11}/10^{-12}$	$\sim 1 \times 10^{-11}$
STABILITY (ALLEN VAR) $\sigma_F(\tau)_{AT\ 1\ DAY}$	$\sim 1 \times 10^{-10}$	$\sim 1 \times 10^{-12}/10^{-13}$
DRIFT/DAY	$\sim 1 \times 10^{10}$	$\sim 1 \times 10^{-12}/10^{-13}$
DRIFT/YEAR	$\sim 1 \times 10^{-7}$	PARTS IN 10^{10}
RETRACE	$\sim 1 \times 10^{-9}$	$\sim 1 \times 10^{-11}$
WARM-UP TIME TO PARTS IN 10^{10}	HOURS	< 2 MIN TO PARTS IN 10^{10}

Table 2. Comparison of Quartz Crystal Oscillator & Rubidium Clock System Parameters

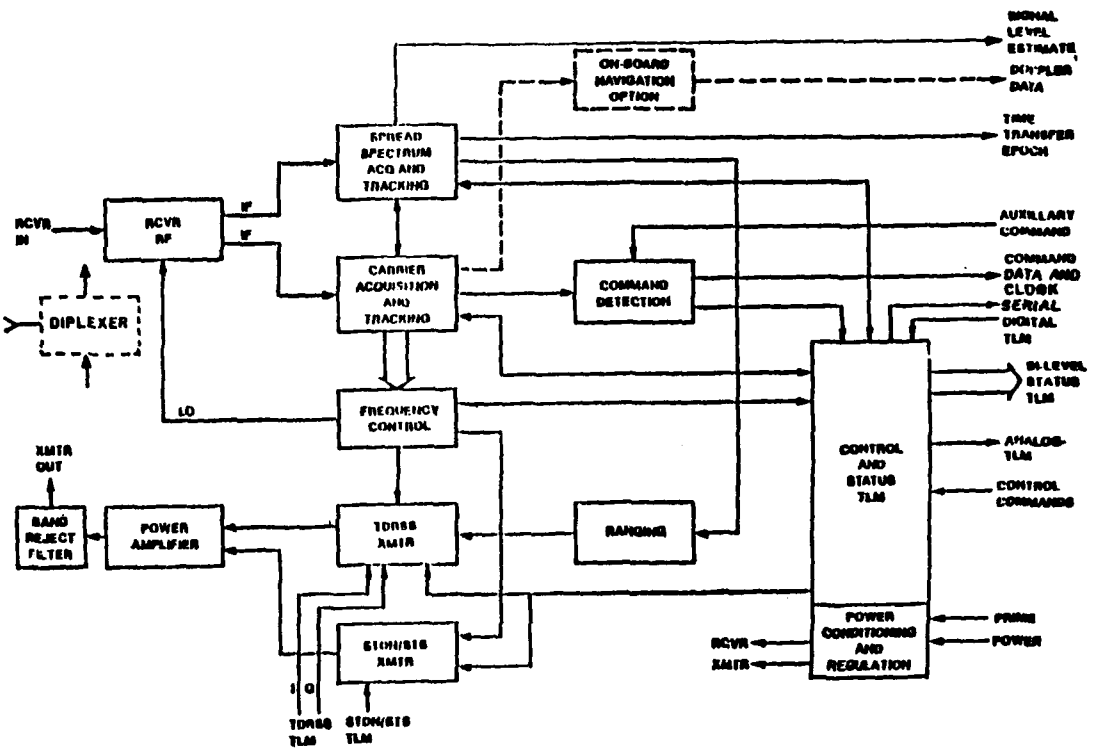

Figure 10. TDRSS User Transponder Functional Block Diagram

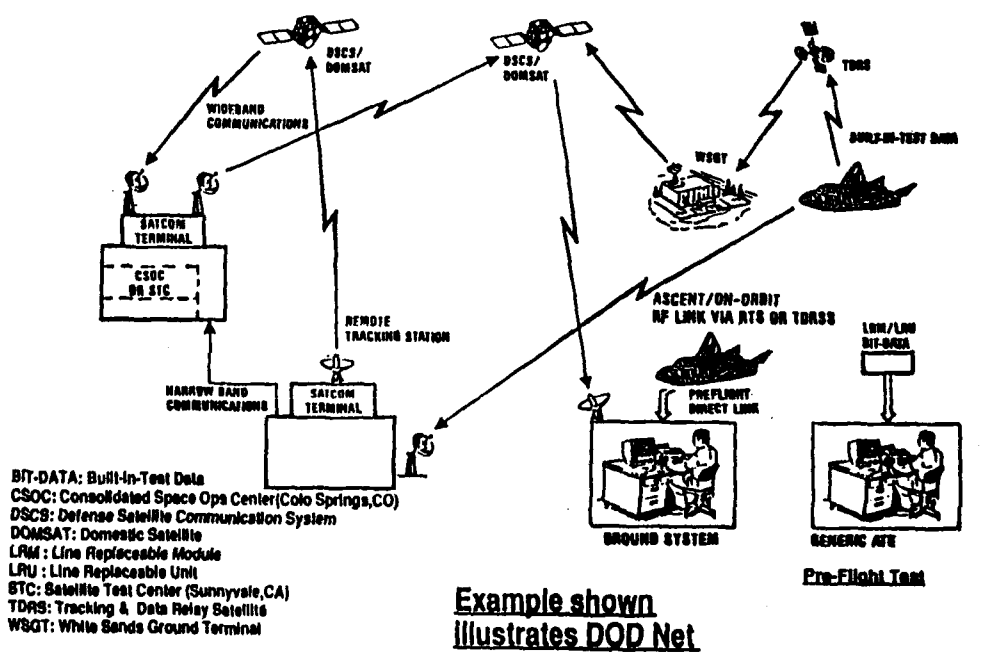

Example shown illustrates DOD Net

Figure 11. Universal GPS Time Reference Usage Will Aid Communications Synchronization

QUESTIONS AND ANSWERS

R. Keating, USNO: It seems to me that tight integration of such complex systems can produce some rather adverse effects. For example, in the GPS system, if you have tight control you can mask relativistic effects. It seems to me with your system you are also creating a very grave danger of masking poorly understood physical effects - such as relativistic effects.

A. Anderman, Rockwell Space Systems Division: Basically I was trying to see to what extent such a platform could be used for various kinds of measurements. I mentioned for those type of measurements you probably could not ever have the right stability and constancy and so on. Plus the fact that even having personnel on board would provide certain amount of vibration and other noise effects. There are some areas which I did not get into on mapping other quantities where some very useful measurements might be performed.

UNDERWATER HYDROPHONE LOCATION SURVEY

Jack B. Cecil
Naval Undersea Warfare Center Detachment AUTEC
West Palm Beach, FL 33402–7517

INTRODUCTION

The Atlantic Undersea Test and Evaluation Center (AUTEC) is a U.S. Navy test range located on Andros Island, Bahamas, and a Division of the Naval Undersea Warfare Center (NUWC), Newport, RI. The Headquarters of AUTEC is located at a facility in West Palm Beach, FL.

AUTEC's primarily mission is to provide the U.S. Navy with a deep–water test and evaluation facility for making underwater acoustic measurements, testing and calibrating sonars, and providing accurate underwater, surface, and in–air tracking data on surface ships, submarines, aircraft, and weapon systems. Many of these programs are in support of Antisubmarine Warfare (ASW), undersea research and development programs, and Fleet assessment and operational readiness trials. Most tests conducted at AUTEC require precise underwater tracking (plus or minus 3 yards) of multiple acoustic signals emitted with the correct waveshape and repetition criteria from either a surface craft or underwater vehicle.

BACKGROUND

At AUTEC, there are two separate underwater tracking ranges located in the Tongue–of–the–Ocean (TOTO) and adjacent to Andros Island, Bahamas. A combination of the narrow shoreline shelf and a deep (5,000 feet) body of water isolated from the open ocean by shallow reef boundaries makes these areas ideal for acoustic analysis, detection, and tracking. Both tracking areas are instrumented with several underwater bottom–mounted hydrophones cabled directly to shore facilities where signal processing and recording equipment are located. The processed data are transmitted by microwave communications to the Main Base facility where computers process and format the data for delivery to range users and display the data for conduct of the test by range personnel.

From January to September 1992, the norther underwater tracking area, instrumented with seven hydrophones spaced at 2,000 yard intervals and in a circular pattern with six on the outer perimeter and one in the center, was enlarged with the addition of seven new hydrophones, two underwater communications transducers, and additional data processing and interfacing hardware. The expansion effort nearly doubled the tracking area for this portion of the AUTEC range from 50 to almost 100 nautical miles and significantly increased AUTEC's data collection capability. Before

this additional area could be integrated and used as part of the operational tracking area, however, a survey was required to establish the precise location of each hydrophone where it had been placed on the floor of the ocean. Average depth of the water in this area of the TOT is 6,000 feet. This paper attempts to give the reader a brief overview of how this survey was accomplished using the Global Positioning System as the Timing source for the emission of tracking source signals, but does not detail the mathematical formulas used to calculate the actual hydrophone positions.

METHOD

The Site One Expansion (SOE) survey processing of received hydrophone signals used a least–squares version of the Vanderkulk mathematical method, developed by Wouter Vanderkulk of International Business Machines (IBM). In this method, propagation delay or "transit" times of the transmitted signal from the source transducer to the bottom–mounted hydrophone were processed to yield baselines and depths for triads (or larger subsets) of hydrophones which were then combined in a least–squares sense to yield a relative set of X, Y coordinates of the hydrophone filed (see Figure 1). This relative set of coordinates was then related, translated, and scaled to optimize agreement (while maintaining the integrity of the Vanderkulk interrelationships) with an independent set of geodetic coordinates that were gathered simultaneously with the acoustic data.

For this survey, the independent set of geodetic reference points (know source locations) was provided by a shore–based, high precision tracking radar that tracked the surface craft. This surface craft, instrumented with a radar beacon, was used as the platform from which the underwater tracking signals or "pings" from a hull–mounted transducer (pinger) were emitted. A parallax offset was used to correct for X and Y positional differences between the radar beacon and the pinger.

Transit times for the Vanderkulk processing were derived from hydrophone arrival times that had been corrected for delays; namely, synchronous pinger emission offset, hydrophone cable delay, and all associated signal processor delays. In the SOE survey, the ping generation delay was compensated for by using a GPS Timing receiver to synchronize an on–board Time Code Generator (TCG) to within 300 nanoseconds of Universal Coordinated Time (UTC). Simultaneously, the shore–based signal processors, used to detect and time tag the pings received from all hydrophones, were clocked from the Central timing facility, also synchronized to within 300 nanoseconds of UTC. Delays in the ping generation hardware were removed by utilizing the propagation delay compensation circuitry in the TCG. The disciplined oscillator (5 MHz) of the GPS receiver was used to clock the TCG and maintain on–time performance. A diagram showing the equipment configuration on–board the surface craft is shown in Figure 2.

Accurate synchronization of the acoustic pinger was of significant importance for this survey because a bias of this nature will go undetected when using the Vanderkulk processing technique, thereby causing a bias error in the mathematical solutions that will manifest itself in the hydrophone depths and the scale factor of the hydrophone filed. An offset of this nature will also manifest itself as a scale factor in the process of mapping the Vanderkulk coordinates into the independent reference coordinates because the collected radar tracking data are also time tagged to the Central Timing System clock.

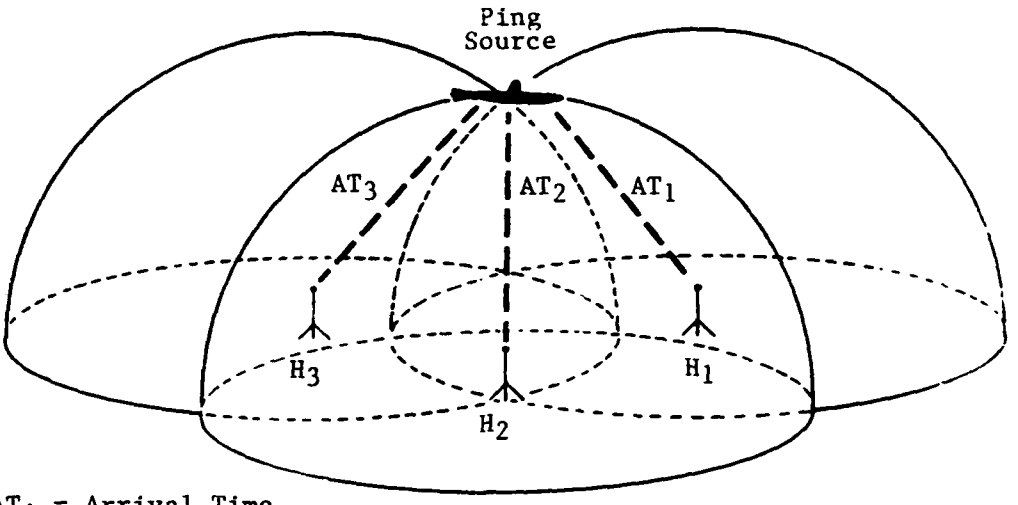

AT_i = Arrival Time

H_i = Hydrophone

FIGURE 1. ARRIVAL TIME DIAGRAM

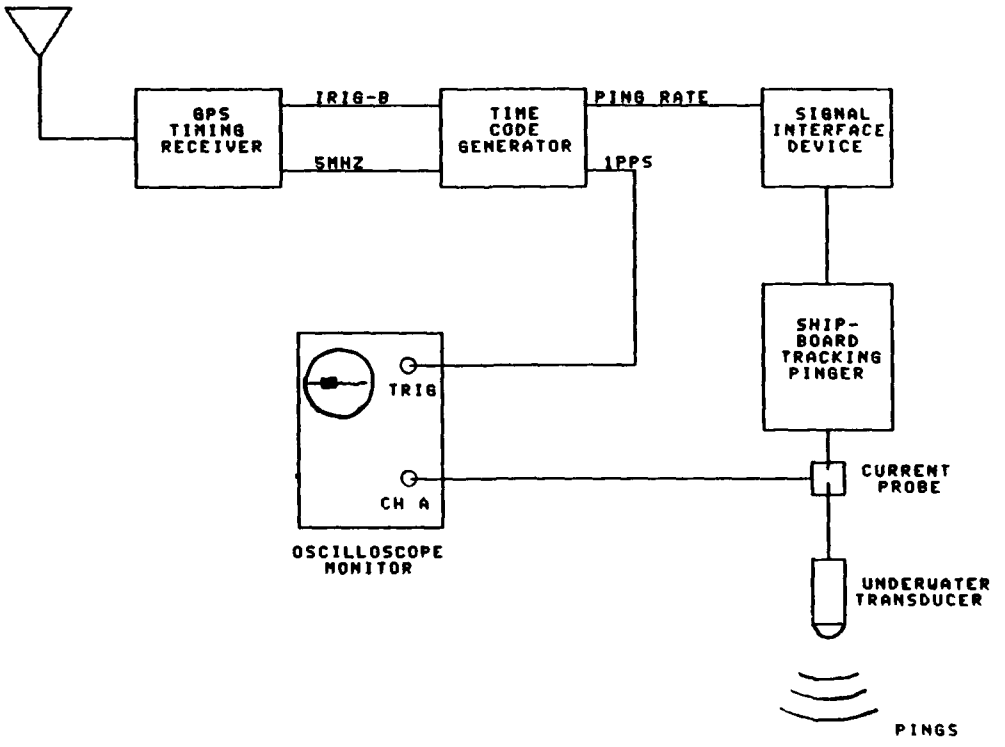

QUESTIONS AND ANSWERS

J. Wisnia, Kernco: I am rather naive on underwater sound but doesn't the speed of sound depend on the temperature of the water and what did you do to account for that?

J. Cecil, Naval Undersea Warfare Center: We take frequent sound velocity profile measurements. We have capability of going down to the full depth and we incorporate that into the data in the software. So there are lots of things that I did not mention, that I did not go into, that are also a part of this formula and part of doing this task. We do consider that as one of the important things that we crank into the software. There are other things like processor delay, that are also injected in there. They are really constants and we do that on a typical basis with our other hydrophones. I tried to emphasize the things we did differently for this exercise because of the survey of surveying these hydrophones in. For the normal tracking that we do at AUTEC, we use a hyperbolic formula and we use four hydrophones per track because the pinger is asynchronous. It is not synchronized to any particular device and we do derive the time with four hydrophones.

D. Allan, Allan Time: Perhaps two comments or questions, one is like GPS why couldn't you use four instead of 3 and have the solution from the four.

J. Cecil: Well because it reduced the amount of processing time and it reduced the complexity of the software involved. Four is just another unknown that you are throwing in there that we would rather not have in the surveying process. Because we do not, we use the hyperbolic method typically when we track on our existing known hydrophones. When we resurvey, we usually use a synchronous pinger. This is really the first time that we used this Vanderkulk technique - this Vanderkulk method. We think we are going to get a significant improvement over the other survey results; and we may. One of the things we are considering is going back over all of our other hydrophones now and surveying all of those in with the same technique. It was just something that we did not want to deal with; the resolution of time in this instance.

D. Allan: The second question: It seems like you could also put the other hardware delay solution into the software like you did with the temperature variations, etc. I was pleased to hear that, very often, these things can be dealt with in the software and get a lot more flexibility, rather than make a hardware solution. In the case you showed you had a hardware solution to a delay problem and that could also be put in the software, I believe, could it not?

J. Cecil: Yes it could. One of the things we wanted to be able to accomplish here was stability. With the stability of the on-board clock to keep in synchronization during the entire exercise because when we go out and survey the hydrophones, we did not survey just three hydrophones, we surveyed seven hydrophones; seven new hydrophones. It took us a period of 12 to 14 hours to complete this survey because the geodetic data that this survey was fitted in with was accomplished through radar track. Precision air tracking radars were tracking the vessels simultaneously; so what I was after was some stability over a long period of time, say over 12 hours. The time code generators that we typically have at AUTEC will not give us that kind of stability. When you can go out and do a pretest measurement and then turn around and do a post test measurement, but that does not tell you what the clock was doing in between. The clock could have been doing this in between; so this gives us a feeling of clock stability.

P. Talley; The Aerospace Corporation: I have a comment regarding this paper, and that I personally was involved in 1959 on the early testing of the Polaris Missile System and we were firing into the hydrophone and we found that the islands were misplaced by over a mile and that the hydrophones had been referenced to the land mass. The inertial guidance of the

Polaris Missiles recalibrated the hydrophone net. That was interesting that GPS is now helping to calibrate the hydrophone net a little further.

J. Cecil: Yes, it is the only constraint here is the fact that have to have a radar fix on the vessel all the time we are going through this exercise. So, if you get into remote areas around the globe you do not have that. Because we have our radar, our existing in air tracking radars, we could tie the data and correlate this data, it made things a lot easier.

A Laser–cooled Cesium Fountain Frequency Standard and a Measurement of the Frequency Shift due to Ultra–cold Collisions

Kurt Gibble, Steven Kasapi, and Steven Chu
Physics Department
Stanford University
Stanford, California 94305-4060

Abstract

A frequency standard based on an atomic fountain of cesium atoms may have an accuracy of 10^{-16} due to longer interaction times and smaller anticipated systematic errors. All of the known systematic effects that now limit the accuracy of the Cs frequency standard increase either linearly or as some higher power of the atom's velocity. The one systematic frequency shift which is dramatically different is the frequency shift due to the collisions between the laser cooled atoms. At a temperature of a few μK, the de Broglie wavelength ($\lambda_{deB} = h/p$, where h is Planck's constant and p is the momentum of the atom) is much larger than the scale of the interatomic potential. Under these conditions the collision cross sections can be as large as λ_{deB}^2/π and the frequency shift due to these collisions has been recently calculated[1].

In our Cs atomic fountain, we laser cooled and trapped 10^{10} Cs atoms in 0.4 s[2]. By shifting the frequencies of the laser beams, the atoms were launched upwards at 2.5 m/s and a fraction of the atoms were optically pumped into the F=3 ground state. The unwanted atoms in the F=4 ground state were removed from the fountain with radiation pressure from a laser beam tuned to excite only those atoms. The Cs atoms in the F=3 state traveled ballistically upwards, were excited by the microwave cavity, and then returned back through the same cavity in the atomic fountain configuration[3].

By varying the cold atom density, we measured a density dependent shift of -12.9 $\pm$ 0.7 mHz or -1.4 $\times$ 10–12 for an average fountain density of (2.7 $\pm$ 1.5) 10^9 atoms/cm^3. This measurementwas made with uniformly populated Zeeman sublevels, while only the atoms in the m_F=0 sublevel contributed to the signal. We also made frequency measurements where the atoms in the F=3 $m_F \neq 0$ states were removed since those atoms do not add to the signal but contribute to the frequency shift. A 97% pure m_F=0 state was made in the following way: after cooling the atoms in optical molasses, they are in the F=4 hyperfine level. Atoms from the F=4 m^F=0 state were then transferred to the F=3 m^F=0 state with microwave radiation and the remaining F=4 atoms

in the other Zeeman sublevels were again pushed out of the way with radiation pressure. By varying the number of atoms transferred to the F=3 m_F=0 state, we determined the frequency shift due to the collisions between atoms in the m^F=0 states as a function of density. At a density of $(3.5 \pm 2.0)\times 10^8$ cm^{-3} (where the signal size is comparable), we measured a shift of -5.5 ± 0.5 mHz.

The extrapolation of the frequency shift to zero density is reproducible with an uncertainty of 4×10^{-14} and can be improved, indicating that it may be possible to control the cold atom density at the 0.1% level and to continuously evaluate the shift at this level.

1. E. Tiesinga, B. J. Verhaar, H. T. C. Stoof, and D. van Bragt, Phys. Rev. A 45, (1992).
2. K. E. Gibble, S. Kasapi, and S. Chu, Opt. Lett. 17, 526 (1992).
3. M. A. Kasevich, E. Riis, S. Chu, and R. G. DeVoe, Phys. Rev. Lett. 63, 612 (1989); A. Clairon, C. Salomon, S. Guellati, and W. D. Phillips, Europhys. Lett. 16, 165 (1991).

QUESTIONS AND ANSWERS

Question: You mentioned that density of the atoms is going to have pulling effects. Is it ultimately going to be a stability limitation as well?

K. Gibble, Stanford University: At the moment it looks like we can control the density and is in a sense automatically controlled by the laser cooling to an accuracy of about 1%. That is what we see at the moment. It might in fact be better than that. Clearly, much more evaluation needs to be done but we are encouraged at this point to see where it will go.

DISCIPLINED RUBIDIUM OSCILLATOR WITH GPS SELECTIVE AVAILABILITY

Wayne P. Dewey
TrueTime, Inc.
3243 Santa Rosa Avenue
Santa Rosa, California 95407

Abstract

A U.S. Department of Defense decision for continuous implementation of GPS Selective Availability (S/A) has made it necessary to modify Rubidium oscillator disciplining methods. One such method for reducing the effects of S/A on the oscillator disciplining process has been developed which achieves results approaching pre-S/A GPS.

This paper describes the Satellite Hopping algorithm used in minimizing the effects of S/A on the oscillator disciplining process, and compares the results of using this process to those obtained prior to the implementation of S/A. Test results are from a TrueTime Rubidium based Model GPS-DC timing receiver.

INTRODUCTION

Our goal in the disciplining process is to maintain a frequency accuracy of better than 10^{-11} at all times and to do this with a minimal effect on oscillator stability. In disciplining the Rubidium oscillator, the philosophy is one of limited intervention. During normal operation, the Rubidium oscillator is sampled and adjusted once per day. This technique takes full advantage the Rubidium oscillator's short term stability, correcting only for frequency errors accumulated during the one day period.

Prior to the implementation of S/A, each daily frequency sample was 16 minutes 40 seconds in duration. The results were good as the Rubidium oscillator remained well within the 10^{-11} design limit, with an average frequency error of 3×10^{-12} and an Allan Deviation of 2.5×10^{-12} at a τ of 1 day[1]. When S/A was was implemented, however, the disciplining algorithm included the S/A term in the Rubidium control solution and misadjusted the oscillator. In an attempt to correct the apparent Rubidium oscillator frequency error, the disciplining algorithm reduced the control period, allowing multiple samples per day which only exacerbated the errors. Rubidium oscillator performance was degraded by almost an order of magnitude.

S/A was also degrading the time transfer accuracy of the GPS-DC (GPS-Digital Clock) in which the disciplined Rubidium oscillator is installed. A method was needed that would reduce the effects of S/A on the disciplining process and the time transfer process as well.

SELECTIVE AVAILABILITY

At current levels, satellites with S/A enabled show typical time transfer errors of ±200 nanoseconds, occasionally peaking to ±350 nanoseconds.

Figures 1 and 2 show typical time transfer stability of two satellites, one with S/A applied and one without. Both satellites are referenced to the Rubidium Oscillator. The satellite with S/A shows peak to peak timing variations of more than 400 nanoseconds over the 2 hour period, while the satellite without S/A applied has normally less than 70 nsec.

Figure 3 compares the Allan Deviation of both satellites (the SatHop plot is discussed later). The difference in time transfer stability over 10 to 50,000 seconds in this graph shows a four times degradation in stability at current S/A levels.

SATELLITE HOPPING

A Satellite Hopping (SatHop) Algorithm has been developed to reduce the effects of S/A on time transfer and frequency disciplining processes. Satellite hopping takes advantage of the fact that a timing receiver requires only one satellite for accurate time transfer. However, any one satellite can transfer a timing error of 300 nanoseconds or more for a random period of time. If several satellites are sampled sequencially and averaged into a composite satellite solution, the effects of the satellites with S/A should be reduced. Additionally, the satellites without S/A will tend to further reduce the errors caused by the satellites with S/A.

Figure 4 is a typical plot of the output directly from the GPS receiver during the Satllite hopping process. Timing solutions from satellites with S/A enabled can be seen mixed with those satellites without S/A. Note that the frequency of the S/A component in this composite satellite has been increased by the hopping period, making it easier to average.

The SatHop Algorithm has two components, a satellite seqeuncer and a solution averager. The sequencer scans the list of satellites currently being tracked and selects one satellite for the GPS receiver to use for timing solutions (user deselected and unhealthy satellites are skipped). As the GPS receiver can track up to seven satellites simultaneously, all visible satellites are normally on the list. After a dwell period of 30 seconds which generates 30 samples for the selected satellite, the next satellite in the sequence is selected. The sequencer continuously loops through the satellite list, which is updated by the GPS receiver as satellites rise and set.

The solution averager creates a composite satellite Clock Bias solution by averaging the phase solutions from all of the tracked satellites into a single 400 sample average. Clock Bias, in units of meters, represents the phase comparison between the Rubidium Oscillator and GPS and is described under System Hardware.

The output of the SatHop solution averager can be seen in Figure 5. This output is an averaged composite phase measurement between all tracked satellites and the Rubidium oscillator. The graph shows how quickly the effects of Selective Availability can be reduced. Averaging a single satellite with Selective Availability enabled will not produce these results. The Allan deviation of the SatHop solution averager can be seen in Figure 3. When tracking three or more satellites this plot tends towerds the non-S/A satellite plot.

SYSTEM HARDWARE

Referring to Photograph 1, the unit under test is a GPS Digital Clock with the Disciplined Rubidium option installed. Referring to Photograph 1, the GPS satellite receiver and Rubidium oscillator are both contained within the Clock, along with other clock electronics.

The oscillator being disciplined is an FRS–C Rubidum oscillator manufactured by Ball Corporation, Efratom Division. It is an integral component of the GPS–DC and is the clock's timebase (located in center of clock).

The GPS receiver is a TTM (Tans Timing Module), manufactured by Trimble Navigation(located in front center of clock). The receiver uses the Disciplined Rubidium oscillator as its' timebase when performing position and timing solutions. Thus, when the GPS receiver performs time transfer solutions, variations in the solution can be attributed to the Rubidium oscillator, Selective Availability, variations in GPS signal path, and system noise.

The variable the TTM uses to report the phase difference is Clock Bias, and has units of meters. Clock Bias os directly converted to seconds using the speed of light in free space ($3.335640952 \times 10^{-09}$ seconds/meter) as the conversion factor. Clock Bias has a usable resolution of a few nanoseconds.

THE DISCIPLINING PROCESS

The disciplining algorithm is a variable period frequency locked loop which controls the Rubidium for zero frequency error. The disciplining algorithm adjusts the Rubidium once each control period. At the end of a control period, a 4000 sample average of Clock Bias is taken (ten sample averages from the SatHop solution averager). Used in conjunction with a previous control period sample, a frequency error is calculated and an adjustment is made to the Rubidium C–field control voltage using a 16–bit D/A converter.

The disciplining algorithm also contains a control period calculator. This calculator is designed to determine the shortest possible control period allowable for an accurate frequency measurement at the current Rubidium oscillator frequency error. The control period is calculated using a simple hyperbolic curve:

$$\text{(Control Loop Period)} = \text{K}/\text{(Rubidium Frequency Error)}$$

where K is a constant calculated to ensure S/A does not impact the required measurement accuracy. The control loop period is limited to minimum and maximum period values. The minimum control period limit is calculated to satisfy the allowable worst case oscillator accuracy, and is currently set at 6000 seconds. The maximum period value is set at 86400 seconds. This one day period is desirable as it allows for cancellation of most daily variances, including those due to daily temperature variations. Once an oscillator has reached the maximum control loop period it tends to remain there unless the oscillator is disturbed.

A hardware temperature compensation circuit reduces the temperature sensitivity of the Rubidium. This circuit measures the temperature of the Rubidium oscillator baseplate and sums a temperature

correction voltage into the Rubidium oscillator C-field adjust input as a feed-forward term. The gain of the temperature compensation circuit is characterized for each Rubidium oscillator. The circuit removes a substantial portion of the temperature sensitivity of the Rubidium oscillator. The temperature sensitivity of the Rubidium oscillator in this test was reduced to better than 2.0×10^{-12} per degree Centigrade.

TEST RESULTS AND CONCLUSIONS

Data taken during the months of August and October 1992 consists of:

- Clock Bias directly from the GPS receiver as it sequenced through the visible satellites,
- Phase measured between the Rubidium 1 PPS and a Cesium 1PPS
- Cesium 1PPS compared to the GPS-DC 1PPS.

The Rubidium remained within $+5.5 \times 10^{-12}$ and -6.8×10^{-12} with variances due to temperature, the Disciplining algorithm, and the Rubidium oscillator frequency stability.

Figure 6 is an Allan Deviation plot of the Rubidium 1 PPS compared to the Cesium 1PPS. The plot shows a degredation in stability at 100,000 seconds which is caused by daily disciplining algorithm adjustments and by daily temperature variations.

The peak frequency error of the Rubidium oscillator during the testing period, assuming all errors belong to the Rubidium, was -6.8×10^{-12} during a 6 degree Centigrade ambient transient. Test performed using the frequency locked loop prior to the advent of Selective Availability (June of 1989) resulted in a value of 2.2×10^{-12}.[1] Note that the temperature did not vary by more than 2 degrees C during the June 1989 test. Also included are results of a test performed in August of 1992. the August and October tests used the same equipment but in different locations. The June 1989 test was performed prior to S/A and is included here for comparison.

Disciplined Rubidium Oscillator Frequency Accuracy

TEST DATE	S/A ENABLED	PEAK FREQ ERROR	FREQUENCY STABILITY @ 1 DAY	PEAK TEMPERATURE VARIATION, DEGREES C
OCTOBER 1992	YES	-6.8×10^{-12}	2.51×10^{-12}	7
AUGUST 1992	YES	5.6×10^{-12}	—	5
JUNE 1989	NO	3.0×10^{-12}	2.5×10^{-12}	2

The stability of the disciplined Rubidium oscillator in an S/A environment are approaching the pre-S/A results. The temperature variations in the tests are once again the predominant variable in the disciplining process.

Improving Rubidium oscillator temperature compensation and/or controlling the temperature of the oscillator baseplate is necessarily the next step in the disciplining process. Improving temper-

ature performance will reduce the peak frequency errors and improve the frequency stability over the 1/2 to 2 day region.

It is interesting to note that the Rubidium Oscillator used in the GPS–DC exhibits a thermal hysteresis on the order of 1×10^{-12} to 3×10^{-12} such that the frequency at a specific temperature will be different depending upon which direction in temperature the final temperature was approached.

The June, 1989 test was performed at a facility with an environmentally controlled labortory.

The August, 1992 test was performed in the TrueTime Engineering offices where the office temperature is controlled by a wall thermostat which was set for the range of 69–71 degrees F.

The October, 1992 test was performed inside an environmental chamber in order to minimize temperature effects on the test. The chamber failed during the test, allowing variations in temperature larger than either previous test. The worst of the failed temperature controller data occurred during the final week of the test and was subsequently truncated.

The GPS Digital Clock 1 PPS output corrects for the accumulated time error of the Rubidium Oscillator and does not pass it on to the user.

References

[1.] Dewey, W.P., *"A GPS Disciplined Rubidium Clock"*, Proc. of the 21st Annual Precise Time and Time Interval (PTTI) Application and Planning Meeting. Washington D.C., (November 1989), 149-160.

SELECTIVE AVAILABILITY TIME ERROR PLOT
SATELLITE WITH S/A

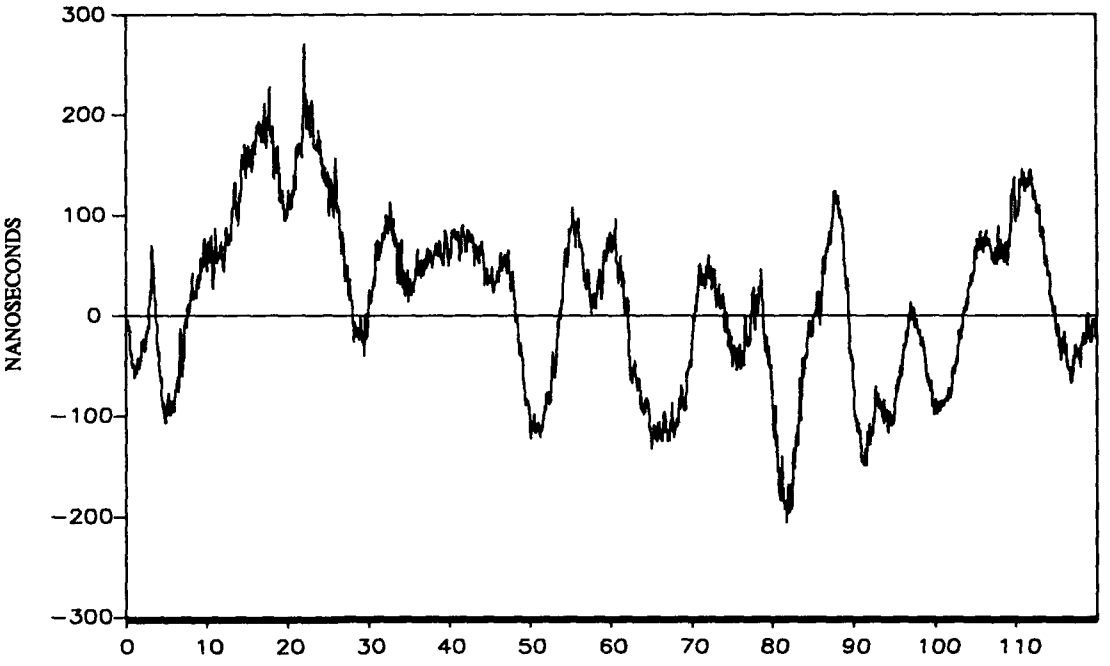

FIGURE 1

SELECTIVE AVAILABILITY TIME ERROR PLOT
SATELLITE WITHOUT S/A

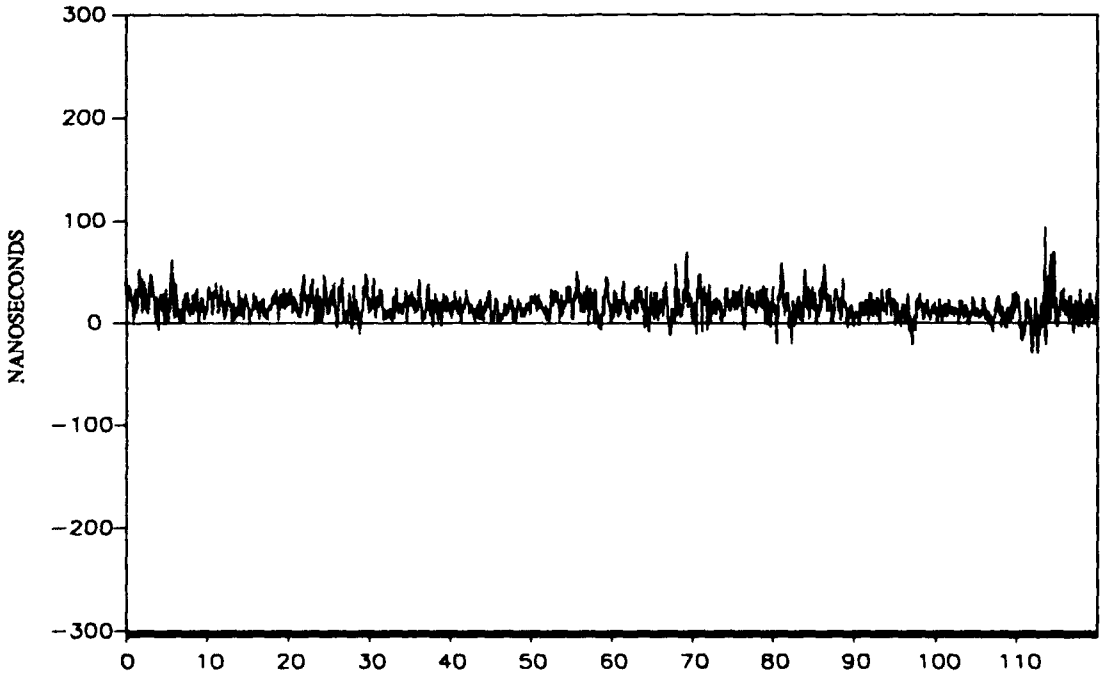

FIGURE 2

SAT WITH S/A, SAT W/O S/A, & SATHOP
LOG ALLAN DEVIATION

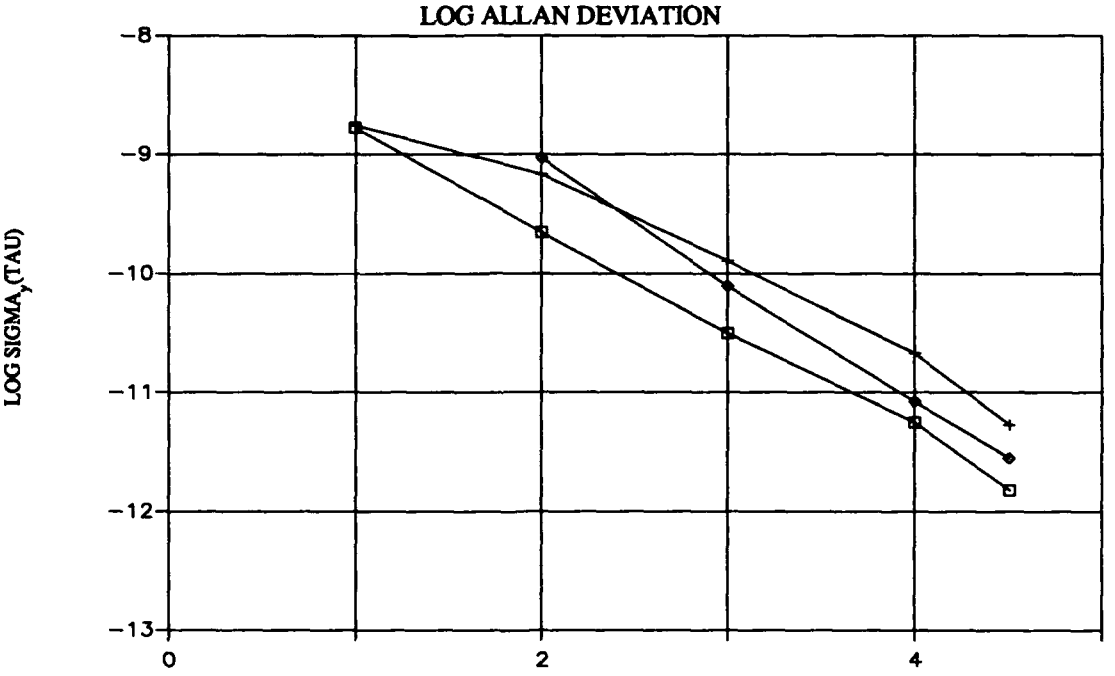

FIGURE 3

SATELLITE HOPPING ALGORITHM OUTPUT
CLOCK BIAS FROM ALL SATELLITES

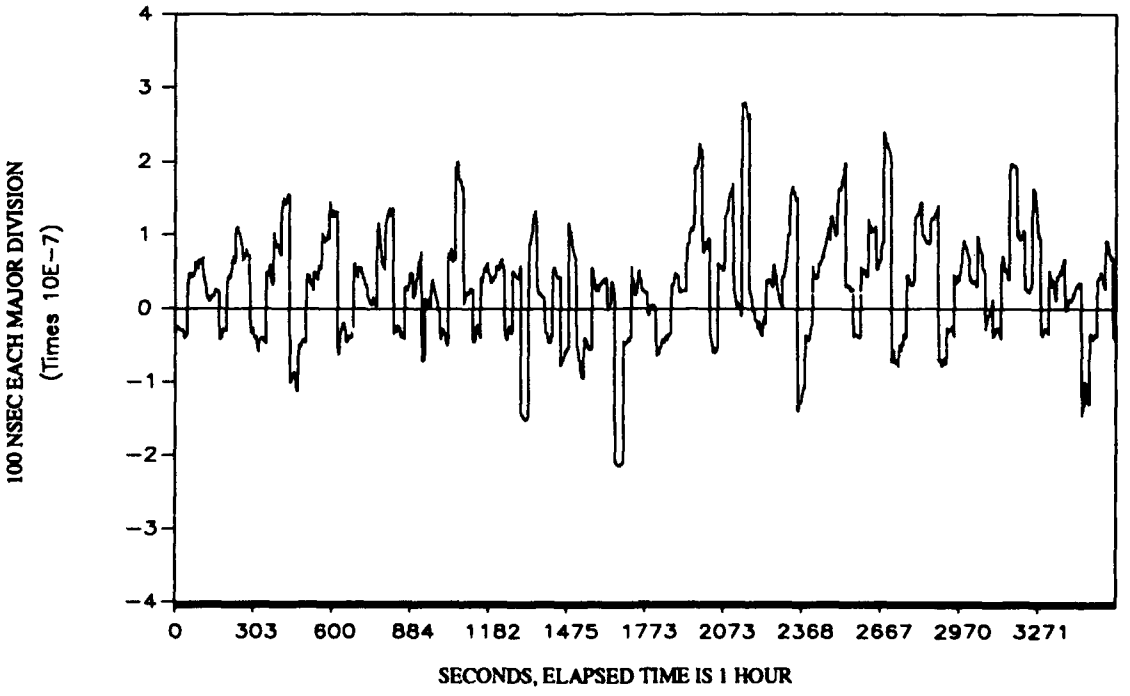

FIGURE 4

SATELLITE HOPPING ALGORITHM OUTPUT
400 POINT AVERAGED CLOCK BIAS

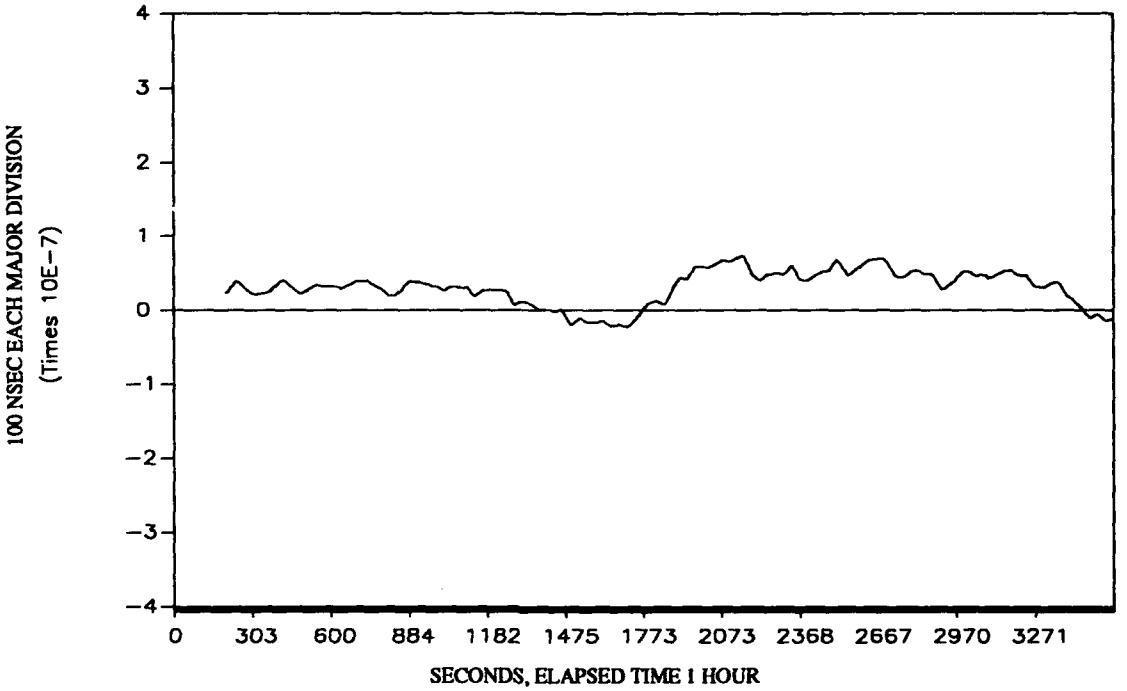

FIGURE 5

RUBIDIUM FREQUENCY STABILITY
ALLAN DEVIATION COMPARED TO CESIUM

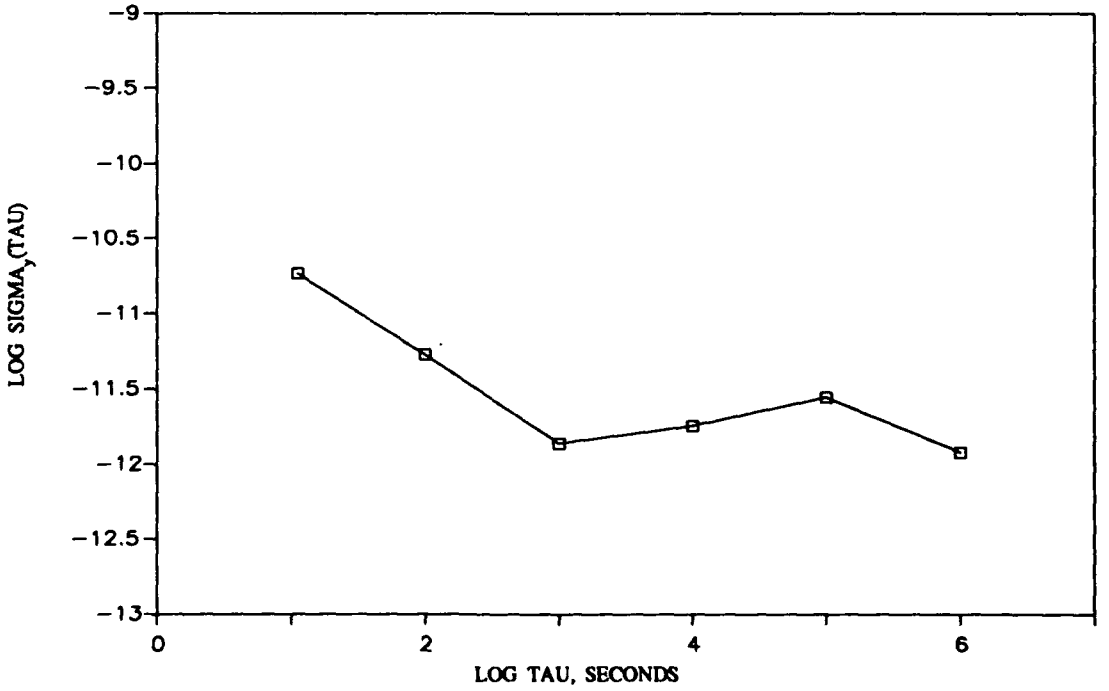

FIGURE 6

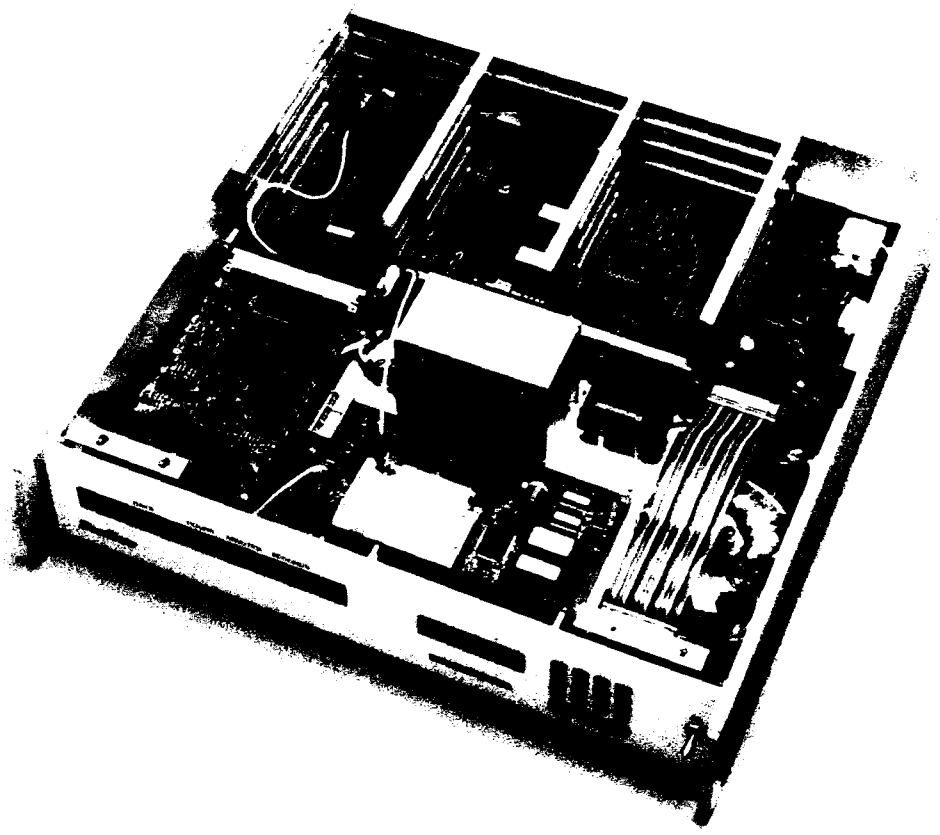

GPS DIGITAL CLOCK

A PRECISE GPS–BASED TIME AND FREQUENCY SYSTEM

Jack Mc Nabb & Earl Fossler
TRAK Systems
Division of TRAK Microwave Corp.
Tampa, Florida, USA

Abstract

This paper describes an approach to implementing a compact, highly reliable and precise Master Time and Frequency subsystem usable in a variety of applications. These applications include, among others, Satellite Ground Terminals, Range Timing Stations, Communications Terminals, and Power Station Timing subsystems. All time and frequency output signals are locked to Universal Time via the GPS Satellite system. The system provides for continued output of precise signals in the event of GPS signal interruption from antenna or lead-in breakage or other causes. Cost/performance tradeoffs affecting system accuracy over the short, medium and long term are discussed. A unique approach to redundant system design provides an architecture with the reliability advantage of triple-redundant majority voting and the cost advantages of dual-redundant elements. The system can be configured to output a variety of precise time and frequency signals and the design can be tailored to output as few, or as many, types and quantities of signals as are required by the application.

I. INTRODUCTION

Overview

This paper first presents a background of precise time and frequency generation and briefly lists current–day applications. The GPS system concept is then introduced and the needs in precise frequency and timekeeping that are filled by the GPS system are discussed. Various accuracy alternatives are presented. Next, a practical Station Clock that meets these needs is described. The discussions then proceed to the implementation of a highly reliable, relatively low cost redundant time and frequency system.

Background

The art of precise frequency generation and timekeeping using electronic means has been with us for several decades, with achieved precision steadily improving as new frequency standards and synchronization methods have been developed. Since 1967, the length of a second has been defined in terms of the resonance of the cesium atom, and since the 1970's, cesium beam standards have been used in all applications requiring the most precise frequencies and precise timekeeping. Maintenance of frequency calibration and precise time setting have been a matter of some difficulty

and great expense, requiring the use of standard frequency radio broadcasts, portable clocks, and extensive manpower allocation. With the advent of the GPS system, ultra–precise frequency generation and timekeeping is with us at immeasurably reduced effort and at a fraction of the costs of previous methods. *When GPS synchronization is used, all generated frequency and time outputs, worldwide, are precisely locked to a common source.*

The GPS system is making all older methods of precise frequency and time generation obsolete and has, with the help of CPU-based instruments, brought precise frequency and timekeeping to a myriad of new applications that could not have afforded the old methods. Present day applications include, among others, the following:

SOME GPS TIME & FREQUENCY APPLICATIONS

* Satellite ground terminals
* Communications terminals
* TV and radio networks
* Astronomical observatories
* Electrical power system monitoring
* Telecommunications systems
* Cellular radio
* Frequency-hopping systems
* Telemetry data acquisition stations

II. GPS CLOCK BASICS

Definitions

The word "clock" has many definitions and connotations. In this paper, we use the term to denote a self–contained electronic instrument that provides a user with precise frequency and (usually) time signals. A GPS Clock is an instrument that synchronizes to GPS to produce precise frequency and time signals. Often, when such an instrument provides all of the signals required at a given site, it is called a GPS Station Clock. Add redundancy, backup power supplies and/or multiple output signal units and we have a GPS Station Clock System (sometimes the word "system" is left off).

Clock Elements

The basic Clock has several necessary elements, as listed below. When only reference frequency outputs are required, the elements related to time accumulation, correction, and generation are not required.

* A reference frequency source
* Frequency counters and time accumulators
* A synchronizing source
* Time correction mechanisms
* Output signal generators

Reference Frequency Source

Being self–contained, the Clock has an internal frequency source (oscillator) and, since this paper addresses a GPS–based system, GPS disciplining of the oscillator is assumed. Crystal or rubidium

based oscillators are normally used. A disciplined cesium frequency standard can provide a clock that eliminates almost all the time inaccuracies due to SA. With GPS disciplining, using properly designed disciplining hardware and software, the long term accuracy, i.e.; 24 hours, of the Clock is equal to that of the core GPS system standard. This results from the fact that long–term phase–locked disciplining locks the local oscillator to the GPS standard over the long term and the fact that the core GPS standard does not vary. Loss of GPS disciplining for periods of even several hours does not degrade long term accuracy as long as oscillator–inherent (free running) drift is not excessive, and this can be controlled by selecting a good oscillator for the application.

Now, "long–term" must be defined. With SA active, the resulting signal distortions last from a few seconds to a few hours. The most visible indication of these distortions is a plot of the 1 PPS output of a GPS receiver against a local cesium standard over a period of several days. Experience has indicated that 1 PPS phase returns to "neutral" at intervals not exceeding two–to–three hours and that the summation of deviations integrates to zero over a 16 to 24 hour period. The conclusion is that the accuracy will be on the order of one part in 10^{12} to 10^{13} when measured over a period of 10 to 20 hours.

Reference Frequency Source

Next we come to the situation of expected intermediate term (one second to several minutes) frequency accuracy while tracking satellites. The figure here is determined by the oscillator characteristics. Typically, in this application, voltage control is used to discipline the oscillator, and the disciplining process is one of continually varying the oscillator voltage to track the inherent drifts (primarily aging and temperature stability). The poorer the oscillator stability, the poorer the intermediate term accuracy will be. Ovenized crystal oscillators typically have accuracies in the range of 1 X 10^{-9} through 5 X 10^{-11}. Rubidium oscillator accuracy is approximately 1 X 10^{-11}. Table 1 lists the characteristics for a representative set of oscillators.

Short term stability is totally determined by the oscillator characteristics. Many different suitable oscillators for this application with a great variation of characteristics are available. Data on typical oscillators are given in Table 1.

Knowing the coasting drift is important in some applications. Coasting drift is defined as the total 1 PPS phase drift at the Clock output during those periods when the oscillator is not being actively disciplined by GPS. Since there is worldwide coverage by at least one satellite 24 hours a day, this situation arises only under unusual circumstances, but it is useful information for those cases. Two possible situations where satellite data may not be available are (1) the temporary disconnection of an antenna and (2) the placement of the antenna at a location where all satellites are obscured for periods of time. The coasting drift for various types of oscillators is given in Table 1.

Table 1 gives data for oscillators available from TRAK Systems Division of TRAK Microwave Corporation. If an instrument has accumulated an offset of less than 10 microseconds while drifting, when a satellite is reacquired corrections are applied smoothly to return the phase difference to zero and to reestablish long term accuracy. Conversely, if, at the time of satellite reacquisition, accumulated offset is greater than 10 microseconds, all counters are reset to zero and a new baseline for long term accuracy measurements is established. As can be seen from Table 1, even the least-

precise of

the oscillators offered can withstand greater than four hours without disciplining and still maintain integrity of long term accuracy.

Frequency Counters and Time Accumulators

Clocks of the type described herein contain, as a minimum, the frequency counters to produce a 1 PPS output. Producing a 1 PPS by countdown from the oscillator is required to implement the disciplining process. Figure 1 is a simplified block diagram showing the disciplining circuits.

Clocks producing time of year outputs also contain time accumulators for seconds through years. Modern time Clocks use software accumulators.

Synchronizing Source

As described above, the internal oscillator and 1 PPS output are synchronized to the GPS received 1 PPS signal. The GPS receiver also outputs the data to initially synchronize the time accumulators. It is important to note that, once synchronized, the Clock and its time accumulators can run for periods of many hours without resynchronization. In other words, the Clock does not merely process received GPS data and output it — the Clock uses the GPS received signals for synchronization and, without loss of long term accuracy, bridges periods of no GPS input.

Time Correction Mechanisms

The various time correction factors are described below.

LEAP YEAR: Leap year data for the next century are stored in memory, and proper updating is provided at each year end.

LEAP SECOND: In order to reconcile the time scale produced by the atomic second with the solar scale (Universal Time, UTC), a second is added approximately once a year. This addition is announced in advance and is flagged in the GPS transmission. The internal time clock recognizes this flag and automatically adds one second at the designated time (June 30 or December 31).

TIME ZONE: Many applications use UTC (zero meridian) time regardless of the Clock's location on earth. No adjustments to received GPS time are required in these cases. However, other applications call for local standard time. Provisions are made for front panel or remote computer entry of time zone offset. Once this entry is made, nonvolatile memory maintains the setup data and the Clock automatically produces local standard time.

SUMMER TIME: Some users prefer to correct for and accumulate Summer (or Daylight) time when it is active. Since the dates of change are set by local mandate, provisions are made for front panel or remote computer entry of the required dates. Once these dates are set in for each year, they are stored in nonvolatile memory and corrections are automatically applied at the designated times.

Output Signal Generators

A Clock containing all of the elements described thus far can output a variety of rates and encoded time signals merely by adding circuits that use the basic clock signals to produce the desired outputs. A Clock designed only as a frequency source can output a variety of optional digital and sinewave frequencies. The next section of this paper illustrates a typical GPS Station Clock containing a great variety of outputs.

III. HARDWARE IMPLEMENTATION

A GPS Station Clock

A functional block diagram for a typical production GPS Station Clock incorporating all of the features outlined in the previous paragraphs is illustrated in Figure 2.

On the front panel of a typical GPS Station Clock, keypad and alphanumeric display implement setup of the unit and status display. All desired setups can also be entered by remote terminal or computer. The setup system provides for entering such data as time zone and other optional data differing from default values. Status screens include satellite status, current modes, time and date, latest navigation solution, GPS–lock status, and many others.

Referring to Figure 2, the instrument contains a six–parallel–channel GPS Receiver for frequency disciplining and time presetting, a Disciplined Frequency Subsystem including stable oscillator (crystal or rubidium), a System Processor including receiver interface, executive controller, frequency and time countdown circuits, computer I/O, and other functions. A great variety of signals, including digital rates, sinewave rates, serial time codes, and parallel time codes can be generated and supplied as outputs.

GPS Antenna System

Three primary choices of antenna system exist: (1) passive, (2) active with preamp at antenna and (optionally) in line, and (3) with downconverter at antenna. These are described in the following paragraphs. For lower-accuracy applications, it is possible to mount the GPS receiver in the antenna, but this approach is outside the scope of this paper.

PASSIVE: The GPS frequency of 1.5 GHZ precludes using a passive antenna with more than just a few feet of lead-in cable, and this type of system is restricted to field and vehicular applications.

ACTIVE WITH PREAMP: This is the most common type of system. It is not uncommon to multiplex a dc voltage up the antenna lead–in conductor to power preamps in the line and at the antenna. A well–designed system can use inexpensive coaxial cable to lengths of 200 feet with a preamp in the antenna and to 400 feet with the addition of a line amplifier at midpoint. This distance is more than adequate for most applications. A view of two typical antennas is shown in Figure 4. Lead-in distance can be extended to over 1000 feet using low-loss (expensive and cumbersome) cable and/or additional line amplifiers, but dynamic range decreases with added amplifiers.

DOWNCONVERTER: Lead–in distance can be extended to a few thousand feet if a downconverter is used at the antenna. Typically, the 1.5 GHZ signal is converted to the range of 10–to–80

MHz to greatly reduce cable losses. An upconverter can then be used at the receiver if it has a standard 1.5 GHz front end, or a special receiver made to accept the downconverted frequency can be used. Some systems send an LO signal up to the antenna on a separate cable.

IV. A REDUNDANT TIME AND FREQUENCY SYSTEM

Reliability And Redundancy

The GPS Station Clock and active antenna described above use highly reliable components and the system has a calculated Mean Time Between Failure (MTBF) of 25,000 hours; however, some applications have a required probability of success unachievable with a single unit. This high probability can be achieved by using a well-designed redundant system having only a few single points of failure. For some applications, it is necessary to back up only critical frequency and timekeeping while for others, backup is required for the entire system. All ac power supply paths should have redundancy and/or the primary ac supply should be backed up by batteries. Variations between these two approaches are also used. One quite common variation is described below.

A Practical Redundant System

For many people, the thought of using a redundant system brings visions of a very high expense and a waste of money. However, there are those situations that demand redundancy and, fortunately, redundant timing systems are far less costly today than they were ten years ago. Such a system is described below.

A typical redundant time and frequency system is shown in the block diagram of Figure 3. Two identical GPS Station Clocks (Clock A and Clock B), each with its own antenna, produce all of the types of signals required for system output. All signals from each of the clocks, along with internal status information, are fed to the Fault Sensing and Switching Unit (FSSU).

One exception to using two completely identical Clocks is to use a rubidium oscillator in Clock A and a crystal in backup Clock B; however, the cost savings of this approach hardly justifies the increased logistic costs.

Within the FSSU, the signal set is examined for phase errors, time bit errors, setup bits, and dropouts. The signals from Clock A are placed on line at the outputs of the FSSU. In the event of a signal failure or bad status message from Clock A, the outputs from Clock B are placed on line. Fault lines from other parts of the system are also fed to the FSSU, and any detected system fault is displayed on the FSSU front panel and an audible alarm is sounded.

Each of the signals passing through the FSSU from Clock A or Clock B connects via a simple, highly reliable, switch element. Elements used are reed relays and simple TTL gates. This technique extends the mean time between failure of individual signals at the output of the FSSU to well over 1,000,000 hours.

High–Isolation Low–Noise Frequency Outputs

Some applications demand reference–frequency (typically 5 or 10 MHz) outputs that have very low phase noise and extremely high output–to–output and output–to–input isolation. These are applications where the reference frequencies are being multiplied to much higher frequencies used

by station radars and other equipments. The system architecture shown in Figure 3 provides this isolation. In this approach, the signals to be protected are routed directly from Clocks A and B to a special high–isolation precision frequency distribution unit (FDU). This unit has dual–redundant input buffers followed by a high–isolation electronic switch. Selection of Clock A or Clock B signals is via remote command lines from the FSSU or by local signal dropout detectors in the FDU. Output isolation of greater than 125 dB assures trouble–free system operation. This approach is costly and should be used only if required; however, it can save a lifetime of problems at many radar and communication station applications.

Fault Sensing and Switching Unit

The FSSU, Figure 4, uses an internal reference source (Clock C) to implement digital signal fault location. The unit initially checks for time and phase agreement of Clock A and Clock B outputs. When agreement has been verified, Clock C is synchronized to the agreeing inputs. After this initial synchronization, all of the Clock C frequency dividers and time accumulators free run, using an internal oscillator disciplined to the on–line input Clock. This provides a third independent clock source to continuously check the digital signals against Clock A and Clock B.

The FSSU initially routes Clock A signals to its outputs. In the event of a failure report on the Clock A status line, the detection of a Clock A phase or time difference (vs agreeing Clocks B & C), or a Clock A signal dropout, the FSSU automatically places Clock B signals on line and activates both local and remote alarms. In the event of a failure of Clock B or C, the outputs from Clock A remain on line and the alarms are given.

The FSSU has several features built in to preclude false alarms and switching without sacrificing fault detection capability. For instance, the operator can enter a desired delay time between the detection of a low Status line and declaring a fault. If both status lines go low, a common antenna problem is assumed and automatic switching is inhibited. Provisions are made for properly operating through leap second, leap year, and summer-time corrections and to enter parameters as required.

Another feature of the FSSU is fault collection and alarm for timing buffer units and other units in the system. Also, two RS–232 I/O ports allow for remote setup and status output.

To assure that a single power supply failure does not cause a system failure, the FSSU must be equipped with a dual power supply system, all the way from the power input connectors to the point where the redundant supply lines are diode–OR'ed to the dc busses. The use of a main ac supply with battery backup is discussed further at the end of this section.

Signal Distribution

In modern timing systems, it is not unusual to have requirements for several hundred separately–buffered signal outputs, all designed for driving long, low impedance lines. Most systems also require each buffer module to have fault sensing circuits. As a result, the distribution subsystem often represents one-half of the total Timing Station cost and size. In specifying a system, the engineer must be careful to assure that all significant design considerations and specifications are considered. Space does not permit detailed coverage of this important subject in this paper.

Power Supply System

It is standard practice to provide battery backup for all critical timekeeping circuits or to use uninterruptible ac power sources. This approach protects the system against recovery problems after restoration of primary power; i.e., the Time Base Subsystem does not require several hours. Beyond this, system designers often allow the system outputs to "die", based on the scenario that all of the users of the signals are also without power and that outputs are fully restored upon restoration of station power.

A second consideration is provision for backup of the power supplies within the units. In a redundant system, backup for failed power supplies is mandatory to preclude unnecessary single-point failures. For those units that already have DC power backup, an additional AC power supply is not required for mission success. The FSSU, however, is in a serial path for all signals and must have redundant power supplies. Finally, system reliability is certainly higher if redundant supplies are used in the Distribution Subsystem, but most system designers elect to permit a short down time while a failed TBU power supply is replaced.

Table 1. GPS Clock Oscillator Performance Comparisons

CHARACTERISTICS	STD CRYSTAL	LO DRIFT	LO DRIFT/ REDUCED NOISE	ULTRA LO DRIFT/ LO NOISE	RUBIDIUM
Accuracy while tracking	1 x 10-9	1 x 10-10	1 x 10-10	5 x 10-11	1 x 10-11
Typical coasting drift (first 2 hours)	1.5 us/hr	250 ns/hr	250 ns/hr	150 ns/hr	40 ns/hr
100 sec Allan variance	5 x 10-11	1 x 10-12	1 x 10-12	1 x 10-12	1 x 10-11
10 sec Allan variance	1 x 10-10	1 x 10-12	1 x 10-12	1 x 10-12	4 x 10-11
1 sec Allan variance	N/C	5 x 10-12	5 x 10-12	5 x 10-12	1 x 10-10
Phase noise @ 1 Hz offset	-80 dBc	-80 dBc	-100 dBc	-100 dBc	-70 dBc
Phase noise @ 10 Hz offset	-85 dBc	-85 dBc	-120 dBc	-120 dBc	-90 dBc
Phase noise @ 100 Hz offset	-100 dBc	-100 dBc	-130 dBc	-140 dBc	-110 dBc
Phase noise @ 1 KHz offset	-105 dBc	-105 dBc	-145 dBc	-155 dBc	-130 dbc
Phase noise @ 10 KHz offset	-115 dBc	-115 dBc	-150 dBc	-160 dBc	-130 dBc
Harmonic distortion	-30 dBc	-30 dBc	-30 dBc	-30 dBc	-40 dBc
Non-harmonic distortion	-40 dBc	-50 dBc	-50 dBc	-60 dBc	-65 dBc

TYPICAL COASTING DRIFT - Oscillator drift when no satellites are in view following two to four days stabilization. Since there is currently full coverage worldwide, this information covers only very unusual conditions.

CHARACTERISTICS	STD CRYSTAL	LO DRIFT	LO DRIFT/ REDUCED NOISE	ULTRA LO/DRIFT LO NOISE	RUBIDIUM
1 hour	1.5 µs	250 ns	250 ns	150 ns	40 ns
2 hours	3 µs	500 ns	500 ns	300 ns	80 ns
4 hours	7 µs	1.5 µs	1.5 µs	750 ns	200 ns
8 hours	20 µs	3 µs	3 µs	1.5 µs	400 ns
16 hours	50 µs	8 µs	8 µs	5 µs	800 ns

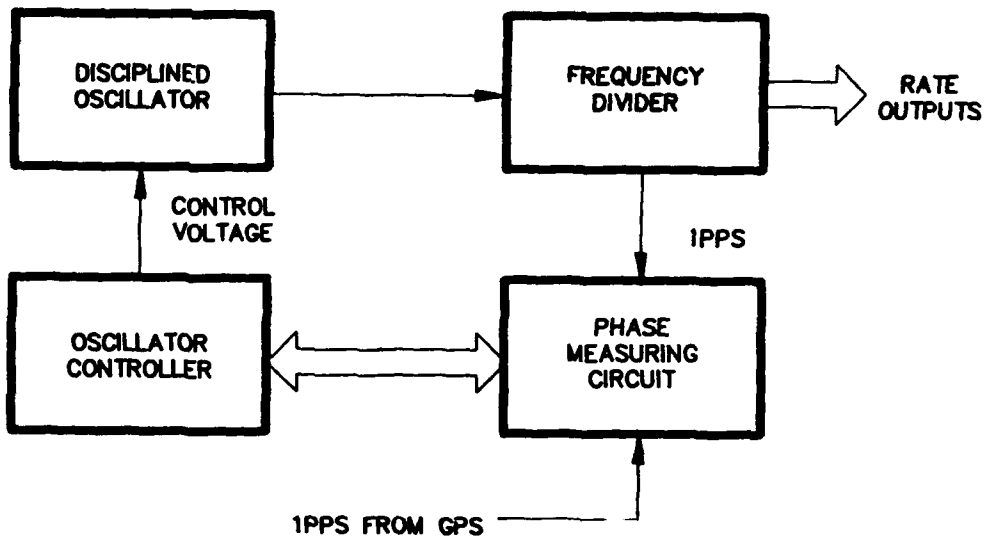

Figure 1. Block Diagram of Disciplining Circuits

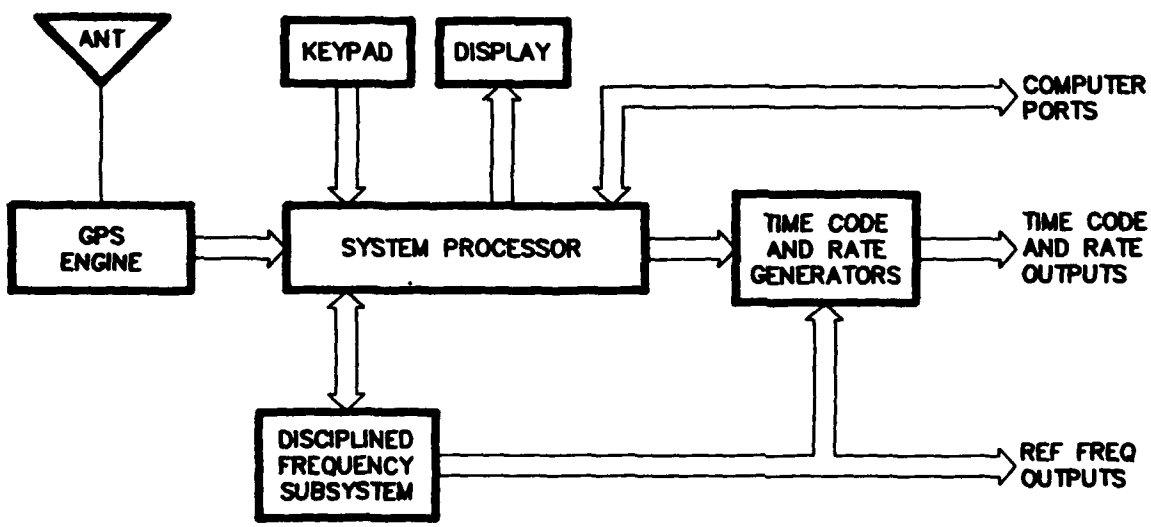

Figure 2. Block Diagram, GPS Station Clock

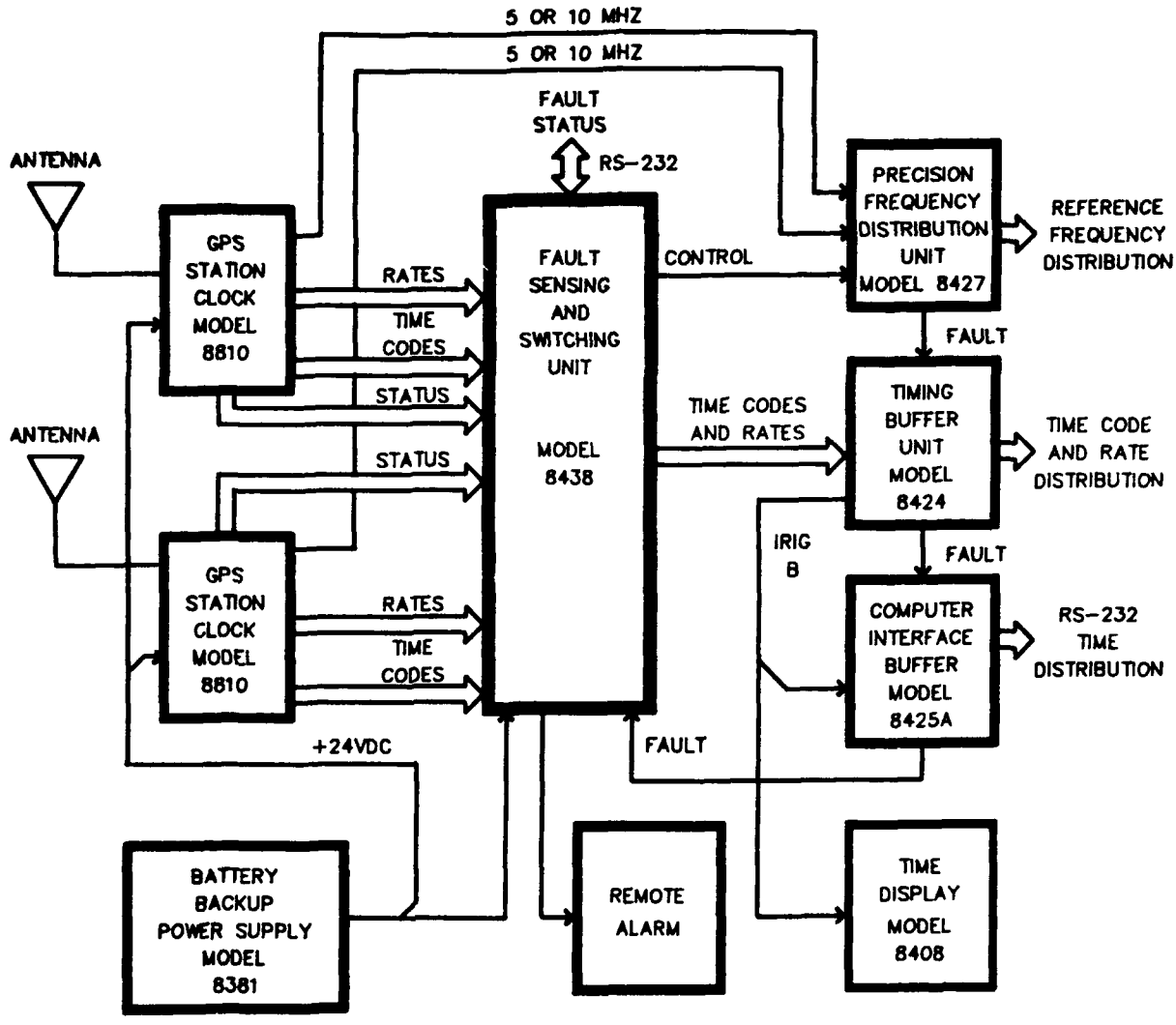

Figure 3. Typical Redundant Timing System

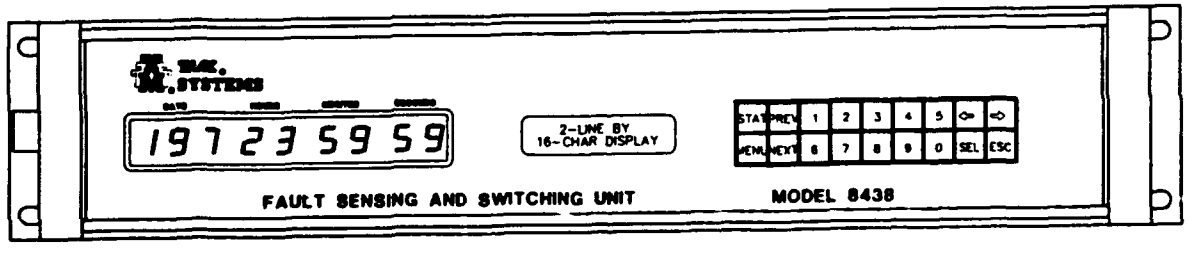

Figure 4. FSSU Front Panel

POSSIBLE APPLICATIONS OF ATOMIC FREQUENCY STANDARDS WITH AN INTERNAL HIGH RESOLUTION DIGITAL SYNTHESIZER

E. Detoma[1], *A.Stern*[2]

1 INTRODUCTION

This paper reviews the applications of Atomic Frequency Standards with an internal synthesizer (thereafter referred as "Synthesized Frequency Standards or Oscillators") with a special emphasis on the Rb oscillator. A fractional frequency synthesizer, developed by SEPA, has been incorporated in the Frequency Locked Loop of a TFL Rubidium Frequency Standard. This combination allows a frequency settability in steps of $1.5 \cdot 10^{-12}$ (optional $1 \cdot 10^{-13}$) over a range of $6 \cdot 10^{-9}$ without having to resort to change the C-field to tune the output frequency of the device. This capability, coupled to the excellent short term stability of the Rb frequency standard, opens new possibilities for time and frequency users in the various fields (time metrology, navigation, communication, etc.) in which stable frequency standards find their application.

In time metrology, the capability to precisely tune the frequency of the atomic standard will provide the same benefits that are now achieved by the combination of a frequency standard and a phase microstepper; the immediate application will be the generation of primary and secondary time scales, by steering the output frequency of the synthesized standard with reference to some other physical device or to a computed time scale: this will provide a hardware implementation of the "paper clock" which constitutes the "ideal" time scale in primary and secondary laboratories.

The high resolution frequency settability of the output signal of the standard may have some uncommon applications, such as the generation of other time scales, as the sidereal time for astronomical uses. Fine frequency and time offsets, the latter with a resolution as small as a few picoseconds, can be generated with the synthesized standard, allowing remote clocks to be precisely set at the same frequency and time, or with controlled offsets in time (and eventually in frequency) to provide a "coordinated" time network. This is important in communications networks, where clocks at the nodes must be kept not only syntonized but synchronized with offsets which account for the relative propagation delays within the same nodes in the network.

Electrical-power generation and distribution systems, and ground-based positioning systems will, for the same reasons, undoubtedly benefit from atomic standards incorporating a synthesizer, but applications exist to exploit the settability and stability of the atomic frequency standard for other navigation applications. In GPS receivers, for instance, where, once synchronized to the GPS System Time, the local oscillator can provide a flywheel to split the solution in its time and space components; in this way, no degradation is expected if the number of available satellites is reduced to 3 because of intentional jamming or satellites masking due to banking manoeuvers.

[1] FIAT CIEI S.p.A., Div. SEPA - Corso Giulio Cesare 300 - 10154 Torino [Italy]

[2] Time & Frequency Ltd., TFL - 14, Habanai Street - Holon 58117 [Israel]

In some particular communication and navigation applications, where minimum exposure is required, keeping the internal Pseudo Random Noise (PRN) generator of the receiver synchronized to the transmitted PRN code, even when this is not actually received, will minimize the exposure by reducing or zeroing the acquisition time when required to track GPS satellites or to communicate through a secure data link.

2 DESCRIPTION OF THE SYNTHESIZED Rb OSCILLATOR

A few frequency standards with a built-in digital frequency synthesizer (for a good review of frequency synthesizers see ref. 20) are currently available on the market: most of the H-masers (refs. 8, 9 and 10) and both Hewlett-Packard (HP) and Frequency and Time Systems (FTS) new cesiums (refs. 16 and 17) incorporate a synthesizer within their frequency locked loop. The HP 5071A Cesium Beam Frequency standard claims a ultra-high resolution of $6.3 \cdot 10^{-15}$ over a range of $1 \cdot 10^{-9}$ and a stability of $2 \cdot 10^{-14}$ for an averaging time of 5 days.

In the Synthesized Rb Oscillator, jointly developed by TFL and SEPA (refs. 1 and 2 and fig. 1), a high resolution fractional frequency synthesizer has been inserted in the frequency locked loop to effectively control the output frequency of the device with a resolution of $1.5 \cdot 10^{-12}$ [optional $1 \cdot 10^{-13}$, since the short term frequency stability of the TFL Rb oscillator may reach $2 \cdot 10^{-13}$ for an averaging time $\tau = 1000\ s$], without resorting to the C-field method for frequency control. In the final device, many other novelties are introduced for the first time in a small Rb oscillator (see the block diagram in fig. 1):

- a.c. C-field modulation, with the aim to reduce the sensitivity of the device to external magnetic fields;
- auxiliary outputs, to provide 50 Ω impedance, TTL-level compatible, 1 pps and standard frequency outputs, in addition to the main 10 MHz sinewave standard output. The TTL output frequency can be electrically selected to be 10, 5, 1 or 0.1 MHz, and the 1 pps output is automatically synchronizable to the leading edge of a reference pulse.

These features make the device ideally suited for stand-alone operation or to be incorporated in timing systems, in the full range of possible applications. For additional informations on the device, the reader is referred to refs. 1 and 2; in the following we will cover in general the benefits deriving from the use of synthesized oscillators in a non-exhaustive list of possible applications.

An immediate benefit, which should be mentioned here since it relates directly to the performance of the atomic standard, derives from the recognition of this basic fact: the operation of an atomic frequency standard can be optimized, even of an order of magnitude, if no constraint is placed on the output frequency derived from it. This means, for instance, that its frequency stability can be improved if we allow a slight detuning of the output frequency due to adjustments in the interrogation RF power, magnetic field, etc. Years of research in this direction, carried on mainly by Andrea De Marchi at NIST, have resulted in an impressive list of papers (refs. 11-14 and 18-19) supporting these claims.

However, the end-user needs a "nominal" output frequency from its reference oscillator, and the incorporation of a synthesizer within the locked loop of the standard allows to "recover" a nominal value for the output frequency, since it controls the output frequency independently from the parameters of interrogation of the atomic resonance. This has been a major factor in improving the performance

of atomic standards, resulting in specifications as those boasted by the HP 5071A Cesium Beam frequency standard.

3 FREQUENCY AND PHASE CONTROL

In the majority of existing frequency standards, based on frequency or phase locked-loops to atomic resonances, the frequency control is achieved by means of changing the magnetic field (C-field control): this may result in unpredictable changes due to residual hysteresis effects and changes in the magnetic susceptibility of the standard. Moreover, the control is non-linear over a wide range, non-repeatable from unit to unit and non-reproducible even in the same unit due to (frequency) aging. These limitations have prevented the precise control of the output frequency of atomic frequency standards; as a matter of fact, for accurate oscillators, like Cs-beam frequency standards, it is strongly advisable not to change at all the C-field setting, if not for very important reasons. As a consequence, precision timing systems had to resort in the past to external devices, such as phase microsteppers, to adjust the output phase and frequency. Neglecting the noise, the output signal of an oscillator can be written as:

$$V(t) = V_0 \cdot sin[2\pi\nu_0 t + \varphi_0] \tag{1}$$

where V_0 and ν_0 are the amplitude and the nominal frequency of the signal, and φ_0 is the initial, arbitrary, phase angle. The frequency $\nu(t)$ [t is used only to indicate a dependency on time] and the phase $\varphi(t)$ are related by a simple equation, namely:

$$\nu(t) = \frac{1}{2\pi} \cdot \omega(t) = \frac{1}{2\pi} \cdot \frac{d\varphi(t)}{dt} \tag{2}$$

where $\omega(t) = \frac{d\varphi(t)}{dt}$ is the instantaneous angular frequency of the signal. If a change $\Delta\nu$ in the nominal frequency of the signal is desired, the resulting equation can be written as:

$$V(t) = V_0 \cdot sin[2\pi\nu_0 t + 2\pi\Delta\nu t + \varphi_0] \tag{3}$$

and the second frequency term can be rewritten in terms of phase drift using (2):

$$V(t) = V_0 \cdot sin[2\pi\nu_0 t + \frac{d\varphi}{dt} t + \varphi_0] \tag{4}$$

A microstepper is capable of stepping the phase of the output signal in precise amounts with extreme resolution, implementing the mechanization of eq. (4); it has been effectively used in timing systems to control the output frequency by applying phase steps at precise intervals in time, in order to simulate the phase drift due to a frequency offset: the main disadvantage of this technique is in the granularity of the control, since phase can be adjusted only in discrete steps, whose minimum value is equal to the resolution of the microstepper. Conversely, frequency control can be applied to adjust the phase of the output signal, using the same basic relationship (2); in this case a continuous phase shift Δx (see the definition below) is obtained, from the current phase to the desired phase, in a predefined time interval Δt, by applying a proper frequency offset $\Delta\nu$ for the duration Δt:

$$\Delta x = \frac{\Delta\nu}{\nu_0} \cdot \Delta t \tag{5}$$

where we have used the definition of the "time deviation" x(t), which represents the phase normalized in units of time, according to the relationship:

$$x(t) = \frac{\varphi(t)}{2\pi\nu_0} \tag{6}$$

Alternatively, the time deviation x(t) can be related to the fractional frequency error $y = \Delta\nu/\nu$ as:

$$x(t) = \int_0^{\Delta t} y(t) \cdot dt \tag{7}$$

Again, two variables ($\Delta\nu$ and Δt in eq. (5)) can be used to control the process, and no discontinuities are apparent in the phase x(t) for any choice of $\Delta\nu$ and Δt; the "granularity" appears in the frequency settability, being a direct consequence of the resolution of the internal synthesizer. Therefore, the resolution on frequency control $\Delta\nu_{min}$ constrains the minimum phase shift allowable, and, since Δt cannot be smaller than the loop time constant of the standard τ_{loop}, this effectively limits the phase resolution Δx_{min} to:

$$\Delta x_{min} = \Delta\nu_{min} \cdot \tau_{loop} \tag{8}$$

In our case, the minimum time step is given by:

$$\Delta x_{min} = 1.5 \cdot 10^{-12} \cdot 196\ ms = 0.3\ ps \tag{9}$$

where: $\Delta\nu_{min} = 1.5 \cdot 10^{-12}$ and $\tau_{loop} = 196\ ms$. However, the rms time-error noise is given roughly by:

$$\sigma_x(\tau) \approx \tau \cdot \sigma_y(\tau) = 7 \cdot 10^{-12} \cdot \sqrt{\tau} \tag{10}$$

for our Rb oscillator, where τ is measured in seconds. The minimum time error noise is obtained at the smallest integration time, which is $\tau_{loop} = 196\ ms$, and:

$$\sigma_x(\tau = 196\ ms) \approx 3\ ps \tag{11}$$

i.e., in order to resolve the time step above noise one has to perform a step larger than 3 ps.

4 APPLICATIONS IN PRECISE TIMING SYSTEMS

A synthesized atomic standard is ideally suited to drive a precise timing system; more than one oscillator can be incorporated into such a system to provide redundancy, with additional benefits compared to a standard, non-controllable oscillator. Consider the situation in which, in a redundant timing system, one oscillator fails and automatic switchover to another unit occurs. If the phase and frequency of the two oscillators are not precisely aligned, a frequency deviation and a phase jump will likely occur, and a disturbance will be generated and propagated downstream to the users of the timing signal. While the frequency offset is usually limited by the relative accuracy and settability of the standards, the phase jump can be as large as the period of the main output of the oscillator, namely 100 ns for a 10 MHz output, if indipendent control of the phase of the oscillators is not accomplished.

This situation can be avoided if precise frequency control is applied, since we can control independently the frequency and phase of each output, with a resolution adequate to keep the output signals aligned; therefore, switchover transients can really be neglected and the failure recovery procedure appears now completely transparent to any user. While these considerations already provide benefits in basic timing systems, sophisticated systems may gain additional benefits; disciplined frequency oscillators can be built, since they rely on intrinsic frequency control of the output signal. Digital versus analog implementation of the control loop is a preferrable mean of locking the output source to one or more indipendent input references, since infinite memory can be provided in the loop and more complex control laws can be easily built in the device.

In many applications of Synthesized Atomic Frequency Standards, we have a phase or frequency locked loop with a very long time constant, from hours to days. This includes also the cases where manual frequency control closes the loop. The long time constant results from the fact that the local oscillator used in the loop, the atomic standard, exhibits the best stability at these long time constants of hours and days. In these applications, the use of a synthesized atomic standard provides the following important benefits:

a. **Digital control**: is the only scheme that can be used to reliably implement very long time constants (analog schemes require high values for resistance and capacitance);
b. **Predetermined fixed frequency steps**: this allows immediate frequency control response: there is no need for experimenting first the loop response to a frequency change and then making a suitable correction.

As an example, we can consider a multiple-input system as the Frequency Combiner Selector described in refs. 3 and 4. The system accepts multiple reference signals as input and performs a near-simultaneous phase intercomparison on the input and output signals with high resolution, since the measurements are carried on using the beat signals (1 Hz) between the various sources and an offset oscillator. The phase relationships are derived by the time of occurrence of the positive zero crossing of the beat signals as measured by a high resolution multichannel event clock, with a total ambiguity (data fold-over) of one full day. A computer steers the output frequency to the best estimate of the input signals, weighted according their accuracy and statistical characteristics, and drives an output crystal oscillator through a high resolution D/A converter. The system works in a closed loop mode, since the system output (from the digitally controlled oscillator) is split and fed back to one of the input (reference) channels; therefore, a continuous measurement of the output phase is provided to effectively servo the output oscillator.

The use of a crystal oscillator as a control element prevents open loop operation of the system; open loop operation is possible only if enough accuracy and repeatability of control is available in the output oscillator: this is the case of synthesized frequency standards, since frequency changes can be programmed (open-loop) with the same accuracy by which the frequency of the standard is known. This does not imply that no measurement feedback is required at all. The frequency of the standard acting as the system output device must be measured and known; however, the time required to precisely measure the frequency of the output oscillator is no longer related to the response time when frequency changes are commanded to the output oscillator. In this case, the system effectively acts as an open loop in terms of servo control, since the output frequency is measured only to steer its nominal value to some preset figure.

The capability **to decouple the time constant of the measurements and of the system response** is the main characteristic that allows a new degree of flexibility in designing redundant timing systems, in which redundancy is not bounded to a local ensemble of oscillators, but is extended to remote clocks as well, providing cost-effective solutions in distributed timing networks. But additional applications are possible, thanks to the capability to effectively and precisely steer the frequency and phase of each oscillator. As an example we can consider another timing system, recently proposed by TFL, in which a novel way of combining reference signals from various clocks is proposed. The arrangement (ref. 5) requires a coarse phase alignement of the signals to be combined. This can be solved with additional hardware: delay lines and switches. But, the introduction of synthesized frequency standards offers this feature for free, without additional hardware and with increased resolution versus what is presently available.

Primary laboratories and national time scales are based on "paper time scales" A **paper time scale** or **software clock** is based on a weighted average of an ensemble of individual clocks. It is convenient to use a synthesized atomic oscillator in such a system in two ways:

1. to implement a **physical output** to the "paper time scale", instead of using a phase microstepper;
2. if the ensemble is constituted of independent Synthesized Atomic Standards (Rb's or Cs's), it is possible to steer all the clocks in the ensemble to follow their weighted average, i.e., to follow the software clock; in this way a very **high redundancy** of the physical output is provided, since system time can be taken from any of the Rb or Cs oscillators in the ensemble.

Indeed, this idea is even more appealing when extended to an **ensemble of distributed clocks**, not clustered in a single location but widely dispersed at the nodes of a telecommunication network. The software clock will act as a single master to the whole network, and each clock in the network will be remotely controlled by it. The frequency and phase of each clock shall be remotely compared at the higher hierarchy nodes, and the comparison made with a long time constant, to improve the filtering of the added noise induced by the communications links. The resulting data will be used to generate the weighted average for the software clock driving the whole ensamble. But more on this subject at para. 6.... The concept of "Software clock" with a physical output provided by a Synthesized Atomic Frequency Standard can be extended to the implementation of time scales related to UTC, such as TAI or Sidereal Time, where a fixed time or frequency offset may exist between the various time scales.

5 SPACEBORNE OSCILLATORS: REMOTE CONTROL

The remote control of the most valued characteristics of a frequency standard, frequency and phase, is especially important in those applications where remoteness adds an additional difficulty to the synchronization and control problems. Current atomic frequency standards used in space applications are tuned through C-field control, with all the disadvantages peculiar to this technique, or via an additional phase microstepper or external synthesizer, which represent a further load to be carried onboard, and are not immune of pitfalls: "granularity" in frequency control is peculiar to a phase microstepper, and a basic synthesizer is not capable of the resolution which can be obtained by placing the synthesis process within the servo loop of the atomic frequency standard.

Again, the possibility of decoupling the sampling time over which the frequency is measured (usually, for remote clocks, via a sequence of phase, or time interval, measurements lasting a few hours if not days) and the capability to precisely control the oscillator with a different time constant, is the main advantage in this situation. Indeed, the intrinsic stability of the oscillator is much better than the capability to measure its frequency, due to the noise on the communication channel and the fact that several effects affecting any synchronization measurement must be removed by post-processing the data, before a reliable estimate of the frequency and phase of the oscillator can be extracted from the raw data.

A typical operational scenario involving such a spaceborne synthesized standard may require a few hours of measurements in order to have a preliminary estimate of its frequency; once this is obtained, any correction to steer the frequency is only limited by the propagation delays of the telemetry and command links, since the frequency can be steered at will with the same accuracy of the estimate of the frequency itself. In comparison, closed-loop operation is less agile, since in a feedback system

the settling time is determined by the slower component in the loop, in this case by the frequency estimation process.

6 NETWORK SYNCHRONIZATION: COMMUNICATIONS AND POWER GENERATION

Other ground-based systems require precise frequency and phase control of remote oscillators in the exceptions noted above. If the oscillators constitute a network, coordination within the network nodes (each oscillator constitute a node in a generalized timing network) adds a degree of complexity to the task of generating and distributing a common reference signal. Examples of networks requiring such a coordination are power generation (electric utilities) and especially telecommunications network.

Electric utilities networks are less demanding: timing must be provided to within a millisecond in the network. In the recent literature, vector measurements techniques place tighter requirements, in the order of microseconds, especially for the applications of fault diagnosis and location within the network (ref. 7).

Telecommunications networks are more demanding (ref. 6); phase noise must be carefully considered when frequency multiplication is involved. Frequency stability and accuracy requires atomic standards as primary standards in the network: for Time Division Multiplexing (TDM) Systems, the CCITT Recommendation G811 demands a frequency accuracy less than $1 \cdot 10^{-11}$ for the long term (> 1 month) accuracy of the network frequency, and less than $20\mu s$ of maximum Time Interval Error (TIE) for sampling times between 1000 s and 1 month.

Redundancy can be achieved by multiple oscillators in one location. Frequency and phase (time) coordination is achieved by use of internal (within the network) synchronization measurements, or by using external timing references, such as Loran-C or GPS timing receivers. Frequency coordination is absolute, in the sense that each node within the network must run at the same frequency (if coordination in relativistic sense is neglected); phase coordination is a more difficult task, since it involves the relative propagation delays between the nodes; for many applications, this is not a serious problem.

Moving toward a network in which redundancy is obtained by the use of distributed oscillators at each node in the network instead of being clustered in local ensembles poses the problem of both frequency and time coordination at the highest level, since failure in any node should be transparent to the users at the node and within the network. No frequency change or phase jump shall be apparent in any point of the network itself. This requires the precise determination not only of the relative frequency and phase between two oscillators at separate nodes, but of the propagation delay between them, corrected by any effect, including relativistic ones, that may affect the accuracy of the determination.

Again, since the measurement time is the slower component of the system and readjustment of phase and frequency in the network oscillators can be independently performed on each oscillator following any failure or restructuration of the network topology, the capability of precise control of frequency and phase of the oscillators is of the greater importance. The capability to decouple the time required to estimate the frequency and the response time associated to the remote control of the oscillators is a tremendous advantage in running such a network, and significant savings and operational benefits can be obtained using this strategy: instead of *clustering* redundant oscillators in one location, these

can be *distributed* in the network, insuring the same numeric redundancy but better frequency/phase coordination, provided that is possible to control these parameters with the highest precision.

7 NETWORK SYNCHRONIZATION: TRACKING SUPPORT

Some of the considerations already made can be extended to the use of frequency standards in satellite tracking networks, with some additional remarks, since accuracy and stability are here important not only for the communications functions (carrier generation, data modulation and demodulation, etc.) but also for the accuracy and correlation of the ranging measurements. The most demanding applications in this field involve precision laser ranging to Earth orbiting satellites for scientific purposes, the most notable of which is the measurement of small deformations of the Earth crust due to the relative movements of tectonic plates.

Two problems arise in this application: high stability and accuracy are required over relatively short time intervals for ranging purposes, while long term stability is needed to generate an accurate local time scale, tied to UTC: this is used to correlate measurements taken at separate tracking sites (no cross-station, or interferometric, ranging is possible using optical links, since the pulse is always reflected back at the transmitting site, and no correlation is possible on the satellite, since this is generally a passive craft carrying an array of retroreflectors)

To achieve centimeter accuracy in ranging a Rb oscillator performs better than a Cs oscillator in many applications; however, laser ranging sites have traditionally used Cs clocks to maintain the long term time accuracy required for range measurements correlation. A disciplined oscillator, based on a frequency-controllable Rb oscillator tied to a GPS timing receiver, can meet all the above requirements at a fraction of the cost of a Cs oscillator, and with a considerable reduction of ancillary costs related to logistics and maintainance. With a synthesized oscillator, it is possible to physically steer the frequency and time, to track **at the station** the nominal values without resorting to timing data post-processing to recover the corrected time of the measurements; this is an additional benefit that can further reduce the operating costs of such a network.

8 APPLICATIONS IN NAVIGATION SYSTEMS

Some interesting considerations find their application when using frequency standards in navigation systems, such as GPS. Neglecting any further considerations on the use of frequency standards in space, already covered before, we will restrict our discussion to the users segment, where additional benefits can be achieved by the use of frequency control in high stability local oscillators.

Multi-channel receivers are used to reduce the exposure time for selected users, namely submarines, during the signal acquisition phase. However, the acquisition and signal tracking steps must be perfomed sequentially, to lock the carrier, SPS (Standard Positioning Service) code, extract the navigation message, lock the PPS (Precision Positioning Service) code and finally perform the pseudo-range measurements. If the PRN code is acquired once, and then continuously updated in the receiver even when the signal from the satellites is not received, the acquisition and lock time of the receiver can be dramatically reduced; this requires that the frequency of the oscillator driving the local PRN code generator is stable enough that, in the time interval between two successive exposures to obtain a fix, the frequency offset between the satellite and the local oscillators is such not to produce a slippage of more than 1 cycle, or a few cycles if some limited search technique is applied when reacquiring

the signal. Since the period of the PPS code is roughly 100 ns, and the time interval between fixes can be one day, the required accuracy for the oscillator frequency is:

$$\frac{\delta f}{f} = \frac{1 \cdot 10^{-7}[s]}{1 \cdot 10^{5}[s]} = 1 \cdot 10^{-12}$$

that can be met only by a Cs standard. However, a greater uncertainty is introduced by the position estimate: current inertial systems can propagate the user position over the same period of time with an uncertainty ranging from a few hundreds meters to a few kilometers. This is the major error factor determining the pseudo-range uncertainty at the time at which the signal is reacquired, since the satellite position can be computed with a better precision by propagating forward the orbital elements. Therefore, it is likely that a limited search is conducted over at least 10-20 cycles of the PPS code when reacquiring the signal. Then a standard Rb oscillator can meet the requirements, provided that some form of frequency control is available to precisely set its frequency to the nominal value and to correct for frequency drift affects (aging).

A second application arises from more basic considerations: the standard GPS navigation solution solves for a minimum of 4 variables, i.e., three spatial coordinates (x,y, z) and time. However, the two sets of coordinates, space and time, are not quite equivalent in their behaviour:

- time changes with a **constant and predictable rate**, the accuracy of the prediction being only a function of the accuracy and stability of the local frequency standard. In contrast,
- space coordinates change in a **completely unpredictable way**, and the main purpose of the GPS is indeed to measure spatial coordinates charges.

Frequency stability in the receiver is not a problem, since the standard navigation algorithm uses the local oscillator only to correlate a minimum of 4 independent measurements, and no stringent requirements are placed on the local oscillator stability or accuracy, as long as a minimum of 4 satellites are in view. However, if a stable and accurate frequency standard is available, the solution can be modified to exploit its capabilities; the navigation estimator time constants should be modified, and the dynamics related to the time solution can be reduced (since the clock is very stable), allowing a heavier filtering of the time offset estimate. As a result, the bulk of the information provided by the pseudoranging measurements contributes to the navigation solution alone.

Taken to the extreme, we are lead to consider two separate solutions running in parallel: one solving for time, as a function of the current position (as provided by the navigation solution), but with heavy filtering and a long associated time constant, and the second solving for position only, the time being available and synchronized to the GPS system time, running with a shorter time constant and using all the data available to improve the precision of the solution: this implies **full decoupling of the time and position solutions**.

The assumption that time and space are separate entities in the GPS solution follows from simple considerations. The first one is rather puzzling when stated the first time: a GPS timing receiver needs to account for the length of the cable connecting the receiver to the antenna, while for a GPS navigation receiver no calibration of the cable is needed, and the coordinates reported are always the coordinates at which the antenna is located (fig. 2), irrespective of the length of the same cable. This rather puzzling behaviour arises from the fact that all common delays in the system (in this case the common propagation delay along the cable) **enter the solution as a clock offset**, i.e. the cable delay appears in the navigation solution as a clock offset, while for the positioning solution this is a term that can be simply neglected.

The fact that considerable benefits can be obtained is apparent by a second example, shown in fig. 4. Here, four GPS satellites are shown at the vertexes of a tetrahedron, equidistant from the user. This provides the best geometry in terms of GDOP (Geometric Dilution of Precision), but results in a total uncertainty in the position of the observer. The uncertainty arises, in such a situation, since any ambiguity in the user position along the axis of the tetrahedron contributes equal delays in the solution, and is simply accounted by a different clock offset; it is like having a cable from the receiver to the antenna of variable length, so that the antenna can be moved in any position along the axis; the coordinates reported will be different and the uncertainty due to the length of the cable will affect the time estimate only.

If the time offset (user clock minus GPS system time) is known, no ambiguity is possible about the location of the user, and from a total uncertainty regarding the user position we move to a situation in which the best possible geometry is exploited to obtain a very good position fix. The situation depicted is extreme in its geometry and consequences for the navigation process; a moving user entering such a situation is aided by its previous estimates of time offset and position to bound the ambiguity to within the error of the previous estimate; nevertheless, the example is striking in the sense that shows what the implications of a synchronized clock are when performing precise navigation. The challenge is therefore to investigate the new possibilities offered by decoupling the time solution from the spatial solution, since:

- the local oscillator is stable, and stability means that we can characterize its behaviour over a longer time constant that is required, for all practical purposes, by the navigation solution; this provides, a better estimate for the time solution and, in turn, a better positioning solution;
- if only three coordinates are to be solved instead of four, marginal geometries can still provide a good solution, since more satellites contribute to the position fix;
- during high-dynamics manoeuvers (such as an aircraft banking rapidly) or shadowing conditions (when one or more satellites are not visible) the "normal" operating conditions can be maintained with a greater margin than that offered by a "conventional" processing receiver.

A possible mechanization is shown in fig. 4, in which the local frequency standard is physically kept in-frequency and synchronized by a solution derived by a "virtual" timing receiver. For high accuracy, this timing processor tracks only the best satellite available, with long time constant and high accuracy, while the current receiver coordinates are provided at a faster rate by the position processor. The latter solves for the spatial coordinates only, by using all the satellites available; the time information is obtained directly from the local clock, synchronized to the GPS Time, so that actual range measurements are performed instead of the pseudo-ranges (biased by the time error). This situation can provide savings also in the implementation of the navigation algorithm. Obviously, the system is initialized by a "classical" GPS solution (position plus time) and the two estimation processes split only when the estimation errors of the combined solution are reduced to within reasonable limits.

9 MILITARY TELECOMMUNICATIONS APPLICATIONS

Military telecommunications systems require precise frequency and time for the very same reasons of civilian telecommunications systems; however, security requirements and data protection place additional constraints on the specifications of reference oscillators in the network. Some communication security (COMSEC) requirements dictate the use of long keys to insure maximum protection of access and information decoding; when keys have a length such that they do not repeat for the

expected lifetime of the system, a "one-time pad" operation results, and no cryptanalytic attack is reputed possible with pure mathematical means without resorting to external intelligence.

"One-time pad" keys, when applied to serial data streams, require precise synchronization of the key generators at both sides, and synchronization can be achieved only after entering the system. This means that it is up to the reference oscillator to maintain the code synchronization when no communication is performed between the two COMSEC terminals. The better the stability and the frequency coordination of the oscillators, the longer the time interval that can be spent without accessing the system, and this is especially important for covert operations, where minimum exposure is required, as is the case of communications to strategic nuclear submarines. Besides communications, the same access and data protection technique is applied to remote control of vital military satellites, since also the command uplinks must be protected against unauthorized access, in addition to jamming and spoofing. Again, the capability to precisely control the frequency and phase of the reference oscillators can increase the protection or lengthen the time interval between resynchronizations, minimizing the exposure and providing additional benefits without the penalty of a sizable increase in costs and hardware complexity.

10 REFERENCES

1. E.Detoma, G.Pedrotto, A.Stern, B.Levi, M.Bootnik, HIGH RESOLUTION DIGITAL SYNTHESIZER FOR A Rb FREQUENCY STANDARD, *Proceedings of the 6th European Time and Frequency Forum (EFTF)* [ESA/ESTEC, Noorwijk - The Netherlands, March 1992]
2. A.Stern, B.Levi, M.Bootnik, E.Detoma, G.Pedrotto, RUBIDIUM FREQUENCY STANDARD WITH A HIGH RESOLUTION DIGITAL SYNTHESIZER, Proceedings of the 46th Frequency Control Symposium [IEEE - Hershey, Pa. - May 1992]
3. V.S.Reinhardt, W.A.Adams, G.M.Lee, R.L.Bush, A MODULAR MULTIPLE USE SYSTEM FOR PRECISE TIME AND FREQUENCY MEASUREMENT AND DISTRIBUTION, Proceedings of the 10th Annual Precise Time and Time Interval Meeting (Washington, D.C., 1978)
4. V.S.Reinhardt, R.J.Costlow, FREQUENCY (STANDARD) COMBINER SELECTOR
5. E.Peled, M.Zelitzki, A.Nemesh, A.Stern, TIME & FREQUENCY SYSTEM FOR SATELLITES GROUND STATIONS
6. P.Kartashoff, FREQUENCY CONTROL AND TIMING REQUIREMENTS FOR COMMUNICATIONS SYSTEMS
7. R.Wilson, PRECISE TIME AND TIME INTERVAL APPLICATIONS TO ELECTRIC POWER SYSTEMS, Proceedings of the 23rd Precise Time and Time Interval (PTTI) Planning and Applications Meeting (Pasadena, Ca. - December 3-5, 1991)
8. V.S.Reinhardt, L.Rueger, THE PERFORMANCE OF NASA RESEARCH HYDROGEN MASERS
9. G.Busca, L.Johnson, A NEW AUTOMATIC CAVITY TUNING FOR ACTIVE H-MASERS
10. Sigma Tau Standards Corporation, ATOMIC H-MASERS mod. 2001 SPECIFICATIONS (Dec. 1989)
11. A.De Marchi, NEW INSIGHTS INTO CAUSES AND CURES OF FREQUENCY INSTABILITIES (DRIFT AND LONG TERM NOISE) IN Cs BEAM FREQUENCY STANDARDS
12. A.De Marchi, G.P.Bava, ON CAVITY PHASE SHIFT IN COMMERCIAL Cs BEAM FREQUENCY STANDARDS, Metrologia, 20, pag. 33 (1984)
13. A.De Marchi, G.D.Rovera, A.Premoli, EFFECTS OF SERVO LOOP MODULATION IN ATOMIC BEAM FREQUENCY STANDARDS EMPLOYING A RAMSEY CAVITY, IEEE Trans. on UFFC (Nov. 1987)
14. E.Bava, P.Tavella, A.De Marchi, DOPPLER EFFECTS IN A MULTI-WAVELENGTH RABI CAVITY FOR THE EXCITATION OF ATOMIC BEAMS IN MICROWAVE FREQUENCY STANDARDS

15. D.A.Howe, H.F.Salazar, A DIGITAL 5.00688 MHz SYNTHESIZER AND SQUARE WAVE SERVO SYSTEM FOR CESIUM STANDARDS, Proc. of the 29th Annual Symp. on Frequency Control, pp. 387-393 (28-30 May, 1975 - Atlantic City, N.J.)

16. HP5071 PRIMARY FREQUENCY STANDARDS: UNSURPASSED STABILITY IN THE LAB OR IN THE FIELD, Hewlett-Packard Specifications (Dec. 1991)

17. FTS 4065, THE MASTER CLOCK DIGITAL Cs TIME AND FREQUENCY STANDARD, FTS Specifications (1991)

18. L.Cutler, A.De Marchi, C.Flory, R.Giffard, FREQUENCY PULLING BY HYPERFINE [SIGMA] TRANSITIONS IN Cs BEAM ATOMIC FREQUENCY STANDARDS, Journ. of Applied Physics, March 1991, pp. 2780-2792

19. L.Cutler, A.De Marchi, C.Flory, R.Giffard, FREQUENCY PULLING IN Cs BEAM FREQUENCY STANDARDS DUE TO [DELTA] M=±1 (SIGMA) TRANSITIONS, Proc. of the 45th Annual Symp. on Frequency Control, IEEE, May 1991

20. V.S.Reinhardt, K.Gould, K.McNab, M.Bustamante, A SHORT SURVEY OF FREQUENCY SYNTHESIZER TECHNIQUES

FIGURE 1:TFL-SEPA Synthesized Rb Frequency Standard

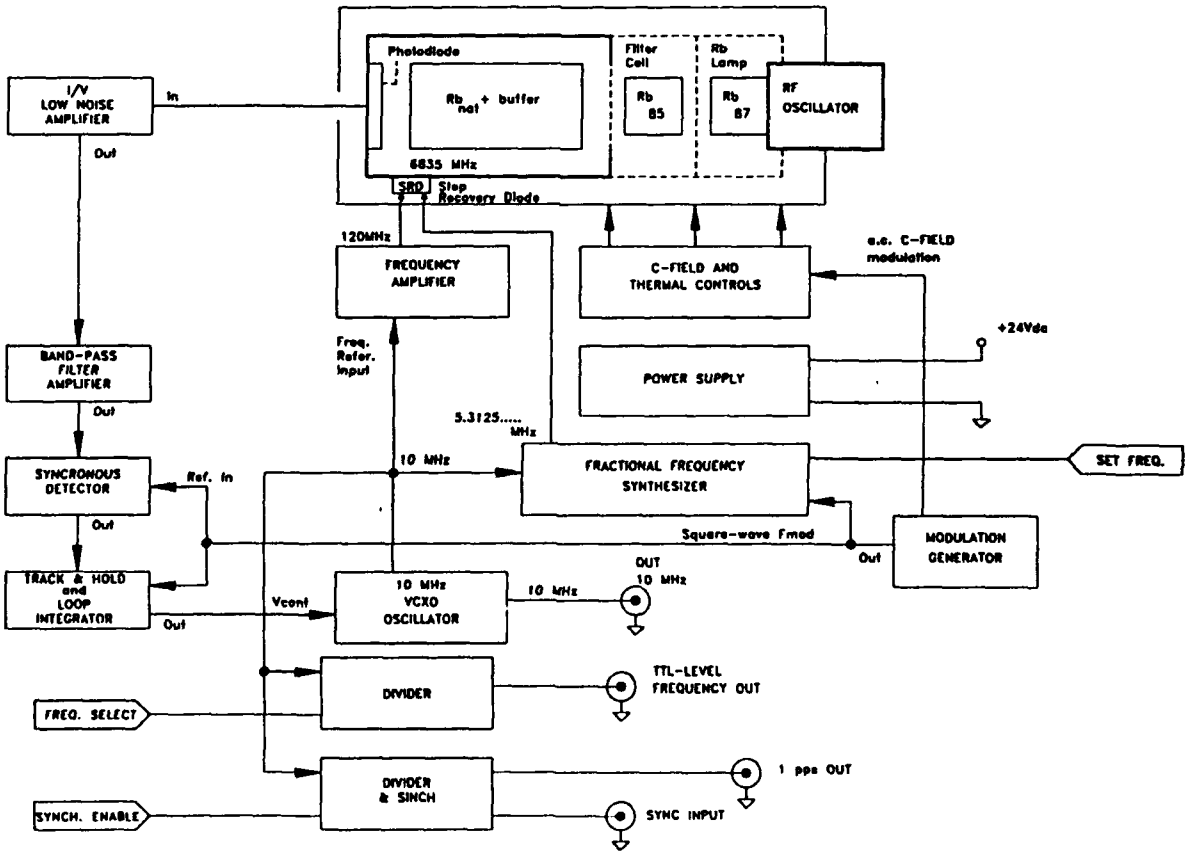

FIGURE 2:GPS System - Non-reciprocity of Antenna Cable Delay

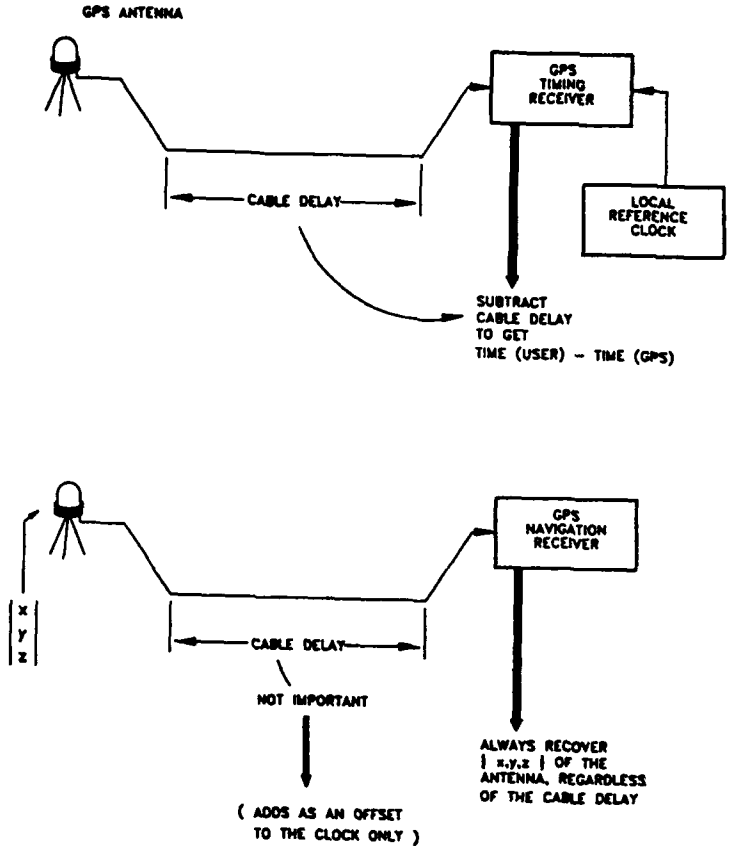

GPS – NON–RECIPROCITY OF ANTENNA CABLE DELAYS IN TIMING AND POSITIONING SOLUTIONS

FIGURE 3:GPS System - Navigation Pseudo-Ambiguity

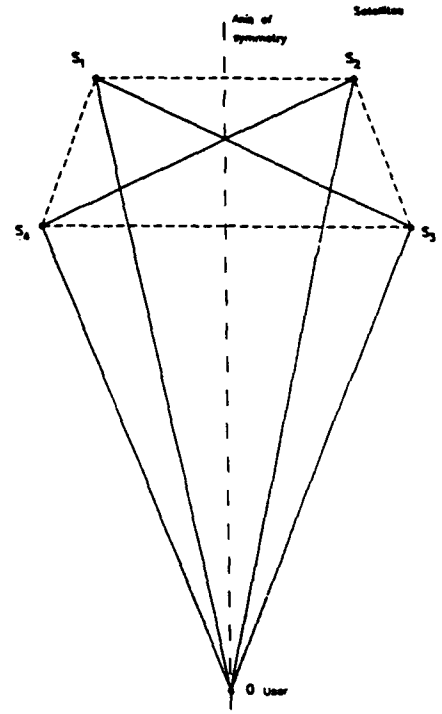

Satellites are equidistant from user at O.

i.e.: $S_1O = S_2O = S_3O = S_4O$

Any position along the symmetry axis is a possible solution; the residual goes into the time component of the solution, i.e the offset becomes completely arbitrary.

FIGURE 4:GPS System - Decoupled Space/Time Navigation Mechanization

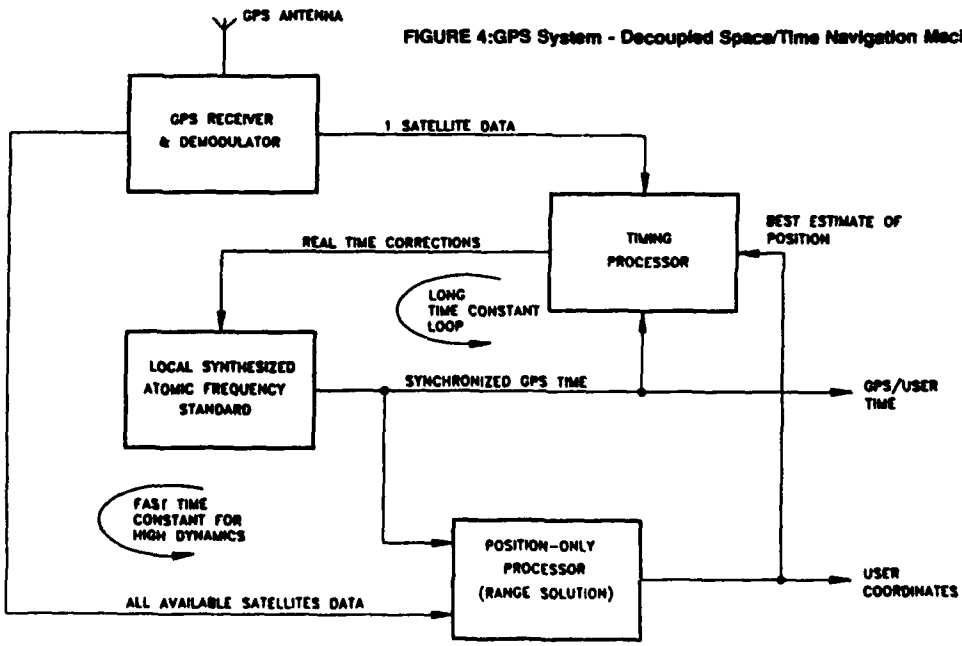

QUESTIONS AND ANSWERS

B. Alam, NRAD: I have a general question regarding the three above papers. In those we were aiding an oscillator from GPS time. Has anyone considered the opposite problem of aiding a GPS receiver with an oscillator or with a frequency standard for direct wide acquisitions for high dynamic platforms. Not only cesium standards but to minimize the size for high dynamic aircraft, for example.

Dr. Winkler, USNO: Yes, in fact several groups have considered that but not merely from that point of view. In the interest of gains of autonomous integrity detection capability by providing additional parameters to the receiver. Not only time as averaged and predicted over periods of 100 or a 1000 seconds which is sufficient but also shows them inertial information. Any parameter which aids the receiver allows you to reduce the dynamic problem to a stationary one, where you can integrate over a longer time constant. The inertial and timing information to the receiver allows you predict in a short time where you are, even if in a very high dynamic environment. You can then reduce the averaging to a stationary problem.

Question: Besides considering the repetition of the P code for example. If you have lost a satellite because of shading or something, what parameters would one need to consider when specifying an oscillator or a rubidium standard keeping in mind a small size for aiding your receiver? What would be the parameters, I am not sure?

G. Winkler: It is efficient for stability of that oscillator to be very good to the one part in ten to the eleventh over periods of 100 to a 1000 seconds.

E. De Toma, FIAT CIEI: There are some other advantages that you may consider from a solution like these. If really all the common mode effects are going into only the timing solution, you can consider also the situation in which you have propagation effects. In the first order tropospheric propagation is common to all the satellites. If the conditions are not too wide the atmospheric propagation is the first order common to all the satellites. Now these affects, if not properly accounted for will contribute to the full solution and mainly to the timing process. Again if you add a longer time the position accuracy also will be degraded. Now if you use this approach you track for time, only the satellites by which these affects are less evident like the one that is directly overhead. So you try to minimize what are the system errors from the timing solution. Then if it is true that all the timing of the common mode effects, just going into time and not the range, you should have a better solution for positioning the satellites which do not have a very high elevation angle. In this case the common mode propagation will not enter into the solution. At least for tropospheric this is certainly true but for atmospheric you have to be more careful because within the time and length of the path and the condition of the propagation.

G. Winkler: I would like to add to that one more point you are absolutely correct. If you compare the situation today with the situation 10 years ago, today it is very much easier to have 8 or even 9 channel receivers because an additional channel is not as expensive as it use to be. By having all the satellites in view at all times for a receiver you not only approve your aim capability, but you also have a system solution which identifies other problems. It is much stronger and much more robust, reliable and it has in fact the capability of giving an internal figure of merit, as if you only use a minimum number of satellites.

E. Detoma: Yes, but remember at this point the position processor solves for real ranges. So you may also have some simplification of the algorithm because it is no longer a completely nonlinear solution that you have to iterate.

CAFS—A CESIUM ATOMIC FREQUENCY STANDARD FOR GPS BLOCK IIR

Jeffry A. Wisnia
Kernco, Inc.
Danvers, Massachusetts

Abstract

Kernco, Inc. was selected to design the Cesium Atomic Frequency Standards (CAFS) for the GPS Block IIR NAVSTAR satellites. These spacecraft are scheduled to be launched in the mid-1990s to replenish and upgrade the existing constellation of Global Positioning System satellites. The Block IIR CAFS output frequency is 13.4003378 MHz, the 686th submultiple of the cesium atomic resonance frequency. Using an integer submultiple simplifies the design of the atomic frequency standard's rf multiplier circuits, eliminating the secondary frequency synthesizer needed in previous designs.

This paper describes the GPS Block IIR CAFS design, particularly the improvements made on our earlier Block II design. Test results are included.

INTRODUCTION

The GPS NAVSTAR Block IIR satellites will replenish and work with the Block II satellites. Cesium atomic frequency standards will provide highly stable timing references for the satellite navigation system.

Kernco was a second source cesium clock supplier to the current generation of Rockwell built Block II satellites. The first of these satellites carrying a Kernco cesium standard is scheduled for launch in December 1992. The Block II design served as a baseline for the current CAFS unit.

General Electric Astro Space Division is the prime USAF contractor for the Block IIR satellites and the ITT Aerospace/Communications Division is the subcontractor for the GPS navigation system. Kernco is the designer of the cesium atomic frequency standards (CAFS) for this program.

Two complete prototype CAFS have been built and subjected to many qualification level tests, including Flash X-ray test on both units. The full spectrum of qualification tests will be run on a production unit.

TECHNICAL REQUIREMENTS

The key performance and environmental/survivability requirements are summarized in Table 1.

TABLE 1 — FUNCTIONAL REQUIREMENTS GPS BLOCK IIR CESIUM ATOMIC FREQUENCY STANDARD (CAFS)	
ITEM	SPECIFICATION VALUE
Frequency	13.4003378571 MHz
Frequency Offset	$-0, +1 \times 10^{-9}$ df/f
Frequency Drift	5×10^{-14} df/f per day (after 30 days)
Frequency Repeatability	Less than 5×10^{-12} df/f
Temperature Stability	Less than 2E-13 per degree C (0 to 256oC)
User Output	50 ohms, +18 dBm +/- 1.5 dB
Phase Noise (maximums)	L(1 Hz): -85 dBc/Hz L(1 kHz): -90 dBc/Hz
Harmonic Output	-50 dBc maximum
Input Power (maximums)	28vdc; 26 watts maximum operating 50 watts maximum warmup (1 hr.)
Size	16.5 x 5.25 x 4.75 inches
Weight	17 lbs. (without radiation shielding)
Life	7.5 years
Reliability	0.755 for 7.5 years (minimum)
Survivability	± 10 nanoseconds (max prompt error) -10 dB max prompt output level change 2.6 meters (maximum 24 hour URE) 36.3 meters (maximum 14 day URE)
SOURCE: ITT A/CD Specification 30072-134L	

Orbital stability requirements for the CAFS are shown by the "spec line" in Figure 1. The Figure also shows the frequency stability performance achieved on one of the prototype units.

CHANGES AND IMPROVEMENTS

Reduced Size, Weight and Power (See Figure 2) Denser electronic packaging resulted in reducing the size of the Block IIR CAFS by 35%. Reducing the size of mechanical structures lowered the unit's base weight to 17 pounds from the previous Block II weight of 26 pounds. Adding 4 pounds of nuclear radiation shielding brings the total flight weight to 21 pounds. Power consumption was reduced 14% to less than 23 watts.

Automatic Start–up Cold turn–on of the previous (Block II) cesium atomic frequency standards needed ground control uploading of a tuning voltage word to set the unit's VCXO frequency. This initial tuning was needed so that the cesium beam excitation frequency, derived from the VCXO by a combination of multiplication and frequency synthesis, was within 500 Hz of cesium resonance (9.192667... GHz). A preset tuning voltage could not accomplish this because orbital aging and radiation effects during the 7.5 year mission life could cause the VCXO to drift as much as 2 Hz from its initial ground value.

Since the Block IIR satellites provide no control signals to the CAFS beyond turning on 28 Volt spacecraft power, the CAFS has an automatic system to obtain the proper initial setting for the

VCXO control voltage, and automatically achieves cesium locked operation about 20 minutes after power is applied. Frequency is within 1×10^{-11} df/f of final value one hour after a cold turn–on.

BLOCK DIAGRAM

A block diagram of the CAFS is shown in Figure 3. The circuitry follows traditional cesium standard design, using 102 Hz square wave frequency modulation of the 9.192 GHz cesium excitation to sense frequency error.

An analog/digital servo system processes the cesium beam tube's output signal to lock the VCXO to the cesium resonance. The servos loop time constant is 13 seconds, allowing the VCXOs short time performance to dominate the frequency stability profile for averaging times below about 50 seconds.

User output at 13.4 MHz is derived from a 6.7 MHz VCXO after frequency doubling and buffering. The VCXO frequency is multiplied directly to produce the 9.192 GHz cesium excitation frequency.

The cesium beam physics package is supported by a cesium oven controller, C–field source, hot wire ionizer current supply, electron multiplier power supply, and an integral ion pump/power supply.

Two telemetry outputs to the satellite's navigation system are derived from the servo system. These are a loop lock status monitor and a linear level monitor of second harmonic modulation (204 Hz) present at the output of the beam signal preamplifier. Signals from two temperature sensing thermistors attached to the bottom of the CAFS are also provided to telemetry.

PHYSICS PACKAGE

The cesium beam tube employs single beam dipole deflection optics. Minor outline changes were made to the long–lived design which had been used in the Kernco Block II cesium units. Some electrical feedthroughs were relocated on the tube shell to optimize lead lengths. Sufficient cesium charge and graphite gettering capacity insures an operating life of at least 20 years. Three units on Acclerated Life tests since 1983 confirm lifetimes in excess of the nominal twenty (20) years.

ELECTRONICS

VCXO

The VCXO uses a 6.7 MHz fifth overtone AT cut swept synthetic quartz resonator in a modified Clapp oscillator circuit. The VCXO is thermally insulated and ovenized, servoed to a fixed temperature near 85 °C. The specific operating temperature of each oscillator is factory set to the zero slope inflection point of its df/dt characteristic.

User RF Output Circuit

The 13.4 MHz user output, a 50 ohm source at +18 dBm, is provided by a push–push doubler and a power amplifier. This part of the CAFS circuitry also supplies buffered 13.4 MHz to the rf

multiplier as well as 6.7 MHz to the servo section; for clocking digital circuits.

RF Multiplier

Square wave FM modulation at 102 Hz produces a servo error signal when the 9 GHz cesium excitation is not precisely at cesium resonance. Modulation takes place at 13.4 MHz in a linear phase modulator driven by a precise triangular waveform.

The 9192.667 GHz cesium excitation frequency is the 686th multiple of the VCXO output. Multiplication is achieved with 36X integer multiplication using doublers and triplers, followed by a step recovery diode harmonic generator. The multiplication factors used are:

$$13.4003...MHz \times ((2 \times 3 \times 3 \times 2 \times 19) + 2) = 9192.6...MHz.$$

Where the final addition of (2 x 13.4003...) is accomplished by mixing action in the SRD multiplier. The upper sideboard of the 19th harmonic is selected by a high–Q cavity filter tuned to the cesium resonance frequency.

Beam Tube Support Systems

The cesium beam tube needs several power sources to support its operation:

- Cesium oven heater supply (temperature controlled)
- C-field current source
- Hot–wire ionizer current supply
- Mass spectrometer accelerating voltage
- Electron multiplier voltage supply
- Ion pump high voltage supply

The function of these supplies is traditional in cesium atomic clocks and will not be discussed in detail here.

Servo Circuits

This is the most complex portion of the CAFS' electronics, containing analog and digital circuits which together control a tuning voltage to keep the VCXO frequency locked to cesium resonance. The servo section also provides several secondary functions including generating the lock indicator and second harmonic level telemetry output signals.

Automatic Starting System (Autostart)

The automatic start–up establishes an initial value in the digital storage register controlling the "coarse" VCXO tuning voltage. After cesium lock is established, this digital register (a 10 bit up–down counter) is incremented or decremented by the servo system to offset VCXO drift.

The cesium oven heater control system is used as a "timer" to initiate the autostart sequence. Autostart begins when the cesium oven regulator comes out of saturation and begins linear tem-

perature control. This occurs about 20 minutes after power is applied to a "cold" CAFS. The VCXO's warm-up is fast enough so that cesium locked frequency is within its tuning range by the time the oven heater circuit comes out of saturation.

The Autostart operates by turning off modulation, zeroing the digital counter/storage register, and clocking 1024 "up" pulses into this register. This sweeps the VCXO through its full tuning range. The maximum value of the cesium beam current signal occuring during the sweep is stored in an analog peak holding circuit. (Maximum beam current occurs when the multiplied VCXO frequency hits the central peak of the field independent transition Ramsey response.) The VCXO is swept a second time and stopped by a comparator circuit when the beam current signal reaches 95% of the stored value. This leaves the digital storage register very close to its cesium locked value. Modulation is switched on, and the servo loop begins steering the VCXO.

Power Supplies

The CAFS runs on 28 vdc spacecraft power and draws 22.5 watts at a temperature of 256oC in vacuum. Power consumption during warm-up is less than 50 watts.

The power supply system uses a single ended flyback switching supply which isolates the CAFS from the input power source. This supply feeds three linear regulators to produce the +15v, -15v and +5v buses which power most of the circuits. The main switching supply also provides power to several secondary supplies with specialized requirements. Examples of these are the 2 kv regulated electron multiplier voltage supply and the hot wire ionizer supply, a downconverting switching supply which sources 2.5 amps to a low impedance (1/3 ohm) load. All power supplies in the CAFS are short circuit tolerant.

Input power filters provide EMI filtering and protect the CAFS power supply from surges and transients.

MECHANICAL DESIGN

Figure 4 shows the CAFS with its outer cover removed.

The cesium beam tube is the largest and heaviest assembly in the CAFS. It measures 13-3/4 x 3 x 3 inches and weighs 9 pounds. The packaging approach placed the electronics against the bottom and sides of the beam tube, so that all beam tube support circuits are close to their respective interfaces with the tube.

Figure 5 is an exploded view identifying the major assemblies. The Base Plate is a machined aluminum part providing the thermal interface with the spacecraft. This assembly contains the main power supply, the input power filter, and the power and telemetry connector filter boxes. The 6.7 MHz VCXO mounts to this assembly.

The Tube Support is a compartmented machined aluminum part housing the rf chain, the user rf output circuits, and the beam tube electron multiplier high voltage power supply. Circuit compartments are fitted with tight covers to prevent rf leakage. The cesium beam tube is rigidly attached to the top of the unit through its central mounting foot.

Printed circuit assemblies containing the servo circuits, cesium oven heater control, and the ionizer power supply are mounted on both sides of the cesium beam tube. Mounting pads on the cesium beam tube shell support these assemblies. The beam tube's ion pump high voltage power supply is mounted in end of the tube, immediately adjacent to the ion pump. All high voltage leads are completely potted to insure corona–free operation.

End panels and covers complete the mechanical assembly and provide additional support and radiation shielding for the printed circuit assemblies mounted on the sides of the cesium beam tube.

RELIABILITY

The CAFS was required to have a 7.5 year mission life, and up to 3 years of pre–launch operation. The predicted MTBF of the CAFS is 601,754 hours, giving a reliability of 0.89657 for the mission life. Several atomic frequency standards are carried on each Block IIR satellite, and can be switched in or out of service by ground commands or on–board computer control.

RADIATION CONSIDERATIONS

A new radiation effects analysis was required because of the tightened autonomous URE specifications. The CAFS circuit designs have been subjected to scrutiny by GE and Jaycor. The critical output circuits were subjected to numerous transient radiation tests at the GE flash X–Ray facility during their development. Both CAFS prototypes were also tested at GE. These analysis and tests have established the shielding and parts screening requirements which enable the CAFS to satisfy the specified radiation requirements.

PERFORMANCE DATA

Stability

Figure 6 shows the SSB phase noise of the CAFS. This plot shows performance well below the spec line with the exception of a power line (60 Hz) spur resulting from imperfect shielding of the measuring setup.

Frequency stability, measured using an HP 5061–004 cesium standard as a reference is shown in Figure 1. Further long–term measurements against a hydrogen maser are anticipated now that developmental performance tests have been completed.

Temperature Stability

The average temperature coefficient of the prototype model measured over 0 to 35°C was less than 1×10^{-13} df/f per degree.

Magnetic Field Sensitivity

The CAFS was subjected to a 3–axis magnetic field sensitivity test, using applied fields of plus and minus two gauss in each axis. A deviation of 7.25×10^{-13} df/f per gauss was measured in the

most sensitive axis.

FUTURE POSSIBILITIES

The Block IIR CAFS design has wrung most of what is available from traditional "unintelligent" cesium atomic standard architecture. We expect that future Kernco Satellite clocks will use microprocessor controlled self–checking techniques to compensate and correct for environmental and aging effects. This technology, now demonstrated in ground–based cesium standards, is the next logical step to achieve further performance improvements in spacecraft clocks.

ACKNOWLEDGEMENTS

The author wishes to acknowledge the contributions of others at Kernco, without whom the Block IIR CAFS development could not have been accomplished. Principal contributors were Tom Hoffman, Michael Delaney and Dan Janssen.

The work described was supported by the United States Air Force via ITT A/CD Subcontracts No. 413928 and No. 414741.

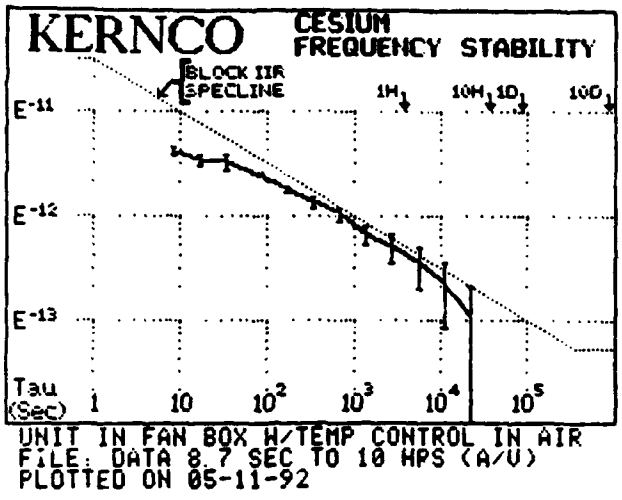

Figure 1. ***CAFS Frequency Stability***

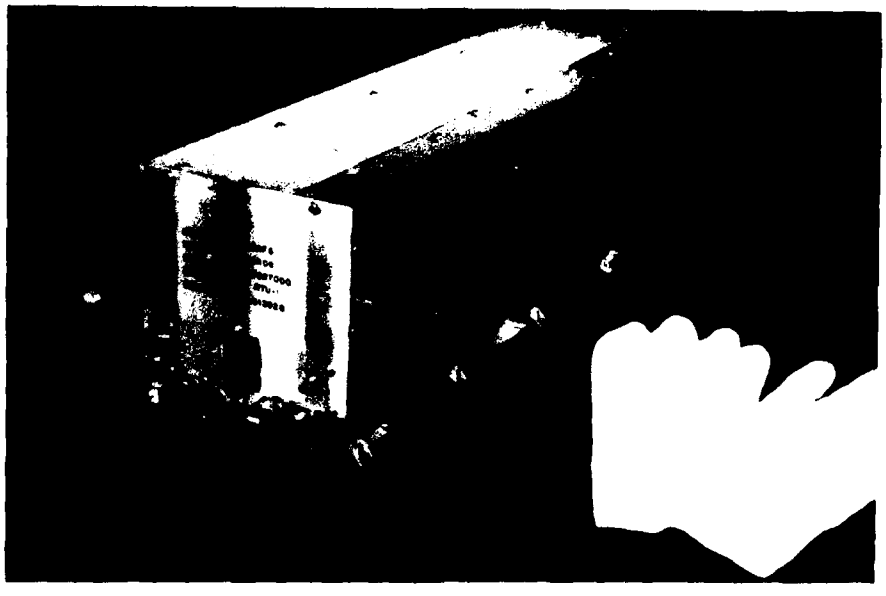

Figure 2. ***GPS-CAFS Unit***

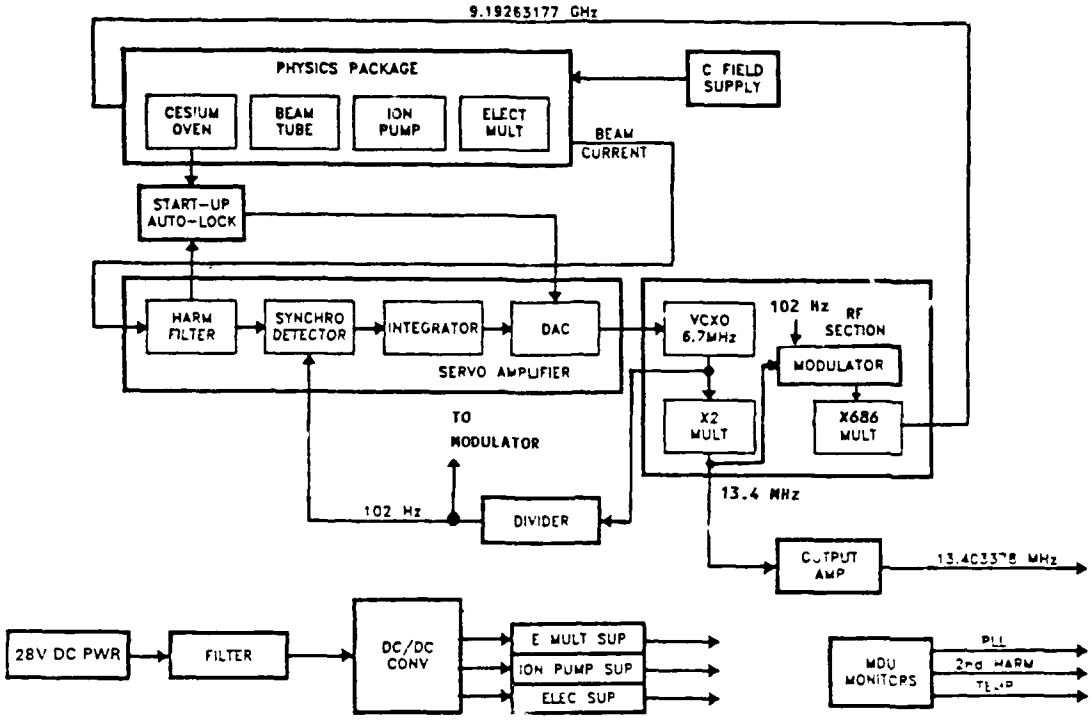

Figure 3. ***CAFS Block Diagram***

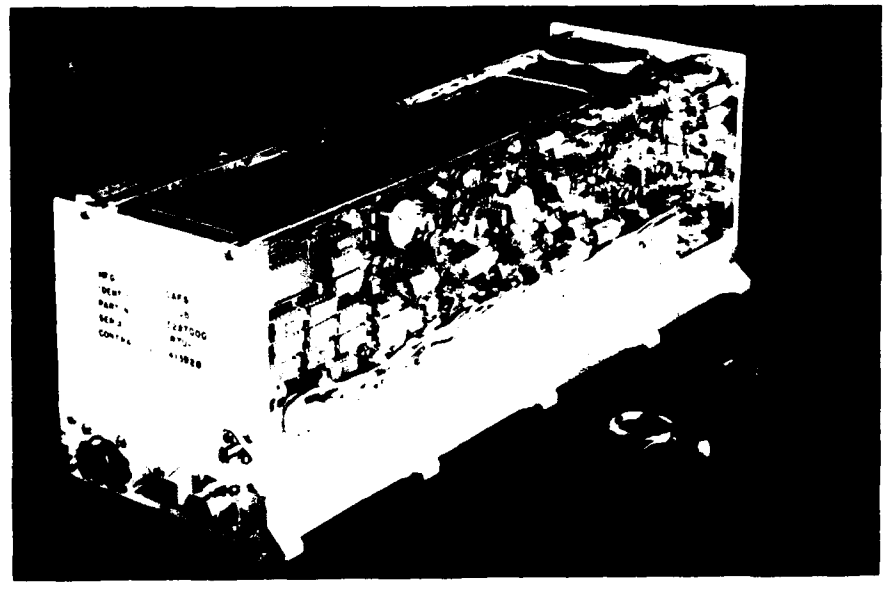

Figure 4. ***GPS-CAFS Showing Servo Electronics***

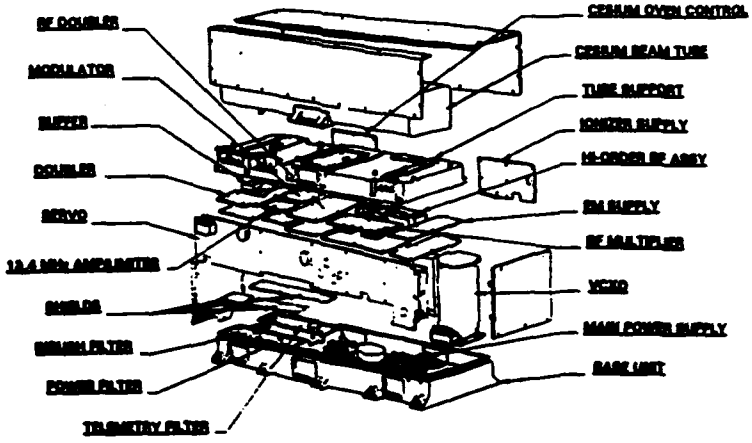

Figure 5. ***CAFS - Construction***

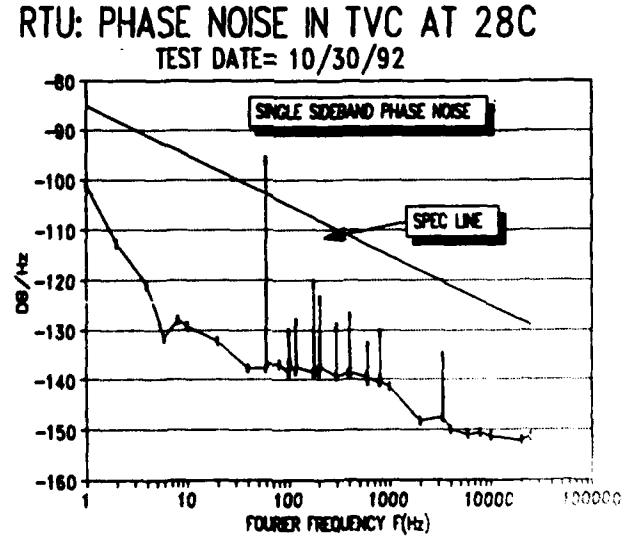

Figure 6. ***CAFS - Phase Noise***

STATUS OF LOCAL OSCILLATORS FOR OPERATING ULTRA–HIGH RESOLUTION FREQUENCY DISCRIMINATORS AS FREQUENCY STANDARDS

R.F.C. Vessot, E. M. Mattison, M.W. Levine and R.L. Walsworth
Smithsonian Astrophysical Observatory (SAO),
Cambridge, Massachusetts 02138

Abstract

The operation of new improved frequency standards based on new ultra–high–resolution frequency discriminators requires high stability local, or "flywheel" oscillators. We review the spectral density of phase fluctuations of existing flywheel oscillators and the related time domain frequency stability of new and proposed cryogenically cooled oscillators suitable for this application. Presently used devices include the quartz crystal oscillator, the room–temperature actively oscillating atomic hydrogen (H) maser and the superconducting maser oscillator. Future devices include the cryogenic H–maser and other cryogenic devices using resonators of superconducting metal or solid crystalline sapphire. The relation of the phase spectral density of these devices to the characteristics of present and proposed frequency discriminators based on trapped cooled ions and cold atoms is discussed in terms of their operation as frequency standards.

1. INTRODUCTION

The advent of several new concepts for frequency standards based on ultra–high resolution frequency discriminators operating at centimeter, millimeter and even optical wavelengths, has refocused attention on local or "flywheel" oscillators needed to generate the signals to be controlled by the discriminator. These signals must have sufficiently narrow frequency spectra compared to the linewidth of the discriminator and adequate frequency stability to stay within the discriminator resonance between interrogations. An important additional requirement of these oscillators is that during the time intervals for a discriminator's frequency interrogation process (including the operational dead–time for quantum state preparation), the phase of the oscillator must not be allowed to drift. Because such phase drifts are cumulative in time, they can seriously compromise the overall long term frequency stability of the frequency standard.[1] Consideration must also be taken to assure that the interrogation process itself causes no appreciable frequency distortion in the discriminator.

New trapped ion[2,3] and cesium fountain[4,5] frequency discriminators enjoy a very high level of immunity from systematic frequency perturbations for very long time intervals ($t > 10^6$ s).

This immunity results from the effective isolation of the atoms or ions from each other and from external perturbations. However, one of the consequences of such isolation to minimize inter–particle collisions is that relatively low densities of particles must be used, resulting in relatively low rates of radiative quantum transitions compared to more conventional devices. This concept has even been extended to the use of a single ion as an optical frequency standard.[2,6] The resulting low signal–to–noise ratio in the frequency discrimination process requires correspondingly longer averaging intervals and puts a premium on the long term frequency stability of the flywheel oscillator.

In general, the frequency stability of an oscillator over very short time intervals (< 1 second) is dominated by thermal noise causing white–phase noise in the output signal. In frequency discriminators the fundamental stability limitation is imposed by stochastic processes, such as shot noise in the detection of an ionized beam of atoms, and the equivalent statistical behavior of photon detectors in optical systems. These processes cause white frequency noise. As in all frequency standards, systematic frequency shifting processes invariably dominate for very long time intervals, but the expectation is that the new discriminators can lengthen the interval before such systematic effects become significant.

Combinations of a number of these systematic processes (including sporadic frequency shifts), will appear in measurements of the Allan deviation, $\sigma_y(\tau)$, and these are often represented as a flicker–noise frequency modulation (FM) , $\sigma_y(\tau) = a_{-1}\tau^0$ and a random walk FM, $\sigma_y(\tau) = a_{-2}\tau^{1/2}$, where a_i is related to a component, h_i, of a power–law spectral density model[7,8,9] of fractional frequency fluctuations, given as:

$$S_y(f) = h_{-2}f^{-2} + h_{-1}f^{-1} + h_0f^0 + h_1f + h_2f^2. \tag{1}$$

Here f is the Fourier frequency and $y = \Delta\nu/\nu_o$, where ν_o is the signal frequency. The units for $S_y(f)$ are Hz^{-1}.

The spectral density of normalized phase (time–interval) fluctuations, $S_x(f)$, is related to $S_y(f)$ by

$$S_x(f) = \frac{1}{(2\pi f)^2} S_y(f), \tag{2}$$

where x represents $\Delta f/2\pi\nu_o$. $S_x(f)$ is in units of $s^2 \cdot Hz^{-1}$ and is related to S_ϕ, the spectral density of phase fluctuations of a signal at frequency ν_o, by $S_x(f) = S_\phi(f)/(2\pi\nu_o)^2$. ($S_\phi(f)$ has units of (radians/s)^2 Hz^{-1}.)

In this spectral representation, h_0, h_1, and h_2 characterize white frequency noise, flicker of phase noise, and white phase noise, respectively. Of these, h_0 and h_2 are easily related to stochastic processes and thermal noise. While there is scant rationalization for the physical origins of the h_{-2}, h_{-1}, and h_1 terms, they are nonetheless useful to represent the Fourier components of observed frequency or phase fluctuations.

The frequency controlling characteristics of frequency discriminators can be described in terms of a *predicted* Allan deviation or in terms of the *equivalent* spectra $S_y(f)$ or $S_x(f)$, calculated from the signal–to–noise ratio and linewidth of the frequency discriminator. It is important to understand

that the *realization of these spectra in an operating piece of hardware*, as manifested in an output signal, will depend both on the interrogation technique and on the limitations imposed by the flywheel oscillator that is controlled by the discriminator.

While it is conventional to describe the frequency stability of frequency locked systems by the Allan deviation in the time domain, $\sigma_y(\tau)$, a better insight into the interactions between flywheel oscillators and frequency discriminators is given by an analysis of the spectral domain of phase (or frequency) fluctuations. In this paper we adopt $S_x(f)$, the spectral density of normalized phase fluctuations, to describe the relationships between frequency discriminators and flywheel oscillators.

2. PRESENT STATUS OF OSCILLATORS USED TO OPERATE FREQUENCY DISCRIMINATORS

Figure 1 shows $S_x(f)$ for commercially available cesium standards, the experimental mercury ion standards at the United States Naval Observatory (USNO)[10], a linear ion trap operated from a superconducting maser oscillator[3,6], a room temperature active H-maser[11], and typical 100 MHz commercial crystal oscillators represented by a band of data. Figure 2 shows the corresponding $\sigma_y(t)$ for these devices.

The quartz crystal-controlled oscillator continues to be the workhorse flywheel oscillator for nearly all frequency standards and clocks in use to date. $S_x(f)$ for 100 MHz voltage-controlled-crystal-oscillators (VCXOs) is shown in Figure 1 over the range of 10^{-1} to 100 Hz. The f^{-3} slope of $S_x(f)$ over these Fourier frequencies indicates a flicker-of-frequency behavior characterized by h_{-1} in Equation 1. At about 10 Hz the VCXO spectra are intersected by the white-phase-noise part of the H-maser spectrum, which steepens to an f^{-2} behavior at lower Fourier frequencies down to about 10^{-3} Hz. This corresponds to white-frequency noise (h_0) in $S_y(f)$, the spectral density of H-maser fractional frequency fluctuations. At still lower frequencies f^{-3} and f^{-4} behaviors are seen in the H-maser $S_x(f)$ spectrum shown in Figure 1. The corresponding behaviors in $S_y(f)$ are flicker-of-frequency noise (h_{-1}) and random-walk-of-frequency (h_{-2}), respectively.

Figure 3 shows a typical phase-lock loop for controlling a VCXO by a low power oscillator (e.g. an H-maser). Such a set-up has good phase stability both at high Fourier frequencies, due to the VCXO, and at low Fourier frequencies, due to the H-maser. In this figure the filter function $g(f)$ represents the loop filter characteristics. Here we see how a 100 MHz crystal oscillator, having a flicker of frequency noise spectrum $S_y(f) = h_1 f^{-1}$, corresponding to a normalized flicker-of-phase spectral-density $S_x(f) = h_{-1} f^3/(2\pi)^2$, can be phase-locked to a room temperature H-maser. To obtain an optimum spectrum, the phase-lock band width should be about 10 Hz, where the white phase noise of the H-maser, at a level 10 log $S_x(f) = -268$, intercepts the flicker-of-phase noise of the VCXO. The design of such phase-lock servo systems is discussed in detail by Vanier and Audoin[12].

3. FREQUENCY LOCK SERVO SYSTEMS

Figure 4 shows a system for frequency–locking an oscillator to a frequency discriminator. Implicit in this process are the requirements that the spectral linewidth of the oscillator's frequency should be narrower than the linewidth of the discriminator, and that the signal from the flywheel oscillator signal should be frequency–modulated to develop an output signal related to the line profile of the discriminator. This signal is then sent to a phase–sensitive detector to control the frequency of the flywheel oscillator, or that of a signal frequency synthesized from that oscillator. The connection between the frequency discriminator and the flywheel is usually made by a second–order servo loop and is depicted by a line with f^{-4} slope in Figure 1 for the H–maser operating the mercury (Hg) ion device. Both the Hg ion trap[10] and the linear ion trap[3] operate their frequency discriminators with a microprocessor. This technique is far more flexible than analog methods for performing complicated routines and permits operation with very long integration times. The goal of such frequency lock servos is to provide an optimum overall connection between the spectrum of the flywheel and the frequency discriminator. Reference 12 discusses the properties of second–order frequency lock servos in detail.

4. APPLICATION OF PRESENT AND FUTURE CRYOGENIC OSCILLATORS AS FLYWHEELS

Operation at low temperatures appears to offer the best prospect to provide flywheel oscillators of sufficient spectral purity and long term stability for use with ultra–high resolution frequency discriminators[2–6] as improved frequency standards.

Low temperature provides improved dimensional stability to materials and tends to freeze out dissipation mechanisms that diminish Q. To obtain levels of frequency stability at the 10^{-15} level from oscillators controlled by microwave resonators, their physical dimensions must be maintained to within fractional dimensions of the same order, smaller than those of atomic nuclei! Under these conditions, variations in power stored in high–Q hollow superconducting metal resonators can produce stress changes and surface heating that affect the dimensions of such resonators. Hollow resonators with Qs of 10^{11} have been developed and operated in oscillators with frequency stability in the low 10^{-16} levels[13,14] for $\tau \approx 10$ s. To reduce the effects of mechanical strain from variations in the radiation pressure caused by the energy confined in hollow resonators, scientists in the former Soviet Union have tried sapphire crystal resonators with superconducting coatings[15,16]. To avoid the need for conductive coatings, ring–shaped sapphire resonators have been developed where the microwave energy is confined by internal reflection from the dielectric boundary in a so–called "whispering gallery" mode. Recent results using this technique show considerable promise[17]. Figure 5 shows the calculated $S_x(f)$ spectrum based on passive Q measurement of a whispering gallery sapphire resonator operated as an oscillator.

The fundamental thermal limit to the frequency stability of a classical, self excited oscillator is

$$\sigma_y(t) = \frac{\Delta\nu}{\nu_o} = \frac{1}{Q}\sqrt{\frac{kT}{2P\tau}} \tag{3}$$

where k is Boltzmann's constant, T is temperature in Kelvins, P is the power driving the oscillation,

and Q represents the inverse of all dissipative processes[18]. The fundamental quantum limit (ql) to frequency fluctuations under conditions where thermal energy, kT, is smaller than $h\nu_o/2$ is[19]

$$\sigma_y^{ql}(t) = \frac{\Delta\nu}{\nu_o} = \frac{1}{Q}\sqrt{\frac{h\nu}{4P\tau}} \tag{4}$$

where h is Planck's constant.

At first sight, it would appear that, by raising the power, the limits on frequency stability given by Eqns. (3) and (4) can be arbitrarily improved. However, there are quantum fluctuations in the radiation pressure in the cavity resonator that increase as $P^{1/2}$. These fluctuations cause dimensional changes in the resonator, and hence frequency fluctuations. For the best cryogenic oscillators, with $Q \sim 10^{11}$ at 10 GHz and operating at an optimum power, and taking into account the mechanical properties of available materials to cope with the quantum fluctuations in the radiation pressure in the cavity, the quantum limit can be as low as[16]

$$\sigma_y^{ql}(\tau) = 2 \times 10^{-20}\tau^{-1/2}. \tag{5}$$

This may not be the final limit on frequency stability, as there are "squeezed state" stroboscopic and quadrature–amplitude measurement techniques that may allow traditional quantum limits to be surpassed; these techniques have been extensively studied by theorists in the former Soviet Union[20].

The combination of a superconducting cavity stabilized maser oscillator (SCMO) with a linear ion trap has been successfully demonstrated at JPL[21,22]. The measured performance of the SCMO is displayed in Figure (1), showing its white phase noise with a signal level given by 10 log $S_x(f) = -276$, and its flicker of frequency noise characterized by f^{-3} behavior between 0.3 Hz and 0.003 Hz. The connection of the SCMO to the linear ion trap at about 0.03 Hz was closed by a "loop in software" using a computer–operated frequency lock servo.

In contrast to oscillators that depend on physical dimensions for determining their output frequency, the cryogenic H–maser[23,24,25] offers considerable immunity from effects related to physical dimensions. Figure 5 shows $S_x(f)$ for estimates of performance based on the present design of the SAO cryogenic H–maser[26]. Here the limiting line Q is taken as 4.5×10^{10}, the storage volume, V_b, is 213 cm^3, and the operating temperature $T = 0.52$ K. The resulting fundamental limit on stability is given by[27]

$$\sigma_y(\tau) = \sqrt{\frac{32\pi kT\sigma_{se}v}{h(2\pi\nu_o)^3V_b}}\tau^{-1/2} = 8.31 \times 10^{-17}\tau^{-1/2} \tag{6}$$

where σ_{se} is the spin–exchange cross section and v is the relative thermal velocity for H–H atomic collisions at 0.52 K. It is interesting to compare this limit with the quantum limit for this oscillator, as defined in equation (4) with the replacement of kT by $h\nu_o/2$:

$$\sigma_y^{ql}(\tau) = 3.03 \times 10^{-17}\tau^{-1/2}. \tag{7}$$

This is well below the limit given in Equation (6).

The output frequency of the cryogenic H–maser is subject to temperature–variable frequency shifts due to H–atom collisions with the superfluid liquid helium wall surface coating and with the helium vapor within the confining maser vessel. The frequency sensitivity to temperature can be minimized by operating at a temperature near 0.52 K, where raising the temperature increases the vapor collision shift and lowering the temperature increases the wall surface effect. Operating at this minimum point, the maser's output frequency is a quadratic function of temperature. To achieve frequency stability at levels about 10^{-18}, temperature stability of a few micro–Kelvins is required; such temperature control is feasible at these low temperatures. There also exists a possible limitation to the stability of the maser that depends on the time of storage of the oscillating atoms[28] and is therefore related to the dimensions of the confining vessel and its collimator. These effects are an important aspect of our present SAO research on the cryogenic H–maser.

Figure 6 shows the projected Allan deviation of new frequency standards based on some of the new ultra–high resolution frequency discriminators discussed in the present paper. It is clear that many precautions must be observed in order to make use of the capability of these new discriminators and to realize standards in the 10^{-18} domain of frequency stability[29]. In addition to the use of appropriate flywheel oscillators, these precautions will likely require new types of technology related to signal transmission and signal processing. Assuming that the projected performance is realized, the new frequency standards will have substantially improved accuracy and stability relative to existing devices.

5. CONCLUSION

Progress continues in the development of flywheel oscillators for use with new ultra–high resolution frequency discriminators. Use of cryogenic techniques is becoming commonplace and should not be considered as a serious roadblock in the operation of such oscillators, even in future spaceborne applications.

ACKNOWLEDGEMENTS

The preparation of this paper was supported by the Smithsonian Institution's Scholarly Studies Program and Research Opportunities Fund. We gratefully acknowledge support from the US Air Force Office of Scientific Research for work on the cryogenic H–maser.

REFERENCES

[1] G.J. Dick, J.D. Prestage, C.A. Greenhall, and L. Maleki, *"Local oscillator induced degradation of medium–term stability in passive frequency standards"*, Proceedings of the 22nd Annual Precise Time and Time Interval (PTTI) Applications and Planning Meeting, NASA Conf. Prec. 3116 (U.S. Naval Observatory, Washington, DC, 1990), p. 487.

[2] D.J. Wineland, W.M. Itano, J.C. Berquist, J.J. Bollinger, F. Diedrich, and S.L. Gilbert, *"High accuracy spectroscopy of stored ions"*, in Frequency Standards and Metrology, A DeMarchi, ed. (Springer–Verlag, Berlin, 1989), p. 71.

[3] J.D. Prestage, G.J. Dick and L .Maleki, *"Ultra–stable trapped ion frequency standard"*, Proceedings of the 22nd Annual Precise Time and Time Interval (PTTI) Applications and Planning Meeting, NASA Conf. Prec. 3116 (U.S. Naval Observatory, Washington, DC, 1990), p. 171.

[4] S Chu, *"Laser manipulation of atoms and particles"* Science 253, 861 (1991).

[5] S.L. Rolston and W D. Phillips, *"Laser–cooled neutral atom frequency standards"*, Proc. IEEE 79, 943 (1991).

[6] D.J. Wineland, J.C. Bergquist, J.J. Bollinger, W.M. Itano, D.J. Heinzen, S.L. Gilbert, C.H. Manney, and M.G. Raizen, *"Progress at NIST toward absolute frequency standards using stored ions"*, IEEE Transactions on Ultrasonics, Ferroelectronics, and Frequency Control 37, 515 (1990).

[7] J.A. Barnes, et al., *"Characterization of frequency stability"*, IEEE Transactions on Instrumentation and Measurement IM–20, 105 (1971).

[8] D.W. Allan, *"Time and frequency (time–domain) characterization, estimation, and prediction of precision clocks and oscillators"*, IEEE Transactions on Ultrasonics, Ferroelectronics, and Frequency Control UFFC–34, 647 (1987).

[9] Characterization of Clocks and Oscillators, D.B. Sullivan, D.W. Allan, D.A. Howe, and F.L.Walls, eds., NIST Technical Note 1337 (NIST, Washington, DC, 1990).

[10] L.S. Cutler and R.P. Giffard, *"Initial operational experience with a mercury ion storage frequency standard"*, Proceedings of the 41st Annual Symposium on Frequency Control (IEEE, New York, 1987), p. 12.

[11] A.A. Uljanov, N.A. Demidov, E.M. Mattison, R.F.C. Vessot, D.W. Allan, and G.M.R. Winkler, *"Performance of Soviet and U.S. hydrogen masers"*, Proceedings of the 22nd Annual Precise Time and Time Interval (PTTI) Applications and Planning Meeting, NASA Conf. Prec. 3116 (U.S. Naval Observatory, Washington, DC, 1990), p. 509.

[12] J. Vanier and C. Audoin, The Quantum Physics of Atomic Frequency Standards (Hilger, Bristol, 1989) pp. 1115–1125 (phase lock) and pp. 752–791 (frequency lock).

[13] J.P. Turneaure, Proceedings of IEEE Conference on Applied Superconductivity (IEEE, New York, 1972), 154.

[14] S.R. Stein, *"Application of superconductivity to precision oscillators"*, Proceedings of the 29th Annual Symposium on Frequency Control (Electronics Industries Association, Washington, DC, 1975), p. 321.

[15] V.M. Pudalov, *"Superconducting SHF resonators and their use in metrology"*, Meas. Tech. 23, 600 (1980).

[16] V.B. Braginsky, V.P. Mitrofanov, and V.I. Panov, Systems With Small Dissipation (University of Chicago, Chicago, 1985).

[17] G.J. Dick and D.G. Santiago, *"Microwave frequency discriminator with cryogenic sapphire resonator for ultra–low phase noise"*, Proceedings of the 6th European Frequency and Time Forum, ESA Document SP–340 (ESA, Paris, 1992), p. 35.

[18] W.A. Edson, *"Noise in oscillators"*, Proc. IRE 48, 1454 (1960).

[19] W.E. Lamb, *"Theory of optical masers"*, in Quantum Optics and Electronics, C. DeWitt, A. Blandin, and C. Cohen–Tannoudji, eds. (Gordon and Breach, New York, 1965), p. 331.

[20] V.B. Braginsky, *"Resolution in macroscopic measurements: progress and prospects"*, Sov. Phys.–Usp. 9, 836 (1988).

[21] G.J. Dick, *"Calculation of trapped ion local oscillator requirements"* Proceedings of the 19th Annual Precise Time and Time Interval (PTTI) Applications and Planning Meeting (U.S. Naval Observatory, Washington, DC, 1987), p. 133.

[22] G.J. Dick and R.T. Wang, *"Ultra–stable performance of the superconducting cavity maser"*, IEEE Transactions on Instrumentation and Measurement 40, 174 (1991).

[23] R.L. Walsworth, I.F. Silvera, H.P. Godfried, C.C. Agosta, R.F.C. Vessot, and E.M. Mattison, *"Hydrogen maser at temperatures below 1 K"*, Phys. Rev. A 34, 2550 (1986).

[24] H.F. Hess, G.P. Kochanski, J.M. Doyle, T.J. Greytak, and D. Kleppner, *"Spin–polarized hydrogen maser"*, Phys. Rev. A 34, 1602 (1986).

[25] M.D. Hürlimann, W.N. Hardy, A.J. Berlinsky, and R.W. Cline, *"Recirculating cryogenic hydrogen maser"*, Phys. Rev. A 34, 1605 (1986).

[26] R.F.C. Vessot, E.M. Mattison, R.L. Walsworth, I.F. Silvera, H.P. Godfried, and C.C. Agosta, *"A hydrogen maser at temperatures below 1 K"*, IEEE Transactions on Instrumentation and Measurement IM–36, 588 (1987).

[27] A.J. Berlinsky and W.N. Hardy, *"Cryogenic masers"*, Proceedings of the 13th Annual Precise Time and Time Interval (PTTI) Applications and Planning Meeting, NASA Conference Publication 2220 (NASA, Washington, DC, 1981), p. 547.

[28] B.J. Verhaar, J.M.V.A. Koelman, H.T.C. Stoof, O.J.T. Luiten, and S.B. Crampton, *"Hyperfine contribution to spin–exchange frequency shifts in the hydrogen maser"*, Phys. Rev. A 35, 3825 (1987); J.M.V.A. Koelman, S.B. Crampton, H.T.C. Stoof, O.J.T. Luiten, and B.J. Verhaar, *"Spin–exchange frequency shifts in cryogenic and room temperature hydrogen masers"*, Phys. Rev. A 38, 3535 (1988).

[29] F.L. Walls, L.M. Nelson, and G.R. Valdez, *"Designing for frequency and time metrology at the 10–18 level"*, Proceedings of the 6th European Frequency and Time Forum, ESA Document SP–340 (ESA, Paris, 1992), p. 477.

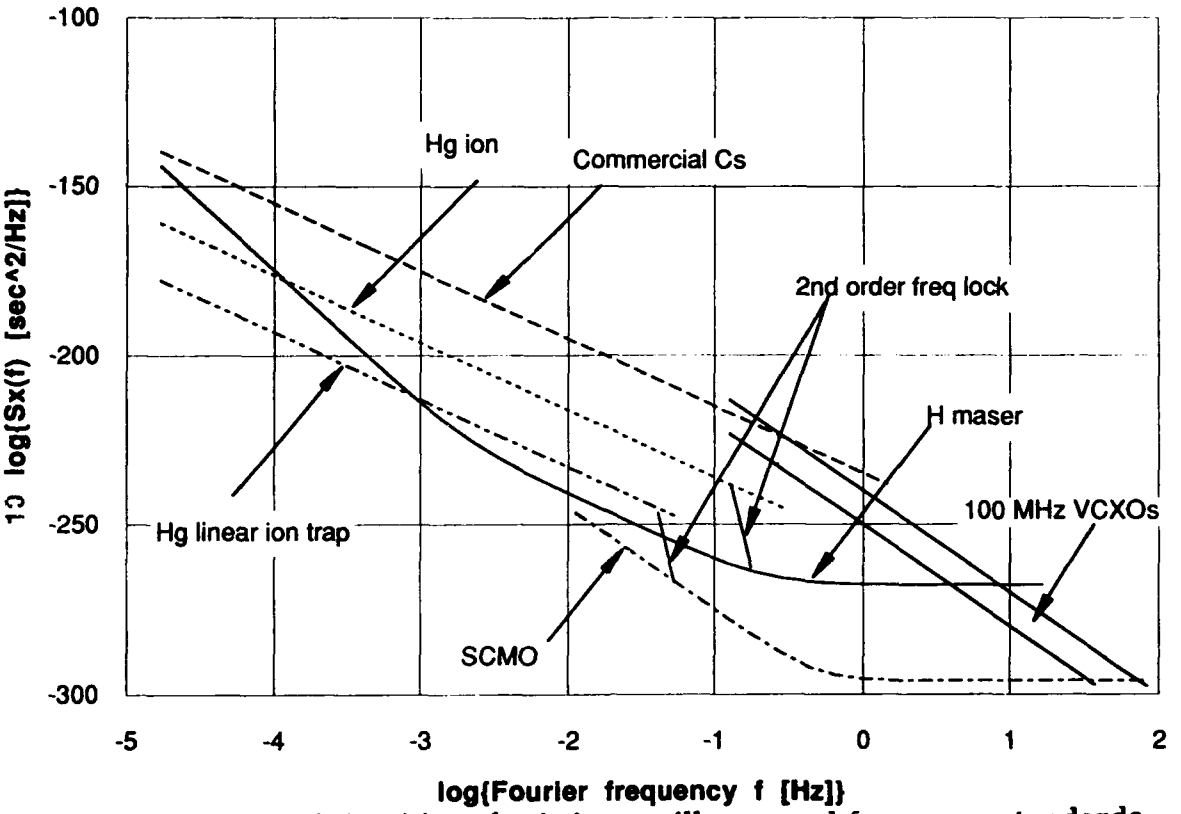

Fig. 1. Phase spectral densities of existing oscillators and frequency standards.

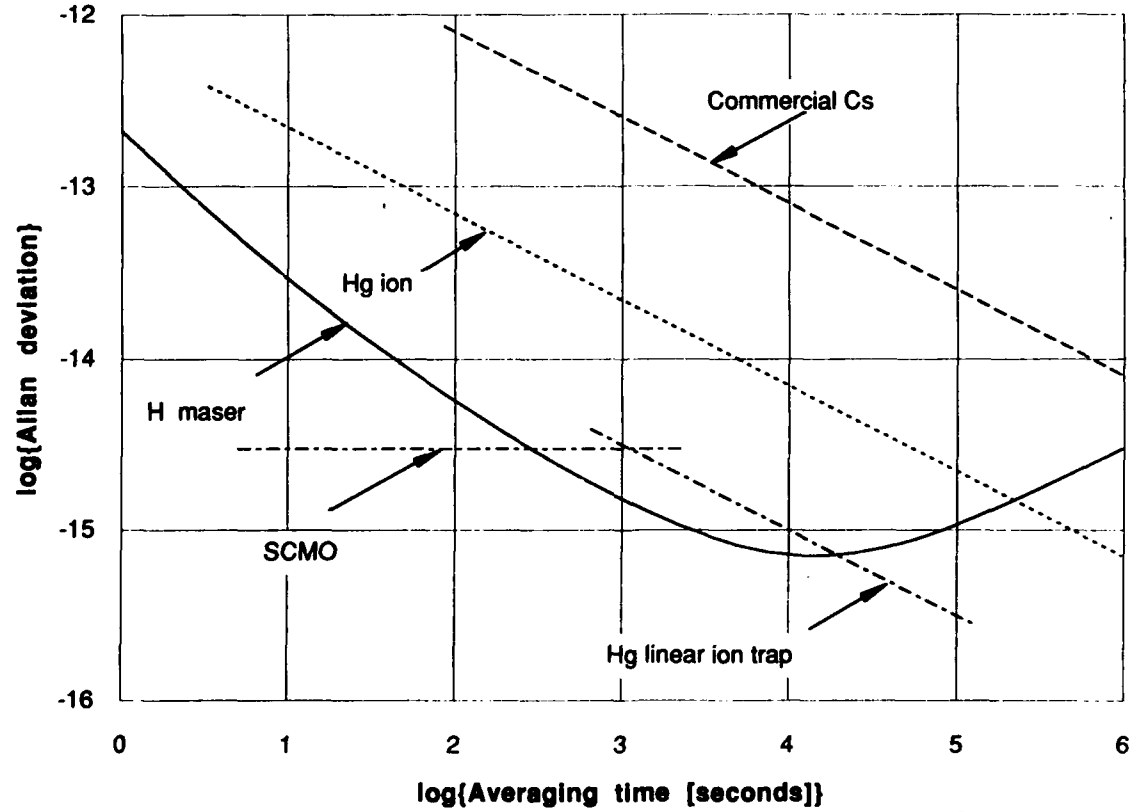

Fig. 2. Allan deviations of existing frequency standards.

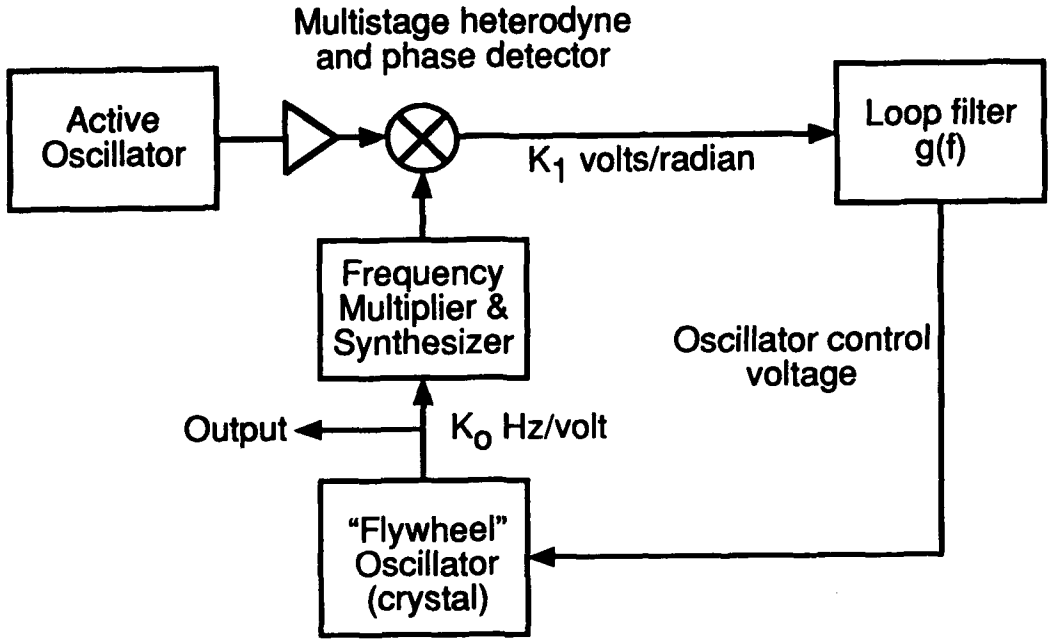

$S_x(f)_{out}$ ~ $S_x(f)_{flywheel}$ for high frequencies (short times)

~ $S_x(f)_{active}$ for low frequencies (long times)

Fig. 3 Typical phase lock loop for active oscillator.

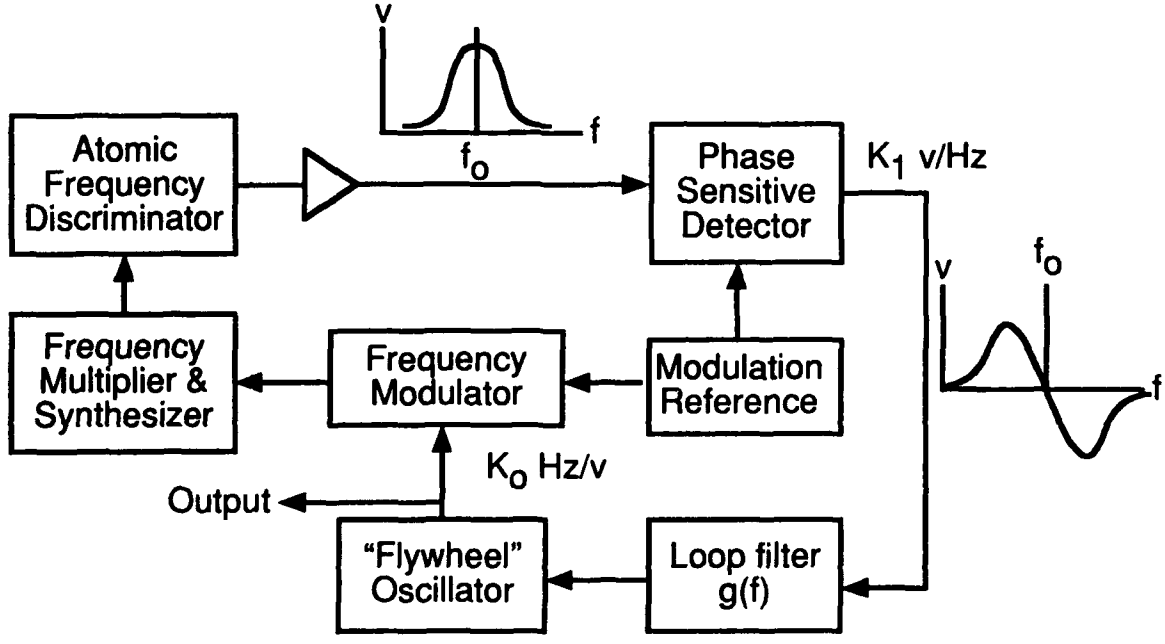

$S_y(f)_{out}$ ~ $S_y(f)_{flywheel}$ for high frequencies (short times)

~ $S_y(f)_{discriminator}$ for low frequencies (long times)

Fig. 4. Typical frequency lock loop for frequency discriminator.

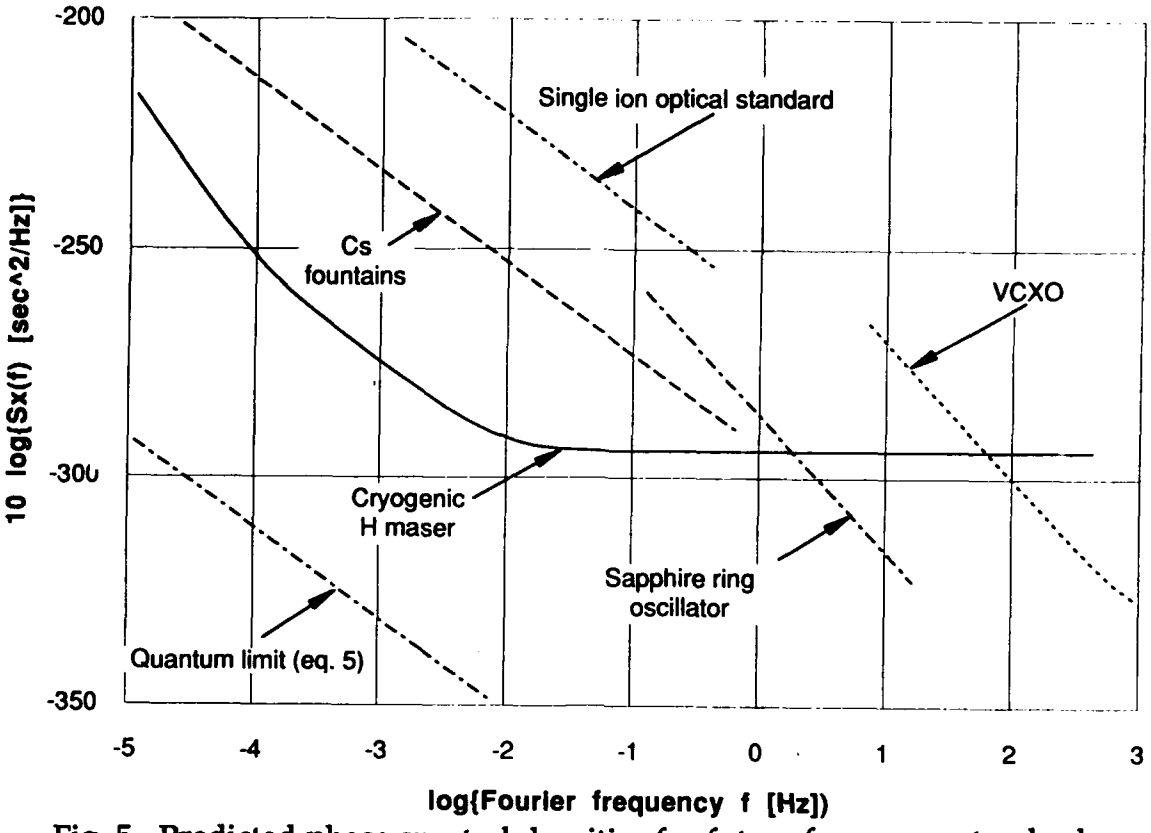

Fig. 5. Predicted phase spectral densities for future frequency standards.

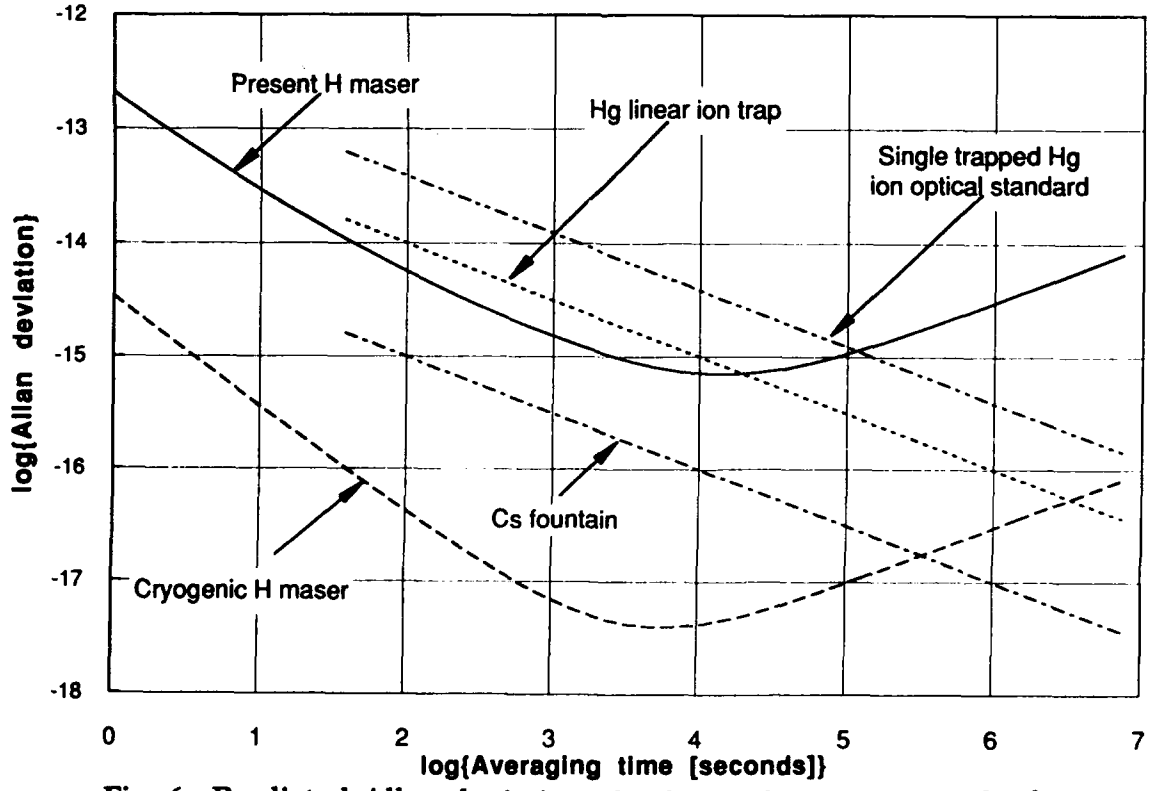

Fig. 6. Predicted Allan deviations for future frequency standards (assumes no systematic effects in Cs and Hg devices).

QUESTIONS AND ANSWERS

D. Allan, Allan Time: Two Comments. Some work at NIST would indicate that some breakthrough potentials for rubidium short term rubidium performance that's quite exciting, short term stabilities in the parts of 10^{-14} at a few seconds. On your long term stability performance, it seems that the linear ion trap potential which was not shown on the one curve for future stability prospects seems very promising as well. The one second stability on it is like 3 parts in $10^{15}/\tau^{-1/2}$, so that might be included as well.

E. Mattison, SAO: I will certainly do that for the paper. I can get more up to date information.

Question: I would be interested in knowing your source for these trapped ion stabilities because I have been trying to find information on that and they seem to be very scarce and it seems to be word of mouth.

E. Mattison: No, that is John Dick at JPL.

Question: People at APL are involved in the work but they are not willing to sort of venture any stability numbers at all. I was just wondering if there was some sort of disagreement between the two scientists.

E. Mattison: All I know is what I got in the paper from John Dick.

D. Stowers, JPL: I have a general question and it is open to anybody in terms of whose giving thought to distribution of these signals. How are we going to get such stabilities to a user? I guess I do not need an answer, but I am sort of concerned about that in the future.

E. Mattison: I suppose an additional question is not only who is going to get it to the user but which user is going to need it. Well one of them is sitting right here, but of course it depends upon the time scale you are talking about.

L. Cutler, Hewlett Packard: JPL is also very interested in this area and I wonder if Dick Sydnor might comment on it or someone else from JPL.

R. Sydnor, JPL: Yes, we see future requirements for this sort of level and of course as you will see in some future papers here we are working on distribution systems that will work at that level and better.

E. Mattison: That being what Dick? You said that level but what level are you referring to?

R. Sydnor: 10^{-17} or thereabouts.

L. Cutler: I have a question or comment. You did not mention the noise of the second harmonic of the modulation frequency as a contributor to the long term performance of the passive resonator. That noise when heterodyned down is indistinguishable from the noise of the resonator itself and does cause a problem. So that is an additional reason why oscillators have to be very good.

Development of a Cryogenic Hydrogen Maser at the NPL

Dr. R. Mossavati
Centre for Basic Metrology
National Physical Laboratory
Teddington
TW11 0LW
UK

Abstract

We have been developing a prototype Cold Hydrogen Maser(CHM) for the past year. The novel features of this CHM, which is designed to operate initially at 4.2 K, are the use of low loss alumina, and later sapphire, in the fabrication of the microwave cavity; possible use of superconductors for shielding; use of a cryogenic amplifier; possible novel coating material; and a reliable rf discharge circuit for the dissociation of hydrogen. A numerical simulation has been performed to find the dimensions of the microwave cavity for the TE011 mode and the model was confirmed experimentally. The system will be used to test various wall coatings adsorbed on top of a PTFE buffer underlayer.

The CHM is expected to be used as a flywheel frequency standard at the NPL with medium-term stability of one part in 10^{14} ***or better.***

INTRODUCTION

Following its initial discovery in 1960 by Goldenberg, Kleppner and Ramsey [1] the hydrogen maser quickly established itself as the most stable of all atomic frequency standards for short and intermediate times, with stabilities of a part in 10^{15} for measuring times between 10^3 to 10^5 seconds. The high stability of the atomic hydrogen maser is due to the following:

(i) the atoms remain in the storage volume for about 1 sec, which is much longer than the storage time in an atomic beam apparatus, so the resonant line is narrower;

(ii) the atoms are stored at low pressure so they are relatively free and unperturbed while radiating;

(iii) the first order Doppler shift is removed because the atoms are exposed to a standing wave and the average velocity is very low for atoms stored for 1 sec;

(iv) the maser noise level is very low when the amplifying elements are isolated atoms.

Cooling the hydrogen maser down to 4K can potentially lead to 3 orders of magnitude improvement in its frequency stability. This is obtained firstly, through an increase in the storage time of the atoms; secondly, by a substantial reduction in the spin exchange collision cross section, which limits the line Q and the power radiated in conventional masers; thirdly, by the use of more uniform and stable storage surfaces which give reproducible wall shifts; and finally; by the improved noise performance of cryogenic rf amplifiers. Thus far three research groups have set up and tested cold hydrogen masers.[2], [3], [4]

The stability of a frequency standard is expressed in terms of the two-sample Allan derviation which is given by:

$$\sigma_y(\tau) = \frac{1}{Q}\sqrt{\frac{kT}{2P\tau}}$$

where Q is the maser line quality factor, k is the Boltzmann constant, T the absolute temperature, P the power delivered by the atoms, and τ the averaging interval. The quality factor of the transition depends on the total transverse relaxation time of the H atoms. This is determined by the storage bulb, the wall and the spin exchange relaxation rates, and is proportional to $T^{1/2}$. The Allan variance depends linearly on T and cooling from room temperature would gives a significant improvement in frequency stability for intermediate measuring times.

The main drawbacks of the hydrogen maser are the change in the hyperfine frequency caused by the occasional collision of atoms with the walls which can give rise to wall shifts of the order of parts in 10^{11}, and the low level of the output signal, which at 10pW puts stringent requirements on the detection system.

Aside from its standards applications the maser has uses in fields as diverse as Very Long Baseline Interferometry, tests of general relativity, satellite navigation systems, telecommunications, and other fundamental research which should lead to a better understanding of spin-exchange, atom-surface interactions, and other relaxation phenomena.

THE COLD HYDROGEN MASER

The Cryogenic Hydrogen Maser (CHM) project was started in October 1991, after the completion of a feasibility study[5], with the following longer term objectives: (i) to develop a flywheel time and frequency standard using recent advances in technology; (ii) investigate the physics and the absolute reproducibility of the standard. Our immediate objective is to acquire the necessary technology by constructing a prototype system before going on to a more sophisticated system.

The CHM assembly is displayed in Fig.1. Hydrogen molecules are dissociated in a discharge bulb energised by the rf circuit shown in Fig.2. They are then formed into a beam of atoms in their ground state having approximately equal populations in each of the four hyperfine sublevels (Fig.3). After flowing down the PTFE transport tube into the cryostat, they are state selected by a hexapole magnet. Atoms in the (F=1) states travel into the maser bulb where they decay into the (F=0) state and radiate power at 1420MHz. If the storage cell is located within a sufficiently high–Q microwave cavity, an oscillation at the resonant frequency will build up until an equilibrium value is reached. The oscillation is picked up by a probe positioned near one end of the cavity, preamplified and transmitted out of the cryostat through a low loss microwave transmission line.

Following a further stage of amplification, the signal is mixed down to audio frequencies and detected.

We will now give a detailed description of the system. The hydrogen discharge system consists of a bulb connected via copper tubing to the hydrogen gas supply and a Pirani gauge. The bulb is capacitively coupled to the rf circuit. We were able to obtain a discharge with 1 mbar pressure of hydrogen in the bulb and 5W rf power at 25MHz. The colour of the discharge changed from bluish red to purplish red with continuous operation.

The state-selector hexapole magnet is displayed in Fig.4. Its appearance was influenced by C. Audoin's original design[6] and specially adapted for operation at low temperatures. The shape of the pole pieces ensures that a uniform positive field gradient is seen by the atoms as they move away from the centre of the magnet. The flux density maximises near the pole tips. We used a NdFeB magnet pieces inserted into soft magnet frame made out of Vanadium Permendur 49. The inter-pole field was measured to be approximately 1.1T using a moving coil galvanometer arrangement with an area of 9.4mm x 0.7mm.

A numerical simulation program was written to find the best configuration of an alumina cavity for use in the CHM. The frequency of the operating mode has to coincide with the hyperfine frequency of the hydrogen, which is 1420.405MHz in a field of 1 mG. The requirements of the hydrogen maser determine the ideal cavity mode to be the TE011. The variation in the cavity frequency of this mode with temperature is shown in Fig.5. This had to be included separately in our numerical model which is only valid at room temperature because of the unknown temperature dependence of the relative permittivity of alumina below 100K. The finished cavity is displayed in Fig.6. The outer surface of the cavity was then silvered to improve its Q factor. We intend to use sapphire in the longer term.

Wall coating of the masing volume is another important factor influencing the overall performance of the CHM. We have performed extensive PTFE coating trials using a solution of Teflon AF1600[7] dissolved in Fluorinert FC77[8]. It was found that 0.75% by weight of the AF1600 dissolved in Fluorinert yielded the best coverage on a thoroughly cleaned surface. Three applications of the solution was found to give the optimum coating. The solution has a transparent, non-viscous appearance when initially mixed. The preparation is comparatively easy; although care has to be taken in the mixing and pouring of the solution onto the surface to be coated. The uniformity of the coating was measured using a nanosurf surface profilometer and found to be smooth to 200nm over a distance of 0.5mm(see Fig.7). Tests of the Teflon film for pinholes using water at room temperature, and cool down as far as 4.2K, were successful; We are about to investigate its performance with atomic hydrogen; and are hoping to test frozen hydrogen and superfluid helium as wall surfaces on top of the Teflon buffer layer.

FUTURE PLANS

Following initial tests, the focusing of the hydrogen beam after the state selector will be observed using a sensitive thermometer made out of phosphorus doped silicon which is capable of measuring 0.5pW at 4.2K over an area of about 0.2 mm^2. The sensitivity of the microcalorimeter arises out of its low heat capacity at low temperatures. The detection threshold corresponds to a flux of 10^6 hydrogen atoms per second impinging and recombining on the device. Since we expect a flux of

10^{12} to 10^{13} atoms per second entering the maser bulb, this gives us a very sensitive hydrogen atom sensor. Preliminary tests are encouraging but its longer term performance is yet to be evaluated.

In preparation for the design of the magnetic shields required for the maser, we have written a program based on Dubber's work[9] which calculates the type and number of shields needed to keep out stray fields and the earth's field. This suggests that a three layer nested arrangement of mu-metal shields which will give a shielding factor of approximately 10^4. Additional low temperature protection is will be provided by a Cryoperm[10] shield.

The electronics for the detection of the free induction decay signal in the passive mode of the maser are assembled and we hope to observe the signal at 4.2K by the middle of next year. Our expectation is that changes to the cavity and in the detection electronics will then become necessary in order to observe the masing action.

ACKNOWLEDGEMENTS

I would like to thank Brian Petley and John Gallop for their advice and support whenever it was asked for. Paul Hardman has been instrumental in much of the recent experimental progress and the NPL workshops have also played their part in realising some difficult designs such as the hexapole magnet.

REFERENCES

[1] H.M. Goldenberg, D. Kleppner, and N.F. Ramsey, Phys, Rev, Lett. 5, 361–2, 1960

[2] R.F.C. Vessot, E.M. Mattison, R.L.Walswoth, and I.F. Silvera, Proc. 4^{th} Symposium on Frequency Standards and Metrology, Italy, 88, 1988

[3] M.D. Hurlimann, W.N. Hardy, A J Berlinsky, and R.W. Cline, Phys. Rev. A 34,2550, 1986

[4] S.B. Crampton, T.J. Greytak, D. Kleppner, W.D. Phillips, D.A. Smith, and A. Weinrib, Phys. Rev Lett. 42, 1039, 1979

[5] R. Mossavati, *Feasibility Study on the Cold Hydrogen Maser*, NPL Report QU89, 1991

[6] C. Audoin, Revue Phys. Appl. 1, 2, 1966

[7] ©Dupont Corporation

[8] ©3M Company, 1991

[9] D. Dubber, *Nuclear Instrumentation and Methods in Physics Research A234, 511–7*, 1986

[10] ©Vacuumschmelz Gmbh.

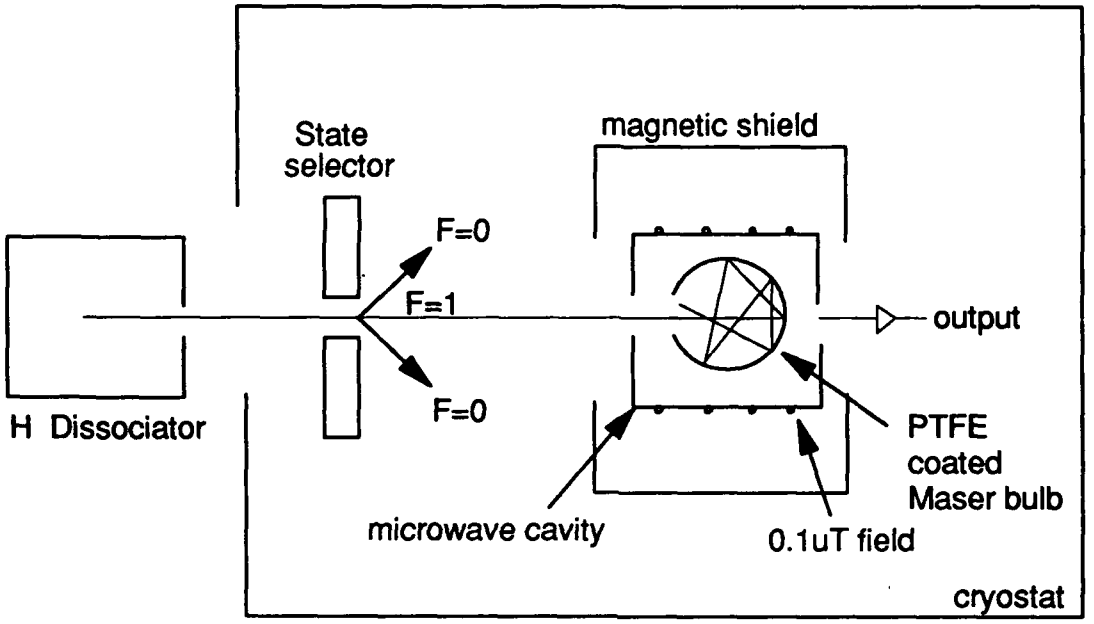

Fig.1 Schematic diagram of the CHM assembly

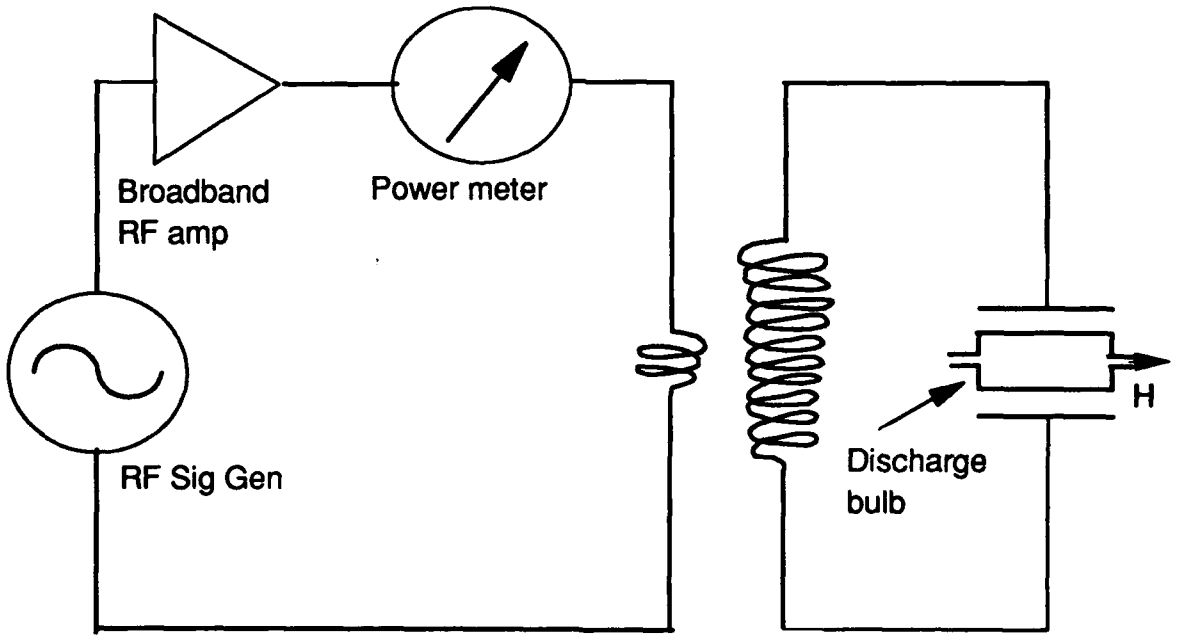

Fig.2 Hydrogen rf discharge circuit

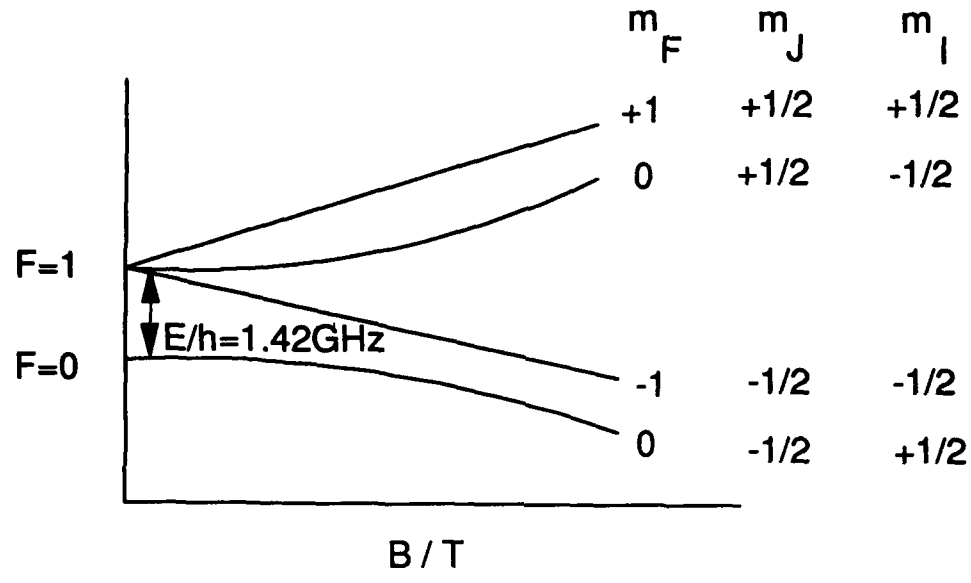

Fig.3 Hyperfine levels of the H atom

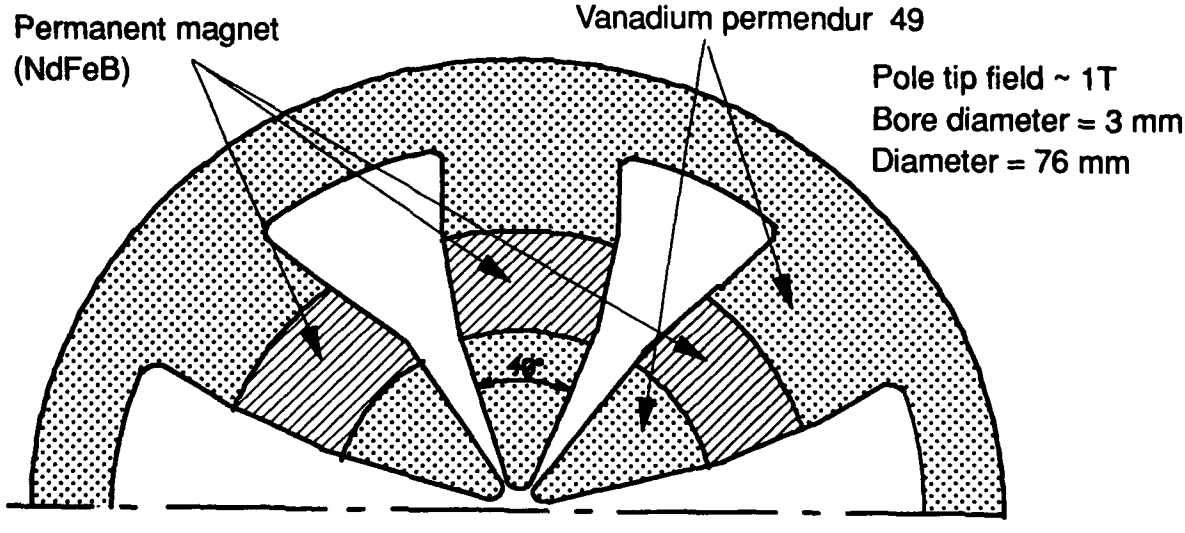

Fig.4 Half section view of hexapole magnet

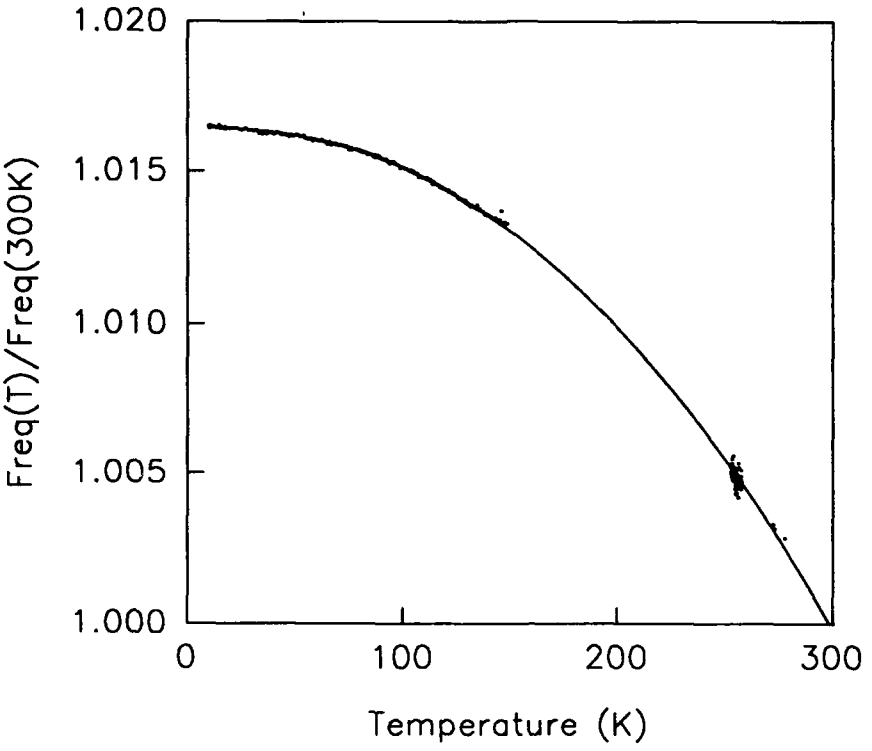

Fig.5 Temperature dependence of the TE011 mode of the alumina microwave cavity.

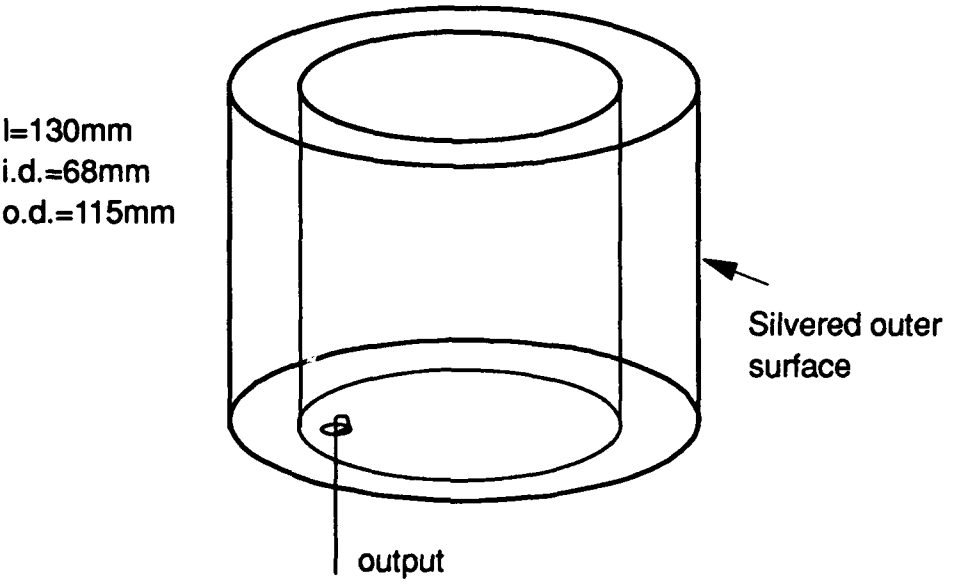

Fig.6 The alumina microwave cavity

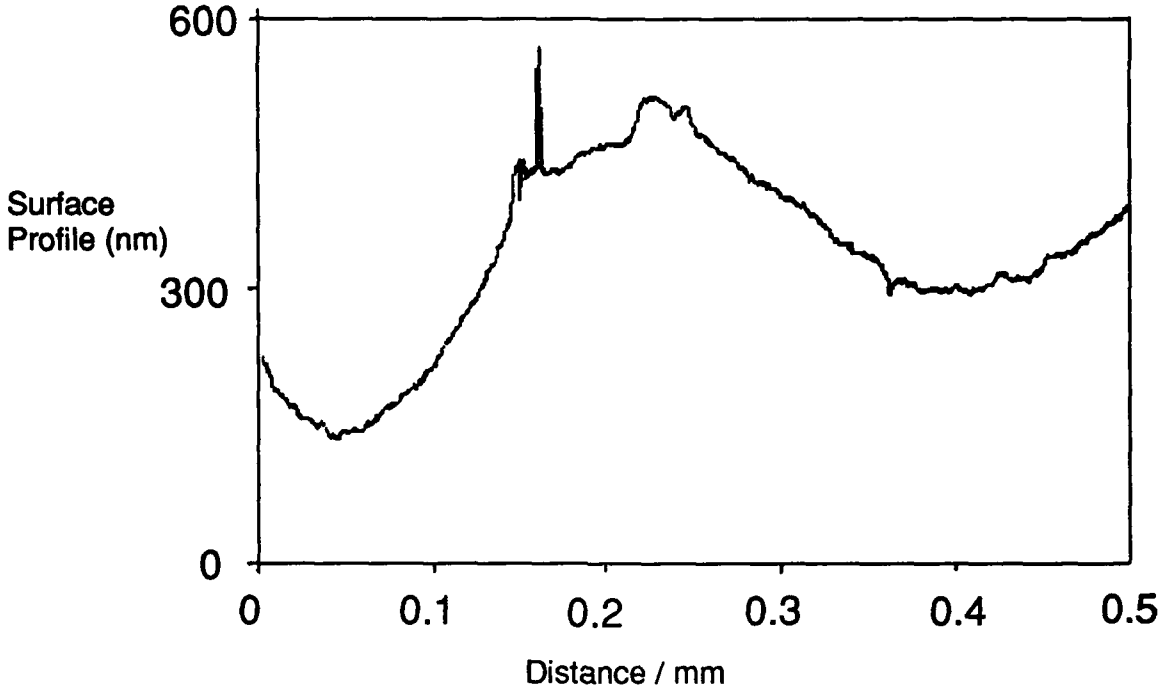

Fig. 7. Profile of the Teflon coating on microscope slide showing the smoothness of the surface.

QUESTIONS AND ANSWERS

E. Mattison, SAO: Do you plan to use liquid helium coating on your walls or just use the teflon?

R. Mossavati, National Physical Laboratory: That is one of the questions which I hope would be discussed at a meeting such as this and what the situation is we had hoped to work at 2.7 Kelvin which is very nice temperature in terms of temperature stability to work at with helium. As you probably know that the vapor pressure of helium goes up exponentially at about 0.6 or 0.7 Kelvin. Therefore we are praying for some new material to be discovered which will work at those set of temperatures. We have to consider so the moving on down in temperature to 0.6 to 0.7 Kelvin. That would be a shame because we would lose the lambda transition stability which we would have otherwise at 2.7 Kelvin. Frozen hydrogen is something that I have considered but I don not think getting masing action with frozen hydrogen is a very easy thing or at all possible.

A. Kirk, JPL: How many of these cold masers are you assembling and if the answer is one, how are you going to test it?

R. Mossavati: It is very much a research effort in terms of finding out the pitfalls with the cold hydrogen maser. We hope to, and as I said I have funding until the beginning of 1995. By that stage, I hope to have enough to show so that I can get additional funding to go on to develop a more sophisticated system. I would like to emphasize that this is a research and development effort and it is very much based in a scientific and research laboratory environment rather than an industrial application type of environment.

Two Way Time Transfer Results at NRL and USNO

Ivan J. Galysh and G. Paul Landis
Naval Research Laboratory
Code 8152
4555 Overlook Ave. S.W.
Washington D.C.20375-5354

Abstract

The Naval Research Laboratory (NRL) has developed a two way time transfer modem system for the United States Naval Observatory (USNO). Two modems in conjunction with a pair of Very Small Aperture Terminal (VSAT) and a communication satellite can achieve sub nanosecond time transfer. This performance is demonstrated by the results of testing at and between NRL and USNO. The modems use Code Division Multiple Access (CDMA) methods to separate their signals through a single path in the satellite. Each modem transmitted a different Pseudo Random Noise (PRN) code and received the others PRN code. High precision time transfer is possible with two way methods because of reciprocity of many of the terms of the path and hardware delay between the two modems. The hardware description was given in a previous paper [1].

Introduction

Three different experiments were performed with the time transfer modems. The first experiment was to verify that the basic operations of the modem were satisfactory. The second experiment was to determine the performance level of the modems. The third test came about because of problems in the second experiment.

Experiments

The first experiment was to determine how well the modems would operate through a satellite. Figure 1 shows the diagram of the configuration. Both modems operated from a common clock source. The two modems transmitted on the same VSAT through a combiner module. The received signal was split to the two modems.

There were two purposes to performing this experiment. The first was to determine how repeatable the modems were in determining the time difference. The second was to determine how well the modems re–synchronized to their one Pulse Per Second (PPS) signal. Tests were run over 6 days with typically two sessions in a half hour of satellite time.

The results show that the modems performed quite well in the experiment configuration. The standard deviation on the second to second time transfer of a single session was no higher than 205 picoseconds with a typical level of about 170 picoseconds as shown in Figure two. The time transfer

between modems was repeatable to within 0.5 nanoseconds peak to peak (Figure 3) with a noise level of about 144 picoseconds. The modems did re–synchronize themselves within 0.5 nanoseconds peak to peak (Figures 4 and 5). The variations in the re–synchronizing were probably due to the long rise times of the 1 PPS signal (Figure 6).

The second experiment was to perform a series of two way time transfers between NRL and USNO. NRL is located about seven miles from USNO and line of sight time transfer methods between the two locations have been used for years. Each location contains a variety of atomic clocks and the performance of the clocks and the time transfer link has been well documented. This configuration provides an almost perfect method of independently verifying the time transfer performance of the modems. Figure 7 shows the block diagram of the modem configuration.

A second measurement system used for verification is shown in Figure 8. The channel 5 television transmitter carrier from WTTG is synchronized to a cesium frequency standard. The carrier signal is received by both NRL and USNO and compared with a local signal synthesized from the house reference but offset from the carrier by 2250 Hz. The 2250 Hz beat is detected at both ends and USNO sends its beat over a dedicated phone line as a 2250 Hz tone. The tone is compared with the beat generated by the NRL system using a phase meter. Resolution is better than 1 nanosecond with a noise level of about 2 nanoseconds. This system is based on the work described in reference 2.

Figure 9 shows the plot of the time difference between NRL and USNO using the modems along with the time difference measurements using the other system. The modem measurements are plotted on the solid line. The channel 5 data is plotted on the dotted line. Figure 10 shows the difference of these two measurements. Figure 11 shows the one second noise plot of the experiment. The long period of no data is where satellite time could not be allocated. The channel 5 measurement system data was offset to match the start of the modem data. The modem tracked the channel 5 measurements somewhat, but not accurately enough. After the experiment, it was determined that a piece of equipment supplying the 5 MHz and 1PPS to the modem at NRL malfunctioned.

With equipment problems corrupting the second experiment, a third experiment was devised. The third experiment took place at USNO using their base station antenna and a VSAT. Both modems were placed side by side. Each was connected to its own cesium standard and individual antenna (Figure 12). This allowed direct measurements on the two modems with a time interval counter. The cesiums were intentionally offset. On each time transfer, the time difference between the two clocks was measured. This measurement was compared with the data generated by the modems. Figure 13 shows the plot of the modem data and the time interval counter. The solid line is the modem measurements. The dotted line is the time interval counter measurements. With the drift of the two clocks and the procedures of measuring the time differences, the peak to peak extremes were within two nanoseconds as shown in Figure 14. The noise level was 528 picoseconds. Since the two modems had never been calibrated this also shows that the absolute calibration or the two modems is very close.

Figure 15 shows the one second data plot of the modem operating on the VSAT. It's noise is at 275 picoseconds. The plot of the earth station data is shown in figure 16. The data is much noisier at 1535 picoseconds. The reason for this is that the earth station is transmitting more power to

the satellite than the VSAT. The satellite retransmits the signal back along with the VSAT signal. The earth station modem has to extract the smaller VSAT signal from its own larger signal. It's own signal appears as a noise source. Figure 17 shows the difference plot of the previous two plots with a noise level at 798 picoseconds approximately half the larger one way noise.

Conclusion

The first experiment has shown that the modem can re–synchronize themselves repeatable at less than 500 picoseconds. The last experiment has shown that the modems can do precise time transfers. More experimentation is needed to see just how precise the modems can be.

References

[1] G. Paul Landis and Ivan Galysh, *"NRL/USNO Two Way Time Transfer Modem Design and Results"*, IEEE Frequency Control Symposium, Hershey Pennsylvania, 27–29 May 1992, pp. 317–326.

[2] A. Gabry, G. Faucheron, B.Dubouis and P. Petit, *"Distance Comparison of Stable Frequency Standards by Means of the Transmission of a Beat Note Between the Carrier of a TV Broadcast Signal and a Frequency Synthesized from the Frequency Standard"*. 31st Annual Symposium on Frequency Control, Atlantic City, New Jersey, 1–3 June 1977

Colocated Time Transfer Configuration

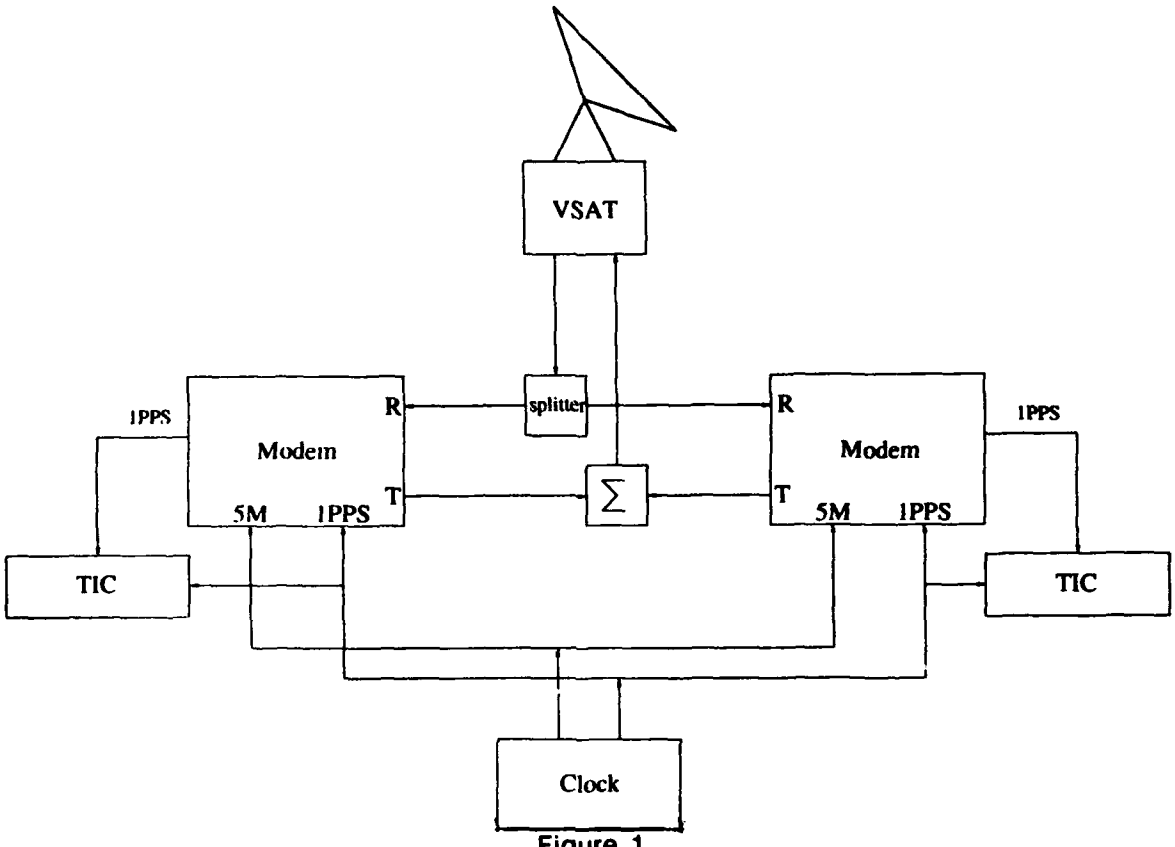

Figure 1.

Colocated Time Difference, One Second Noise

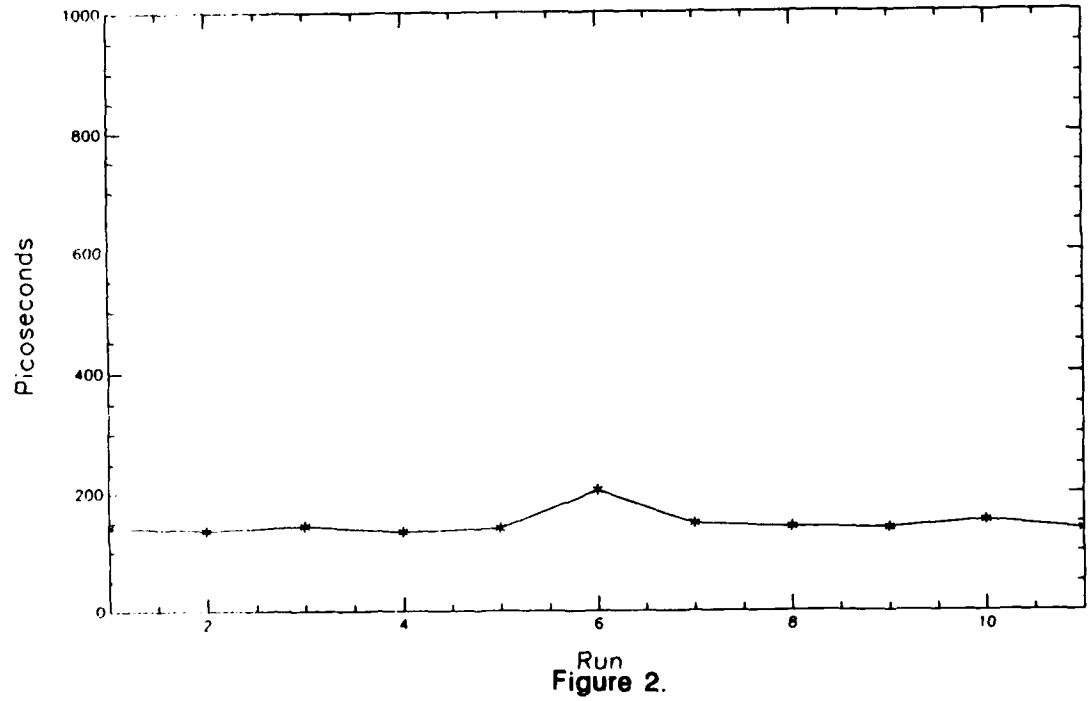

Figure 2.

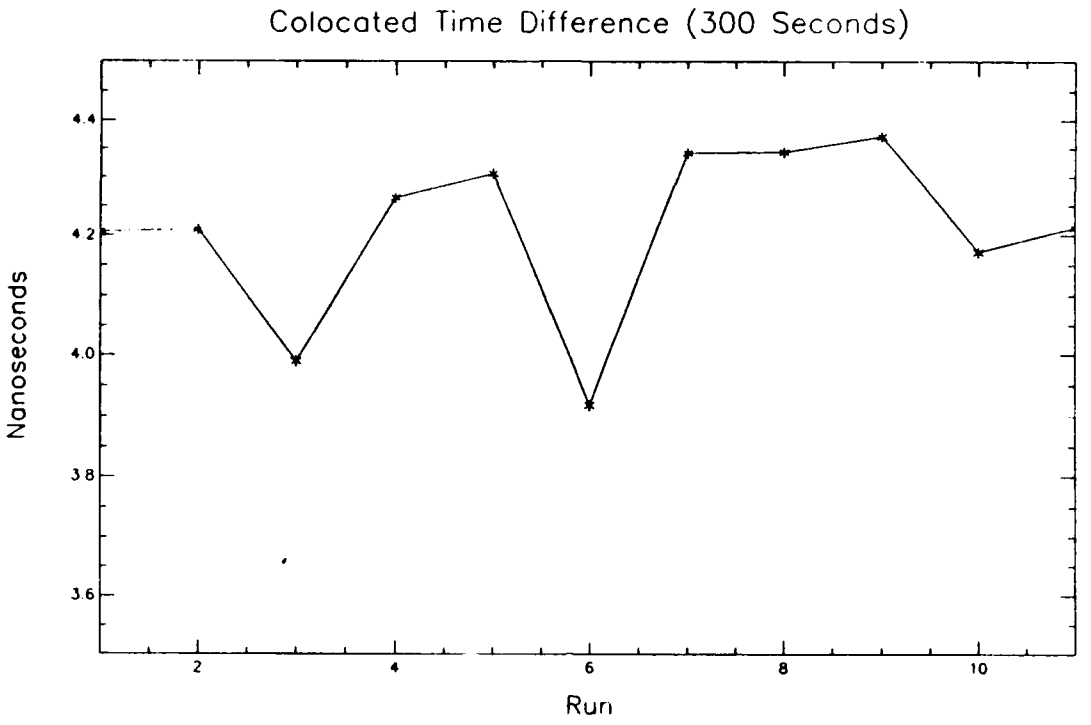

Figure 3.

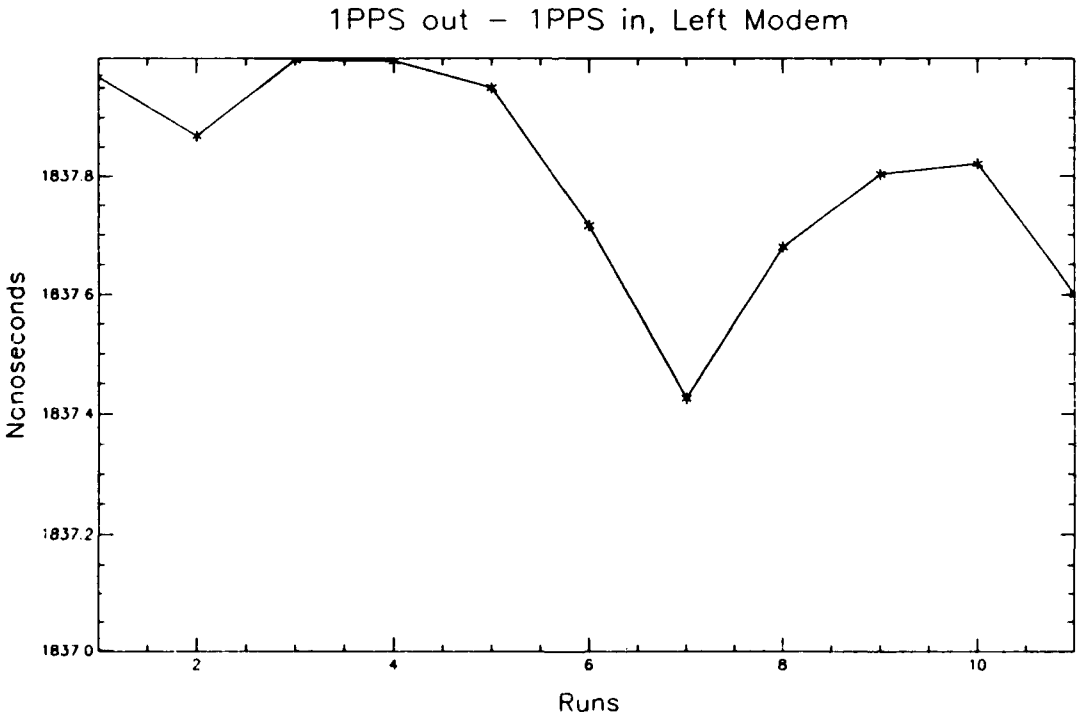

Figure 4.

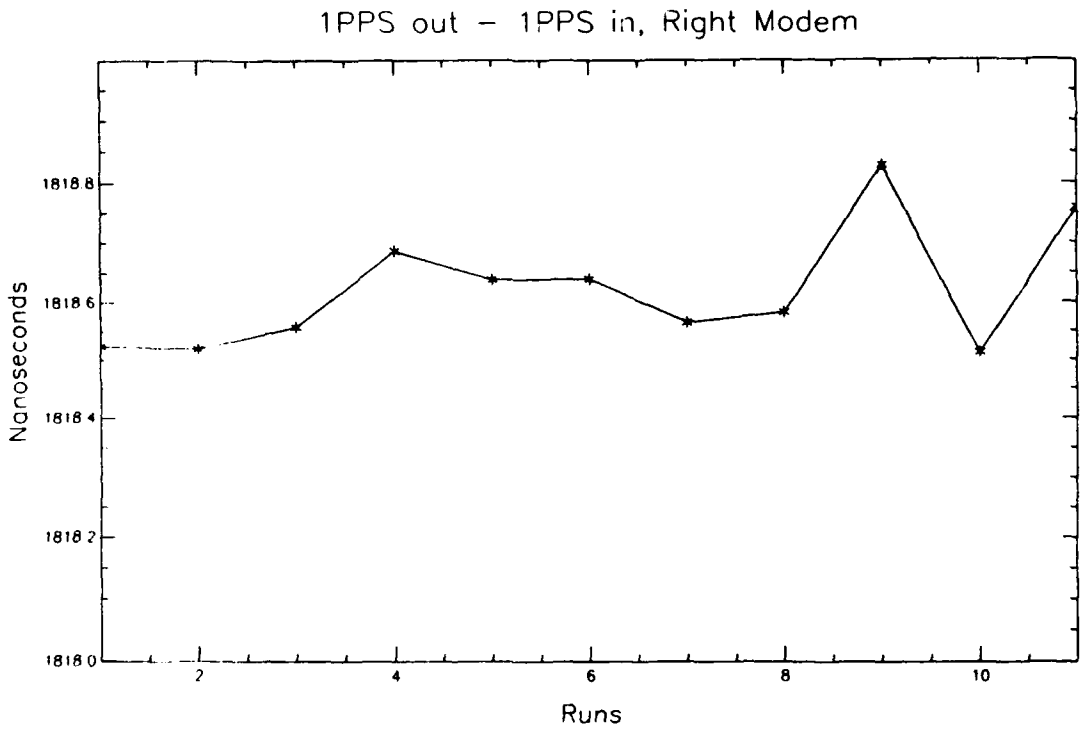

Figure 5.

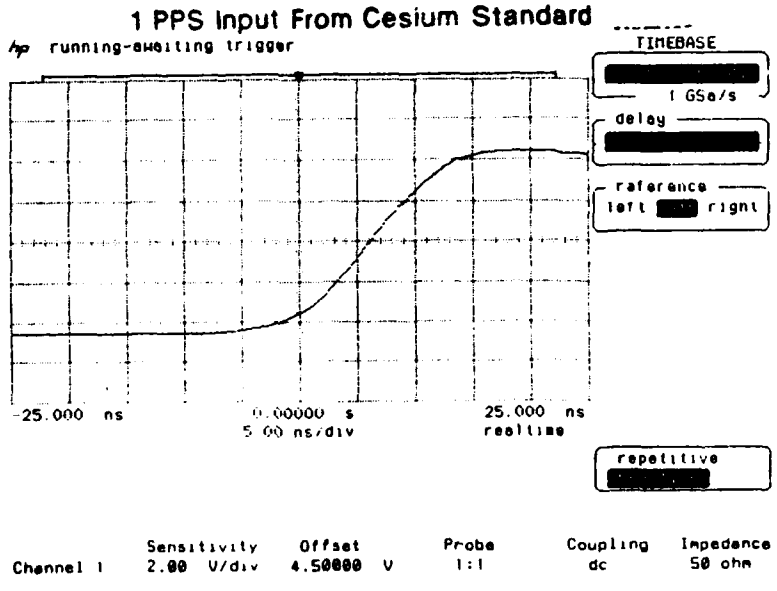

Figure 6.

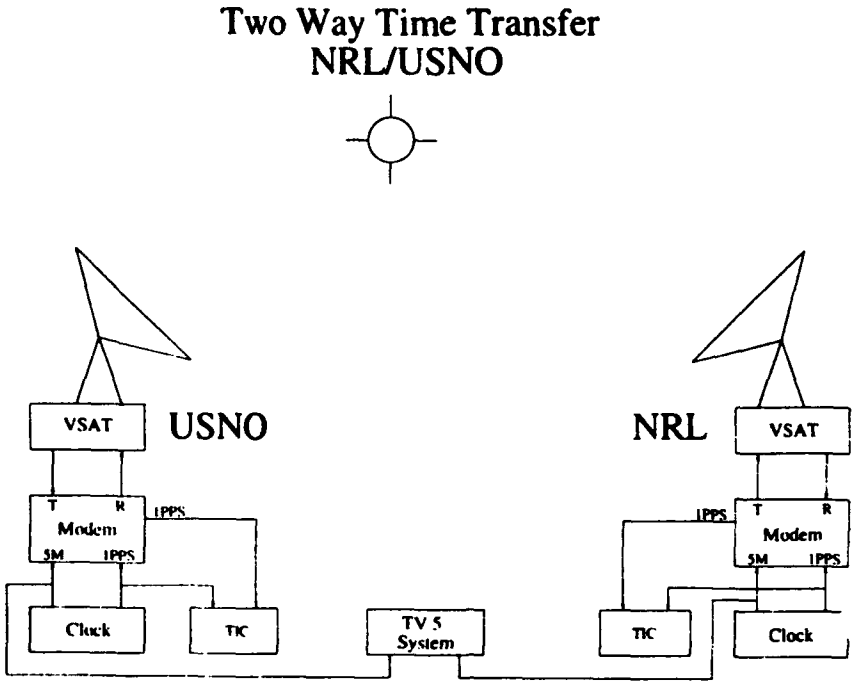

Figure 7.

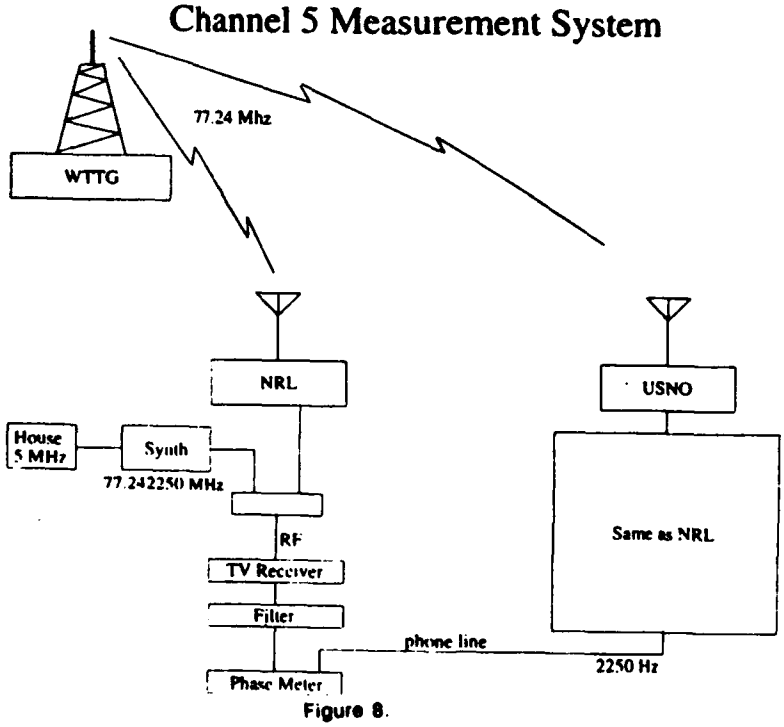

Figure 8.

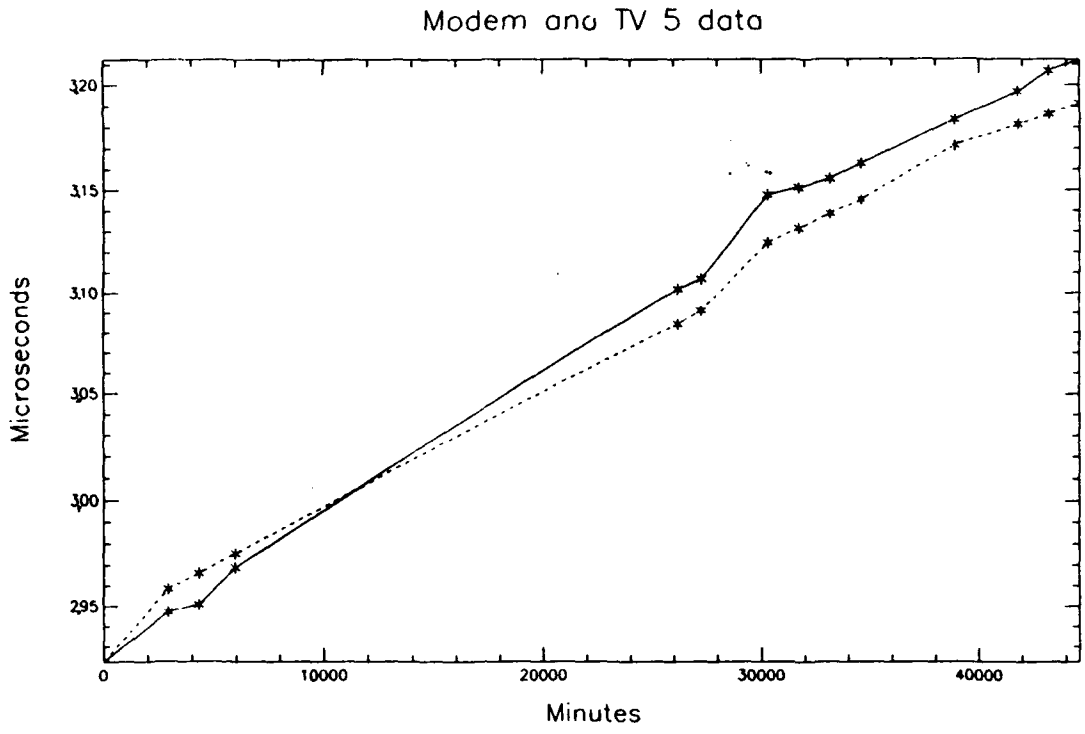

Figure 9.

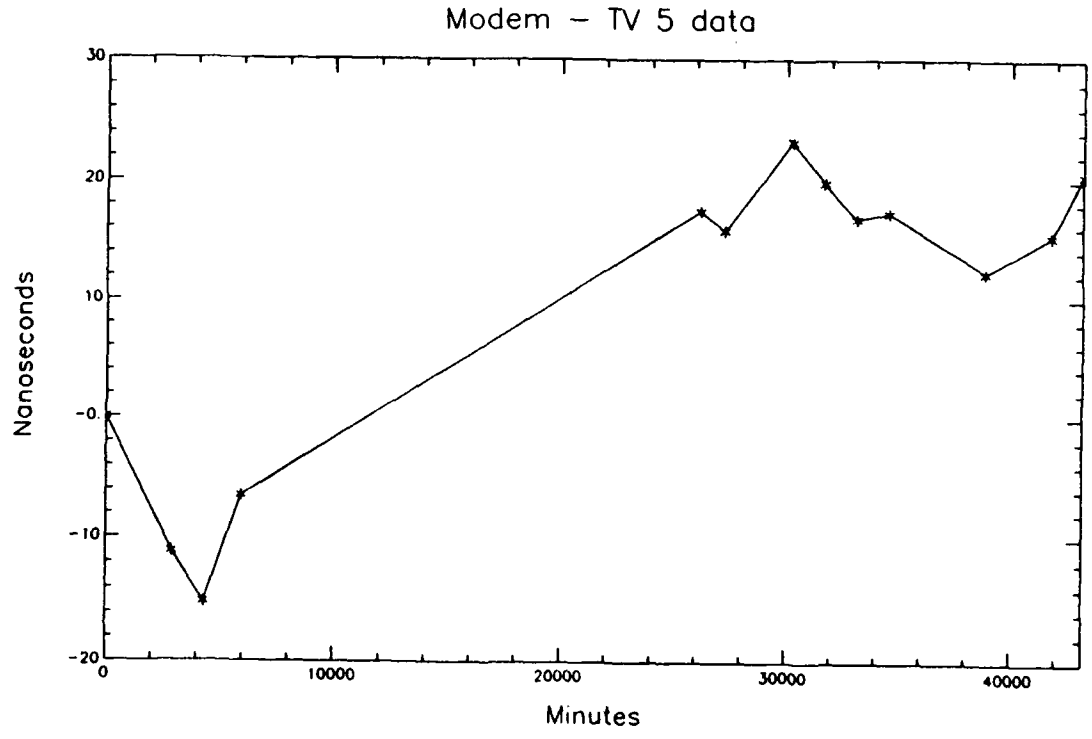

Figure 10.

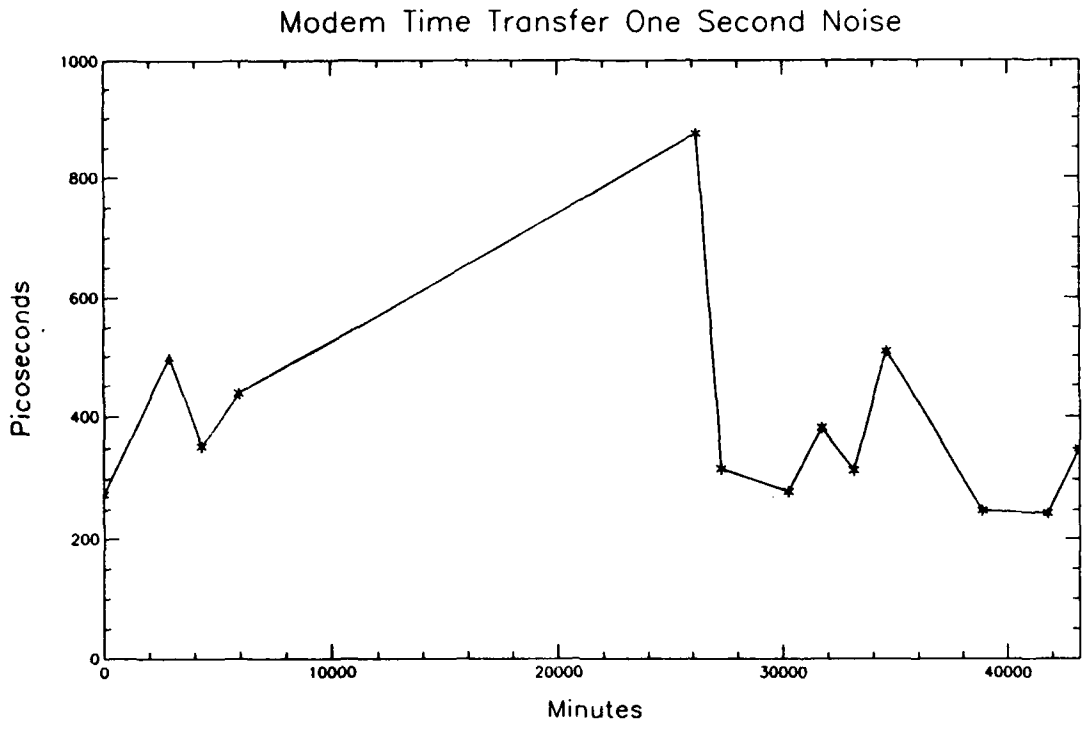

Figure 12.

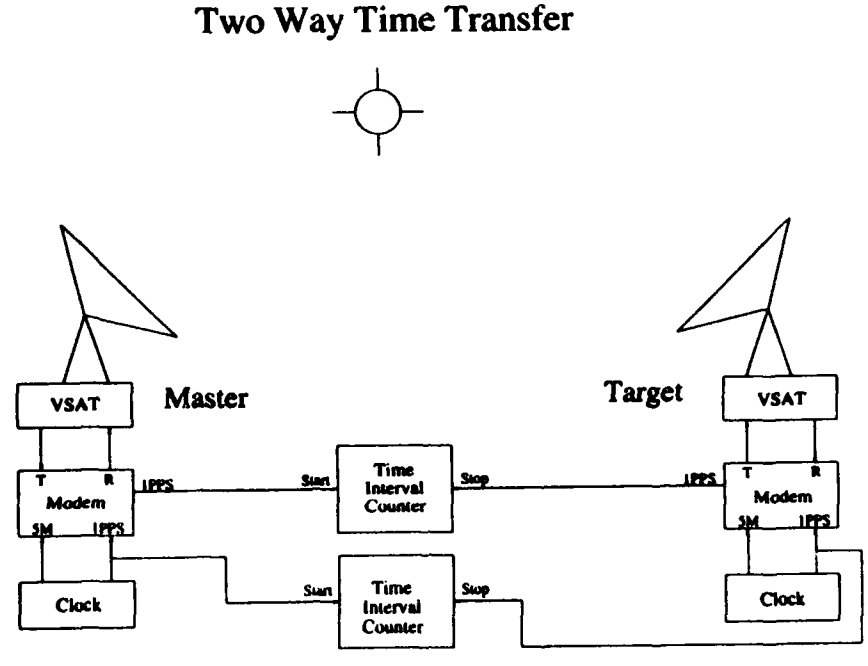

Figure 11.

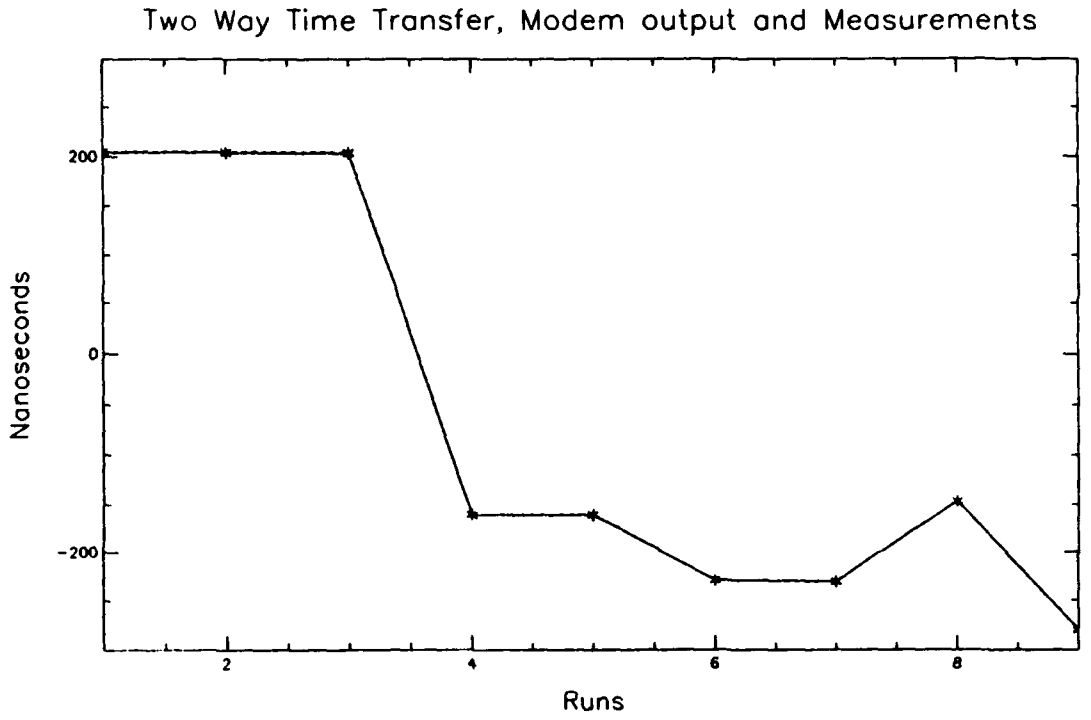

Figure 13.

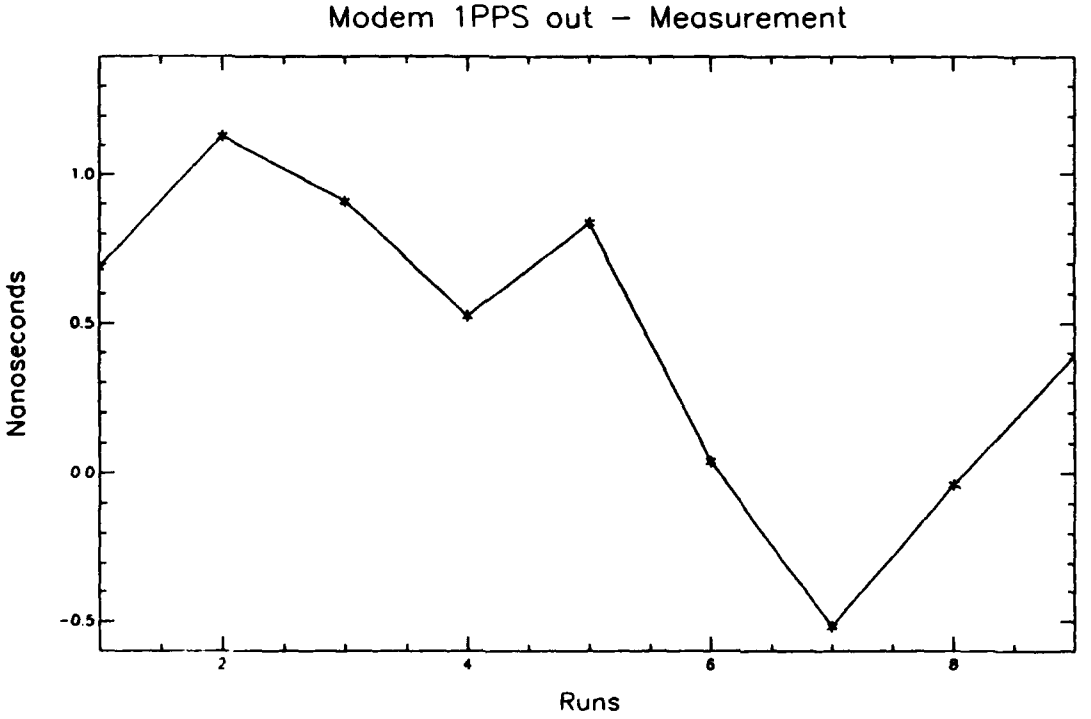

Figure 14.

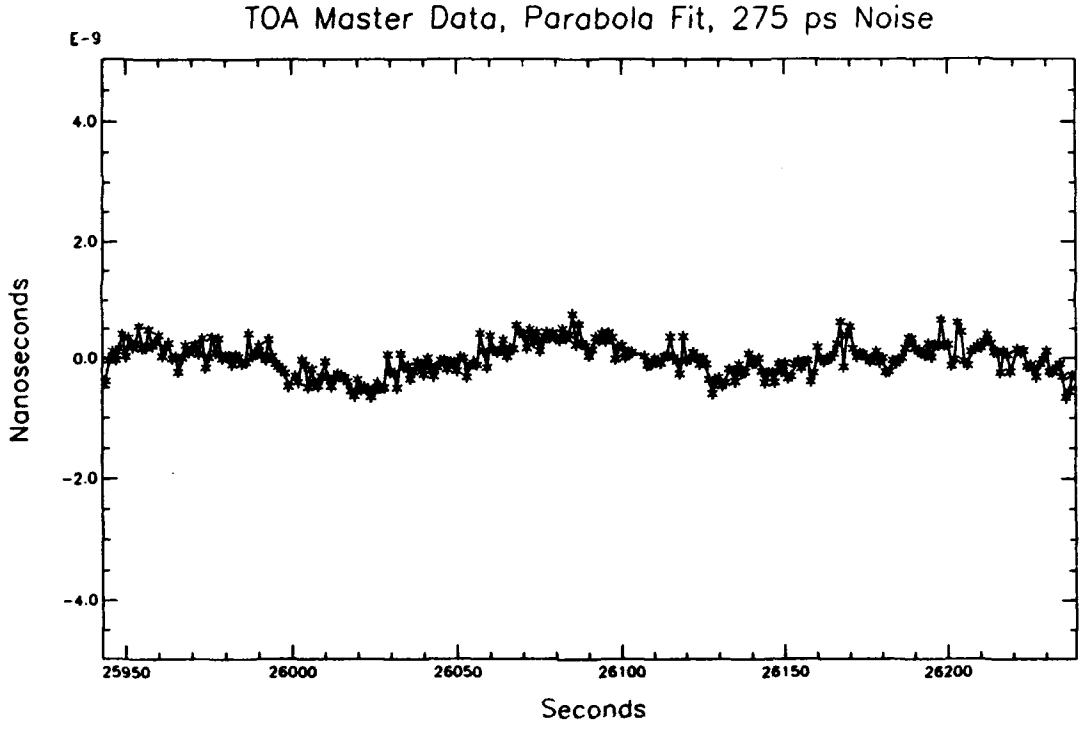

Figure 15.

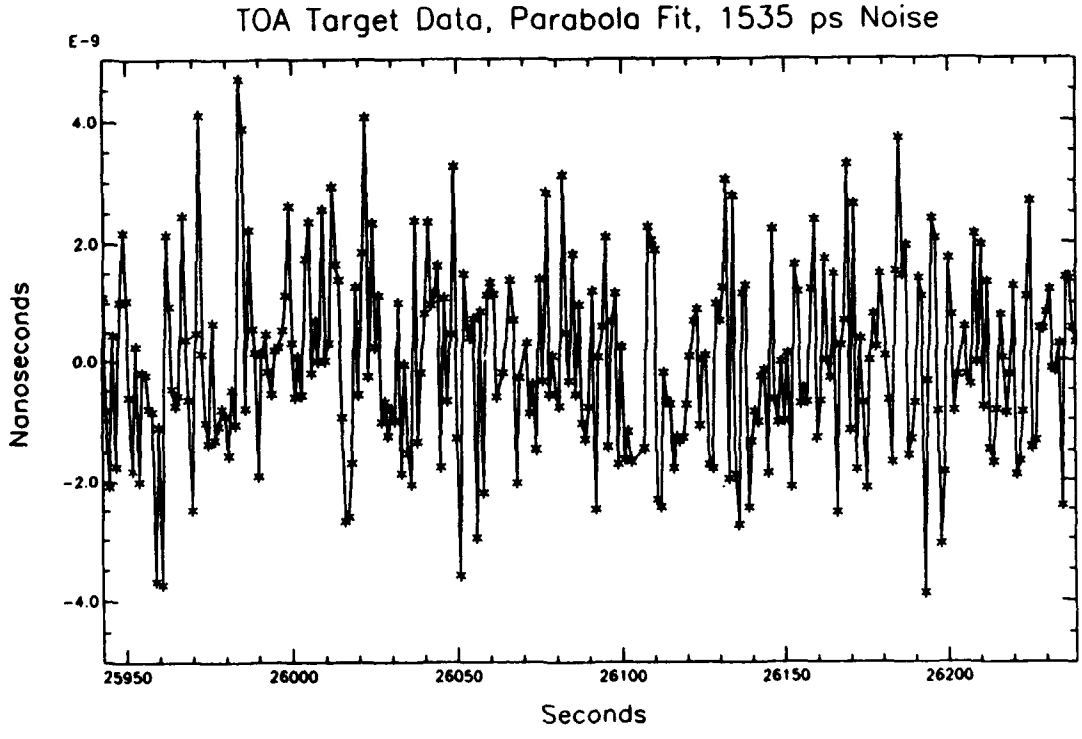

Figure 16.

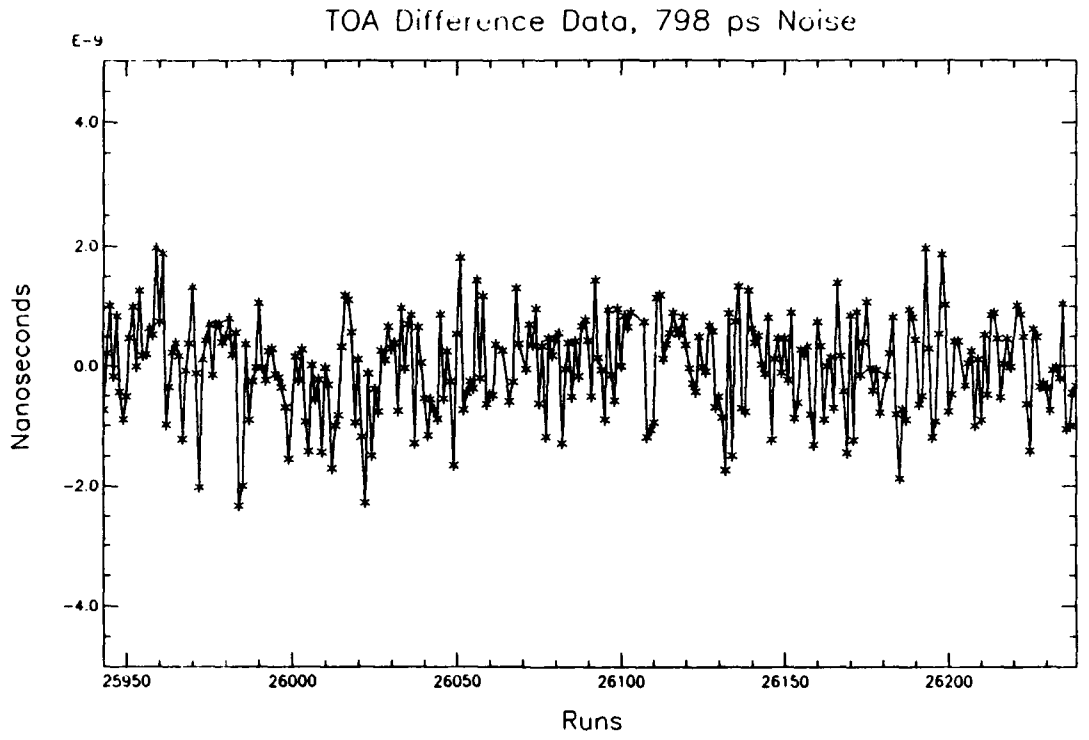
TOA Difference Data, 798 ps Noise
E-9
4.0
2.0
0.0
-2.0
-4.0
Nanoseconds
25950
26000
26050
26100
26150
26200
Runs

Figure 17.

Performances of a Date Dissemination Code on Telephone Lines Using Commercial Modems

F. Cordara, V. Pettiti,
Istituto Elettrotecnico Nazionale Galileo Ferraris
c.so Massimo D'Azeglio no. 42
I-10125 Torino, Italy

R. Quasso, E. Rubiola
Politecnico di Torino
Dipartimento di Elettronica
c.so Duca degli Abruzzi no. 24
I-10129 Torino, Italy

Abstract

A coded time/date information dissemination system (CTD), based on telephone lines and commercial modems, is now in its experimental phase in Italy at IEN. This service, born from a cooperation with other metrological laboratories (TUG, Austria, SNT, Sweden, VSL, The Netherlands), represents an attempt towards an European standardization.

This paper will give some results of an experimental analysis in which a few modems have been tested, both in laboratory conditions and connected to the telephone network, in order to evaluate the timing capability of the system.

When the system is used in a one-way mode, in many practical cases the modems delay turns out to be the main factor which limits the accuracy, even more than the telephone line delays. If the two-way mode is used, the modems asimmetry, i.e., the delay difference between transmission and reception, is almost always the most important source of uncertainty, provided the link is not including a space segment.

Comparing the widely used V.22 modems to the old V.21 ones, the latters turn out to be better both in delay time (30–100 ms V.22, and 7–15 ms V.21) and asimmetry (10–50 μs V.21, and 10 ms V.22).

Time transfer accuracies of 10 μs (same town) to 100 μs (long distance calls) have been obtained in two-way mode with commercial V.21 modems.

1 Introduction

In 1991, four European time and frequency laboratories, namely IEN, SNT, TUG and VSL, that perform standard time dissemination in Italy, Sweden, Austria and the Netherlands respectively, agreed upon a format for the distribution of a coded date and time information on telephone lines using commercial modems [1].

This dissemination service, designed to synchronize computer clocks or digital terminals, is capable to attain accuracies ranging from low to medium (100 ms to 1 ms), as reported in previous papers dealing with symilar synchronization systems realized in Canada [2] and in the USA [3].

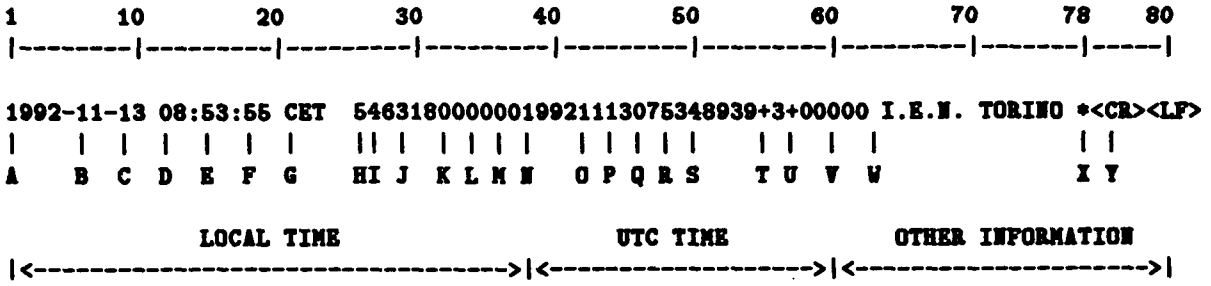

LOCAL TIME INFORMATION

- **A** year
- **B** month
- **C** day
- **D** hour
- **E** minute
- **F** second
- **G** local time identifier
  CET (Central Europe Time)
  CEST (Central Europe Summer Time)
- **H** day of the week
- **I** week of the year
- **J** day of the year
- **K** month of the next change from CET to CEST or viceversa
- **L** day of the next change from CET to CEST or viceversa
- **M** hour of the next change from CET to CEST or viceversa

UTC INFORMATION

- **N** year
- **O** month
- **P** day
- **Q** hour
- **R** minute
- **S** Modified Julian Date (MJD)
- **T** DUT1: time difference, in tenth of seconds, between UT1 and UTC time scales
- **U** month of the next leap second; contains also the sign (+/-)

OTHER INFORMATION

- **V** propagation time compensation (in millisecond), if not performed the digits are: 000
- **W** message (15 characters)
- **X** visible time marker: can change to "#" when advanced to compensate for the propagation delay
- **Y** electrical time marker, CR/LF sequence (CR = Carriage Return, LF = Line Feed)

Figure 1: CTD format and features.

The Istituto Elettrotecnico Nazionale (IEN), which is responsible for the national time scale in Italy, has implemented since mid 1991 this coded time information for telephone lines (CTD) that is presently accessible dialling number (+39) 11 3487892.

It has been demonstrated that the delays introduced by telephone lines are very stable compared to those due to the telephone network equipment, and that the modems used both at the code generation side and at the users end are by far the most influential factor in the synchronization error of these services.

To evaluate the accuracy achievable by using this code in the Italian telephone network, special care has been therefore devoted to modems delays and their asymmetries. The network behaviour has also been tested performing round-trip delay measurements both for in-town and long distance calls.

Modems of different CCITT standard (V.21 and V.22) and manufacturer have been tested using as reference signals both the CTD timing reference and ASCII characters generated by a personal computer.

The following sections describe in details the format of the CTD and its realization, the measurement setup used, the results obtained in the delay measurements of the modems and of the telephone line and some consideration about the accuracies that could be obtained by users of CTD in the field of time and frequency.

2 The coded date information for telephone lines

The European code, implemented at IEN and operative also in Austria [4] and Sweden [5], consists of a 80 ASCII characters line transmitted each second, supplying the date, the time and some information relative to the corrections performed on the legal time or special warnings regarding time scales.

The code format and access protocol have been agreed so as to allow a user terminal to connect via a CCITT V.22 modem configured for 1200 bit/s, 8 bits, 1 stop bit, no parity, and the time information trasmitted is relative to the incoming second. The reference of time is given by the last three characters, namely "*", Carriage Return (CR) and Line Feed (LF). The leading edge between the stop bit of CR and the start bit of LF is "on time" with the UTC(IEN) second. This reference point can be advanced to compensate for the transmission delay if this feature is implemented.

A sample of one line of the code as generated at IEN with full details is shown in Fig. 1.

The characters from 1 to 37, identified in Fig. 1 by letters from A to M, give the date and time information in Italian legal time, meanwhile those from 38 to 59 (letters N to U) supply the time information according to the UTC time scale together with the Modified Julian Date and the DUT1 difference between UT1 and UTC time scales.

It can be noticed that the format of the timing sequence has been chosen so as to leave the first 24 characters, giving the date and time, easily readable. Concerning the characters from 60 to 77 (letters V and W), the first three give the amount of the propagation delay compensated by advancing the time marker, and fifteen can be used for messages.

Finally, character no. 78, "*", is changed in "#" if the delay compensation is performed by the generator side.

The duration of a character is 833 μs and the beginning of the time code string occurs 50 ms after the UTC(IEN) second. The timing of the last three characters of the string can vary to compensate for a maximum delay of about 0.3 seconds.

The block diagram of the CTD generator is shown in Fig. 2.

Two standard frequencies from IEN cesium clocks are supplied to the device to phase-lock its internal 10 MHz clock oscillator that is used as time base for the microprocessor unit generating the time code string. The clock functions can be checked and updated by a keyboard or a PC interface.

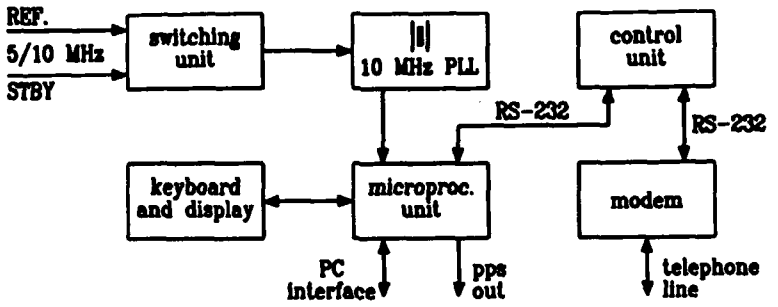

Figure 2: CTD generator block diagram.

The output signal, available on an RS-232 interface, is synchronized to UTC(IEN) within 0.2 μs and sent to a control unit and succeedingly to the modem input. The control unit checks the user's connection time, presently limited to one minute, and allows for counting the daily number of calls and their distribution in time.

The 1200 bit/s rate at the CTD/RS-232 interface, is synchronized with the reference time base and the time marker jitter is below 1 μs.

The definitive generation scheme, that will be ready for the beginning of 1993, will rely upon three devices and a switching unit to check the time code sent to the telephone line.

3 Experimental methods and equipment

When using the classical one-way scheme in telephone network synchronizaton, we define the propagation time t_p between laboratory A (source) and B (user) as

$$t_p = t_a + t_l + t_b \tag{1}$$

where t_a and t_b are modem delays (laboratories A and B respectively) and t_l is the line delay, as seen at the telephone twisted pairs extremes.

In the two-ways scheme, the propagation time $\tilde{t_p}$ from A to B is estimated as half the echo time

$$\tilde{t_p} = \frac{1}{2}\left(t'_p + t''_p\right) \tag{2}$$

where t'_p and t''_p are the path delays from A to B and from B to A respectively.

The residual error is

$$\epsilon = \frac{1}{2}\left(t'_a - t''_a\right) + \frac{1}{2}\left(t'_l - t''_l\right) + \frac{1}{2}\left(t'_b - t''_b\right) \tag{3}$$

where the terms in brackets highlight asimmetry contributions of each element, either line or modem.

Unfortunately, t_a and t_b are hardly measurable separately because there are no suitable time markers on the signal; there are modulated waveforms only, with a given duration and bandwidth. Moreover, any attempt to measure these delays seems somewhat misleading because the modem front-end interacts with the line; this interaction involves bandwidth, impedance matching and equalization. Hence the sum $t_a + t_b$ was measured as a single quantity.

The basic scheme adopted in all measurements is shown in Fig. 3, where an arming circuit, not shown, ensures that start ans stop events are related to the same edge. In a first set of measurements the line (dashed box in the scheme) was simulated by attenuating the signal by 10 dB, which is the

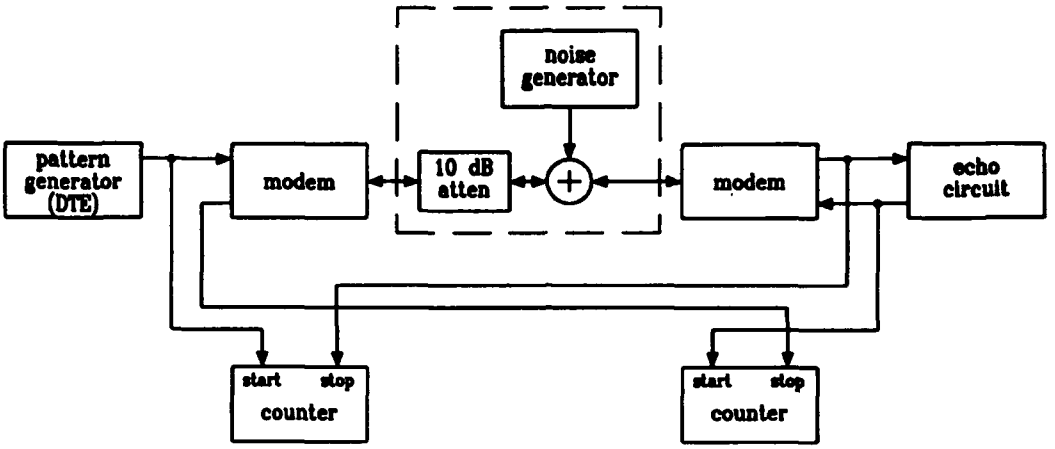

Figure 3: Experimental setup.

factory and type		standard	analog or digital	no. available devices
AET	MD 300	V.21 only	analog	2
AET	2.4 Must	V.21 / V.22	digital	1
Dataconsyst		V.21 / V.22	digital	1
Hyunday	MD 2404	V.21 / V.22	digital	2
Smartlink	1200 S	V.21 / V.22	digital	1

Table 1: Modems under test.

typical line loss [6], and adding noise. Later on, a line simulator (passive RC network) and a true line were used.

Three test patterns were adopted: (i) a stream of "U" characters, which appears as a squarewave on the RS-232 interface, giving the maximum number of measurements per second, (ii) a stream of NUL characters (ASCII 0), which is a sequence of pulses (start bits), and (iii) the CTD.

Experiments were performed with some modems (Table 1), available both at the Politecnico and at the IEN. These equipment are representative of the low speed class of modems. High speed modems were not considered because they often use sophisticated coding and buffering techniques which make time delay more unpredictable.

Time delays were averaged on suitable block sizes, say 5000, in order to keep the noise effect at a negligible level.

Time jitter σ was measured as the standard deviation of the average values of blocks; its value depend on the block size n. Allan variance was not considered because no diverging process is involved in our experiments.

4 Modem measurements

4.1 CCITT standard V.22

These equipment work at 1200 bit/s with Q-PSK (quad phase shift keying) modulation. Their internal circuits are often based on sampling processes and digital hardware. Bits are packed in dibit (2 bits)

symbols after a scrambling process [7] defined by

$$B = S_0 \oplus S_{-14} \oplus S_{-17} \tag{4}$$

where B is the current output bit, S_0 is the current source bit, S_{-i} the i^{th} previous one and $\oplus$ means ex-or. The duration of 18 bits is needed for the complete scrambling process. Since unscrambling needs the same time, the complete scrambling/unscrambling operation takes 36 bits time, which lasts 30 ms. This is the lower bound for $t_a + t_b$. Additional delays are due to modulation/demodulation, filtering, impedance equalization. Some equipment are capable of adaptive equalization during the communication, others have a complex buffering mechanism. Both of these features, not present in our measurements, could affect time jitter and repeatability.

When the modems, working in full duplex asynchronous mode, were connected via a 10 dB attenuator, the following averaged time delays for two couples of equipment were measured using 5000 samples.

couple	$t'_a + t'_b$	$t''_a + t''_b$	asimmetry error $\lvert (t'a + t'b) - (t''a + t''_b) \rvert /2$
no. 1	46.6 ms	31.6 ms	7.5 ms
no. 2	34.0 ms	58.7 ms	12.35 ms

4.1.1 Time jitter and related problems

In a V.22 asynchronous communication only the DTE/modem connections are actually asynchronous, while the two modems are synchronized each other by means of the data flow. Focusing our attention on the transmitting side (source DTE and modem) we observe that the data rate is driven by the DTE on the DTE/modem connection, and by the modem on the telephone line. Since each equipment works under control of its internal quartz oscillator, stuffing idle bits are added or removed in order to ensure the same data flow for the two devices.

The main consequence of this is that the term $(t_a + t_b)$ shows a sawtooth behaviour whose period T_{beat} is related to the DTE and modem oscillators relative frequency offsets, and whose peak-to-peak value is the duration T_s of one bit (833 μs at 1200 bit/s). This sawtooth behaviour has been observed in all the modems considered; T_{beat} fits exactly to its calculated value, which is based on the measurements of the DTE and modem oscillators offsets. Moreover, changing the frequency of an oscillator we got different T_{beat} in agreement with the foreseen values.

The beat phenomenon gives to the time jitter a contribution symilar to a random variable uniformly distributed between $\pm T_s/2$, whose standard deviation is $\sigma_{\text{beat}} = T_s/(2\sqrt{3}) \simeq 240$ μs. When measuring time jitter, we expect that the contribution of σ_{beat} is flat (slope 0) for observation time (i.e., the time needed for acquiring one data block) $\tau \leq T_{\text{beat}}$, and that is reduced a factor $1/n$ (slope -1) for $\tau \gg, T_{\text{beat}}$.

The experimental results, shown in Fig. 4A (plot □), are in agreement to the foreseen behaviour. Since $\sigma \simeq 240$ μs for small τ, any "true" noise phenomena seem to give a contribution that is negligible when compared to the beat effect. Changing the data flow rate, plots similar to that shown in Fig. 4A (plot □) were obtained, but the cross point between slopes 0 and -1 occured for the same τ — with different values of n — because it depends on τ only.

When modems are synchronously connected to the DTE, the effect of oscillators offset vanishes. Variations of 30–80 μs peak-to-peak are still present on $t_a + t_b$, probably due to modulation/demodulation processes. Figure 4A (plot △) shows typical experimental jitter values.

Finally, the effect of the telephone line noise was simulated by injecting white noise into the modem/modem connection. Figure 4B shows typical results measured in extreme conditions, S/N = 8 dB

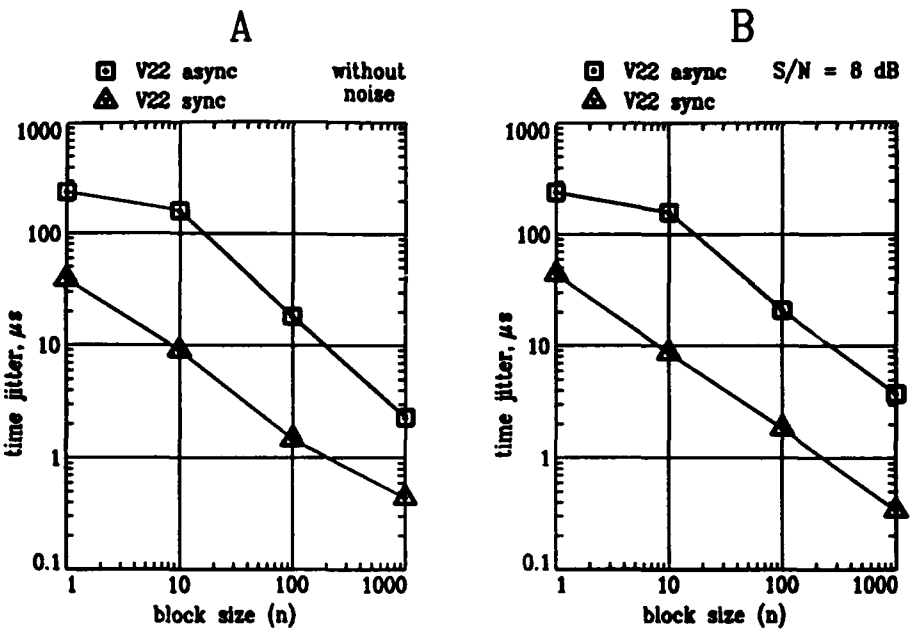

Figure 4: Typical time jitter measured sending 3 NUL characters per second on a V.22 modems connection.

in the 300–3400 Hz band, for both asynchronous and synchronous connections. When V.22 modems operate synchronously, the plot overlaps almost exactly to the previous one, measured without noise. When the asynchronous mode is chosen, a small noise contribution to the time jitter appears for $n = 100$ to $n = 1000$.

4.2 CCITT standard V.21

In this standard, almost in disuse, information is sent at 300 bit/s in FSK (frequency shift keying). Since frequency modulation is directly driven by the source bits, the DTE/modem connection is, in principle, synchronous.

Because of different behaviours observed for timing applications, we divided the V.21 equipment in two categories, based on internal circuits type. Thus we name *analog* the oldest equipment, based on fully analog circuits, and *digital* the new ones, which are actually V.22 modems set in the V.21 mode. The last ones often include digital waveform synthesis and sampling.

Digital modems connections delay show a sawtooth behaviour similar to what observed in the V.22 ones. However, peak-to-peak delay variations are about 300 μs, which is far less than the bit duration of 3.3 ms. This behaviour is supposed to be due to a difference in relative frequency offset between modem and DTE, which is compensated by steps by the modem synthesizer. This statement is supported by the fact that T_{beat} is properly related to these frequency offsets.

Analog modem were found to be free from any beat phenomena.

Figure 5A shows the typical $t_a + t_b$ jitter for couples of analog and digital modems connected through the 10 dB attenuator.

The effect of the noise, tested in the same conditions as for V.22 modems, is shown in Fig. 5B; these results are to be compared to those measured without noise (Fig. 5A). Injected noise (S/N = 8 dB) increases the jitter nearly by a factor three in digital modems, while the analog equipment show

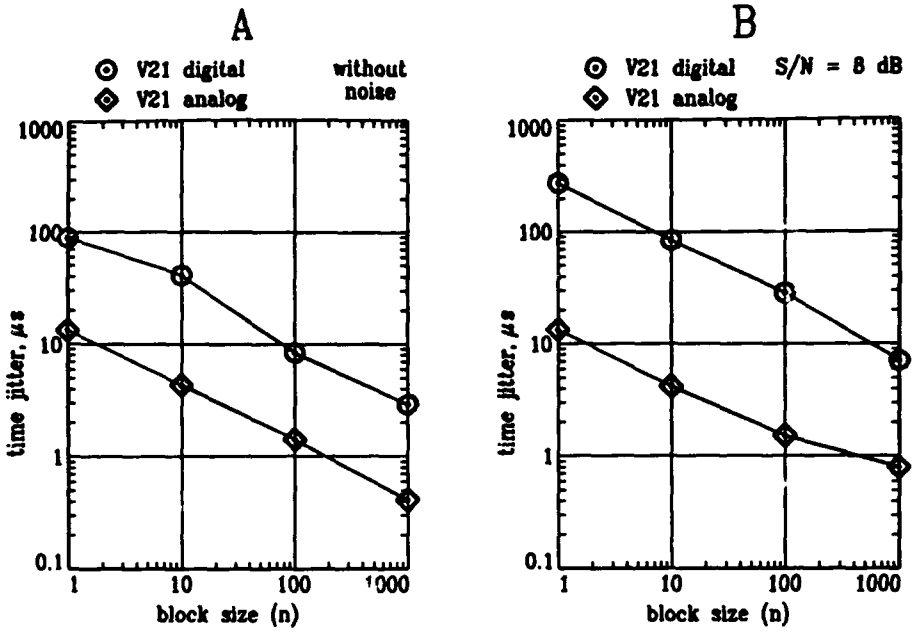

Figure 5: Typical time jitter measured sending 3 NUL characrters per second on a V.21 modems connection.

a small difference for large n only. When connecting analog modems through a local loop — i.e., two links from IEN to the same telephone switch, some kilometers apart — jitter resulted to be higher by a factor 1.5 compared to that measured in absence of noise.

As regards to delay and simmetry, the following values were measured.

type	$t'_a + t'_b$	$t''_a + t''_b$	asimmetry error $\|(t'a + t'b) - (t''a + t''_b)\|/2$
†digital	12.55 ms	12.48 ms	35 μs
†analog	6.889 ms	6.990 ms	50 μs
‡analog	6.889 ms	6.869 ms	10 μs
† full duplex		‡ half duplex like connection	

Results shown in the first two rows of the table can be compared directly because both digital and analog couples of modem were measured in full duplex mode. Analog modems were also tested (3rd row) exchanging the calling and answering role, thus keeping the same frequency modulation for the two directions; this is roughly equivalent to a half duplex connection.

5 Telephone line measurements

Cables have a remarkable potential in time transfer, as it was shown in past works using a dedicate coaxial cable (accuracy of some microseconds at 700 km distance [8]) and a dedicate telephone twisted pair (stability of 10 ns at 10 km [9]). Conversely, a telephone network, although based on cables and amplifiers symilar to those of dedicated links, gives additional problems due to FDM (frequency division multiplexing) or TDM (time division multiplexing) equipment, switches and other devices.

cable or equipment type	delay
coax cable under ground	4 ns/m
FDM modulation or demodulation	750 μs
PCM coding or decoding	300 μs
digital exchange (connection)	450 μs
digital exchange (ending)	800 μs
for each analog interface add	300 μs

Table 2: Tipical delays of the Italian telephone network.

Table 2, taken from [6] gives the typical delays for the Italian network. Unfortunately, information on the network configuration and signal paths are not available in most cases. Comparing a rough estimate of path delays, based on the geographic distance, to modem delays, these last ones turn out to be far bigger; consequently, it was decided to measure the connection in some cases.

All experiments were done with two analog V.21 modems carefully calibrated in order to evaluate the delay due to the line only. In spite of this, it has been impossible to separate modem and line contributions to the measurement instabilities.

A first set of measurements was done at the IEN, using the local loop. An average delay $t_l = 219$ μs was measured in half duplex mode, with small variations — less than 5 μs peak-to-peak — during the same call. Exchanging the two modems, but keeping the same modulation frequencies, line asimmetry was always less than 5 μs, which implies a maximum contribution of 2.5 μs to the two-ways synchronization error ϵ. When hanging up and redialling, t_l showed slight changes, with a standard deviation between calls of 7.5 μs (carrier 1750 Hz) and 20 μs (carrier 1080 Hz).

A more significant asimmetry ($t_l' = 219$ μs and $t_l'' = 356$ μs) arose when modems were set in full duplex mode. This is due to the line response to the different carriers used for the two directions.

In a second experiment, we measured the link between IEN and a calibration laboratory in Milano (SIRTI), whose distance is about 130 km, using the same couple of modems in half duplex. Path delay was $t_l \simeq 4$ ms, stable within ± 200 μs when hanging up and redialling. Line asimmetry error was between 25 and 75 μs, depending on the time of the day, and consequently on the telephone traffic on the network.

timing error		modem type	distance call	sync. method
30–120	ms	V.22	long	
30–100	ms	V.22	short	one
7–30	ms	V.21	long	way
7–14	ms	V.21	short	
10	ms	V.22	long/short	
200	μs	V.21 digital	long	two
100	μs	V.21 digital	short	ways
100	μs	V.21 analog	long	
10	μs	V.21 analog	short	

Table 3: Time transfer errors.

6 Conclusions

Timing accuracies, taken from the last two sections, are combined in Table 3. It has been assumed that no propagation estimate is used in one-way mode, and no care is taken about simmetry for two-ways mode.

The CTD service, as presently implemented (one-way, using 1200 bit/s V.22 modems), ensures timing accuracies of 100–120 ms. A correction, based only on the lower bound of the modems delay and made either by the IEN or by the user, reduces the error to 70–90 ms.

When the system is used for frequency calibration, timing accuracy is replaced by repeatability in the errors budget. Taking two averaged time values over one day, frequency accuracies from some units 10^{-9} to 10^{-10} can be expected.

A two-ways extension of the CTD service is under study. A timing accuracy of 10 ms is achievable without calibrating modem asymmetries. It seems that an improvement by a factor 10 can be obtained if the nominal asymmetry of the user's modem type (factory and model) is specified.

References

[1] CCIR Study Group 7/A, Document 7/A TEMP 15 - Proposed amendment to Report 363–7, Geneva, 1991.

[2] D. Jackson, R. J. Douglas, "A telephone based time dissemination system," *Proc. 18th PTTI Meeting*, USA, Dec. 1986, p. 541–552.

[3] J. Levine, M. Weiss, D. D. Davis, D. W. Allan, D. B. Sullivan, "The NIST digital time service," *Proc. 21st PTTI Meeting*, USA, Nov. 1989, p. 181–190.

[4] D. Kirchner, "Genaue Zeit für rechner über telephonmodems," *Proc. Mikroelectronik 89*, Springer-Verlag, 1989, p. 103–108.

[5] E. Brännström, "European Computer Time Service," *Proc. 5th European Frequency and Time Forum*, France, 1991, p. 284–287.

[6] F. Caviglia, *Prestazioni della rete analogica mista*, CSELT internal report, May 1992.

[7] M. Malcangi, *Il modem, teoria, funzionamento e applicazioni*, Jackson, 1989.

[8] S. Leschiutta, "Long term accuracy of time comparisons via TV signals along radio links," *IEEE Trans. on Instr. and Meas.*, vol. IM-22 no. 1, p. 84–87, March 1973.

[9] E. Rubiola, "Short distance frequency distribution systems," Proc. *2-nd European Frequency and Time Forum*, Switzerland, 1988, p. 263–270.

QUESTIONS AND ANSWERS

M. Weiss, NIST: Do you have plans to implement a service that allows you to adjust the transmission of the on time marker?

F. Cordara, Instutito Elettrotecnico Nationale Galileo Ferraris: Yes; we also have this plan for the end of 1993. The most widespread service is truly devoted to the one way users which seems to be the most in our account. We have several inquiries about this kind of service in the 1 second to 0.1 second region.

M. Weiss: So we have jumped from the nanosecond time transfer to the 1 second time transfer. Apparently as you get less accurate there are a lot more users.

TimeSet: A Computer Program That Accesses Five Atomic Time Services on Two Continents

P.L. Petrakis
Life Sciences Software
Camano Island, Washington 98292

Abstract

TimeSet is a shareware program for accessing digital time services by telephone. At its initial release, it was capable of capturing time signals only from the U.S. Naval Observatory to set a computer's clock. Later the ability to synchronize with the National Institute of Standards and Technology was added. Now, in Version 7.10, TimeSet is able to access three additional telephone time services in Europe — in Sweden, Austria, and Italy — making a total of five official services addressable by the program. A companion program, TimeGen, allows yet another source of telephone time data strings for callers equipped with TimeSet version 7.10. TimeGen synthesizes UTC time data strings in the Naval Observatory's format from an accurately set and maintained DOS computer clock, and transmits them to callers. This allows an unlimited number of "freelance" time generating stations to be created. Timesetting from TimeGen is made feasible by the advent of Becker's RighTime, a shareware program that learns the drift characteristics of a computer's clock and continuously applies a correction to keep it accurate, and also brings .01 second resolution to the DOS clock. With clock regulation by RighTime and periodic update calls by the TimeGen station to an official time source via TimeSet, TimeGen offers the same degree of accuracy within the resolution of the computer clock as any official atomic time source.

INTRODUCTION

The introduction of modem timing services for computers, first by the U.S. Naval Observatory, then by the National Institute of Standards and Technology, has created a need for software to interpret the data strings put out by these services and to set the computer clock with maximum accuracy.

Both the Naval Observatory and NIST are very helpful in supplying programs and programming code for accessing their modem time services, but my first exposure to such a program was early in 1987, when I downloaded a program called CallTime, written by a programmer in New England. As it turned out, the version I got was for a millisecond time service of the Naval Observatory that had already been discontinued.

At that point I decided to write TimeSet, which I first put out on computer bulletin boards in the summer of 1987. The appreciative response from the computing community, particularly on Compuserve, was most gratifying. Interest on the part of users has driven TimeSet development ever since. Ability to call the NIST's service was added in 1989, which for a time made TimeSet the only program of its kind that could work with both telephone time sources in the United States. Now, with Version 7.10, three European services — in Sweden (Swedish National Time and Frequency Laboratory), Austria (Technical University of Graz), and Italy (National Electrotechnical Institute) — have been added.

Inclusion of European services in TimeSet was at the suggestion of Mr. Erland Brannstrom of the Swedish National Time and Frequency Laboratory. He developed the modem time generator used in Sweden and

participated in the establishment of the standard data string format used in Sweden, Austria, and Italy. The standard has also been adopted in The Netherlands, though it has not yet been installed there, and it is thought likely that other European time services will adopt it in the future. Of the three European services using this standard format, only the Swedish and Austrian services offer the capability of measuring line delays at this time. The long-term development goal for TimeSet is to include as many of the world's atomic time services as possible. As new modem-accessible time services come online, they will be added to TimeSet.

In addition to these official time sources, Timeset 7.10 can set computer clocks from time data strings generated by a companion program called TimeGen, which generates UTC time data strings in Naval Observatory format. TimeGen allows any PC computer to become in effect a "substation" of any official atomic time service transmitting over the telephone system. The computer running TimeGen automatically updates its own clock by means of periodic calls via TimeSet to a selected atomic time service. The rest of the time it waits for the phone to ring so it can transmit data strings by modem to other computers calling it with TimeSet. Details on TimeGen are presented later in this article.

TIMESET OPERATION

Program Configuration

A copy of TimeSet that has never been configured before presents a configuration menu screen when it is first run (Figure 1). Scrolling up or down the list of configuration items is done by pressing the Up and Down arrow keys to highlight the next line. For most configuration items, selections are made by pressing the Right or Left arrow keys when a particular configuration line is highlighted. For example, when the line for modem speed is highlighted, each press of the Right or Left arrow key brings a new modem speed into view. The selectable modem speeds range from 1200 bps to 115200 bps (the high-speed options are to accommodate newer modems that can be "locked" at high speed locally while allowing the line speed to drop to 1200 bps to match the usual speed of a time service's modem).

Another configuration item that allows options to be toggled is the one for manual or automatic operation. If manual operation is selected, the user intitates a call to one or another of the time services by pressing a certain keys or key combinations at the main program menu, and on completion of a call the program remains loaded. If automatic operation is toggled, the program calls the selected time service, sets the computer clock, and immediately exits to DOS. A number of automatic options are available at the configuration screen. There are two options for each time service, specifically with or without line delay measurement. Thus one can select the NIST with or without line delay measurement, the Naval Observatory with or without line delay measurement, a selected European time service with or without line delay measurement, and a selected TimeGen service with or without line delay measurement. Automatic operation is mainly for the convenience of those who wish to include a TimeSet call in their AUTOEXEC.BAT file as part of the boot-up procedure.

A few lines may be edited. These include the lines containing time service telephone numbers, since it is not uncommon for telephone users in institutional settings to have to insert codes and pauses before and after an outside phone number, or, as in the case of those using the Federal telephone system, to revise the phone number to conform to that system's rules. One phone number configuration line is reserved for one of the European time services, Although the default for this line is "NULL", pressing the Right or Left arrow key successively produces current phone numbers for the Swedish, Austrian, and Italian time services, which, as noted, share the same data format. If a European phone number is selected on this line, it must be edited to remove the '+' sign in front of the phone number if one is calling from the host country, or to replace it with an international calling code if one is calling from another country. The last telephone number line is for calling a computer equipped with TimeGen. Here one simply types a phone number to replace the default "NULL."

Another line that allows editing is the one where users select their local time zone, which the program needs to know to convert UTC to local time. Although any of the named North American time zones can be obtained by toggling with the Right or Left arrow key while that line is highlighted, provision is made for TimeSet users outside North America to write in their time zone's offset from UTC (a positive number if east of 0 degrees longitude, negative if west of 0 degrees longitude).

Another line that often requires editing is the modem initialization string. Two alternative strings for modem initialization are built into version 7.10 of Timeset. The string '&C1&D2X4' is the default and is intended for users who have simple basic asynchronous modems, with no speed option higher than 2400 bps and no error checking/data compression protocols. &C1 instructs the modem to wait for a carrier, not to assume one is already present. &D2 instructs the modem to hang up when the DTR status is set to 0, which is TimeSet's method of hanging up quickly after it has obtained a time data string for parsing and clock setting. X4 selects a result code set that includes CONNECT, NO CARRIER, BUSY, and NO DIALTONE.

Toggling with the Right or Left arrow key while user's modem initialization line is highlighted will bring another modem initialization string for users who have one of the new high-speed modems that use data compression and error-checking protocols such as MNP or LAP-M. These protocols must be turned off and the modem placed in basic asynchronous mode when TimeSet makes a call to one of the time services. The string, '&Q0&B1&C1&D2X4' accomplishes this with the majority of high-speed modems. &Q0 is the modem command for basic asynchronous mode in most high-speed modems (a few brands use &M). &B1 is the command most high-speed modems use to keep the local speed high while allowing the line speed to adjust to match the speed of the remote modem; it is essential that &B1 be present if the TimeSet user has selected a high dial-up speed such as 38,400 bps. (It is also essential, if a high dial-up speed is selected, that the line that allows toggling YES or NO for locking the local speed be toggled to YES, because it will prevent any attempt to adjust the serial port to 1200 bps after connection is made.)

A variety of other options exist on the configuration screen. For example, users in the United States can select automatic adjustment for time season changes. Installing this feature would have been no problem with the data strings from the NIST, since that service has a time season flag embedded in its data string. However, since many TimeSet users have requested automatic season adjustment for the Naval Observatory data as well, and since the Naval Observatory has no flags for it in its data string, it was necessary to develop an algorithm to calculate when switches to daylight savings time and standard time will occur. To reduce code size, TimeSet applies this algorithm to both the Naval Observatory data and the NIST (ignoring the flag for season changes in the NIST string). This algorithm is good for the next 74 years, or until Congress changes the switch days again, whichever comes first.

No automatic time season adjustments are available for the European services, since it is not certain that all countries that might adopt the current European standard in the future will change time seasons on the same day. However, with any of the time services a season adjustment can be made manually from TimeSet's main menu merely by pressing function key F7. Whatever the current time season, a press of F7 reconfigures the program to the opposite season and adjusts the computer's clock accordingly.)

When the user has finished configuring TimeSet, a press of F10 saves the configuration to TimeSet's own file and brings the user to the program's opening menu.

The Main TimeSet Menu

If TimeSet is configured for manual operation, the program will always show the main menu (Figure 2) and will wait there for the user's keyboard input. If the user has configured TimeSet for automatic operation, however, as from a batch file, the main TimeSet menu normally will not be seen. Instead, the program will immediately begin initializing the modem and dialing the phone number of the selected time service. (The main menu is accessible even while dialing is in process, however, just by pressing the Back Space key.)

The main menu screen features a running time display with numbers for hours, minutes, and seconds typically 3/4" to 1" high, depending on monitor size. Fractions of seconds, to two decimal places, are displayed with standard characters.

Keystrokes needed to call one of the time services, with or without line delay measurement, are also displayed. The keys for each service are mnemonic: pressing W calls Washington (USNO) without line delay measurement, Alt-W calls the USNO with line delay measurement; pressing B calls Boulder (NIST) without line delay measurement, Alt-B calls Boulder with line delay measurement; pressing E calls the selected European time service (identified by country name on the menu screen) without line delay measurement, pressing Alt-E calls the selected European service with line delay measurement (except for the Italian service, which does not provide it); pressing T calls the selected TimeGen service, Alt-T with line delay measurement.

A variety of function key options are available at the main menu. F1 produces a help screen. F2 brings the configuration screen, allowing the user to change any configuration item. F7 toggles daylight saving time and standard time, simultaneously adjusting the computer clock by one hour. F8 toggles monochrome and color display. F9 allows a pulse to be generated at the parallel port at the instant of timesetting, useful for calibrating external equipment.

Figures 4 and 5 show a call in progress to the NIST, with line delay measurement requested.

After a call to a digital time service is completed, TimeSet summarizes the results on its final screen (Figure 6). The summary screen displays the last data string captured, the UTC information extracted from it, the measured line delay (if that option was chosen), and the local computer's time and date before and after.

Interaction with RighTime

RighTime is a remarkable program developed by Tom Becker of Air System Technologies, Inc. (see Mr. Becker's paper elsewhere in these Proceedings). It is a small memory-resident program that overcomes two glaring deficiencies in the PC's timekeeping system: (1) the typically appalling drift rate of the DOS clock, which can be as much as 15 seconds a day or more, and (2) the poor resolution of the DOS clock, no better than 55 ms. Mr. Becker's program makes getting highly accurate time from an atomic source with a program like TimeSet meaningful, because RighTime learns the computer clock's drift rate and refines a correction for it over a series of precision clock settings with TimeSet, and it applies this correction incrementally every few seconds as long as the computer is turned on. It can even learn the drift rate when the computer is turned off and only the CMOS clock, driven by a battery, is maintaining the time. As a result, RighTime can, after only a few TimeSet calls spaced over a few days, hold both the CMOS and DOS clocks within a few hundredths of a second of true time for a week or more. In addition, the latest version of RighTime breaks the .055 second granularity of the DOS clock and gives it true .01 second resolution.

Version 7.10 of TimeSet is able to detect the presence of RighTime and interact with it. If RighTime is loaded, TimeSet presents another function key option (F5) at its main menu screen that allows the user to see the current RighTime correction and the time that has elapsed since the last time set, which is useful in judging whether it is time to call a time service (Figure 3). The F5 option also allows the user to control certain functions of RighTime, including disabling RighTime learning for the next time and date set, forcing the system to ignore the next time and date sets completely, suspending all of RighTime's DOS clock maintenance actions, and suspending RighTime's maintenance of .01 second resolution in the DOS clock. All keys controlling RighTime functions in TimeSet have a toggle action; that is, pressing a designated key once changes the state of a RighTime function, and pressing the same key again causes reversion to the previous state.

THE TIMEGEN PROGRAM

RighTime's ability to bring sustained high accuracy to the computer clock, together with the ability of the latest version (version 2 or higher) to provide .01 sec resolution in the DOS clock, has stimulated further development of TimeGen, a program that allows any DOS computer to serve as a time source for any other computer equipped with TimeSet ver. 7.10 and a modem. I developed an early version of TimeGen several years ago, but abandoned it in consideration of the typically high drift rate of computer clocks. Computers with such a serious limitation would need to call an atomic time source several times a day to maintain only moderate accuracy.

The advent of RighTime has made further development of TimeGen feasible and desirable, and TimeGen is now included in the TimeSet version 7.10 distribution package. Once RighTime has learned the drift rate of the clock and has optimally refined its correction for it, a single call daily to an atomic time source should be sufficient to maintain accuracy high enough to be worth sharing with other computers via TimeGen and TimeSet. Indeed, since the latest version of RighTime provides .01 second resolution for the DOS clock, timesetting from a TimeGen source is as precise as timesetting from the NIST, the USNO, or any other atomic time source, provided the calling computers also have TimeGen installed and therefore have .01 second resolution. Although atomic clocks are accurate in the nanosecond range, this extremely high accuracy has no practical use in a device like a computer that can resolve time to no better than two decimal places. For this reason, when two computers are connected via modem, with one of them running TimeGen and the other running TimeSet, and both obtaining clock stability and .01 second clock resolution from RighTime, computer timesetting via TimeGen can be just as accurate as from a telephone time service based directly on a cesium beam clock.

To ensure accuracy of TimeGen's generated data strings, the program features daily automatic clock update calls to a preselected atomic time service. The trigger for these timed calls is a memory resident program called AutoDial, which can be loaded into memory with instructions to generate an alarm signal to TimeGen at a specified time each day. The alarm signal includes information on which service is to be called — the NIST, USNO, a selected European time service, or even another TimeGen service. On receipt of this signal, TimeGen runs TimeSet through a shell to call the specified time service and update the computer's clock. If RighTime is installed and its clock correction value has been well learned, this daily setting is sufficient to maintain very high accuracy for the rest of the day. As soon as TimeSet has completed its update work, which takes less than a minute, TimeGen regains control and resumes its wait for incoming calls. As soon as the phone rings, TimeGen begins to generate UTC time signals in Naval Observatory format. If the caller is TimeSet version 7.10 installed on another computer, TimeSet captures a data stream, extracts the time information, and uses it to set the calling computer's clock.

(Note: The memory-resident trigger program AutoDial also interacts with TimeSet, causing TimeSet to dial a specified time service at a specific time each day. If AutoDial is loaded, all that is necessary is to have TimeSet loaded and waiting when the specified time arrives.)

Repeated tests in which TimeSet, using line delay adjustment, alternately called the NIST, USNO, a European service, and a TimeGen service (maintained by RighTime and a daily update call to an atomic service) produced practically identical before/after decimal time readings on the final summary screen (within .01 second, which is the variance usually encountered even with purely atomic time sources in this version of TimeSet). Only the minutes and seconds were different on successive calls, reflecting the time it takes to place and complete a timesetting call. The fractional times at the instant of timesetting were practically identical in all cases, indicating the feasibility of using TimeGen to make any RighTime-equipped personal DOS computer the equivalent of an atomic time service "substation".

It remains to be seen how many individuals will find practical uses for TimeGen. A number of possibilities come to mind. The majority of countries in the world lack a digital time service accessible to the general computing public; even in Europe only three countries provide them. It is conceivable that individuals in

many countries could set up TimeGen "substations" to distribute accurate time from another country's publicly available atomic time service locally. Commercial and governmental organizations with multiple branch offices in a metropolitan area — banks, utilities, precinct police stations, for example — could provide a central TimeGen service available through a local call to computers in the various outposts. In both situations, only one computer would need to make a periodic long–distance or international call, but TimeGen and TimeSet would allow the accurate time to be shared by many others. Although a computer could be dedicated full time to this function, it is also feasible to provide TimeGen services only during specific hours, freeing the host computer for other uses the rest of the time. Finally, we will soon begin development of a computer bulletin board version of TimeGen that will allow any caller to a BBS to access TimeGen from a menu to set his computer clock.

Since the UTC time data streams sybthesized by TimeGen are based on DOS time, they can be no more accurate than the DOS clock itself. Therefore, in all instances it will be the responsibility of the TimeGen operator to ensure that RighTime is installed for clock stability and that the host computer's clock is updated regularly, preferably daily, with a call to an atomic time source.

PERFORMANCE

A reasonable test to perform with a program that can call as many time services as TimeSet version 7.10 is to see how much agreement exists in the decimal portion of the time before and after clock setting when several calls are made to the same time source in quick succession, and when calls are alternated between different time sources in quick succession. Such a test requires line delay adjustment with each time service to cancel out varying distance and modem effects. The results of several such tests, involving calls to the NIST, the USNO, and the Swedish National Time and Frequency Laboratory from a site 60 miles north of Seattle, are shown in Tables 1–6.

Tables 1–3 show the results from quickly repeated measures made with the NIST, the USNO, and the Swedish National Time and Frequency Laboratory. In nearly every instance, and with all three services, the difference between the time reading before and after the time set was either .00 or -.01 second.

Table 4 shows the results of calls alternating between the Swedish National Time and Frequency Laboratory and the NIST. Again the before/after discrepancy is either .00 or -.01 second. The results suggest that if the clock is set by the Swedish service, a call to NIST moments later produces the same setting that another call to Sweden would have produced, and vice versa.

Table 5 shows the results from calls alternating between the Naval Observatory and the NIST. Again, the discrepancy ranged between .00 and -.01 second. It is very gratifying to see this level of agreement, since line delay measurement with the NIST is made by that sophisticated service, which then advances its on–time mark to compensate for it. In contrast, line delay measurements with the Naval Observatory are made by TimeSet using the modem's remote digital loopback feature, and TimeSet adds the measured one–way delay to the time just before setting the system clock. To make these RDL measurements with high accuracy, Timeset reprograms the system timer to produce a tick rate such that the successive ticks are only about 838 nanoseconds apart. Measuring line delay is a matter of counting the ticks between the transmission of a character to the Naval Observatory's modem and the arrival of its echo, dividing the result by two, and applying appropriate factors to convert the result to time (to four decimal places). The excellent agreement between the results of calls alternating between the two services indicates the accuracy and precision of TimeSet's line delay measurement procedure.

Finally, Table 6 shows the results of alternating calls to the Naval Observatory, the NIST, and the Swedish time service made in rapid succession through four cycles. Before/after time readings never varied by more than .02 second and usually less, despite the widely disparate distances of the three services from the Seattle area and the apparent involvement of a satellite link with the Swedish service (as suggested by a consistent line delay measurement of approximately .14 second).

CONCLUSION

TimeSet is a shareware program that has reached a mature stage of development since its inception and initial release in 1987. With version 7.10, TimeSet can now access by telephone five atomic time resources on two continents, as well as freelance time sources operating the companion program TimeGen, which generates UTC data in Naval Observatory format and thus can act as a substation of the Naval Observatory or any other atomic time service. TimeGen ensures the accuracy of its synthesized UTC data strings by regularly running TimeSet through a shell to call a selected atomic time service and update the system clock. Its accuracy can be further ensured by installation of the clock regulating program RighTime. TimeGen can thus provide for many a reliable local alternative to an official atomic time source that might be a continent or an ocean away. They need only call a local TimeGen station with TimeSet and set their computer clock from it with the same accuracy they would get by calling an atomic time service themselves (provided the TimeGen service operator takes the necessary steps to maintain accuracy).

Two major factors limiting the utility of setting a computer clock to an atomic time service, namely the notorious drift rate in computer clocks (which often made the effort to get highly accurate atomic time seem not worthwhile) and their poor time resolution, have been eliminated by the release of version 2 of Becker's RighTime clock-regulating program, which learns and continually corrects for the drift and also provides .01 second resolution to the DOS clock. TimeSet version 7.10 is aware of the presence of RighTime and is designed to interact with it for maximum timesetting accuracy.

Table 1. Repeated Measures with the NIST

Conditions: Line delay enabled
RighTime 2 installed, optimal correction
System clock resolution: .01 second
Calls made in rapid succession

Time before set	Time after set	Error*
15:02:40.02	15:02:40.02	.00
15:04:51.02	15:04:51.02	.00
15:06:00.01	15:06:00.02	-.01
15:07:09.02	15:07:09.02	.00
15:08:18.01	15:08:18.02	-.01
15:09:20.02	15:09:20.02	.00
15:10:26.01	15:10:26.02	-.01
15:11:31.01	15:11:31.02	-.01
15:12:36.01	15:12:36.02	-.01
15:13:47.02	15:13:47.02	.00

Calls with zero error: 50%
Calls with -.01 error: 50%

* Error is difference between set time and previous time.

Table 2. Repeated Measures with the Naval Observatory

Conditions: Same as in Table 1

Time before set	Time after set	Error
15:15:32.11	15.15:31.11	.00
15:19:41.10	15:19:41.12	-.02
15:21:11.11	15:21:11.11	.00
15:22:37.10	15:22:37.11	-.01
15:24:07.11	15:24:07.11	.00
15:25:32.10	15:25:32.12	-.02
15:27:02.11	15:27:02.12	-.01
15:28:38.12	15:28:38.12	.00
15:30:02.11	15:30:02.11	.00
15:31:28.10	15:31:28.12	-.02

Calls with zero error: 50%
Calls with -.01 error: 20%
Calls with -.02 error: 30%

Table 3. Repeated Measures with Swedish Time Service

Conditions: Same as in Table 1

Time before set	Time after set	Error
20:33:10.12	20:33:10.12	.00
20:35:41.10	20:35:41.11	-.01
20:38:33.11	20:38:33.12	-.01
20:40:34.12	20:40:34.12	.00
20:41:54.12	20:41:54.12	.00
20:43:12.11	20:43:12.12	-.01
20:44:34.11	20:44:34.12	-.01
20:46:14.12	20:46:14.12	.00
20:47:34.11	20:47:34.12	-.01
20:48:50.12	20:48:50.12	.00

Calls with zero error: 50%
Calls with -.01 error: 50%

Table 4. Calls Alternating between Swedish National Time & Frequency Laboratory and NIST

Conditions: Same as in Table 1

Baseline calls to Sweden
from Seattle, Washington

	Error
Sweden	.00
Sweden	-.01
Sweden	.00
Sweden	-.01

Begin alternating calls

	Error
Boulder	.00
Sweden	-.01
Boulder	.00
Sweden	-.01
Boulder	.00
Sweden	-.02

Calls with zero error: 50%
Calls with -.01 error: 33%
Calls with -.02 error: 17%

Table 5. Calls Alternating between the Naval Observatory and the NIST

Conditions: Same as in Table 1

Baseline calls to NAVOBS
from Seattle, Washington

	Error
Washington	-.01
Washington	.00
Washington	.00
Washington	-.01

Begin alternating calls

	Error
Boulder	-.01
Washington	.00
Boulder	-.01
Washington	-.01
Boulder	-.01
Washington	.00

Calls with zero error: 33%
Calls with -.01 error: 67%

Table 6. Results of "round-robin" calls to Naval Observatory, NIST, and Swedish National Time and Frequency Laboratory, from Seattle, Washington.

Conditions: Same as in Table 1

Call to:	Time before set	Time after set	Error
Washington	01:08:34.11	01:08:34.11	.00
Boulder	01:09:46.01	01:09:46.02	-.01
Sweden	01:11:08.12	01:11:08.13	-.01
Washington	01:14:33.12	01:14:33.11	+.01
Boulder	01:15:42.01	01:15:42.02	-.01
Sweden	01:17:01.11	01:17:01.12	-.01
Washington	01:18:39.11	01:18:39.11	.00
Boulder	01:19:54.00	01:19:54.02	-.02
Sweden	01:21:16.11	01:21:16.12	-.01
Washington	01:22:56.12	01:22:56.11	+.01
Boulder	01:24:04.01	01:24:04.02	-.01
Sweden	01:25:24.11	01:25:24.13	-.02

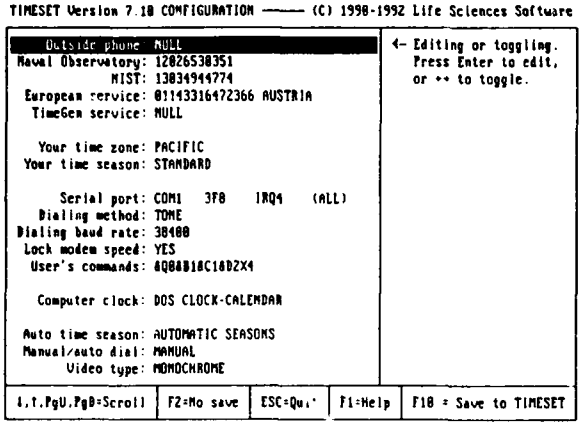

Figure 1. TimeSet 7.10 configuration screen. Most selections are made by toggling new values with the right or left arrow key. A few are made by editing existing values.

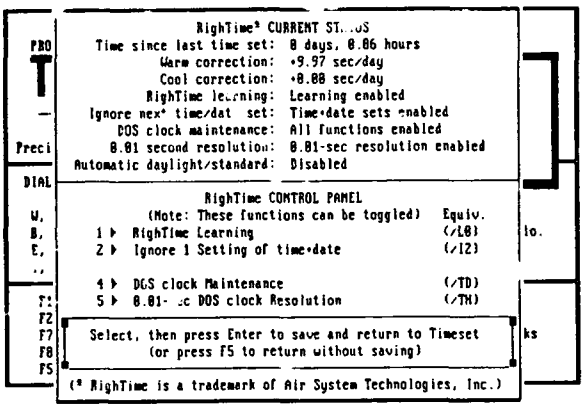

Copyright 1987-1992 Life Sciences Software, Stanwood, Washington, USA

Figure 3. Pop-up window showing current RighTime settings and control options. Control options include temporarily disabling RighTime learning for the next call to a time service, ignoring the next pair of time and date sets, suspending RighTime's maintenance of the DOS clock, and suspending 0.01-sec DOS clock resolution. This window does not appear unless TimeSet detects the presence of RighTime.

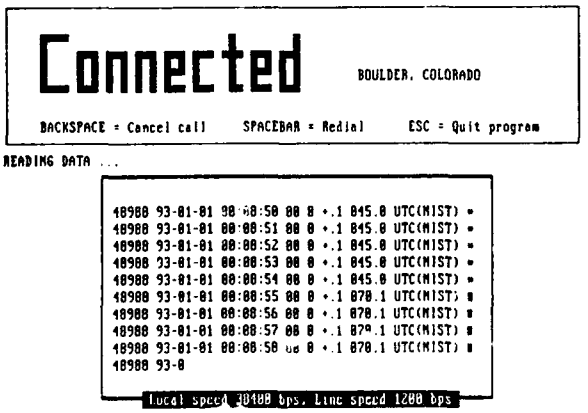

Figure 5. Data string capture in progress. Unless there is line noise, TimeSet receive nine data strings and captures the tenth for parsing and timesetting.

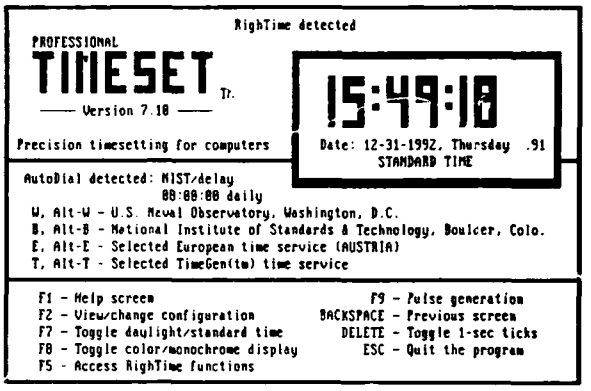

Copyright 1987-1992 Life Sciences Software, Stanwood, Washington, USA

Figure 2. TimeSet 7.10 menu screen. Selecting and calling a time service is done by mnemonic key strokes (e.g., W = Washington, Alt-W = Washington with line delay measurement; B = Boulder, Alt-B = Boulder with line delay measurement; etc.). Several control options are available by pressing function keys.

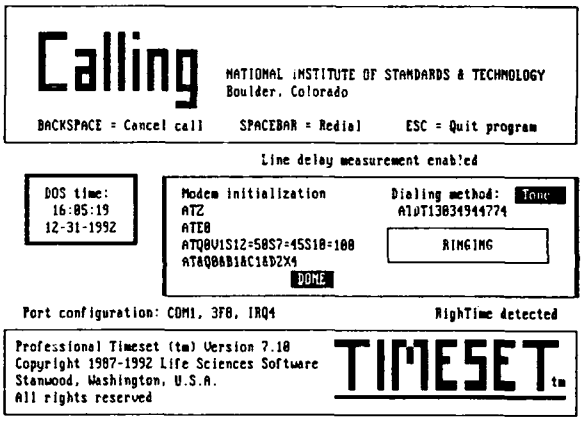

Figure 4. Modem initialization and dialing the NIST with line delay request.

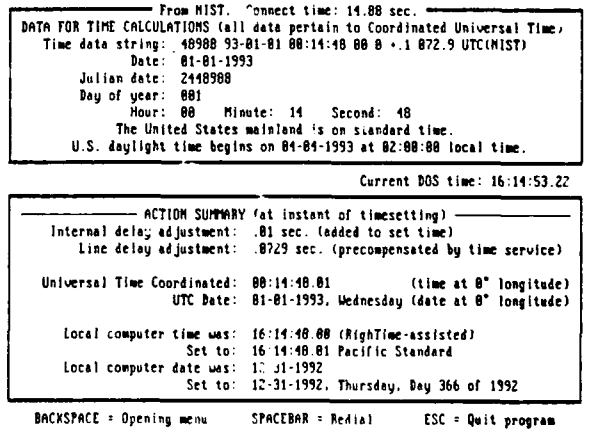

Figure 6. TimeSet 7.10 summary screen. If the program is configured for automatic operation it exits to DOS at this point.

QUESTIONS AND ANSWERS

Ralph Partridge: Los Alamos National Laboratory: We have tried your program before. We have a need to work with a rather different time format using the same thing. We have written our own program to do it but we wondered if it is feasible to work with you recompiling with a different time format?

R. Petrakis: Yes. I will give you my phone number and we can talk.

RighTime[tm]
A Real Time Clock Correcting Program For MS–DOS–Based Computer Systems

G. Thomas Becker
Air System Technologies, Inc.
14232 Marsh Lane, Suite 339
Dallas, Texas 75234–3899

Abstract

A computer program is described which effectively eliminates the misgivings of the DOS system clock in PC/AT–class computers. RighTime is a small, sophisticated memory–resident program that automatically corrects both the DOS system clock and the hardware "CMOS" real time clock (RTC) in real time. RighTime learns what corrections are required without operator interaction beyond the occasional accurate time set. Both warm (power on) and cool (power off) errors are corrected, usually yielding better than one part per million accuracy in the typical desktop computer with no additional hardware, and RighTime increases the system clock resolution from approximately 0.0549 second to 0.01 second. Program tools are also available which allow visualization of RighTime's actions, verification of its performance, display of its history log, and which provide data for graphing of the system clock behavior. The program has found application in a wide variety of industries, including astronomy, satellite tracking, communications, broadcasting, transportation, public utilities, manufacturing, medicine and the military.

Introduction

Most MS–DOS, PC–DOS and DRDOS users have long ago learned to live with, and generally regard as inadequate, the system time–of–day clock that is a standard component of these operating systems. The typical DOS–based computer system clock exhibits inaccuracies that can range from a few seconds to several minutes per day, and the system can lose track of days at a time (on Friday, leave a DOS–based computer running at the office and go home for the weekend; when you return to the office Monday morning, the machine will very likely tell you it's Saturday). These errors are the result of a combination of compromises at several steps in the IBM PC design process, *circa* 1980. The consequences remain with users to this day.

No autonomous RTC hardware was implemented in the original IBM PC announced in August, 1981. Instead, software (partially in ROM–based BIOS firmware and partially in RAM–resident DOS) counted regular interrupts which were generated by an interval timer. DOS converted the resulting "tick" count to conventional expressions of time of day when application software called for it, and, if during a request for the time DOS determined that midnight had passed, it

incremented the system date. Whenever the system was booted, the date and time was initialized to 1980/01/01 00:00:00; the user was expected to set both at each boot.

With the introduction of the PC/AT in August, 1984, a hardware clock system — a Motorola MC146818 CMOS RTC and some associated circuitry — was included. The part was powered by a battery when the system was not operating so it would maintain date and time continually. Released at the same time, DOS Version 3 automatically read the CMOS RTC clock date and time at system boot and set its date and tick counts to match; aside from that initialization at boot, the hardware clock was not used. When the DOS date or time was changed by the user, the change was not reflected in the CMOS RTC clock; it needed a separate setup utility program. Later DOS versions set the CMOS RTC clock at the same time the DOS clock was set, but the CMOS RTC clock time was still read, and is still today, only at boot.

No other changes have been made to the time-of-day clock mechanisms of the AT-class PC-compatible computer since 1984, except as have been applied to the CMOS RTC clock hardware itself. (Dallas Semiconductor and Motorola now produce several compatible lithium-powered clock modules and Intel and other semiconductor producers have incorporated the RTC logic within large-scale integrated circuits that support the current microprocessors.) The hardware manufacturers and software publishers moved on as if whatever few difficulties that existed were solved with the advent of the PC/AT. The problems were neither solved nor few.

The Problems of The DOS Clock

The interval timer that DOS uses to generate the regular tick that it counts is driven by an uncalibrated, unconditioned and usually non-adjustable 1.193 MHz source (1.193 MHz is one quarter of the original PC system clock frequency of 4.77 MHz, and it is also one third of the NTSC television standard color burst frequency, 3.579 MHz). The interval timer is programmed to divide that frequency by 65,536 to produce an interrupt rate of approximately 18.206 ticks per second which determines the resolution of the standard DOS clock, approximately 54.925 milliseconds. DOS allows for the expression of time in 0.01 second increments, but it cannot internally maintain that resolution nor represent decimal times exactly due to the tick resolution.

DOS depends upon the cooperation of all software that runs on the machine to allow sufficient time for each interval timer tick interrupt to be counted. This is not always possible, so some interrupts are missed and are not counted. On a computer whose interrupt system is heavily loaded, the accumulation of lost interrupts makes the DOS clock appear to run slowly.

The tick interrupt is normally intercepted by a routine in the ROM BIOS which increments a 32-bit tick count in RAM and determines if a value that represents approximately 24 hours has been exceeded (the tick duration makes 24 hours indeterminable exactly). If so, the tick count is set to zero and a single bit flag, representing the passing of midnight, is set and provided to DOS when it next asks for the tick count. These DOS requests only occur when the system is in need of the current time of day. At that time, if the bit is set, DOS increments the date. If more than 24 hours have elapsed between two requests for time of day, DOS is unable to recognize that more than one midnight has passed. If the user displays the date after a system has been running, but idle for more than a day, DOS will indicate that the date is one day after the last day the machine was used.

The interval timer has found itself reprogrammed by a number of applications, usually games that require dynamic video presentations. In these programs, the interrupt that the interval timer yields is used to refresh the video screen at a high rate. At the termination of the game, the DOS clock is rarely where it should be. Some of the more responsible programs make an attempt at resetting the DOS clock to compensate for the game session duration, but others leave it in disarray. If the game increased the tick rate and left the intercepting BIOS interrupt "hook" in place, the DOS clock will have advanced greatly; in the worst examples, the rate is left accelerated as well.

The Problems of The CMOS RTC

The CMOS RTC clock resolves only to whole seconds. When DOS reads it at boot, one second of ambiguity is set in the DOS clock even if the CMOS RTC clock is accurate. Conversely, when the DOS clock is set, DOS transfers whole seconds to the CMOS RTC clock but makes no attempt to deal with the fractional part of the seconds, nor does it synchronize the seconds transition, so even if the DOS clock is set accurately, the CMOS RTC clock won't be.

The CMOS RTC clock is usually paced by a 32.768 kHz quartz crystal which is loaded by a pair of capacitors. The crystal is often an inexpensive watch–type device, characterized for operation at room temperature (typically 25 degrees C). At temperatures either above or below the characterized temperature, the crystal's resonance change will slow the clock. The loading capacitors are generally not temperature compensated and add to the detuning. Except in the case of the modern CMOS RTC modules mentioned earlier, no provision is made to allow trimming the crystal frequency. Dallas Semiconductor RTC modules are internally trimmed at the factory to +20 seconds per month at room temperature, anticipating an environment that will slow the clock; in use, the computer system internal temperature is widely varying, ranging from perhaps 10 degrees C when the system is not powered to 55 degrees C when it is. Dallas Semiconductor's data indicates that the part can be expected to run as much as 2.5 minutes per month slow at these temperatures.

The CMOS RTC clock oscillator is powered by the system's +5 volt supply when the machine is powered and by a lower voltage when it is on battery backup. Typically, an additional six parts per million error can be expected when the clock is running on battery power.

The CMOS RTC clock part provides an option that will automatically advance or retard the time at 0200 on the appropriate Sunday morning when Daylight Savings Time and Standard Time, respectively, start in the USA. This feature is usually not used, since no mechanism to invoke it exists in DOS. DOS does, nevertheless, include a bit in its internal time data structure that indicates whether this automatic time change feature is enabled or not (many documents incorrectly state that the bit indicates that the time is Daylight Savings Time). The rule was changed in 1986 and many computers — even current models — contain parts that still adopt the pre–1986 rule. Even if the feature is enabled, many machines will change on the wrong Sunday morning in April (the last rather than the first). Dallas Semiconductor's DS1287 RTC module was introduced with the currently correct rule. Motorola corrected its part with the announcement of the MCCS146818B1M RTC module in 1991.

The Solution to the Problems

RighTime approaches the solution to these problems by making best use of the better qualities of each of the two clocks. Two foremost qualities of the CMOS RTC are its relative stability and its autonomy. The DOS clock has a high resolution interval timer available to it, although its availability is conditional, subject to loss of power and to software that commandeers it.

With these resources, RighTime does four fundamental things:

1. RighTime slaves the DOS clock to the CMOS RTC, frequently referring the DOS date, tick count and interval timer count to the CMOS RTC date and time;
2. RighTime operates the interval timer in a disciplined mode that allows deriving a higher resolution than standard while maintaining the standard tick rate and count for compatibility;
3. RighTime maintains accuracy by regularly calculating and applying corrections to the DOS clock and adjustments to the CMOS RTC; and
4. RighTime intercepts and monitors time set commands to learn and refine the CMOS RTC correction rate.

RighTime is loaded each time DOS is booted, makes itself resident in system memory, and hooks a number of system interrupts. (A hook is a logical tap in the execution chain of some specific event or class of events.) For its time–keeping tasks, RighTime hooks an interrupt from the CMOS RTC, one from the interval timer, and several that convey the time set and read commands from an application program or the user to DOS. Other interrupts are intercepted to disallow functions that could otherwise change resources that RighTime must exclusively control. Since DOS is not ordinarily a multitasking operating system, several other interrupts are hooked to determine when system activities are momentarily idle. These logical pauses are often very brief, but occur frequently and allow RighTime to do its manipulations as a transparent background function without noticeably affecting work that is ongoing in the foreground.

The CMOS RTC is programmed to produce an interrupt once per second, immediately after its internal seconds update. Every four seconds, RighTime reads the CMOS RTC date and time, calculates the equivalent DOS clock values, and sets the tick count and interval timer count and mode accordingly. This regular update prevents the DOS clock from wandering far from the CMOS RTC time and corrects whatever ills might come from a game or other application that reprograms the interval timer. Between these periodic updates, the DOS tick count is incremented by the BIOS interval timer interrupt handler — just as it is without RighTime — and is available to those programs that use the tick count directly.

RighTime augments the routines that handle the conversions of tick count to time–of–day and time–of–day to tick count with its own routines. These routines process the Get DOS Time and Set DOS Time functions, respectively, and provide resolution that far exceeds the 0.01 second resolution of the DOS clock data structure. Any program that gets the time via the DOS calls will benefit from the additional resolution that RighTime provides.

Although the CMOS RTC is relatively stable, its rate is rarely highly accurate. Since, under RighTime, the DOS clock mimics the CMOS RTC, the DOS clock would exhibit the same rate error unless corrected. RighTime handles this by incorporating a calculated correcting offset in

each of the DOS clock updates. The result is a deliberately increasing divergence of the two clocks. Assuming that the corrected DOS clock rate is accurate, the CMOS RTC must be occasionally adjusted to match the DOS clock. The CMOS RTC is advanced or retarded when the difference between the two clocks has reached one second; the DOS clock offset is adjusted accordingly. If the DOS clock is set to the correct time, and the CMOS RTC rate correction is proper, the result is a DOS clock whose expression is within 0.01 second of the correct time and a CMOS RTC that is within one second of the correct time. Actually, the calculated DOS clock offset is bipolar, so the CMOS RTC is never more than +/-0.5 second from the correct time.

Since the CMOS RTC rate can vary with changes in temperature and voltage, the theoretically perfect correcting algorithm would account for both in appropriate complex terms. In practice, two rates are maintained by RighTime, and suffice; one represents the system power–off state and the other represents power–on. We refer to them as "cool" and "warm", though, since most users seem intuitively familiar with temperature effects. RighTime applies a single calculated adjustment when it is loaded at system boot that corrects for CMOS RTC error that accumulated while the system was in the power–off state; if the program has not been running for more than 30 minutes, the cool correction rate is employed, otherwise the warm correction rate is applied. With that exception, the warm correction rate is used in each DOS clock update.

The CMOS RTC rate correction values are learned. RighTime assumes that whenever the DOS clock is set, it is set accurately. At the moment of set, then, the existing DOS clock error is a function of the CMOS RTC rate error, the current cool and warm correction rates, the time elapsed since the last accurate time set, and the ratio of warm and cool operation in that period. The correction rates are refined with each time set, yielding decreasing error as they close on the "ideal" values. These values, and others that are necessary for the process, are stored in a suitable place within the machine hardware or in a small dedicated file.

For those users who want one less clock to change twice each year, RighTime offers support for the American Daylight/Standard time change feature of the CMOS RTC. Since the change itself is handled by the hardware, the program does not need to be running when the change needs to occur. The user is cautioned, though, that the change might not occur on the prescribed day in April due to an outdated hardware component.

Although RighTime can usually be used effectively with the defaults, the program accepts a wealth of options and user–provided parameters that can detail the function to a specific machine environment, and a logical interface is included that allows the time setting functions to be automated. A system can be easily designed that will continually adjust itself to a slowly changing operational environment as might be encountered with seasonal temperature changes at a remote data acquisition site.

Conclusion

RighTime is an effective software solution to the poor time–keeping performance of the PC/AT–compatible, DOS–based computer system. The cesium beam and hydrogen maser clock industries will remain unchallenged by your computer, but it should be easy to achieve error rates of 0.5 second per week or better. We regularly hear reports of one tenth of that error rate from stable systems, but these represent the best that can be expected in the current form of the program.

The current version (v2.46) requires only 6.5K of RAM, and the program can be loaded into high memory.

RighTime is a commercial software product that is currently distributed via shareware. An evaluation copy is available electronically on the Air System Technologies BBS, 214/869–2780 (300–9600 bps, 8N1), free of charge. The evaluation program is fully functional and may be used for up to 30 days. Usage beyond that period requires payment of a registration fee.

Development of the RighTime process is ongoing. We anticipate reliable accuracies on most hardware to exceed 0.001 second, allowing DOS clock time to be expressed to the millisecond in a future revision. An OS/2 version is in planning, with a summer 1993 anticipated delivery.

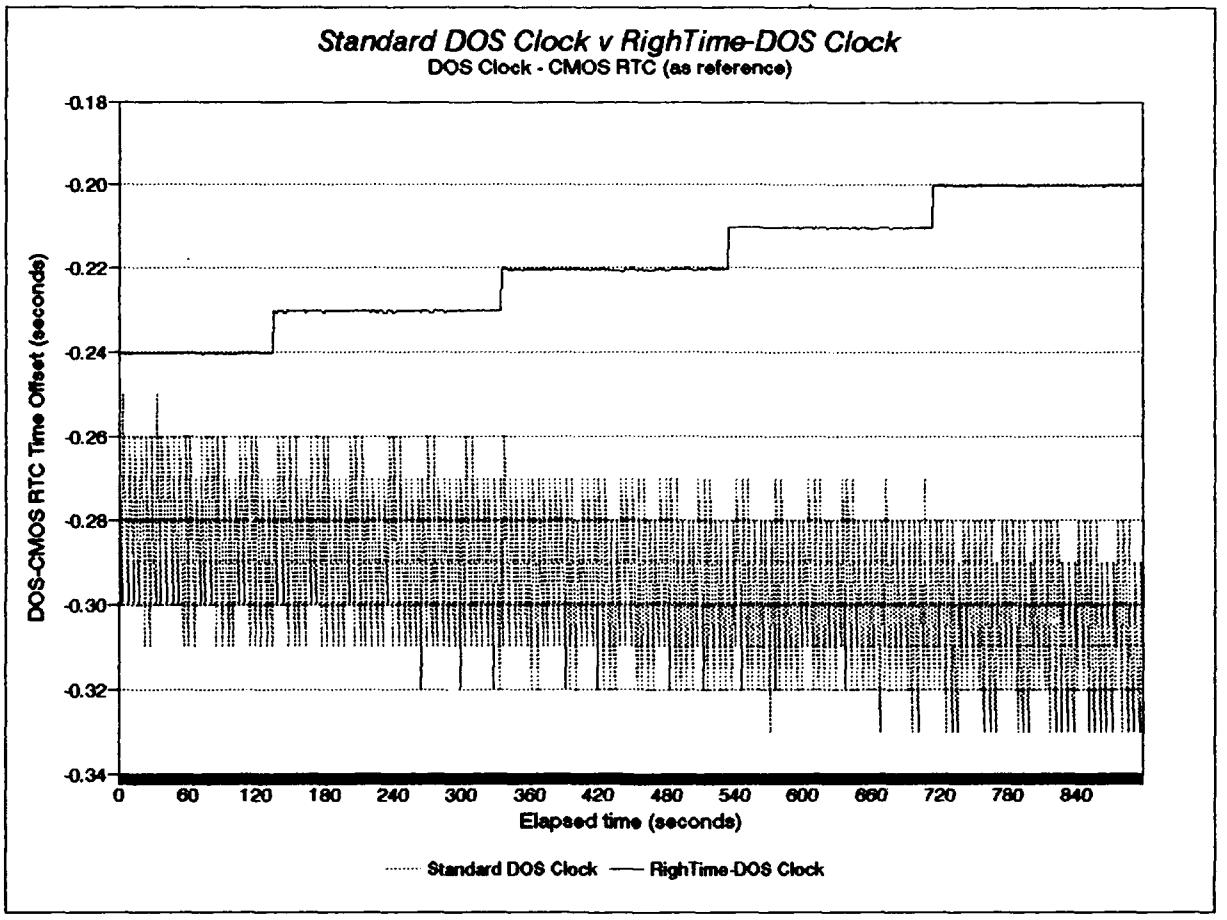

Figure 1. Comparison of the uncorrected, standard-resolution DOS clock to the RighTime-corrected DOS clock. The data is the difference between the indicated DOS clock time and the CMOS RTC time, measured at the moment of the CMOS RTC seconds update. The broad swath of the standard DOS clock is due to its inability to express decimal time values as a result of its poor resolution. The general downward trend results from the combined rate error of the DOS clock and the CMOS RTC. The comparatively fine, stepped RighTime-corrected DOS clock data shows the tight regulation (typically well within 1 ms) and the deliberately increasing applied time offset that compensates for the CMOS RTC rate error. These data were taken from a machine whose CMOS RTC runs about four seconds per day slow.

```
C:\RT2>rightime

RighTime: Indicated DOS clock date and time is 1993/01/05 20:54:31.91.
RighTime: Warm correction rate is -0.62 second per day.
RighTime: Cool correction is defeated. All adjustments use warm rate.
RighTime: Current applied DOS-CMOS RTC offset is -0.03 second.
RighTime: Last DOS clock correction was 1.94 seconds ago.
RighTime: Last CMOS RTC adjustment was 0.07 hour ago.
RighTime: Last timeset was 1.94 hours ago.
RighTime: Stack A headroom is 146 bytes; Stack space used is 62 bytes.
          Stack D headroom is 158 bytes; Stack space used is 50 bytes.
RighTime: /?=Help; Version 2.46; DEVELOPMENTAL PROGRAM: DISTRIBUTION PROHIBITED
RighTime: Copyright 1991-92 GTBecker, Dallas 214/402-9660. All Rights Reserved.
RighTime: Selftest passed.
RighTime: ** Already resident. **

C:\RT2>testtime

TestTime: Version 2.46; DEVELOPMENTAL PROGRAM: DISTRIBUTION PROHIBITED
TestTime: Copyright 1991-92 GTBecker, Dallas 214/402-9660. All Rights Reserved.
TestTime: RighTime v2.46 is resident.
TestTime: CMOS RTC mode is normal.
TestTime: "Appl" data is the current DOS-CMOS RTC offset applied by RighTime.
          "Meas" data is the current DOS-CMOS RTC offset measured by TestTime.
TestTime: If = in CMOS data below is flashing, CMOS RTC interrupts are normal.
          Flashing ! indicates the moment of DOS clock correction.
TestTime: Press any key to exit.

TestTime: CMOS=930105:20:55:46 DOS=930105:20:55:46.54 !Appl=-0.03 Meas=-00.0301

C:\RT2>testincr

TestIncr: Version 2.45 Copyright 1991-92 GTBecker, Dallas. All Rights Reserved.

TestIncr: Difference of successive unique DOS clock reads (seconds):
          58.49 - 58.48 = 0.01

TestIncr: There were 500 unique values over 5 seconds, or 100.000 per second.
TestIncr: The average increment over this period was 0.01000 seconds.
```

Figure 2. Screen prints of RighTime (when resident), TestTime, a diagnostic program, and TestIncr, a DOS clock resolution verification program. A log program (not shown) also displays all system time-related activities while RighTime is resident.

QUESTIONS AND ANSWERS

J. Levine: NIST: It should work just as well; you have done a very nice job with it. There are two comments that I was going to make which have nothing to do with your program, rather with people who might not realize two consequences of your program. First of all is that if your clock is fast, then your program will be continuously setting it backwards. That may confuse utilities like MAKE and that is not a bug of the program. That is simply a feature that you just have to be aware of, that you can wind up in which a derivative file is a time that is earlier than is apparent; because the clock was set backwards. The second thing that I wanted to point out is that there are some versions of that real time clock chip which have an incorrect daylight saving time algorithm. They used the old U. S. daylight saving time algorithm rather than the new U. S. daylight saving time algorithm. If you have the older type PC's and you do not call somebody you will be wrong by an hour for a few weeks in April.

G. Becker, Air Systems Technologies, Inc.: Yes, as a matter of fact the Motorola MC146818 was unfortunately modeled; it uses the old rule, it went out of date in 1986. It unfortunately was modeled by many of the VLSI manufacturers for modern machines, so we have machines that were designed in 1990 and manufactured in 1991 that use a 1986 rule. The Motorola chip has been fixed. There is a 146818 MCCS1B, I think that has the new rule in it and the Dallas Semiconductor DS1287 series are also correct. You are quite right if you adopt to use this slash A option on the command line level and you find that the clock has suddenly sprung forward. It will miss the first Sunday, instead will spring forward on the last Sunday of April. It is not the program's fault. It is either an old chip or you can blame your hardware manufacturer for not being up to date. It still is a very common error. I think it was published in Computer Language Magazine, which went to great lengths to publish an algorithm so you could adopt this erroneous rule in C language.

G. Winkler, USNO: I have two questions and one comment. The comment is first. Since there are several computer people here, we have to do something about that awful custom of calling the Gregorian Date a Julian Date. It has been somehow introduced about 20 to 25 years ago to call the day of the year and the year combination the Julian Date. This is of course a Gregorian Date. There is complete confusion about this; there is a modified Julian Date which we discussed before. There is a Julian Date in use for the last 400 years in astronomy. I think you ought to keep these things clearly separated. That is the first thing. Another question is what happens when you have your computer turned off and then is turned on. The rate of your CMOS clock would be different because of the different temperature inside the computer. Does your program correct for that also?

G. Becker: There are actually variables. One is temperature and the other is the power supply voltage. The clock module falls back to usually 3.6 volts (a lithium cell). Sometimes, however it is backed up by four AA cells, or something like that (six volts). In any event, the voltage changes as does temperature. Yes, Right Time developed both warm and cool corrections and will, given enough opportunity, correct adequately for both of those.

G. Winkler: That is wonderful and I am really impressed by that. Now comes another question. I have three operating systems on my computer; DOS, OS2 and Coherent. Of course, I boot up alternately by using the Boot Manager. Is it correct to say that your program will only come into action when we boot using the ALT Executive file on drive C?

G. Becker: Yes, at this moment, it is only in a MS-DOS program. There is an OS2 version coming that will be executionally compatible. You will be able to switch between those two operating systems. The data that one produces can be used by the other. Going into a third, perhaps UNIX or some other operating system, Right Time will not be running. However,

there is a facility so that you can tell Right Time when you come back into either of the operating systems that it will run in, that it has not in fact been comatose. The system still has been running and warm and so it will not mistake that dead period for a cool correction but instead apply the appropriate warm correction to span the lapse of the real time correction.

Measurement Methods and Algorithms for Comparison of Local and Remote Clocks*

Judah Levine
Time and Frequency Division
and
Joint Institute for Laboratory Astrophysics
National Institute of Standards and Technology
Boulder, Colorado 80303

Abstract

We will discuss several methods for characterizing the performance of clocks with special emphasis on using calibration information that is acquired via an unreliable or noisy channel. We will discuss time–domain variance estimators and frequency–domain techniques such as cross–spectral analysis. Each of these methods has advantages and limitations that we will illustrate using data obtained via GPS, ACTS and other methods. No one technique will be optimum for all of these analyses, and some of these problems cannot be completely characterized by any of the techniques we will discuss.

We will also discuss the inverse problem of communicating frequency and time corrections to a real–time steered clock. Methods have been developed to mitigate the disastrous problems of data corruption and loss of computer control.

Introduction

Measuring the time or frequency of a clock inevitably involves transmitting the clock signal through a channel of some sort. The channel may consist of nothing more than a measurement system if the clock is nearby, while the channel for a remote clock is likely to be much more complex. In either case it is important to characterize the performance of the channel and to remove its effects if possible. This is quite difficult to do in general; we will discuss methods that are useful in several important special cases. None of these methods is optimal in all situations.

Differential Comparisons

One of the simplest methods of separating the contributions of the channel and the clock is to observe the same clock through two nominally independent channels. Figure 1 shows the difference between two channels, each of which is measuring the time of a single cesium standard with respect to a reference oscillator. Since the input signals are identical, the difference should consist primarily of a constant value that depends only on the differential delays in the cables and the measurement

hardware, and a mean value has been removed from the data set to account for this. The residual fluctuations are channel noise. If the channels are independent and identical, we can estimate the channel performance by assigning 50% of the remaining variance to each channel.

We may characterize the data of Fig. 1 using the standard two–sample (Allan) variance. The magnitude of the Allan variance is 6×10^{-16} at 2 hours, and it decreases approximately as $1/\sqrt{\tau}$ for longer times (Fig. 2), suggesting that the difference between the two measurement systems can be modeled as white frequency noise. Although this is not impossible, the response of the hardware is more likely to be approximated by white phase noise, which would fall off more rapidly with averaging time. If we assume a white phase noise model for the channel, then the observed excess power at long periods must be the response of the channel to some other signal. The more detailed analysis below shows that the measurement systems are in fact responding to fluctuations in ambient temperature.

The air temperature in the vicinity of the measurement hardware is shown in Fig. 3; there is a clear qualitative correlation between these data and the data of Fig 1. This temperature sensitivity may be quantitatively estimated using correlation analysis in either the time or the frequency domains.

Analysis in the Time Domain

The simplest assumption is that the measurement hardware responds linearly to fluctuations in the ambient temperature, possibly with some time lag. If $R(t)$ is the perturbation in the measurement at time t when the ambient temperature differs from its long–term average value by $T(t)$, then we estimate $R(t)$ by

$$\hat{\mathbf{R}}(\mathbf{t}) = \mathbf{C_0 T(t)} + \mathbf{C_1 T(t-\tau)} + \ldots + \mathbf{C_k T(t - k\tau)}. \quad (1)$$

The parameter τ is the time interval between measurements of both R and T. The C_k coefficients in eq. 1 are usually called admittances. They are generally not linearly independent of each other since the temperature series itself has a non–zero auto–correlation at finite lag. As a result, it is usually sufficient to use only a single term on the right–hand side of eq. 1. This choice may also be necessary to achieve numerical stability in the solution if the auto–correlation function of the temperature varies only slowly with lag time (which is the usual situation). We can estimate both k and C_k in the simple 1–term case by finding the value of k for which the cross–correlation function $< R(t)T(t-k) >$ is an extremum. The value of the cross–correlation for this value of k divided by $< T(t)T(t) >$, the variance in the temperature series itself, is then an estimate of C_k. The sharpness of this extremum depends on $< T(t)T(t-k) >$, the auto–correlation of the temperature function, and on how well eq. 1 models the variance in the measurement channel.

We have computed the cross correlation between R and T (data in Figs. 1 and 3), and the result is shown in Fig. 4 as a function of lag $k\tau$, where $\tau = 2$ hours. We find a clear extremum at about $k = 2$; the normalized admittance at that lag is -6.59 ps/°C. As we should expect, the extremum is rather broad because the temperature changes slowly in time and peaks at a non–zero lag because of the thermal inertia of the measuring hardware. We can use eq. 1 to model the temperature–induced variance in Fig. 1 and to remove the temperature–dependence from the data. This operation reduces the Allan variance by a factor of 3 and whitens the time difference data by removing much of the longer–period structure. The Allan variance now decreases more rapidly than $1/\sqrt{\tau}$, suggesting that we are approaching the underlying white phase noise of the

channel. There is still some residual long–period structure in the measurements, however, and we can do better.

Analysis in the Frequency Domain

The constant time–delay used in eq. 1 is phenomenologically useful, but does not accurately model the actual system. We inserted the delay to model the thermal inertia of the hardware, but this inertia does more than just introduce a time delay—it also acts as an integrator of the fluctuations in the ambient temperature. This integration acts as a low–pass filter. In addition, the correlation analysis does not recognize that both of the time series have high–frequency uncorrelated noise which nevertheless contributes to the computation. Both of these considerations imply that the actual admittances are likely to decrease at higher Fourier frequencies (shorter period perturbations). This dependence is not incorporated into eq. 1, which estimates a frequency–independent average admittance. The admittance estimated using that model is therefore likely to be too small at long periods where the temperature fluctuations are significant and too large at short periods where the data are largely noise due to other causes.

The simplest way of incorporating these considerations into the model is to assume a linear frequency–dependent admittance. If R' and T' are the Fourier Transforms of R and T, respectively, then the admittances will be estimated to satisfy

$$\mathbf{R'(f) = C'(f)T'(f)}, \tag{2}$$

where $C'(f)$ is the admittance as a function of frequency. The admittance at each frequency may be complex to incorporate both a magnitude and a phase shift; the phase shift is the frequency–domain analog of the time delay in eq. 1.

If R' and T' are computed using standard Fast Fourier Transform methods, then each will have n degrees of freedom, where n is the number of points in the time–domain functions R and T. (These frequency–domain degrees of freedom are normally assigned to $n/2$ amplitudes and $n/2$ phases, but other assignments are possible.) Equation 2 can then be solved for $n/2$ complex admittances, all of which will be approximately linearly independent of each other:

$$\mathbf{C'(f) = \frac{R'(f)}{T'(f)}} \tag{3}$$

This process would reduce eq. 2 to an identity, but it would result in an admittance estimate that was not physically reasonable, since $C'(f)$ should not vary rapidly with frequency. We can introduce this constraint by averaging $C'(f)$ both in frequency and in time. The frequency averaging is motivated by the fact that the hardware and its surroundings are a non–resonant thermal system and cannot have a response that is a rapidly–varying function of frequency. The time–averaging recognizes that the admittance to temperature should depend on the mechanical and electrical design of the system and its surroundings and should therefore be time–independent. (This latter condition may not be true if the system is also sensitive to the spatial gradient of the temperature. This quantity may vary in time even if the temperature does not.)

It is possible to satisfy both of these averaging criteria simultaneously by breaking the time series into blocks and by averaging the admittances computed in each block. The blocks are usually chosen to be consecutive, non–overlapping subsets of the data. The frequency resolution of a Fourier transform is inversely proportional to the length of the input time series, so that shorter blocks implies a wider bandwidth for each estimate and hence greater frequency averaging. In addition, as the length of each block decreases the number of blocks in a given data set increases, thereby increasing the number of admittance estimates that are averaged to yield the final value. The admittances that make up each average are computed using data from different times, resulting in an averaging of the admittances over the time period of the full data set.

Fig. 5 shows the coherence between the two data sets as a function of frequency. The coherence is simply the average of $C'(f)$ computed as above and then normalized by the average power in the time series at frequency f. Each block contained 64 measurements (128 hours). If $C'(f) = 1$ then the two series are perfectly coherent at that frequency, which means that there is a constant relationship between the two amplitudes and phases. A measurement of the amplitude and phase in one series can be used to construct a perfect prediction of the corresponding parameters in the other. Note that $C'(f) = 0.82$ at very low frequencies, so that most of the observed variance in the time difference data at low frequencies is due to temperature fluctuations and could be removed using the temperature observations. The rather surprising peak in the coherence at 1.25 c/day is not a resonance — it is due to the fact that the temperature spectrum itself has a peak in its power spectrum at that frequency, perhaps because of harmonics generated by the interaction of the underlying diurnal temperature cycle with the slower weekday/weekend cycle.

The admittance analysis shows that the effects of temperature are largest at periods of several hours and longer, and it is possible to remove these effects from the data by low–pass filtering the temperature data and then subtracting them from the time–difference measurements with a time shift of a few hours as indicated in the previous analysis. The coherence analysis is used to estimate the characteristics of the filter function and the scale factor that should be applied to the low–passed data.

Discussion

Each of the preceding analyses modeled the data differently. A two–sample Allan variance computation, for example, is most useful if the power spectrum of the variance in the data set can be approximated by a polynomial in frequency. The correlation analysis models the relationship using a constant time–delay independent of frequency, and is usually appropriate only if the data to be examined are band–limited signals with appreciable broad–band coherence. The frequency–domain analysis is the most general of the three approaches, but it may produce numerically unstable estimates without lots of averaging. In addition, the coherence estimates are not normally distributed if the "true" coherence is small — the estimates tend to be too large when the actual coherence is less than about 0.55. While all describe the same data set, the interpretations are quite different in each case.

A common assumption in all of the analyses is that the characteristics of the data set are time invariant, so that the entire series can be described by a single set of global parameters. These

methods will not be useful for modeling isolated transmission errors, for example, and problems of this type must be treated with some form of time–dependent analysis. Kalman techniques and moving–average models are well–known methods of detecting these problems, but all of these methods tend to require surprisingly large quantities of data to function reliably. Since there is no reliable means of predicting when a glitch will occur, the measurement interval is usually driven by how long a large glitch can be allowed to remain undetected rather than by the more usual statistical considerations derived from an Allan variance computation. This problem is more difficult than the choice between Type I and Type II errors in conventional statistical analyses because the magnitude of a channel error is not governed by a statistical distribution and is at least potentially unbounded.

Another situation that is difficult to model using the techniques we have described is a channel that has significant multi–path effects, such as a radio channel or a wide–area computer network. There is a lower bound but essentially no upper bound to the channel delay in both of these situations, so that it is not the mean but the minimum value of a group of measurements that is an invariant of the system and hence represents the "correct" delay. The mean is unbounded in principle, but it will always be too large even if some artificial bound is enforced. The channel delay can be estimated by comparing measurement data received via several independent routes, but it is often quite difficult to construct several independent channels to the same system since the local hardware tends to be common to all of these channels.

Application to a Steered Clock

Time–difference data are often used to steer a remote clock so that it is kept on time or on frequency with respect to some other system. Although the channel is "inside" this servo loop in principle, the loop gain does not attenuate offsets and phase shifts of the type we have been discussing. These offsets in the measurement channel are transmitted to the control system without attenuation. In addition, the control loop must be designed to minimize the effects of a channel failure.

Both of these problems tend to be more serious if frequency steering is used, since the measurement error or channel failure is converted to a control signal whose effect grows linearly with time. Although time steering does not have this problem, it introduces step–like discontinuities into the output of the steered device which complicate the analysis of its performance and degrade its spectral purity.

Our steered clocks are currently controlled using a combination of time and frequency steering. The frequency component of the steering is designed to control the long–term performance of the clock while the time corrections have a limited range and are only intended to compensate for the short–term fluctuations in the output. The steering system that realizes UTC(NIST), for example, is steered in this way. Using a measurement interval of 12 minutes, the average time correction that must be applied is 200 ps. The frequency steering is designed to realize UTC(NIST) in long term, so that if the system fails, the divergence of the output from UTC(NIST) is on the order of ns/day and is governed by the free–running stability of a cesium standard rather than by a frequency steering command that was intended to be applied for 12 minutes but in fact remained in force because the channel failed. The performance of this servo is nearly optimum in the sense that the short–term (< 2 hours) RMS deviation in the steered output is essentially the same as the

frequency noise in the cesium standard itself while the long–period performance is better than this and is limited by the performance of the AT1 time scale that is used as the reference for estimating UTC(NIST).

References

Julius S. Bendat and Allan G. Piersol, Measurement and Analysis of Random Data, New York, John Wiley and Sons, Inc., 1966, Chapter 9.

Alan V. Oppenheim and Ronald W. Schafer, Digital Signal Processing, Englewood Cliffs, New Jersey, Prentice–Hall, Inc., 1975, Chapter 11.

A. D. Whalen, Detection of Signals in Noise, New York, Academic Press, 1971, Chapter 9.

Fig. 1. Time Difference Between Two Channels

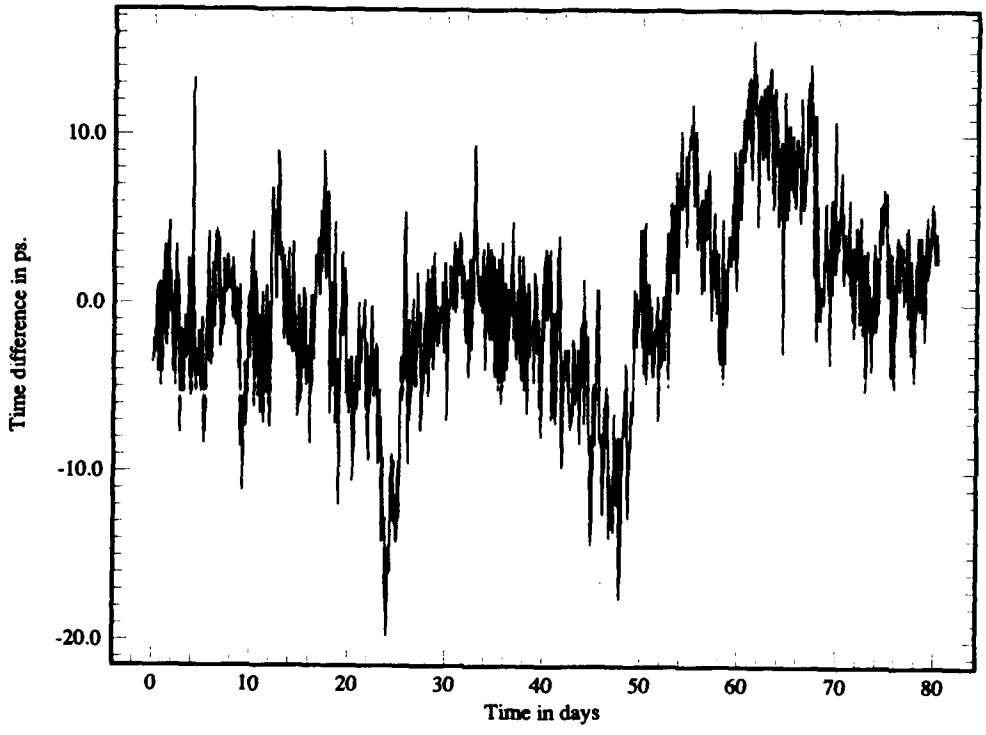

Fig. 2. Two-Sample Variance of Data in Fig. 1

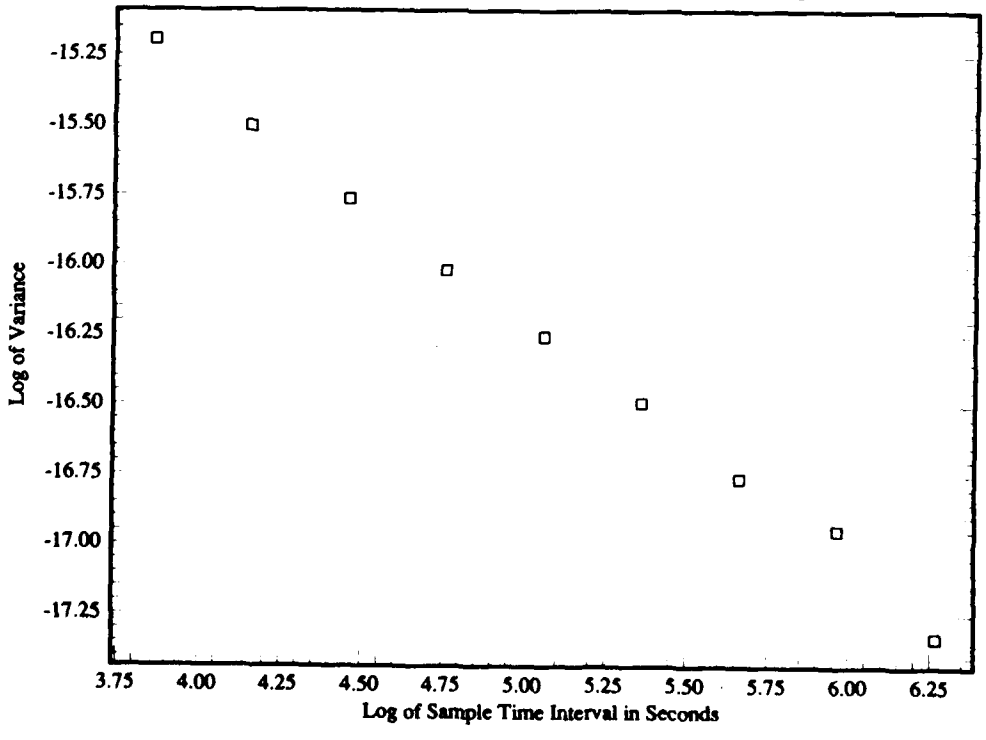

Fig. 3. Ambient Temperature

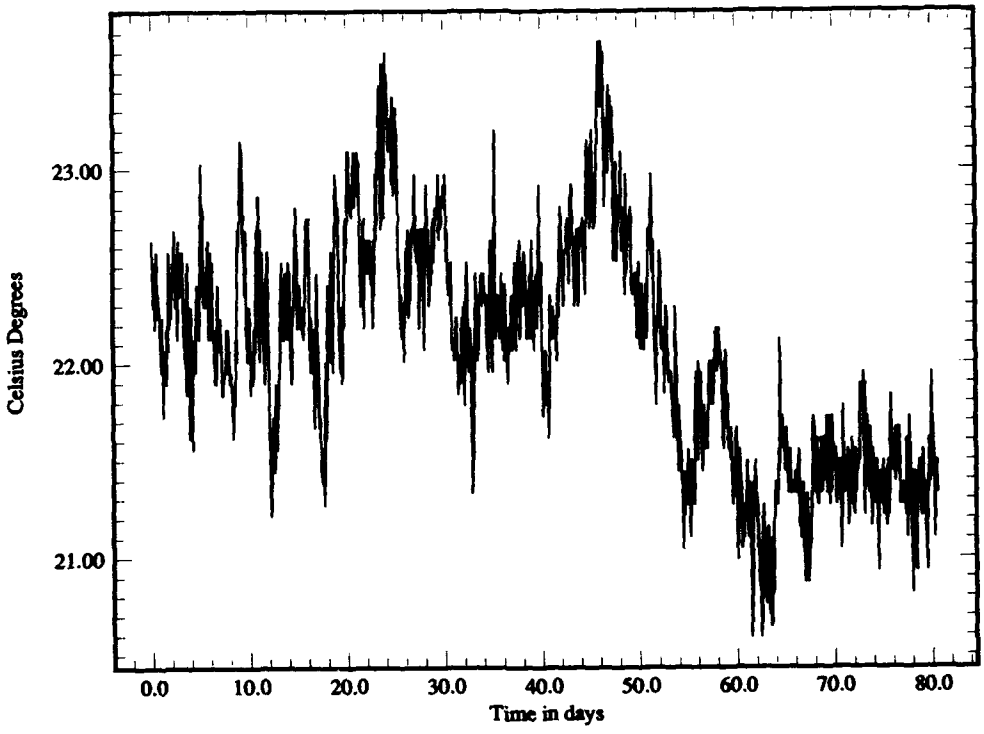

Fig. 4. Correlation as a Function of Lag

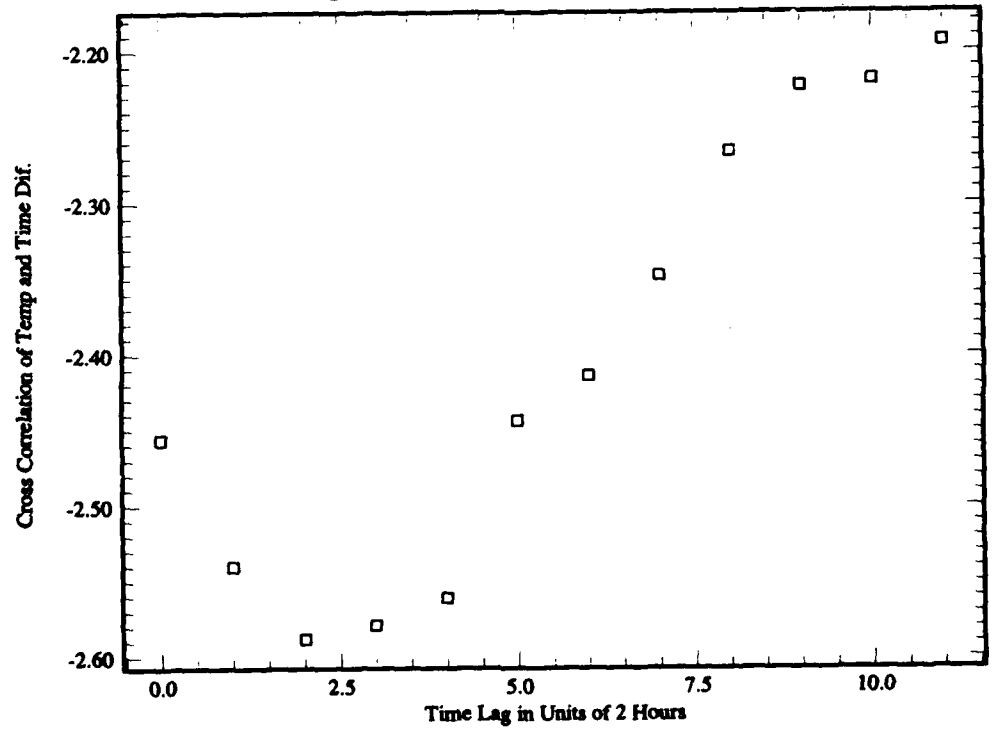

Fig. 5. Coherence as a Function of Frequency

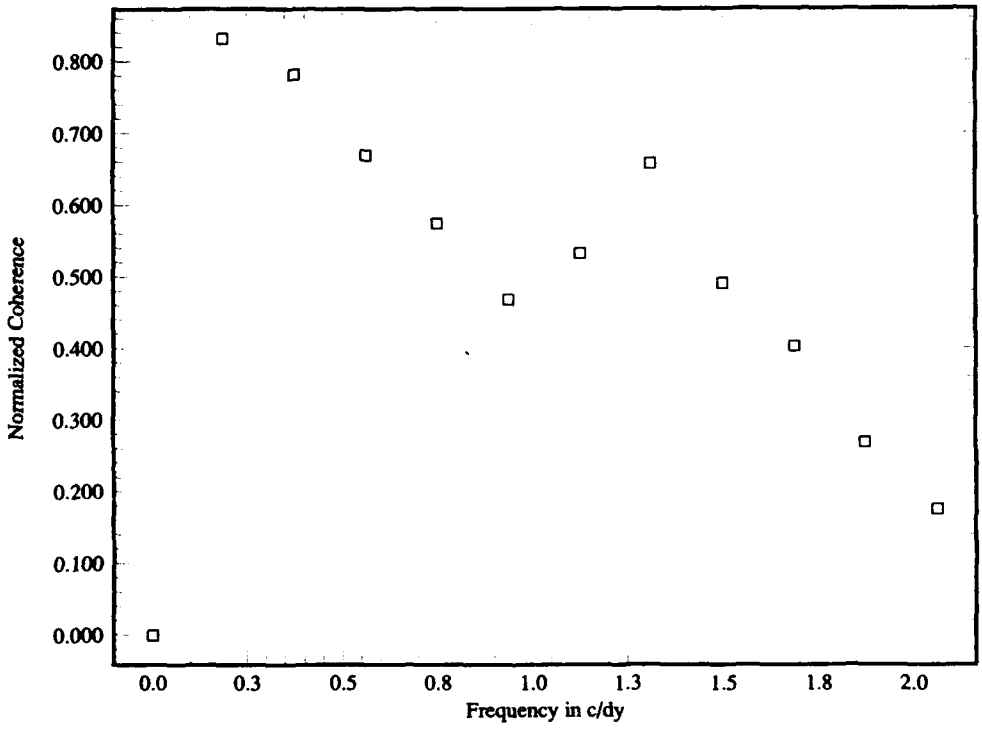

QUESTIONS AND ANSWERS

J. Barnes, Austron Incorporated: First a comment on using regression analysis on data that has low energy content and not looking at the residuals to finally tell you the residuals are not white which says the regression should not be believed anyway.

J. Levine, NIST: I agree but I am not sure what you ...

J. Barnes: Take two random walks that are independent of each other, they are most certainly highly correlated. The task of looking at the residuals that are white tells you they are a poor model.

J. Levine: In this case, I pass that test. I do not have the data but the temperature really does work. The residuals are really white.

J. Barnes: You maybe right, but I would be surprised if it were. It obviously has too much energy at the low frequencies.

J. Levine: Let us discuss this after this meeting.

C. Jacques, NRC, Canada: I am not sure if I understood very well your experience of steering the (?) network but I am a bit surprised by a meterology laboratory like NIST Time Division could steer clocks by a network on which they have no control.

J. Levine: Yes.

C. Jacques: So, what was the purpose of the experiment?

J. Levine: This is not what we intended to happen. Namely we did not know this when we started. This is what came out. This was a test of how well we could send packets and get them received. It was not a test of problems in the Internet. This is the NIST primary backbone; this is the real Internet or what we have. It has now been upgraded to (?) but at the time it was totally saturated but nobody knew it.

G. Zampetti, Telecom Solutions: The last result, the failure, so to speak! As I look at that data, if you change the scale to a different scale that is not quite tenth's of a second but the shape and the (?) characteristics looks exactly like data you would see coming out of a DS1 timing signal generically anywhere in the telecommunications network. So we talk about this real life scenario where things get overloaded, buffers are mismanaged, SONET is going to come down the pipe with pointers. All these erratic adjustments makes the channels truly a challenge. This is real life for some people.

J. Levine: I agree with you. Those are exactly SONET slips. They are the same as SONET slips – they come from the same thing. They are basically the same. There is a way of dealing with those slips but it is extremely complicated. It is an ad hoc kind of basis and basically in order to cope with a slip like that you have to have a better model of what your local clock is doing. So you have confidence that when you detect a slip that really was a slip. In fact we manage to get something out of that kind of data using that kind of model. I think the SONET problem has different aspects. I would suggest that a SONET problem can be approached a different way.

S. Stein: I would reiterate what George Zampetti just said that in fact it really did not matter in the first part of Judah's talk that he was talking about picoseconds and the last part about

seconds. The whole problem scales, the problems are so similiar; analysis techniques are really what is important here and it can be applied to your situation; whatever your problems are and whatever the level of performance of your system is.

Advances in Time-Scale Algorithms

S. R. Stein
Timing Solutions Corporation
1025 Rosewood Avenue, Suite 200
Boulder, CO 80304

Introduction

The term clock is usually used to refer to a device that counts a nearly periodic signal. A group of clocks, called an ensemble, is often used for time keeping in mission critical applications that cannot tolerate loss of time due to the failure of a single clock. The time generated by the ensemble of clocks is called a time scale. The question arises how to combine the times of the individual clocks to form the time scale. One might naively be tempted to suggest the expedient of averaging the times of the individual clocks, but a simple thought experiment demonstrates the inadequacy of this approach. Suppose a time scale is composed of two noiseless clocks having equal and opposite frequencies. The mean time scale has zero frequency. However, if either clock fails, the time-scale frequency immediately changes to the frequency of the remaining clock. This performance is generally unacceptable and simple mean time scales are not used.

This paper will first review previous time-scale developments and then present some new methods that result in enhanced performance. The historical perspective is based upon several time scales: The AT1 and TA time scales of the National Institute of Standards and Technology (NIST), the A.1(MEAN) time scale of the US Naval Observatory (USNO), the TAI time scale of the Bureau International des Poids et Measures (BIPM), and the KAS-1 time scale of the Naval Research Laboratory (NRL). The new methods have been incorporated in the KAS-2[1] time scale recently developed by Timing Solutions Corporation. The goal of this paper is to present time-scale concepts in a nonmathematical form with as few equations as possible. Many other papers and texts discuss the details of the optimal estimation techniques that may be used to implement these concepts.

Clock Models

The perfect integrator is widely used as the mathematical model representing a precision clock. The fundamental model describes the continuous states of the clock. The time (or phase) is the integral of the frequency and the frequency is the integral of the frequency aging. For

[1]KAS is a tradename of Timing Solutions Corporation

some clocks, the frequency aging state may be zero for all time and can be deleted from the model. Most often, the continuous model is integrated to form a discrete model that is an explicit function of the time between observations. Let us call the phase-time of the clock x, the dimensionless frequency of the clock y, and the frequency aging, w. Then we write the discrete deterministic model as follows:

$$x_i(t+\delta) = x_i(t) + \delta y_i(t) + \frac{\delta^2}{2} w_i(t) \quad (1a)$$

$$y_i(t+\delta) = y_i(t) + \delta w_i(t) \quad (1b)$$

$$w_i(t+\delta) = w_i(t) \quad (1c)$$

We will also use two special symbols: $\hat{x}_i(t|t)$ is the estimate of clock i based on all data through time t and $\hat{x}_i(t+\delta|t)$ is the forecast of clock i at $t+\delta$ based on all data through t. The perfect integrator deterministic model is not always used. Several investigators have used the ARIMA modelling technique to study clocks [1,2]. This approach may use the perfect integrator model, or it may use model identification techniques to fit a model to the observations.

There are several methods of including the effects of noise on the system. One way is to add a random shock on the right hand side of each line in Eq. 1. These shocks are assumed to be uncorrelated in time and cause each clock state to behave as a random walk. This type of noise model is most commonly used for both Kalman filtering and ARIMA modelling of precision clocks. An alternative noise model was used as the basis for A.1(USNO,MEAN). In this model the frequency is given by a series of steps plus white noise. The frequency steps occur at random times. Mixtures of the two approaches have also been used and there is not yet a definitive answer to the question of what is the optimal noise model for precision clocks.

Review of Prior Techniques

With only one exception, all the major time-scale algorithms use the same approach to combine the individual clock times into the time scale. The current estimates of the clock times with respect to the time scale are determined by the requirement that the weighted sum of the differences between the current time estimates and their predicted values is zero. The mathematical expression of this requirement is called the basic time-scale equation:

$$\sum_{i=1}^{N} a_i \hat{x}_i(t+\delta|t+\delta) = \sum_{i=1}^{N} a_i \hat{x}_i(t+\delta|t) \quad (2)$$

If optimal estimation techniques are used as the basis for prediction, the differences between the current estimates and the predictions form a white sequence and averaging is the appropriate method of combining the contributions from different clocks. Combining the residuals instead of the clock times themselves results in time continuity upon addition or deletion of clocks. The basic time-scale equation is also responsible for establishing the weights, a_i, that control the contribution of each clock to the time scale.

The only time-scale algorithm that doesn't use the basic time-scale equation is TA(NIST) and a similar algorithm called the Composite Clock. This algorithm defines state equations

that describe the time evolution of the states of the ensemble members including the effects of noise. Optimal statistical techniques are used to estimate the times of each constituent clock. However, the results are not good. In fact, the estimation problem of TA(NIST) is underdetermined. This situation results from the failure of the algorithm to implement the basic time-scale equation or some alternative and is not the result of the statistical estimation techniques (Kalman filter) that are employed. As a result, the effective weighting that controls how the clocks are combined is different from the intuitive weighting schemes used in the other algorithms and can't be controlled by the user. In addition, the time scale is hard to manage. Addition of new clocks is a particular problem. Another time scale called the Composite Clock is used to compute GPS time. It is based on the TA(NIST) approach and suffers from the same problems.

The question of how to form the forecasts needed by the basic time-scale equation has been ignored throughout the preceeding discussion. Unfortunately, the same question was not dealt with sufficiently carefully by any of the time-scale algorithms. Instead, ad hoc procedures have been used to estimate the clock frequencies used in predicting the future clock times. The ad hoc procedures limit time-scale performance. In particular, these algorithms do not solve the problem of how to form a time scale that has optimum performance for both long and short sampling times when some clocks have good short-term stability and others have good long-term stability. Recent developments, described in the New Techniques section, have eliminated this limitation.

New Techniques

The problem of determining the clock times and frequencies would be trivial if it were possible to make absolute time measurements of the clocks. However, it is only possible to measure the time differences between pairs of clocks. This situation may be described by saying that the states of the clocks are not observables of the system. One way to view the problem is as follows. Each clock is perturbed by two noise inputs at every observation. One random shock contributes to the evolution of the clock time and the other to the evolution of the clock frequency. Suppose that there are N clocks that have no noise on the frequency. Then there are N-1 clock time difference measurements. One cannot uniquely determine the N random shocks that perturb the time. However, when one uses the basic time-scale equation in addition to the N-1 measurements, there are N relations among N unknowns and one obtains a unique estimate for each random shock and therefore for the clock times themselves.

At first it might appear that, knowing the times, one may unambiguously calculate estimates of the clock frequencies. However, this is not the case when there are independent noises on both the time and the frequency states. The time difference measurements, together with the basic time-scale equation, suffice to determine the total noise input to each clock's time. However, that total noise input is composed of a direct contribution to the time and a contribution via the noisy frequency. There is insufficient measurement information to separate these two noise sources. Thus, with certain limitations, there is freedom in determining the clock frequencies. For example, one could require that all the frequencies are zero for all time and still be consistent with all the measurements. The problem is how to allocate the

noise between the time and the frequency states.

The allocation of the noise between time and frequency is partially accomplished by requiring that the model of each clock has the appropriate statistics. This requirement is sufficient, for example, to exclude the case of all clocks having constant frequency but is not sufficient to allocate the frequency noise on a detailed basis in such a way that the time scale has all the desired properties. If nothing further were done, the frequency noise would be allocated according to the weights used in the basic time-scale equation. Independent detailed allocation of the frequency noise is accomplished by adding a supplemental time-scale equation that also guarantees that the time-scale frequency is continuous when clocks are added to or dropped from the time scale. By analogy with the clock times, one requires that the weighted sum of the differences between the current frequency estimates and their predicted values is zero. The same technique must be extended to the frequency aging state if it is nonzero. The supplemental time-scale equations are written:

$$\sum_{i=1}^{N} b_i \hat{y}_i(t+\delta|t+\delta) = \sum_{i=1}^{N} b_i \hat{y}_i(t+\delta|t) \quad (3)$$

$$\sum_{i=1}^{N} c_i \hat{w}_i(t+\delta|t+\delta) = \sum_{i=1}^{N} c_i \hat{w}_i(t+\delta|t) \quad (4)$$

The basic time-scale equation and the supplemental time-scale equations have been incorporated in the KAS-2 time-scale algorithm developed by Timing Solutions Corporation. Using this approach, each clock's contribution to the time-scale is determined by a set of weights, one for each state that is perturbed by noise. There are always at least two weights per clock. As a result KAS-2 may be independently optimized in both the short term and the long term. It can therefore utilize clocks with very different frequency stability without degrading the stability of the time scale. U. S. Patent 5,155,695 has been issued covering time scale systems utilizing the supplemental time-scale equations. Other patent applications are pending.

Implementation

There are two basic approaches to time-scale algorithms — real time *v.s.* after the fact. Real-time algorithms are required for applications that need a physical signal derived from the time-scale. This is true, for example, if the time-scale is used to provide stable and fault tolerant time and frequency for a communications network. Other applications are amenable to post processing of the data. In this case it is possible, in principle, to compute time-scale estimates with smaller mean-squared errors since more data are available. TA(NIST), A.1(MEAN,USNO), and ALGOS(BIPM) are computed after the fact. They do not use smoothing techniques but they do use both subjective and objective techniques to detect "unhealthy" clocks and modify the ensemble membership before performing the final time-scale estimates. KAS-1(NRL), KAS-2(TSC), and AT1(NIST) all produce estimates in real time. Other experimental algorithms utilize smoothing techniques to attempt to improve their estimates compared to a real-time filter.

Optimal State Estimation

The deterministic clock model, the noise model, the basic and supplemental time-scale equations, and the observations are sufficient to calculate the time scale. Since the problem is stochastic in nature, the solution is not unique. However, there are several methods for calculating minimum squared-error estimates of the clock states. Among these are: least squares estimation, Bayesian estimation, maximum likelihood estimation, Kalman filtering, and Wiener filtering. All these techniques are equally good in the sense that they minimize the mean square estimation error as long as the assumptions are the same in each case [3].

Robust Statistics

Inevitably, the data presented to the time-scale algorithm will be deviant in some way. Perhaps one of the clocks changes characteristics dramatically due to an internal failure or perhaps the observations are corrupted during a data transfer. It is desirable for the time scale to be robust under these conditions. By this we mean that deviant behavior in a small number of observations does not unduly influence the performance of the time scale [4].

Robustness is ensured by a two step process. First we generate an estimate of the expected observations and then we act to reduce the effect of any observation that is far from our expectation. Both parts of the process must be robust. Consider the problem of detecting outliers in a set of measurements of a constant such as the length of a rod. One might think to compare each measurement with the mean of the set. However, when one measurement is bad, the mean may differ arbitrarily from its expectation value making the deviation from the mean an undesirable measure of deviant behavior. The median is much more robust.

The most common method of dealing with outliers is to reject observations that appear deviant. But this procedure leads to a discontinuity in the estimation procedure where small changes in an observation can produce significant changes in the resulting estimate. This discontinuity can produce transients and even instability and should be avoided. Continuity is ensured by continuously deweighting observations over a range of values.

Finally, it is sometimes argued that if one has a wealth of data, it is desirable to discard large amounts of good data to enhance the probability of rejecting the bad data. This must not be done if the residuals from the estimation process are used to determine the noise of the clocks. If good data are discarded under these circumstances, the clock noise will inevitably be underestimated.

Parameter Estimation

The function of time-scale algorithms is to allocate the observed clock noise among the contributing clocks. This can only be done if the parameters of the clock models of each clock are accurately known. These parameters are the spectral densities of each of the noise sources that perturb the clock and any of the commonly used techniques for estimating the noise of clocks may be applied. For example, one may characterize the Allan variance of clock pairs and use the three corner hat technique to separate the variances. The principal drawback of this approach is that Allan Variance estimation requires uniformly sampled data.

The Maximum Likelihood method [5] is a more sophisticated approach. It relies on the fact that the likelihood function computed from the residuals of the time-scale estimation process is maximized when the correct parameters are used. The model itself can also be checked for validity by this method since the correct model used with the correct parameters results in Gaussian white residuals. Standard statistical techniques can be used to analyze the residuals for whiteness. The principal drawbacks of the maximum likelihood method are that it requires storing large amounts of historical data and substantial processing time.

Other techniques have been developed for real-time algorithms that are incompatible with storing and processing large amounts of historical data. For example, AT1(NIST) uses the one step ahead prediction error as its sole measure of clock noise. The value is updated recursively in an exponential filter after each cycle of time-scale computation. An extension of this technique is the analysis of the one step ahead prediction error as a function of the prediction interval [6]. Since different noise sources dominate the time prediction error as the interval varies, it is possible to estimate all the important noise spectral densities of each clock.

Performance of the KAS-2 Time-Scale Algorithm

The best way to evaluate the performance of a time-scale algorithm is to simulate the clocks in the ensemble since simulation makes it possible to know the true times of the clocks. There are several appropriate simulation techniques [6,7]. The method developed by this author has been used to test KAS-2. However, simulation testing should be supplemented with tests using actual clock data. The comparison of several different time scale algorithms on real clock data provides the ultimate reassurance that something important has not been overlooked.

Figure 1 shows the simulated performance of KAS-2 with an eight clock ensemble composed of four clocks with good short-term stability and poor long-term stability and four additional clocks with poor short-term stability and good long-term stability. The resulting time scale is better than the best clocks everywhere.

Figure 2 compares the times of three independent time scales computed from the measurements of the clock ensemble at the National Institute of Standards and Technology using data supplied by NIST. The test period was the first 10 months of 1992. The AT1(NIST) time scale was computed in real time while TA(NIST) was computed after the fact using the information generated by AT1 to adjust the ensemble. KAS-2(TSC) was run on the historical data as if it were running in real time. It used the same estimates for the clock noises that were used in TA(NIST). All three scales were adjusted so that they had the same rate as TAI at the beginning of the year. In addition, an intentional frequency steer of 3.98 ns/day in AT1(NIST) was removed in order to compare the free time scales. One should not jump to conclusions since there is only one year of comparative data, but the results certainly support the theoretical claims of the advantages resulting from the implementation of the supplemental time scale equations.

Figure 3 illustrates the performance of a Cs clock at the Naval Research Laboratory that was steered in real time to the KAS-2 time scale. The time scale was computed every 5 minutes and approximately one-tenth of the estimated phase error was removed each sample

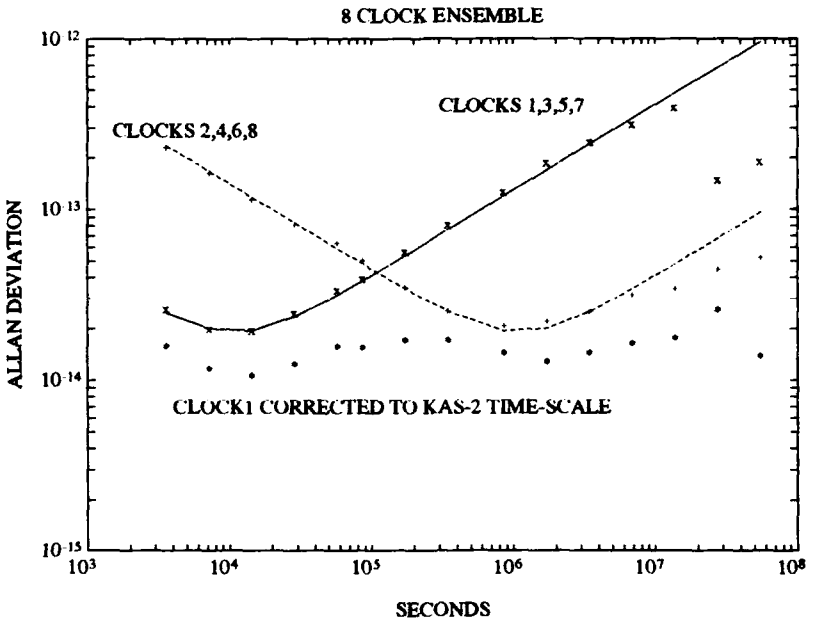

Figure 1: The simulated frequency stability of a time scale composed of four clocks with good short-term stability and four clocks with good long-term stability.

by a second order phase-lock loop. As a result, the frequency stability of the Cs standard equals its free running value for times shorter than three thousand seconds (10 sample intervals). At longer times, the frequency stability improves until it reaches the performance of the KAS-2 time scale.

Comparison of Time-Scale Algorithms

Table 1 summarizes the features of the time-scale algorithms discussed in this paper. Some of the more important differences and similarities will be discussed in more detail here.

All the algorithms except for TA(NIST) and the similar GPS Composite Clock implement the basic time-scale equation. Neither do these two algorithms implement a suitable alternative. As a result, they both perform worse than the others. First of all, they do not provide user control of the weights that determine the clock contributions to the time scale. Second, they have difficulties when clocks enter or leave the ensemble. Finally, they are likely to be unstable when adaptive filtering is used.

The algorithms that implement the basic time-scale equation fall into two categories. TAI(BIPM) and A.1(USNO,MEAN) are computed after the fact. In practice, human judgement supported by objective statistical analysis is used to filter the input data in an attempt to improve the time-scale performance. AT1(NIST), KAS-1(NRL), and KAS-2(TSC) are real-time time scales. In principle, after the fact time scales are capable of performing bet-

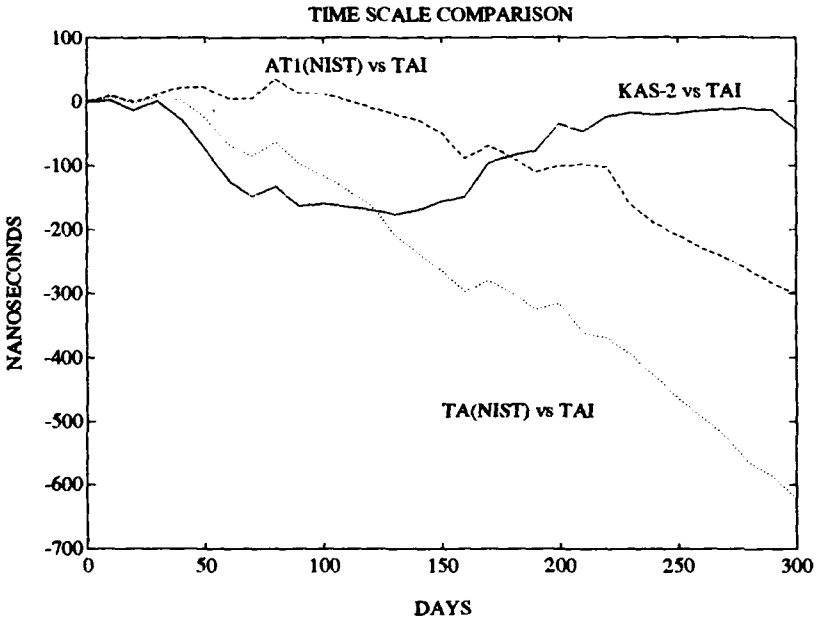

Figure 2: The times of KAS-2, AT1(NIST), and TA(NIST) *v.s.* International Atomic Time (TAI) for the first 10 months of 1992.

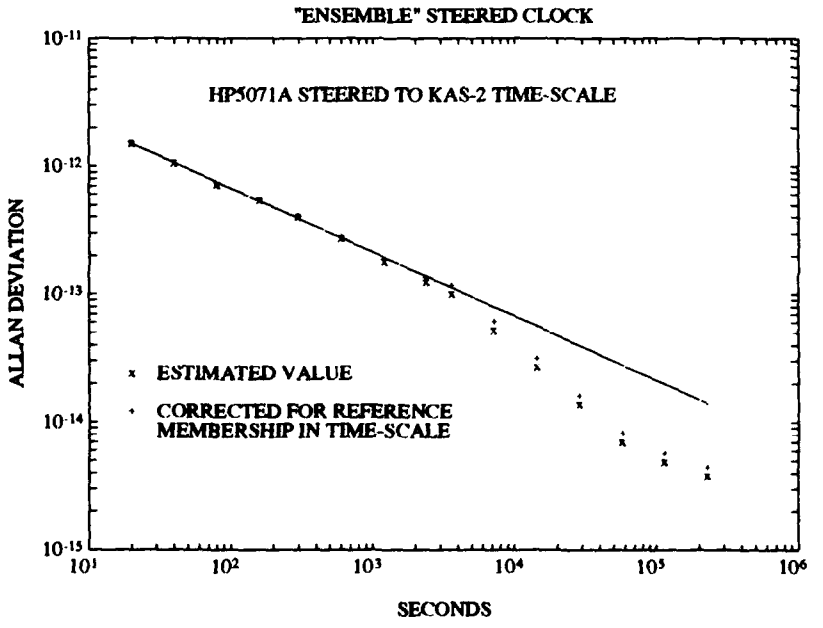

Figure 3: Stability improvement of a cesium clock steered to the KAS-2 time scale.

Table 1: Comparison of time-scale algorithms

	USNO A.1	BIPM ALGOS	NRL KAS-1	TSC KAS-2	NIST AT1	NIST TA
deterministic clock model is an integrator	√	√	√	√	√	√
uses explicit noise model	√		√	√		√
uses basic time-scale equation for the time state	√	√	√	√	√	
uses supplemental time-scale equation for the frequency state				√		
uses supplemental time-scale equation for the frequency aging				√		
protects against outliers	√	√	√	√	√	√
uses robust statistics			√	√		
accounts for measurement noise			√	√		√
estimates true clock performance				√		√
estimates weighted time-scale		√	√	√	√	
uses separate weights to optimize short, medium, long-term stability				√		
accepts frequency measurements				√		
solves an observable problem	√	√	√	√	√	
accepts aperiodic data				√		√
time-scale available in real-time			√	√	√	
available commercially				√		

ter than their real-time counterparts because they have available more information. However, real-time time scales are necessary whenever the time scale is used to control physical clocks or for synchronization. Each approach has its advantages and should be used in the appropriate circumstances.

Many of these time scales differ in their implementation of robust statistics. The after the fact scales typically use rejection rule techniques to exclude bad clocks entirely. Use of rejection rules in real-time algorithms is inappropriate since the discontinuity of the rejection rule introduces a potential instability that can result in rejection of all the clocks in the ensemble and require human intervention to restart the time scale. AT1(NIST) has suffered from this problem. KAS-1(NRL) and KAS-2(TSC) eliminate this discontinuity by implementing Percival's outlier deweighting method. Large outliers are still rejected, but there is a continuous transition between full acceptance and full rejection of data.

Different clock models are used in the time scales discussed in this paper. The USNO A.1

time scale models the frequency noise as a series of discrete steps of random amplitude and time of occurrence. The other time scales model the frequency noise as either a continuous or a discrete random walk process. An advantage of the random walk model is the existence of straightforward filtering and smoothing techniques that can provide objective estimates that are optimum in the minimum squared-error sense. Several state estimation techniques have been used in these time scales. However, regardless of the state estimation method, the update equation used for the states is always an exponential filter. Thus, the only issue is the proper selection of the filter time constant. Despite the simple description of this problem, the solution is quite difficult except in special situations such as an ensemble consisting of several identical clocks. TAI(BIPM) and AT1(NIST) utilize restricted operating conditions and approximate formulas for the required filter lengths. The approach works well as long as the restrictions are not violated. TA(NIST), KAS-1(NRL), and KAS-2(TSC) utilize the Kalman filter approach. This guarantees that the filter lengths are correctly determined as long as the clocks fit the models and the parameters are correctly estimated. However, TA(NIST) and the GPS Composite Clock are often intentionally mismanaged by changing the parameters of the clocks since they do not have explicit user controlled weights.

Acknowledgements

The author wishes to thank the Naval Research Laboratory for prior support. Several people made large contributions to the testing and evaluation of the KAS-2 algorithm. G. A. Gifford at the Naval Research Laboratory tested the UNIX version and J. Levine at the National Institute of Standards and Technology tested the VAX VMS version. Their feedback was invaluable.

References

[1] G. E. P. Box and G. M. Jenkins. *Time Series Analysis: Forecasting and Control, revised ed.* Holden-Day, San Francisco, 1976.

[2] Donald B. Percival. The U. S. Naval Observatory clock time scales. *IEEE Trans. Instr. and Meas.*, IM-27:376–385, December 1978.

[3] Arthur Gelb, editor. *Applied Optimal Estimation.* The M. I. T. Press, Cambridge, 1974.

[4] Donald B. Percival. Use of robust statistical techniques in time scale formation. *Second Symposium on Atomic Time Scale Algorithms*, June 1982.

[5] Peter V. Tryon and Richard H. Jones. Estimation of parameters in models for cesium beam atomic clocks. *NBS Journal of Research*, 80:3–16, January / February 1983.

[6] L. A. Breakiron, G. A. Gifford, and S. R. Stein. Report on the timescale algorithm testbed at USNO. *Proc. 21st Annual PTTI Applications and Planning Meeting*, 269-287, December 1989.

[7] James A. Barnes. Simulation of oscillator noise. *Proc. 38th Annual Frequency Control Symposium*, 319–326, 1984.

QUESTIONS AND ANSWERS

Question: M. J. Van Melle, Rockwell International: I was interested in the table you had on comparison of time scale algorithms and also your CAS1 which was on your last chart. I am also working at (??) and you know the Air Force has partitioned all the GPS's into different partitions or ensembles. Up to six they can handle and now down to five and they have three partitions. But they can only work if they have the Cesium clocks in there. Once they put a Rubidium in there, it doesn not work. I was wondering if you could explain why that is the case.

Question: S. Stein: I really did not pay you enough for that question. The composite clock algorithm that IBM did is esssentially the same as the NIST TA algorithm. It has some differences in the way they treat the renormalization of the covariance matrix to get around this problem of the covariance matrix blowing up, but fundamentally the problem with that type of algorithm is it implements the clock model – perfect integrator clock model - and it estimates the time of the clock based on the measurements, but it does not implement the basic time equation. The solution is not constrained to be the waited average of the times of the clocks based on user selectable weights. Thats the fundamental reason for the what I would call instabilities you will see in the state predictions of algorithms of that type. So I think is what happens is you have both additional burden operationally on the Air Force personnel at the Master Control Station and try to maintain the algorithm and you have limitations on not being able to include different types of clocks with different characteristics. The algorithm only works on a limited set of circumstances. I do not know what to do about that except to fix that algorithm so indeed the basic time scale equation is incorporated.

Question: Richard Keating (USNO): Have you ever studied the sensitivity of the basic time scale equation as you call it to round off and loss of significance. Some remarkably disparate numbers in the sense of very large numbers and very small numbers play a role when you start averaging. I was wondering if you ever made a study of that or if you know anybody who has.

Answer: S. Stein: I have done to date approximately two hundred seventy simulations studies of the performance of these algorithms. The problem you raise is possibly the most difficult problem of all in the computation of system time. I am not sure I can remember the exact figures but the asymetry in the covariance matrix occurs depending on the number of clocks and the difference in the performance of the clocks in the eighth or tenth digit while computing in double precision. Once one cycle through the recursion costs you eight digits of precision. Yes, this is a terrible problem because the fundamental approach to generating the gains, the filter time constants, is differencing large numbers against small numbers. You can treat that problem, for instance one of the ways of treating that problem and Kalman Filter methods is to go ahead and resymmetrize the covariance matrix each time. You also must treat the problem in special cases. For example we provide the facility for the user to carry along clocks which we call not members of the ensemble. That means that the clock is defined as not effecting the time scale computation, no matter how large a deviation it makes. It can move one second and shall not move the ensemble one nanosecond. There is simply not enough computational accuracy to do that, so what we do is we go in and we fix the Kalman gains directly to cope with that situation. You always have to do some special things, there are some special things we do, and that is one of them. Fortunately the statistical analysis that has been done for much more important applications than this for navigating spacecraft and flying airplanes, have dealt with all of these problems and you can use a more sophisticated version of a standard Kalman Filter that allows you to go in and change the gains and still correctly compute the recursion, and to correctly take into account the ad hoc changes you

have made in the gains. We do that.

Manuel Aparicio (ITT): I have two questions. The first one is if you have a non-evenly spaced sample for the Kalman Filter that you are using, you mention that you will have some problems. What type of problems are they? The second one is if your estimates of the noise processes in the Kalman Filter are not absolutely correct for one of the members of the ensemble, what kind of effects will you see?

S. Stein: The first is a potential problem. Box Jenkins or ARIMA modeling requires evenly spaced data. The typical way around that is if you are missing data you interopolate it. It biases your results. We use the approach that was done by Dick Jones and (Petrian?) for the TA algorithm and that is we use a noise model which is the integration of continuous white noise and so the Kalman Filter runs optimally for any spacing of data, therefore you do not need equally spaced data. Your second question. The effect of inaccuracies in the estimates of the parameters. Of course you never know the parameters – you only estimate them. The values of the spectral densities of clocks determine the filter time constants. The bottom line, forget everything else, the reason is why ad hoc algorithms work is that all of these techniques result in simple exponential filters for estimating the states. The actual filter that performs the state estimates is an exponential filter. Incorrect parameter estimate results in having a slightly non optimun filter link. The worst your estimate of the parameter, the more non optimun it is. That is it's effect and so it is upsetting, but not tragic. It is serious, but not catastrophic.

P. Tavella (IEN, Italy): You spoke of the possibilities of using different states to optimize the things, maybe short, medium and long term stability. In the definition, you describe but do you use different equations with different ways, and it seems to me that in this way you define two or three different in different time scales. How can you obtain a unit time scale - do you make a sort of frequency lock of one on the other.

S. Stein: No! They are not different scales. All three equations can be satisfied simultaneously. It is as simple as that.

P. Tavella: That if you solve the three equation, you will obtain the redefined ensemble time scale.

S. Stein: No! Remember you have a weighted average of the phases of the clock that is constrained. You have a weighted average of the frequencies that are constrained and you have a weighted average of the frequency aging that are constrained and they may all be constrained and achieve a single solution. Each of the states is independently perturbed. So we have one solution and there is no funny steering to combine them.

P. Tavella: In the equation for phase continuity in the prediction of the phase that you also put frequency and (?) or also phase.

S. Stein: You use the frequency in there to make the forecast. In the basic time scale equation we say the weighted average of the time of the clock with respect to the time scale is equal to the weighted average of the forecasts. That is the equation you wrote in your paper two years ago. It is the same except that I use "a" and you use "p". The forecast depends on the frequency estimate. The forecast is the old phase estimate, plus the old frequency estimate, times the interval delta, plus one half delta squared, times the old frequency aging estimate. We constrain independently now the current frequency estimate to be the weighted average of the frequency forecast. This equation and the basic equation are all required simultaneously - the same solution. I have lots of degrees of freedom.

R. Clark (USNO): When you have subgroups of clocks that are exposed to environmental

effects and that type. There is a correlation between groups of clocks. How is this treated and is that looked for and sometimes that is just entirely not obvious - things like preventive maintenance that is done on the first of the month or third Tuesday of the month with clocks that are not even in the same area.

S. Stein: I think the answer to that question is at the present time nobody has a tentative process for that kind of information. We do not.

Time Signal Distribution in Communication Networks Based on Synchronous Digital Hierarchy

Atsushi Imaoka and Masami Kihara
NTT Transmission Systems Laboratories
1-2356 Take, Yokosuka, Kanagawa 238-03, Japan

Abstract

A new method that uses round-trip paths to accurately measure transmission delay for time synchronization is proposed. The performance of the method in Synchronous Digital Hierarchy networks is discussed. The feature of this method is that it separately measures the initial round-trip path delay and the variations in round-trip path delay. The delay generated in SDH equipment is determined by measuring the initial round-trip path delay. In an experiment with actual SDH equipment, the error of initial delay measurement was suppressed to 30ns.

1. INTRODUCTION

Timing (frequency) signals are currently distributed in digital telecommunication networks as the reference clocks needed by digital switching and multiplexing equipment. The phase stability of the reference clocks must be better than 10μs [1]. The existing NTT (Nippon Telegraph and Telephone corporation) network has over 2000 offices that must receive timing signals. As the number of synchronous offices increases, precise timing signal distribution (phase or time distribution) without excessive delay variation is demanded for ensuring reference clock phase stability. Accurate time signal distribution is also useful for many applications such as time management in network operation systems and time stamping in distributed computer networks [2].

The Synchronous Digital Hierarchy (SDH) has been standardized by the International Telegraph and Telephone Consultative Committee (CCITT) [3] and is the basis of many existing communication networks. Timing signals for frequency synchronization are conventionally carried by 1.544Mbit/s or 6.312Mbit/s signals which are multiplexed into the digital traffic signals. In SDH systems, the frequencies derived from SDH line signals, such as 155Mbit/s, 622Mbit/s and 2.488Gbit/s, are currently being used as the reference signals for frequency synchronization.

This paper reports a time distribution method that uses the Virtual Container (VC) signals multiplexed into the SDH line signals, as the time reference signals. Time synchronous networks can be constructed flexibly to cover a wide area if VC signals are used to replace SDH line signals as the time reference signals. The delay imposed on VC signals by SDH equipment, however, varies much more widely than the waiting time jitter [4] generated in asynchronous digital networks. Precise time synchronization is only possible if the equipment delay and its variation can be accurately measured. A new method to measure VC signal transmission delay accurately is proposed in this paper. The performance of the proposed method is presented together with experimental results.

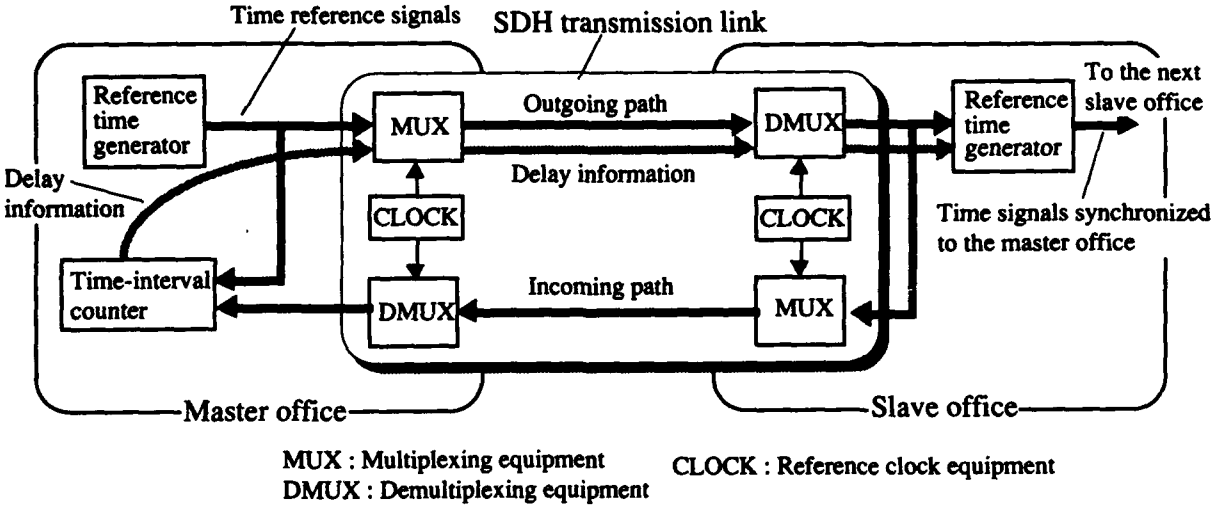

Fig. 1 Basic principle of time synchronization in SDH networks.

2. TIME SYNCHRONIZATION IN SDH NETWORKS

2.1 Basic principle of time synchronization

Figure 1 shows the basic principle of time synchronization in SDH networks. The reference time generator in a slave office is synchronized to the original time generator in the master office. The master and slave offices are connected by an SDH digital terrestrial transmission link. The outgoing path delay is estimated to be one half of the round-trip path delay as measured by the master office. The round trip delay is measured continuously and the current delay information is sent to the slave office. The time signals output by the slave office are advanced by the received delay information. Time synchronization radiates outwards from the master office to all slave offices. To achieve this effect, a synchronized slave office acts as a master office to its designated neighbors. Because the delay information is updated continuously, the accuracy of time synchronization is limited by the delay difference between outgoing and incoming paths in the round-trip path. This problem is discussed in section 3.

2.2 Time signal transfer in SDH networks

In SDH networks, transferred signals are multiplexed into higher bit rate line signals which are multiples of 155Mbit/s, such as 622Mbit/s and 2.488Gbit/s. SDH line signals have a frame structure termed the Synchronous Transport Module (STM) which repeats every 125μs as shown in Fig. 2. The STM frame is a structure of 9 rows by 270 byte columns in the case of 155Mbit/s STM signals. Each STM frame consists of an information payload and overhead. The information payload includes the data signals being transferred. The overhead includes block framing information and information for maintenance, monitoring, and other operational functions. Transferred signals are structured as Virtual Containers (VCs) which also repeat every 125μs. VC signals are carried only within the STM information payload and are not carried in the overhead. The pointer included in the overhead locates the start of the VC signal within each STM frame. Because they employ pointers, STM signals can flexibly carry either synchronous or asynchronous signals.

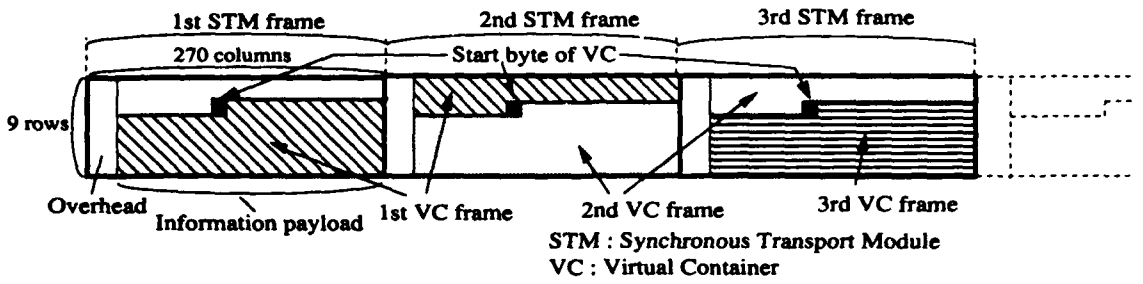

Fig. 2 Frame structure of SDH signals. Each frame has a 125μs period. The start byte of VC is indicated by the pointer included in the overhead. The phase of the VC frame is independent of the STM frame phase.

In each office, the reference clock synchronizes the SDH node, such as multiplexing and demultiplexing equipment. Reference clock in this paper means reference timing (frequency). The SDH equipment must be accurately synchronized to handle STM signals. The STM signals are synchronized to the reference clock. When an STM signal is received by an SDH node, the phase of the STM signal is terminated. The phase is not passed through the SDH equipment but is regenerated by the equipment.

VC signals "float" within the STM information payload. "Float" means that the start of the VC signal is independent of the STM frame phase as shown in Fig. 2. Because the start of the VC signal does not correspond to the start of STM information payload, the VC signal extends over two STM payloads. When a VC signal embedded in an STM signal passes through a node, the phase of the VC signal is also passed through. Thus, VC signals are more suitable to carry time reference signals than STM signals. Time synchronous networks using VC signals as time reference signals can be constructed flexibly over a wide area. This paper reports a time distribution method that uses the VC signals as time reference signals.

3. ERROR FACTORS IN DELAY MEASUREMENT

3.1 Asymmetry of transmission lines

The accuracy of measuring the round-trip delay is limited by the delay difference between outgoing and incoming paths. This delay difference is caused by delay dispersion in the SDH equipment, asymmetry of transmission line length, and the difference in delay variation of the transmission lines. We assume that two optical fibers within the same transmission cable are used as outgoing and incoming lines. Fibers included in a single cable have the same length and are set in the same environment. Thus, differences in transmission line length and delay variations are small.

Asymmetry of line length depends on the number of fiber fusion splices, in-line connectors, and equipment connections. The typical delay difference is reported to be 100ns between two SDH nodes [5]. The delay of a transmission line mainly varies with temperature. The delay variation characteristics of two fibers are very similar if they are part of the same cable. For an installed optical fiber cable 2000 km in length, the difference in delay variation between outgoing and incoming lines is reported to be below 10ns [6].

3.2 Delay dispersion in the SDH equipment

When an STM signal that is carrying a VC signal traverses an SDH node, the VC signal is embedded in a new STM signal and a new pointer must be generated to indicate the start of the VC signal. The new STM signal is synchronized to the node's reference clock. The SDH equipment delay equals the time difference between the VC signal embedded in the original STM signal and that embedded in the STM signal output from the node as shown in Fig. 3. The STM signal pointers locate the start of the VC signal to the nearest byte unit equivalent to 52Mbit/s. Hence, the use of the pointer can cause a delay difference of up to 150ns, or eight unit intervals for 52Mbit/s signals.

Figure 3 (a) and (b) show how the equipment delay of a VC signal can vary widely. When the data signals in the original payload are embedded in a payload of the new STM frame, the data in region A is little delayed, as shown in Fig. 3. The data in region B, however, is delayed by about 3 to 4 bytes (52Mbit/s) because the overhead cannot carry the data signals. Figure 3 (a) shows the delay of the VC signal when the start of the VC signal is located in region A. In this case, VC signals are delayed no more than one byte (52Mbit/s). Figure 3 (b) shows the case when the start of the VC signal is located in region B. In the case of Fig. 3 (b), the VC signal is delayed by about 3 to 4 bytes. The source of this equipment delay is the signal buffer for pointer operation. The buffer capacity is about 8 bytes (52Mbit/s), hence the maximum delay variance is about 1.2μs per node. It is necessary to measure this equipment delay accurately if we are to use VC signals as time reference signals.

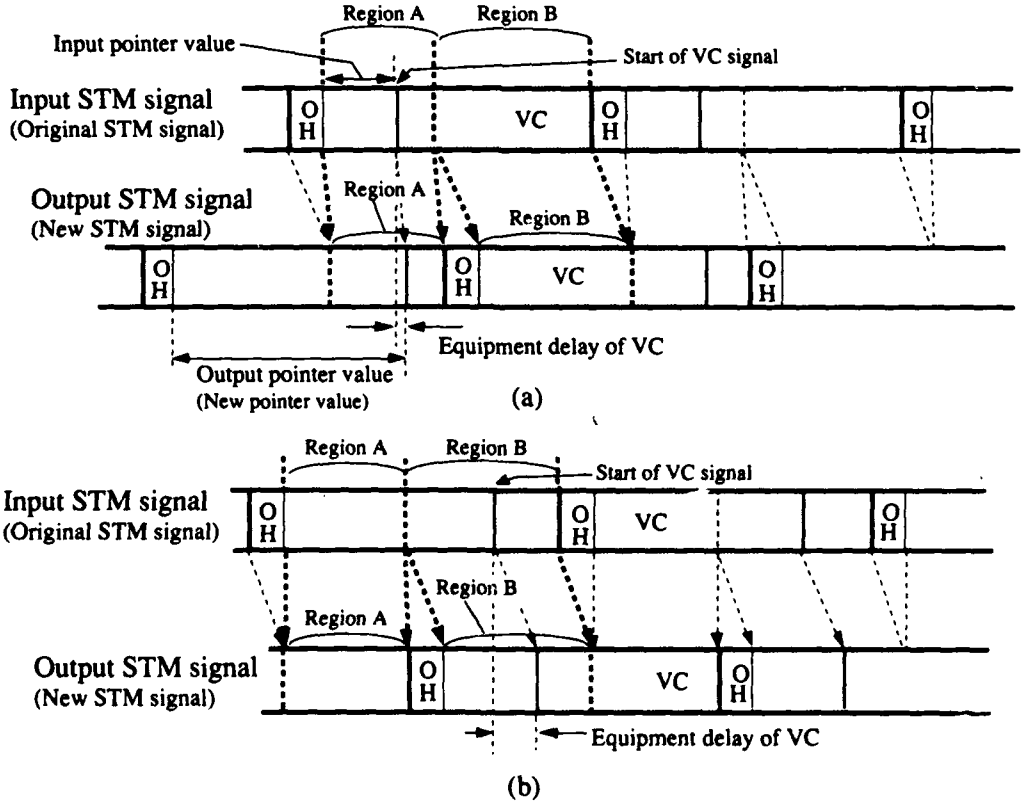

Fig. 3 Equipment delay of VC signals. Output STM signals are synchronized to the node's reference clock.

4. ACCURATE DELAY MEASUREMENT METHOD

4.1 Basic configuration

This section proposes an accurate delay measurement method using round-trip paths. Figure 4 shows the basic configuration of the proposed method. We consider here the measurement of the transmission delay between office A and office B. The feature of this method is that it measures the initial round-trip path delay and the round-trip path delay variations separately. In this method, VC signals embedded in STM signals are used to carry the reference time signals and to measure the initial round-trip path delay. The clock signals derived from STM line signals are used to measure the delay variations. The delay variations are measured after determining the initial delay. We assume that the reference clock in office B is usually synchronized to the frequency derived from the line signals output by office A in Fig. 4

4.2 Initial delay measurement

Before measuring the initial round-trip delay, three operations are performed to determine multiplexing and demultiplexing equipment delay accurately. Each step controls the phase difference between input signals to the equipment and the reference clock of the equipment. The phase of the input signal is delayed to minimize the equipment delay by ensuring that the signal buffer for pointer operation is empty. After determining the equipment delay, the phase of the input signal is fixed to the reference clock phase.

In the first step, B's reference clock is controlled to equalize the demultiplexing delays of office A and B. In this operation, the phase of B's reference clock is continuously advanced at a constant rate. Then, the B's reference clock is fixed when the demultiplexing delays of office A and B are equalized. The second step is to delay the phase of the reference clock of the signal generator at a constant rate. After a short time, the signal buffer for pointer operation of A's multiplexing equipment is emptied. The reference clock is then fixed when

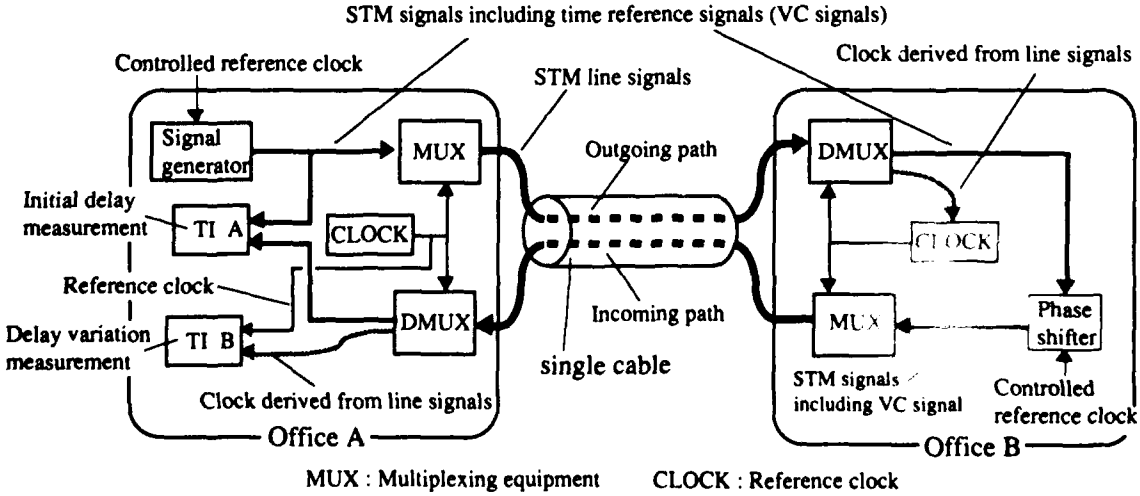

Fig. 4 Basic configuration of the proposed method.

the delay of A's multiplexing equipment is minimized. In the third step, the phase of the time reference signals received by the multiplexing equipment in office B is controlled by the phase shifter to minimize the delay of the multiplexing equipment in office B.

These steps are performed in such a short time that we can assume that the phase difference between the reference clocks in office A and B is stable. After the three phase control steps, the initial round-trip delay can be accurately measured. Accuracy of this measurement is confirmed in section 5 with experimental results.

4.3 Delay variation measurement

Delay variations of the round-trip path are measured by comparing the phase of the reference clock in office A and the frequency derived from incoming STM line signals. The reference clock in office B is synchronized to the frequency derived from the STM line signals received from office A. The STM signals output by office B are synchronized to B's reference clock. Hence the phase variations of the STM line signals received by office A from B, as measured in office A, equal the sum of outgoing path delay variations and incoming path delay variations. If the outgoing path delay variations are assumed to be one half of the variations measured by office A, the precision of this measurement is limited by the difference between outgoing delay variations and incoming delay variations. The precision can be below 10ns if the outgoing and incoming lines are part of the same cable [6].

The equipment delay mentioned in section 3.2 depends on the phase difference between the received STM frame and the node's reference clock. When the frame phase of the STM signal received by office B is changed by variations in transmission delay, the phase of B's reference clock varies with the frame phase of the received STM signal. Hence the demultiplexing equipment delay of office B does not change when the delay of the transmission line changes. Therefore, transmission delay and delay variations can be accurately determined by measuring round-trip delay variations after measuring the initial delay.

5. EXPERIMENT OF THE INITIAL DELAY MEASUREMENT

5.1 Setup

The initial delay measurements mentioned in section 4.2 were performed in a laboratory using the setup shown in Fig. 5. Two 622Mbit/s SDH line terminals including multiplexing and demultiplexing devices and two 20km optical fibers were used to connect the SDH terminals. One pulse per second (1pps) signals were used as the time reference signals and they were carried in 50.112Mbit/s Virtual Containers (VC-3) embedded in 155.52Mbit/s STM signals (STM-1). The STM-1 signals were multiplexed into 622Mbit/s STM line signals (STM-4) by each SDH terminal. The four reference clocks of the two SDH terminals, one for the time signal generator and one for the phase shifter, were separately controlled by four synthesizers. The phase differences of the time reference signals were measured by time-interval counters. One half of the round-trip path delay was captured by counter A while the true outgoing path delay was recorded by counter B.

5.2 Results

Figure 6 is a plot of the difference between one half of the round-trip path delay and the true outgoing path delay. The effects of the three phase control steps are shown in Fig. 6. The delay measurement error before the three steps indicates the difference in equipment delay

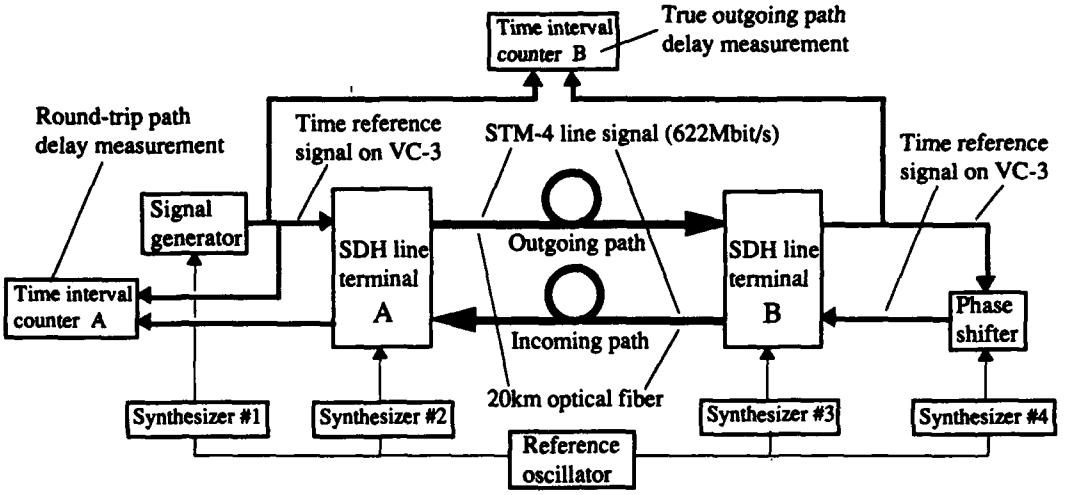

Fig. 5 Experiment setup of the initial round-trip measurement. In the first step, the phase of SDH terminal B is controlled by synthesizer #3.
In the second step, the phase of input time signals to SDH terminal A from the signal generator is controlled by synthesizer #1.
The phase of input time signals to SDH terminal B is controlled by synthesizer #4 in the third step.

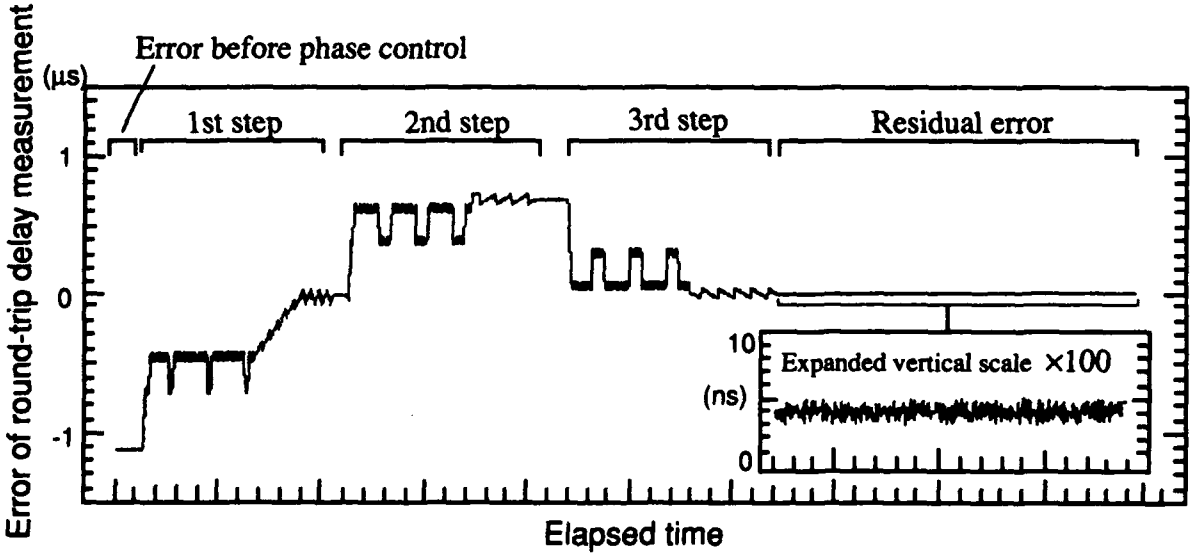

Fig. 6 The effect of the three phase control steps and the error of the round-trip delay measurement. The error before phase control was about -1.2μs and the residual error after the phase control was 5ns in this experiment.
The error before the control varied in the range from -1.2μs to +1.2μs as determined by repeated experiments. The residual error after control varied only 30ns in repeated experiments.

of the outgoing and incoming paths. The absolute value of maximum error before the three steps was 1.2μs as determined by repeated experiments. The residual error of the initial delay measurement after the three steps lay within the range of -15ns to +15ns in repeated experiments. The residual error is probably caused by phase control error and delay variations below the unit interval of the 50Mbit/s VC signals in the two SDH terminals.

Because actual measurements will be made on actual transmission paths, asymmetric path lengths will cause a residual error in initial delay measurement. Typical delay asymmetry is reported to be 100ns [5],[6], hence it will be the dominant source of initial delay measurement error.

6. CONCLUSION

An accurate delay measurement method that uses round-trip paths for time signal distribution in SDH networks was proposed. The feature of this method is that it measures the initial round-trip path delay and round-trip path delay variations separately. In an experiment using actual SDH equipment, the fluctuation of the equipment delay was suppressed to 30ns with a new three step process. This residual fluctuation is smaller than the typical delay asymmetry, which is reported to be 100ns, of actual paired transmission lines that will be used to effect the round-trip paths. The accuracy of absolute time synchronization is limited by the residual fluctuation of equipment delay and the delay asymmetry of the paired lines. On the other hand, the precision of delay variation measurement can be below 10ns. Hence the instability of time synchronization will be within 10ns.

ACKNOWLEDGEMENTS

The authors would like to thank Dr. Haruo Yamaguchi and Mr. Ikuo Tokizawa of NTT Transmission Systems Laboratories for their encouragement.

REFERENCE

[1] CCITT Recommendation G.824, Blue Book, Oct. 1988.

[2] W. D. Grover and T. E. Moore, "Precision Time-Transfer in Transport Networks Using Digital Cross-Connect Systems," IEEE Trans. Communications, vol. 38, pp.1325-1332, Sep. 1990.

[3] CCITT Recommendation G.707, G.708, G.709, Blue Book, 1989.

[4] R. D. Hall and M. J. Snaith, "Jitter Specification in Digital Network," Post Office Electrical Engineers' Journal, vol. 72, pp.96-101, July 1979.

[5] M. Kihara and A. Imaoka, "Time Concurrency / Phase-Time Synchronization in Digital Communications Networks," Proc. 22nd PTTI, pp. 367-374, 1990.

[6] A. Imaoka and M. Kihara, "Long Term Propagation Delay Characteristics of Telecommunication Lines," IEEE Trans. Instrumentation and Measurement, vol. 41, Oct. 1992 (in press).

QUESTIONS AND ANSWERS

R. Brown, Bellcore: I was wondering on your jitter of one nanosecond; was that optical line jitter?

A. Imaoka: It was not line jitter. It was equipment jitter.

R. Brown: Is it payload jitter like the virtual container jitter or is it optical line jitter?

A. Imaoka: The jitter includes all those.

SYNOPSIS OF TIMING MEASUREMENT TECHNIQUES USED IN TELECOMMUNICATIONS

George Zampetti
Telecom Solutions

Abstract

Historically, Maximum Time Interval Error (MTIE) and Maximum Relative Time Interval Error (MRTIE) have been the main measurement techniques used to characterize timing performance in telecommunications networks. Recently, a new measurement technique, Time Variance (TVAR) has gained acceptance in the North American (ANSI) standards body. TVAR was developed in concurrence with NIST to address certain inadequacies in the MTIE approach. This paper describes the advantages and disadvantages of each of these approaches. Real measurement examples are presented to illustrate the critical issues in actual telecommunication applications. Finally, a new MTIE measurement is proposed (ZTIE) that complements TVAR. Together, TVAR and ZTIE provide a very good characterization of network timing.

1. MEASUREMENT CRITERIA

A good starting point in evaluating timing analysis techniques is to set objectives of what constitutes a good approach. A good measurement technique is one that efficiently extracts the useful information from the timing signal in a repeatable and cost effective manner. The usefulness of the information extracted is closely tied to the use of a good practical model. Historically, the model used to described timing signals in non telecommunications applications is based on a simple decomposition of the signal into two components:

- Systematic components (Phase Offset, Frequency Offset, and Frequency Drift)
- Stochastic Power Law noise components, $S_x(f) = \sum_{n=0}^{4} \alpha_n f^{-n}$ (white pm, flicker pm, white fm, flicker fm, random walk fm).

This model permits the characterization of a complex timing signal with a handful of parameters. The premise that this model can be extended to telecommunication synchronization distribution applications is reasonable. Conceptually, one can treat a distributed network of clocks as a single composite super clock. The dominant sources of noise and bias may be different, but the resulting timing signal will still be characterized by this model. This approach has recently been adopted by ANSI committee T1X1 . Extensive field phase data has been analyzed using TVAR (described

later) as the measurement tool to extract the key parameters of the model [ANSI T1X1.3/91-074]. The dominant noise types found in the network are white PM, flicker PM and white FM.

The fact that more divergent noise processes (such as random walk FM) are not significant indicated that the network is reasonable traceable in frequency to the primary reference sources.

1.1 Dual Role of Measurement/Modeling Approach

One role that the measurement approach fills is the need to extract the timing model parameters. The critical issues in this role are:

- Does the measurement approach extract the essential parameters ?
- Does it use the data efficiently (fast convergence of parameter estimates)?
- Is it practical to compute?
- Is it robust to practical measurement anomalies (glitches, gaps etc.)?

A key role that the modeling approach fulfills is the need for timing specifications and standards. The critical issues in this role are:

1. Is the parameter set compete (does the model allow for timing signals that meet the parameters but have undesirable attributes)?
    - Is the parameter set excessive (does the model over–constrain the design of the network or the elements)?
    - Does the model permit networking of elements and subnetworks (can one interconnect clocks and/or subnetworks and determine overall performance)?

2. MEASUREMENT TOOL DESCRIPTION

Three measurement approaches are compared in the paper:

1. M[R]TIE (Maximum [Relative] Time Interval Error) ,
2. TVAR (Time Variance),
3. ZTIE (Z–transformed processed Time Interval Error)

2. 1 M[R]TIE

M[R]TIE is the established measurement approach for telecommunications. The bracketed [R] (Relative) is used to distinguish the reference timing signal. When the term is used with the [R] (MRTIE) the reference timing signal is the input to a timing element and the signal under test is the network element output. When no [R] is used (MTIE), the reference is considered to be ideal (practically a primary reference source). For simplicity, MTIE will be used as a general description of both measurements.

MTIE is fairly straightforward to describe. For a given observation interval (usually termed S) the phase error between two timing signals is observed. The peak to peak phase (delay) variation of

the error signal is the MTIE for that sample interval. The observation interval can be considered as window function. As the window slides through the phase error signal, the next sample of MTIE is calculated. The MTIE for the overall phase data set is the maximum of all the individual MTIE samples. For full overlapping processing of MTIE, there is a greater than linear growth in computation resulting from the need to search for minimums and maximums.

MTIE appears to be a useful approach when considering conventional network controlled slip rates. The maximum peak to peak delay variation impressed on a frame alignment (slip) buffer is directly related to MTIE . However, the controlled slip mechanism is a function not only of peak to peak buffer movement, but also of the type of movement. Monotonic movement will result in a slip rate governed by the frame size (typically 125 microseconds) and the rate of phase movement (frequency offset). But, cyclical movement results in a slip rate governed by the hysteresis in the buffer control (which can be as small as 18 microseconds). MTIE provides little information regarding the underlying model controlling the phase motion in the buffer. The basic attributes of MTIE are:

1. Monotonically increasing with increasing observation intervals.
2. Suppresses Phase bias; asymptotically converges to frequency or drift bias for long observation intervals.
3. Captures peak information regarding delta time variation.

2.2 TVAR

TVAR (Time Variation) is a new term to some, but it is based on the well established Modified Allan Variance (MVAR). TVAR can be viewed as a filtering operation applied to the raw phase error signal. The filtering operation is diagramed in Figure 1. The following notation is used:

1. f is normalized in units of T^{-1} where;
2. T is the observation interval (averaging interval),
3. $T = n \bullet T_0$ where T_0 is the sampling period, and n is the number of samples in the observation interval.

The TVAR filter can be viewed as consisting of three sections:

1. Block Averaging,
2. First Difference, and
3. Second Difference.

The block averaging provides a T dependent low pass filter characteristic. The transfer function of the block averaging function is illustrated in Figure 2.

The block averaging function has the characteristic main lobe with a zero at 1/T. The main function of the block averager is to provide a Tau dependent low pass filter to suppress jitter and provide for discrimination between flicker PM and white PM. As will be shown in section 3 this low pass function is critical in telecommunications as timing signals can be dominated by these higher frequency noise components.

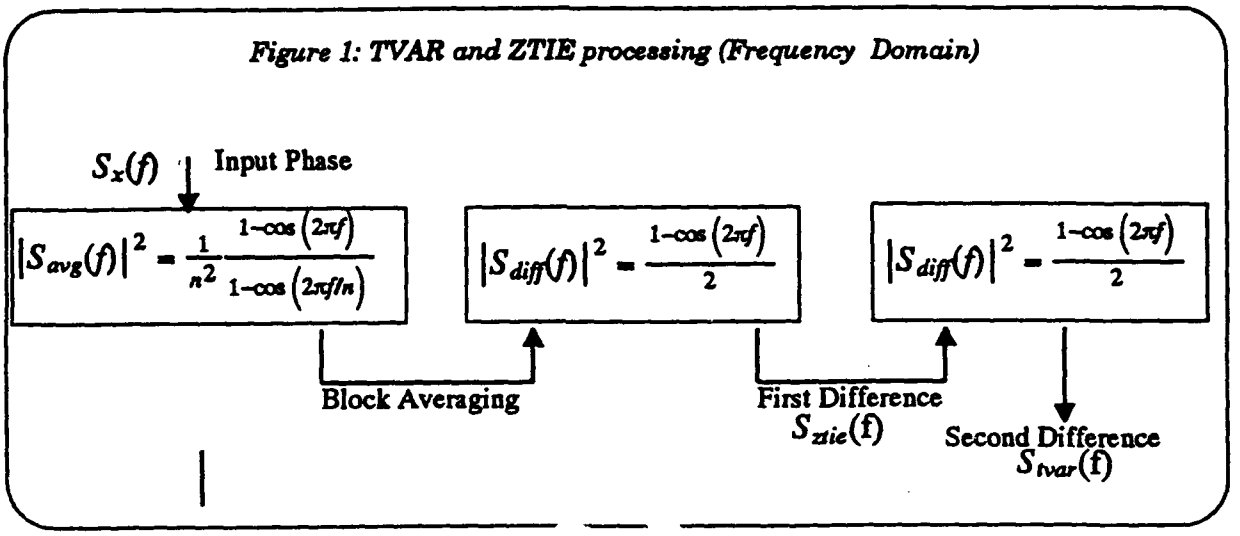

The next operation is the first difference. The first difference transfer function is shown in Figure 2. The main purpose of the difference operator is to provide suppression of the f^n divergent power law noise processes. The first difference provides 20 dB per decade suppression . This is adequate to ensure a stationary noise power process for input phase noise with white noise FM as the most divergent noise (which is the expected case for traceable timing signals). The first difference operation also suppresses phase bias. In TVAR processing the difference operator is applied twice yielding an overall second difference. This ensures stationarity for noise processes up to random walk FM which is the most divergent noise expected in general oscillator applications. The second difference also suppresses frequency bias. Since frequency bias is a critical parameter, TVAR needs to be complemented with another measurement in describing telecommunication timing signals.

The composite TVAR transfer function is shown in Figure 2. It is essentially a bandpass filter with a center frequency and bandwidth controlled by the averaging time T. To complete the calculation of TVAR the variance of the filtered output signal is calculated for each observation interval (T). A close analogy can be drawn to an FFT based spectral analysis. The bandpass filter function can be viewed as a window function centered at a specific frequency (approx $T/2$). Normally TVAR is calculated in a geometric series of $2^{-n}T_0^{-1}$ frequency bins. An FFT is based on a arithmetic series of 2^n frequency points. In an FFT the bandwidth of the window function is fixed. In TVAR analysis the bandwidth is proportional to the frequency bin. TVAR is tailored to being an efficient method to extract broadband power noise processes. FFTs are in general better suited for analyzing frequency over a smaller dynamic range.

2.3 ZTIE

The basic concept behind ZTIE is that a peak power measure is needed to complement TVAR. ZTIE is one possible approach to providing a bandpass measure of peak power. ZTIE measures the peak power using a bandpass filter controlled by the averaging time T. Figure 1 shows that ZTIE is calculated from the output of the first difference function used in calculating TVAR. The reason that the first difference output was selected over the second difference is that it does not

suppress the frequency bias term of the model. The importance of this will be seen in the examples in the next section. ZTIE is calculated by simply measuring the peak output of the first difference operator. The peak information is critical to providing bounds to the model parameters. As the examples will show, it is risky to assume that the peak to rms ratio is gaussian in telecommunication networks.

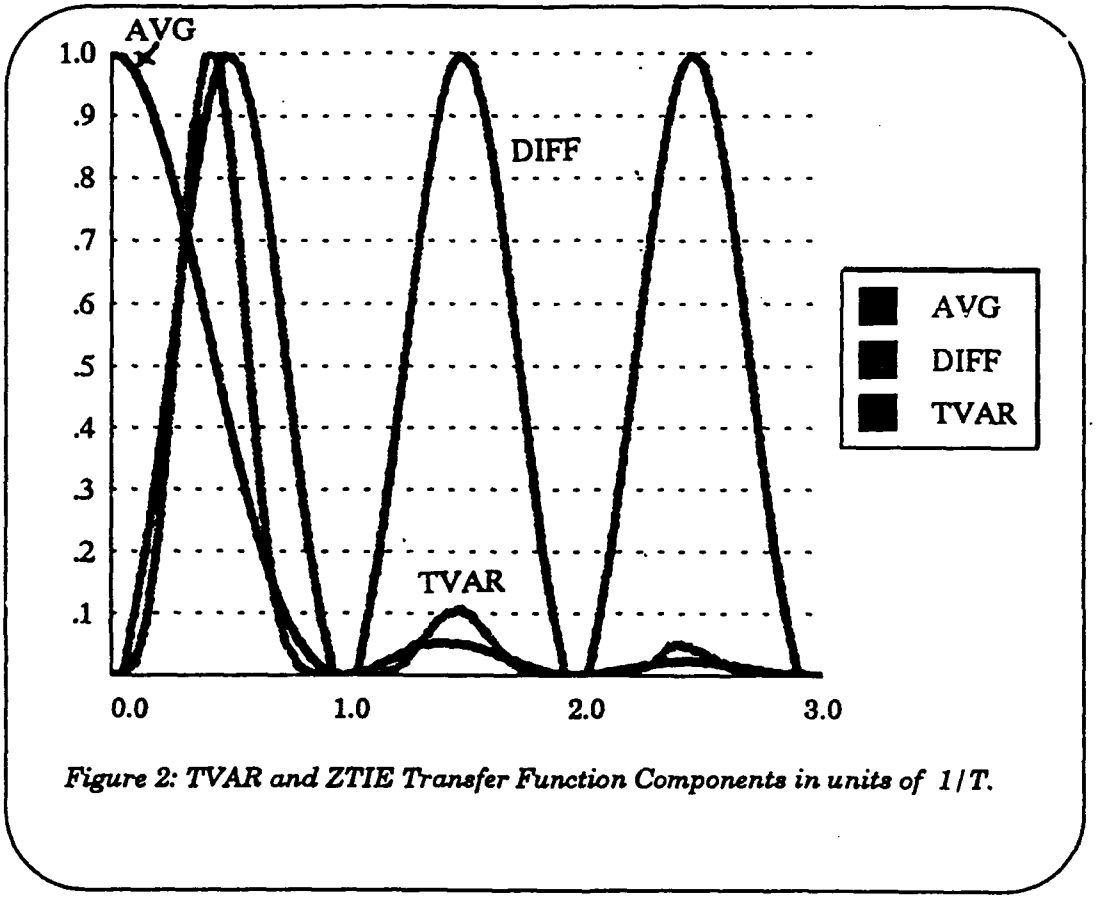

Figure 2: TVAR and ZTIE Transfer Function Components in units of 1/T.

3. MEASUREMENT EXAMPLES

This section provides a selection of measurement examples to illustrate the key attributes of each measurement method. The measurement examples were generated using a simulation approach.

3.1 Power Law Noise Examples

Figures 3a, 3b and 3c illustrate the measurement behavior for White PM, Flicker PM and White FM respectively. Each simulation was run for 86,400 sample points.

Figure 3a shows the results for a gaussian white PM input signal. In addition to the TVAR, ZTIE and MTIE results, an asymptote showing the -1/2 expected slope is plotted. The TVAR result shows the expected behavior:

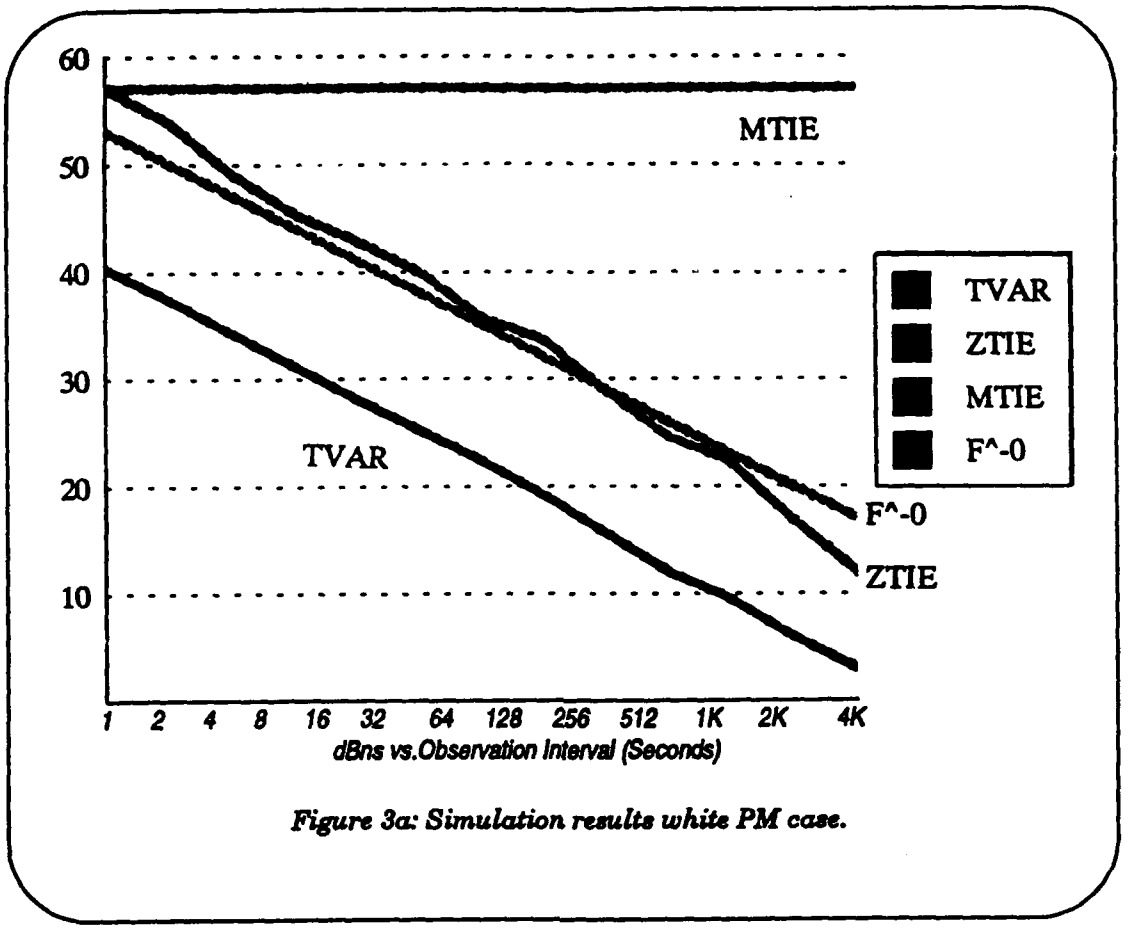

Figure 3a: Simulation results white PM case.

1. At T_0 the TVAR (actually the root TVAR) value 40dBns (100 ns) equals the noise level of the input jitter.
2. The -1/2 slope shows the root law reduction in rms error associated with averaging .

The ZTIE result shows the same trend as the TVAR data. The slight droop at longer averaging times is explained by the reduction of independent peak power measurements (fewer measurements reduce the likelihood of finding a point on the tail of the distribution). The TVAR curve is running about 14 dB above the ZTIE curve showing a well behaved peak to rms ratio.

The MTIE result highlights the inadequacy of MTIE in extracting useful data for white PM noise. The MTIE shows a slight increase for longer observation intervals. Naturally, since the bandwidth of the measurement increases with observation interval there is increasing probability of finding a higher noise peak.

Figure 3b shows the results for Flicker PM. The TVAR results show the flicker PM noise floor as a horizontal asymptote. This is a very practical feature of TVAR. The flicker PM floor represents the best time error calibration that can be realized for a given timing signal. This is important when we consider issues like phase error during rearrangement of clock timing inputs. A clock cannot resolve phase better than the flicker PM noise floor of the reference input.

ZTIE shows a similar behavior as with white PM. The peak to rms ratio is well behaved. The

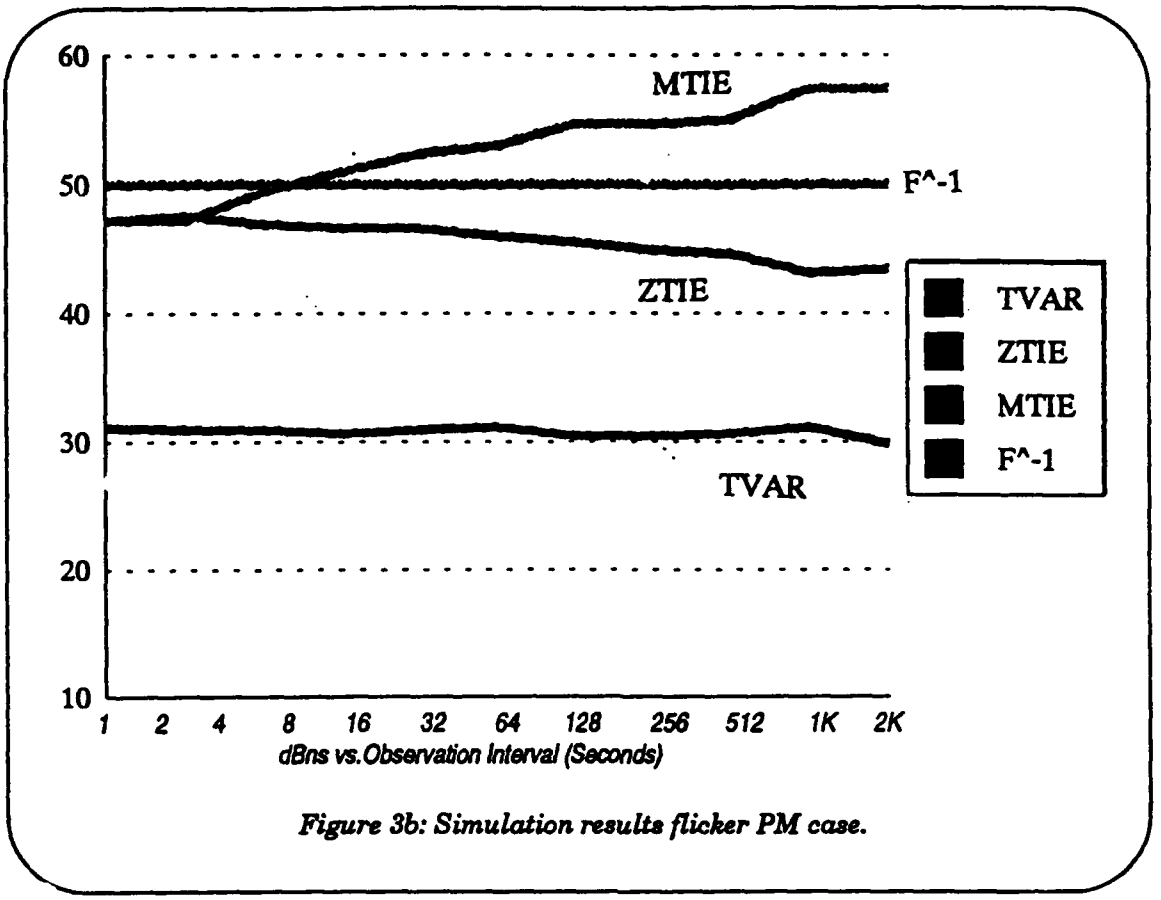

Figure 3b: Simulation results flicker PM case.

peak information is very useful in this case as it bounds the peak phase error achievable during rearrangement (approx 220 ns in this case).

MTIE behaves much better with a divergent noise process input. However, it still shows a 10 dB positive skew for longer observation intervals.

With white FM all three measures show the $+1/2$ slope divergence of the timing error expected (Figure 3c). Note that ZTIE and MTIE converge for white noise FM. ZTIE has been designed to converge with MTIE for longer observation intervals where either white FM or frequency bias dominate.

3.2 Telecommunication Network Examples

The examples in this section are constructed to illustrate issues related to the telecommunications network.

3.2.1 Transient Glitch

In measuring actual network timing data there is the practical issue of managing transients. The transient may be part of the measurement system, disruption in the transport path or a clock anomaly. Regardless, a good measurement approach should not completely mask transients or let

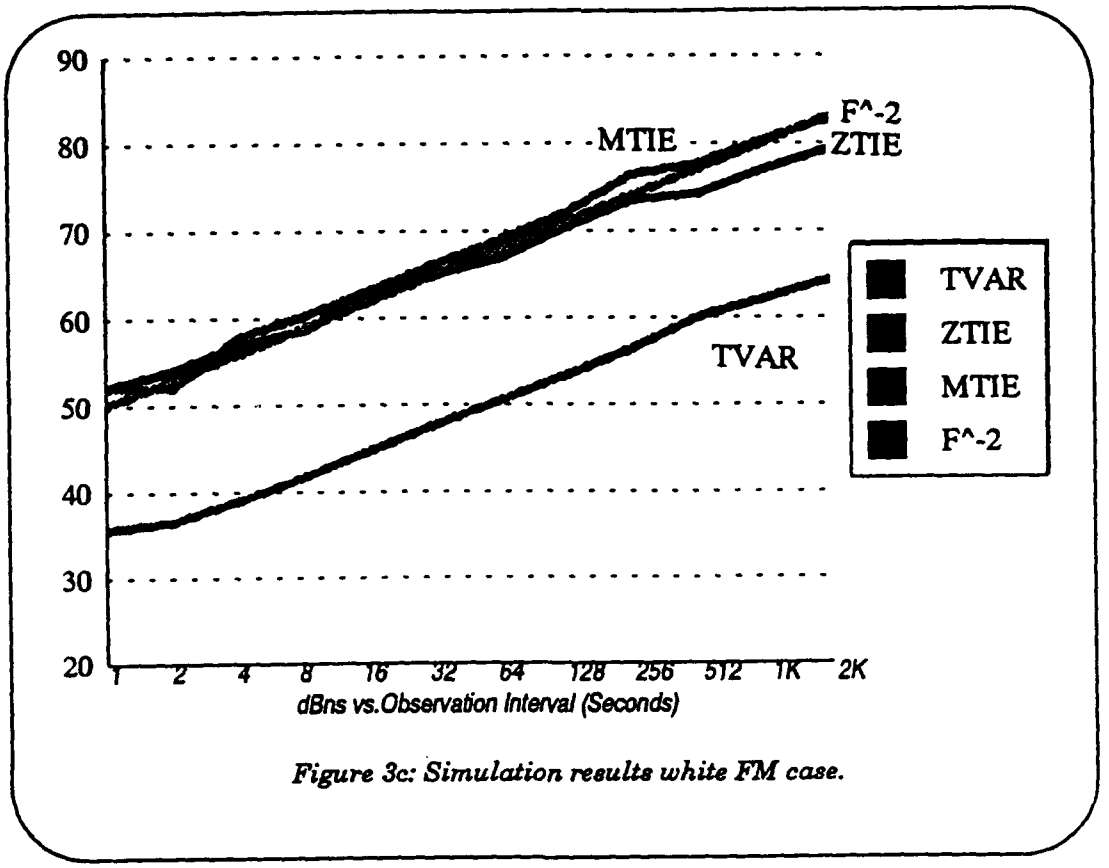

Figure 3c: Simulation results white FM case.

transients mask steady state performance. Figure 4 shows the response of the three measurement approaches to a simple phase impulse event.

TVAR is plotted for two data collection intervals (one hour and one day). Since TVAR is an rms power estimator, it tends to remove transient impulses (which are finite energy zero average power). Thus, TVAR needs to be complemented with a peak estimator to capture transient information.

ZTIE shows an interesting response to the impulse. The total peak level of the impulse is shown at T_0 (10,000 ns). The power level is then linearly suppressed for longer observation intervals.

MTIE is extremely sensitive to transients. A single transient can completely mask out the underlying noise model for the timing signal. This is a serious weakness in the application of MTIE to actual network timing analysis.

3.2.2 Jitter plus Frequency Offset

Figure 5 illustrates an example of a realistic network timing signal.

The timing signal is constructed with nominally 1 UI of peak to peak timing jitter. This level of jitter is well within worse case network limits (5 UI), and is a reasonable bound for expected network transport jitter over the existing plesiochronous digital network. The frequency bias (1×10^{-10})

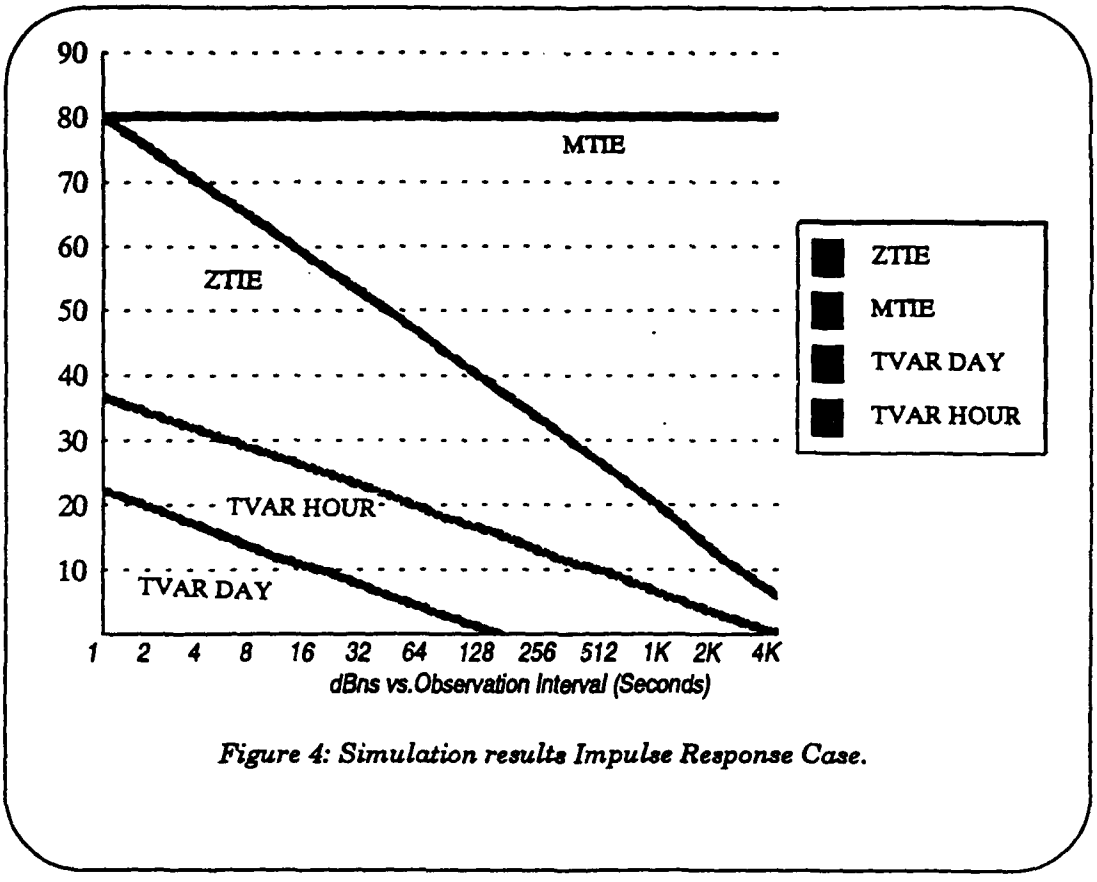

Figure 4: Simulation results Impulse Response Case.

represents a timing signal that has impaired frequency traceability to the primary reference source (the next example suggests one of a number of mechanisms for this to occur).

TVAR effectively suppresses the frequency offset and correctly reports the underlying white PM transport jitter. ZTIE is very effective in showing both the short term peak jitter noise component and the long term frequency bias. MTIE again is inadequate to show the true underlying noise process.

This is a good example to consider from the point of view of timing specifications and standards. One can consider how well this measurement results would function as network timing interface standards. A key question is how well one can calibrate the frequency of slave clock to a network timing reference? The ability to calibrate directly impacts slip performance during reference outage conditions. For sake of illustration let us consider a clock with a 128 second averaging algorithm. At 128 seconds the MTIE value is 488 ns. Since the MTIE mask provides no insight on the underlying noise process, one can't assume white PM. In fact, the only safe assumption is that this 488 ns phase instability cannot be effectively filtered. This leads to frequency calibration error bound of 3.8×10^{-9}. In contrast, at 128 seconds ZTIE has a value of 30 ns. A mask based on ZTIE would constrain the worse case frequency calibration to 2.4×10^{-10} (over an order of magnitude tighter).

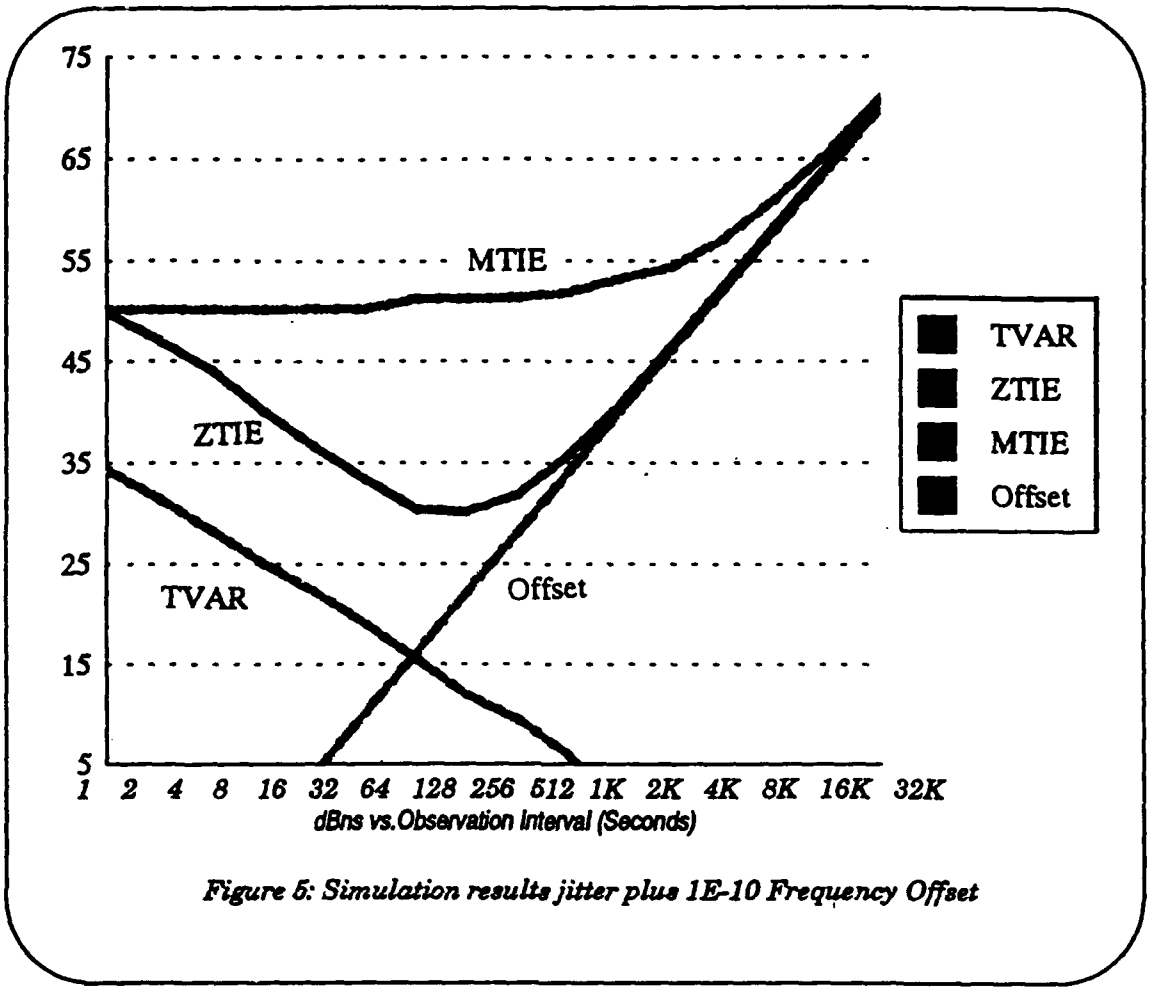

Figure 5: Simulation results jitter plus 1E-10 Frequency Offset

3.2.3 Network Timing Signal (Stress Condition)

Figure 6 shows the measurement results for a network timing signal under stress conditions.

CCITT G.812 defines a clock under stress conditions. One stress condition is frequent transient disruption on the reference transport. For constructing the simulation for network stress one reference disruption per hour was used. This level of disruption is within the maintenance performance action limits for network transport. The disruption activity will lead to reference rearrangement transients. The following model for reference rearrangement was simulated:

1. The maximum total phase movement at the clock output in response to a transient is assumed to be either plus or minus 1 UI (488ns). This is within the current maximum of 1,000 ns allowed for in network timing standards.
2. The direction of the phase step is assumed to be a bias with positive steps occurring with a 75% probability. Bias errors can result from numerous hardware and software sources in a clock.

In addition to the hourly reference disruptions, white PM was added to the timing signal to simulate network transport jitter (the jitter distribution was assumed to uniform with a 1 UI peak to peak magnitude.

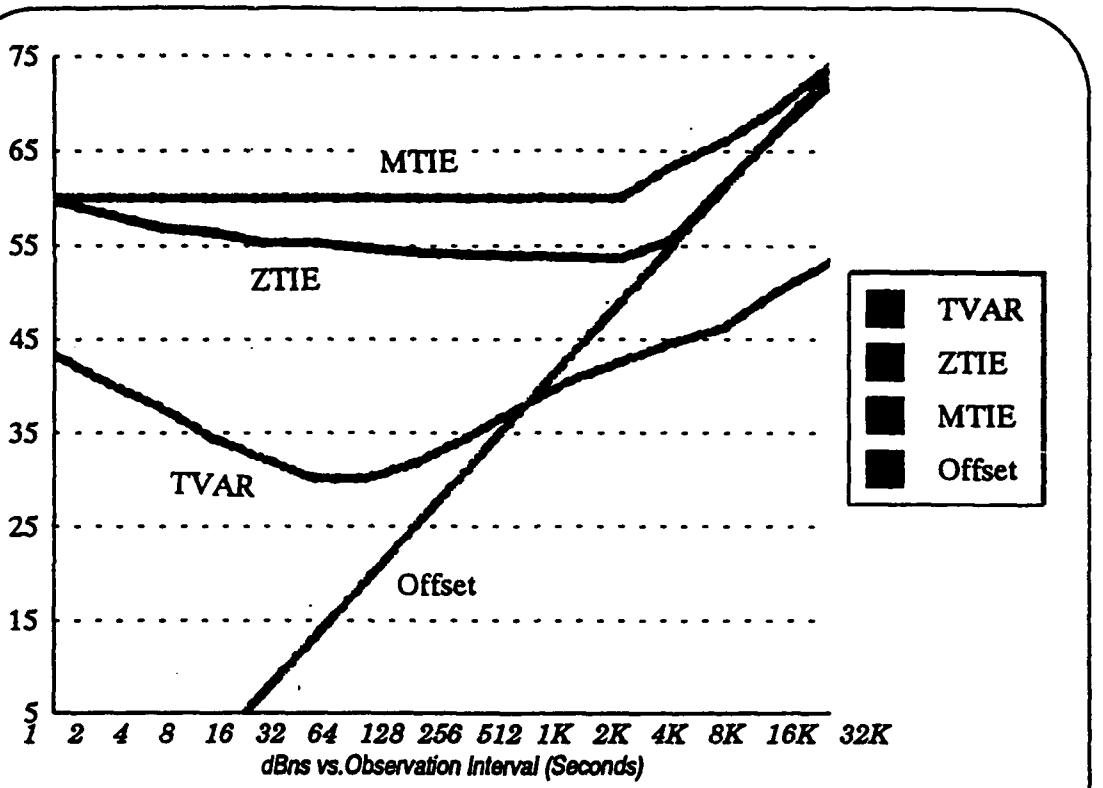

Figure 6: Simulation results Network Stress Conditions

The TVAR result clearly shows two dominant noise processes. The white PM transport jitter dominates for short observation intervals, and the white FM associated with the reference rearrangements dominates for longer observation intervals.

The ZTIE result shows that timing signal error distribution is definitely non-gaussian. The random walk in phase is quantized in 1 UI steps. These phase steps manifest themselves as impulsive noise. ZTIE complements TVAR by showing that the peak error is dominated by non-filterable transient steps rather than the underlying white FM noise process. The TVAR results suggest that the best time calibration error is 32 ns. ZTIE shows the true achievable timing calibration performance is actually limited to 500 ns.

MTIE performs fairly well for this constructed example because the phase walking process dominates. However, ZTIE still provides a correct estimate of the underlying frequency offset (which in this case is 6×10^{-11}), about ten times faster than MTIE.

4. SUMMARY

Measurement and modeling are closely related. The use of the power law model in conjunction with TVAR as a measurement technique provides a very effective platform to characterize network timing performance. However, TVAR is inadequate for establishing network timing specifications

and standards as it fails to extract important information concerning peak noise power, frequency biases and transients. MTIE has been shown to be inadequate as measurement tool for a variety of practical network scenarios. ZTIE is proposed as one measure of peak power. It complements TVAR by providing information on peak noise power, frequency bias and transient activity. It is designed to converge with MTIE for longer observation intervals. The use of both TVAR and a bandlimited peak power measurement like ZTIE in telecommunication applications is increasingly critical as new synchronous optical transport (SONET and SDH) require more accurate and tighter specification of network timing.

QUESTIONS AND ANSWERS

G. Winkler, USNO: A single characterization is sufficient. What I wonder is what actually is wrong in using structure functions. That has been proposed some 15 years ago by Lindsey, as I remember; probably David Allan will remember that. This discussion entered, at that time, to use a different set of differencing in measures of these differences. The maximum value of the RMS values and so on.

Comment: I think from the scientific community there is a much better parameter set that could be obtained. From where the telecommunication's community is, I think this introduction of TBAR by itself, which is very simple to cause a major conniption. One of the things I mentioned that ZTIE behaves just like MTIE does on the long term. That was one of the attributes that, I knew, I had to have a connection there, so it's a very simplistic measurement is trying to take the most logical step. So it is a practical issue as to why this step is the way they are currently. That is a good point.

R. Brown, Bellcore: Just as a side to that, the telecommunication community has adopted using time variance or time deviation as an additional parameter to MTIE. We are very indebted to the National Institute and Standards and Technology: Dave Allan, Mark Weiss for their help in that. We are not time and frequency people, we kind of dabble in it, we are getting a feel for it. We needed some help with that and greatly appreciate the efforts of NIST.

TIMING IN PRIVATE DIGITAL TELECOMMUNICATION NETWORKS

J. E. Abate, C. D. Near, M. S. Russo
AT&T Bell Laboratories, Holmdel, NJ, USA

Abstract

For proper operation of today's large digital private networks, high quality synchronization must be achieved. A general telecommunication performance objective is to maintain long-term frequency accuracy of ten parts per trillion at all synchronous digital equipment in the network. Many times, however, this is not achieved in private networks. Low quality clocks, errored transmission facilities, and incorrectly designed synchronization plans are often cause for poor performance. It is shown that properly-designed private networks can operate with long term frequency averages between ten parts per trillion to ten parts per million.

These performance levels can adversely impact customer applications. The most demanding applications are digital and voiceband data, encrypted voice, facsimile and video. In a typical private network operating at 0.01 parts per million, the user would experience reduced data throughput, dropped encrypted calls, unreadable facsimile pages, or interrupted video transmission dozens of times per day.

The major contribution to poor private network synchronization performance is the interaction of Customer Premises Equipment (CPE) clocks and the network facilities used to distribute timing. The performance of typical CPE clocks and facilities, and their impact on customer applications, are discussed. CPE clock performance issues, along with private network architectural constraints, make synchronization planning extremely difficult. Planning is usually costly and requires specialized expertise.

CUSTOMER EXPECTATIONS

Intelligent digital networks which can consist of the public switched network's facilities and services, as well as customer owned equipment must provide nearly error free performance under a variety of operating conditions. This includes automatic reconfiguration of the network (which may occur under software control, without operator intervention) during normal operations and failure modes.

The robustness of a network can be improved against observable degradation of services during failure modes, if a quality synchronization plan is in place. To attain such a plan, one must consider synchronization performance at each level in the network including:

1. The synchronization performance of the public switched network,

2. The private network's synchronization architecture, and

3. The performance of individual, CPE clocking systems.

AT&T has strived to improve the synchronization performance of both the public switched network and CPE [1-5]. Thus, customers can expect and get the best possible error–free performance from digital networks.

NEED FOR SYNCHRONIZATION IN DIGITAL NETWORKS

Synchronization is the means used to keep all the equipment in a digital telecommunications network operating at the same average rate. If the receiving end is to receive and properly interpret the digital signals transmitted over a communications link, it must stay in step, or be synchronized, with the transmitting end. When digital signals are transmitted over a network of digital communications links, switching nodes, and transmission interfaces, all entities must be synchronized. This is known as network synchronization [5].

We refer to the loss or repetition of an entire frame of data as a slip. (The loss or repetition of an entire frame of data along frame boundaries is more accurately called a controlled slip. For purposes of this paper, slips and controlled slips are synonymous). Slips are caused by differences in clock rates within a network and by the effect of transmission–induced impairments on clocks.

The primary methods used to control the slip rate and limit it to an acceptable level are:

1. Operate all clocks in the network at the same average rate.

2. Place buffers at the receiving end to absorb small phase variations.

In the United States, equipment clocks are categorized by ANSI standards according to accuracy and performance level [4]. Stratum 1 clocks have the highest accuracy requirements: stratum 2, 3, and 4 clocks have progressively lower accuracy and performance requirements [5]. Timing references are passed hierarchically from high–performing clocking systems to equivalent or lower performing clocking systems within a network to synchronize many equipment clocks to one, nominal reference frequency. Most of the clocking systems used in the AT&T switched network are stratum 1 and stratum 2. Most clocks found in CPE, such as PBX's and multiplexers, are stratum 4.

However, even when all the equipment clocks are synchronized to a single master clock, it still is impossible to eliminate slips in a digital network. Therefore, synchronization plans are developed to minimize and control the rate at which slips occur. A synchronization plan specifies the timing flow through the network and takes into account equipment performance, facility performance, and network topology.

PRIVATE NETWORK SYNCHRONIZATION PLANNING

Customer digital private networks present additional complexities for synchronization planning. Typically, these networks have diverse architectures; i.e., the equipment and facilities they contain come from multiple vendors and carriers and are interconnected in complex arrangements [7].

In addition, the quality of the clocks in CPE tends to be poor in private networks. Most CPE currently use stratum 4 clocks, which are not designed to transfer timing references between equipment. Consequently, the private network arena is the most difficult one in which to obtain high quality synchronization performance and is the one most susceptible to overall performance problems.

SYNCHRONIZATION ARCHITECTURE

Ideally, timing flow in digital private networks follows the hierarchical source to receiver method. That is, synchronization references are passed from high performing clocks to the low performing clocks. While most private network equipment is usually equipped with stratum 4 clocking systems, some CPE have stratum 3 systems.

Most public switched network services contain traceable, stratum 1 timing (i.e. timing that originates from a stratum 1 primary source). Hence, if the timing source in a private network originates from a traceable, stratum 1, public switched network link, then such timing should be distributed to all CPE throughout the network. Ideally, intra–building timing will be distributed via a hierarchical arrangement. In such an architecture, the best performing clock in a building is used to distribute timing to all office equipment via dedicated lines in the office. The clock is referred to as a BITS (Building Integrated Timing Supply). The BITS receives its timing reference from outside the office. This architecture is used for the AT&T public network. In private networks, a BITS type arrangement is unlikely to happen because most CPE do not have a dedicated timing interface and can only derive timing from a traffic–carrying signal.

Figure 1 illustrates a typical private network location. This location is connected to four other locations in the private network, as well as to three public–switched–network services. Each public–switched–network service contains timing that can be traced to a stratum 1 clock. All equipment at the location requires synchronization, and the diagram shows a reasonable synchronization plan for the site. This plan adheres to the hierarchical timing–flow requirements and permits diverse timing sources into the location.

However, the location does not contain a true BITS architecture. Instead, the location illustrated in Figure 1 has two BITS clocks: the PBX, and the digital cross–connect system (DCS). A BITS architecture offers several advantages:

1. Maximum use of the highest performing clock at the location (without intralocation cascading of timing references)

2. The BITS clock serves as a central point for maintaining synchronization within the location.

Because of implementation problems, private network BITS designs are unlikely. Customer premises lack bridging repeaters for routing timing signals within the site. In addition, some stratum 3 and most stratum 4 CPE systems lack dedicated timing interfaces.

A major focus for any synchronization plan is to overcome topological complexity and constraints. Private networks can suffer from excessive cascading of CPE, lack of diversity of timing references,

and hierarchical conflicts. There may be limited connectivity within the private network and to public switched networks. They may lack provisioning for BITS architectures.

Before a good synchronization plan can be developed for a given network, we must consider these issues in detail. But we must understand that these problems may be compounded because equipment and facility performance will also vary and affect network performance. The stratum 4 clock is one of the consistently poor performers in private networks[7].

CPE CLOCKS

Originally, stratum 4 clocks acted as the CPE receive clock, which terminates timing; they were not designed to transfer timing references between systems. But as the private customer–owned networks have grown more complex, the clocks in CPE (such as PBX's and multiplexers) have been used to transfer timing. Private networks often have long chains of stratum 4 systems through which timing is cascaded.

The main problem with stratum 4 clocks is not their low oscillator accuracy (typically 32 parts per million), but rather their inability to switch cleanly between timing references. If the timing reference for a stratum 4 clock is sufficiently impaired, the clock will switch to its backup timing source, which may be either another timing reference or the clock's internal oscillator. Stratum 4 clocks do not have a phase build–out mechanism that would slowly correct for the phase difference between the previous and current sources of timing. Therefore, the reference switch would cause a phase hit at the CPE's digital interfaces. If this CPE is providing a timing reference to another piece of equipment, the receiving CPE will react to this degradation (which looks like an error burst) by inducing a reference switch of its own. Thus, these impairments will propagate through the chain of cascaded stratum 4 clocks, seriously affecting the network's performance [8].

Stratum 3 and stratum 2 clocks do not suffer from this phenomenon. If a reference switch occurs, these clock systems correct for phase differences between references [6].

Today, digital network standards define a new level of stratum 4 clock that incorporates phase build–out when references are switched. For example, AT&T's TR 62411 (the interface specification for Accunet T1.5 service), which was last published in December 1988, defined an enhanced stratum 4 clock that can be used for timing transfer [8]. This clock, which TR 62411 calls stratum 4, type I, met the requirements for maximum time–interval error (MTIE), which regulates the total phase movement and the rate of change of phase movement of the timing signal under reference–switching conditions. In addition, a new EIA/TIA standard defines the same enhanced stratum 4 system [10].

PRIVATE NETWORK PERFORMANCE

Overall, the typical synchronization performance of a digital private network can be up to 100,000 times worse than the performance of the AT&T network (in terms of frequency accuracy). When new CPE synchronization standards for the telecommunications industry are implemented in private networks, this performance should improve by several orders of magnitude. Generally, a high–quality synchronization plan is needed to minimize the occurrence of slips, error bursts, and phase hits in private networks.

SYNCHRONIZATION PLAN DESIGN CONCEPTS

Some basic concepts need to be considered during the design of a synchronization plan:

1. Whenever possible, it is important to adhere to the hierarchical rules of timing transfer. That is, timing should always be passed from low numbered stratum devices (e.g. stratum 1, stratum 2) to equivalent or higher numbered stratum devices (e.g. stratum 3, stratum 4).

2. Traceable, stratum 1 timing sources need to be used whenever possible, and timing sources should be diverse whenever possible.

3. Timing loops must be avoided. These loops occur when two or more CPE transfer timing to each other and form a loop without a designated master source.

4. The cascading of timing references through CPE should be minimized.

These are some of the fundamental concepts that are the basis of over 6000 rules that AT&T has developed for synchronization planning of digital private networks. The rules have been incorporated into an expert system, called PRINCE–S, that was developed by AT&T Bell Laboratories. PRINCE–S, stands for **PRI**vate **N**etwork **C**omputer–based **E**xpert–system for Synchronization[9].

EXPERT SYSTEM FOR SYNCHRONIZATION PLANNING

AT&T developed the PRINCE–S system to mechanize the task of synchronization planning for a private network in a consistent, accurate, and reliable way. AT&T synchronization engineers have used the system to help them design synchronization plans and maintain synchronization networks.

The system generates network maps that specify primary and backup timing reference distribution for each CPE, and estimates the synchronization performance of the network end–to–end (and for each CPE). The system's recommendation represents the best synchronization performance attainable, based on information used to model the network topology, equipment, facilities, and public–switched–network connectivity.

SUMMARY

We have explained how AT&T provides the means to give the best possible synchronization performance in digital customer–owned private networks. This includes consideration of synchronization planning for customer–owned networks and CPE clock–performance issues.

ACKNOWLEDGMENTS

We would like to thank the following for their contributions to the body of knowledge described in this paper: Pablo Alcivar, Jack Amoroso, Ed Butterline, and Elie Khawand.

REFERENCES

[1.] J. E. Abate, et al, *"The Switched Digital Network Plan,"* The Bell System Technical Journal, Vol. 56, No. 7, September 1977, pp. 1297–1320.

[2.] J. E. Abate et al., *"AT&T's New Approach to the Synchronization of Telecommunications Networks,"* IEEE Communications Magazine, April 1989, pp. 35–45.

[3.] G. J. Grimes, et al, *"Synchronization in Intelligent Digital Networks,"* AT&T Technical Journal, Vol. 70, No. 5, September/October 1991, pp. 59–68.

[4.] AT&T, *"Digital Synchronization Network Plan,"* AT&T Technical Reference PUB 60110, December 1983.

[5.] J. E. Abate et al, *"Use of GPS to Synchronize the AT&T National Telecommunications Network,"* Proceedings of 20th Annual Precise Time and Time Interval (PTTI) Applications and Planning Meeting, Washington, D.C., November 29, 1988,

[6.] *"Synchronization Interface Standards for Digital Networks,"* American National Standard for Telecommunications, ANSI T1.101–1987, American National Standards Institute, Washington, D.C., 1987.

[7.] *"Private Digital Network Synchronization,"* EIA/TIA SP–2198, Electronics Industries Association, December 1990.

[8.] AT&T, *"ACCUNET T1.5 Service Description and Interface Specifications,"* AT&T Technical Reference TR 62411, December 1988.

[9.] F. Myers, *"A PRINCE–ly Solution,"* Bell Labs News, October 16, 1989, p. 7.

[10.] ANSI/EIA/TIA–594–1991, *"Private Digital Network Synchronization,"* August, 1991.

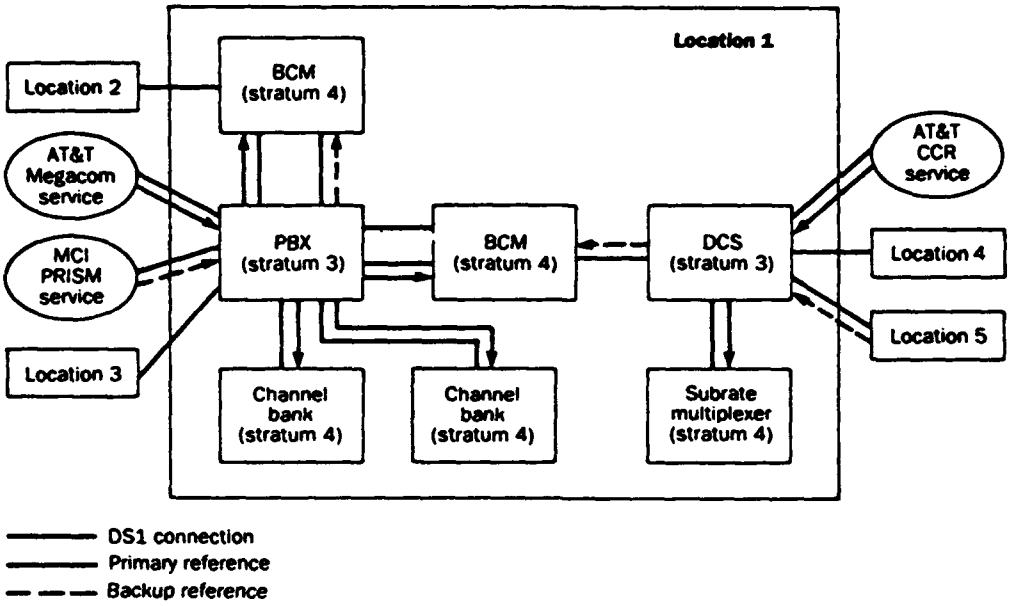

Figure 1. Synchronization plan for all equipment at a representative location in a private network. This location is connected to four other locations in the network and to three public-switched-network services. The timing for each network service can be traced to a stratum 1 clock.

QUESTIONS AND ANSWERS

D. Allan, Allan's Time: This is a broader question than just a private network but perhaps you can address it. If the timing community could provide for telecommunication a clock or clock system which would allow you to synchronize the network with even a broad network say at the 100 nanosecond level forever for all the nodes. What would that mean to telecommunication, if it could be done inexpensively?

C. Near, AT&T Bell Laboratories: It depends upon how inexpensive is inexpensive. It is in a normal carrier environment, for long distance carriers or your locals where they can afford clocking systems, that could be of benefit. If they were in a few (?) range, that is fine. Private networks is where you are going to be getting a much larger customer basis. They are not going to spend that much money. They will spend maybe a $1000.00 for a clock and will not want to spend a whole lot more than that. Sometimes you can get them to spend maybe $5000.00 on a clock but those are cases where you are lucky. If it is in a few hundred to a $1000.00 range and offer that; then they will go for it.

R. Brown: Just my two cents on that Dave. The one thing that I would like to emphasize a little bit from Chris's talk is this is a field with a huge number of players in it. If you look at our specifications I think you people might say that performance is lousy, these guys have got to be dumb if they can not achieve this. We are not dumb, it is just we have a lot of players. We have got different carriers, we have got different vendors. Any circuit that is going to go across the country, you have got local exchange carriers and inter-exchange carriers. Those carriers buy equipment from different vendors and so you are looking at a chain of clocks that is managed by possibly three management entities and the equipment might be built by a dozen different vendors. It might be possible for us to say this is good clock design but we can not force people to implement a design. As far as something at every node, our clients themselves are looking at LORAN receivers. This is a fairly inexpensive thing that might be implemented at every node. Right now their impression is, that is not cost effective. Something has got to be cheaper than to be at every node.

G. Winkler, USNO: This is very right but on the other hand if you have a huge number of customers that is going to bring the price down tremendously. Don not forget all the clock technology today is based on a customer base which can absorb maybe several thousand precision clocks per year. If they can absorb five hundred thousand clocks per year, the price is going to drop as precipitously as the GPS receivers have dropped. Today, only three years after a GPS receiver cost $50,000.00, it is down to $900.00. I would predict to you that a clock which will have one part and 10^{11} capability will cost you less than $500.00 seven years from now, if you have that kind of a customer base and if you will completely turn around all these considerations.

W. Harding, Naval Electronics Systems: That customer base is just right around a corner for you because with the advent of the telephone systems and the pictures that you are going to be able to see years from now by the person that you are talking to on the other end. Also the individual customers as far as VHS communications will all be through satellites. So you are going to have a big base.

R. Kern, Kernco: I have a question. I am new to telecommunications but I have not heard any of you fellows talk about reliability. What is your experience? What MTBF do you need? You can talk about a $100.00 but if it is only going to last a week you are in trouble. Could you comment on reliability or have you guys got standards on that?

R. Brown: I am going to comment on that real quickly and then we will get to Bob's talk and save any other questions to the end. Just on reliability, what we have done at Bellcore is we

write requirements for equipment. We require a lot of duplication of equipment so that no single failure will cause the system to fail. That is really the way we have gone after reliability and it seems to have worked out ok, that you don not get any duplicated failures. As far as specific MTBF numbers, the clocks and the function they are serving are very critical so it has to be very high. The way we have attacked it, is to require duplication of equipment.

SONET Synchronization: What's Happening

Robert W. Cubbage
Alcatel Network Systems, Inc.
Richardson, Texas

Abstract

Almost everyone that has heard of SONET knows that the acronym stands for Synchronous Optical NETwork. There has been a host of magazine articles on SONET rings, SONET features, even SONET compatibility with digital radio. What has not been highly publicized is the critical relationship between SONET, network synchronization, and payload jitter. This paper will address this topic.

Introduction

Almost everyone that has heard of SONET knows that the acronym stands for Synchronous Optical NETwork. There has been a host of magazine articles on SONET rings, SONET features, even SONET compatibility with digital radio. What has not been highly publicized is the critical relationship between SONET, network synchronization, and payload jitter. This topic has been jointly studied by T1X1.3 and T1X1.6 Working Groups. Recently, these two groups have been combined into one group which is called T1X1.3 Synchronization and Tributary Analysis Working Group.

Still No Jitter Specification

The work T1X1.3 is currently doing in SONET payload jitter is extremely important to the successful deployment of SONET equipment in the network. If the badly needed DS3 payload jitter specifications are not specified by ANSI soon, manufacturers will be free to output levels of jitter in their equipment that may cause unacceptable service in the network. In addition, these problems can be extremely difficult to trace. Some people may be surprised to learn that standardization of SONET began in 1985, and it is now 1992 and there still is no SONET payload jitter specification from ANSI. The industry is getting close and is expected to release these badly needed jitter specifications for letter ballot in March of 1993. This paper explains the relationship between synchronization and payload jitter in SONET systems and how important these specifications are.

Asynchronous vs. Synchronous Multiplexing

In the past, network synchronization quality did not have an adverse effect on payload transport systems because these transport systems operated asynchronously. In other words, the transport system did not require external synchronization to properly operate. They used a free running oscillator in each terminal to drive the output frequency such as a 1.2 Gb/s fiber optic terminal (e.g. Alcatel's LTS-21130). But SONET has changed all this. The "S" in SONET stands for synchronization and now the SONET transport system requires synchronization engineering (except in some simple point-to-point cases).

SONET uses synchronous multiplexing to go from lower rate signal (e.g. STS-1 or OC-3) to higher rate signals (such as OC-12). This allows efficient Add Drop Multiplexers (ADM) to be built. Because the synchronization network has frequency and time phase variations, SONET uses an STS-1 pointer processor to synchronously multiplex "N" STS-1s to an OC-N signal in a slipless manner. A pointer processor uses positive/zero/negative pulse stuffing to

accommodate differences in STS-1 frequencies when synchronously multiplexing them together to form the high speed output.

Figure 1 shows an OC-3 terminal with three STS-1 inputs and one OC-3 output. The three STS-1s go through a pointer processor to frequency synchronize them so that they may be multiplexed in a synchronous manner to form the OC-3 output signal. One of the drawbacks of this technique is that jitter is encoded into the signal that is being transported when an STS-1 pointer adjustment occurs. This is similar to jitter caused in an M13 except it is more severe.

This jitter, being much more severe than the jitter caused in an M13, can cause service degradation. Simply put, time phase noise on the synchronization network can cause STS-1 pointer adjustments in SONET systems. These pointer adjustment cause 8 unit interval of phase discontinuity (or jitter) to be encoded in the payload signal being transported (e.g. DS3). This jitter, if not properly bounded, will cause severely errored seconds (bit errors or mis-frames) to occur on payload being carried. Thus, giving the end customer poor quality of service. This has been one of the major issues T1X1.3 has been addressing (i.e. how synchronization performance affects service quality in a hybrid network).

Service Affecting Jitter Across SONET Islands

Figure 2 shows an example of a hybrid network which is a network with mixed asynchronous and SONET transport equipment. In a hybrid network, a DS3 is transported by traditional asynchronous transport equipment (e.g. 565 Mb/s lightwave system) and SONET islands. A SONET island is a collection of SONET equipment interconnected at the OC-N or STS-1 interface. This can be as small as a point to point SONET transport system or as large as ten to a hundred SONET network elements interconnected. Jitter accumulation of a DS3 signal across multiple SONET islands must be bounded, or the current network jitter specifications will be exceeded. This may cause the service being transported to degrade to a point were it is unreliable. There are many complex variables which can have an influence on jitter accumulation in a hybrid network, and two primary factors are the quality of the synchronization input and the payload jitter produced per single pointer adjustment. Before going into any detail, it is important to understand how synchronization is distributed in the network today.

Typically, synchronization timing is distributed from one Central Office (CO) to another Central Office via traffic carrying DS1 facilities. When synchronization timing signals are distributed using traditional transport equipment (fiber terminals, multiplexers, digital cross-connects, etc.), phase noise is added to the signal. This phase noise is caused by various sources which include waiting time jitter cause by multiplex pulse stuffing, thermal noise, etc.

Historically, the phase noise on synchronization sources did not cause serious service degradation on digital switching systems because they used large slip buffers. Most NE's which require slip buffers, have 1 or 2 DS1 frame storage buffers. This large amount of buffering can easily accommodate the short-term phase noise introduced in the network. Now, because of the way that SONET systems handle short-term phase noise variations, there is a need to specify and limit the short-term phase noise on a signal used to synchronize a SONET NE. The phase noise of most interest to SONET network is in the observation range of 0.1 to 1000 seconds. Specifications for this range have recently been adopted and are currently being letter balloted at the T1 level. High levels of short-term phase noise, on either the synchronization input or the OC-N input to a SONET NE, can cause excessive pointer movements to occur in STS-1 or VT pointer processors, which in turn can cause excessive jitter in the payload signal. This jitter can cause degradation to or loss of customer service

altogether. As a result, SONET is sensitive to this phase noise which the existing network can tolerate.

Phase Noise, Jitter, and Wander

Network phase noise which has high speed frequency components (> 10 Hz) is called jitter. Slower speed phase noise is called wander. Both jitter and wander routinely exist in the network and can cause data impairments to occur. In today's network, excessive jitter can cause bit errors or signal frame loss whereas wander can cause buffer spills or slips to occur. Although SONET is no more sensitive to jitter than any other network element, it does react to low speed wander. SONET, in effect, translates low speed wander on the synchronization input to high speed jitter on the payload being transported. The jitter shows up on DS1s and DS3s which traverse a SONET system. The mechanism in SONET which does this translation is the STS-1 or VT pointer processors.

One of the benefits of the STS-1 (or VT) payload pointer is to provide the ability for SONET NE's to operate properly in a plesiochronous environment without the need for slip buffers. This avoids the delays and data impairments that can be caused by frame slip buffers. This is accomplished in a similar manner as an M12 (a DS1 to DS2 multiplexer). An M12 can account for differences in DS1 and DS2 frequencies by using positive pulse stuffing technique. But one of the major differences between the STS-1 payload pointer and an M12 multiplexer is that the STS-1 payload pointer operates on the highest theoretical jitter peak with positive/zero/negative stuffing. To further compound this, SONET uses byte stuffing rather than bit stuffing. This causes the waiting time jitter to be an order of magnitude higher than single bit stuffing. As a result, severe jitter can appear in the payload signal. SONET requires sophisticated desynchronizers which can attenuate the 8 bits of phase discontinuity (or jitter) caused by STS-1 (or VT) pointer adjustments.

Important Role of T1X1 Committee

T1X1 has been studying the relationship of synchronization quality, STS-1 pointer adjustment, DS3 payload jitter, and service performance in a hybrid network that will occur while transitioning the network to SONET. It has been through industry cooperation and participation that has help T1X1 solve this complex problem. First, network synchronization measurements needed to be taken in the actual network. Important data on synchronization quality (short-term stability) was not available. Several network providers spent months collecting needed data to help specify synchronization network performance. T1X1 contracted the services of NIST (National Institute of Standards and Technology) to help analyze the data, and NIST provided T1X1 with a new metric on how to specify synchronization quality in the region of interest. This new metric is called Time Variance (TVAR), and is currently being used to specify synchronization performance levels for SONET. In addition, a clock noise model was developed which was based on the characteristics of the synchronization network data. This clock noise model was used to simulate the jitter performance of a DS3 being transported in a hybrid network similar to that shown in Figure 2.

Results of Two Years Work

After collecting synchronization network data and extensive network simulation, it is recommended that the best manner to control DS3 payload jitter accumulation in a hybrid network is to limit the jitter at the source. That is minimize the jitter caused by a single STS-1 pointer adjustment. This would allow network providers to use their existing synchronization network without requiring costly replacement for SONET deployment. In other words,

SONET equipment could be deployed and synchronized with current synchronization network if the proposed tighter DS3 payload jitter specifications are adopted..

The current proposed DS3 payload jitter specification for a single pointer movement is 0.25 unit interval peak-to-peak. This specification is expected to begin the T1X1 letter ballot process by March 1993 and is tighter than the previous proposed 1.5 unit interval SONET payload output jitter specification. But recent analysis has shown that the tight specifications are needed for achieving satisfactory network performance and will most likely be adopted as ANSI standards later next year. The new tighter jitter specification affects the point were DS3s are extracted from a SONET transport system (i.e. at the DS3 input/output conditioning circuits). To avoid and minimize possible network problems caused by excessive jitter, it is important equipment be checked to see if it complies with the new anticipated jitter specification.

Summary

SONET has not only gained national acceptance, but world wide acceptance. The industry understands the benefits that SONET promises to offer with efficient ADM, transport of new broadband services, extensive performance monitoring and fault location capability. But one very important specification overlooked is the DS3 payload jitter specification for SONET. This can have a major impact on quality of service as SONET is deployed in network. Network jitter problems caused by STS-1 pointer adjustment can be extremely difficult to pinpoint. Tighter jitter specification can give the network the margin needed to guarantee grade of services customers are demanding. Network operators need to consider supporting and adopting the 0.25 unit interval single pointer adjustment proposed specification in T1X1 because it will help ensure that proper network performance is maintained as the network migrates towards an all SONET network.

Definitions

Phase Noise -	Perturbations of a digital signal's "1s" and "0s" as compared to an ideal source.
Jitter -	The short term phase variations of the significant instants (e.g. zero level crossings) of a digital signal from their ideal position in time. Here short term implies phase oscillations of frequency greater that or equal to 10 Hz. Jitter is a potential source of bit errors and mis-frames in a digital network.
Wander -	The long term phase variations of the significant instants (e.g. zero level crossings) of a digital signal from their ideal position in time. Here long term implies phase oscillations of frequency less than 10 Hz. Wander is a potential source of slips in a digital network.
Pointer Adjustment -	Technique for accommodating timing differences within SONET.
Pointer Processor -	A device which performs pointer adjustment to frequency synchronize an STS-1 input to an OC-N output rate.
Plesiochronous -	Two signals are plesiochronous if their corresponding significant instants occur at nominally the same rate, any variation in rate being constrained within specified limits. In other words, two signals whose frequency is almost synchronous.
Bit/Byte stuffing -	a technique used to frequency synchronize a signal's rate to some other rate. An M13 uses bit stuffing when multiplexing 28 DS1s to one DS3. A SONET STS-1 pointer processor uses byte stuffing (eight bits at a time) when multiplexing an STS-1 to OC-N output. Both of these techniques cause phase noise in the signal, except byte stuffing is eight times worse.

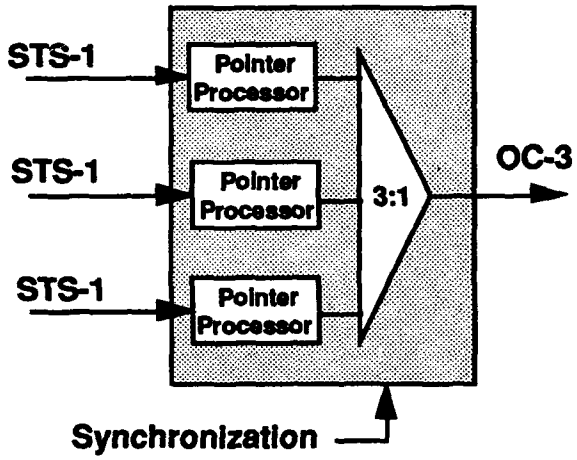

Figure 1: SONET synchronous multiplexing with STS-1 pointer processors

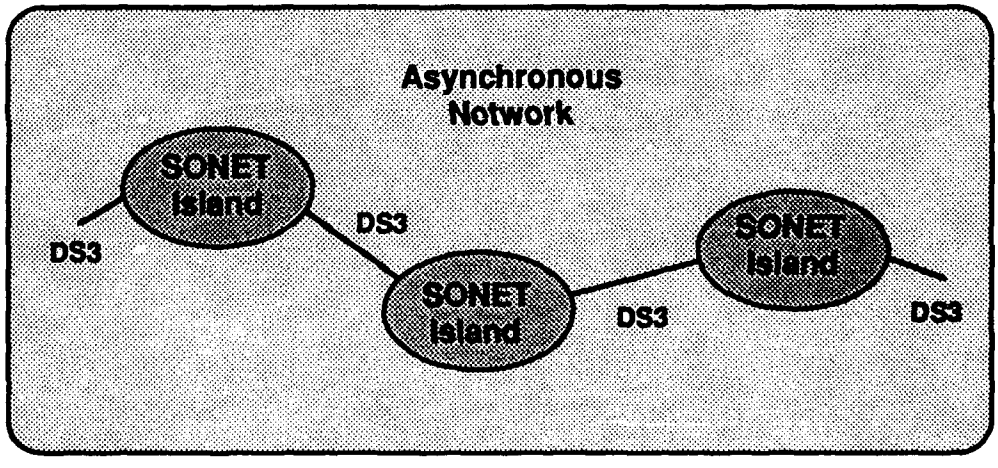

Figure 2: Hybrid Network used to study network DS3 jitter accumulation

QUESTIONS AND ANSWERS

K. Martin, Bonneville Power Administration: I am curious with the SONET why they do that stuffing like that, it seems like it throws all your timing off.

R. Cubbage, Alcatel Network System Inc.: Yes, some hind sight there. we would rather have had bit pointers but if you look at why we do that type of stuffing and SONET. Since we are using synchronous transport systems and synchronous multiplexing, we have to be able to account differences in frequency or phase between an input signal we are multiplexing and the output signal. The way we do in today's switch network is a slip buffer. The only other alternative of using pointer processors is to use a slip buffer. A slip buffer at the SONET rate leads to the DS1 rate. It is only a 193 bits at the DS1 rate. At the SONET rate since it's 51.84 megabits it would be 6,480 bits. So a slip buffer would be over 6000 bits in length and at every transport multiplexing circuit you would have at least 125 microseconds of delay. When you look at the number of elements you would go through in a network, that delay would be unacceptable. So pointer processors, a fraction of a size, minimizes the delay and reduces the buffer storage.

Performance of Low-Cost Commercial Fiber–Optic Transceivers for Reference Frequency Distribution

Richard Dragonette and Joseph J. Suter
The Johns Hopkins University Applied Physics Laboratory
Laurel Maryland 20723-6099

Abstract

Precision time and frequency reference signals have been effectively disseminated using high–quality intricate fiber–optic distribution systems. The quality of signals distributed by such systems is excellent, but the cost of these systems makes them unavailable to many potential users. In this paper, a study of signal quality maintained using inexpensive commercial transmitter/receiver pairs is undertaken. Seven different transmitter/receiver pairs obtained from four different manufacturers have been thoroughly tested using a 5 MHz sinusoid derived from a precision, temperature–controlled, crystal–controlled oscillator. The electrical signal output from each fiber–optic receiver was tested for spectral purity, single–sideband phase noise, and AM noise, and the results are tabulated and discussed without identification of the manufacturer or the equipment model number.

INTRODUCTION

One advantage of maintaining atomic frequency standards is that their reference frequency signals can be distributed to a number of users who need an precision common time base, accurate time, or a local oscillator with minimal long–term drift. At the Applied Physics Laboratory (APL), for example, atomic frequency references are distributed to the calibration laboratory for the calibration of long–term drift in quartz oscillators that are in precision measurement equipment, and also to satellite communications and tracking facilities for use as a local oscillator. One of the difficulties associated with a remotely located atomic frequency standard is that its signals tend to be degraded by transmission over long distances. The time and frequency laboratory at APL, for example, distributes 1, 5, and 10 MHz frequency references to eight facilities over distances up to 3000 feet.

Unfortunately, long interbuilding connections typically share cable trays and underground conduits with digital computer–network cables and 60 Hz power cables. Frequency–reference signals are often badly distorted by induced electrical interference as they are distributed via coaxial cables. At APL, for example, the 60 Hz sine wave superimposed on some distributed 5 MHz signals was large enough to trigger, and be displayed by, an oscilloscope.

A typical application at APL usually requires the distribution of both 5 MHz and 1 pps signals in the same cable bundle. When these signals travel side by side for 3000 ft in parallel coaxial cables, the potential for cross talk exists.

To minimize electrical interference and distortion, construction of a multichannel fiber–optic transmission network was initiated at APL. Currently over 75 channels of information (including 1, 5, and 10 MHz frequency references, and IRIG B and 1 pps reference signals) are distributed by APL's time and frequency laboratory; 30 of these lines are interbuilding connections. Monetarily, it is impractical to implement 30 interbuilding connections with customized analog fiber–optic links, which would cost thousands of dollars per channel. We therefore began testing inexpensive commercial fiber–optic transmitters and receivers that were designed for video signal transmission as a means of disseminating our reference signals.

In this study, seven different fiber–optic transmitter/receiver pairs from four different manufacturers were tested to verify the extent to which they degrade the single-sideband phase noise, harmonic distortion, spurious noise, and AM noise of a 5 MHz sinusoid derived from a precision, temperature–controlled, crystal–controlled oscillator. The test results are summarized here without identification of the manufacturer or the model number. The systems we tested ranged in price from $600 to $10,000 per transmitter/receiver pair, with most of the systems priced at the low end of that range. The prices per transmitter–receiver pair of the systems were as follows:

System A	$600	System B	$700
System C	$700	System D	$2850
System E	$3800	System F	$10,000
System G	$700		

By comparison, the cost of APL's commercial 50Ω buffer–amplifier system with coaxial–cable distribution (when fully populated, resulting in minimum cost on a per–channel basis) is approximately $350 per channel.

APL currently maintains 14 fiber–optic distribution lines, consisting exclusively of equipment costing less than $1000 per transmitter/receiver pair. In each case, the fiber–optic systems have improved the reliability of signal transmission through the elimination of either electrical surges caused by induced voltages (such as lightning) or mismatched terminations (or a direct short) by the user at his end of the distribution cable. Fiber–optic distribution has also drastically improved the quality of the distributed signals by greatly reducing electrical interference.

EXPERIMENTAL PROCEDURE

The seven systems tested here are designated System A through System G. The output of each system was tested for single–sideband phase noise performance, harmonic and spurious noise, and AM noise. All tests were performed using the transmitter/receiver pair to transmit a low–phase–noise 5 MHz sinusoid derived from a precision, temperature–controlled, crystal–controlled oscillator. The same reference oscillator was used to test each system and to determine the noise floor of each. The oscillator was used instead of an atomic frequency standard because it exhibits better phase–noise performance and lower–level harmonics in its output than does a typical atomic frequency standard. The oscillator's performance is illustrated in Figures 1, 2, and 3.

For the tests, each transmitter and receiver pair was connected by a short fiber-optic cable (less than 50 feet long). When possible, the tests were repeated using a 3200 ft, 250/62.5μm diameter

multimode fiber. When availability allowed, more than one transmitter/receiver pair representative of each system was tested.

Phase noise tests were conducted using an HP3048A phase noise test system, which was calibrated (traceable to NIST) to be accurate to within ±2 dB over the frequency range of interest. The fiber–optic systems were tested over the frequency range of 0.1 Hz to 100 kHz from the carrier frequency. The results of each test are presented individually in graphical form and are discussed collectively. It is clear from Figure 1 and Figures 5a through 10a that the fiber–optic systems measurably degraded the phase noise of the reference oscillator at frequencies greater than 1 Hz from the carrier.

In some phase noise tests, buffer amplifiers were required to maintain specified signal levels. Whenever buffer amplifiers were used, the HP3048 phase noise system was recalibrated with the amplifiers included to ensure that the noise floor of the system with the buffers was well below that exhibited by the outputs of the fiber–optic systems. AM noise tests were also performed using the HP3048A phase noise system over the frequency range of 1 Hz to 100 kHz from the carrier frequency.

The spectral purity of the reference oscillator and the systems under test was verified with an HP8560A spectrum analyzer that was set for a frequency range of 1 to 51 MHz, with a video bandwidth and resolution bandwidth of 10 kHz. These settings provided a clear picture of the frequency spectrum of the devices under test.

The single–sideband phase noise of the reference oscillator used throughout the testing is shown in Figure 1, a plot of its spectral purity appears in Figure 2, and its AM noise is presented in Figure 3. As will be seen, the reference oscillator exhibits much better phase noise performance beyond 1 Hz from the carrier and has a much cleaner frequency spectrum than any of the fiber–optic systems can maintain, so the numbers seen in the test results are truly attributable to the optical transmitters and receivers being tested.

DESCRIPTION OF THE SYSTEMS

SYSTEM A

System A consists of a stand–alone transmitter and receiver pair that cost $600. Three identical models were available and tested. The system uses an LED light source at 850 nm for light transmission, and light is transmitted through 205/62.5-μm diameter multimode fibers. The system has an input frequency range of DC to 60 MHz, and its electrical output can be adjusted from 50 mV to 2 V p-p.

SYSTEM B

System B consists of a rack–mounted system that costs approximately $700 per transmitter/receiver pair when the rack chassis is fully populated. The rack chassis holds approximately 10 plug–in cards, with up to two transmitters or receivers on each card. Its operational frequency range is from near DC to 20 MHz, with an electrical output amplitude that is adjustable up to 3 V p-p. This system uses an LED operating at 850 nm as its light source and 62.5 μm multimode fibers connected the transmitter and receiver. Two System B transmitter/receiver pairs were available for testing. The performance of this system was partially limited by the presence of noise added by a 1 pps signal

being distributed by a transmitter on the same chassis, although the manufacturer claims that this system is capable of distributing both sinusoidal and pulsed signals from the same chassis.

SYSTEM C

System C consists of the same equipment as System B, but with the transmitter distributing the 1 pps signal removed. There is a noticeable improvement in the system's performance with the removal of the 1 pps signal lines. A comparison of the system with and without the 1 pps lines active is important because it is not uncommon for a timing station to distribute both 5 MHz frequency references and 1 pps timing references.

SYSTEM D

System D consists of a stand–alone transmitter/receiver pair that costs $2850, and operating with an 1300-nm LED as its light source. Only one transmitter/receiver pair of this type was available. The system's frequency range is 5 to 125 MHz, and its electrical output is approximately -10 dBm. Connector incompatibility prevented this system from being tested over the 3000 ft cable.

SYSTEM E

System E consists of a stand–alone transmitter/receiver pair that costs $3800. This system uses a 1350-nm laser transmitter and single-mode optical fiber for interconnection; therefore, it could not be tested with the 3000-ft multimode cable. Only one such system was available for test. Its operating frequency range is 5 to 300 MHz, with an output power near -25 dBm.

SYSTEM F

System F is also a stand–alone system using a 1350-nm laser light source, and single-mode optical fiber interconnection. The system costs $10,000 per channel, and only one transmitter/receiver pair was available. Its operating frequency range is 5 MHz to 3 GHz.

SYSTEM G

System G is a rack–mounted system that consists of a chassis with ten plug–in slots, and the ability to house two transmitters or receivers in each slot. When the chassis is fully populated, the system costs $700 per channel, and uses an 850-nm LED as a light source. Although similar, System G and System B were supplied by different manufacturers.

EXPERIMENTAL RESULTS

The results of the single–sideband phase noise tests and spectral analyses of each individual system appears in Figures 5 through 11, and is summarized in Table 1. Figure 5a shows the single–sideband phase noise of System A's output when transmitting the reference oscillator through a short optical fiber, and Figure 5b shows the spectral purity of its output when transmitting the same signal. Figures 6 through 11 show the similar two measurements for Systems B through G, respectively. Table 2 summarizes the AM noise measured in the outputs of the reference oscillator and in the fiber–optic links as a function of frequency.

Three pairs of System A equipment were available for testing. Each one was tested with both a 10 ft and a 3200 ft multimode fiber. Figure 5 is representative of the results of the six test runs performed on System A. The single–sideband phase noise curves obtained from all three receivers with the long and short fibers exhibited a noise floor of 115 ± 4 dBc/Hz for frequencies greater than 10 Hz from the carrier frequency. In all three cases, the phase noise floor was 2 to 3 dB lower when the 3200 ft fiber was used for signal transmission.

The frequency spectrum shown in Figure 5b is typical of that seen in all six tests of the transmitter/receiver pairs of the type used in System B. The first harmonic ranged from 36 to 50 dB below the carrier, and the second harmonic ranged from 35 to 45 dB below the carrier. The higher harmonics were insignificant, if present at all, and there were no cases with spurious signals other than those that were harmonically related.

The excessive spurious signals seen in the phase noise characteristic of System B (Figure 6a) were caused by the presence of a 1 pps transmitter in the rack chassis used to supply power to the plug–in transmitter–receiver pairs under test. Two pairs of equipment were available for testing, and both showed similar phase noise response; the phase noise of the two transmitter/receiver pairs were within 3 dBc/Hz of each other. The presence of the 1 pps transmitter in the system chassis caused an excessive number of spurious signals in the systems phase noise between 5 and 100 Hz; similar spurious signals were seen over the same frequency range in the AM noise measurements for System B. In both receiver's outputs, the first and second harmonics are between 37 and 44 dB below the carrier.

In order to find the ultimate performance of the equipment being tested, the tests were repeated with the 1 pps transmitter removed from the rack chassis that housed the transmitter/receiver pairs. After the 1 pps transmitter was removed, the System B equipment was redesignated as System C to differentiate the test results from the original System B tests. When the systems were tested with a short optical fiber interconnection, the first System C transmitter/receiver pair achieved a noise floor of -115 dBc/Hz. The second System C transmitter/receiver pair exhibited a noise floor of -125 dBc/Hz, 10 dBc/Hz below the noise floor the same transmitter/receiver pair achieved with the 1 pps transmitter in the chassis. Phase noise tests were repeated with the 3200 ft optical fiber, a length slightly longer than System C's specified range, which resulted in the phase-noise floor rising to -100 dBc/Hz.

The first harmonic was roughly 45 dB below the carrier level, and the second harmonic was near 50 dB below the carrier. As is evident by comparing Figures 7b and 8b, the noise floor in the frequency spectrum of System C was 10 dB below that of System B, showing the effect of the 1 pps signal's presence in System B.

Only one transmitter/receiver pair representative of System D, System E, and System F were available for testing. System D and System E were manufactured by the same manufacturer for analog transmission over a similar frequency band. The primary difference between the systems is the light source; System D uses an LED and System E uses a laser. Both systems achieved a noise floor of -120 dBc/Hz. The first and second harmonics in the output of System D were 40 and 50 dB below the carrier level, respectively, whereas in System E both the first harmonic and the second harmonic were 37 dB below the carrier level.

System F, which is considerably more expensive than all the other systems, exhibited a noise floor of

-125 dBc/Hz, with the first and second harmonics 38 and 50 dB below the carrier level, respectively.

System G has 75-Ω electrical inputs and outputs, but both the reference oscillator and the HP3048A are configured for 50-Ω systems, requiring impedance matching networks to interconnect the devices. In is possible that those impedance matching networks may have limited the test results of System G, although its measured performance compares favorably with the other systems. System G exhibited a single–sideband phase noise floor of -118 dBc/Hz, with the first harmonic 36 dB below the carrier level.

As can be seen in Table 2, each of the transmitter/receiver pairs significantly degraded the AM noise characteristics of the reference oscillator. With the exception of System B, each system achieved an AM noise floor in the neighborhood of -120 dBc/Hz. The reference oscillator's AM noise floor was closer to -150 dBc/Hz. No AM noise measurements were made on System A. During the time System A was available for testing, the AM noise measurement system was being calibrated and was not available for use.

CONCLUSIONS

The most interesting result of testing these many fiber–optic systems is that they all achieved a single–sideband phase noise floor of -115 to -125 dBc/Hz. This noise floor was amazingly consistent across the tests even though these systems used different light sources and frequencies, they varied widely in cost, and they were manufactured by many different manufacturers. Since a number of examples representative of Systems A and C were available, they were tested in the full permutation of configurations; that is, System A transmitter 1 was tested with System A receiver 1, 2, and 3, *etc.* From these tests, it is clear that, at least for these systems, the phase noise in the output signal is not completely limited by either the transmitter or the receiver, but rather by a combination of both elements.

It is also interesting to note that fiber–optic cable length can have a measurable effect on the signal quality. As was seen in System A, for example, the phase noise for frequencies greater than 10 Hz from the carrier frequency was approximately 3 dBc/Hz lower at the longer fiber lengths than it was for the shorter fibers.

It is clear that all the fiber–optic systems significantly degrade the single–sideband phase noise, AM noise, and harmonic distortion of a quality oscillator. The levels of performance achieved by these systems is acceptable for reference frequency distribution if the transmitted signals are being used as a common time base for test equipment, or as a reference for a system that phase locks its own internal voltage controlled oscillator to the transmitted reference.

BIBLIOGRAPHY

[1.] R. Simons, Optical Control of Microwave Devices, Artech House, Boston (1990).

[2.] E. Udd, Fiber Optic Sensors, John Wiley, New York (1991).

[3.] H. W. Yen et al., *"High-Speed Optical Modulation Techniques"*, Optical Technology for Microwave Applications II, SPIE, 645, 2-9 (1985).

[4.] G. Keiser, Optical Fiber Communications, McGraw-Hill, New York (1983).

Table 1. Single-sideband phase noise performance of the fiber-optic systems.

	Single-sideband phase noise (dBc/Hz)							
Freq. (hz)	Reference	System A	System B	System C	System D	System E	System F	System G
0.1	- 90	- 85	- 90	- 90	- 90	- 90	- 90	- 80
1	-120	-115	-115	-115	-115	-110	-117	-113
10	-145	-115	-116	-125	-120	-118	-124	-118
100	-152	-115	-116	-125	-120	-118	-124	-119
1k	-153	-115	-116	-125	-119	-119	-124	-119
10k	-153	-115	-116	-125	-120	-119	-124	-119
100k	-153	-115	-116	-125	-118	-119	-124	-119

Table 2. AM noise response of the fiber-optic systems.

	AM noise response (dBc/Hz)						
Frequency (Hz)	Reference	System B	System C	System D	System E	System F	System G
1	-125	-112	-115	-108	-90	-120	-110
10	-133	-115	-121	-110	-100	-120	-115
100	-140	-112	-121	-115	-105	-120	-117
1000	-148	-113	-120	-118	-115	-120	-117
10k	-153	-112	-119	-118	-120	-120	-117
100k	-154	-111	-117	-118	-120	-120	-117

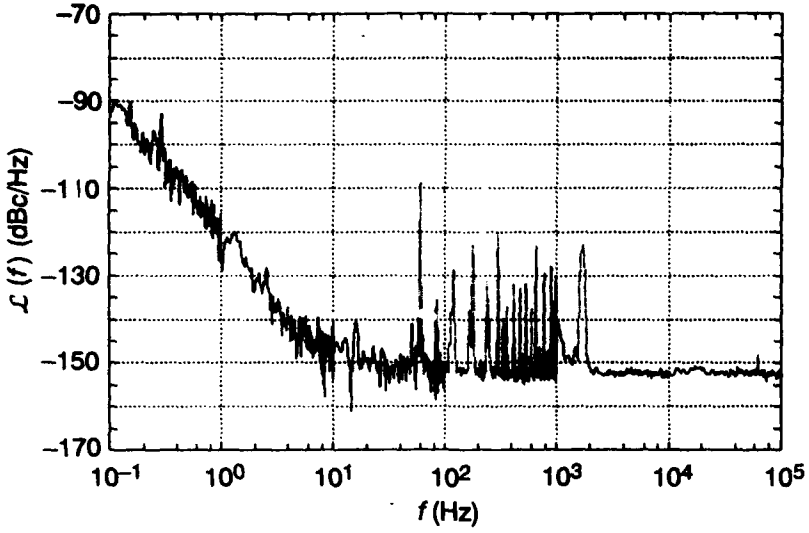

Figure 1. Reference oscillator single-sideband phase noise.

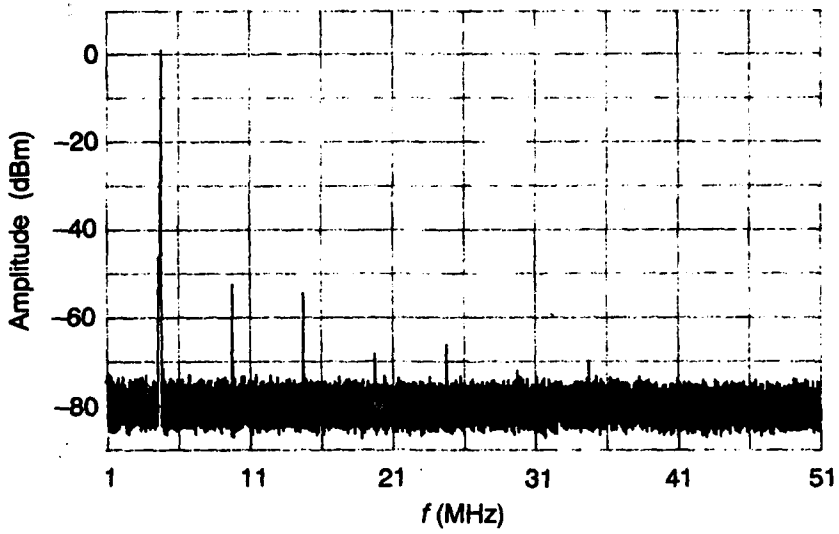

Figure 2. Reference oscillator frequency spectrum.

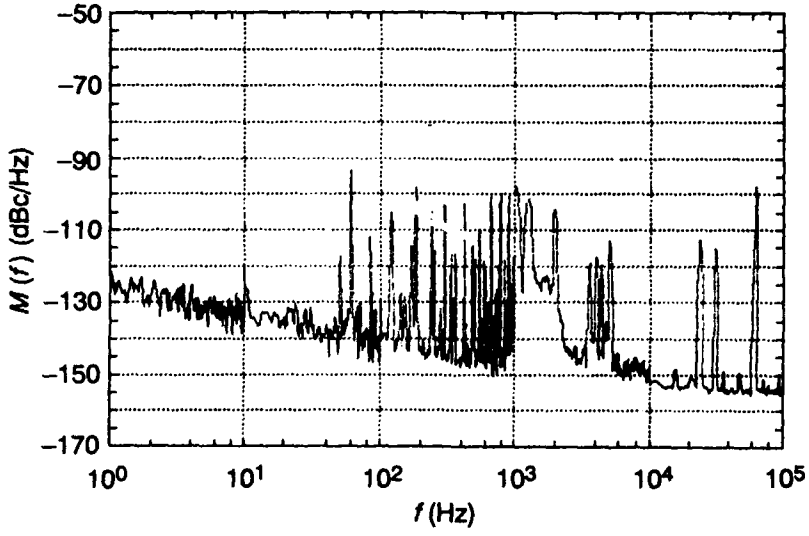

Figure 3. Reference oscillator AM noise.

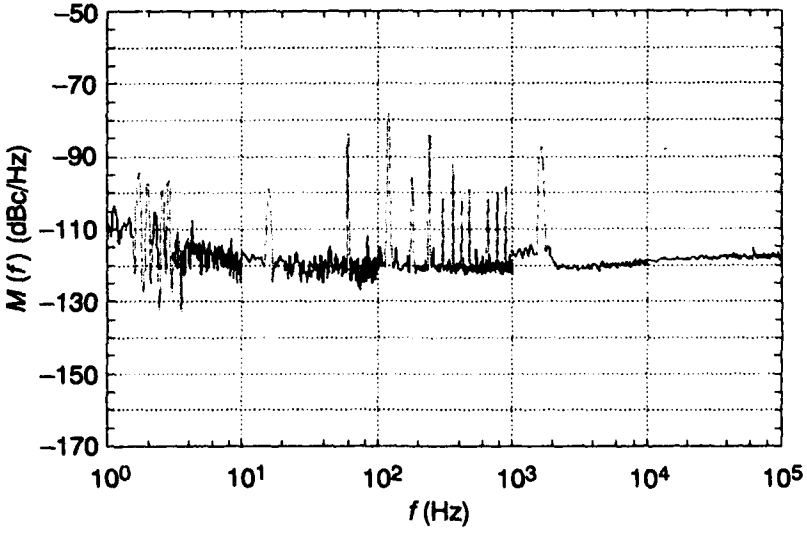

Figure 4. System C AM noise.

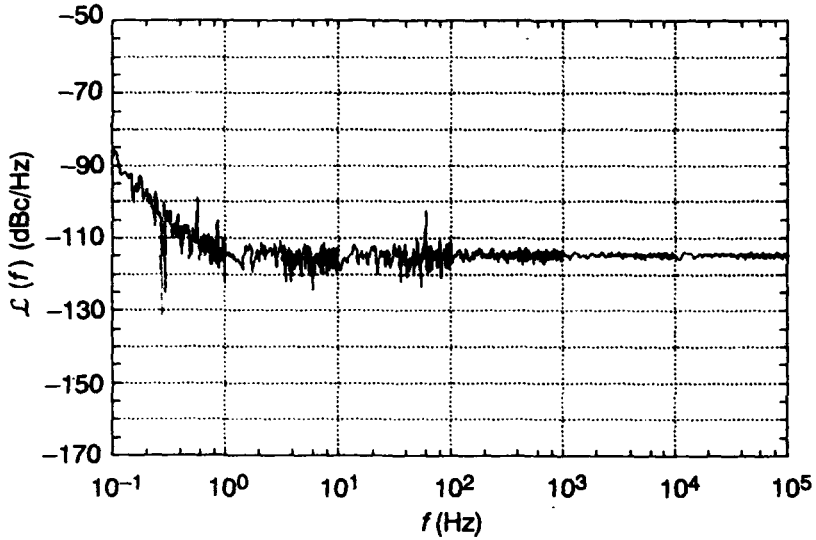

a. Single-sideband phase noise.

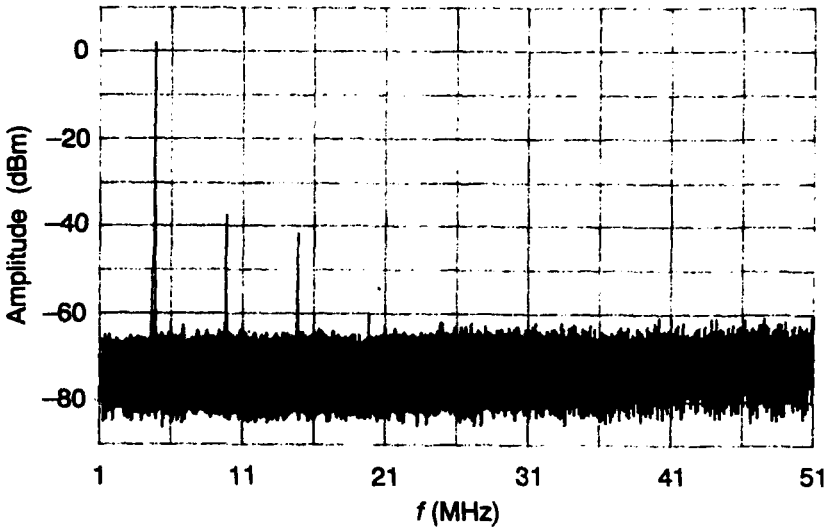

b. Output frequency spectrum.

Figure 5. System A performance.

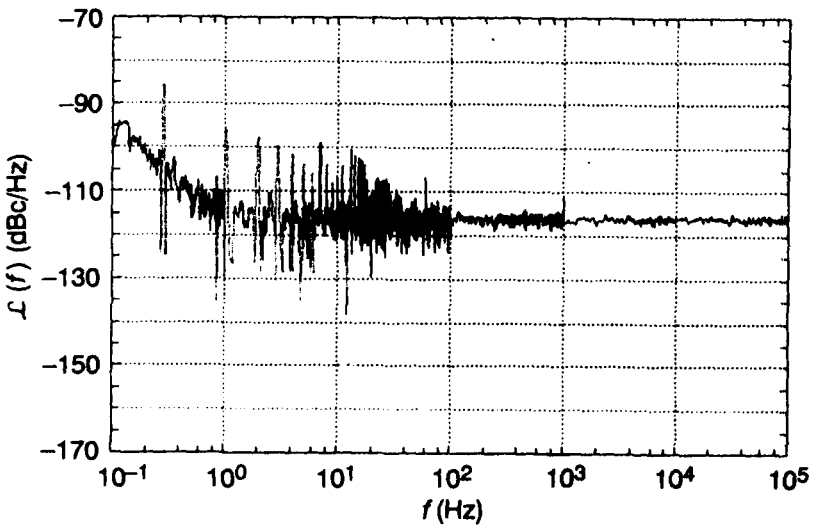

a. Single-sideband phase noise.

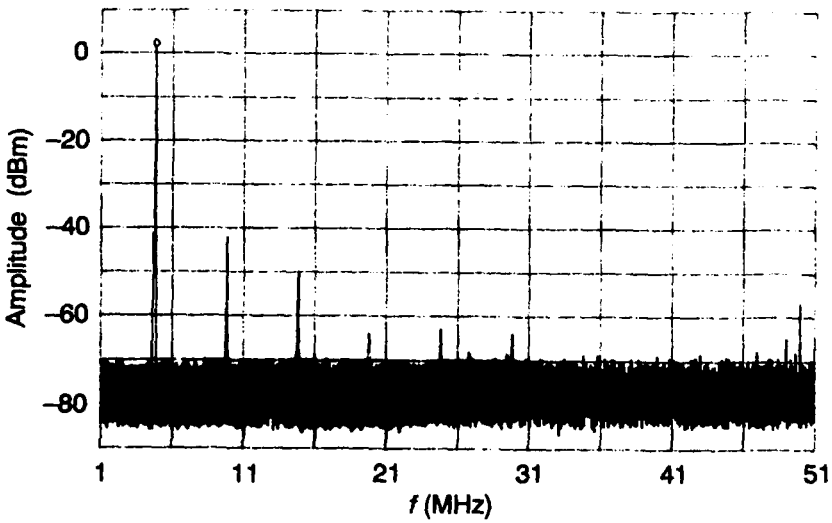

b. Output frequency spectrum.

Figure 6. System B performance.

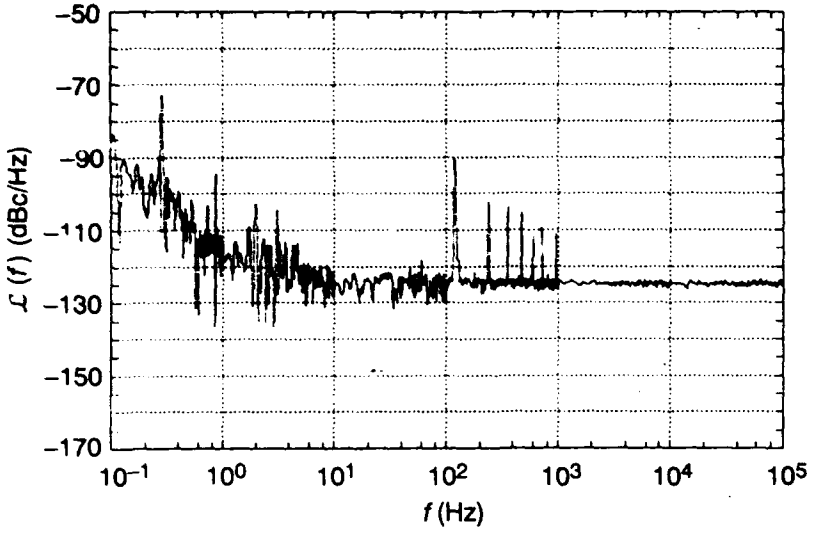

a. Single-sideband phase noise.

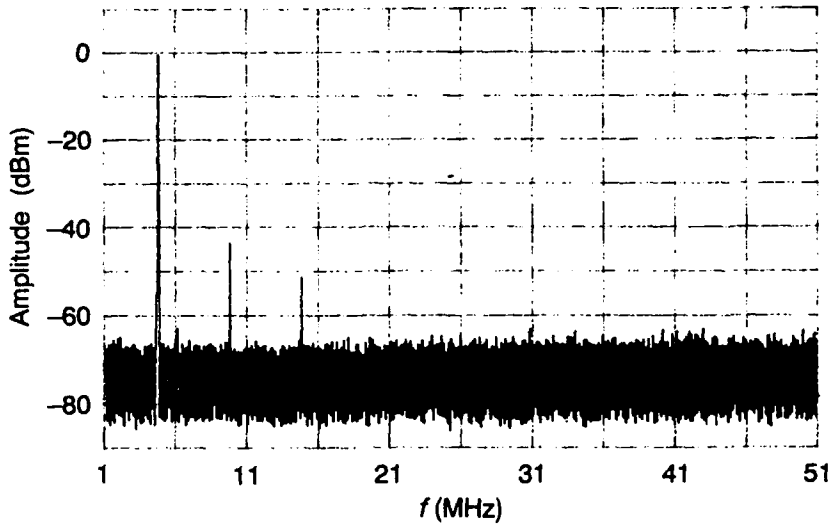

b. Output frequency spectrum.

Figure 7. System C performance.

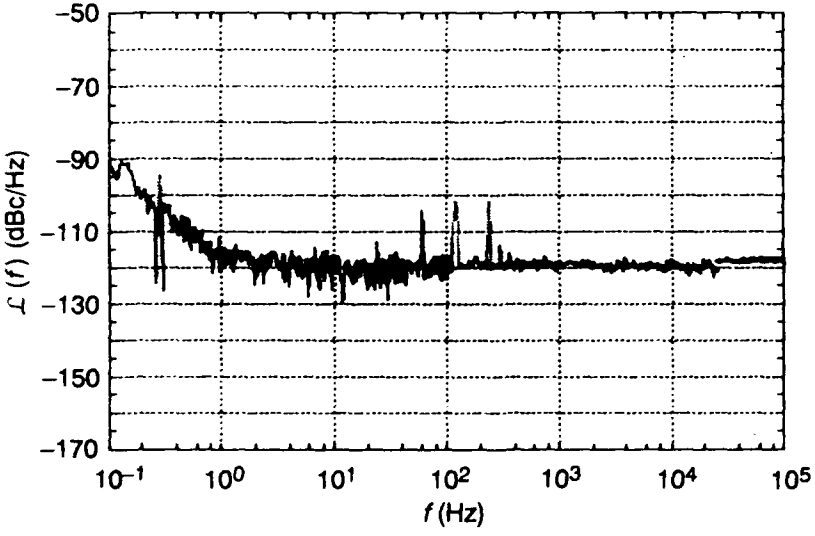

a. Single-sideband phase noise.

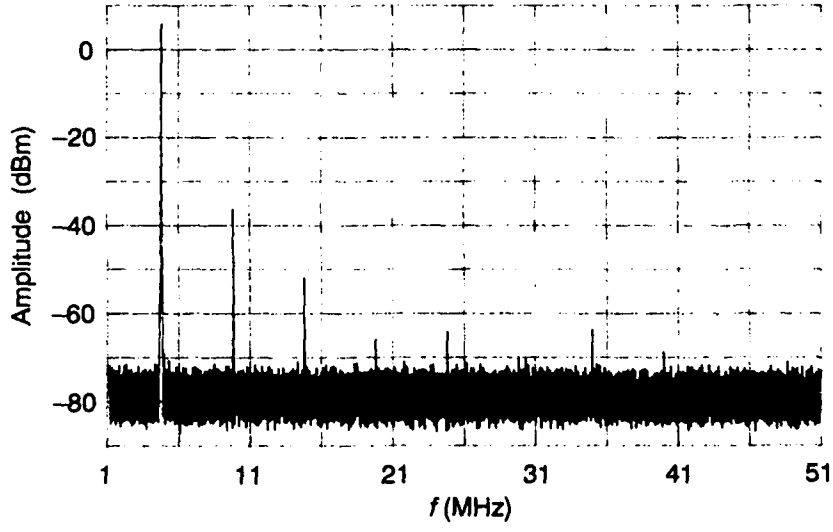

b. Output frequency spectrum.

Figure 8. System D performance.

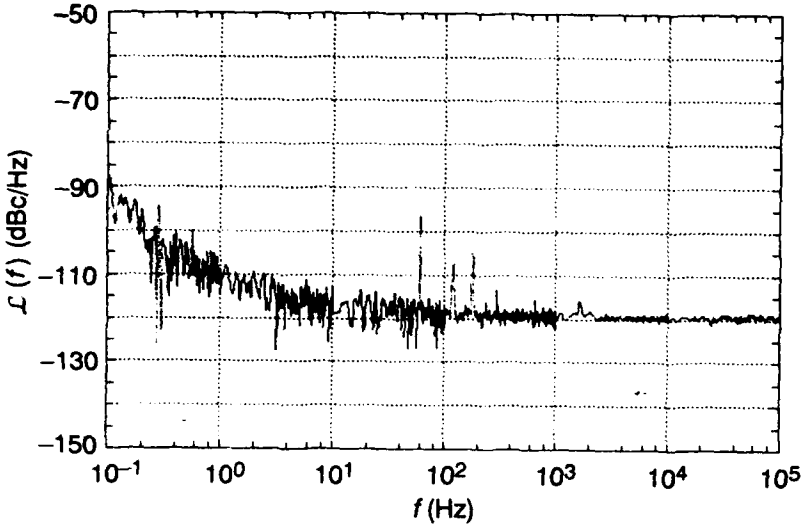

a. Single-sideband phase noise.

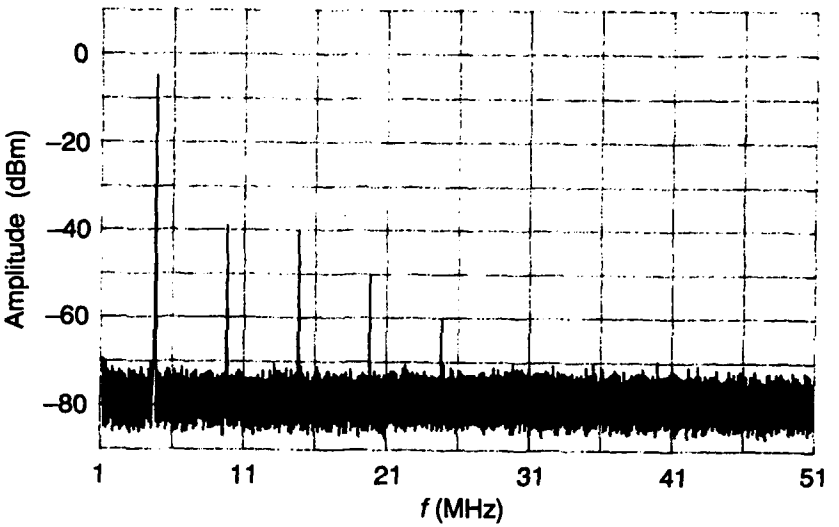

b. Output frequency spectrum.

Figure 9. System E performance.

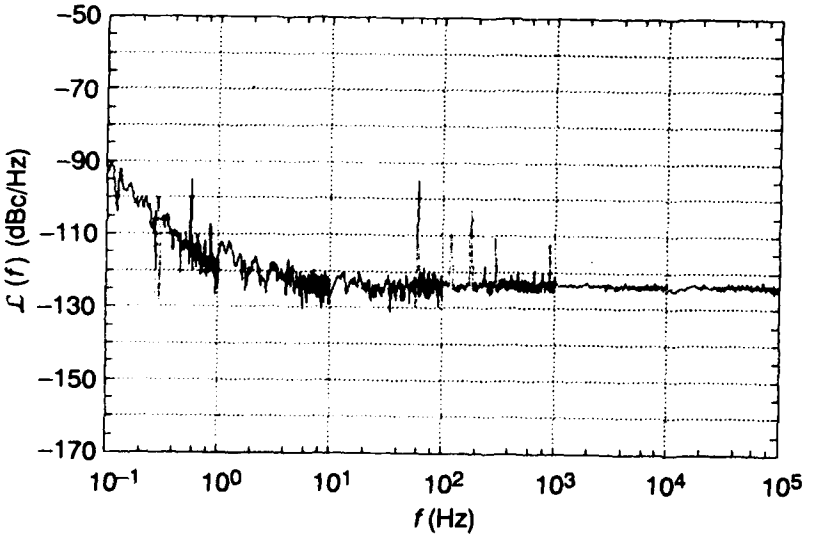

a. Single-sideband phase noise.

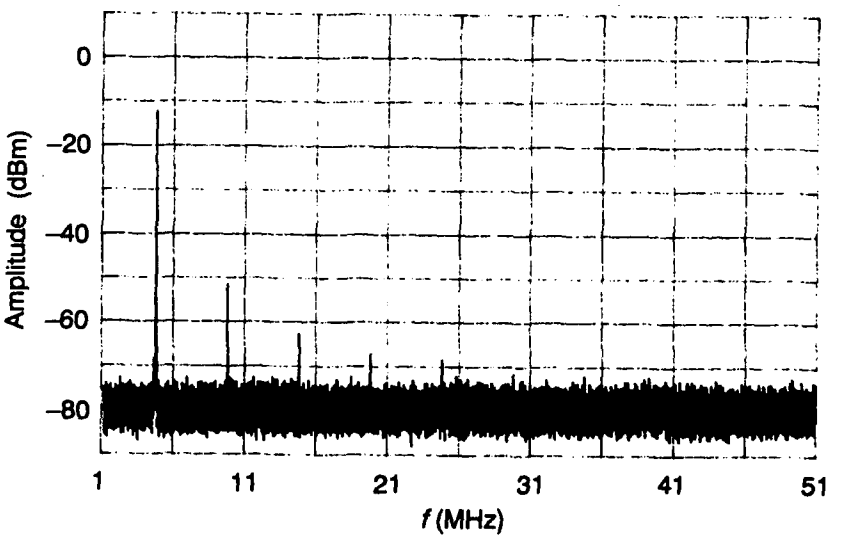

b. Output frequency spectrum.

Figure 10. System F performance.

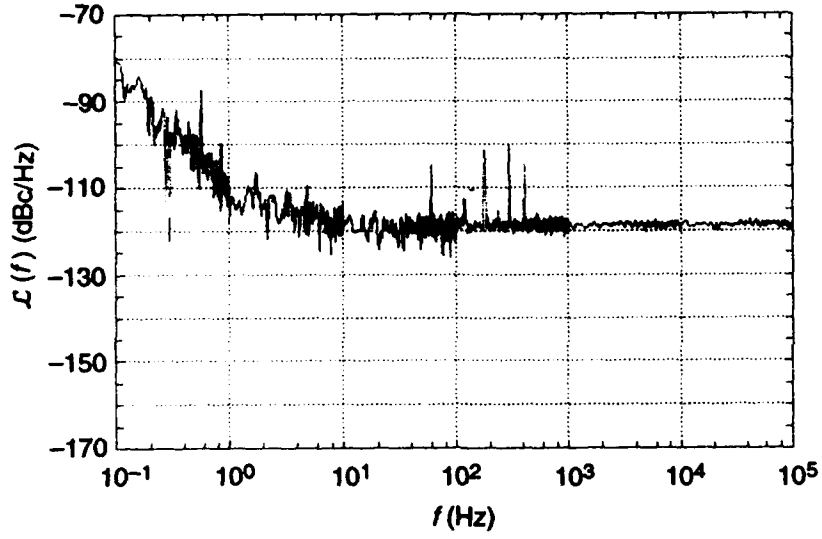

a. Single-sideband phase noise.

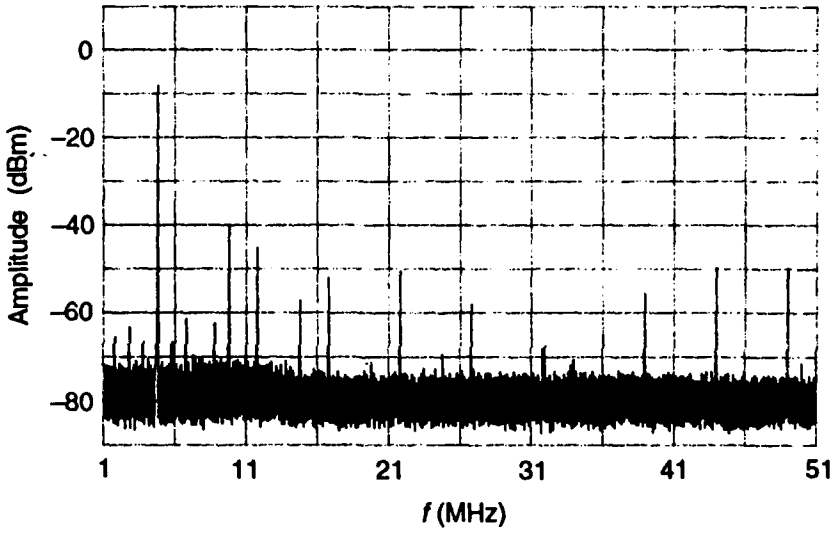

b. Output frequency spectrum.

Figure 11. System G performance.

QUESTIONS AND ANSWERS

Question: In many cases it's a noise performance characteristic which is not only parameter of interest and have you also checked the delay stability for example with dependence on

Answer: We didn't do that in this particular test because our particular application is to use as a frequency reference, we're not really worried about the delay so much between the start and stop as we are as just a clean signal for for the user. It's also because these systems were demo and some of the demos were borrowed systems so I didn't have a good underground insulation to test a lot of the good thermal chamber to test temperature fluctuations. So no we didn't do this test.

Bill Riley, EG&G: It would seem that one of the advantages of using the fiber optic distribution would be to avoid hum. That wasn't really apparent in your data, I assume that most of those power lines spurs were from the measuring system but could you comment on the effectiveness of that length to avoid hum contamination?

Answer: Yes, that was the primary reason we sort of go into these systems because some of our clocks and lines where you could see 60 Hz superimposed on the signals, and the fiber optics obviously are immune to that but the problem you have to be careful of is that the receivers and transmitters aren't immune so you have to watch the chassis. The spikes and the plots were due to the phase and measuring system because it's plugged into a 60 Hz power supply so of course it's got hum. But the system is very effective in illuminating that cause the same we basically have parallel lines of coax and the fiber and the coaxial lines are essentially useless because there is almost as much 60 Hz as there was 5 MHz. And when we replace the same lines we're into the same conduits with these fibers and these transmitters. The signals are now you know they are fine, they're useable in the automatic about two years of use. They perform admirably. So they are definitely good for illuminating that as long as you keep your transmitter power supplies isolated from 60 Hz noise.

ULTRASTABLE REFERENCE FREQUENCY DISTRIBUTION UTILIZING A FIBER OPTIC LINK*

MALCOLM CALHOUN and PAUL KUHNLE
California Institute of Technology
Jet Propulsion Laboratory
Pasadena, California 91109

Abstract

The Frequency Standards Laboratory at the Jet Propulsion Laboratory (JPL) is responsible for the generation and distribution of ultra-stable reference frequency in NASA's Deep Space Network (DSN). Certain assemblies and components of the Radio Science and VLBI systems are located in the cones of tracking antennas hudreds of meters from the Frequency and Timing Subsystem's frequency standards. The very stringent requirements of these users challenge the performance of state-of-the-art frequency sources as well as the associated signal distribution system. The reference frequency distribution system described in this paper is designed around a low temperature coefficient of delay (TCD) optical fiber. On-site measurements of the fiber optic link alone indicate 100 MHz phase noise performance on the order of -120 dBc at 1 Hz from the carrier and Allan deviation on the order of parts in 10^{16} at 1000 seconds averaging time. The measured phase noise and stability of the link indicate that the performance characteristics of the hydrogen maser frequency standards are not degraded by the distribution system. Thus, optical fibers and electro-optic devices as distribution media appear to be a viable alternative to the classical coaxial cable distribution systems.

INTRODUCTION

Reference signals for Radio Science experiments in the NASA/JPL Deep Space Network are provided by hydrogen masers. These masers are located centrally at the DSN tracking stations in a controlled environment. The signals which drive the Radio Science local oscillators and up/down convertors must maintain maser quality for equipment which is located hundreds of meters from the maser source and in an environment which subjects this equipment to temperature variations as well as vibration. Cable runs from the base of the antennas to the cone areas may be exposed to a temperature differential as great as 40° C over a twelve hour period. Additionally, the equipment located in the antenna is subjected to mechanical vibration and flexing of the cables. Reference

*This work represents one phase of research carried out at the Jet Propulsion Laboratory, California Institute of Technology, under a contract sponsored by the National Aeronautics and Space Administration.

frequency distribution via coaxial cable does not provide the required stability at the point of use for some of the more sophisticated deep space investigations such as very long–base interferometry (VLBI), gravity waves, and planetary rings and occultation experiments. This paper describes a reference frequency distribution scheme which has proven to be a successful alternative to methods used previously. The new distribution system is based upon a single–mode fiber optic link employing a temperature compensated fiber along with state–of–the–art electro–optic devices. The fiber optic reference frequency distribution has been installed and tested at two DSN antennas and is scheduled for installation at four more locations.

DESIGN APPROACH

The terminal equipment hardware in the distribution links consists of single–mode laser transmitters located near the frequency standards in the DSN Signal Processing Center (SPC); compatible fiber optic receivers are located at the antennas near or in the cone areas. In addition to the optical transmitters and receivers, operational requirements dictate that certain critical system parameters be monitored and made available to DSN operations personnel at the SPC. Figure 1 is a block diagram of the fiber optic reference frequency distribution assembly showimg the major subassemblies and their locations.

A 100 MHz reference frequency signal derived from the station's primary frequency standard (typically, a hydrogen maser) is applied to the fiber optic transmitter unit. The 100 MHz signal is applied to a laser diode through a rf matching network where the light intensity is varied by direct intensity modulation. The principal component of the transmitter is a single–mode, distributed feedback (DFB) laser diode with an integral optical isolator [1]. The laser is commercially available as a modular unit including bias circuitry and temperature control. A second optical isolator external to the laser provides approximately 60 dB isolation to prevent optical back–reflection from degrading the laser performance. The laser emits light at 1300 nm which is launched into a single–mode optical fiber; optical interfaces between the system optical fiber and the transmitter and receiver employ slant–polished connectors to reduce back reflection. The rack–mounted fiber optic transmitter along with the monitor interface and monitor computer are located in the control room of the SPC.

The fiber optic receiver is located several hundred meters from the transmitter in the cone area of the antenna. The photodetector in the receiver is optically matched to the 1300 nm light signal from the transmitter. The impinging 1300 nm light is converted from optical to 100 MHz rf at the p–i–n photodetector. The optical loss over the fiber between the transmitter and receiver typically is less than 1 dB, thus care must be exercised to prevent overdriving the photodetector. An optical attenuator located in the transmitter unit is set so that the received optical power is approximately 1 mW, resulting in -30 dBm of at the photodiode output. A low–noise rf pre-amplifier is employed to raise the signal to a higher level for subsequent distribution to users. A low–pass filter is used to mitigate any non–linear effects of the laser diode and photodetector. Typically, second and third harmonics of the 100 MHz output signal are 45 dB or more below the fundamental. The 100 MHz reference signals to the users are distributed through low–noise power amplifiers which provide greater than 100 dB isolation between output ports. Temperature control has been provided at the receiver since the antenna location is subject to variations in temperature. A

Peltier temperature device, temperature sensor, and control circuit provide a factor of twenty–five times reduction in ambient temperature effects. The optical receiver and the rf distribution circuits are contained within an emi/rfi shielded box to prevent stray rf radiation and/or magnetic fields from corrupting the 100 MHz signal. Measurements made in the field indicate that the distributed reference signals are virtually free of non–harmonic spurious signals including power line related frequencies.

Power supplies for the fiber optic receiver assembly are located in a separate emi/rfi shield box to isolate them from the receiver. The power supply assembly also houses the data acquisition circuits for the monitor functions. Monitor signals are feed from the antenna to the SPC via multi–mode fiber optic modems.

DISTRIBUTION SYSTEM OPTICAL FIBER

The longest run of fiber optic cable in the network is approximately 800 meters. Surface temperature variations at the stations are so great that exposed cable trays cannot be used for reference frequency distribution cable runs. In order to minimize phase variations due to temperature effects on the cable, the optical fiber cable run is in a duct which is underground at a depth of 1.5 meters. Temperature profiles of the ground near the antenna indicate that at this depth the cable is not affected by diurnal variations in temperature; however, seasonal effects are observed. The cable run from the base of the antenna to the cone area is exposed to the maximum outside temperature variation. This cable run is between 50 and 70 meters in length.

The optical fiber used in this distribution system is a special commercial fiber which has been treated to reduce the temperature coefficient of delay (TCD). Measurements in the laboratory indicate that the TCD of this particular fiber is approximately 0.3 ppm/°C for temperatures below 25°C and less than 1 ppm/°C in the range from 25°C to 35°C [2]. The TCD of typical commercial optical fiber is approximately 7 ppm/°C while the coaxial lines used presently for reference distribution are 15 ppm/°C or greater. Thus, the special low TCD optical fiber performs very well in locations where there are extremes of temperature such as exposed cable runs on the antennas. Figures 2 and 3 show results of tests using the low TCD optical fiber under operating conditions at DSS 14. The test period for the data shown in the figures is three days. Figure 2 shows the actual phase variation at 100 MHz. Stability test results are shown in the Sigma–Tau plot of Figure 3. The hump in the Allan deviation is due to the diurnal temperature variations. Note that the 1000 second Allan deviation is just slightly greater than 1 part in 10^{16}. During this test, surface temperature variations were 30°C peak–to–peak over a twelve hour period.

LINK PERFORMANCE RESULTS

Following installation of the fiber optic distribution equipment and cables at Deep Space Station 15 (DSS 15) and Deep Space Station 45 (DSS 45) extensive testing was done to verify that system requirements were satisfied. Figure 4 is a graph of phase noise spectral density at DSS 15. The single–sideband power spectral density at 1 Hz from the carrier frequency of 100 MHz is -120 dBc with a floor of -140 dBc; the Radio Science System requirement at the receiver first local oscillator is -92 dBc with a floor of -125 dBc. Thus, the fiber optic reference frequency distribution does not

degrade the noise performance of the reference signal from the hydrogen maser.

Figure 4 is a plot of Allan deviation for the same distribution link. It is worth noting that a second test link from the antenna to the SPC was employed in order to measure Allan deviation and phase noise since there is no better quality reference signal available at the antenna. The test link carries the reference signal from the distribution amplifier at the output of the receiver in the antenna back to the reference maser at the SPC. Thus, the actual stability of the reference signal as graphed in Figure 4 is better by at least 3 dB due to the extra test link used. Stability measured at 1000 and 3600 seconds indicate approximately 2 parts in 10^{16} which is an order of magnitude lower than Radio Science System requirements.

SUMMARY

Fiber optic reference frequency distribution installations at two of six DSN stations are complete with the remaining four to be installed in 1993. Low TCD optical fiber must be employed in the link to meet stability requirements. The bulk of the cable run between the SPC and the antenna is underground at a depth of 1.5 meters. An alternative to the low TCD optical fiber is active phase stabilization of the fiber links [3]. Test results indicate that fiber optic reference frequency distribution is superior to coaxial cable and that stability and noise performance requirements for very sophisticated radio science experiments can be met.

REFERENCES

[1] Operator's Manual, Model 3612B Laser Transmitter, ORTEL Cororation

[2] Data Heet #88–31 supplied to Jet Propulsion Laboratory by Sumitomo Electric Industries, Inc, June 1, 1988

[3] D. Johnson , M. Calhoun, R. Sydnor, and G. Lutes, "A Wide–band Fiber Optic Frequency Distribution System Employing Thermally Controlled Phase Compensation," Proceedings 24th Annual Precise Time and Time Interval Applications and Planning Meeting, December 1992.

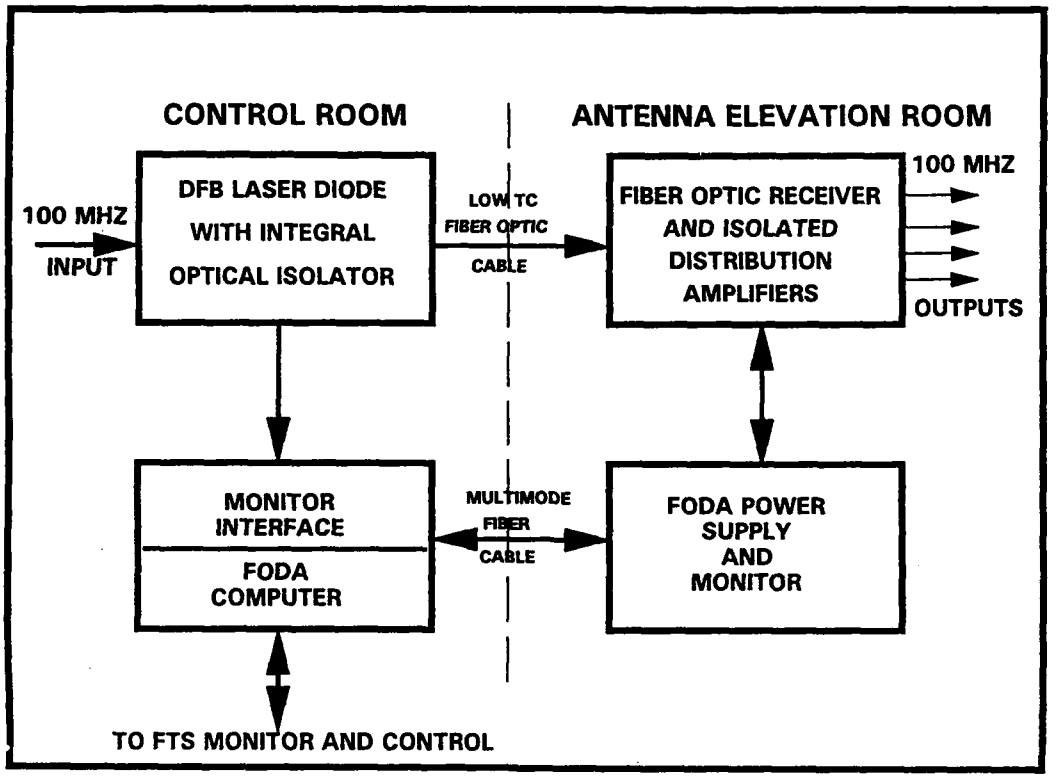

Figure 1. Block Diagram, Fiber Optic Reference Frequency Distribution Assembly

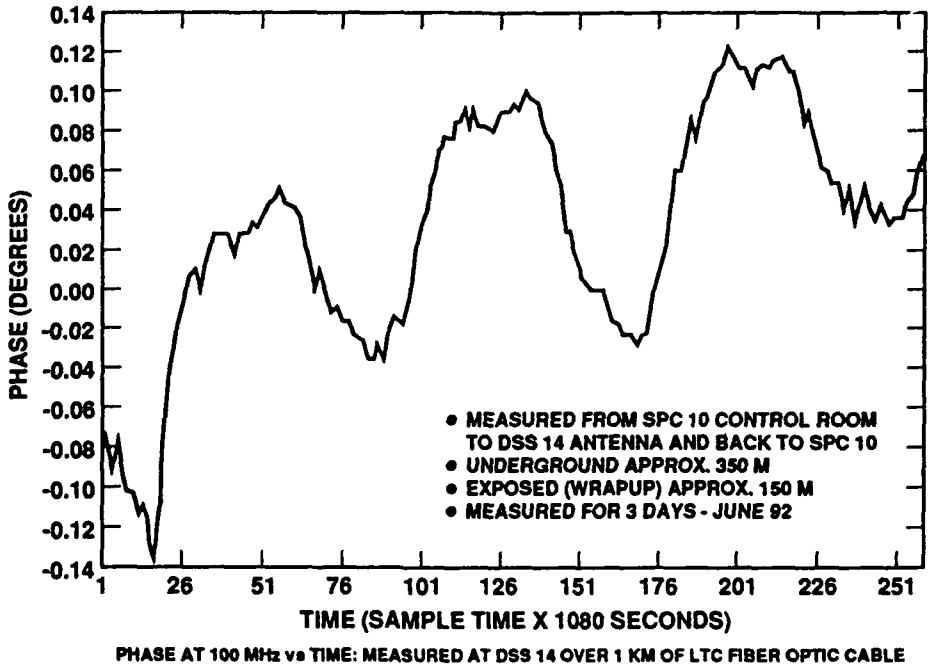

Figure 2. Phase Variations at 100 MHz Over Low TCD Optical Fiber

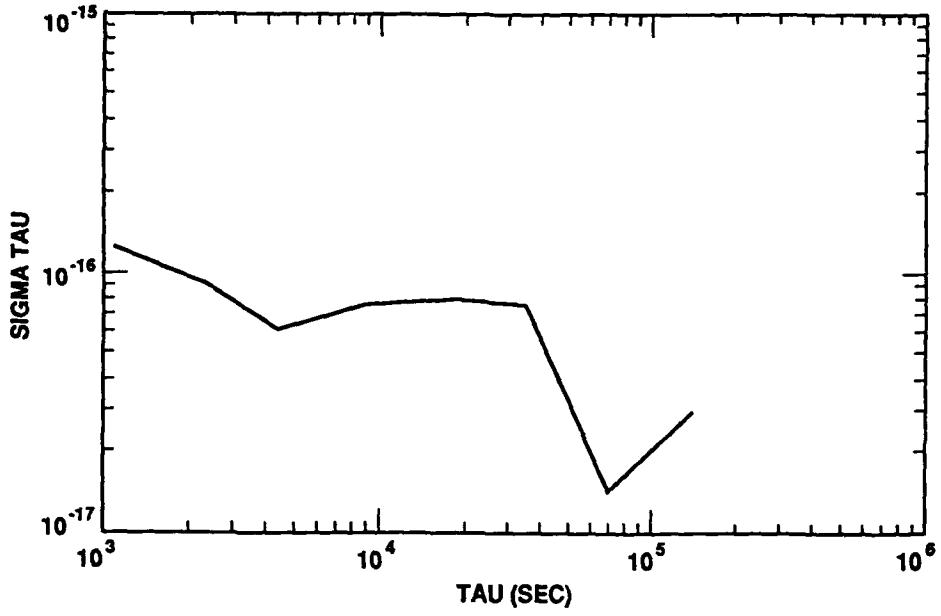

ALLAN DEVIATION COMPUTED FROM PHASE DATA TAKEN AT DSS 14 OVER 1 KM FIBER OPTIC LINK USING LTC FIBER

Figure 3. Allan Deviation of Low TCD Optical Fiber

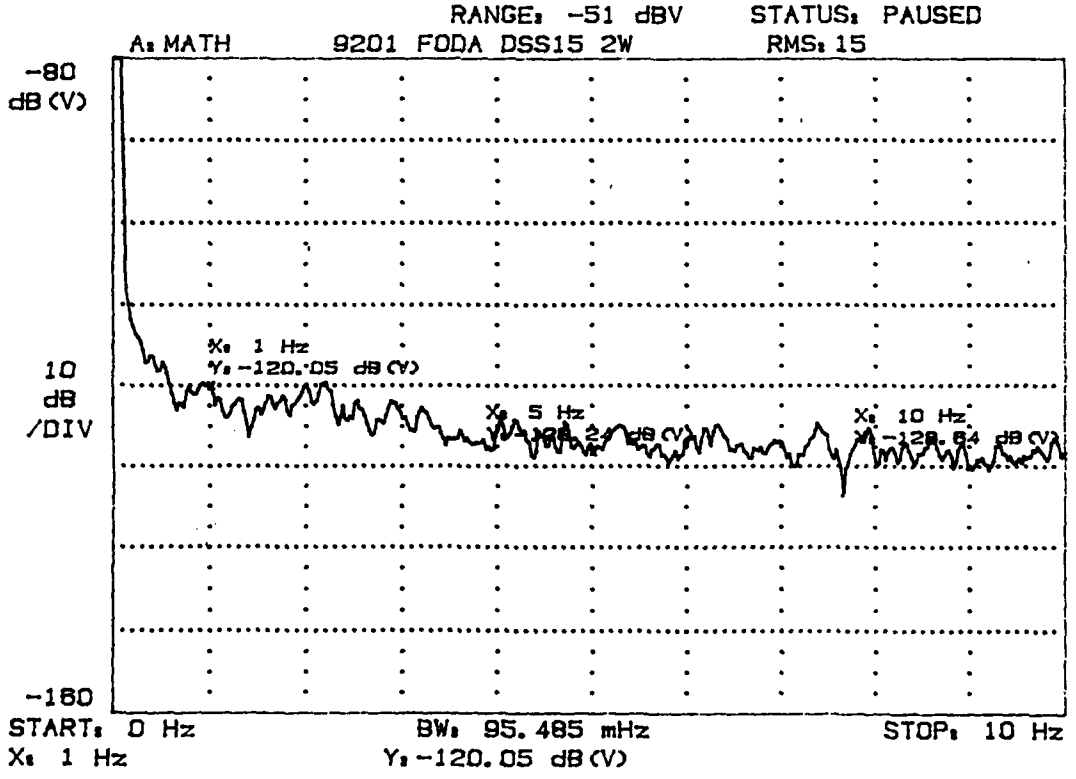

Figure 4. Phase Noise Density Measured Over Fiber Optic Reference Frequency Distribution

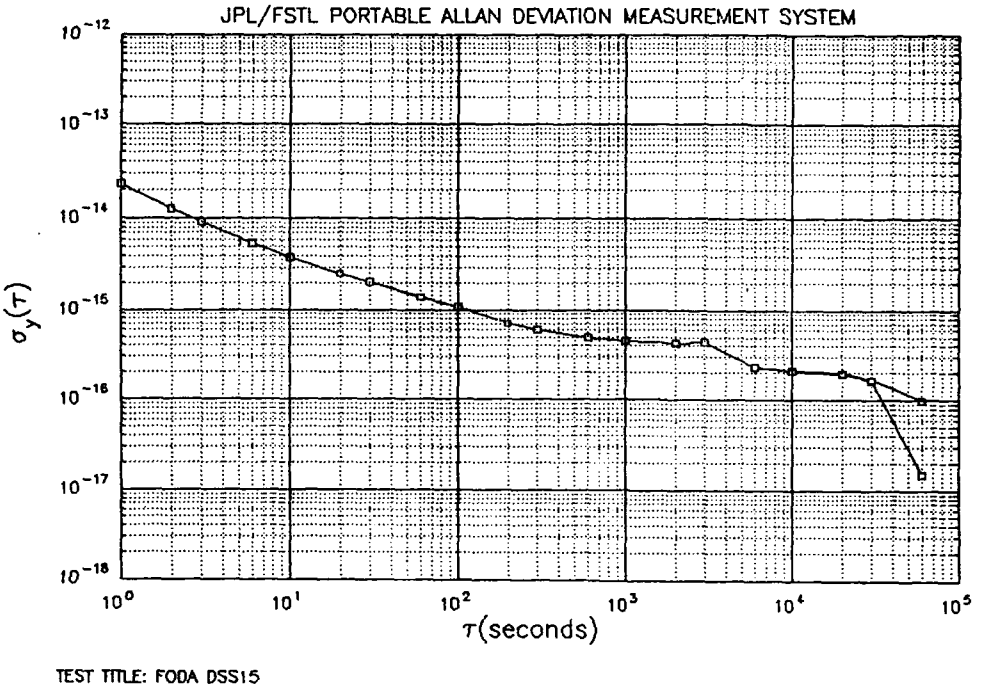

Figure 5. Allan Deviation Measured Over Fiber Optic Reference Frequency Distribution

A WIDE–BAND FIBER OPTIC FREQUENCY DISTRIBUTION SYSTEM EMPLOYING THERMALLY CONTROLLED PHASE COMPENSATION*

Dr. Dean Johnson
Department of Electrical Engineering
Western Michigan University
Kalamazoo, Michigan 49008

Drs. Malcolm Calhoun, Richard Sydnor, and George Lutes
California Institute of Technology
Jet Propulsion Laboratory
Pasadena, California 91109

Abstract

An active wide–band fiber optic frequency distribution system employing a thermally controlled phase compensator to stabilize phase variations induced by environmental temperature changes is described. The distribution system utilizes bidirectional dual–wavelength transmission to provide optical feedback of induced phase variations of 100 MHz signals propagating along the distribution cable. The phase compensation considered here differs from earlier narrow–band phase compensation designs in that it uses a thermally controlled fiber delay coil rather than a VCO or phase modulation to compensate for induced phase variations. Two advantages of the wide–band system over earlier designs are (1) that it provides phase compensation for all transmitted frequencies, and (2) the compensation is applied after the optical interface rather than electronically ahead of it as in earlier schemes. Experimental results on the first prototype shows that the thermal stabilizer reduces phase variations and Allan deviation by a factor of forty over an equivalent uncompensated fiber optic distribution system.

INTRODUCTION

The Frequency Standards Laboratory at the Jet Propulsion Laboratory is interested in developing ultrastable fiber optic frequency distribution systems for the Deep Space Network, which would allow for the distribution of high quality microwave local oscillator signals to several antennas from a central distribution point. To meet the requirements of such systems which will transmit

*The research described in this paper wascarried out by the Jet Propulsion Laboratory, California Institute of Technology, under a contract with the National Aeronautics and Space Administration.

over several tens of kms and require parts in 10^{17} stability for 1000 s averaging times, fiber optic frequency distribution systems employing active phase compensation techniques are being studied.

This paper describes an active wide–band fiber optic frequency distribution system which employs a thermally controlled phase compensator to stabilize phase variations arising from environmental temperature changes occurring along the distribution cable. The distribution system utilizes bidirectional dual–wavelength optical transmission to provide optical feedback of induced phase variations of 100 MHz signals propagating along the distribution cable. The phase compensation considered here differs from earlier narrow–band phase compensation designs in that it uses a thermally controlled fiber delay coil rather than a VCO or phase modulation to compensate for induced phase variations. Two advantages of the wide–band system over earlier designs are (1) that it provides phase compensation for all transmitted frequencies, and (2) the compensation is applied after the optical interface rather than electronically ahead of it as in earlier designs. In the next section, the design issues of passive and active frequency distribution schemes are discussed. Following this, the design of a thermal stabilizer and corresponding linear transfer function describing the dynamics of a thermally controlled frequency distribution system are presented. Finally, experimental results obtained from a thermally stabilized 3.8 km distribution system are given.

PASSIVE VERSES ACTIVE DESIGNS

The preferred transmission medium for distributing RF frequency standards at JPL's Goldstone Deep Space Network Antenna Complex is optical fiber cable. Fig. 1(a) describes a typical optical fiber frequency distribution system installation. A Hydrogen maser located at a signal processing center (SPC) is used to impress a highly stable 100 MHz RF reference signal on an optical carrier by intensity modulation of a semiconductor laser. This signal is subsequently transmitted and distributed to a remote antenna via a buried optical fiber. However, because of environmental temperature variations the optical path length between the SPC and antenna is unstable. This effect is observed at the antenna in the form of a induced, time–varying disturbance phase angle on the distributed RF standard.

For transmission systems employing superior optical isolation at the laser transmitter output as well as an adequate signal to noise ratio, the frequency stability of the distributed standard is predominately dependent upon the amplitude and time characteristics of the thermal disturbance effects [1]. For passive transmission distribution designs, thermal environmental effects can be reduced by burying the optical fiber underground and employing fibers having small thermal coefficients of delays. Two–way transmission tests (those that are independent of the stability of the frequency reference) performed by Calhoun [2] on ultrastable field installed distribution links employing these methods have shown to be capable of achieving parts in 10^{16} stabilities for 1000 second averaging times.

Two–way tests performed on distribution systems employing state of the art fiber optic transmitters and receivers under ideal, thermally stable laboratory conditions at JPL have shown the capability of achieving parts in 10^{17} stabilities over 1000 seconds. To maintain these levels of stabilities in a field installation where the environment is thermally unstable and transmission distances may span several tens of kilometers, distribution system designs employing active phase compensation techniques have been a subject of research and development. Fig. 1(b) illustrates the principle of

operation employed by a distribution system utilizing active phase stabilization. In this scheme, optical feedback is employed to sense the thermal disturbance along the distribution cable through the use of a backward travelling optical carrier supporting the distributed RF standard at the antenna. The resulting feedback signal then drives special stabilizer circuitry at the SPC which in turn adjusts the RF phase at the transmission end to actively compensate for the disturbance angle induced along the forward direction of distribution. Narrow–band stabilization schemes employing a VCO or phase modulation to generate the necessary compensating phase angle have been designed in the past at JPL by Lutes [3], Primas [4], and others with varying amounts of success. In each of these schemes, the compensation was performed on the narrow–band RF distribution signal ahead of the optical interface. An alternative wide–band scheme shall now be presented which provides compensation for wide–band RF signals and involves manipulating only the optical signal itself.

THERMAL STABILIZER DESIGN

While the optical fiber used to transport the RF standard between the SPC and antenna has proven to be sensitive to environmental temperature changes (and thus susceptible to thermally induced phase disturbances), one might consider employing the thermal sensitivity of the fiber also to provide the necessary compensation to nullify outside disturbances. A stabilization system based upon this premise is illustrated in Fig. 2. Shown in series with the distribution cable is an additional length of fiber located inside a thermal electric cooler (TEC). The purpose of this special section of thermally controlled fiber is to compensate for length changes induced in the distribution cable by heating (or cooling) the small fiber coil so as to keep the optical path length between the SPC and antenna constant. The control loop is manifested by providing a secondary transmission link between the antenna and the SPC. In this case the primary transmission system transmits the frequency reference through the TEC and distribution cable to the antenna receiver, while the secondary transmission system returns the distorted antenna signal back to the reference end through the same optical fiber path. To isolate the forward and backward transmissions, the primary and secondary links are supported by two different optical wavelengths and signals generated by each system are routed to appropriate receivers by use of wavelength division multiplexers (WDMs) at each end of the common transmission path. Phase detection of the feedback RF signal from the secondary transmission system provides an error signal used to drive the TEC.

RF signal flow through the active distribution system is illustrated in Fig. 3. Ignoring phase differences arising from average transit delays, it is observed from this diagram that the phase of the RF signal received at the antenna along the primary transmission path (path 1) is $\theta_{1R} = \theta_{Ref} + \phi_{1C} + \phi_{1D}$. The phase observed at the second receiver at the front end resulting from the feedback transmission path (path 2) is $\theta_{2R} = \theta_{Ref} + \phi_{1C} + \phi_{1D} + \phi_{2C} + \phi_{2D}$. Under conditions where the compensation and disturbance phase angles are approximately equal for the two wavelength carriers, a closed loop transfer function describing the output phase angle of the active distribution system may be written as

$$\Phi_{out} = \frac{\Phi_D}{1 + 2K_{PD}H(s)} + \Phi_{ref} \tag{1}$$

where K_{PD} is the phase detector gain and $H(s)$ describes the transfer function of the thermal phase

compensator. Note that in the active configuration, the effect of disturbance angle is reduced by a factor $1 + 2K_{PD}H(s)$ over an equivalent passive distribution system.

A simple linear model describing H(s) may be constructed by assuming that the TEC cold plate behaves as a leaky integrator (heat storage plus heat loss) and that the thermal interface between the cold plate and the fiber behaves as a simple first order thermal lag network. The front end of the TEC consists of a current driver which is controlled by an input voltage. Thus the thermal phase compensator transfer function (Volts in to phase out) may be modeled as

$$H(s) = \frac{K_{TEC}ab}{(s+a)(s+b)} \tag{2}$$

where K_{TEC} is the TEC current driver gain, $1/a$ is the cold plate temperature time constant resulting from a step current input and $1/b$ is the time constant of the RF phase induced by the TEC fiber resulting from a step temperature cold plate change. This model is undoubtedly overly simple, but it provides a starting point for the analysis to follow. Employing Eq. (2) for $H(s)$ into the overall transfer function of Eq. (1) for the active frequency distribution system yields a second order system having an underdamped natural frequency described by

$$\omega_n^2 = 2K_{PD}K_{TEC}ab + ab - \frac{(a+b)^2}{4} \approx K_{ab} \tag{3}$$

where $K = 1 + 2K_{PD}K_{TEC}$ is the disturbance phase compensation factor corresponding to the DC gain of Eq. (1). The natural frequency and phase compensation factors are parameters which may be easily measured and employed to characterize the system as will be seen in the next section.

If the disturbance phase angles induced along the two transmission paths are significantly different because of differential dispersion effects between the two optical carriers, then the compensation will be degraded. In this case $\phi_{2D} \neq \phi_{1D}$ and in liu of any other advantage, it can be seen that it is only possible to compensate for the average of the forward and backward induced disturbance phase angles. However, the ideal compensation of Eq. (1) may be recovered if the dispersion effect behaves approximately linear such that $\phi_{2D} \approx \alpha\phi_{1D}$ and $\phi_{2C} \approx \alpha\phi_{1C}$ for some constant α over the compensation temperature ranges. The reciprocal linear compensating effect supposed here requires that the thermal stabilizer employ the same fiber as utilized in the distribution cable.

EXPERIMENTAL RESULTS

A frequency distribution system incorporating thermally controlled phase compensation was constructed and tested in the test chambers of the Frequency Standards Laboratory at JPL. The distribution cable was 3.8 kms in length and utilized an optical fiber having a thermal coefficient of delay of 7 ppm/°C . The distribution cable was located in a temperature controlled test chamber which could be programmed to maintain a constant temperature or thermally cycle 1°C sinusoidally over a 24 hour period. The rest of the distribution system was located outside the test chamber. This included an AT&T 1300 nm laser and in house receiver for the primary transmission path and a Fujitsu 1550 nm laser and BTD receiver for the secondary feedback path. The 1300 nm laser was installed with 55 dB of optical isolation, while the 1550 nm laser possessed 35

dB isolation. The frequency stability of this system under constant temperature conditions was estimated to be 1 x 10^{-16} at 1000 s averaging times. The supplied RF reference frequency was 100 MHz, obtained from a Hydrogen maser.

The thermal phase compensator consisted of 200 m of 7 ppm/°C Corning fiber wrapped in a 6 inch loop pressed down on the cold plate of a TEC. To improve the thermal coupling between the cold plate and the fiber, thermal paste was applied between the winds of the fiber and the cold plate. The thermal compensation unit was located in series with the 3.8 km fiber to produce a total mean optical path length between transmitters and receivers of approximately 4 km. The laser transmitters and receivers were interfaced to the 4 km common transmission path through the use of two WDMs manufactured by JDS. By disturbing the electrical drive to the TEC the underdamped response of the distribution system could be observed. These experiments revealed natural oscillations having a period of approximately 50 s. Employing this result with a phase compensation factor of K = 40 (see later) in Eq. (3) yields $1/(ab) = 2533\ s^2$ which gives a measure of the product of the internal time constants of the thermal stabilizer (TEC and delay fiber coil).

Figs. 4 and 5. show the theoretical and experimental Allan deviation curves resulting from cycling the 3.8 km distribution cable 1°C. Time residual measurements revealed a 115 ps oscillation corresponding to a 4.14° peak to peak diurnal phase shift at 100 MHz. The resulting theoretical Allan deviation equation for this diurnal variation is, from Greenhall [5], $\sigma(\tau) = 2X_0/\tau \sin^2(\pi\nu\tau)$ where $2X_0 = 115$ ps and $\nu = 1/86400$ Hz. This expression is plotted in Fig. 4. The experimental curve of Fig. 5. shows evidence of the thermal disturbance starting about $\tau = 1000$ s, where it emerges from the baseline phase noise characteristic, finally peaking near $\tau = 43200$ s.

Fig 6. shows the experimentally derived Allan deviation curve arising from the thermally cycling 3.8 km distribution system after the 200 m stabilizing fiber coil was activated. Peak to peak RF phase variations at the distribution system output were observed to be 0.104° which correspond to a 40 fold reduction over the uncompensated case. This compensation factor may also be inferred by comparing Figs. 5 and 6, although there are no data points at the theoretical peak at $\tau = 43200$ s in Fig. 6 where this observation should be made directly. Note that the stability of the system for $\tau = 1000$ s is 1 part in 10^{16}. Comparing these same curves for small τs also reveals that the stabilizer added no amount of significant phase noise beyond that produced by the uncompensated system.

As the distribution cable was cycled 1°C, the TEC was observed to vary just under 20°C which is consistent with the 19 to one ratio of optical fiber lengths employed in the distribution cable and thermal stabilizer. However for experiments lasting 24 hours or more, the temperature characteristic of the thermal stabilizer was observed to drift upward in temperature and resulted in somewhat higher values of Allan deviation. We believe that this thermal drift could be corrected with some additional work. The present data shown in Fig. 6 is a record of the best data that was observed.

CONCLUSIONS

A 3.8 km active fiber optic frequency distribution system employing thermally controlled phase compensation has been built and tested. The prototype system demonstrated a 40 to one improvement in frequency stability over an equivalent uncompensated frequency distribution system when

subjected to a diurnal thermal disturbance. One advantage of this design over earlier compensation schemes is that it provides compensation over a wide-band of transmitted RF frequencies since the compensation afforded by this system purposes to maintain a constant optical path length between the frequency reference and the distribution point. Also the compensation is applied after the optical interface rather than in the electronics (before the optical interface), as provided by earlier narrow-band stabilization schemes. Another advantage of the thermal phase compensator is its simple and low cost design, employing only a coil of fiber in a TEC. The thermal stabilizer also possesses very little intrinsic phase noise of its own. Unfortunately, the compensation provided by the thermal stabilizer design is relatively slow, and thus disturbances varying less than several tens of seconds cannot be properly compensated. However, for most applications in the Deep Space Network, the largest source of frequency distribution instabilities arise from diurnal environmental temperature variations. In this case, the thermal controlled stabilizer provides a simple, low noise, and low cost mechanism for actively maintaining ultrastable frequency reference distribution in thermally unstable environments.

ACKNOWLEDGEMENTS

The authors wish to thank Michael Buzzetti for his invaluable assistance in the laboratory.

REFERENCES

[1] G. Lutes, *"High Stability Frequency and Timing Distribution Using Semiconductor Lasers and Fiber Optic Links,"* SPIE Proc.Laser Diode Technology and Applications, vol. 1043, pp.263-271, 1989.

[2] M. Calhoun and P. Kuhnle, *"Ultrastable Reference Frequency Distribution Utilizing a Fiber Optic Link,"* Proc. 24th Ann. Precise Time and Time Interval Applications and Planning Meeting, December, 1992.

[3] G. Lutes, *"Optical Fibers for the Distribution of Frequency and Timing References,"* Proc. 12th Ann. Precise Time and Time Interval Applications and Planning Meeting, pp. 663-680, NASA Conference Publication 2175, Goddard Space Flight Center, December 1980.

[4] L. Primas, R. Logan, G. Lutes, *"Applications of Ultra-Stable Fiber Optic Distribution Systems,"* IEEE 43rd Annual Symposium on Frequency Control - 1989, pp. 202-210, June, 1989.

[5] C. Greenhall, *"Frequency Stability Review,"* The Telecommunications and Data Acquisition Progress Report 42-88, pp.200-212, October-December, 1986.

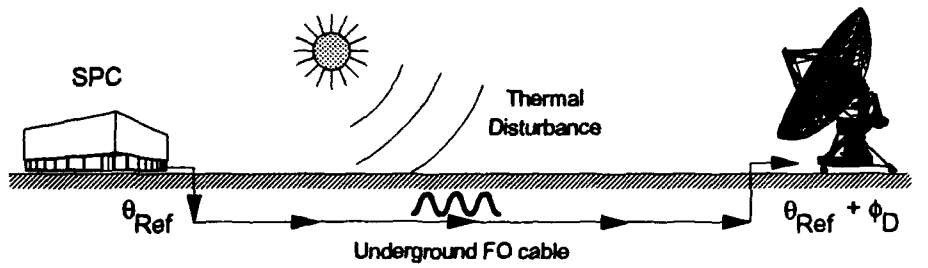

(a) *Passive distribution*

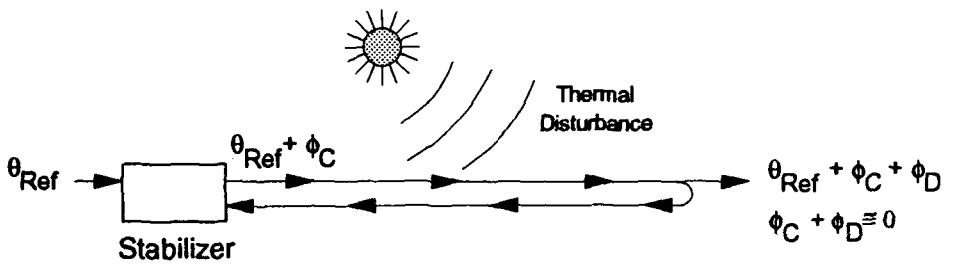

(b) Frequency distribution with active phase compensation

Figure 1. Fiber optic frequency distribution systems.

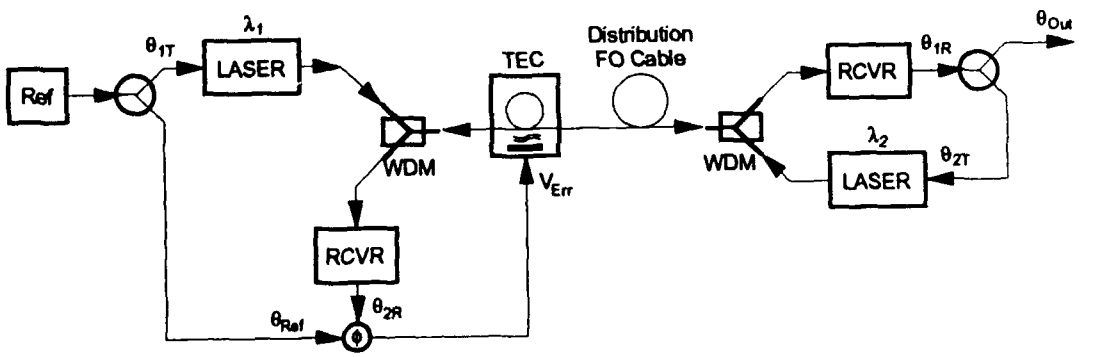

Figure 2. Block diagram of a fiber optic frequency distribution system employing thermally controlled phase compensation.

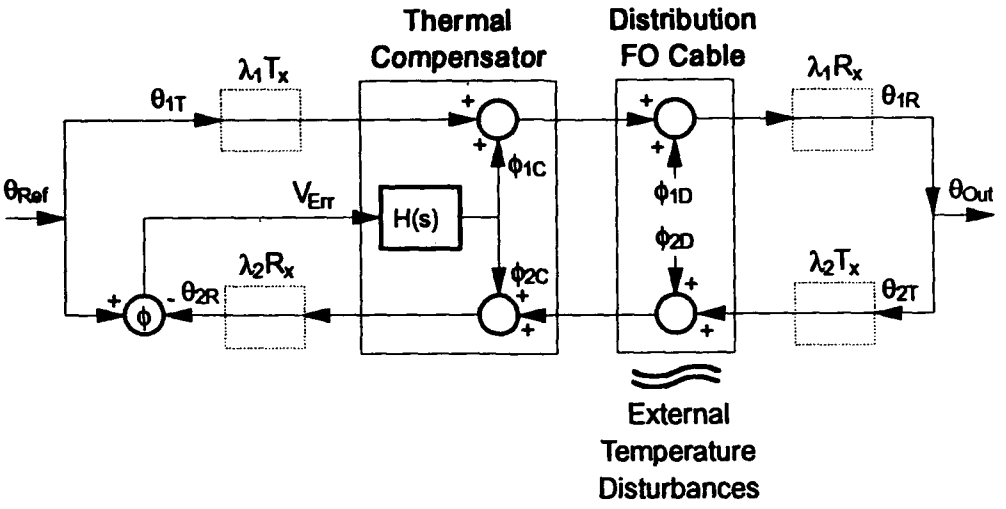

Figure 3. Signal flow diagram of thermally stabilized fiber optic frequency distribution system.

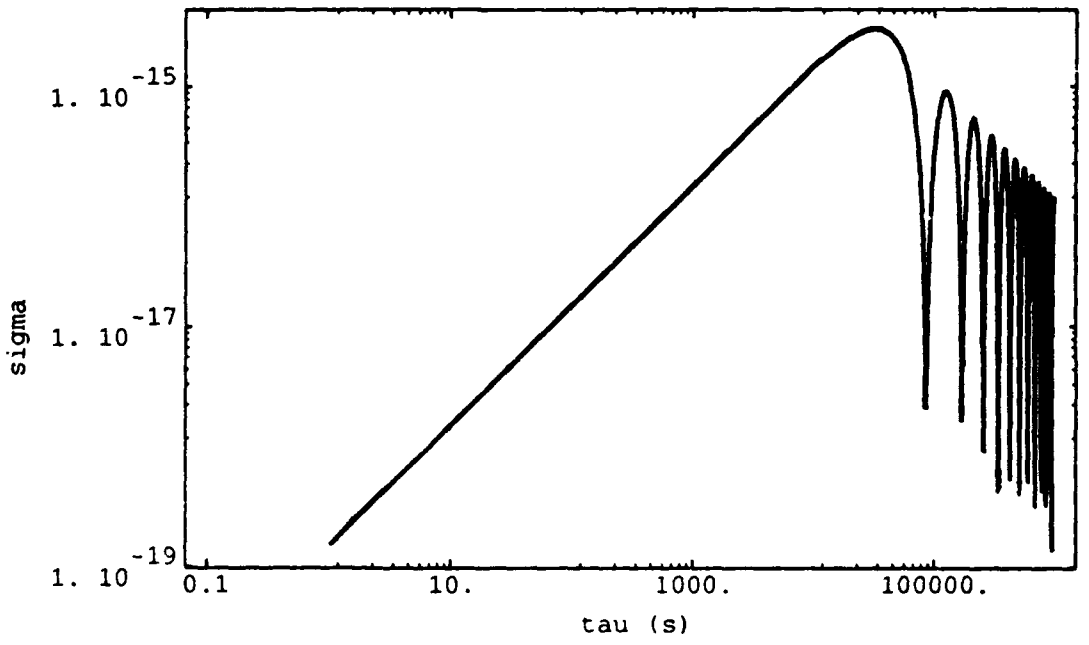

Figure 4. Theoretical Allan deviation curve arising from a diurnal phase variation having a peak to peak time residual of 115 ps (4.14° at 100 MHz).

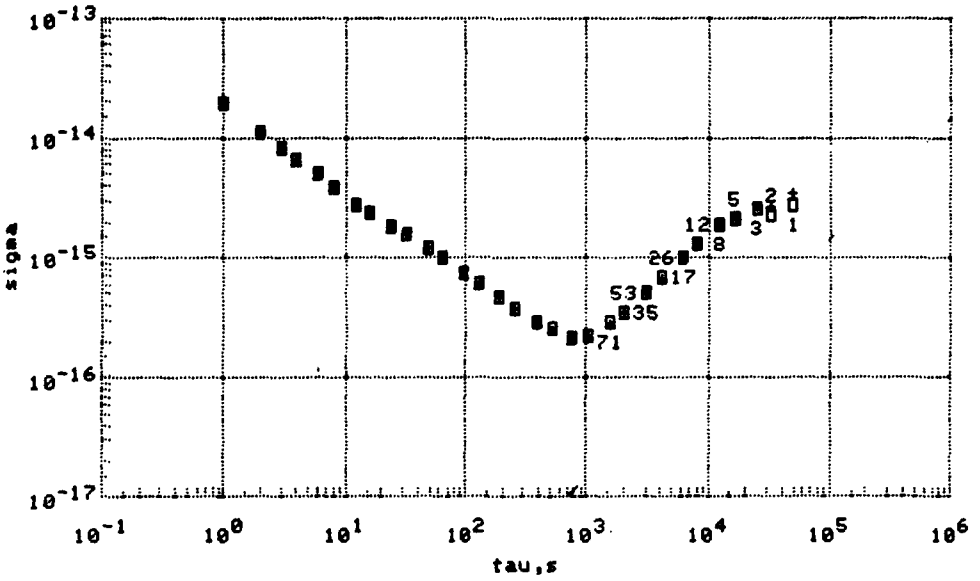

Figure 5. Experimental Allan deviation curve arising from a 3.8 km, 100 MHz passive frequency distribution system cycling 1°C over a 24 hour period.

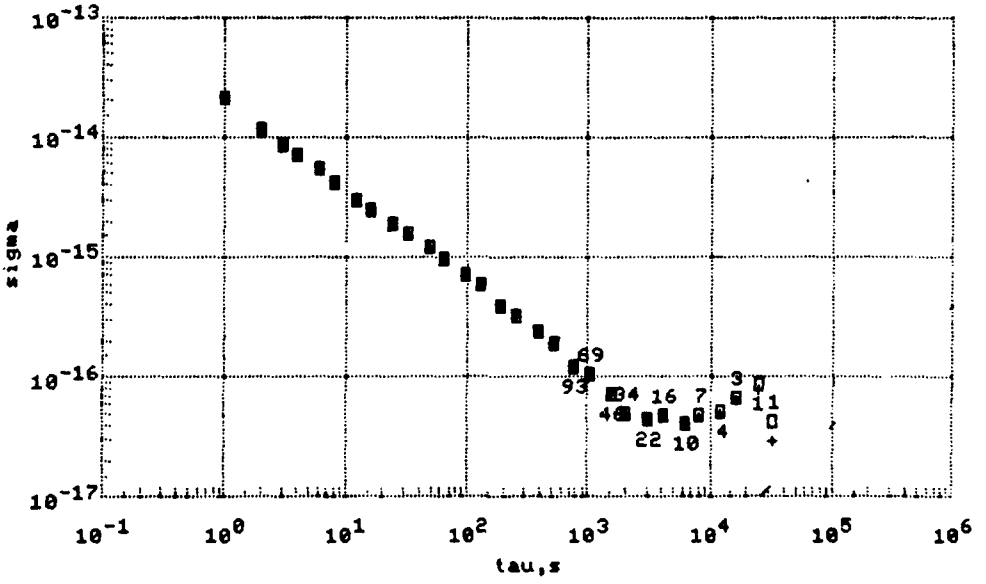

Figure 6. Experimental Allan deviation curve arising from a 3.8 km, 100 MHz actively compensating frequency distribution system consisting of a 3.8 km distribution cable (cycling 1°C over 24 hours) stabilized by a 200 m coil under thermal electric control.

QUESTIONS AND ANSWERS

Question: Did you get the opportunity to look at the temperature coefficient of the transmitter on the antenna end?

Answer: No

Comment: It would seem your that your compensation scheme might take out those affects at the expense of stability from that.

Question: I have a question about the compensation scheme. What did you use for lasers, because that laser is not compensated for. No change in that laser will provide an over compensation which should not be provided. Why did you use that active amplication and couldn't be done with the passive optical signal.

Answer: You're speaking about primarily reflecting the signal back. One of the earlier researchers, Lori Primas, actually looked at that system. That uses the same wave length and by using the second laser sources at different wave lengths we got better isolation between the two channels and better noise performances, so that system has been looked at in the past.

Lutes: I might add that the stability of these highly isolated lasers is extremely good, on the order of 0.01 dB over a day's time so they are very stable.

Question: Did you measure the Allan variance noise performance when you weren't modulating noise temperature?

Answer: I don't have any data to show.

Comment: You only did the test?

Answer: Yes.

Lutes: We have data on other systems that are similar to that one that show that and this one falls right on that line.

Comment: When we did these tests we had only the cable inside the temperature chamber, the electronics were outside the chamber. They were in a very well temperature controlled room within 50 millidegrees at set point at all times. If we were to go into doing more work we will of course compensate or temperature control the transmitters and controls at both ends and the rest of the electronics to prevent phase drift.

ANALYSIS OF THE EASTERN RANGE MULTIPLEXED FIBER OPTIC IRIG B120 DISTRIBUTION SYSTEM

Michael J. Duncan
John S. Martell
James L. Wright

Computer Sciences Raytheon
Patrick Air Force Base Florida

Abstract

A study was conducted to assess the effects of transmitting a precision clock synchronization signal over a commercial multiplexed fiber optic communication system. This study is an evaluation of the distortion and jitter introduced into the signal by this type of transmission system. An analysis comparing signal quality at the multiplexing and demultiplexing ends of the fiber optic communication system shows that the amplitude and phase distortion added to the clock synchronization signal by the transmission system is minimal.

BACKGROUND

The Eastern Range (ER) provides launch and tracking support for commercial and Department of Defense missile launches from Cape Canaveral Air Force Station, Florida (CCAFS). In addition to the facilities at CCAFS, the ER consists of Florida mainland assets at Patrick Air Force Base (PAFB), the Jonathan Dickinson Tracking Annex, and the Malabar Tracking Annex. Down range stations are located in the British West Indies (Antigua Air Station) and at Ascension Island (Ascension Auxiliary Air Field) in the South Atlantic. These stations may be augmented with a range instrumentation ship, the USNS Redstone, to provide additional tracking coverage depending on the launch mission. In all, the ER tracking network provides over 4,000 nautical miles of coverage.

The ER timing system comprises a CCAFS range clock with subordinate station and site clocks. This system provides precise time and time interval signals that conform to the IRIG (Inter-Range Instrumentation Group) standard formats and are correlated to the DoD master clock to within 0.1 microseconds on the UTC (Universal Coordinated Time) scale. The station clocks distribute an IRIG B120 time-of-year signal to synchronize subordinate clocks. The IRIG B120 signal contains 100 bits per second of pulse width modulated serial data that is then amplitude modulated onto a 1 KHz sine wave carrier for transmission. Beginning each second, a reference marker in the signal indicates "on time". This is followed by days, hours, minutes, and seconds data. A formal description of this signal is available in document 200-89, *IRIG STANDARD TIME FORMATS*, available from the Range Commanders Council, White Sands Missile Range, New Mexico 88002.

INTRODUCTION

As part of ER modernization, a FIBERMUX FX4400 multiplexed fiber optic communication system was installed in the Range Operations Control Center (ROCC) to transmit voice, data, and video information between the ROCC and the CCAFS communications distribution hub (XY Bldg.). The relevant portions of this system are shown in Figure 1. In this application, the system is configured as a FX4400 network utilizing approximately 120 single-mode fiber lines to provide communication services. One module in this system is used to distribute the IRIG B120 clock synchronization signal from the ER master clock. As part of the fiber optic system acceptance testing, a study was conducted to assess the capability of the communication system to transmit an IRIG B120 signal with minimal degradation.

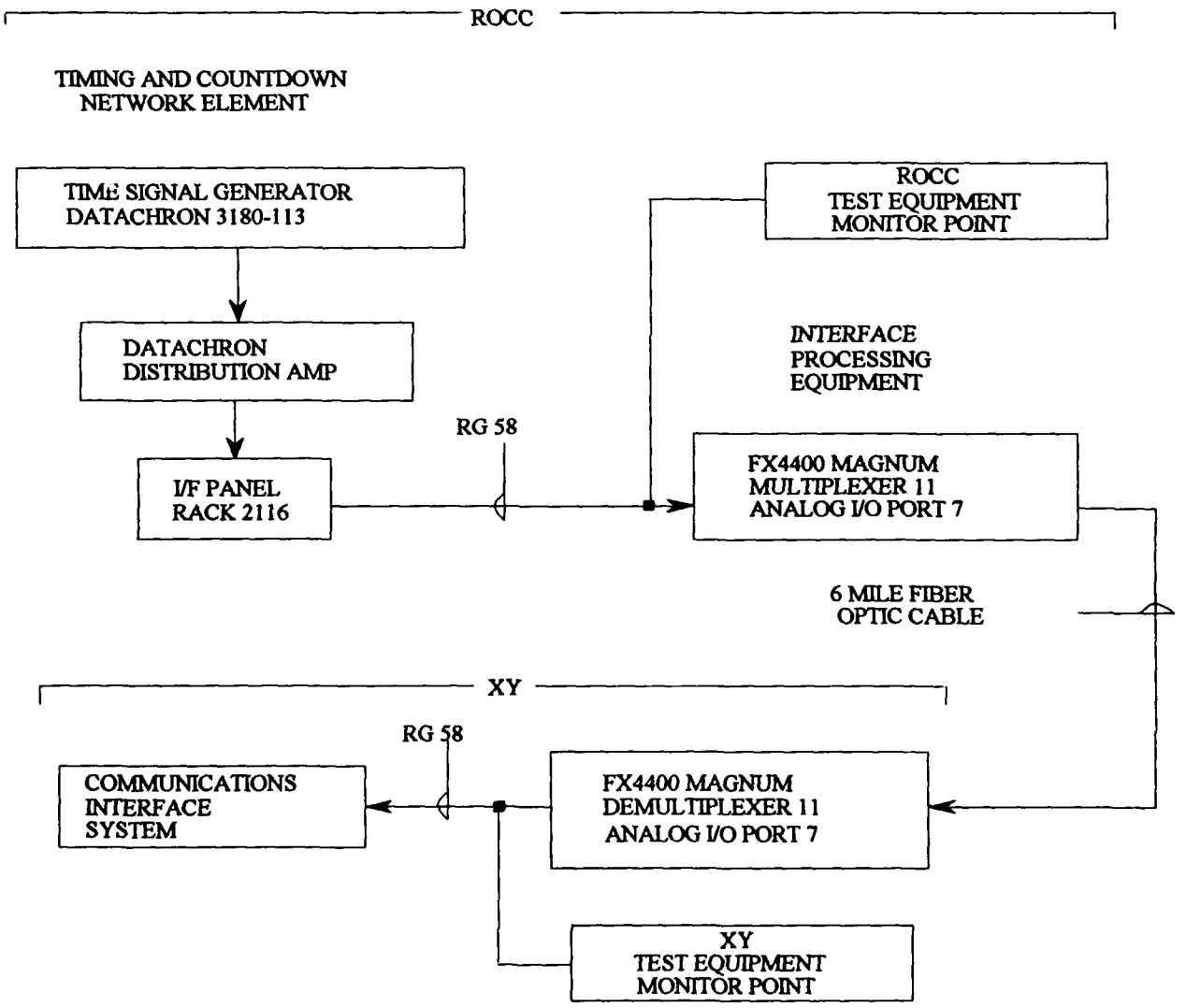

Figure 1. System Configuration.

The transmission of an amplitude modulated IRIG B signal over a commercial communication system is more difficult than it may first appear. The signal contains significant lower frequency (less than 300 Hz) components. The relatively large amplitude and importance of these low frequency components is due to the fact that the carrier is not sufficiently high in frequency to prevent negative frequency side-band harmonics from "folding over" into the signal. The loss of these low frequency components leads to unacceptable levels of amplitude and phase distortion. This precludes the use of a voice channel to transmit the signal. Instead, a FIBERMUX two channel CC4461G analog input card is used to multiplex the IRIG B120 signal onto the fiber optic system. This card has a 0 - 10 KHz bandwidth and has been optimized for use with a 1 KHz amplitude modulated signal. Reproduction at the demultiplexing end of the fiber is accomplished using a complementary CC4461 G/S card.

ANALYSIS PERFORMED

The IRIG B120 signal was analyzed at the input to the multiplexed fiber optic communication system and at the demultiplexing end of the system approximately six miles away. These measurements were taken to evaluate the waveform shape, data errors, and the phase stability of the IRIG B120 signal after transmission over the fiber optic system.

Figure 2 shows the test configuration used at both ends of the system. The "IRIG B120 signal source" refers to the IRIG B120 signal provided to the CC4461G analog input card in the fiber optic multiplexing equipment at the transmitting end, and to the IRIG B120 signal reproduced by the CC4461G/S analog output card in the fiber optic demultiplexing equipment at the receiving end. At both ends, the IRIG B120 signal source was supplied to a Hewlett-Packard 54112D digital storage oscilloscope (DSO), a Hewlett-Packard 5372A frequency and time interval analyzer, and a Kinemetrics 972-303 time code reader/tester. A reference one pulse per second (1 PPS) square wave was generated from a Hewlett-Packard 5061B cesium beam flying clock. This 1 PPS signal was provided as a trigger to the DSO and as a reference signal to the frequency and time interval analyzer.

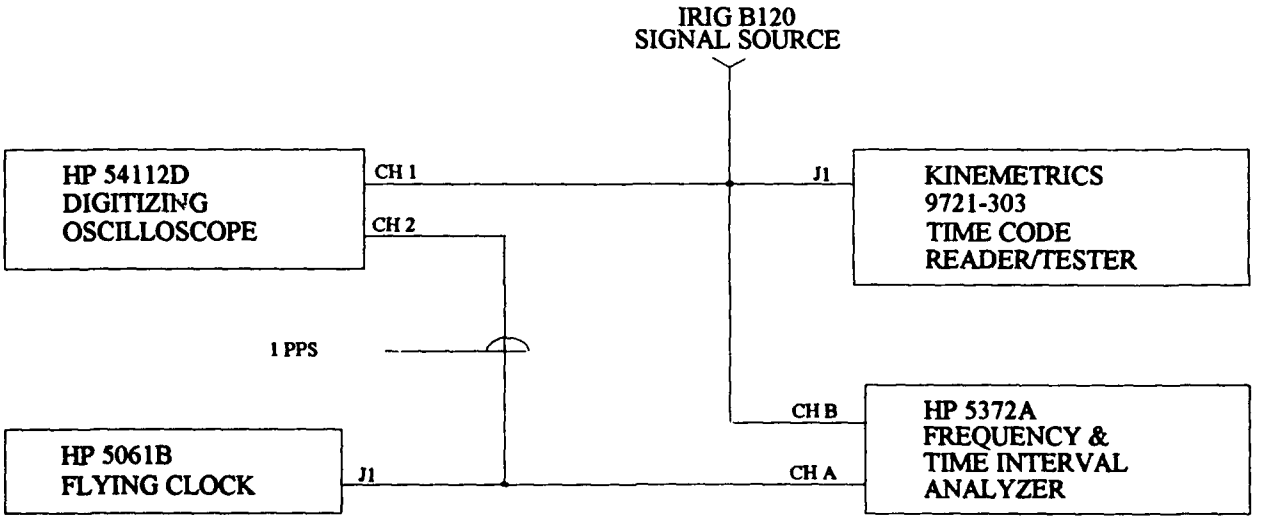

Figure 2. Test Configuration.

The IRIG B120 signal was first checked for distortion at both ends of the transmission system using the DSO. The analysis consisted of looking for signal deformation at nine specific points in the waveform. First, the IRIG B120 source signal was provided as input to channel 1 of the DSO. The 1 PPS signal from the flying clock was then aligned with the range master clock 1 PPS output and provided to DSO channel 2. Finally, the DSO was set to trigger on the leading edge of the flying clock reference 1 PPS. Several measurement sets were taken at both ends of the system for comparison. Figure 3 shows the nine areas where signal distortion typically occurs during transmission.

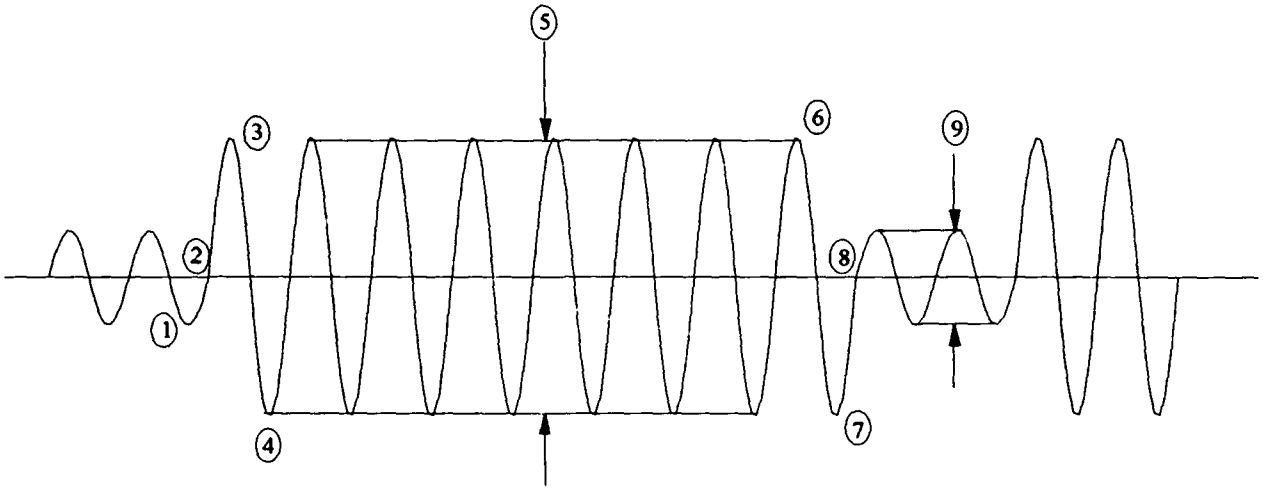

1. pre-exalted cycle distortion
2. zero cross-over distortion
3/4. exalted cycle distortion
5. exalted cycle stability
6/7. post-exalted cycle distortion
8. zero cross-over distortion
9. non-exalted cycle stability

Figure 3. Typical IRIG B120 Signal.

A second series of tests were performed to evaluate the short term and longer term frequency stability of the IRIG B120 signal. The 1 PPS output of the cesium beam flying clock was aligned with the range master clock 1 PPS output. The 1 PPS output of the flying clock was then used as the start reference in performing direct time interval measurements versus the "on time" point (first positive zero crossing in a frame) of the IRIG B120 signal. In each test, one hundred measurements were made. Five series of tests were performed at each end of the fiber optics network. The time between samples (Tau) was increased after each test series. The first series was conducted with a Tau of one second. For each subsequent test series, the Tau was increased by an order of magnitude. In the final series of tests, a Tau of ten thousand seconds was used. This provided data on both short term signal stability and the long term signal stability trends. Tests were conducted sequentially, first at the transmitting end, and then at the receiving end of the fiber optic cable.

While the above test series were performed, the signal under test was monitored by the Kinemetrics 972-303 Time Code Reader/Tester. This unit was used to monitor the signal for bit errors and code dropout.

RESULTS

A comparison of results from the transmitting and receiving ends of the fiber optic cable showed no discernible distortion at any of the nine points of interest in the IRIG B120 signal (refer to Fig. 3). In addition, there were no bit errors or code dropouts detected at any time during the testing.

For the frequency stability tests, a statistical analysis was performed on each group of samples taken. The frequency and time interval analyzer was used to perform these calculations and display the results. The square root of the Allan Variance (Rt Al Var) was calculated to characterize the stability of the IRIG B120 signal. This variance was determined from the time interval measurements of the IRIG B120 signal versus the reference 1 PPS from the flying clock. This sampled square root Allan variance is the primary measurement used in the comparison tests between sample groups at the two ends of the transmission system. Table 1 describes the test series performed.

SAMPLE RATE, TAU (seconds/sample)	SAMPLE SIZE	TIME OF TEST (in seconds)
1	100	100
10	100	1,000
100	100	10,000
1,000	100	100,000
10,000	100	1,000,000

Table 1. Test Series Performed.

Table 2 shows the average results obtained from the transmitting and receiving ends of the fiber optic system. At the transmitting end, the average value for the standard deviation was 1.82304 microseconds, and the average value for the square root Allan variance was 1.73734 microseconds. The receiving end showed an average standard deviation value of 1.86320 microseconds, and an average square root Allan variance of 1.80689 microseconds.

	TRANSMITTING END		RECEIVING END	
Tau	Std. Dev. ($x10^{-6}$ sec.)	Rt. Al. Var. ($x10^{-6}$ sec.)	Std. Dev. ($x10^{-6}$ sec.)	Rt. Al. Var. ($x10^{-6}$ sec.)
1	1.89787	1.83203	1.79326	1.74611
10	1.90233	1.89802	1.85756	1.80097
100	1.71966	1.59866	1.90140	1.81727
1,000	1.69359	1.70912	1.78028	1.83392
10,000	1.90176	1.64888	1.98354	1.83620

Table 2. Frequency Stability Test Results.

Graph pairs 1a,b through 5a,b show the test measurement sets taken at the multiplexing and demultiplexing ends of the transmission system. Each of these graph pairs shows test samples on the x-axis, and has been scaled to show a time interval range of 20 microseconds on the y-axis. Please note that the time interval values show a fixed delay at both the transmitting and receiving ends of the system. At the transmitting end, this delay (approximately 115 microseconds) is caused entirely by the choice of triggering level used in the testing. The same triggering level was used at both test locations, and was chosen to minimize spurious readings caused by noise at the zero-crossing point. The magnitude of the delay is due to the slope of the IRIG B120 signal. At the receiving end the delay is approximately 305 microseconds. This includes a transmission delay in addition to the triggering level delay.

CONCLUSION

Comparisons of the data collected at the multiplexing and demultiplexing ends of the transmission system indicate that a commercial multiplexed fiber optic communication system can successfully transmit a modulated IRIG B timing signal. The communication system tested in this study did not cause significant signal degradation or cause additional phase instabilities in the transmitted signal.

GRAPHS

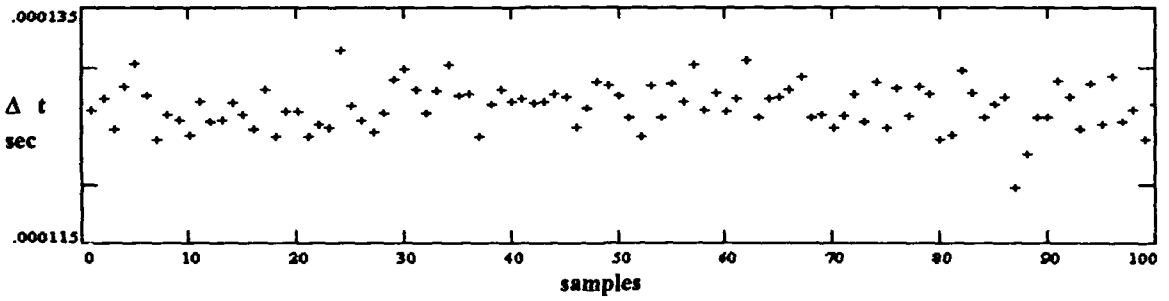

Graph 1a. Transmission End Time Interval Measurements (Tau = 1 seconds).

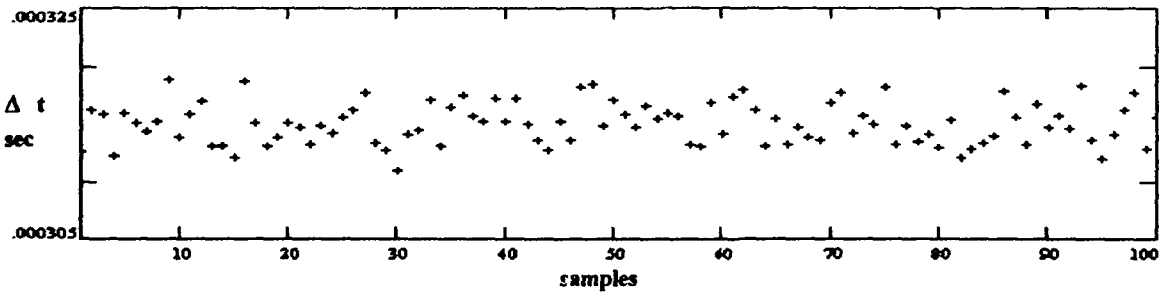

Graph 1b. Receiving End Time Interval Measurements (Tau = 1 seconds).

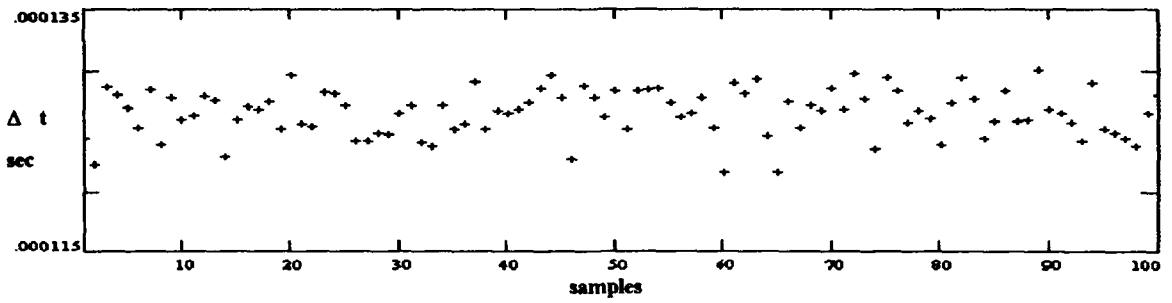

Graph 2a. Transmission End Time Interval Measurements (Tau = 10 seconds).

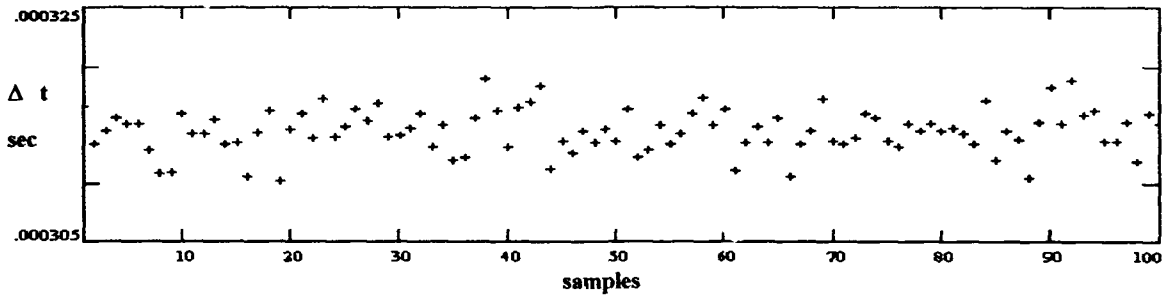

Graph 2b. Receiving End Time Interval Measurements (Tau = 10 seconds).

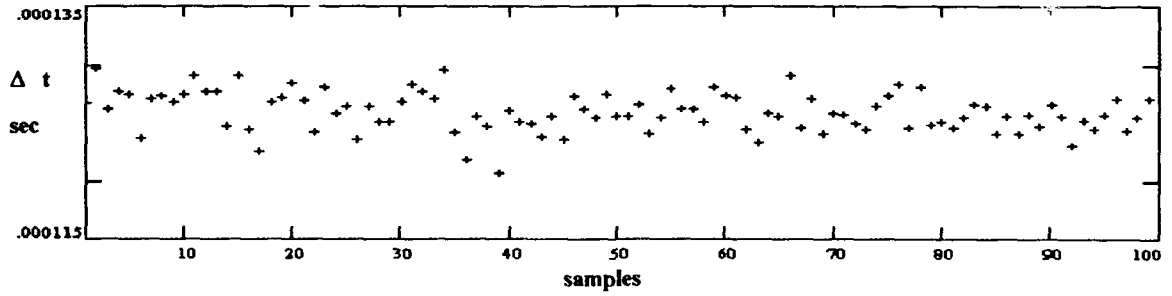

Graph 3a. Transmission End Time Interval Measurements (Tau = 100 seconds).

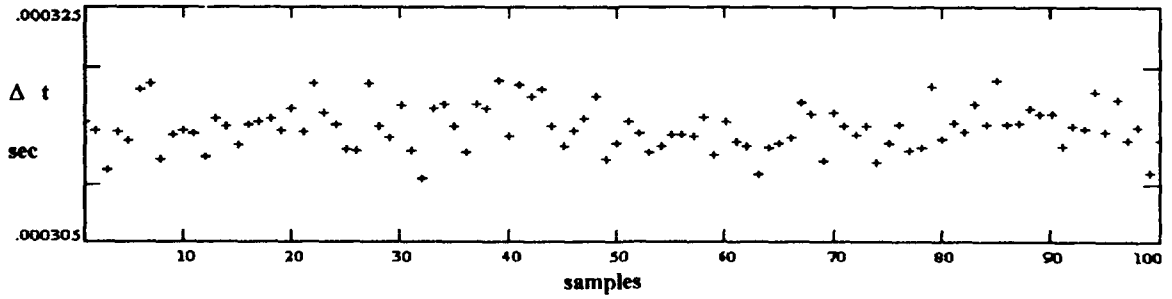

Graph 3b. Receiving End Time Interval Measurements (Tau = 100 seconds).

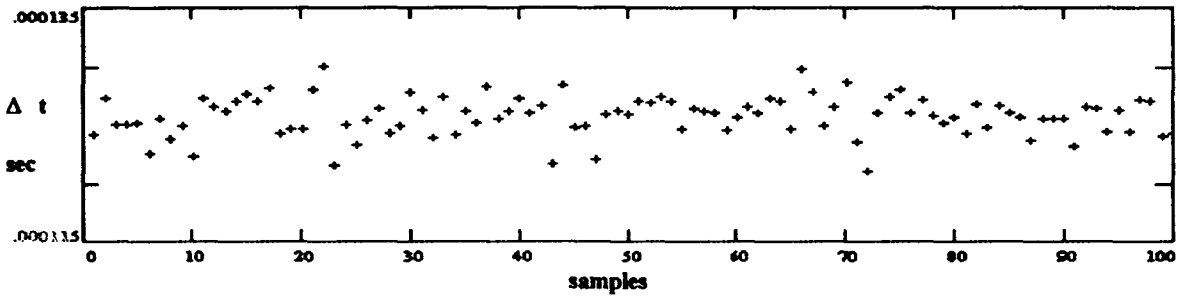

Graph 4a. Transmission End Time Interval Measurements (Tau = 1,000 seconds).

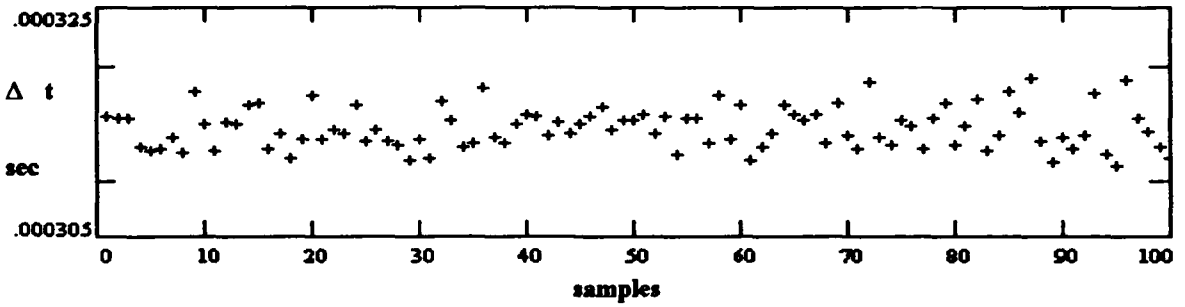

Graph 4b. Receiving End Time Interval Measurements (Tau = 1,000 seconds).

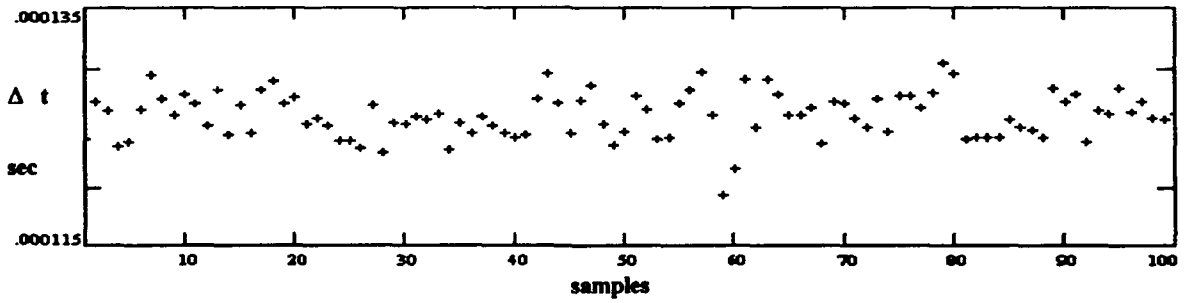

Graph 5a. Transmission End Time Interval Measurements (Tau = 10,000 seconds).

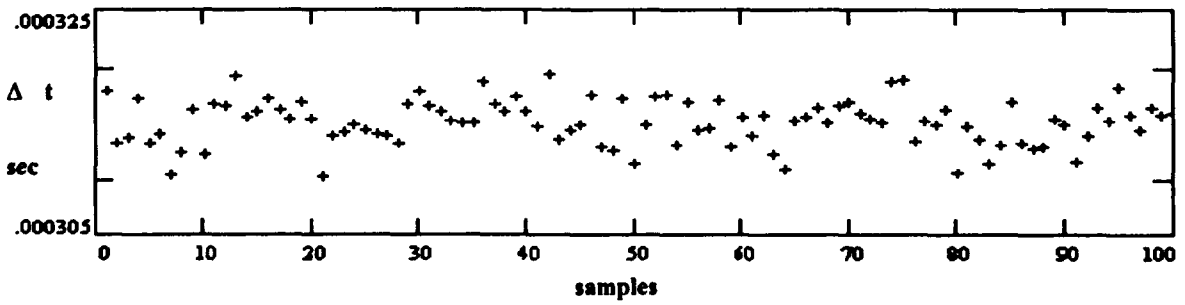

Graph 5b. Receiving End Time Interval Measurements (Tau = 10,000 seconds).

REFERENCES

D. A. Howe and D. W. Allan, *Methods of measuring frequency stability*, NIST Time & Frequency Seminar, chapter 2, pp. 1-43, 1989.

D. A. Howe, D. W. Allan, and J. A. Barnes, *Properties of signal sources and measurement methods*, Proceedings of the 35th Annual Symposium of Frequency Control, 1981.

IRIG Standard 200-89, *IRIG Time Code Formats*, Timing Committee, Range Commanders Council Telecommunications Group, White Sands Missile Range, New Mexico, 1989.

Technical Report, *Transmission of IRIG Timing*, Communications and Data Transmission Committee, Range Commanders Council Tele-Communications Working Group, White Sands Missile Range, New Mexico, 1968.

ESTIMATING THE INSTABILITIES OF N CLOCKS BY MEANS OF COMPARISON MEASUREMENTS.

Amedeo Premoli
Dip. di Elettrotecnica, Elettronica ed Informatica
Università di Trieste, Via A. Valerio 10, 34127, Trieste, Italy

Patrizia Tavella
Istituto Elettrotecnico Nazionale G. Ferraris
Strada delle Cacce 91, 10135, Torino, Italy

Abstract

The estimation of individual instabilities of N clocks, compared by measuring the differences of their readings, is here considered without assuming a priori any hypotheses on their uncorrelation. Instabilities of the N clocks are described by a complete (non-diagonal) NxN covariance matrix R. Only differences of clock readings are available in order to estimate R. Statistical processing of these data allows one to calculate the (N-1)x(N-1) covariance matrix S of the differences relative to the N-th(reference) clock. By analyzing the relationships tying R and S, several pieces of information can be inferred and, in particular, the conditions for the validity of the uncorrelation hypothesis are established. The estimation of R from S is not unique: in any case R must be positive definite. A theorem states that R is positive definite if and only if its determinant is positive. Nevertheless infinitely many acceptable choices of R still fulfil the condition of positive definiteness. This paper shows that, by increasing the number N of compared clocks, the amount of arbitrariness in estimating R is reduced. The analysis of some experimental data illustrates the capability of the method.

1 INTRODUCTION

The evaluation of frequency standard instability is often performed by comparing N clocks and measuring differences in their signals. Results depend on the simultaneous contributions of all N standards and it is often desirable to estimate the noise contributions of any single units. In the past years, this problem has been considered in several papers, which introduced the popular "3–cornered hat" method [1], successively investigated and extended to N clocks [2, 3, 4, 5, 6].

The application of these methods often results in an unpleasant situation: some estimated clock variances turn out to be negative, violating the positiveness restriction intrinsic to their definition.

The assumption of uncorrelation of clocks, necessary in the above methods, seems to be too stringent and not always supported by experimental evidence ([7], see also [8]). Moreover, when more than 3 clocks are compared, the uncorrelation hypothesis leads to the formulation of an overdetermined linear system of equations [2, 3, 6, 9] and this overdetermination seems incompatible with the inconsistency of some results.

Here a new, consistent and more general mathematical model is proposed, suited for statistical processing of measured differences. The entire *NxN* covariance matrix **R** of the clocks along with the *(N-1)x(N-1)* covariance matrix **S** of the differences are introduced. Their relationship, and the possibility to estimate **R** from the knowledge of **S**, are then discussed. A diagonal structure of **R** can result, a posteriori, from the most desirable situation of truly uncorrelated clocks. This model abides by the CIPM recommendation [10] in which it is recognized that "where appropriate, the estimated covariances should be given".

The examination of matrix **S** helps understanding the validity of the uncorrelation hypothesis. When such hypothesis is acceptable, the problem can be reduced to the classical case of the *N*-cornered hat, while in the other cases, the complete matrix **R** must be solved. In this second case the problem is underdetermined because the number of unknowns exceeds the number of equations. In any case there is an important constraint which binds the domain of acceptable solutions: the matrix **R**, as any covariance matrix, must be positive definite. A theorem, specifically devised, is here presented showing that **R** is positive definite if and only if its determinant is positive. This constraint has been geometrically interpreted giving an insight of the features of the solution domain.

The interesting case of an increasing number of compared clocks is then examined showing how a larger number of clocks reduces the solution domain of **R**.

2 STATEMENT OF THE PROBLEM

Let us denote by x^i the process related to the i-th clock and x^i_m its realization at the instant t_m. If M consecutive equispaced samples of the process are considered, they can be arranged in the vector $\mathbf{x}^i = [x^i_1,\ x^i_2, \ldots,\ x^i_M]^T$, where superscript ^{T} denotes the transposition. The expected value $\bar{x}^i$ of process x^i can be estimated in terms of the elements of $\mathbf{x}^i$ as $\bar{x}^i = (1/M)(x^i_1 + x^i_2 + \ldots + x^i_M)$ and arranged into the M-vector $\bar{\mathbf{x}}^i = [\bar{x}^i,\ \bar{x}^i, \ldots, \bar{x}^i]^T$. The M samples of the N clock processes are then cast in the $M \times N$ matrix $\mathbf{X} = [\mathbf{x}^1,\ \mathbf{x}^2,\ \ldots, \mathbf{x}^N]$. Similarly, the $M \times N$ matrix $\bar{\mathbf{X}}$ is introduced as $\bar{\mathbf{X}} = [\bar{\mathbf{x}}^1,\ \bar{\mathbf{x}}^2,\ \ldots,\ \bar{\mathbf{x}}^N]$. With these definitions the covariance matrix of the processes x^i, $i = 1,\ 2, \ldots,\ N$ is estimated by **R**:

$$\mathbf{R} = [1/(M-1)][\mathbf{X} - \bar{\mathbf{X}}]^T[\mathbf{X} - \bar{\mathbf{X}}] \tag{1}$$

The diagonal element r_{ii} ($r_{ii} > 0$) denotes the variance of the i-th clock, while, for $i \neq j$, r_{ij} denotes the covariance between the i-th and the j-th clock. In order to obtain a good estimation of the matrix **R**, it is required that the number of samples M be much larger than the number N of clocks.

When clocks are compared by measuring differences between their readings, the available data are the time differences $y^{ij} = x^i - x^j$. Also y^{ij} is statistically characterized by its expected value $\bar{y}^{ij}$

and by its variance: the estimates of these values are tied to the estimates of the variances r_{ii} and r_{jj} of the two single clocks and of their covariance r_{ij}.

One of the clocks, for instance clock $\#N$, is chosen as the reference, and it is compared at M different instants with clocks #1, #2,..., #(N-1) giving $(N-1)$ distinct time difference measure M-vectors $\mathbf{y}^{1N} = \mathbf{x}^1 - \mathbf{x}^N$, $\mathbf{y}^{2N} = \mathbf{x}^2 - \mathbf{x}^N, \ldots$, $\mathbf{y}^{(N-1),\,N} = \mathbf{x}^{(N-1)} - \mathbf{x}^N$. Under the assumptions of contemporary and noiseless measurements, the other possible measure vectors $\mathbf{y}^{ij}$ $(i, j \neq N)$ are redundant, since they can be obtained as linear combination of those involving clock $\#N$ and they don't add any information, as proved in [11].

The M samples of the $N-1$ clock differences are cast in the $M \times (N-1)$ matrix $\mathbf{Y} = [\mathbf{y}^{1N}, \mathbf{y}^{2N}, \ldots, \mathbf{y}^{N-1,\,N}]$. Similarly the $M \times (N-1)$ matrix $\bar{\mathbf{Y}}$ is introduced as $\bar{\mathbf{Y}} = [\bar{\mathbf{y}}^{1N}, \bar{\mathbf{y}}^{2N}, \ldots, \bar{\mathbf{y}}^{(N-1),\,N}]$, where $\bar{\mathbf{y}}^{iN}$ is the M-vector whose elements are coincident with $\bar{y}^{iN}$.

The processes y^{iN}, $(i = 1, 2, \ldots, N-1)$ are statistically characterized by the estimation of the $(N-1) \times (N-1)$ covariance matrix $\mathbf{S}$ defined as:

$$\mathbf{S} = [1/(M-1)][\mathbf{Y} - \bar{\mathbf{Y}}]^T[\mathbf{Y} - \bar{\mathbf{Y}}] \tag{2}$$

A generic element s_{ij} denotes either a variance (for $i = j$) and it is always positive or a covariance (for $i \neq j$) and may assume any real value. Note that the index N of the reference clock has been dropped in any element of $\mathbf{S}$.

The relationship between matrices $\mathbf{S}$ and $\mathbf{R}$ is easily determined by observing that $\mathbf{Y}$ can be derived from $\mathbf{X}$, according to the following relationship:

$$\mathbf{Y} = \mathbf{X}\,\mathbf{H} \tag{3}$$

where $\mathbf{H}$ is the $N \times (N-1)$ matrix:

$$\mathbf{H} = \begin{bmatrix} \hat{\mathbf{I}} \\ -\mathbf{u}^T \end{bmatrix} \tag{4}$$

where $\hat{\mathbf{I}}$ is the $(N-1) \times (N-1)$ identity matrix and $\mathbf{u}$ is the $(N-1)$-vector $[1, 1, \ldots, 1]^T$. A similar relationship ties the corresponding matrices $\bar{\mathbf{X}}$ and $\bar{\mathbf{Y}}$.

From (1), (2), and (3), the covariance matrix $\mathbf{S}$ can be expressed in terms of $\mathbf{R}$ as:

$$\mathbf{S} = \mathbf{H}^T\mathbf{R}\mathbf{H} \tag{5}$$

For sake of generality here we discuss the covariance matrices of the processes themselves, but the same properties hold also for any covariance matrix defined from prefiltered data as is generally the case in the estimation of clock instability, where the Allan variance is used.

3 CONSIDERATIONS ON R AND S

By taking into account the symmetry of $\mathbf{R}$ and $\mathbf{S}$ it appears that $\mathbf{R}$ is defined by $N(N-1)$ scalars and $\mathbf{S}$ by $(N-1)N/2$ ones, then the knowledge of $\mathbf{S}$ is not sufficient to fix a unique estimation

of $\mathbf{R}$ because ∞^N solutions satisfy (5) (underdetermined problem). A way to isolate the N free parameters consists in partitioning $\mathbf{R}$ according to:

$$\mathbf{R} = \begin{bmatrix} \hat{\mathbf{R}} & \mathbf{r} \\ \mathbf{r}^T & r_{NN} \end{bmatrix} \tag{6}$$

where $\hat{\mathbf{R}}$ is the leading $(N-1)\times(N-1)$ submatrix; $\mathbf{r} = [r_{1N},\ r_{2N}, \ldots,\ r_{N-1,\ N}]^T$ is the $(N-1)$-vector, grouping the covariances involving the N-th clock and r_{NN} is the variance of the N-th clock. With this partition, and by substituting (4), equation (5) can be rewritten as:

$$\mathbf{S} = [\hat{\mathbf{I}} - \mathbf{u}] \begin{bmatrix} \hat{\mathbf{R}} & \mathbf{r} \\ \mathbf{r}^T & r_{NN} \end{bmatrix} \begin{bmatrix} \hat{\mathbf{I}} \\ -\mathbf{u}^T \end{bmatrix} = \hat{\mathbf{R}} + r_{NN}[\mathbf{u}\ \mathbf{u}]^T - \mathbf{u}\ \mathbf{r}^T - \mathbf{r}\ \mathbf{u}^T \tag{7}$$

This equation shows that $\mathbf{R}$ can be uniquely reconstructed from $\mathbf{S}$ if the (co)variances related to the N-th clock, i.e. $\mathbf{r}$ and r_{NN}, are known. In fact, (7) can be transformed in the following expression:

$$\hat{\mathbf{R}} = \mathbf{S} - r_{NN}[\mathbf{u}\ \mathbf{u}^T] + \mathbf{u}\ \mathbf{r}^T + \mathbf{r}\ \mathbf{u}^T \tag{8}$$

With a deeper look into (7), some qualitative information about $\mathbf{R}$ can be immediately deduced when $\mathbf{S}$ is known:

1. If the N clocks are uncorrelated, $\mathbf{S}$ assumes the form:

$$\mathbf{S} = \begin{bmatrix} r_{11} + r_{NN} & r_{NN} & \ldots & r_{NN} \\ r_{NN} & r_{22} + r_{NN} & \ldots & r_{NN} \\ \ldots & \ldots & \ldots & \ldots \\ r_{NN} & r_{NN} & \ldots & r_{N-1,\ N-1} + r_{NN} \end{bmatrix} \tag{9}$$

   All the covariances s_{ij} (with $i \neq j$) are equal and positive, because $s_{ij} = r_{NN} > 0$. Moreover each variance $s_{ii} > s_{ij}$ (with $i \neq j$). These conditions are necessary to validate the assumption of uncorrelation of the N clocks. Unfortunately they are not sufficient to conclude that the clock are uncorrelated because, together with a unique diagonal solution, infinitely many other non–diagonal matrices $\mathbf{R}$ would drive to the same matrix $\mathbf{S}$, but if these conditions are satisfied one can "reasonably" assume the uncorrelation.

2. If the reference clock is "quasi–ideal" (that is $r_{NN} \ll r_{ii}$ for $i = 1,\ 2, \ldots,\ N-1$) and all the clocks are uncorrelated, then $s_{ij} \ll s_{ii}$ for any $i \neq j$ and $\mathbf{S}$, as well as $\mathbf{R}$, can be considered diagonal. So, if $\mathbf{S}$ is almost diagonal, the reference clock is of high quality. In this case, the submatrix $\hat{\mathbf{R}}$ almost coincides with $\mathbf{S}$ and $\mathbf{r} \cong 0,\ r_{NN} \cong 0$.

3. For the same reason, when the hypothesis of uncorrelation holds, if the reference clock is changed and $\mathbf{S}$ is computed again, it gives an idea of which one of the clocks is less noisy, because it results in a matrix $\mathbf{S}$ with minimum off–diagonal terms.

4. If any s_{ij} (with $i \neq j$) is negative, then the uncorrelation hypothesis is certainly to be excluded at least between the $(i,\ N)$-th or the $(j,\ N)$-th pair of clocks.

5. If all the terms s_{ij} (with $i \neq j$) are equal and positive except one, for instance s_{kl}(with $k \neq l$), which is positive but differs from the others, that indicates that all the clocks can be considered uncorrelated except the pair $(k,\ l)$.

6. If the terms s_{ij} (with $i \neq j \neq k$) are coincident and positive, and the terms s_{ij} (with $i \neq j,\ i = k,$ or $j = k$) are coincident but different from the previous ones, the k-th clock is possibly correlated with the reference one while all the others are uncorrelated.

From the theoretical point of view, the above considerations suggest clear interpretations. By handling experimental data, it can be difficult to recognize the points above because of round-off error, not perfect contemporaneity of measurement, low noise introduced by the measurement system but, above all, the low number of statistical samples that give a considerable uncertainty bar on the estimates.

4 POSITIVE DEFINITENESS OF S AND R

The estimation of the complete matrix $\mathbf{R}$ asks for a suitable choice on the N free parameters in (8). In any case, there is an important constraint which bounds the solution domain $\mathcal{D}$ in the space of the N free parameters and which guarantees a significant result: as any covariance matrix [13], *the estimated covariance matrix* $\mathbf{R}$ *must be positive definite.*

Some significant properties of positive definite covariance matrices are here reminded. Let $\mathbf{A}$ be an $N \times N$ symmetrical matrix and $\mathbf{A}^{(n)}$ $(n = 1,\ 2, \ldots,\ N)$ be the leading $n \times n$ submatrices of $\mathbf{A}$, extracted from $\mathbf{A}$ by considering the elements belonging to the first n rows and n columns (with $\mathbf{A}^{(N)} \equiv \mathbf{A}$). The matrix $\mathbf{A}$ is positive definite if and only if [13]:

$$|\mathbf{A}^n)| > 0 \qquad \text{for } n = 1,\ 2, \ldots,\ N \tag{10}$$

where $|\ .\ |$ denotes the determinant.

Then the positive definiteness of $\mathbf{A}$ requires the validation of N scalar inequalities. In the case of $\mathbf{R}$ and $\mathbf{S}$, since they are both positive definite and they are linked by (5), a theorem holds [11]:

Theorem 1: The $N \times N$symmetrical matrix $\mathbf{R}$, related to the known positive definite $(N-1) \times (N-1)$ symmetrical matrix $\mathbf{S}$ by the relationship (5), is also positive definite if and only if $|\mathbf{R}| > 0$.

This theorem allows one to verify the positive definiteness of $\mathbf{R}$ by considering only one of the inequalities (10); moreover this inequality can be geometrically interpreted. In fact, the relationship $|\mathbf{R}| = 0$ appears to be an equation of second degree in the $N-1$ elements of $\mathbf{r}$ and in r_{NN}.

With the partition of $\mathbf{R}$ used in (6), it can be demonstrated [11] that its determinant can be expressed as:

$$|\mathbf{R}| = |\mathbf{S}|(r_{NN} - [\mathbf{r} - r_{NN}\mathbf{u}]^T\mathbf{S}^{-1}[\mathbf{r} - r_{NN}\mathbf{u}]) \tag{11}$$

with $\mathbf{u}$ defined in (4). The boundary of the solution domain $\mathcal{D}$ is therefore described by the surface $|\mathbf{R}| = 0$:

$$[\mathbf{r} - r_{NN}\mathbf{u}]^T\mathbf{S}^{-1}[\mathbf{r} - r_{NN}\mathbf{u}] = r_{NN} \tag{12}$$

If r_{NN} is fixed, this expression represents an ellipsoid in the $(N-1)$dimensional space described by the variables $r_{1N},\ r_{2N}, \ldots,\ r_{N-1,\ N}$ because the matrix $\mathbf{S}^{-1}$ of the quadratic form is positive definite.

This ellipsoid is centered at the point of coordinates ($r_{1N} = r_{NN}$, $r_{2N} = r_{NN}, \ldots, r_{N-1,N} = r_{NN}$), the principal axes are rotated and the squared length of the axes is proportional to r_{NN}. As far as the parameter r_{NN} is concerned, the domain $\mathcal{D}$ takes the form of an elliptic hyper-paraboloid in the N-dimensional space. The intersection with a plane ($r_{NN} = \text{constant}$) leads to an $(N-1)$-dimensional ellipsoid, the increase of r_{NN} increases the surface and shifts the center of the ellipsoid (12), and it doesn't rotate its axes. Fig. 1 shows an example of the domain $\mathcal{D}$ in the case of $N = 3$.

The constraint of positive definiteness of $\mathbf{R}$ bounds the domain of choice of the N free parameters $\mathbf{r}$ and r_{NN} and only the set of values of $r_{1N}, r_{2N}, \ldots, r_{N-1,N}, r_{NN}$ situated inside the surface described by (12) guarantees acceptable solutions.

5 EFFECT OF AN INCREASING NUMBER OF COMPARED CLOCKS

Knowing the expression of the boundary of the domain $\mathcal{D}$, it can be interesting to test how it is modified by varying the number of clocks involved in the measurements. Within a set of N clocks let's individuate the N-th clock as the reference one and two subset $\mathcal{C}^a$ of N^a clocks and $\mathcal{C}^b$ of N^b clocks. $\mathcal{C}$ denotes the union of $\mathcal{C}^a$ and $\mathcal{C}^b$ and $N = N^a + N^b + 1$. With the above notation, the $N \times N$ covariance matrix $\mathbf{R}$ of the N clocks is partitioned as follows:

$$\mathbf{R} = \begin{bmatrix} \mathbf{R}^{aa} & \mathbf{R}^{ab} & \mathbf{r}^a \\ [\mathbf{R}^{ab}]^T & \mathbf{R}^{bb} & \mathbf{r}^b \\ [\mathbf{r}^a]^T & [\mathbf{r}^b]^T & r_{NN} \end{bmatrix} \tag{13}$$

where $\mathbf{R}^{aa}$ and $\mathbf{R}^{bb}$ are the covariance matrices related to the clocks in $\mathcal{C}^a$ and $\mathcal{C}^b$ respectively. $\mathbf{R}^{ab}$ contains the covariances between clocks in $\mathcal{C}^a$ and $\mathcal{C}^b$ versus the N-th clock; they represent a partition of the vector $\mathbf{r}$ introduced in (6). The element r_{NN} is the variance of the N-th clock.

Analogously, the $(N-1) \times (N-1)$ covariance matrix $\mathbf{S}$ of the differences can be partitioned as:

$$\mathbf{S} = \begin{bmatrix} \mathbf{S}^{aa} & \mathbf{S}^{ab} \\ [\mathbf{S}^{ab}]^T & \mathbf{S}^{bb} \end{bmatrix} \tag{14}$$

where $\mathbf{S}^{aa}$ and $\mathbf{S}^{bb}$ are the covariance matrices of the differences related to the clocks in $\mathcal{C}^a$ and $\mathcal{C}^b$ respectively.

If the clocks in $\mathcal{C}^a$ and $\mathcal{C}$ (jointly with the reference one) are considered, the respective solution domains $\mathcal{D}^a$ and $\mathcal{D}$ are:

$$[\mathbf{r}^a - r_{NN}\mathbf{u}^a]^T[\mathbf{S}^{aa}]^{-1}[\mathbf{r}^a - r_{NN}\mathbf{u}^a] \leq r_{NN} \tag{15}$$

$$[\mathbf{r} - r_{NN}\mathbf{u}]^T\mathbf{S}^{-1}[\mathbf{r} - r_{NN}\mathbf{u}] \leq r_{NN} \tag{16}$$

where $\mathbf{u}^a$ is the N^a-vector $[1, 1, \ldots, 1]^T$.

Expression (16) can be rewritten in terms of the submatrices of $\mathbf{S}$ in (14). In fact, the vector $\mathbf{r} - r_{NN}\mathbf{u}$ can be partitioned as:

$$[\mathbf{r} - r_{NN}\mathbf{u}] = \begin{bmatrix} \mathbf{r}^a - r_{NN}\mathbf{u}^a \\ \mathbf{r}^b - r_{NN}\mathbf{u}^b \end{bmatrix} \tag{17}$$

where $\mathbf{u}^b$ is the N^b-vector $[1,\ 1,\ldots,\ 1]^T$ and the inverse of $\mathbf{S}$ can be written as:

$$\mathbf{S}^{-1} = \begin{bmatrix} [\mathbf{S}^{aa}]^{-1} + [\mathbf{S}^{aa}]^{-1}\,\mathbf{S}^{ab}\,[\mathbf{D}^{bb}]^{-1}\,[\mathbf{S}^{ab}]^T\,[\mathbf{S}^{aa}]^{-1} & -[\mathbf{S}^{aa}]^{-1}\,\mathbf{S}^{ab}\,[\mathbf{D}^{bb}]^{-1} \\ -[\mathbf{D}^{bb}]^{-1}\,[\mathbf{S}^{ab}]^T\,[\mathbf{S}^{aa}]^{-1} & [\mathbf{D}^{bb}]^{-1} \end{bmatrix} \tag{18}$$

where the matrix $\mathbf{D}^{bb}$ is defined as [12]:

$$\mathbf{D}^{bb} = \mathbf{S}^{bb} - [\mathbf{S}^{ab}]^T[\mathbf{S}^{aa}]^{-1}\mathbf{S}^{ab} \tag{19}$$

Now the idea is to compare the extension of the domains delimited by the elliptic paraboloids $\mathcal{D}^a$ and $\mathcal{D}$, defined by (15) and (16), respectively. The domain $\mathcal{D}^a$ is defined in the space of N^a+1 variables $r_{1N},\ r_{2N},\ldots,\ r_{N^aN},\ r_{NN}$, while $\mathcal{D}$ is defined in the space of N variables $r_{1N},\ r_{2N},\ldots,\ r_{N-1,N},\ r_{NN}$. To the aim of comparison, it is necessary to individuate a sub-domain $\bar{\mathcal{D}}$ obtained from $\mathcal{D}$ by a suitable projection in the subspace of N^a+1 variables $r_{1N},\ r_{2N},\ldots,\ r_{N^aN},\ r_{NN}$.

Domain $\bar{\mathcal{D}}$ is obtained by the projection of the intersection of $\mathcal{D}$ with the N^b-dimensional subspace defined by the hyperplane $r_{NN}\mathbf{u}^b = \mathbf{r}^b$. Since this choice corresponds to the largest intersection of $\mathcal{D}$, $\bar{\mathcal{D}}$ results in the largest possible subdomain in the (N^a+1)-dimensional subspace and therefore it yields the least favourable case in the comparison of the two domains.

By substituting (17), (18), (19) and $r_{NN}\mathbf{u}^b = \mathbf{r}^b$ in (16), the equation defining domain $\bar{\mathcal{D}}$ is obtained as:

$$[\mathbf{r}^a - r_{NN}\mathbf{u}^a]^T[\mathbf{S}^{aa}]^{-1}[\mathbf{r}^a - r_{NN}\mathbf{u}^a] + [\mathbf{r}^a - r_{NN}\mathbf{u}^a]^T\{[\mathbf{S}^{aa}]^{-1}\mathbf{S}^{ab}[\mathbf{D}^{bb}]^{-1}[\mathbf{S}^{ab}]^T[\mathbf{S}^{aa}]^{-1}\}[\mathbf{r}^a - r_{NN}\mathbf{u}^a] = r_{NN} \tag{20}$$

By comparing $\bar{\mathcal{D}}$ (20) with $\mathcal{D}^a$ (15), it appears that the only difference is in the second quadratic form in the l.h.s. of (20). From the properties of the definite positive matrices, since $\mathbf{S}$ and its submatrix $\mathbf{S}^{aa}$ are positive definite, so are their inverses, and it can be demonstrated that also the matrix $[\mathbf{S}^{aa}]^{-1}\mathbf{S}^{ab}[\mathbf{D}^{bb}]^{-1}[\mathbf{S}^{ab}]^T[\mathbf{S}^{aa}]^{-1}$ of the second quadratic form in (20) is positive definite. So it necessarily results that $\bar{\mathcal{D}}$ is contained inside $\mathcal{D}^a$. As a result, an increased number of compared clocks reduces the solution domain and therefore the amount of arbitrariness in the determination of the covariance matrix $\mathbf{R}$, even in the worst considered case, i. e. with the largest possible intersection. It must be stressed that the reduction ratio of the solution domains depends only on the elements of matrix $\mathbf{S}$ and not on the value of r_{NN}. Intuitively, if the clocks in $\mathcal{C}^b$ are completely correlated with any clock in $\mathcal{C}^a$ or with the reference one, their measurement doesn't add any further information to the problem and the reduction of the solution domain will be very poor. On the contrary, the addition of independent clocks can result in a significant shrinking of the solution domain.

6 EXAMPLE

Five commercial cesium clocks have been compared. Three of the clocks are maintained at IEN, Turin, Italy (Cs4, Cs5, Cs6), the other two clocks are maintained at ISPT, Rome, Italy and Telespazio, Matera, Italy and data are regularly transmitted to the IEN for traceability. The comparison at distance is obtained with GPS or TV link. An appropriate smoothing procedure has been applied to reduce the additive noise due to the synchronization link and, for integration times larger than five days, this noise can be assumed to be negligible. The Allan covariance matrix

has been computed for different integration times, with overlapping samples, by using one year (1991) of daily measurement data. (The Allan covariance matrix is an extension of the well-known Allan variance in the sense of (1)). In the present example the set $\mathcal{C}^a$ is composed of clocks Cs4 and Cs5 of IEN, the set $\mathcal{C}^b$ is composed of the two external clocks and the clock Cs6 of IEN is the reference one. When the clocks in $\mathcal{C}^a$ jointly to the reference are used, the 2x2 matrix $\mathbf{S}^{aa}$ is obtained while, with the five clocks, the 4x4 matrix $\mathbf{S}$ is obtained.

To investigate how the increased number of clocks reduces the solution domain, $\bar{\mathcal{D}}$ is compared with $\mathcal{D}^a$ in the plane (r_{15}, r_{25}), with a fixed value for the variance r_{55}. Here we report only some of the most significant examined cases.

The first case regards the Allan covariance matrix evaluated for integration time $\tau = 10$ days. The following matrices $\mathbf{S}^{aa}$ and $\mathbf{S}$ are obtained, where numerical values have been scaled by 10^{28}:

$$\mathbf{S}^{aa} = \begin{bmatrix} 11.8 & 4.78 \\ 4.78 & 9.34 \end{bmatrix} \qquad \mathbf{S} = \begin{bmatrix} 11.8 & 4.78 & 8.64 & 7.10 \\ 4.78 & 9.34 & 7.38 & 1.31 \\ 8.64 & 7.38 & 96.7 & -23.7 \\ 7.10 & 1.31 & -23.7 & 218 \end{bmatrix} \tag{21}$$

Since matrix $\mathbf{S}^{aa}$ satisfies conditions (9), the uncorrelation hypothesis is acceptable for the clocks in $\mathcal{C}^a$ and the reference one. We can choose $r_{55} = s_{12}$, $r_{15} = 0$, and $r_{25} = 0$ driving to the classical solution. By choosing $r_{55} = s_{12}$, the two domains $\mathcal{D}^a$ and $\bar{\mathcal{D}}$ delimiting the possible choices for r_{15} and r_{25} are compared in Fig. 2. As expected, the classical solution corresponding to $r_{15} = 0$ and $r_{25} = 0$ is inside the domain $\mathcal{D}$, and it is also inside the domain $\bar{\mathcal{D}}$. It also means that from the comparisons of the five clocks it results that the clocks in $\mathcal{C}^a$ and the reference one may be considered uncorrelated. That is not the case for the other clocks because the complete matrix $\mathbf{S}$ has not all equal and positive off-diagonal elements.

From Fig.2 it can be verified that the addition of the (co)variances of the clocks in $\mathcal{C}^b$ slightly shrinks the solution domain and therefore also the arbitrariness in the choices of the free parameters r_{15} and r_{25} is reduced.

The second case concerns the instability estimation of the same clocks for $\tau = 100$ days. The following matrices $\mathbf{S}^{aa}$ and $\mathbf{S}$ are obtained:

$$\mathbf{S}^{aa} = \begin{bmatrix} 104 & 20.3 \\ 20.3 & 16.1 \end{bmatrix} \qquad \mathbf{S} = \begin{bmatrix} 104 & 20.3 & 97.4 & 103 \\ 20.3 & 16.1 & 19.8 & -41.6 \\ 97.4 & 19.8 & 97.3 & 88.9 \\ 103 & -41.6 & 88.9 & 433 \end{bmatrix} \tag{22}$$

where the values are again scaled by 10^{28}.

Here the conditions (9) are not satisfied neither in the comparison of three clocks ($\mathbf{S}^{aa}$), nor with five clocks ($\mathbf{S}$). The solution domain of the covariances r_{15} and r_{25} is represented in Fig. 3. Here we see a significant reduction of $\bar{\mathcal{D}}$ with respect to $\mathcal{D}^a$ when five clocks are compared. The clocks in $\mathcal{C}^a$ add so much information that the range of acceptable values for r_{15} and r_{25} is reduced by a factor of 5. Inside the domain $\bar{\mathcal{D}}$, the arbitrariness in choosing r_{15} and r_{25} is so much reduced that it seems not so much crucial the criterion to be used for the final choice. This situation is also

depicted in Fig. 4 where the two 3–dimensional elliptic paraboloids describe the boundaries of the solution domains for r_{15}, r_{25}, and r_{55}.

7 CONCLUSIONS

This work has considered the estimation of clock instabilities when 3 or more clocks are compared by measuring signal differences. From the measure covariance matrix **S** several information about the instability of the individual clocks can be inferred and, in particular, the uncorrelation hypothesis can be accepted or rejected. The estimation of the individual clock covariance matrix **R** from the knowledge of **S** is an underdetermined problem and an appropriate optimization criterion ought to be formulated to fix the remaining free parameters, but the solution domain is constrained by the request of positive definiteness for the resulting **R**. Such a constraint has been deeply analyzed and, with a theorem, it has been possible to give a simply geometrical illustration. Moreover the importance of the comparison of a larger number of clocks is outlined, showing how, in some cases, it results in a significant reduction of the arbitrariness in estimating clock instability.

REFERENCES

[1] J. E. Gray, D. W. Allan, *"A method for estimating the frequency stability of an individual oscillator,"* in Proc. 28th Frequency Control Symposium, 1974, pp. 243–246.

[2] J. A. Barnes, *"Time scale algorithms using Kalman filters – Insights from simulation,"* presented at the 2nd Atomic Time Scale Algorithm Symposium, Boulder, CO, 1982.

[3] C. A. Greenhall, *"Likelihood and least–squares approaches to the M–cornered hat,"* in Proc. Precise Time and Time Interval Planning Meeting, 1987, pp. 219–225.

[4] J. Groslambert, D. Fest, M. Olivier, J. J. Gagnepain, *"Characterization of frequency fluctuations by crosscorrelations and by using three or more oscillators,"* in Proc. 35th Frequency Control Symposium, 1981, pp. 458–463.

[5] D. Fest, J. Groslambert, J. J. Gagnepain, *"Individual characterization of an oscillator by means of cross–correlation or cross–variance method,"* IEEE Trans. Instrum. Meas., vol. 32, n. 3, pp. 447–450, Sept. 1983.

[6] D. W. Allan, *" Time and frequency (time domain) characterization, estimation, and prediction of precision clocks and oscillators,"* IEEE Trans. Ultr. Ferr. Freq. Control, vol. UFFC–34, n. 6, pp. 647–654, 1987.

[7] A. Premoli, P. Tavella, *" A revisited 3–cornered hat method for estimating frequency standard instability,"* to appear on IEEE Trans. Instrum. Meas., Feb. 1993

[8] P. Tavella, A. Premoli, *" Characterization of frequency standard instability by estimation of their covariance matrix,"* in Proc. Precise Time and Time Interval Planning Meeting, 1991, pp. 265–276.

[9] J. Mck. Luck, " *Construction and comparison of atomic time scale algorithms,*" Tech. Report 32, Dept. Resources and Energy, Nationai Mapping Div., Camberra, Australia, 1983.

[10] CIPM Comite International des Poids et Mesures, Proc. Verb., v. 49, p.26, 1981.

[11] P. Tavella, A. Premoli, in preparation.

[12] F. Ayres, Jr., *"Matrices,"* Schaum's outlines series, Mc.Graw–Hill, 1962, chapter 17, pp. 131–145.

[13] R. Bellman, *"Introduction to matrix analysis,"* Mc.Graw–Hill, 1970, chapters 1 and 5, pp. 4 and 75.

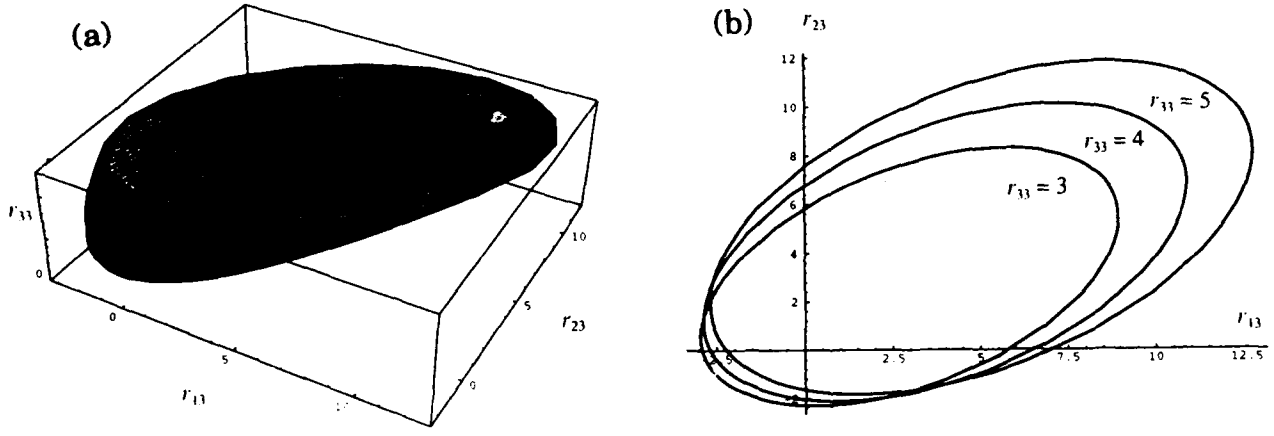

Fig.1: Solution domain $\mathcal{D}$ corresponding to a particular matrix S obtained from the comparison of 3 different clocks.
(a) the domain $\mathcal{D}$ in the space of variables r_{13}, r_{23}, and r_{33}.
(b) boundaries of $\overline{\mathcal{D}}$ for some fixed values of r_{33}.

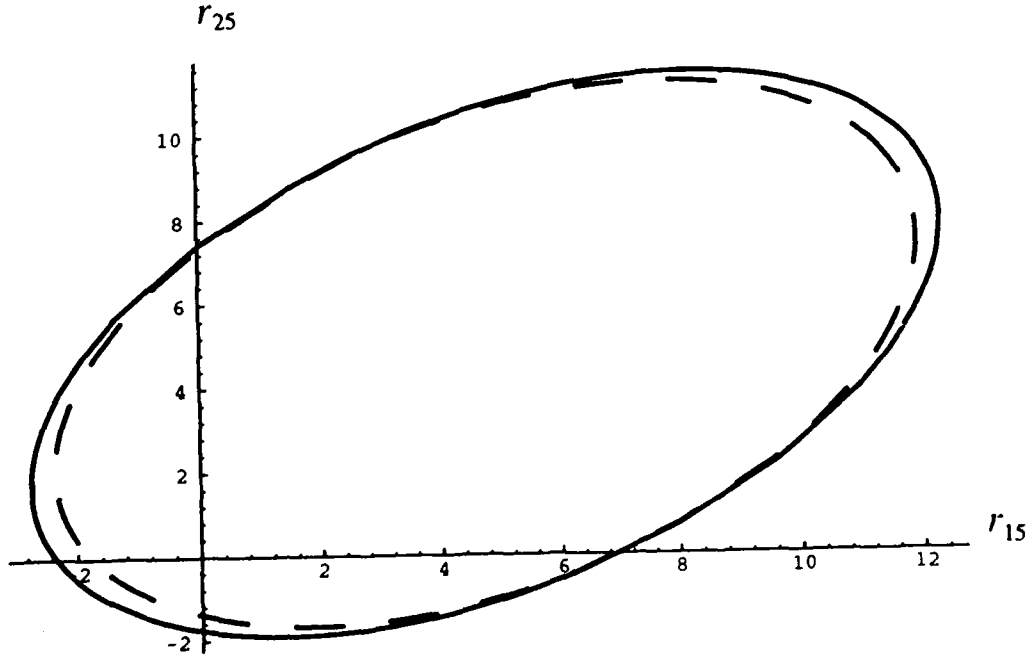

Fig.2: Domains $\mathcal{D}'$ (solid line) and $\overline{\mathcal{D}}$ (dashed line) in the plane (r_{15},r_{25}) for integration time $\tau = 10$ days and $r_{55} = 4.78*10^{-28}$.

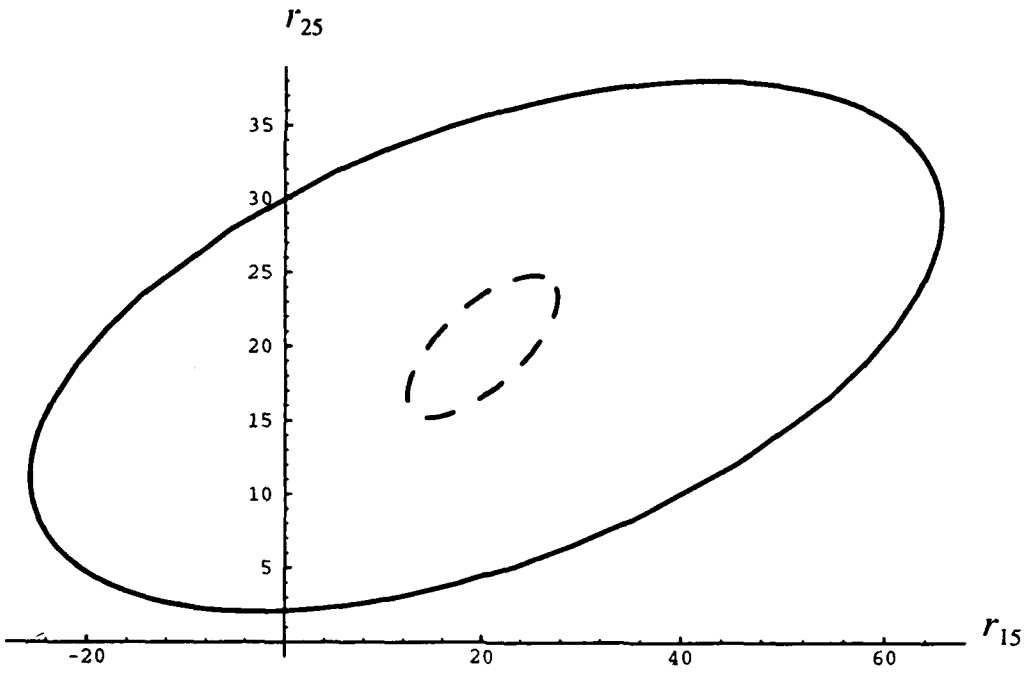

Fig.3: Domains $\mathcal{D}^a$ (solid line) and $\overline{\mathcal{D}}$ (dashed line) in the plane (r_{15}, r_{25}) for integration time $\tau = 100$ days and $r_{55} = 20*10^{-28}$.

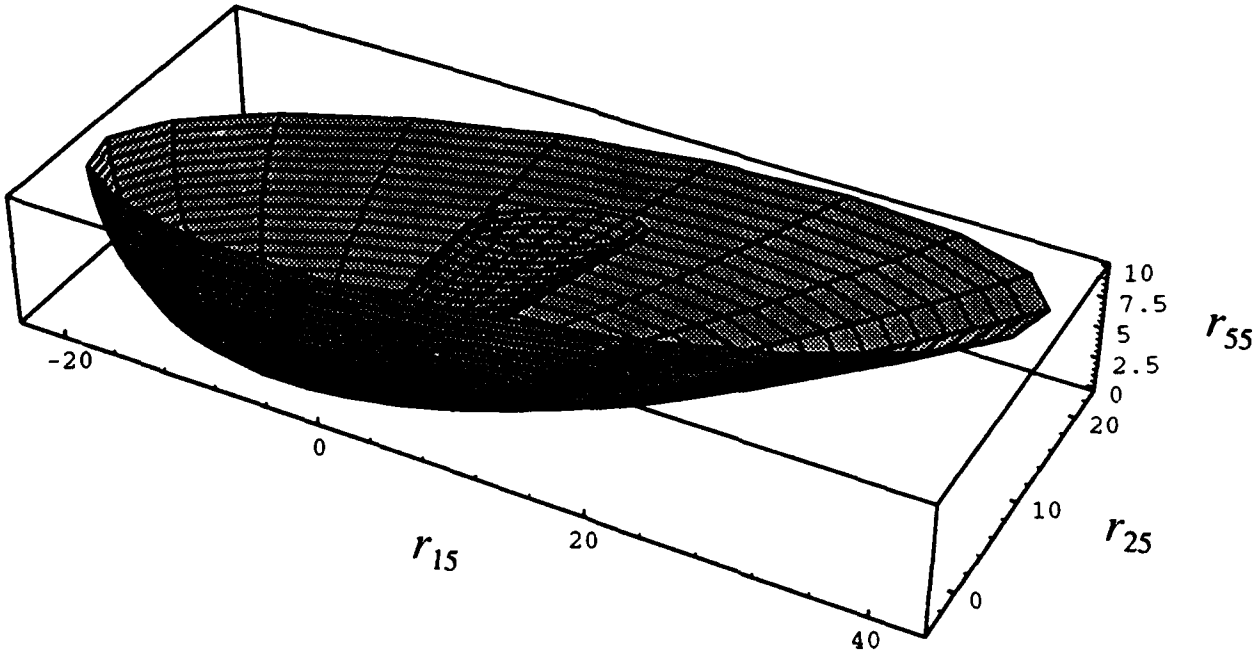

Fig.4: Domains $\mathcal{D}^a$ (external paraboloid) and $\overline{\mathcal{D}}$ (internal paraboloid) in the space described by r_{15}, r_{25}, and r_{55}.

QUESTIONS AND ANSWERS

Question: Is it possible for the domain to shrink to zero?

P. Tavella, Instituto Elettrotecnico Nazionale: Yes, in fact for example, I suppose that one correlation is possible. You just shrink to the region when all the covariances term are zero. You just have no more degrees of freedom.

Time Scale Algorithms for an Inhomogeneous Group of Atomic Clocks

C. Jacques, J.-S. Boulanger, R.J. Douglas, D. Morris,
S. Cundy, and H.F. Lam
Time and Frequency Standards Group
Institute for National Measurement Standards
National Research Council of Canada
Ottawa, CANADA K1A 0R6

Abstract

Through the past 17 years, the time scale requirements at NRC have been met by the unsteered output of its primary laboratory cesium clocks, supplemented by hydrogen masers when short-term stability better than $2 \times 10^{-12} \tau^{-1/2}$ has been required. NRC now operates three primary laboratory cesium clocks, three hydrogen masers and two commercial cesium clocks.

NRC has been using ensemble averages for internal purposes for the past several years, and has a real-time algorithm operating on the outputs of its high-resolution (2×10^{-13} s @ 1 s) phase comparators. The slow frequency drift of the hydrogen masers has presented difficulties in incorporating their short-term stability into the ensemble average, while retaining the long-term stability of the laboratory cesium frequency standards.

We report on this work on algorithms for an inhomogeneous ensemble of atomic clocks, and on our initial work on time scale algorithms that could incorporate frequency calibrations at NRC from the next generation of Zacharias fountain cesium frequency standards having frequency accuracies that might surpass 10^{-15}, or from single-trapped-ion frequency standards ($Ba^+, Sr^+, \ldots$) with even higher potential accuracies.

We present and discuss the requirements for redundancy in all the elements (including the algorithms) of an inhomogeneous ensemble that would give a robust real-time output of the algorithms.

Introduction

Time scale algorithms are of wide interest because an ensemble average should behave better than the best clock of the ensemble, in terms of accuracy, stability and reliability: to some extent the misbehavior of any clock of the ensemble can be filtered out without disturbing appreciably the ensemble average. The stability of a new clock can be added to the ensemble average without major disturbance.

Historically, at NRC, the implementation of a time scale algorithm at NRC has been delayed by the excellent behavior of the laboratory cesium clocks of the Cs V and Cs VI designs. Used alone, they met most of the needs of TA(NRC) and UTC(NRC), with the other needs being met by NRC's masers. The advantages of developing a good time scale algorithm were not as evident as the advantages of maintaining a "good clock".

Nonetheless, a time scale algorithm was developed for the NRC ensemble, and used to assist in primary clock evaluations. It was particularly beneficial for evaluations when the NRC ensemble was operating

in a degraded mode caused by problems either with our building's environment or with the clocks themselves.

This algorithm was developed to exploit the short-term characteristics of the NRC clock ensemble for the purposes of clock diagnostics, initially to run with the NRC three-channel phase comparators at 10^{-12} s resolution, taking phase data every 10 s. With the new NRC masers, a higher resolution phase comparator was desirable, and the old design [1] was improved to give a unit which gives phase differences each second (averaged over one second) with 0.1 ps resolution, and a short-term noise level of less than 0.2 ps. We have built, and are commissioning two phase comparator systems for full redundancy. Each phase comparator system can record 32 phase differences taken from up to 16 5 MHz sources, and has standard serial output at 9600 bps. The main data acquisition software runs on MS-DOS computers under Deskview. We wrote a driver to accept and check the phase comparator data, and write the files to disk. The data acquisition computer system also runs the ensemble average software in real-time (with less than 1.5 s delay from any phase step to the ensemble average: up to 1 s delay in the phase comparator, up to 0.3 s in serial transmission, and up to 0.2 s for the recalculation of the ensemble average). The same computer system flexibly displays the phase difference results in a wide variety of formats.

Other operational advantages of real-time time scale algorithms also became evident at NRC as automated inter-laboratory time transfer with resolutions of better than 200 ps came on line in our laboratory. Also a real-time algorithm promises advantages during evaluations or during repairs to the primary laboratory cesium standards.

An algorithm seems attractive for exploiting the superior timekeeping characteristics of NRC's two new masers, and could gracefully incorporate frequency calibrations from the initially short periods of operation of the new cesium frequency standards — cesium Zacharias fountains — and single-ion frequency standards, which are under development at NRC and will likely have frequency accuracy capabilities in the 10^{-15} range. An algorithm based on Kalman filtering seems to be a promising candidate to meet our requirements of good stability in both the short term and long term while keeping the accuracy that cesium beam frequency standards and their successors provide.

Kalman Filtering

Of the many time scale algorithms used in different institutions and laboratories [2, 3, 4, 5, 6, 7], an algorithm based on Kalman filtering seemed the most promising to meet our needs. It is an optimum estimator in the minimum squared error sense, it applies to dynamic systems with a proper adaptive filtering technique, it has the optimum transient response, and it can address the requirements of both short and long term stability.

We have used Kalman filtering at NRC for several years, for algorithm evaluation purposes although the ensemble average has been a very helpful tool for clock evaluations from early in the development. We have set up a full project to pursue the development of the algorithms, and fine tune an algorithm that we envisage will include rejection and correction of outliers for both phase and frequency jumps.

The purpose of this paper is not to develop the Kalman filter equations. This development can be found in many good books[8, 9]. Briefly, if we have a linear system with the state-space description

$$\begin{cases} \mathbf{x}_{k+1} &= A_k \mathbf{x}_k + \xi_k \\ \mathbf{v}_k &= C_k \mathbf{x}_k + \eta_k \end{cases} \tag{1}$$

where A_k, C_k are $n \times n$, and $q \times n$ constant matrices, respectively the state transition matrix and the connection matrix between the measurement $\mathbf{v}_k$ and the state vector $\mathbf{x}_k$, and $\{\xi_k\}$ and $\{\eta_k\}$ are respectively system and observation noise sequences, with known statistical information such as mean, variance, and covariance, we can derive the following Kalman filtering process:

$$\begin{cases} P_{0,0} &= \mathrm{Var}(\mathbf{x}_0) \\ P_{k,k-1} &= A_{k-1} P_{k-1,k-1} A_{k-1}^{\mathsf{T}} + Q_{k-1} \\ G_k &= P_{k,k-1} C_k^{\mathsf{T}} (C_k P_{k,k-1} C_k^{\mathsf{T}} + R_k)^{-1} \\ P_{k,k} &= (I - G_k C_k) P_{k,k-1} \\ \hat{\mathbf{x}}_{0|0} &= \mathrm{E}(\mathbf{x}_0) \\ \hat{\mathbf{x}}_{k|k-1} &= A_{k-1} \hat{\mathbf{x}}_{k-1|k-1} \\ \hat{\mathbf{x}}_{k|k} &= \hat{\mathbf{x}}_{k|k-1} + G_k (\mathbf{v}_k - C_k \hat{\mathbf{x}}_{k|k-1}) \\ k &= 1, 2, \ldots \end{cases} \tag{2}$$

where

$P_{k,k-1} = \mathrm{Var}(\mathbf{x}_k - \hat{\mathbf{x}}_{k|k-1})$ the variance of the difference between the state vector and the prediction $\hat{\mathbf{x}}_{k|k-1}$,

$P_{k,k} = \mathrm{Var}(\mathbf{x}_k - \hat{\mathbf{x}}_{k|k})$ the variance of the difference between the state vector and the estimation $\hat{\mathbf{x}}_{k|k}$,

$Q_k = \mathrm{Var}(\xi_k)$,

$R_k = \mathrm{Var}(\eta_k)$.

Equation 2 is a recursive scheme that, when applied to the incoming data $\mathbf{v}_k$, produces predictions $\hat{\mathbf{x}}_{k|k-1}$ and estimations $\hat{\mathbf{x}}_{k|k}$ of the state vector $\mathbf{x}_k$. The difference $\mathbf{v}_k - C_k \hat{\mathbf{x}}_{k|k-1}$ is called the innovation. It can be shown that

$$\mathrm{Var}(\mathbf{v}_k - C_k \hat{\mathbf{x}}_{k|k-1}) = C_k P_{k,k-1} C_k^{\mathsf{T}} + R_k. \tag{3}$$

For a description of a clock, we need to know its phase and frequency; in some case the frequency aging is needed. Since absolute time is not known, the exercise is equivalent to comparing two or more clocks together: that means that the state vector components are the phase difference $x(t)$ and the relative frequency $y(t)$. The following equations are for the phase difference and relative frequency between two clocks. A generalization to more clocks is straightforward.

$$\mathbf{x}(t) = \begin{pmatrix} x(t) \\ y(t) \end{pmatrix} \tag{4}$$

and

$$\hat{\mathbf{x}}_{k|k-1} = \hat{\mathbf{x}}(t \mid t - \delta) \tag{5}$$

where $\hat{\mathbf{x}}(t \mid t - \delta)$ is the prediction on $\mathbf{x}(t)$ given $\hat{\mathbf{x}}(t)$ from $t = 0$ up to $t - \delta$. The state transition matrix is:

$$A_k = \begin{pmatrix} 1 & \delta \\ 0 & 1 \end{pmatrix}; \tag{6}$$

and since we measure the phase difference between two clocks, the connection matrix between the measurement and the state vector is

$$C_k = \begin{pmatrix} 1 & 0 \end{pmatrix}. \tag{7}$$

R_k is the variance of the measurement error:

$$R_k = \sigma^2_{v_x}. \tag{8}$$

Now, if we have a careful look to the equations 2 of the Kalman filtering process, we see that the second, third and fourth equations are self-sufficient as a group: the matrices $P_{k,k-1}$, $P_{k,k}$ and G_k are updated independently of the data v_k! There is nothing wrong with that if the description of the model is right, and if the behaviour of any clock in the ensemble is unchanging. The latter is practically impossible to realize, at least on a long term basis. The development of adaptive filtering is needed in our case. This means that the parameters of the model, specifically the variance matrix Q_k of the system noise, must be continuously evaluated. The frequency of evaluation depends on the type of noise process involved.

Although we are still evaluating different adaptive filtering approaches, the one developed by Stein[5] looks the most appropriate of all the adaptive filtering approaches we have studied until now[9, 10, 11]. The approach is based on the fact that the variance of the innovation, equation 3, links the measurement v_k with $P_{k,k-1}$, which is defined in terms of Q_{k-1} in equation 2. Our next step will be to implement a slightly modified version of Stein's approach, the modifications are more on the procedure of calculating the parameters rather than on the underlying principles.

Results using the current algorithm

We present here an analysis of our internal time scale algorithm based on Kalman filtering by looking at two different sets of clock data — relative phase measurements between six pairs of clocks taken at 10 minute intervals — taken respectively between MJD=48795 and 48865 for 70 days (from 92-06-22 to 92-08-31), and between MJD=48895 and 48915 for 20 days (from 92-09-30 to 92-10-20). These two sets of clock data correspond to periods of relatively stationary behaviour of the clocks. Of the different clocks included in the calculation of the time scale, there are the two new NRC hydrogen masers, H3 (H) and H4 (h), on which there are still experiments done, often resulting in frequency steps; for that reason, H3 has been included in the calculation of the first period of 70 days for only 37 days, between MJD=48795 and 48832. H4 is not included at all in the 70 day period. Besides the two hydrogen masers, the time scale algorithm is calculated from the relative phase measurement of three primary laboratory cesium beam atomic clocks, Cs V, Cs VI A and Cs VI C, and two commercial cesium beam atomic clocks P and p (HP5061-A's with super tubes). The six phase differences were taken with two three-channel phase comparators with 1 ps resolution, and the calculations were done using phase difference data taken every 10 minutes.

The time scale algorithm evaluation includes also Cs VI C (undergoing a full evaluation during part of this period) and the two commercial cesium clocks. For that period, though, their measured stabilities were not good enough to give them important weights in the calculation, and we will not present results for them.

To analyze the time scale algorithm, we present the Allan deviation graphs of each of the other clocks vs the ensemble. As expected from Figs. 1-3, the hydrogen masers H show a very good short term stability that is reflected in the algorithm. Fig. 1 shows the Allan deviation of free- running maser H3 vs the ensemble. In Figs. 2 and 3 the Allan deviations are for the masers under cavity servo control. In Figs. 1-5, the upper and lower traces show the limits of the interval of confidence (95 %) in the evaluation of the Allan deviation. After a week, Cs V starts to take over when it reaches the $\sigma_y(\tau) = 2 \times 10^{-14}$ level, Fig. 4. A longer term analysis, of the order of 1 year, would show a larger contribution of Cs V, and also of Cs VI A and Cs VI C, since their long term stability is better than the hydrogen masers. A comparison of Figures 1, 4 and 5 shows that the cesium clocks and the hydrogen maser H3 are at the same level of stability after a week, defining the beginning of a cross-over region before the long term stability of the hydrogen maser deteriorates. At this level of stability, $\sigma_y(\tau) = 2 \times 10^{-14}$, and on a period of 70 days, it is easy to appreciate the difficulties of determining from the Allan deviation over this period which clock(s) should be pulling the algorithm the most. This time scale algorithm allows a maximum weight of 0.8 for the contribution of the best clock.

Other long-term questions have not been resolved in this algorithm. It does have built-in consistency from the continuous evaluation of the weights from predictions and estimations for the calculation of the phase of the ensemble. However, the same standard of consistency is not implemented for frequency, nor for aging or related effects. The consequence is that the long term behavior of the time scale is not optimally controlled, with phase comparisons taken every ten minutes as clock data. The algorithm could be pulled by the hydrogen masers even if the long term stability of a cesium clock is better. This problem will be addressed in the further developments in our time scale algorithm.

Additional requirements for a real-time system

The results of our experience with ensemble averaging, such as that presented above, has encouraged us to undertake a project aimed at implementing a real-time algorithm for UTC(NRC). Our old system has used the proper time output of our "best" primary cesium clock, as PT(NRC), adjusted for our 100 m elevation by a microstepper to convert to UTC(NRC). We have examined the requirements of a time scale system, and we are building a system shown in Fig. 6. It measures phase differences each second and controls a quartz oscillator giving UTC(NRC) by calculating and outputting a correction to the quartz oscillator frequency with a delay of less than 1.5 s. Most components of the system have on-line backup, both to minimize the effects of component failure and to simplify component maintenance and upgrading. Most of the hardware has been operating for over a year, and the algorithm presented above has been re-implemented on the redundant PC's (switching from the Hewlett-Packard Basic (Rocky Mountain Basic) and Infotek compiler to Microsoft's Quickbasic and Basic System 7 for MS-DOS 80486 computers). We have encountered more difficulties than expected with compiler errors as well as the normal coding errors. We are in the process of independently re-coding the algorithm in FORTRAN, both for speed and as a further check on the coding and compilers: we plan to use the greater portability of the FORTRAN code to run the algorithm on VAX VMS, IBM VM, Silicon Graphics UNIX as well as PC's under MS-DOS. The greater speed will expedite the offline examination

of different strategies for algorithms running on our small, inhomogeneous ensemble of atomic clocks.

When one examines the behaviour of clocks, what looks simple is in fact more complicated. The stability of a clock, mostly evaluated by the Allan variance, varies with the time interval on which it is evaluated. If a phase or frequency step happens, it must be not only detected but also determined as being either phase or frequency. A time scale algorithm must deal with changes in stability, both in time and in time interval, and in phase and frequency. The evaluation of the parameters of the algorithm, the system noise and the weights of the clocks, must be as automatic as possible without loss of control. A well designed algorithm lets the human operator keep track of all the evaluated parameters to keep control in case the algorithm behaves inappropriately. The reliability is one of the aspect on which the algorithm will be evaluated extensively. Initially we expect to be running different real-time algorithms in parallel, constrained to lie within a time window around the old "best clock" algorithm. The time window would have to be manually set and reset when necessary.

Conclusion

Until now, UTC(NRC) has been derived from one of the three laboratory primary cesium beam clocks, Cs V, Cs VI A and Cs VI C. Their excellent capabilities has delayed the implementation of a time scale algorithm. The advantages of a time scale algorithm for NRC's inhomogeneous group of atomic clocks were not as evident as the advantages of maintaining a "good clock".

We presented in this paper some ideas for the development of a timescale algorithm based on Kalman filtering. The choice of Kalman filtering is dictated by our requirement for both short and long term stability of the ensemble. By taking phase differences between pairs of clocks instead of time of clocks, we make sure that the different variance matrices involved in the recursive calculation of the time scale do not diverge. The system noise variance matrix must also be updated dynamically to take into account the change in behavior of any clock of the ensemble. Continuity, not only in phase but also in frequency, and aging if measured, must be implemented in the algorithm. This is to avoid pulling of the algorithm by clocks which have the best short term stability, like the hydrogen masers, but poorer long term stability. We have presented an analysis of the time scale algorithm, used internally only, for two periods of time of 20 and 70 days respectively. The algorithm was found to give the most weight to the best clocks in the short term, but the analysis didn't allow us to evaluate the algorithm on the long term.

We considered also the requirements of an on-line time scale system generating UTC(NRC), from the measurement of phase differences to the control of the quartz oscillator. Many of the components will be redundant, the measurement system and the computer calculating the algorithm, to detect any phase comparator or computer error. The program and its coding will be checked against different source of errors like coding, compiler, and the algorithm itself. For that matter, the coding will be checked on different computer architectures, not only on a PC DOS 80486 where it will be implemented.

In the future, a time scale algorithm will have be optimized to facilitate exploiting the initially short periods of operation of NRC's new frequency standards: cesium Zacharias fountains and single-ion frequency standards, which will likely have frequency accuracy capabilities in the 10^{-15} range. Unless there are surprising advances in time intercomparisons, the promises of good algorithms will have to be realized to allow inter-laboratory frequency intercomparisons at this level. Subsequent work will focus on the optimal inclusion of the intervals of operation of these higher accuracy frequency standards into the ensemble average of our inhomogeneous group of atomic clocks.

References

[1] D.W. Allan, and H. Daams, Proceedings of the 29th Annual Symposium on Frequency Control, Fort Monmouth, New Jersey, U.S.A., 1975, pp. 404-11

[2] P.A. Clements, and B.P. Gibbs, in *Third International Time Scale Algorithm Symposium*, Turin, Italy, 1988, pp. 289-310

[3] M. Mnackri, and C. Thomas, in *Third International Time Scale Algorithm Symposium*, Turin, Italy, 1988, pp. 313-26

[4] S.R. Stein, in *Third International Time Scale Algorithm Symposium*, Turin, Italy, 1988, pp. 345-57

[5] S.R. Stein, Research and Development Technical Report SLCET-TR- 89-0717-F, US Army Laboratory Command, 1989

[6] P. Tavella, and C. Thomas, Metrologia **28**, 57-63 (1991)

[7] M. Weiss, and T. Weissert, Metrologia **28**, 65-74 (1991)

[8] C.K. Chui, and G. Chen, *Kalman Filtering with Real-Time Applications*, Second Edition, Springer-Verlag, 1991

[9] R.G. Brown, *Random Signal Analysis and Kalman Filtering*, John Wiley & Sons, 1989

[10] D.T. Magill, IEEE Transactions on Automatic Control AC-10(4), 434-9 (1965)

[11] R.K. Mehra, IEEE Transactions on Automatic Control AC-15(2), 175-84 (1970)

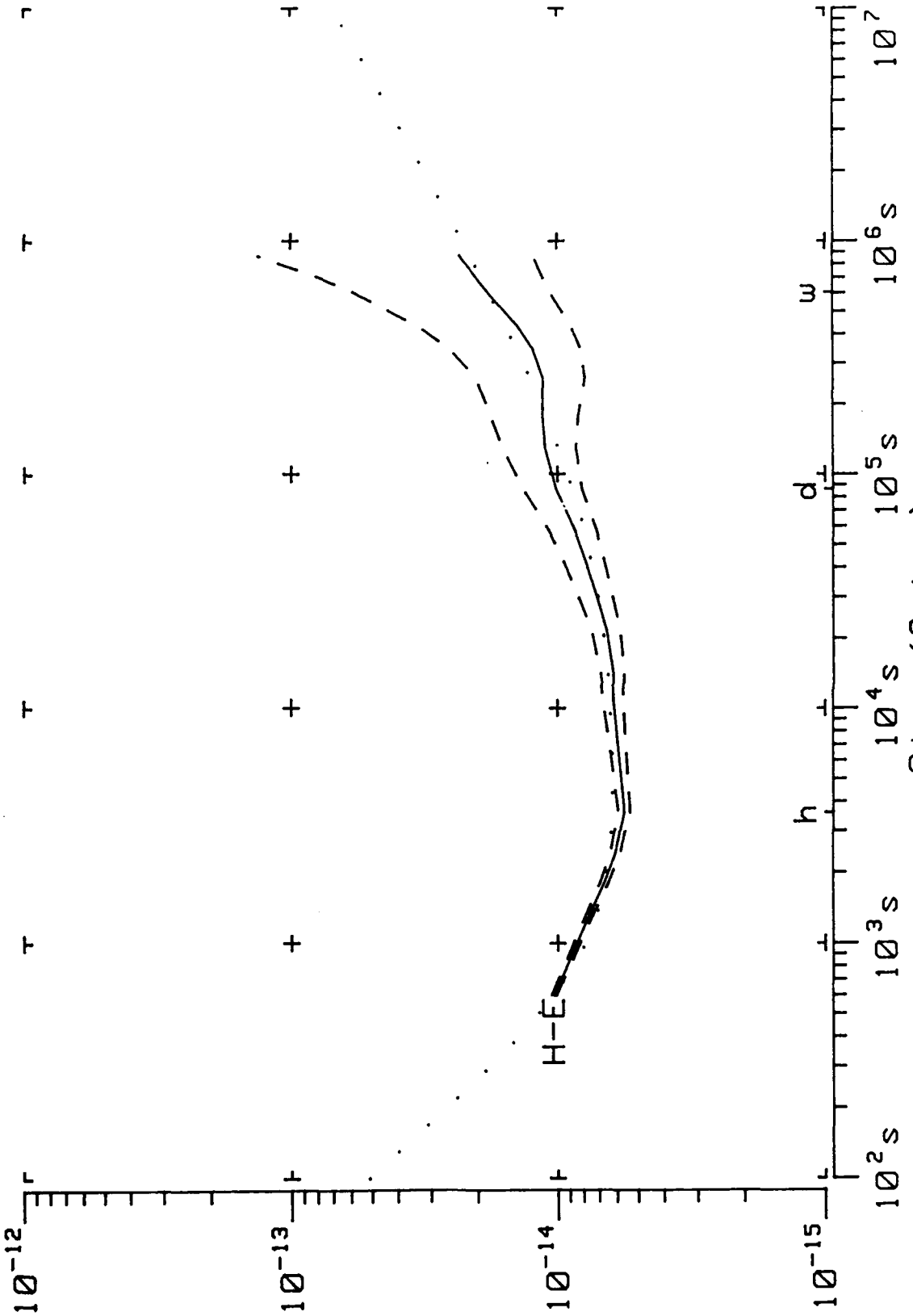

Figure 1. Allan deviation of H3 vs Ensemble for MJD=48795 to 48832 (37 days).

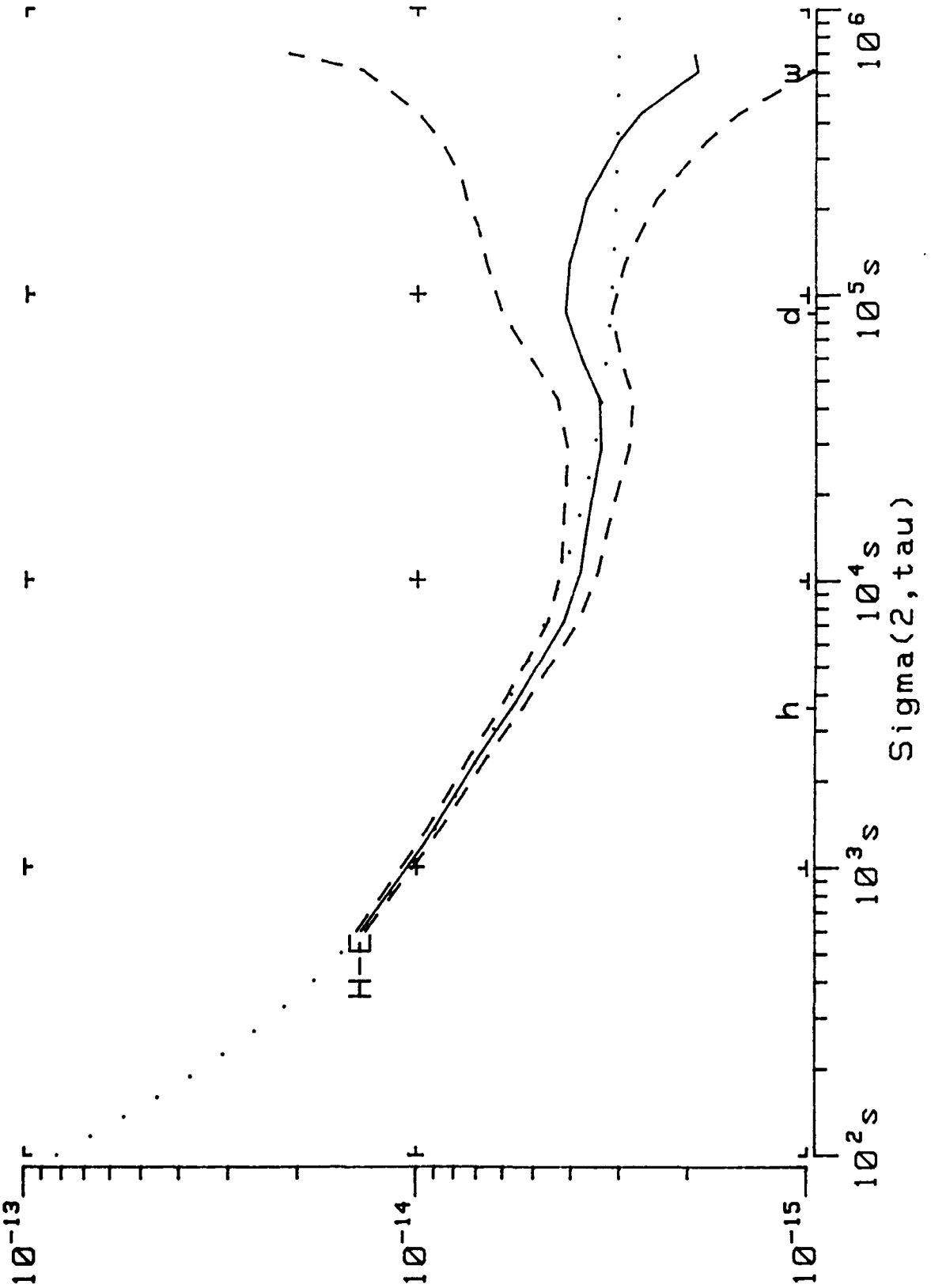

Figure 2. Allan deviation of H3 vs Ensemble for MJD=48895 to 48915 (20 days).

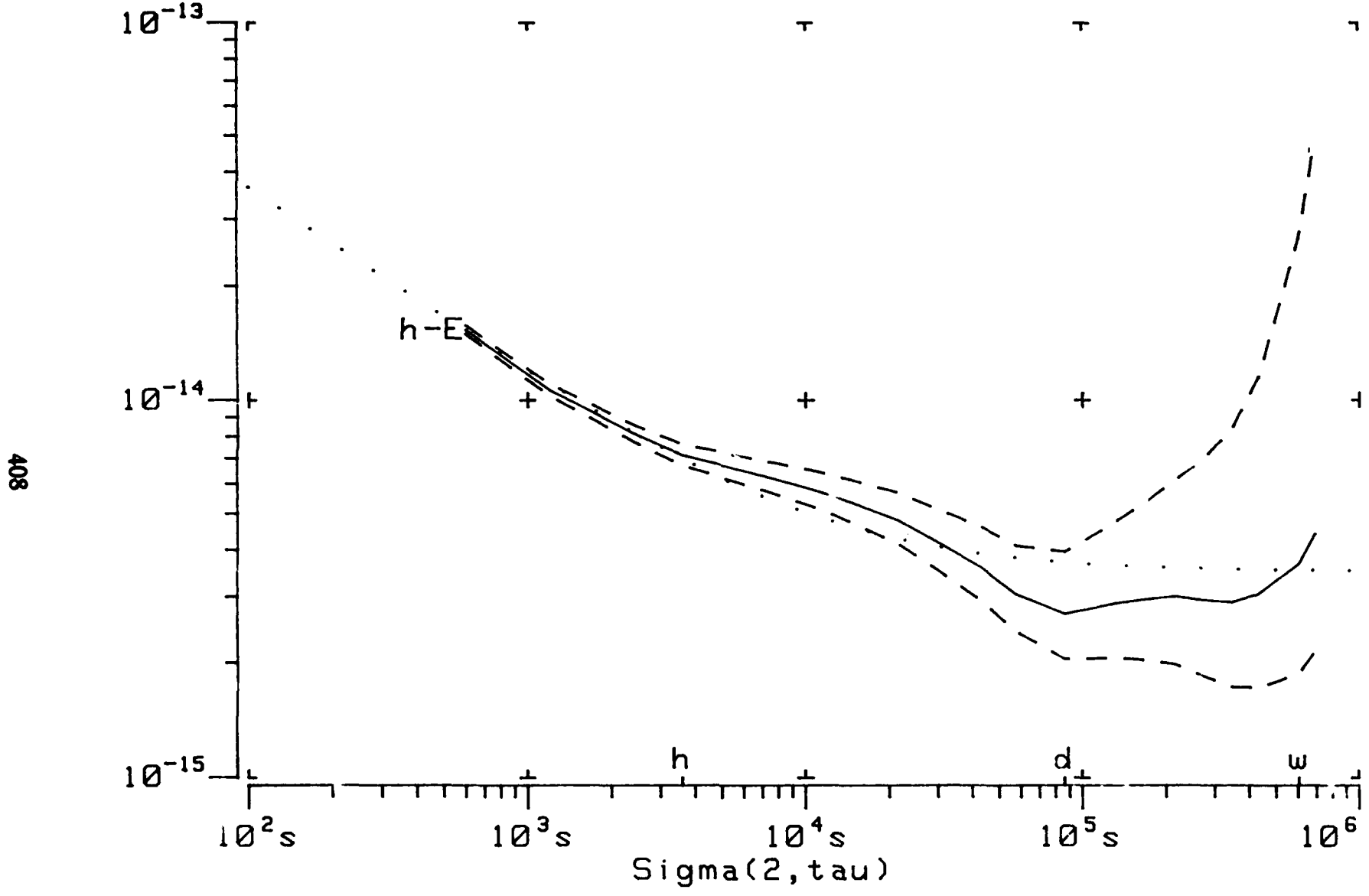

Figure 3. Allan deviation of H4 vs Ensemble for MJD=48895 to 48915 (20 days).

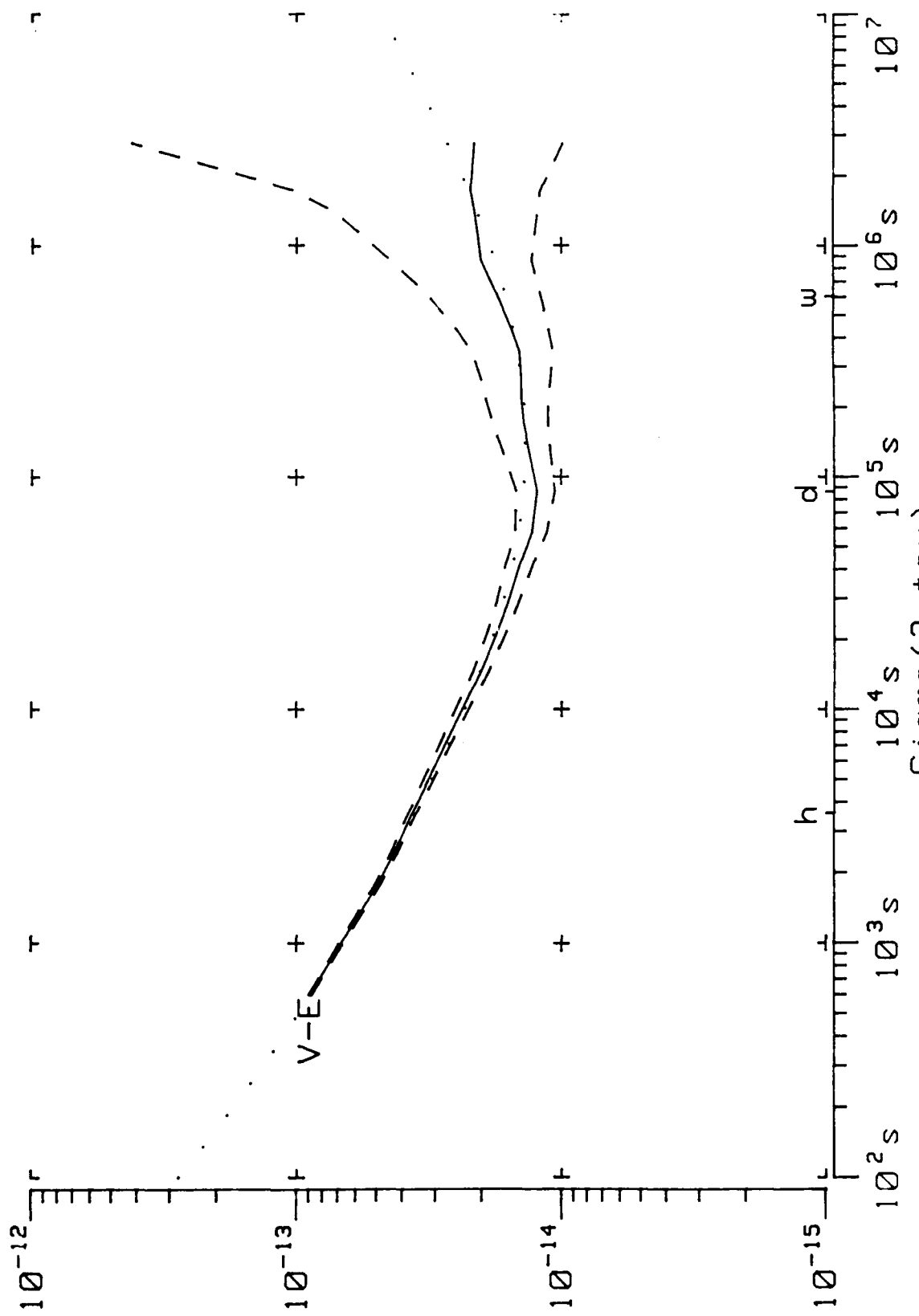

Figure 4. Allan deviation of Cs V vs Ensemble for MJD=48795 to 48865 (70 days).

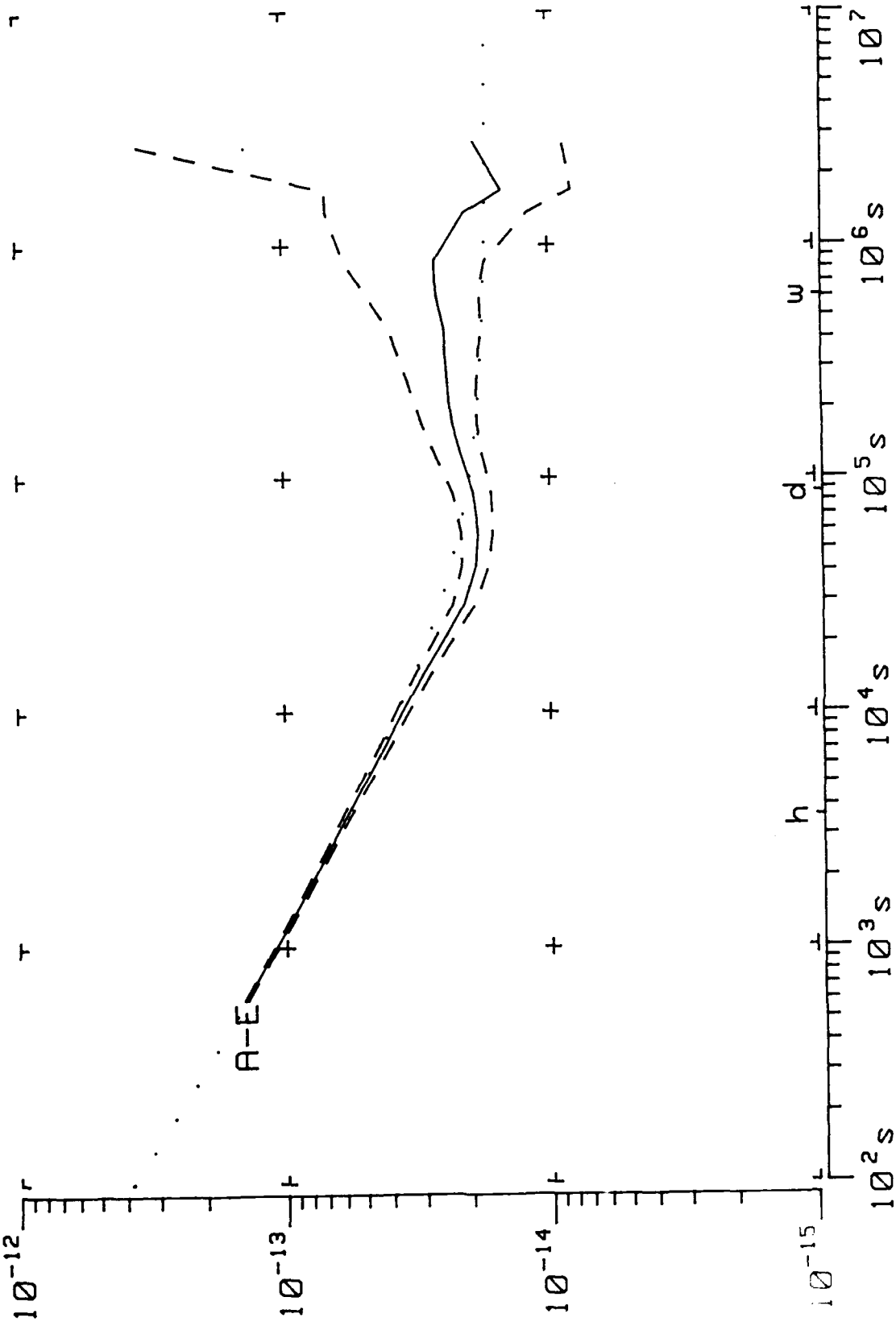

Figure 5. Allan deviation of Cs VI A vs Ensemble for MJD=48795 to 48865 (70 days).

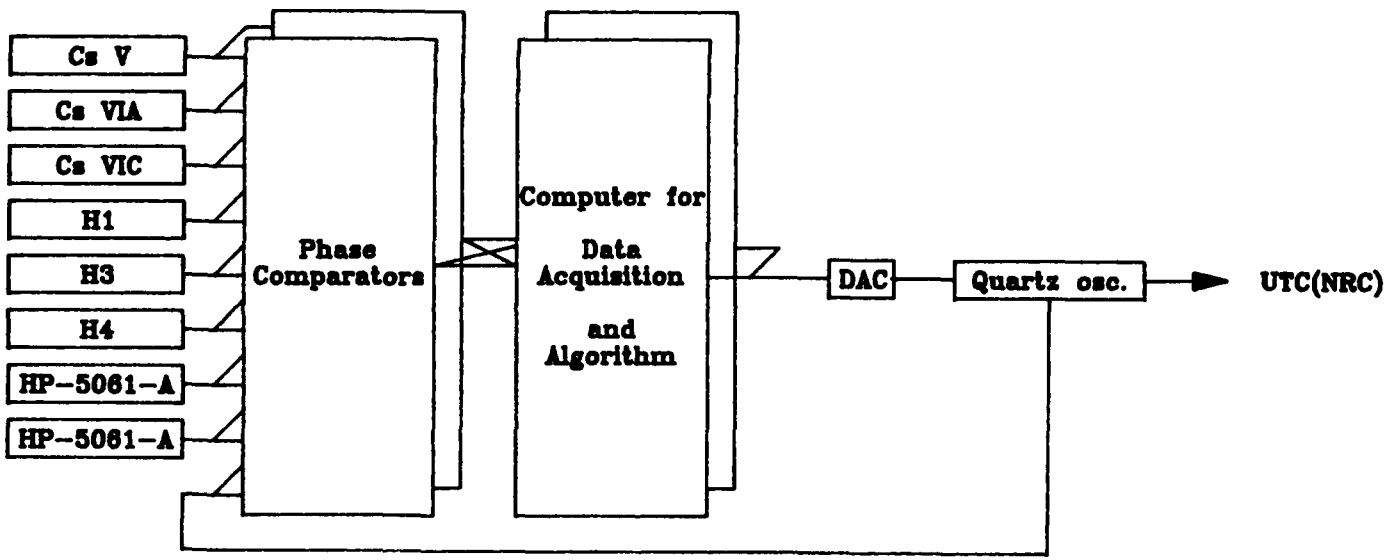

Figure 6. Time scale generation at NRC (project)

A MULTI-VARIANCE ANALYSIS IN THE TIME DOMAIN

Todd Walter

W.W. Hansen Experimental Physics Laboratory
Stanford University, Stanford, CA 94305-4085

Abstract

Recently a new technique for characterizing the noise processes affecting oscillators was introduced [1] [2]. This technique minimizes the difference between the estimates of several different variances and their values as predicted by the standard power law model of noise. The method outlined in this paper makes two significant advancements: it uses exclusively time domain variances so that deterministic parameters such as linear frequency drift may be estimated, and it correctly fits the estimates using the chi-square distribution. These changes permit a more accurate fitting at long time intervals where there is the least information. This technique has been applied to both simulated and real data with excellent results.

I. Introduction

Stochastic noise processes are the dominant source of imprecision in high-performance oscillators. Better information about these noise sources leads to an improved understanding of the estimated stability of the oscillator. Furthermore, information about the level of contribution from each noise type can improve their theoretical description. Some of these processes are well understood (thermal noise, shot noise, etc.), but many are not adequately described by theory. For some processes, when they are understood, there is greater potential for their subsequent reduction. Rudimentary stability analysis of an oscillator is fairly straight-forward. However, placing confidence limits on the stability estimates requires detailed knowledge of the noise types affecting the precision. The processes being characterized are stochastic, and therefore we can only provide a rough statistical analysis. Additionally there may be many contributing noise sources that can have a tendency to obscure one another. Thus there has been a scarcity of good data on the precise contributions of individual noise sources. Recently a new method in noise analysis was introduced. This method, called multi-variance analysis [1], is capable of providing precise measurements of dominant noise sources.

Before examining the details of this new method, we must first understand how noise affecting oscillator precision is measured. The output of an oscillator can be represented by [3] [4]

$$V(t) = [V_0 + \varepsilon(t)] \sin[2\pi\, \nu_0 t + \varphi(t)] + V_I(t)$$

V_0 and ν_0 are the respective nominal amplitude and frequency of the output, $\varepsilon(t)$ and $\varphi(t)$ are amplitude and phase fluctuations respectively and $V_I(t)$ is additive noise. Provided ε and V_I are much smaller than V_0, the instantaneous frequency of the oscillator output can be written

$$\nu(t) = \nu_0 + \frac{1}{2\pi}\frac{d\varphi(t)}{dt}$$

The instantaneous fractional frequency deviation from nominal may also be defined

$$y(t) \equiv \frac{\nu(t) - \nu_0}{\nu_0} = \frac{1}{2\pi\,\nu_0}\frac{d\varphi(t)}{dt}$$

It is the stability of the output frequency that is of primary concern. Stochastic processes that affect this stability will appear in y(t). Another useful quantity is the phase deviation, in units of time,

$$x(t) \equiv \frac{\varphi(t)}{2\pi\,\nu_0}$$

This quantity, the time integral of $y(t)$, is a measure of the time deviations of the oscillator. Averaged values of $y(t)$ can be obtained by differencing two phase measurements and dividing the result by the time interval between the measurements.

The effects of these noise processes manifest themselves in both $x(t)$ and $y(t)$. This paper is concerned with the characterization of these effects rather than their physical cause. Examining the disturbances to $y(t)$ is one of the more common means of characterizing the frequency stability of an oscillator. One method is to look at the power spectral density (PSD) of $y(t)$. It has been observed that the PSD of $y(t)$ often has integer slopes when plotted on a log-log graph. Empirically, five slopes are commonly observed. This has led to the standard power law model which may be written [3] [4]

$$S_y(f) = \sum_{\alpha} h_\alpha f^\alpha$$

where α is an integer that runs from -2 to 2 and the h_α's are the noise intensity coefficients. The five noise categories are respectively white phase modulation, flicker phase modulation, white frequency modulation, flicker frequency modulation and random walk frequency modulation.

This model adequately describes most of the observed noise processes. However the frequency domain is not necessarily the best place for analysis. Forming a PSD estimate from data discretely sampled in the time domain can lead to biases and distortions. Additionally the data is often affected by systematic effects such as frequency offset and linear frequency drift that, if not properly estimated and removed, will also distort the PSD estimate.

The process $y(t)$ is not the most convenient measure because it is not possible to measure the instantaneous frequency. Instead the frequency measurement takes place over a finite time interval τ. Also the measurement of $y(t)$ often involves some dead-time. This causes a reduction in the amount of information obtained. Therefore, the frequency stability is more easily specified through the characterization of $x(t)$ in the time domain.

II. Time Domain Variances

The most common time domain measure of oscillator stability is the Allan (or two-sample) variance. For the process $x(t)$ it is defined by

$$\sigma_y^2(\tau) \equiv \frac{1}{2\tau^2}\left\langle [x(t+2\tau) - 2x(t+\tau) + x(t)]^2 \right\rangle$$

The angle brackets denote an ensemble average or expected value. The Allan variance was chosen because it forms a convergent measure of the fractional oscillator stability as a function of time interval. It is possible to define other variances that meet this criterion. A less familiar measure is the Hadamard variance with binomial coefficients [5]-[8]. I will use a renormalized version given by

$${}_H\sigma_y^2(\tau) \equiv \frac{1}{6\tau^2}\left\langle [x(t+3\tau) - 3x(t+2\tau) + 3x(t+\tau) - x(t)]^2 \right\rangle$$

This measure is convergent for $\alpha > -5$, unlike the Allan variance which is convergent for $\alpha > -3$. Thus it would be possible to use the Hadamard variance to probe for noise beyond random walk frequency modulation. Perhaps the most important feature of the Hadamard variance is that it is unaffected by linear frequency drift. This makes it an excellent tool for investigating noise types whose signatures are similar to and often confused with linear drift.

A new variance is introduced, which I call the alternate difference variance. It is defined by

$${}_D\sigma_y^2(\tau) \equiv \frac{1}{2\tau^2}\left\langle [x(t+3\tau) - x(t+2\tau) - x(t+\tau) + x(t)]^2 \right\rangle$$

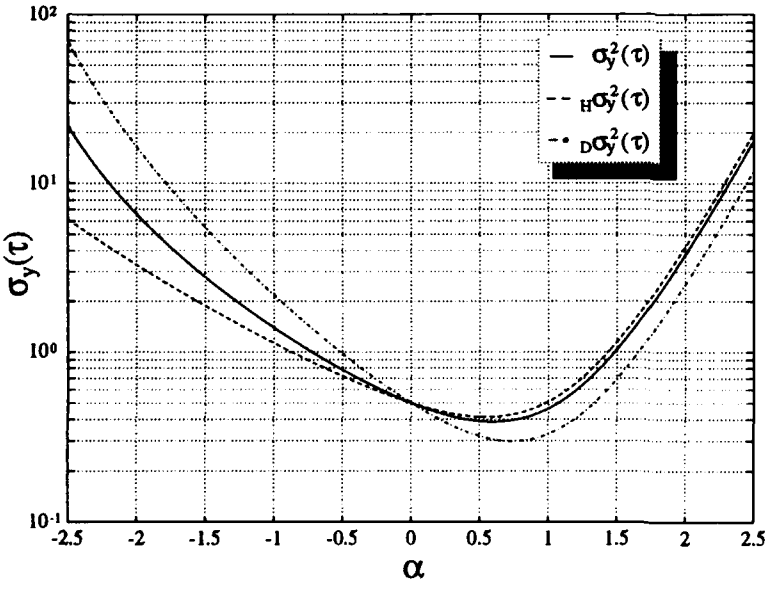

Figure 1. The Allan, Hadamard and alternate difference variances are plotted as functions of α ($h_\alpha = 1$, $\tau = 1$)

Its chief advantage is that it is affected to a greater degree by noise with α below 0 although it too is only convergent for $\alpha > -3$.

Table 1 shows the functional dependence of each variance on the different noise types. In addition Figure 1 plots these three variances as functions of α. Notice that for $\alpha > 0$ all three variances have similar responses, although the Hadamard variance is slightly above and the alternate difference variance is below the Allan variance. At $\alpha = 0$ the variances are equal by definition. For $\alpha < 0$ the three begin to diverge.

All three of these variances have difficulty distinguishing between white phase and flicker phase noise. To aid in this resolution the modified Allan variance was created [4]. It exploits the different dependencies of these two noise types on system bandwidth (f_h). Just as the modified Allan variance was created from the Allan variance it is possible to create the modified Hadamard variance and the modified alternate difference variance from their respective variances.

The time domain variances, as for the PSD, can only be estimated from the observed data. The noise processes will each have some underlying true variance that is unknown to the observer. We use the discretely sampled data of finite length to estimate this true variance. If we have N points each separated in time by τ_0, so that $x_k = x(k\tau_0 + t_0)$, the estimate of the Allan variance is given by

$$\hat{\sigma}_y^2(m\tau_0, N) = \frac{1}{2(N-2m)(m\tau_0)^2} \sum_{k=1}^{N-2m} (x_{k+2m} - 2x_{k+m} + x_k)^2$$

The ^ specifically denotes the fact that this is only an estimate. This estimate has a specific uncertainty associated with it. Clearly as m approaches N fewer points will be included in the estimate and it will have greater uncertainty. For each specific noise type it is possible to calculate the variance of the variance estimate [4] [9] [10]. Similar estimates and uncertainties of estimates can be calculated for each of the other variances.

Noise Type	Allan Variance	Hadamard Variance	Alternate Difference
White Phase $\left(S_y(f) = h_2 f^2\right)$	$\frac{3}{(2\pi)^2 \tau^2} h_2 f_h$	$\frac{10}{3(2\pi)^2 \tau^2} h_2 f_h$	$\frac{2}{(2\pi)^2 \tau^2} h_2 f_h$
Flicker Phase $\left(S_y(f) = h_1 f\right)$	$\frac{3\gamma - \ell n2 + 3\ell n(2\pi f_h \tau)}{(2\pi)^2 \tau^2} h_1$	$\frac{10\gamma - 6\ell n2 + 15\ell n3 + 10\ell n(2\pi f_h \tau)}{3(2\pi)^2 \tau^2} h_1$	$\frac{2\gamma + 2\ell n2 - \ell n3 + 2\ell n(2\pi f_h \tau)}{(2\pi)^2 \tau^2} h_1$
White Frequency $\left(S_y(f) = h_0\right)$	$\frac{h_0}{2\tau}$	$\frac{h_0}{2\tau}$	$\frac{h_0}{2\tau}$
Flicker Frequency $\left(S_y(f) = h_{-1} f^{-1}\right)$	$2\ell n2 h_{-1}$	$(4\ell n2 - \frac{3}{2}\ell n3) h_{-1}$	$(\frac{9}{2}\ell n3 - 4\ell n2) h_{-1}$
Random Walk Freq. $\left(S_y(f) = h_{-2} f^{-2}\right)$	$\frac{2\pi^2 \tau}{3} h_{-2}$	$\frac{\pi^2 \tau}{3} h_{-2}$	$\frac{5\pi^2 \tau}{3} h_{-2}$
Linear Frequency Drift $\left(x(t) = \frac{1}{2} D r\, t^2\right)$	$\frac{Dr^2}{2} \tau^2$	0	$2Dr^2 \tau^2$

Table 1. The functional dependencies of the three variances under the assumption $f_h \tau >> 1$

III. Multi-Variance Analysis

The multi-variance method combines the power law model with the output of several variance estimates. Thus many observations with different variances must all agree within the predicted responses of the power law model. This greatly simplifies the analysis, as all of these observations are used to estimate the five noise intensity coefficients. A single-variance technique separates noise contributions by their differing dependencies on τ. The multi-variance method exploits those τ dependencies in addition to utilizing different responses of each variance for each particular value of τ. Thus the multi-variance method gains more resolution over analysis with a single variance. This powerful new technique was introduced recently by Vernotte et al. [1] [2].

The estimates used in previous work [1] [2], correspond both to the time domain (Allan and modified Allan variances) and to the frequency domain (Band-pass and High-pass variances) [6]. The frequency domain variances are a powerful analytical tool, but, as previously mentioned, they are more susceptible to biases and distortions. Systematic effects such as frequency offset and drift, if not properly accounted for, will also bias the spectral density estimates. We are interested in finding both the frequency offset and linear drift in our analysis of the time series. In order to correctly form the PSD estimate these effects must be subtracted from the time series. Often a least squares fit is performed on the data to estimate these parameters. Unfortunately, the noise is non-white. Non-white noise also has linear and quadratic components which will yield biased estimates and incorrect confidence limits on those estimates [4]. When these false estimates are used to detrend the data, some of the noise contribution will be subtracted out as well. A better approach would be to incorporate these systematic effects in the fitting process, or to estimate the parameters after the fitting process, so that the noise types will be known and can be correctly taken into account.

I have chosen to implement the multi-variance technique using exclusively time domain variances. The five variances used in this analysis are the Allan and modified Allan variances, the Hadamard and modified Hadamard variances, and the alternate difference variance. This change leads to a more robust estimator and allows systematic errors such as linear frequency drift to be solved for as part of the fit. The frequency offset is estimated after performing the fit when we have better knowledge of the noise shape. In the fit routine I present here, I use the five variances at different values of τ, to fit six parameters: the five noise intensity coefficients and linear frequency drift.

IV. Chi-Square Probability Distribution

Standard least squares fit methods return the maximum likelihood solution for estimates that are distributed normally. However, the variance estimates used in oscillator noise analysis follow a chi-square distribution. Therefore fit routines using the standard least squares method will not yield the best solution, particularly when the estimates have few degrees of freedom. Figure 2 shows the chi-square distribution for two different values of the number of degrees of freedom (ν). It is evident from this figure that for low degrees of freedom the distribution is quite different from a normal distribution.

The mechanics of performing a fit on chi-square distributed variables are similar to fitting normally distributed variables. One possible source of confusion is that least-squares fitting of data with normally distributed noise is often referred to as chi-square fitting. This is because the cost function (parameter to be extremized) is chi-square distributed (the sum of the squares of normally distributed variables). I define a new fitting routine, for chi-square

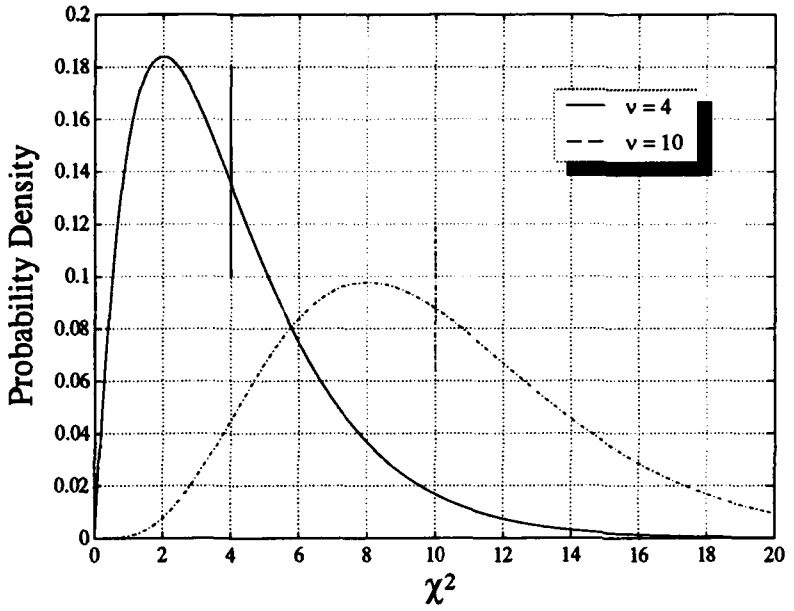

Figure 2. The chi-square probability distribution is plotted for two different values of the number of degrees of freedom (ν). The vertical lines indicate the mean value or 50% point

distributed variables, in which the cost function will have a different distribution. I have termed this type of fit *xi-square fitting*.

The variance estimate contains both stochastic and deterministic effects. It is the stochastic contribution which follows the chi-square distribution. We must subtract out the systematic effects and then properly scale the estimate. The subtraction of systematic components takes place as part of the fit. They do not have to be estimated and subtracted before the variance estimates can be formed, as in the case of the frequency domain measures. After the fit, when the systematic effects have been estimated, they can be subtracted from the raw data and this detrended version can be refit for comparison.

In order to perform the fit we must construct our chi-square variables. Just as in the case of the PSD, the expected value of the k^{th} variance at time interval τ_i can be treated as the sum of five noise contributions

$$\sigma_k^2(\tau_i) = \sum_\alpha h_\alpha \, {}_\alpha\phi_k^2(\tau_i)$$

The functions ${}_\alpha\phi_k^2(\tau_i)$ are the known functional dependencies for a specific noise type (see Table 1). The uncertainty for each noise type $\sigma^2[{}_\alpha\phi_k^2(\tau_i)]$ is also calculable [10] and can be used to construct the variance of the variance estimate

$$\sigma^2[\hat{\sigma}_k^2(\tau_i)] = \sum_\alpha h_\alpha^2 \, \sigma^2[{}_\alpha\hat{\phi}_k^2(\tau_i)]$$

This variance of the variance estimate permits us to calculate the number of degrees of freedom for that variance estimate [4]

$$\nu_{k,i} = \frac{2[\sigma_k^2(\tau_i)]^2}{\sigma^2[\hat{\sigma}_k^2(\tau_i)]}$$

The number of degrees of freedom is important for two reasons: the definition of our chi-square variable depends explicitly upon it and it determines the shape of the probability distribution.

With the number of degrees of freedom and the fit function in hand we have only to subtract off the systematic effects to create our chi-square variable. It is defined in the following manner [4]

$$\chi^2_{k,i} \equiv \nu_{k,i} \frac{\hat{\sigma}^2_k(\tau_i) - [Dr_k(\tau_i)]^2}{\sigma^2_k(\tau_i)}$$

$Dr_k(\tau_i)$ is the contribution from deterministic effects on the variance estimate. $\chi^2_{k,i}$ is a random variable that is distributed according to the standard chi-square distribution.

Figure 2 shows the standard chi-square distribution for two different degrees of freedom. It is evident that although the expected value of $\chi^2_{k,i}$ is $\nu_{k,i}$, the estimate is more likely to be found at the distribution peak that occurs at $\nu_{k,i} - 2$. For small degrees of freedom this is a significant difference. The estimates of the variances at longer values of τ are formed with fewer data points and consequently have lower degrees of freedom. Thus the most likely estimate will be biased below the true value of that variance. Xi-square fitting correctly accounts for this effect.

Another result apparent from Figure 2 is that the distribution is skewed about this maximum likelihood point. The estimate is more often found to the right of the peak than to the left. This can be corrected by multiplying the cost function by an appropriate factor when the estimate is found to be to the left of the peak. Also chi-square distributed variables have zero probability of being zero or negative. The variance of a chi-square distributed variable is twice the number of degrees of freedom. Thus, lower degrees of freedom lead to narrower, steeper peaks. Putting these ideas together leads to the following definition of the cost function.

$$\xi^2 \equiv \sum_{k,i} \frac{[\chi^2_{k,i} - \nu_{k,i} + 2]^2}{2\nu_{k,i}}$$

Now it is ξ^2 that must be minimized. It is a non-linear function of the five h_α's and any deterministic parameters we choose to include. One must remember that not only is $\chi^2_{k,i}$ a function of h_α, but $\nu_{k,i}$ is as well (note that $\chi^2_{k,i}$ is also a function of $\nu_{k,i}$). The deterministic parameters are found only in $\chi^2_{k,i}$. The minimization of ξ^2 can be accomplished in nearly the same fashion as for a non-linear least squares problem.

Non-linear fitting routines require initial values of the parameters being fit. They attempt to step from one set of values to a better set in an effort to minimize the cost function. The fitting routine described in this paper is not excessively sensitive to the initial guesses. It will converge to the same solution as long as the initial guesses are roughly of the right order of magnitude. It has been observed that it is better to overestimate the magnitude of the parameters and have the routine shrink their value down than to start at too small of a value and try to have it grow out to the correct solution. Thus, to initialize this routine, assume that certain variance estimates are caused entirely by one noise source. Because we know the functional dependencies of the variances on the noise sources we can then estimate the noise intensity coefficients. The same can be done for deterministic parameters. This insures that the guesses are exaggerated but not exceedingly distorted.

V. Results

The method outlined in this paper was first tested against simulated data. With real data there is no way of knowing the true parameters. The routine might consistently converge on the wrong answer without our knowledge. It is therefore crucial to test routines such as this one with computer simulated data with a known truth model. Correctly simulating power law noise can be a difficult task. It is not enough for the noise to have the correct shape (e.g., 1/f), but it must be distributed about that shape in the correct fashion. The criteria by which simulated noise is judged and generated is beyond the scope of this paper. There are, however, several good references on the subject [11]. The noise generated for the truth models used in this analysis came from a routine described in [12].

The routine is able to fit the data very quickly. It often takes more time to form the estimates than to fit them. The one drawback is that the calculation of the variance of the variance estimates is very time intensive (roughly an hour for N on the order of a thousand). Fortunately these values need only be calculated once and then can be stored for subsequent use. When taking data, one can attempt to take the same number of points from run to run. Clearly, an area that warrants further investigation is finding simpler functional approximations for these uncertainties as has been done for the Allan variance [4]. These approximations would permit faster calculation and more flexibility in data taking.

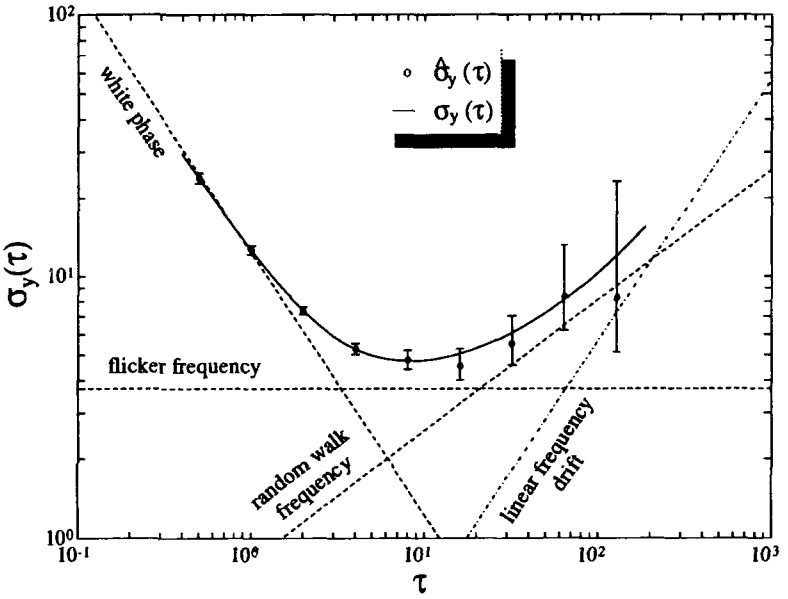

Figure 3. The Allan variance estimates are fit for a particular simulated data set of 1024 points. The solid line is the fit variance. The 90% confidence limits correspond to the fit results. The dashed lines represent the true noise levels and the dash dot line is the true contribution from frequency drift.

Va. Simulated Noise

Various magnitudes of the noise intensity coefficients and linear drift were simulated in combination. There are many combinations in which the contribution of a noise of a certain type is overwhelmed by other noise sources. Also, some noise types may not be observable because a sufficiently long data record was not taken or because the sampling rate was not sufficiently fast. These effects cause such noises to fall below the limits of measurability. Unless one takes an inordinately large amount of data, and none of the noise types completely obscure each other, it will not be possible to precisely determine each noise intensity coefficient and each deterministic parameter. Thus the routine is not always able to resolve each parameter. Obscuration effects are also discussed by Vernotte et. al [1] [2]. When one of these situations occurs, it is important to determine that the parameter has not been well estimated. In these cases, the confidence limits on the estimate are orders of

magnitude larger than the estimate itself. Thus the routine correctly identifies those noise types that have little or no contribution and weights them accordingly. When a noise type is observable, this routine is often capable of correctly estimating the values to within 10% or better.

Parameter	Estimate	Uncertainty	Truth Model	Percent Error
h_2	436	290	500	12.8%
h_1	0.00693	452	0	100%
h_0	25.7	103	0	100%
h_{-1}	9.95	6.17	10	0.5%
h_{-2}	0.0917	0.0662	0.1	8.3%
Dr	0.0752	0.0623	0.08	6.0%
y_0	22.5	5.95	25	10.0%
x_0	-151	17.1	-150	0.667%

Table 2. Best fit coefficients and parameters for the simulated data.

For one particular example of simulated noise, Table 2 lists the estimated parameters, uncertainties, truth model and percent error. Notice that for the two absent noise types (flicker phase and white frequency) the estimated parameters are low and the uncertainties are high. For the noise types that were present, the parameters were well estimated. The comparatively large error for the white phase coefficient is a result of not sampling often enough. This can be seen in Figure 3. More estimates at shorter time intervals are necessary to better resolve this parameter. The fit variance is in excellent agreement with both the estimates and the true variance within the observed time intervals.

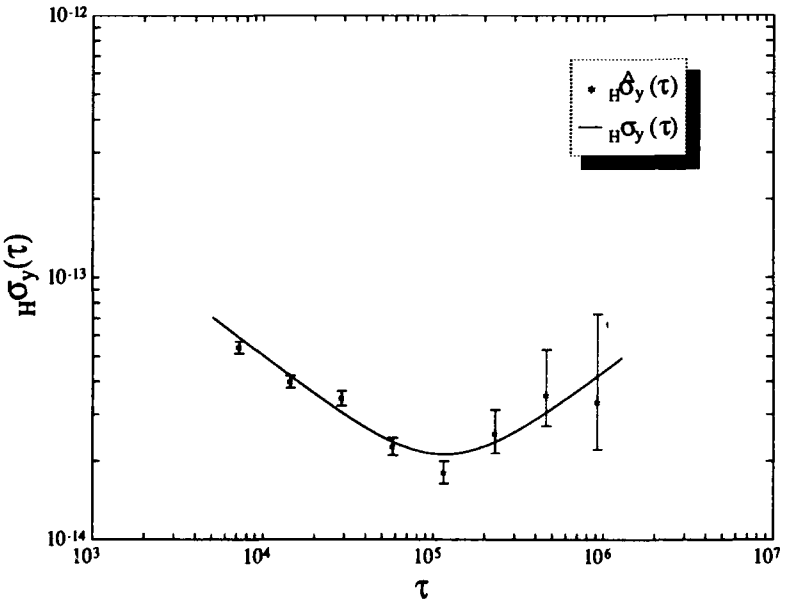

Figure 4. This plot shows the Hadamard variance estimates and fit values from the raw rubidium data. Again the error bars correspond to 90% confidence limits obtained from the fit.

Unfortunately, the confidence intervals on the parameter estimates are excessively large. They are nearly a factor of five too large in the example of Table 2. Some of this error is because the xi-square residuals of the fit are treated as though they are chi-square distributed. While this is a reasonable approximation, more study needs to be done on the true statistics of the residuals to obtain better, stricter estimates of the uncertainties. Another factor is that the different variances are not statistically independent. Probably the best way to place reasonable confidence limits on the parameter estimates would be through computer simulation. By simulating

Parameter	Estimate	Uncertainty
h_2	1.39e-22	1.11e-18
h_1	7.76e-24	2.43e-18
h_0	4.42e-23	4.70e-23
h_{-1}	2.65e-32	2.53e-28
h_{-2}	5.17e-34	3.17e-34
Dr	-2.41e-19	5.9e-20
y_0	2.182617e-10	4.67e-14
x_0	1.18e-09	1.66e-09

Table 3. Best fit coefficients and parameters for the rubidium oscillator vs. AT1 data.

many data sets in the region of the predicted parameters, one could obtain a better feel for what the real confidence limits might be.

This routine is particularly adept at picking out small values of linear drift even when completely buried in the noise. Notice in Figure 3 that the last data point has a large uncertainty and occurs where the linear drift level is still below the random walk frequency contribution. Yet the routine still estimated the drift parameter to better than 10%. If the second difference method of estimating drift [4] [13] had been applied to this data, it would have obtained a value of -0.015. That method is incapable of estimating drift when it is so far buried in the noise. For larger relative values of linear frequency drift, the second difference method yields estimates comparable to, and sometimes better than, those found with this routine.

Also notice in Figure 3 that the last point dips well below the true variance or even below the contribution just from the random walk frequency noise. For this point the number of degrees of freedom is predicted to be 3.135 and the value of the chi-square variable corresponds to 0.731 or right near the distribution peak. Thus the estimate has less than one third the value of the true variance. Because of the scarcity of data for this time interval, the variance estimate is not very good. If the chi-square distribution were not correctly applied to this case, one would obtain an overly optimistic prediction of the stability.

Vb. Rubidium Data

The routine was also tested on real data from an EG&G rubidium oscillator. This oscillator was measured against ensemble time (AT1) at NIST [14]. The raw data was fit reasonably well by this routine. Because of the large drift that was present in this oscillator the Hadamard variance is a good measure of the stability, Figure 4. Unfortunately it can be observed that the fit values lie outside the 90% confidence limits for some of the estimates. Such an effect could have a number of causes: noise that does not follow the standard power law model, environmental effects or other deterministic effects such as periodic modulation of the data. Because the most

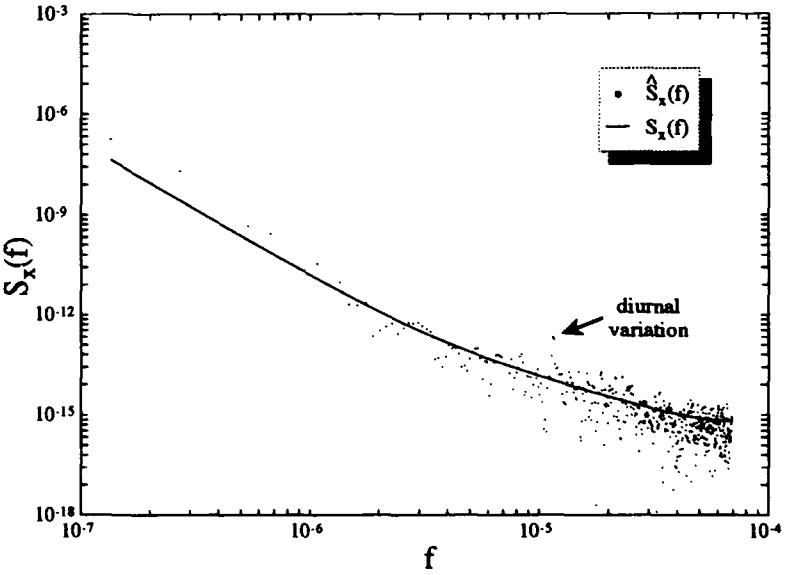

Figure 5. The power spectral density of the partially detrended data is plotted as a function of Fourier frequency. The diurnal variation is clearly visible.

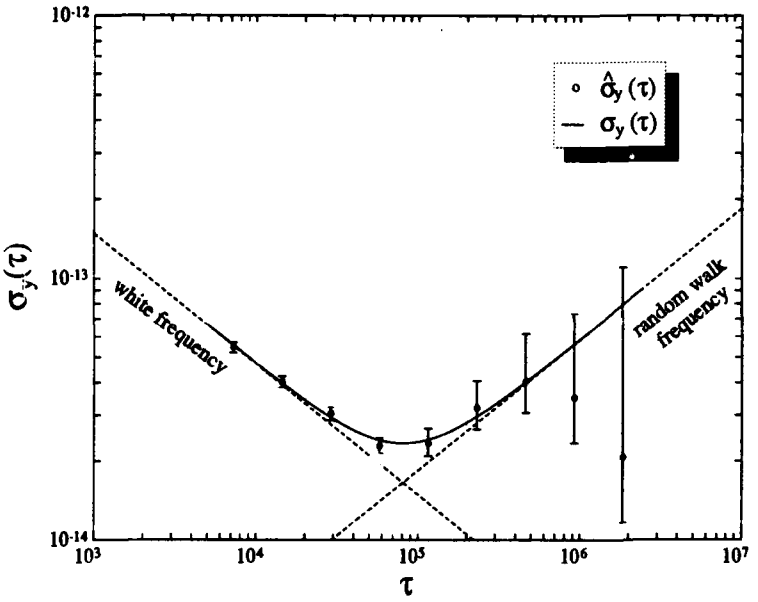

Figure 6. The Allan variance estimates and fit variances are shown for the fully detrended rubidium vs. AT1 data. The dashed lines indicate the estimated level of contribution from each noise type.

affected point corresponds to a time interval of nearly half a day, diurnal variations were suspected. Using the estimates of the drift and frequency offset, these effects were removed from the data. Investigation of the PSD of the detrended data confirmed the suspicion (Figure 5). By fitting a sine-wave response to the PSD, a diurnal modulation with an amplitude of 0.35ns was found and subtracted from the data. The magnitude of the variation is reasonable for an oscillator with a temperature coefficient of 2×10^{-12} and temperature variations on the order of a tenth of a degree Celsius. When this detrended data was refit, the fit variances were in excellent agreement with the estimates (see Figure 6). Thus it was this periodic modulation that had corrupted the initial fit. It is evident that only two significant noise types affect the data. This can also be seen in the estimated noise coefficients in Table 3. Only the estimated coefficients for white frequency modulation and random walk frequency modulation are not well below their confidence limits. Again the confidence limits in this case could probably be reduced significantly. Nevertheless the presented routine was not only able to fit the real data, but it was also able to indicate the periodic modulation that was present.

VI. Acknowledgments

The Author is grateful to the Time and Frequency Division at NIST, particularly Marc Weiss and David Allan, for providing the rubidium data. I am also grateful to Bill Riley at EG&G for providing information about their rubidium oscillator. Finally, I also wish to thank Professor John Turneaure and Dr. Jeremy Kasdin for their many helpful comments and suggestions.

VII. References

[1] F. Vernotte, E. Lantz, J. Groslambert, J. J. Gagnepain, "A New Multivariance Method for the Oscillator Noise Analysis," Proceedings of the 1992 Frequency Control Symposium, pp 284-289, 1992.

[2] F. Vernotte, E. Lantz, "Time Stability: An Improvement of the Multi-Variance Method for the Oscillator Noise Analysis," Proceedings of the 6th European Frequency and Time Forum, pp 343-347, 1992.

[3] J. A. Barnes, et. al., "Characterization of Frequency Stability," IEEE Trans. Instr. Meas., Vol. IM-20, pp. 105-120, May 1971.

[4] D. B. Sullivan, D. W. Allan, D. A. Howe and F. L Walls, Characterization of Clocks and Oscillators, NIST Technical Note 1337, 1990

[5] R. A. Baugh, "Frequency Modulation Analysis with the Hadamard Variance," Proceedings 25th Frequency Control Symposium, pp 222-225, 1971.

[6] J. Rutman, "Characterization of Phase and Frequency Instabilities in Precision Frequency Sources: Fifteen years of progress," Proceedings of the IEEE, vol. 66, no. 9, pp. 1048-1075, Sept 1978.

[7] J. A. Barnes, "Atomic Timekeeping and the Statistics of Precision Signal Generators," Proceedings of the IEEE, Vol 54, pp. 207-220, February 1966.

[8] W. C. Lindsey, C. M. Chie, "Theory of Oscillator Instability Based Upon Structure Functions," Proceedings of the IEEE, Vol 64, pp. 1552-1666, December 1976.

[9] P. Lesage, C. Audoin, "Characterization of Frequency Stability: Uncertainty due to the Finite Number of Measurements," IEEE Trans. Instr. Meas., Vol. IM-22, pp. 157-161, June 1973.

[10] T. Walter, "Characterization of Frequency Stability: A Continuous Power Law Model with Discrete Sampling," submitted to IEEE Trans. Instr. Meas.

[11] N. J. Kasdin, "Discrete Simulation of Colored Noise and Stochastic Processes and $1/f^{\alpha}$ Power Law Generation," *submitted to* Proceedings of the IEEE.

[12] N. J. Kasdin, T. Walter, "Discrete Simulation of Power Law Noise," Proceedings of the 1992 Frequency Control Symposium, pp 274-283, 1992.

[13] M. A. Weiss, D. W. Allan, D. A. Howe, "Confidence on the Second Difference Estimation of Frequency Drift," Proceedings of the 1992 Frequency Control Symposium, pp 300-305, 1992.

[14] D. W. Allan, J. Levine, "A Rubidium Frequency Standard and a GPS Receiver: A Remotely Steered Clock System with Good Short-Term and Long-Term Stability," Proc. of the 44th Ann. Symp. on Freq. Cont., pp 151-160, 1990.

QUESTIONS AND ANSWERS

Question: I imagine it is hard to estimate drift in the presence of random walk. They start looking the same. I am wondering if I have not seen anybody do this, but can you imagine a way to estimate drift from random walk, and remove it that would not automatically bias the variance low. That would at least give some deviation ....

T. Walker, Stanford University: I can imagine a way that would work. I think a slightly better way to implement it, rather than subtracting the drift the way I do, would be to actually detrend the data after every step. This would be computationally impossible or not worth doing but if you actually detrend the data as you go along, optimize that way rather than subtracting, there is cross terms that can get in there. But you can expect from random walk frequency that the last point will be biased low because you essentially have only degree of freedom, or something very low that will be biased very low. What you have to realize ....

Questioner: Just because it is Chi-Square?

T. Walker: Well I think that the statistics for the Allan variance estimate is almost worthless for just one estimate. You really do not have enough information to say anything meaniful about what the stability is.

Questioner: Why bias low?

T. Walker: Well it could be high but is more likely to be found at that.

D. Allan, Allan's Time: It is interesting to look back at classical statistics for these low frequency processes. They turn out to be incredibley sensitive to low frequency. In fact they diverge but we know they diverge as a function of a number of samples and if you look at that independence you can get estimates of some of these low frequency properties for the very low frequency components; ie: one cycle per data length. The standard deviation is a very good measure and it is sensitive to the number of samples and the kind of parallel processes. I wonder if we could exploit this some to help us. It is a measure we have kind of forgotten, that has information in it.

T. Walker: I think that you could, providing you have a model, like this, where you assume the noise type. You certainly can do a lot with the statistics in analyzing what you are seeing.

H. Fliegel, The Aerospace Corporation: I may be wrong. I am trying to remember something from a long time ago. I wonder if it is mathematically even possible to separate linear drift from random walk. The only way I ever thought it might be handled is through the arc sine law. If you have a fantastic amount of data, then the number of zerocrossings you get from a pure random walk is predictable. You could use that to estimate roughly where your line should go. I do not know if that is practical.

T. Walker: Right, it is probably not practical and I think what you are saying is correct. What I attempted to do in this, is use some of the information by fitting them at the same time. Then you do have some information on each level. You may be able to subtract them again. You need to detrend the data after you find the drift and verify that has been correctly done.

R. Keating, USNO: I just want to compliment you on a fine and interesting paper. It is not very often that we get comments from the people that ask questions. What I would like to know, what are your plans for the future, what are you going to do now?

T. Walker: That is a perfect question. I am a graduate student at Stanford right now and I am finishing up my thesis, hopefully in the spring. I actually do not have plans beyond that.

I am working on the gravity B project, and I may be continuing with that. I definately would like to stay involved with some of this work. I already see some things that could potentially be done in extending this. So I would have to say my plans are not set. If anyone has any offers for plans, I would gladly accept them.

SPACECRAFT SIGNAL SOURCES PORTABLE TEST SYSTEM*

Albert Kirk, Paul Kuhnle, Richard Sydnor
William Diener and David Stowers

California Institute of Technology
Jet Propulsion Laboratory
Pasadena, California 91109

Abstract

There is a frequent need to measure the frequency stability and phase noise levels of very high performance signal sources that are required for certain spacecraft missions. These measurements need to be done at different locations as the spacecraft subsystems progress through the various stages of development, assembly, test and integration.

Allan Deviation and Phase Noise of high performance sources are generally measured by comparing the unit under test to a reference standard. Five basic requirements are associated with making these kind of measurements:

1. *The reference standard performance needs to be equal or better than the unit under test.*
2. *The measurement system needs to accomodate odd, non- standard measurement frequencies that can range from 4 MHz to 35 GHz.*
3. *Warm–up frequency drift and aging can corrupt a measurement and must be dealt with.*
4. *Test equipment generated noise must be understood and prevented from limiting the measurements.*
5. *Test equipment noise performance must be verifiable in the field as needed.*

This paper describes a portable measurement system that has been built by JPL and used in the field. The methods of addressing the above requirements are outlined and some measurement noise floor values are given.

This test set has recently been used to measure state of the art crystal oscillator frequency standards on the TOPEX and MARS OBSERVER spacecraft during several stages of acceptance tests.

INTRODUCTION

The Frequency Reference Unit (FRU) of the Topex/Poseidon spacecraft and the Ultrastable Oscillator (USO) of the Mars Observer spacecraft are high performance signal sources that needed to be measured in their final environment to assure compliance with previously established specifications.

*This work represents one phase of research carried out at the Jet Propulsion Laboratory, California Institute of Technology, under a contract sponsored by the National Aeronautics and Space Administration.

The objective was to design and build a portable measurement system that would meet the following requirements:

A. Perform all required measurements on the Mars Observer USO and the Topex/Poseidon FRU at designated spacecraft assembly and checkout facilities including thermal/vacuum and pre launch sites.

B. Measure output frequencies of 4.096 MHz, 5.00 MHz and 19.056 MHz on the FRU; at 0 dBm $\pm$ 5 dB power levels.

C. Measure the transmitter output at 8.423 GHz and 8.417 GHz on the Mars Observer spacecraft. Power levels range from -70 dBm to +10 dBm depending on configuration and modulation.

D. Use existing equipment and available commercial instruments when possible for maximum cost effectiveness.

E. Avoid customizing in order to reconfigure and reuse equipment for future tests.

F. Provide flexibility to facilitate unexpected last minute changes in scope when in the field.

G. Simplify and minimize calibration procedures as much as possible without sacrificing confidence and accuracy.

REQUIRED MEASUREMENTS

1. ALLAN DEVIATION, τ=1 s to τ=10000 s
2. PHASE NOISE, AT 1 Hz to 10 KHz OFFSETS FROM THE CARRIER
3. DETECTION OF SPURIOUS, UNDESIRABLE PHASE MODULATION
4. DETECTION OF CROSSTALK
5. DETECTION OF ENTRAINMENT
6. AGING
7. WARM-UP CHARACTERISTICS
8. ABSOLUTE FREQUENCY

SPECIFICATIONS

It is beyond the scope of this paper to list all specifications. Figures 1 and 2 show typical Allan Deviation and Phase Noise for the signal sources under test. It is evident that these are extremely low noise crystal oscillator units.

BASIC APPROACH

We decided to use the mixer/phase detector method of comparing the UUT to available references. The block diagram in Figure 3 shows the basic test configuration.

Phase noise measurements are made by establishing phase quadrature between the two mixer inputs. The DC voltage fluctuations at the output are proportional to phase noise between the two input signals. With proper calibration and processing the spectral density of phase can be measured directly with a commercial spectrum analyzer at the required offset frequencies. The detailed procedures and limitations of this method are well documented in the literature.[1, 2] Continuous observation of these phase fluctuations can detect crosstalk and other spurious undesirable phase modulation on the unit under test.

Allan Deviation, Frequency Offset, Frequency and Phase Residuals are measured by establishing a 1Hz beat between the two mixer inputs. The Zero Crossing Detector (Z/C) provides a fast, one time only, transition at this beat period which can be counted to yield frequency offset data at selected averaging times. In our system, the output of the Z/C is also fed to a time interval counter which measures the time difference between each positive going or negative going zero crossing transition and subsequent 10 PPS pulse. This is known as the "Picket Fence" method of measuring the Allan Deviation. This process also yields residual phase and frequency data in the time domain.[3]

There are five basic requirements associated with making these kind of measurements.

1. The reference source must be equal or better than the UUT.
2. The system must accommodate the output frequency of the UUT.
3. The mixer noise must not limit the measurement sensitivity.
4. The UUT. must not drift too much. (See explanation below)
5. Test system performance must be verifiable in the field.

(Allan Deviation measurements are corrupted if tau is not held constant during the duration of the test. A rule of thumb is to maintain the minimum tau at 1 s $\pm$ .01s. For a 12 hour test run this would require a frequency offset drift between the reference and the UUT of less than 2.4×10^{-12}/day at 8.4 GHz. At a 5 MHz test frequency, this requirement diminishes to about 4×10^{-9}/day.)

AVAILABLE REFERENCES

Figure 4 shows the Allan Deviation of four different reference standards that were available to us. Also shown are the typical specified and expected values of the units under test. Only the Hydrogen

Maser qualifies as the reference that is equal or better than the units under test. Although Hydrogen Masers are portable, the costs and time factors associated with moving one from site to site was unacceptable. The high performance Cesium is not good enough over the tau range of interest. A compromise solution was adopted by splitting each Allan Deviation test into two parts. For tau values of less than 50 s the Crystal Oscillator was used; and for tau values of greater than 50 s the Rubidium Standard was used as the reference. The Rubidium also qualified as the absolute frequency measurement Standard. Although, the exact performance of the units under test could not be established in the field, it was acceptable to verify that the units met the minimum specified performance.

LOW FREQUENCY TEST SYSTEM CONFIGURATION

Figure 5 shows the Low Frequency Test System Configuration that was used to measure the Topex/Poseidon FRU signal characteristics. Each output signal was multiplied to about 95 MHz and mixed with the 100 MHz reference signal. This way we achieved two objectives: The noise contribution of the first mixer was not significant at this frequency and the use of a synthesizer at the 5 MHz intermediate frequency provided for the correct 1Hz offset capability at each test frequency with 0.1 Hz resolution. It should be noted that we could not find a synthesizer that could be used directly at the first mixer input because of noise limitation. A Fluke model 6160B was tested and found to be acceptable at the 5 MHz intermediate frequency. Frequency drift at the 95 MHz level was no problem once the system was warmed up.

The system was tested in the field as often as needed by measuring the known 5 MHz test oscillator and or by feeding the 5 MHz reference into the x19 configuration multiplier. Phase Noise, Crosstalk and Spurious Signals were measured by closing the loop with a less than 1Hz BW and using the 5 MHz VCO as the reference.

Allan Deviation, Frequency Offset, Frequency and Phase Residuals, Entrainment, Aging and Warmup Characteristics were measured with the loop open using the free running VCO or the Rubidium as a reference.

HIGH FREQUENCY TEST SYSTEM CONFIGURATION

Figure 6 shows the High Frequency Test System Configuration used to measure the Mars Observer Transmitter output at 8.423 and 8.417 GHz. Aging and warmup characteristics were estimated to be at least 5×10^{-11} per day. The corresponding frequency drift at 8.4 GHz during a 12 hour period is .21Hz. It turned out during actual testing that the drift was often much more because of unscheduled power off/on cycles. The configuration of Figure 6 solved this problem by effectively dividing the 8.4 GHz output to a lower frequency for Allan Deviation measurements. This was done by hardlocking the precision 5 MHz VCO to the 8.42 GHz test signal. Any convenient multiple of this 5 MHz, such as the 100 MHz output shown, preserves the inherent stability of the signal input within the loop bandwidth. The Allan Deviation, Frequency Offset, Frequency and Phase Residuals, Entrainment, Aging and Warmup Characteristics were measured at 100 MHz against either the Rubidium or Crystal Oscillator Reference. Thus we were able to maintain the beat frequence within limitations. Mixer and synthesizer noise contributions are negligable at these frequencies and frequency ratios.

The system noise floor and the x84/ref multiplier noise levels were measured in the field as needed to verify measurement system integrity. (See Figures 7 & 8)

UNIVERSAL LOW NOISE FREQUENCY MULTIPLIER

Figure 9 shows the Frequency Multiplier Module that was used. External, high isolation distribution amplifiers are not shown. A string of x2 sections, each consisting of a commercial 2way power splitter and frequency doubler, followed by a JPL designed low temperature coefficient bandpass filter and high isolation amplifier are mounted inside a magnetically shielded box. The input to each x2 is +10 dBm. The bandwidth and center frequency of the 5 pole filters are chosen so that with a minimum number of units a large range of input frequencies and multiplication factors can be configured in the field by simply selecting the appropriate bandpass filter, The noise of this multiplier is well below Hydrogen Maser levels. We use this multiplier with input frequencies in the range of 1 to 50 MHz and output frequencies in the range of 10 to 500 MHz.

REFERENCES

[1] Allan, D.W., Shoaf, J.H., and Halford, D., *"Statistics of Time and Frequency Data Analysis"*, chap. 8, Time and Frequency: Theory and Fundamentals (B.E. Blair, ed.), 1974, National Bureauof Standards Monograph No. 140, pp 151-204.

[2] Walls, F.L., Felton, C.M., Clements, A.J.D., *"Accuracy Model for Phase Noise Measurements"*, Proceedings of the 21st Annual Precise Time and Time Interval (PTTI) Applications and Planning Meeting, 28-30 November,1989, Redondo Beach, CA, pp 295–312.

[3] Greenhall, C.A., *"A Method for Using a Time Interval Counter to Measure Frequency Stability"*, IEEE Trans. on Ultrasonics, Ferroelectrics, and Frequency Control, UFFC-36, No 6, September 1989.

SPECIFICATIONS

Figure 1. ALLAN DEVIATION

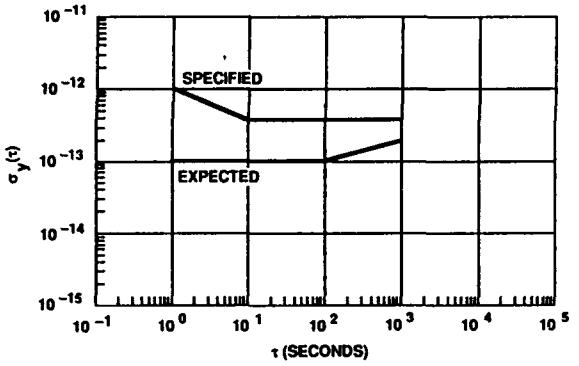

Figure 2. PHASE NOISE, NORMALIZED TO 5 MHz

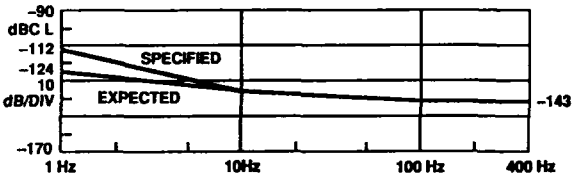

Figure 3. BASIC TEST CONFIGURATION

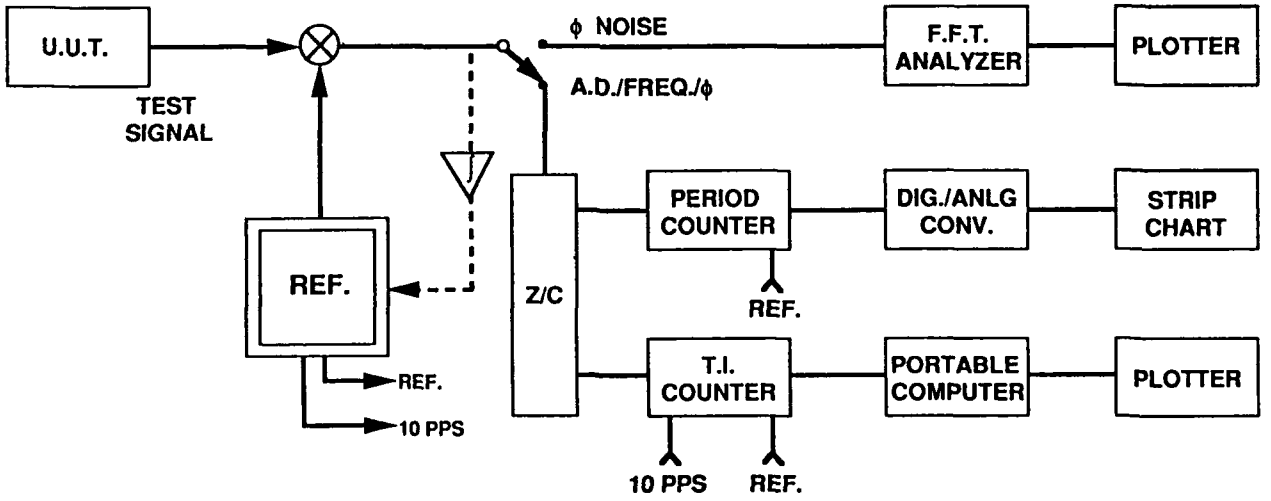

WHAT ARE THE PROBLEMS?

1. U.U.T. MUST NOT DRIFT TOO MUCH
2. MIXER NOISE MUST NOT LIMIT MEASUREMENT
3. REF. SOURCE MUST BE EQUAL OR BETTER THAN U.U.T.
4. SYSTEM MUST ACCOMMODATE OUTPUT FREQ. OF U.U.T.
5. MEASUREMENT SYSTEM PERFORMANCE MUST BE VERIFIABLE

Figure 4. AVAILABLE REFERENCES

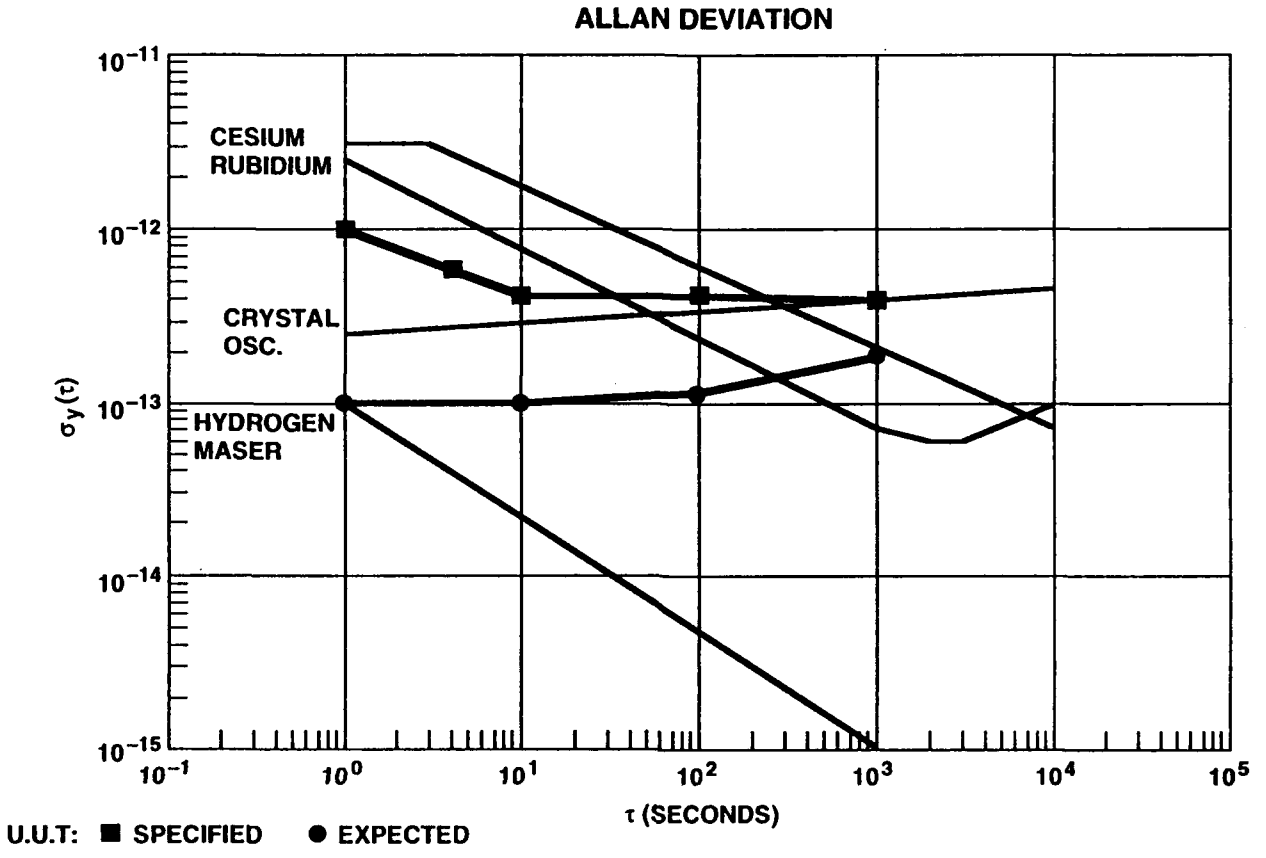

Figure 5. LOW FREQUENCY TEST SYSTEM CONFIGURATION

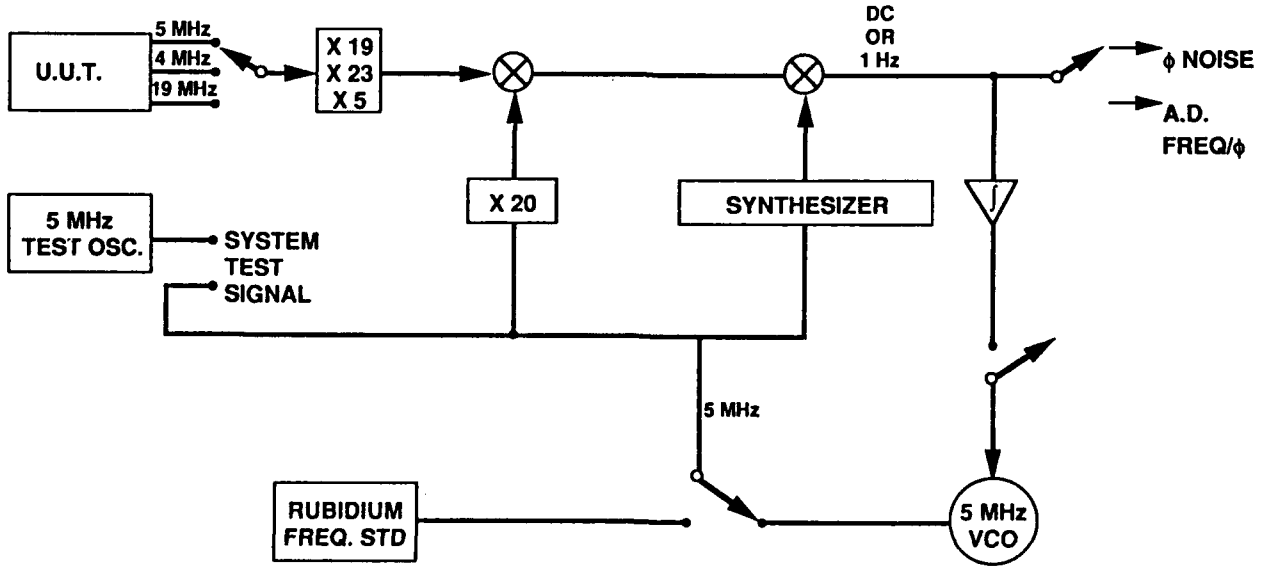

Figure 6. HIGH FREQUENCY TEST SYSTEM CONFIGURATION

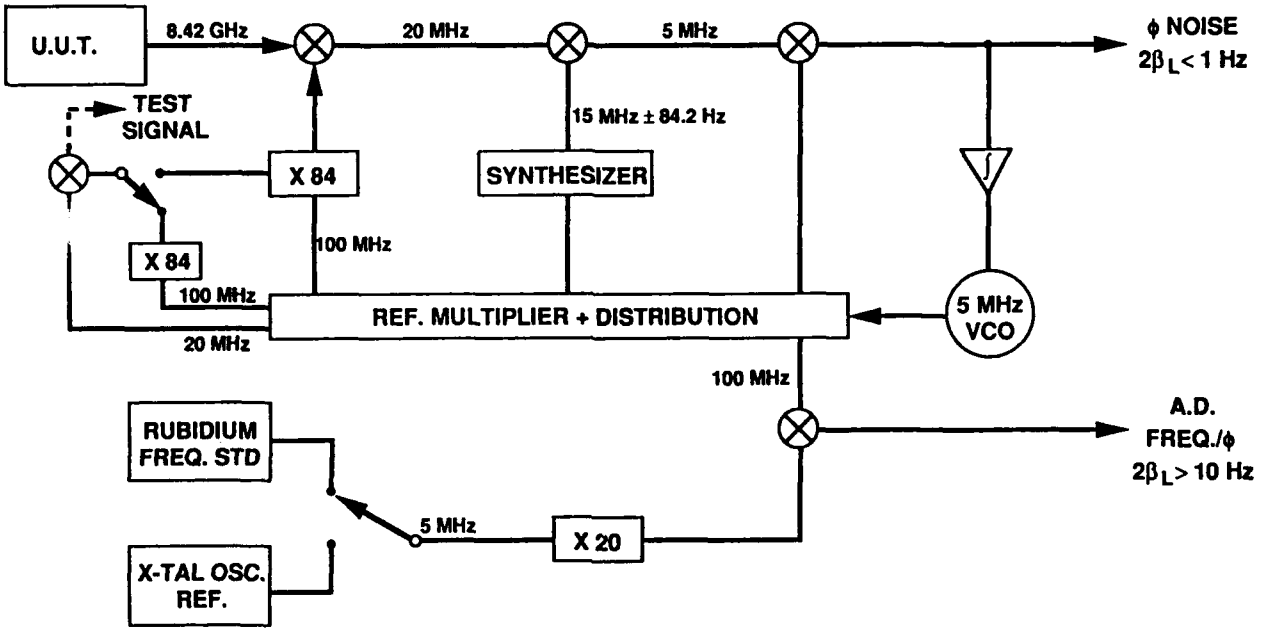

Figure 7. TEST SYSTEM NOISE FLOOR AT 8.42 GHz

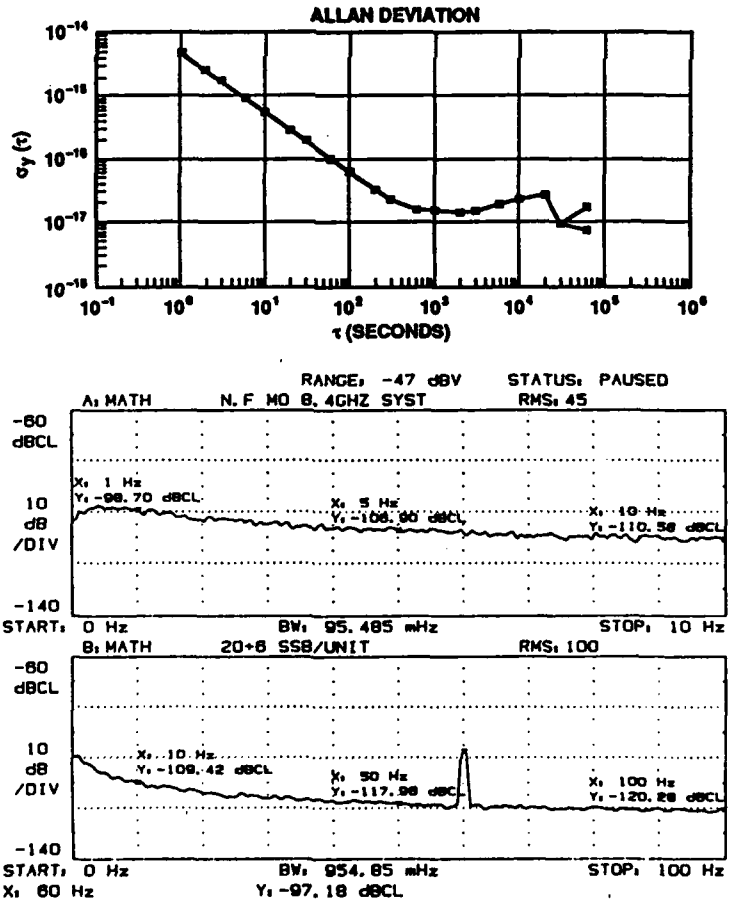

Figure 8. x 84 MULTIPLIER NOISE AT 8.4 GHz

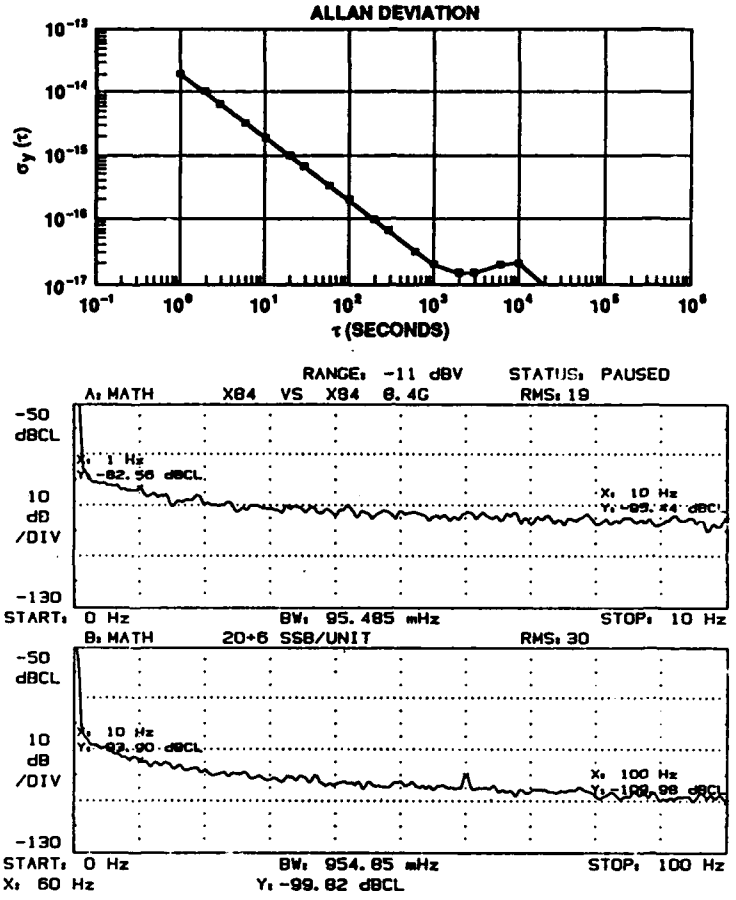

Figure 9. UNIVERSAL LOW NOISE FREQUENCY MULTIPLIER

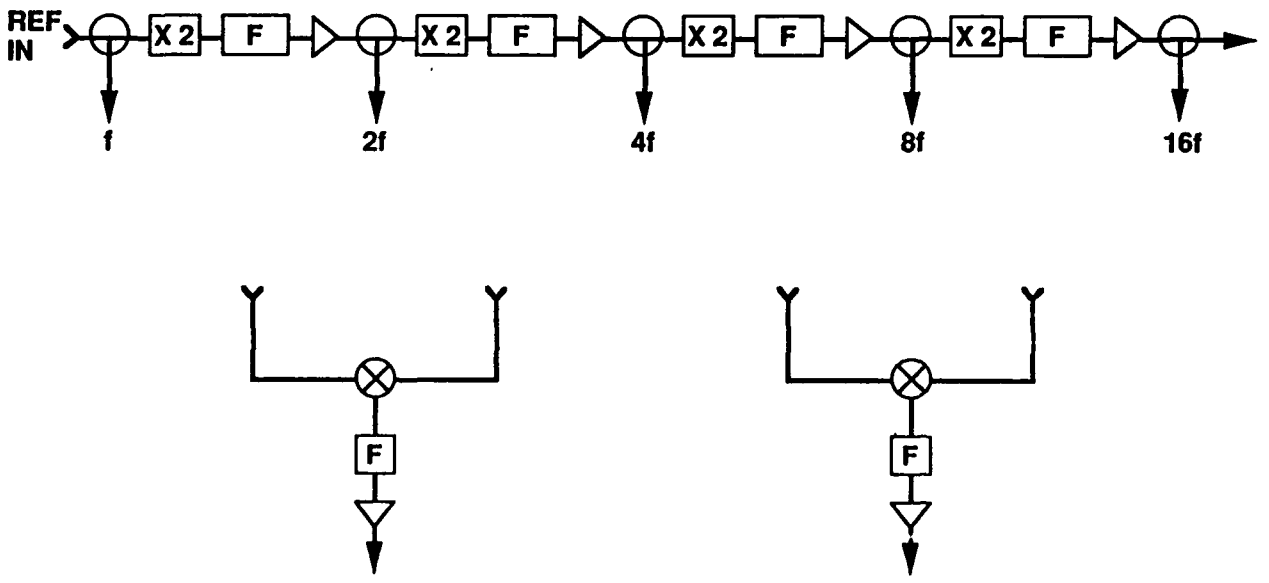

X 19 = 16f + (f + 2f)
X 23 = 16f + (8f – f)
X 5 = 4f + f

The Limit of Frequency Estimation

Wei Guo
Shaanxi Astronomical Observatory, Academia Sinica
P. O. Box 18 Lintong, 710600 Shaanxi, P.R. China

Abstract

In phase and frequency measurements, the measured phase and frequency are not the true phase and frequency but the ones which are disturbed by noises, due to the effects of the noise processes. In this paper, we discussed the effects of three noise processes, i.e., White PM, White FM and Random Walk FM, on the estimations of phase and frequency. It is indicated that the properties of these two estimations are very different. In phase estimation, the error can be reduced by properly selecting suitable smoothing length NT and smaple interval T. But in frequency estimation, the error cannot be reduced arbitarily by means of improving estimator or measurement equipment. The precison of frequency is limited by the intrinsic noises in the clock.

I. Introduction

In phase and frequency measurements, the measured phase and frequency are not the true phase and frequency but the disturbed ones, due to the effects of the noise processes. Before an atomic time scale being computed, the phase and frequency of each clock should be measured. So it is necessary to give proper estimations of the true phase and frequency.

In this paper, we discussed the effects of three noise processes, i.e., White PM, White FM and Random Walk FM, on the estimations of the phase and frequency. It is indicated that the properties of these two estimations are very different.

II. The Noise Model

The basic model, so called Power-law Model, is presented in frequency domain[1],

$$S_y(f) = h_{-2}f^{-2} + h_{-1}f^{-1} + h_0 + h_1 f + h_2 f^2 \qquad (1)$$

In time domain, the Dynamic Model is more convenient[2],

$$\begin{aligned} T(k) &= x(k) + r(k) \\ x(k+1) &= x(k) + y(k)\,T + q(k) \\ y(k+1) &= y(k) + f(k) \end{aligned} \qquad (2)$$

where $r(k)$ are phase modulation noise processes which contain White PM and Flicker PM; $q(k)$ are frequency modulation noise processes including White FM, Flicker FM and Random Walk FM; and $f(k)$ is Random Walk FM. The sampling interval is T.

The two flickers are not considered in the following disscusion, because the other three noise processes in different levels are enough to demenstrate the properties of the phase and frequenbcy estimations. So $r(k)$ represents the White

PM only,

$$Dr(k)^2=Er(k)^2=\frac{1}{(2\pi)^2}h_2f_h \tag{3}$$

and $q(k)$ represents the White FM and the Random Walk FM,

$$Dq(k)^2=Eq(k)^2=\frac{1}{2}h_0T+\frac{1}{6}(2\pi)^2h_{-2}T^3 \tag{4}$$

III. Phase Estimation (finite-memory smoothing)

For a set of $2N+1$ phase measurements of $T(k+i)(i=-N,...,0,...,N)$, the linear estimation of $x(t)$ is

$$\hat{x}(k)=\sum_{i=-N}^{N}C_iT(k+i) \tag{5}$$

There is a set of cofficients, $C_i(i=-N,...,0,...,N)$, which enables the estimation error to be minum,

$$E[T(k)-\hat{x}(k)]^2\rightarrow \min \tag{6}$$

But we do not care about the optimal solution here, because the properties of the estimation are more important. For convenience, a simplified smoother, average smoother, is used here. That is,

$$C_i=\frac{1}{2N+1} \qquad i=-N,\cdots,0,\cdots,N \tag{7}$$

and

$$\begin{aligned}\hat{x}(k)&=\frac{1}{2N+1}\sum_{i=-N}^{N}T(k+i)\\&=\frac{1}{2N+1}\sum_{i=-N}^{N}x(k+i)+\frac{1}{2N+1}\sum_{i=-N}^{N}r(k+i)\end{aligned} \tag{8}$$

If T is not large, the effect of Random Walk FM, $f(k)$, can be ignored in phase estimation. It is easy to show that

$$x(k+i)=x(k)+\sum_{l=1}^{i}q(k+l-1) \tag{9}$$

So the estimated phase can be expressed as true phase plus a serier of noise processes.

$$\begin{aligned}\hat{x}(k)=x(k)&+\frac{1}{2N+1}\sum_{i=-N}^{N}r(k+i)\\&-\frac{1}{2N+1}\sum_{i=1}^{N}q(k-i)(N-i+1)\\&+\frac{1}{2N+1}\sum_{i=1}^{N}q(k+i-1)(N-i+1)\end{aligned} \tag{10}$$

According the assumption of independence between noise processes, the estimation error is

$$
\begin{aligned}
&E[x(k)-\hat{x}(k)]^2 \\
&=\frac{1}{(2N+1)}\cdot Er^2(k)+\frac{2}{(2N+1)^2}\sum_{i=1}^{N}(N-i+1)^2\cdot Eq^2(k) \\
&=\frac{1}{2N+1}\cdot\frac{1}{(2\pi)^2}h_2f_h+\frac{N(N+1)}{2(2N+1)}h_0T \\
&\approx\frac{1}{2N}\cdot\frac{1}{(2\pi)^2}h_2f_h+\frac{1}{4}NTh_0
\end{aligned}
\tag{11}
$$

This is the property of phase estimation that a small NT, smoothing length, can reduce the effect of White FM and also when NT is fixed, increasing N, i.e., decreasing T, can reduce the effect of White PM. Therefore, a suitable selection of N and T will make the error of phase estimation small enough.

IV. Frequency Estimation-I (Finite-memory smoothing)

We assume the measured phase has been carefully filtered before the frequency estimation being done. Thus the phase noise can be ignored and the noise model of Eq.(1) is rewritten as

$$
\begin{aligned}
d(k)&=y(k)+\frac{1}{T}q(k) \\
y(k+1)&=y(k)+f(k)
\end{aligned}
\tag{12}
$$

where

$$
d(k)\triangleq\frac{1}{T}[x(k+1)-x(k)] \tag{13}
$$

For a set of $2N+1$ frequency measurements of $d(k+i)(i=-N,\ldots,0,\ldots,N)$, the linear estimation of $y(t)$ is

$$
\hat{y}(k)=\sum_{i=-N}^{N}C_id(k+i) \tag{14}
$$

We also consider an average smoother, similar to the case in phase estimation. That is,

$$
\begin{aligned}
\hat{y}(k)&=\frac{1}{2N+1}\sum_{i=-N}^{N}d(k+i) \\
&=y(k)+\frac{1}{T}\cdot\frac{1}{2N+1}\sum_{i=-N}^{N}q(k+i) \\
&\quad-\frac{1}{2N+1}\sum_{i=1}^{N}f(k-i)\,(N-i+1) \\
&\quad+\frac{1}{2N+1}\sum_{i=1}^{N}f(k+i-1)\,(N-i+1)
\end{aligned}
\tag{15}
$$

The estimation error is

$$
\begin{aligned}
&E[y(k)-\hat{y}(k)]^2 \\
&=\frac{1}{(2N+1)T^2}\cdot Eq^2(k)+\frac{2}{(2N+1)^2}\sum_{i=1}^{N}(N-i+1)^2\cdot Ef^2(k) \\
&=\frac{1}{2N+1}\left[\frac{1}{2T}h_0+\frac{1}{6}(2\pi)^2h_{-2}T\right]+\frac{N(N+1)}{2N+1}\cdot\frac{1}{2}(2\pi)^2h_{-2}T \\
&\approx\frac{1}{4}NTh_0+\pi^2h_{-2}NT
\end{aligned}
\tag{16}
$$

It can be seen from Eq.(11) and Eq.(17) that estimations of phase and frequency are very different. In phase estimation, the two noise effects can be reduced simultaneously by small NT and large N. But in frequency estimation small NT may reduce the effect of h_{-2} but the effect of h_0 will increase, while large NT will lead high h_{-2} and low h_0. Therefore, the precision of frequency estimation cannot be improved arbitarily by change N or T for certain noise levels.

According to Eq.(17), we may choose a suitable NT which can make the estimation error as small as possible,

$$
(NT)_{\min}=\frac{1}{2\pi}\sqrt{\frac{h_0}{h_{-2}}} \tag{17}
$$

Correspondent error is

$$
E[y(k)-\hat{y}(k)]^2_{\min}=\pi\sqrt{h_0h_{-2}} \tag{18}
$$

V. Frequency Estimation-II (Kalman Filtering)

For the noise model shown in Eq.(12), Kalman filter may be considered as an optimal estimator. Obviously, the system of Eq.(12) fulfills the conditions of observability and controllability, so the filter is stable. When the system is in steady state, the frequency estimation is

$$
\hat{y}(k+1/k+1)=\hat{y}(k/k)+K[d(k+1)-\hat{y}(k/k)] \tag{19}
$$

and the estimation error is

$$
E[y(k)-\hat{y}(k/k)]^2=P^+ \tag{20}
$$

In steady state, the filtering error P^+, the prediction error P^- and the gain K fulfill the Riccati Equation as below,

$$
\begin{aligned}
&P^-=P^++F \\
&K=P^-\left(P^-+\frac{1}{T^2}Q\right)^{-1} \\
&P^+=(1-K)P^-
\end{aligned}
\tag{21}
$$

where $F=Df^2(k)$ and $Q=D(q(k)/T)^2$. P^+ is solved as

$$
\begin{aligned}
P^+&=\frac{1}{2}\left(-F+\sqrt{F^2+4F\frac{Q}{T^2}}\right) \\
&=-\pi^2h_{-2}T+\sqrt{\pi^2h_0h_{-2}+\frac{7}{3}\pi^4h_{-2}^2T^2}
\end{aligned}
\tag{22}
$$

There is a $T_{\min}$ which makes P^+ be minium,

$$T_{min}=\frac{1}{\pi}\sqrt{\frac{9h_0}{28h_{-2}}} \tag{23}$$

The correspondent estimation error is

$$E[y(k)-\hat{y}(k/k)]^2=\pi\sqrt{\frac{4}{7}h_0h_{-2}} \tag{24}$$

Because Kalman filter is an optimal estimator, any other estimator will not be better than it. Therefore, Eq.(25) can be regarded as the limit of the frequency estimaton. This limit is related to the intrinsic noises in the clock, not the measurement equipment. In general speaking, the precision of frequency estimation is limited by the noise levels in the clock, which cannot be improved arbitarily by improving measurement.

VI. Conclussion

We have analyzed the effects of clock noises on the phase and frequency estimations, respectively. In phase estimation, the error can be reduced by properly selecting suitable smooth length NT and smaple interval T. But in frequency estimation, the error cannot be reduced arbitarily by means of improving estimator or measurement equipment. The precison of frequency is limited by the intrinsic noises in the clock.

Reference

[1] J. A. Barnes et al., "Characterization of Frequency Stability", IEEE Trans. on Instru. and Measu., Vol. IM-20, No. 2, 1971

[2] WEI Guo, "Characteristic Analysis of Clock Noise: A Dynamic Model", Proc. of Third International Time Scale Algorithm Symposium, 1988

[3] WEI Guo, Ph. D. Thesis, 1991

[4] WEI Guo, Characterization of Frequency Stability: Analysis in Time Domain", Science in China (Series A), Vol. 36, No. 2, Feb. 1993 (to be published)

A New Method of Time Difference Measurement– The Time Difference Method by Dual "Phase Coincidence Points" Detection

Wei Zhou
Dept. of Measurement and Instrumentation, Xidian University
Xi'an, 710071, P.R.China

Abstract

In the high accurate measurement of periodic signals the greatest common factor frequency and its characteristics have special functions. This paper describes a new method of time difference measurement–the time difference method by dual "phase coincidence points" detection. This method utilizes the characteristics of the greatest common factor frequency to measure time or phase difference between periodic signals. It can suit a very wide frequency range. Measurement precision and potential accuracy of several picoseconds have been demonstrated with this new method. The instrument based on this method is very simple, and the demand for the common oscillator is low. This method and instrument can be used widely.

1. Introduction

With the greatest common factor frequency and its characteristics the high accurate measurement of periodic signals can be accomplished easily, and the equipment is very simple. The time difference method by dual "phase coincidence points" detection is a new method of time difference measurement based on the characteristics of the greatest common factor frequency. With this method the high accurate time difference measurement can be accomplished in a very wide frequency range. It is different from some frequency standard measurement method and instruments which can only be used to measure time difference at certain frequency points and the devices are complex, that this new method can be used in a very wide frequency range and the device is simple.

The greatest common factor frequency between two frequency signals is similar to the mathematical greatest common factor between two numbers. To two frequency signals f_1 and f_2, if $f_1 = Af_c$, $f_2 = Bf_c$, the two positive integers A and B are prime with each other, then f_c is the greatest common factor frequency f_{maxc} between f_1 and f_2 . The period of f_{maxc} is the least common multiple period T_{minc} between f_1 and f_2 .

With the characteristics of the greatest common factor frequency to measure frequency and other periodic signals, the main method is to detect the "phase coincidence points" between a standard frequency signal and a measured frequency signal. The "phase coincidence point" does not mean

exact phase coincidence. It means the degree and case of the very near relative phase. It has been demonstrated that the quantized phase shift discriminability between two frequency signals is:

$$\Delta T = \frac{f_{maxc}}{f_1 f_2} \tag{1}$$

where f_{maxc} is the greatest common factor frequency between f_1 and f_2 . In a T_{minc} period the phase difference change between any two frequency signals can be quite different. Maybe it is from large to small or from small to large. Maybe the change is irregular. It depends on the relative relationship between the two frequency signals. If we rearrange the order of the quantized phase difference values by size sequence in a T_{minc} period, the change of the quantized adjacant phase difference is ΔT. According to the measuring accuracy, the "phase coincidence points" are some time difference value decided by the initial phase difference plus 0, ΔT, $2\Delta T$, $3\Delta T$,... respectively. If the measuring gate time is composed of some time interval that starts and stops at the "phase coincidence points", there are the cycle numbers that are very close to many integral periods of the two frequency signals respectively. Using this method some high accurate measurements of frequency and periodic signals can be achieved. The ± 1 count error that occurs in ordinary frequency and time interval measurement instruments can be overcome satisfactorily. Therefore, the new instruments designed by this method can obtain 1000 times higher accuracy than that of ordinary instruments. When the instruments are designed for special purposes, their accuracy is much higher.

2. The time difference method by dual "phase coincidence points" detection

A principle block diagram of the time difference method by dual "phase coincidence points" detection is shown in Fig. 1. Fig. 2 is the waveform diagram of this method.

In Fig. 2, $f_c(t)$ is the common oscillator. Sometimes it can be the standard frequency. $f_1(t)$ and $f_2(t)$ are the two compared signals which are the same in frequency . Sometimes one of them is the standard frequency signal. The "phase coincidence points" between common oscillator signal and two compared signals are detected respectively. The measuring gate time begins with the "phase coincidence point" between $f_1(t)$ and $f_c(t)$, and ends up with the "phase coincidence point" between $f_2(t)$ and $f_c(t)$. If the frequencies of $f_1(t)$ and $f_2(t)$ are unknown (at this time $f_c(t)$ is the standard frequency), their period T_x is measured with $f_c(t)$. The measured whole time is:

$$\begin{aligned} t &= N_{x1}T_x + \Delta t \\ t &= N_{c1}T_c \end{aligned}$$

The measured time difference is:

$$\Delta t = N_{c1}T_c - N_{x1}T_x \tag{2}$$

where T_c is the period of $f_c(t)$, N_{c1} are the cycle numbers of $f_c(t)$ in the gate time t, and N_{x1} are the cycle numbers of $f_1(t)$ in the time interval $t - \Delta t$.

The measuring error is much less than ±1 period of the count pulse, but is the value relating to the quantized phase change between the common oscillator and measurands and the phase detection discriminability of the phase detection circuit.

According to different measuring purposes the standard frequency signal can be used in different positions, and the demand for the common oscillator is different. In the measurement there are two same greatest common factor frequencies f_{maxc} between the common oscillator and the two compared frequency signals which are the same in frequency. In the general time difference, time interval measurements, the standard frequency signal is used as common oscillator. At this time the frequency relationship between common oscillator and compared frequency signals is similar to that of the frequency measurement with "The Frequency Measuring Technique by Broad–band Phase Detection". If the frequency of measured signal is close to the frequency of the standard signal or they have multiple relationship in frequency, the measurement must be accomplished by a frequency synthesizer. Some papers have described this question in detail.

In the time difference measurement of two high stable frequency signals, one of which is the standard frequency signal, the common oscillator can be a stable crystal oscillator. The frequency of the common oscillator and its frequency stability in certain period can influence the measurement. The common oscillator is an important device in the measurement system. Generally its frequency has some little frequency difference with general standard signal frequency or its multiple frequencies. The frequency difference can be chosen according to the measuring demand, and can suit most standard frequency signals. The common oscillator can be locked by the standard frequency signal, also can be not locked. It may influence the measuring accuracy obviously. Generally, in the measurement with the locked common oscillator the measuring period can be controlled easily. If the common oscillator is locked, the locked frequency can be chosen flexibly. But for ordinary synthetic frequency, that has a little integral frequency deviation based on general standard frequency or its multiple frequencies (for example, 5.0001 MHz, 10.001 MHz), the greatest common factor frequency f_{maxc} is large. It is unfavourable to further enhancing the measuring accuracy. In each least common multiple period the phase difference between the common oscillator and the two compared signals changes in one direction uniformly. In this case the measurement is very regular. The least regular period of measurement is equal to the least common multiple period. The measurement can be controlled very easily. According to equations (1) and (2), the measuring accuracy depends mainly on the detection accuracy of the "phase coincidence point" detection circuit and the quantized phase shift discriminability between the common oscillator and the two compared signals. The quantized phase shift discriminability depends on equation (1). It is not very high. Therefore, compared with the ordinary measuring technique, the new measuring method can only get a limited enhanced accuracy. With this method the ±1 count error in the ordinary time–frequency measuring instrument can be overcome. Using a suitable frequency synthesizer, we can measure time difference in a very wide frequency range and obtain 0.2 ns or higher measuring accuracy. Because there is no non–linear circuit for frequency transformation, the direct time difference measurement can be accomplished easily when the two input circuits are identical.

When the unlocked common oscillator is used, the demand for the frequency stability of the common oscillator is high, but the synthesizer can be omitted. In this case we can obtain the very little greatest common factor frequency. It is favourable to further enhancing the measuring

accuracy. We can also get suitable measuring time and interval. When a crystal oscillator is used as the common oscillator that is not locked by the standard frequency signal, its frequency value is composed of three sections. They are the main frequency section which is equal to the frequency value of general frequency standard or its multiples (for example, 5 MHz, 10 MHz), some regular low frequency difference (1 kHz or 100 Hz etc.), and some unfixed little frequency deviation. In this case, a regular distribution of "phase coincidence points" can also be obtained. It is different from a frequency synthesizer as the common oscillator that the unlocked common oscillator has the unfixed little frequency deviation. The third section is important to the measurement. In this case the greatest common factor frequency between the common oscillator and compared signal is very little (is several Hz or much less), and it is much less than the low frequency difference section. Therefore, we can obtain higher measuring accuracy with a phase detection circuit that has a high precision. In a least common multiple period there are many periods of phase change from large to small or from small to large. There are very little differences between these corresponding phase diferences that are in different periods of phase change. The period number of the phase change in a least common multiple period is about equal to the ratio of the second section of the common oscillator frequency to the greatest common factor frequency. The distribution of "phase coincidence points" is uniform.

When the detection precision of the phase detection circuit is higher enough, in a T_{minc} period the detected "phase coincidence points" are less and are concentrated some range in the T_{minc} period. In this case, the distribution of the detected "phase coincidence points" is no longer uniform. Because the greatest common factor frequency f_{maxc} and the quantized phase shift discriminability ΔT are small, we have chance to get higher measuring accuracy, especially in the frequency standard comparison. Fig. 3 is the block diagram of an instrument designed by this new method.

In this instrument, the nominal frequencies of the two compared frequency signals $f_1(t)$ and $f_2(t)$ are known and the same, and one of them is the standard frequency signal. The compared signal frequency can be 10 MHz, 5 MHz, 2.5 MHz, 1 MHz or 100 KHz. These frequency values are stored in EPROM of the microcomputer. The common oscillator is a unlocked crystal oscillator. It has good short-term stability and its nominal frequency is 10.0001 MHz. However its practical frequency has several to several tens Hz deviation from 10.0001 MHz. Therefore the greatest common factor frequency between the common oscillator and the compared frequency signal is from less than 1 Hz to about several tens of Hz, and in most cases it is much less than 1 Hz. The quantized phase shift discriminability $\Delta T'$ between them is less than 1 ps. The delay control signal generated by microcomputer software controls the measurement interval. The "phase coincidence" signal between $f_1(t)$ and $f_c(t)$ starts the gate time generating circuit 1 and the gate time generating circuit 2. The gate time generating circuit 1 is stopped by another "phase coincidence" signal between $f_1(t)$ and $f_c(t)$, and the gate time generating circuit 2 is stopped by a "phase coincidence" signal between $f_2(t)$ and $f_c(t)$ which follows the starting signal. The $f_1(t)$ and $f_c(t)$ signals are counted in 4 counters after 4 gate circuits. From Fig. 3, the gate signals are synchronized by corresponding signals, the counted numbers do not have ± 1 count error. From counted cycle numbers by counter 1 and counter 2, the frequency of the common oscillator can be computed. Its period is:

$$T_c = \frac{N_0 T_0}{N_c}$$

where T_0 is the period of $f_1(t)$ and $f_2(t)$, N_0 is the cycle number of $f_1(t)$ counted by counter 1, and N_c is the cycle number of $f_c(t)$ counted by counter 2. According to a different input compared frequency signal, the computer can choose the different T_0 value which has been stored in its EPROM. From cycle number N_{c1} of $f_c(t)$ counted by counter 3 and the cycle number N_{01} of $f_1(t)$ counted by counter 4, the time difference Δt between $f_1(t)$ and $f_2(t)$ can be computed.

$$\begin{aligned} \Delta t &= N_{c1}T_c - N_{01}T_0 \\ &= (\frac{N_{c1}N_0}{N_c} - N_{01})T_0 \end{aligned} \tag{3}$$

Because the gate time 1 and gate time 2 start at same time, and stop at very close two different times, the frequency stability of $f_c(t)$ almost does not influence the measuring accuracy. It is the frequency fluctuation of the common oscillator in the time interval of not synchronized two finishing gate times that influences measuring accuracy. If the phase fluctuations of the common oscillator are small during this interval as compared to the phase fluctuations between $f_1(t)$ and $f_2(t)$ over a full gate time 2, the noise of the common oscillator is insignificant in the measurement noise error budget, which means in most cases the noise of the common oscillator can be worse than that of either $f_1(t)$ or $f_2(t)$ and still not contribute significantly. The common oscillator $f_c(t)$ is used to generate the suitable greatest common factor frequency and to help to accomplish the high accurate measurement. We only demand its frequency range, but its practical frequency and long term frequency fluctuation do not influence the measurement. The integral section (10 MHz) of the common oscillator $f_c(t)$ is the multiples of the compared frequency. In every T_{minc} period there are many regular phase change which is from small to large or from large to small. It is favourable to the "phase coincidence" detection circuit. Because in this case, it is the stability of "phase coincidence" detection circuit that decides the measuring accuracy. The circuit discriminability is not so important, and it is lower than the circuit stability.

This device can be used in a very wide frequency range, in the comparison of the integral frequency standards it can get very high measuring precision and accuracy. When it is used in the the comparison of 5 MHz or 10 MHz frequency standard, the better than 10 ps measuring precision can be obtained. In the device there are not any frequency transformation circuits or non–linear circuits. Therefore, it is very simple. This new method and instrument can be used widely in the time–frequency measurements.

References:

[1.] Wei Zhou *"The Greatest Common Factor Frequency and Its Application in the Accurate Measurement of Periodic Signals"* 1992 IEEE Frequency Control Symposium, May, 1992

[2.] Wei Zhou *"A New Principle of Linear Phase Comparison — Irregular Phase Discrimination"* 18th Annual PTTI Applications and Planning Meeting, Dec., 1986

[3.] D.W.Allan, Herman Daams *"Picosecond Time Difference Measurement System"* 29th Annual Symposium on Frequency Control, pp.404 - 411, 1975

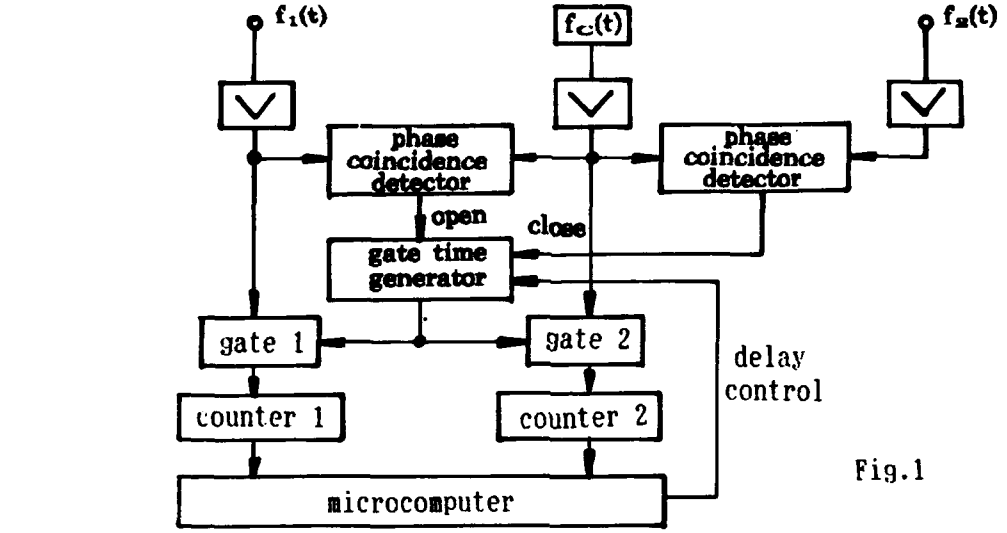

Fig.1

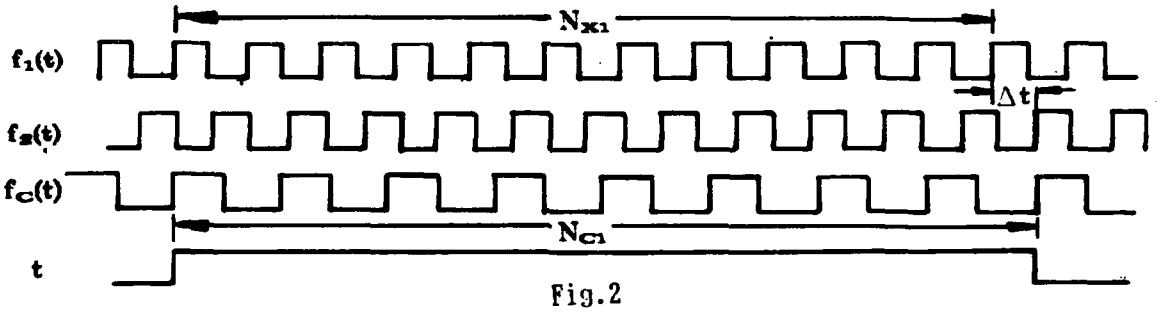

Fig.2

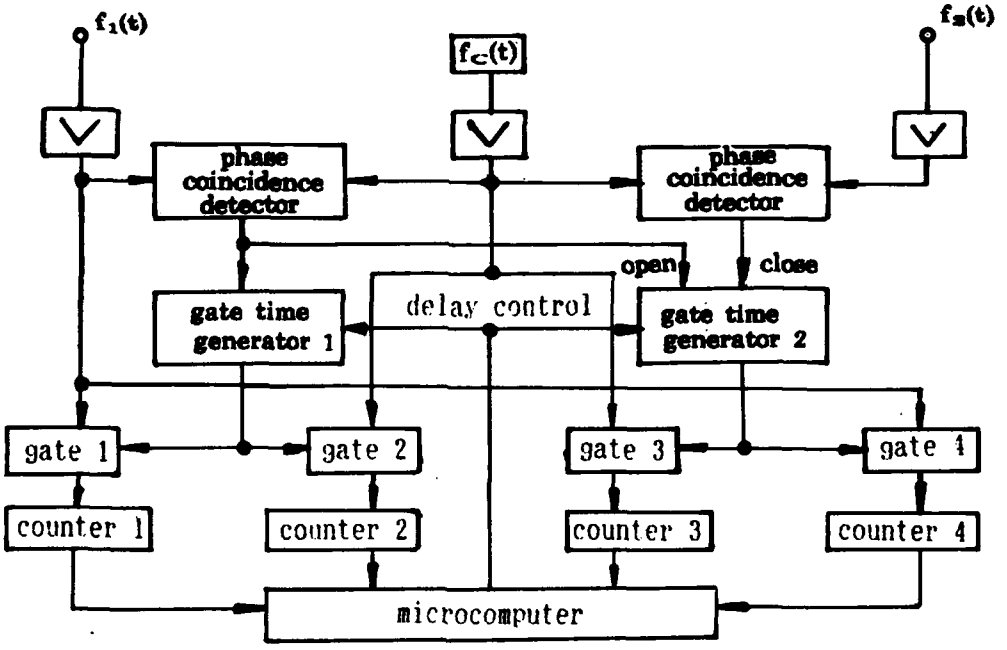

Fig.3

CONFIDENCE ON THE THREE-POINT ESTIMATOR OF FREQUENCY DRIFT*

Marc A. Weiss and Christine Hackman
Time and Frequency Division
National Institute of Standards and Technology
325 Broadway
Boulder, CO 80303

Abstract

It has been shown that a three–point second difference estimator is nearly optimal for estimating frequency drift in many common atomic oscillators. We derive a formula for the uncertainty of this estimate as a function of the integration time and of the Allan variance associated with this integration time.

Theory

The three–point drift estimator is a useful tool for estimating the frequency drift in many atomic oscillators [1]. In this paper we derive a formula for the uncertainty of the three–point drift estimate; as we shall demonstrate, there is a simple relationship between the uncertainty of the drift estimate and the Allan variance of the residuals which remain after the estimated drift is removed. We explain how to apply the uncertainty formula and then we use it to assess the uncertainty of the drift estimate in several examples.

Let us begin by discussing the three–point drift estimator. To define it, let x(t) be a time series of time difference measurements between two oscillators drifting in frequency relative to each other. An optimal estimator, $\hat{D}$, of drift uses the first, middle, and last time–difference points. We estimate the average frequency over the first and second halves of the data, subtract the first frequency from the second, and then divide by τ, the time elapsed between the first and middle or middle and last data points. This yields:

$$\begin{aligned} \hat{D} &= \frac{1}{\tau}\left(\frac{x(2\tau)-x(\tau)}{\tau} - \frac{x(\tau)-x(0)}{\tau}\right) \\ &= \frac{1}{\tau^2}\left((x(2\tau)-2x(\tau)+x(0)\right) \end{aligned} \tag{1}$$

That is, we estimate drift as $1/\tau^2$ times the second difference of the time series x, where we take the second difference over as large an interval as possible.

Let us separate the time offset $x(t)$ into the part due to the frequency drift D and the part due to everything else (initial offsets, stochastic noise, systematics):

$$x(t) = x'(t) \frac{D}{2} t^2 \ . \tag{2}$$

We now will show that the uncertainty of the drift estimate, $\hat{D}$, is functionally related to the Allan variance of the $x'(t)$ time series.

If we substitute (2) into (1) we obtain

$$\hat{D} = \frac{1}{\tau^2} \left(x'(2\tau) - 2x'(t) + x'(0) + D\tau^2 \right) \ . \tag{3}$$

Rearrangement yields:

$$\hat{D} - D = \frac{1}{\tau^2} \left(x'(2\tau) - 2x'(\tau) + x'(0) \right) \ . \tag{4}$$

The expected variance of our drift estimate, $\hat{D}$, around the true drift D will thus be

$$\langle \left(\hat{D} - D \right)^2 \rangle = \frac{1}{\tau^4} \langle \left(x'(2\tau) - 2x'(\tau) + x'(0) \right)^2 \rangle \ , \tag{5}$$

where $\langle \ \rangle$ is the expectation operator. The square root of this quantity is the expected deviation of $\hat{D}$ around the true value.

If we compute an Allan variance of x' for the integration time τ we obtain [2,3]

$$\sigma_{y'}(\tau)^2 = \frac{1}{2\tau^2} \langle \left(x'(2\tau) - 2x'(\tau) + x'(0) \right)^2 \rangle \ . \tag{6}$$

Substitution of (6) into (5) yields our result, the relationship between the expected deviation in the drift estimator, $\hat{D}$, and the Allan variance of x', the drift–removed data:

$$\boxed{\langle \left(\hat{D} - D \right)^2 \rangle = \frac{2}{\tau^2} \sigma_{y'}(\tau) \ ,} \tag{7}$$

where $\sigma_{y'}(\tau)$ is the Allan variance of the x' data, and y' refers to the frequency data derived from x'. Thus we see that the uncertainty in our drift estimate is a function of the Allan variance of the drift–removed data.

Application of Equation 7

The application of (7) requires a bit of finesse. First of all, the alert reader has probably noticed that, since we don't know the value of D, the true drift, we cannot obtain the time series $x'(t)$. To circumvent this problem, we obtain an approximation of $x'(t)$ by removing the estimated drift from the $x(t)$ series. We then compute the Allan variances for the approximate $x'(t)$ series. However, it is at

this point that we encounter another problem: It is generally true that if you 1) use a second–difference estimator (such as the three–point estimator) to estimate drift, 2) remove this estimated drift from the time series, and then 3) compute the Allan variances for the residual time series, the Allan variances obtained for large integration times (such as $\tau = 1/2$ the data length) will be biased low, i.e. the Allan variance will not be an accurate measure of the frequency variability at large integration times. In fact, if we were to take a data set with constant drift, compute $\hat{D}$ using (1), remove $\hat{D}t^2/2$ from each data point, and then compute $\sigma_{y'}(\tau)$ for this same τ, we would obtain exactly zero.

We need to have $\sigma_{y'}(\tau)$ for $= 1/2$ the data length in order to use (7). Yet we know that after removing $\hat{D}$ from $x(t)$, we are going to get the incorrect value of 0 for $\sigma_{y'}2(\tau)$ for $\tau = 1/2$ the data length. However, while $\sigma^2_{y'}(\tau)$ is incorrectly low for large τ, it does accurately represent the frequency variability for smaller τ. Furthermore, the noise processes of atomic oscillators are such that, for a given range of integration times τ, it is usually the case that $\sigma^2_{y'}(\tau) = k\tau^n$, where k is a constant and n is an integer ranging from 1 to -2. The result of this power–law behavior of $\sigma_{y'}(\tau)$ is that log–log plots of $\sigma_{y'}(\tau)$ versus τ exhibit linear behavior. This can be seen in Figure 1. Therefore, in order to obtain $\sigma^2_{y'}(\tau)$ for $\tau = 1/2$ the data length, we look at the log–log plot of $\sigma_{y'}(\tau))$ versus τ and discard the incorrectly–low values of $\sigma_{y'}(\tau)$ which occur at large τ (For example, in Figure 1, we would discard the point for which log τ (seconds) ≈ 7. In Figure 3 we would discard the point for which log τ (seconds) ≈ 6.75). Then, we use the $\sigma_{y'})\tau)$ points which correspond to the largest remaining τ values to determine k and n (i.e., we determine the equation of the line on the log–log plot formed by the remaining valid data points). Then, knowing k and n, we use the equation $\sigma^2_{y'}(\tau) = k\tau n$ to determine the value of $\sigma^2_{y'}(\tau)$ at $\tau = 1/2$ the data length. This value is what we need to apply (7).

For cesium beam and rubidium gas–cell oscillators, the dominant noise types at large integration times are flicker frequency modulation and random walk frequency modulation (FLFM and RWFM, respectively). FLFM corresponds to an n value of 0 and RWFM corresponds to an n value of $+1$. For very large τ, RWFM generally dominates. Therefore, if the last (i.e. largest τ) valid linear trend that we see on the log–log plot is consistent with a model of RWFM, we may use this slope with a measure of confidence to estimate the value of $\sigma^2_{y'}(\tau)$ at $\tau = 1/2$ the data length. If, however, the last linear trend corresponds to FLFM, we need to ask ourselves whether the FLFM noise type continues out to $\tau = 1/2$ the data length, or whether RWFM is the correct noise type for $\tau = 1/2$ the data length. The assumption of RWFM as the noise type always leads to a larger computed value of $\sigma^2_{y'}(\tau)$ than the assumption of FLFM. Thus, simply assuming that RWFM dominates at $\tau = 1/2$ the data length yields a conservative estimate. The uncertainty in the Allan variance estimate will limit the accuracy of our uncertainty estimate. Nevertheless, we can make conservative estimates of uncertainty and obtain meaningful results.

In summary, to use (7) to estimate the uncertainty of we take the following steps:

1. Compute using the second difference estimator (3), where in that equation, $\tau = \tau_{max}$, the time interval for one–half the data length. Remove $\hat{D}t^2/2$ from each of the time–difference data points $x(t)$.

2. Compute the Allan deviations $\sigma_{y'}(\tau)$, for $\tau = n\tau_0$, where n is an integer multiple of the sampling interval τ_0. Make a log–log plot of $\sigma_{y'}(\tau)$ versus τ.

3. Look for abnormally low values of $\sigma_{y'}(\tau)$ at large values of τ. Discard them.

4. Determine the parameters k and n in the equation $\sigma^2_{y'}(\tau) = k\tau n$ for the last valid linear trend

on the log–log plot. Then use this equation to compute $\sigma_y^2(\tau)$ for τ_{max}. Remember to consider the possibility that the noise type might change past the last valid $\sigma_y(\tau)$ value on the log–log plot (i.e., the noise type might change from FLFM to RWFM).

5. Substitute this value of $\sigma_y^2(\tau)$ into (7). Solve (7) for the variance of $\hat{D}$. The square root is the expected deviation.

Examples

As examples we use atomic standards aboard GPS satellites studied from July 1, 1991, to September 15, 1992, a period of 443 d. Satellites are referred to by their pseudo–random code number (PRN), the number by which users identify satellites , or by their satellite vehicle number (SVN), the number used by the GPS control segment. Clocks on the GPS satellites are measured at NIST against the AT1 time scale. For clocks which ran for this entire period, drift could be estimated using a second difference with τ=221.5 d. Not all clocks analyzed were on line for this entire period, in which case shorter τ values were found. We found an assortment of dominant noise types at various integration times, with FLFM, and RWFM dominating at times equal to one–half the data length. Table I gives our example results and indicates associated figure numbers.

PRN#2 and figure 1 illustrate the difficulty in determining noise type. Looking at figure 1, we see that, while FLFM, τ^0, is the probable slope for the last valid $\sigma_y(\tau)$ values, the uncertainty allows for the possibility of a $\tau^{1/2}$ slope, indicating RWFM. Furthermore, RWFM is usually the dominant noise process for cesium frequency standards at integration times such as 221.5 d [6]. We compute a more conservative value in the second line of the table. Similarly for PRN#25 we have assumed FLFM in its first line. If we assume RWFM we see we find only a small change.

Another consideration is that equation (7) applies to the Allan variance, not the modified Allan variance. In figures 1 and 5 we used the modified Allan variance. We can account for this as follows. Asymptotically, if we define

$$R_\infty = \lim_{\tau \to \infty} \frac{\mathrm{mod}\ \sigma_y^2(\tau)}{\sigma_y^2(\tau)}\ , \tag{8}$$

then $R_\infty = 0.91$ for RWFM and $R_\infty = 0.82$ for FLFM [5]. These corrections have been included in the table.

Conclusions

We have derived a relationship that allows us to estimate the uncertainty of the three–point estimator of frequency drift. It does not give a lot of precision but it is adequate for determining a confidence level. With the procedure outlined, we can determine an upper bound on the uncertainty of the estimate of frequency drift.

References

[1] M.A. Weiss, D.W. Allan, and D.A. Howe, *"Confidence on the Second Difference Estimation of Frequency Drift, A Study Based on Simulation,"* Proceedings of the 1992 IEEE Frequency Control Symposium, pp. 300–305, 1992.

[2] D.A. Howe, D.W. Allan, and J.A. Barnes, *"Properties of Signal Sources and Measurement Methods,"* 35th Annual Symposium on Frequency Control, 1981.

[3] Eds. D.B. Sullivan, D.W. Allan, D.A. Howe, and F.L. Walls, NIST Tech Note 1337: Characterization of Clocks and Oscillators, 1990.

[4] S.R. Stein, *"Frequency and Time–Their Measurement and Characterization,"* Precision Frequency Control, vol. 2, chap. 12, pp. 191–232, 1985.

[5] D. B. Sullivan, D.W.Allan, D.A. Howe, and F.L. Walls *"Characterization of Clocks and Oscillators,"* in [3], pp.1–13.

[6] D.W. Allan, *"Time and Frequency (Time-Domain) Characterization, Estimation, and Prediction of Precision Clocks and Oscillators,"* in [3], pp. 121–128.

Table 1

PRN# (Type)	Dates	τ_{max} days	Dominant Noise Type	$\sigma_y(\tau)$ @ τ(s)	Estimated Drift ± σ parts in 10^{-15}/d	Figure Nos.
2 (Cs)	1Jul91 - 15Sep92	221.5	FLFM	$0.4 \cdot 10^{-13}$	-2.7 ±0.3	1
2 (Cs)	1Jul91 - 15Sep92	221.5	RWFM	$0.2 \cdot 10^{-13}$ @ 10^6	-2.7 ±0.6	1
3 (Rb)	1Jul91 - 15Sep92	221.5	RWFM	$2.0 \cdot 10^{-13}$ @ 10^6	-98 ±6	2
12 (Rb)	8Apr - 15Sep92	80.5	RWFM	$2.5 \cdot 10^{-13}$ @ 10^6	-130 ±10	3
19 (Cs)	1Jul - 18Dec91	85.5	RWFM	$1.2 \cdot 10^{-13}$ @ 10^6	35 ±5	4
25 (Rb)	30Jun - 15Sep92	39	FLFM	$0.7 \cdot 10^{-13}$	-183 ±3	5
25 (Rb)	30Jun - 15Sep92	39	RWFM	$0.6 \cdot 10^{-13}$ @ 10^6	-183 ±4	5

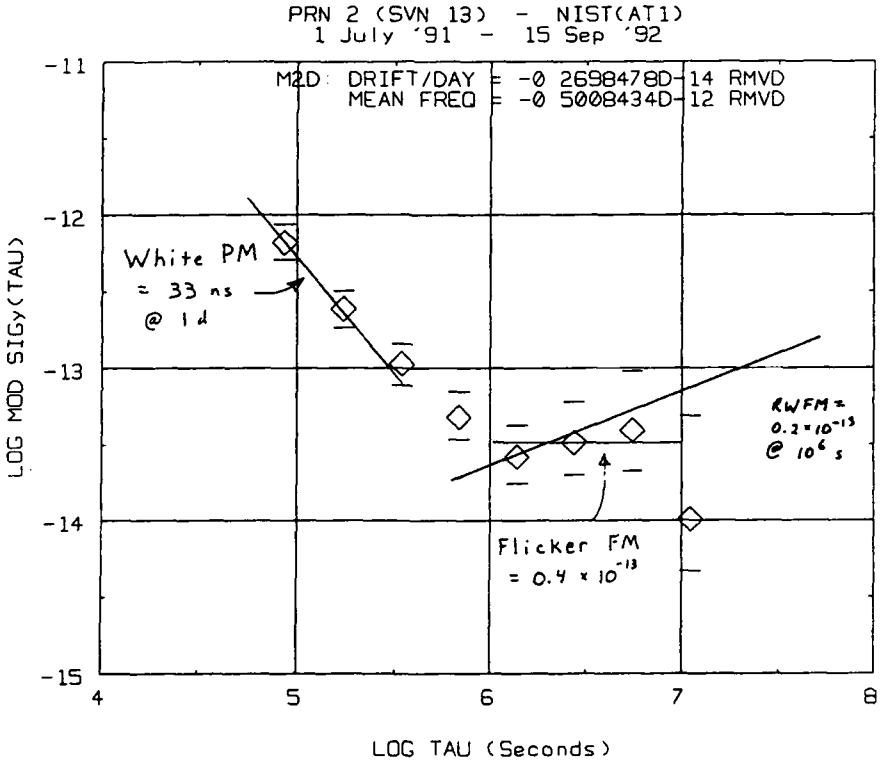

Figure 1: The modified Allan variance of the Cs clock on PRN#2 as measured at NIST against the AT1 time scale from July 1, 1991 to September 15, 1992.

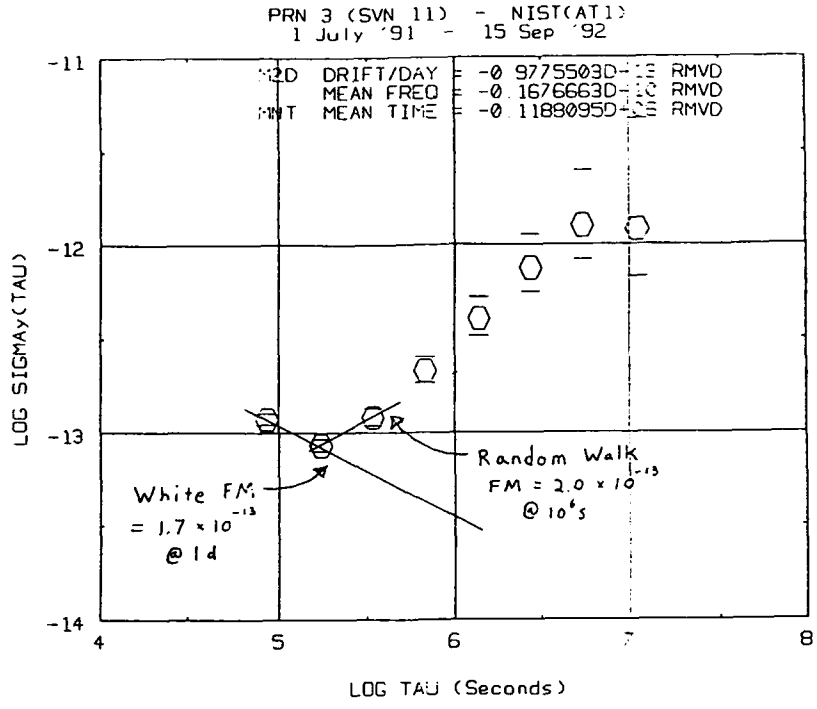

Figure 2: The Allan variance of the Cs clock on PRN#3 as measured at NIST against the AT1 time scale from July 1, 1991 to September 15, 1992.

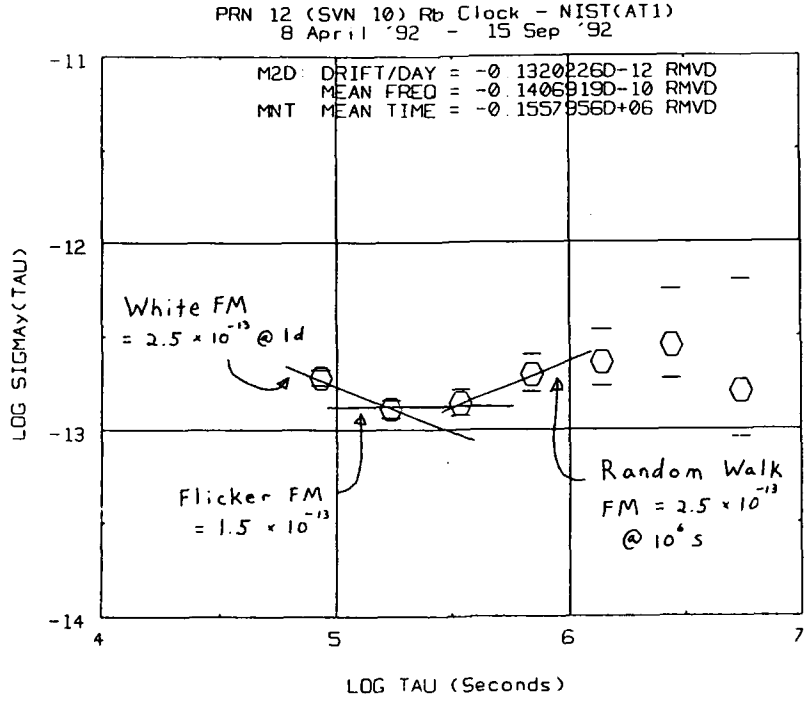

Figure 3: The Allan variance of the Rb clock on PRN#12 as measured at NIST against the AT1 time scale from April 8, 1991 to September 15, 1992.

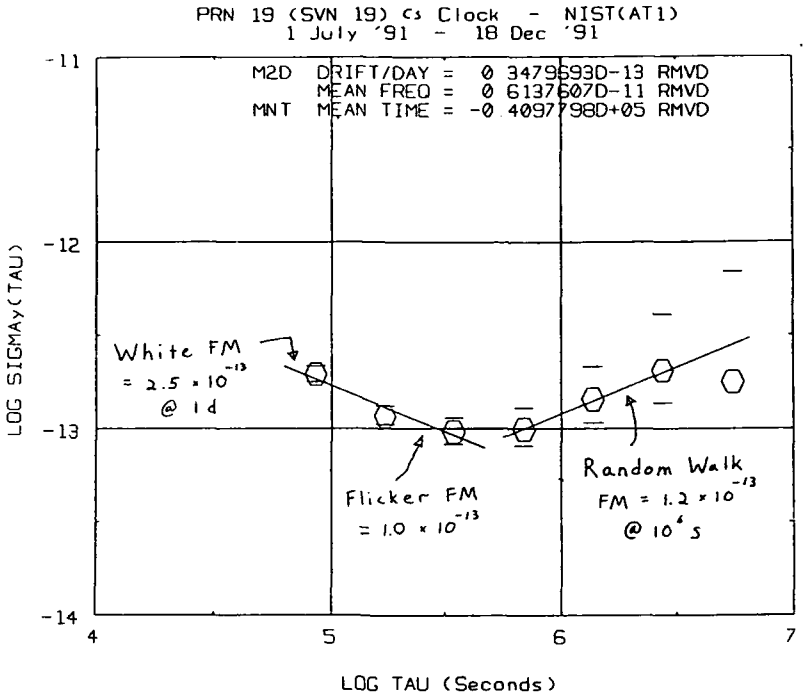

Figure 4: The Allan variance of the Cs clock on PRN#19 as measured at NIST against the AT1 time scale from April 8, 1991 to September 15, 1992.

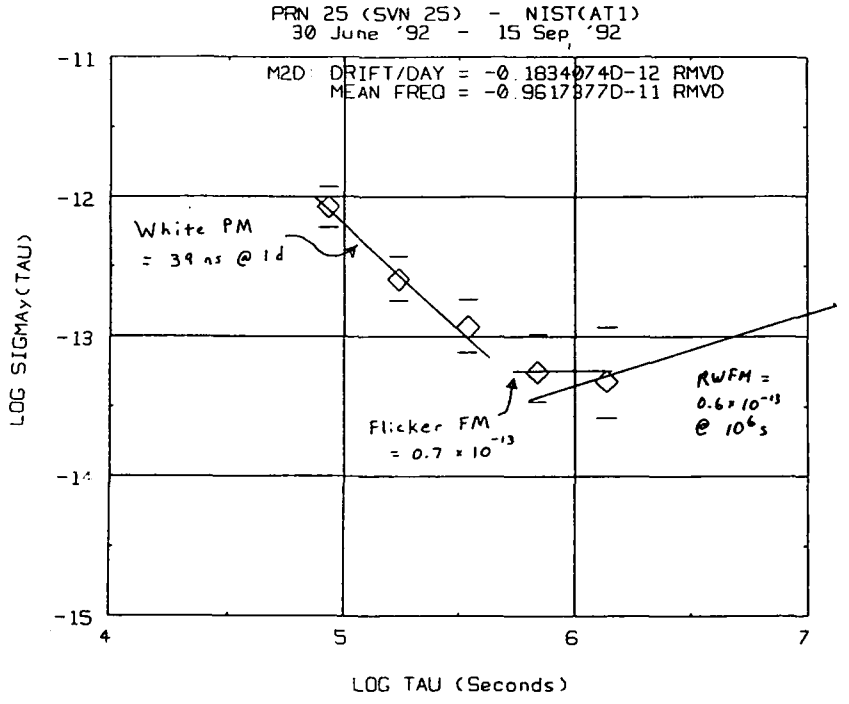

Figure 5: The Allan variance of the Rb clock on PRN#25 as measured at NIST against the AT1 time scale from April 8, 1991 to September 15, 1992.

QUESTIONS AND ANSWERS

J. Barnes, Austron, Incorporated: I want to ask a quick question so I am sure I understand what you are doing with the data. You take a data link and take the first point, minus the last point, plus the last point, minus two times the midpoint.

M. Weiss, NIST: Yes.

J. Barnes: That gives you your estimate of drift.

M. Weiss: Divide by Tau square, but yes.

J. Barnes: Then you take that and calculate a number to take from all of the data to get the residuals.

M. Weiss: Subtract a quadratic based on that number; Yes.

G. Winkler, USNO: I find that discussion very interesting. In fact it is a continuation of a discussion of drifts which started about six or seven years ago, when you gave your paper about how not to measure drift, by not making a parabolic fit, for the phase data; remember that? I think you did that and ever since that time, we have discussed how do you best measure drift. Before there was a question and it was questioned whether you can determine it at all, I believe you should remember that whenever we measure something, we measure it against a hypothesis, about a assumption. You have in your various estimates made various different assumptions. Each of these define ––(Tape ran out)–for it's instability. We have to remember that these numbers always are connected with a assumption, which has been made in the first place. You are starting out with three point estimates. Why is it the best estimate, or the optimun estimate, you can obtain, because it makes the minimun number of assumptions.

M. Weiss: I think you are right about the underlying assumptions. In particular, I think what is most important is to realize there is physics involved and the reason we estimate drift because we believe that what is physically causing the drift is different than what is physically causing the random walk. That they are two separate processes and they should therefore be estimated independately. And sometimes random walk looks an awful like drift and there may not be any drift and it may be random walk.

J. Barnes: I see people like the idea of being explicit in their models. I think that is great. I think I like the comments very much.

CORRECTIONS AND ADDENDA

Large Sample Simulation of Flicker Noise
J. Barnes and C. Greenhall
Proc. 19th PTTI, pp. 203–217, 1987

1. The covariance program on page 215 has two errors. Here are the corrected lines:

```
1260  IF I1<>N THEN F = F/(BET(I1)-BET(N))
1300  D(I,N) = D(I1,N)*F
```

2. Lines 220–290 on page 204 compute the filter poles PH(N) and zeros TH(N), which approach 1 as N increases. Before running the covariance program on page 215, one has to set ALF(N) = 1 - TH(N), BET(N) = 1 - PH(N). The user will get a more accurate covariance matrix if ALF(N) and BET(N) are computed directly from PH(1) as follows:

```
220  REM COMPUTE ALPHAS AND BETAS
230  W = (1# - PH(1))/SQR(PH(1))
235  ALF(1) = 1#: BET(1) = 1# - PH(1)
240  FOR N = 2 TO M
250      W = W/R
260      ALF(N) = .5#*W*(SQR(W*W + 4#) - W)
270      W = W/R
280      BET(N) = .5#*W*(SQR(W*W + 4#) - W)
290  NEXT N
```

One can run the filter directly from the alphas and betas by rewriting line 370 as

```
370 Y(I) = Y(I-1) + Y1(I) - Y1(I-1) - BET(I)*Y1(I) + ALF(I)*Y1(I-1)
```

The user is reminded to use double precision throughout, except possibly for storage of the output sample Y(M).

Lines 520 and 530 in the spectral density routine on page 214 can be rewritten as

```
520  S = S*(4#*(1#-ALF(J))*SIN(.5#*W)^2 + ALF(J)^2)
530  S = S/(4#*(1#-BET(J))*SIN(.5#*W)^2 + BET(J)^2)
```

3. Minor typos
Page 203: The second phi in eq.(1) should be a theta.
Page 212: The title of Table 1 should be ALZ(i,j).

PTTI '92
OFFICIAL ATTENDEES' LIST

John Aasted
European Space Agency
Keplerlaan 1
Noordwijk NETHERLANDS

Bilal Alam
NRAD
Code 312
Street and Jacksonville Roads
Warminster, PA 18974 USA
215/441-1406

David W. Allan
Allan's Time
P.O. Box 66
Fountain Green, UT 84632 USA
801/445-3216

C. O. Alley, Jr.
University of Maryland
Physics and Astronomy Department
College Park, MD 20742

Alfred Anderman
Rockwell International
MS 841-FB32
12214 Lakewood Boulevard
Downey, CA 90244

Ronald J. Andrukitis
U. S. Naval Observatory
Time Service Department
3450 Massachusetts Avenue, NW
Washington, DC 20392-5420 USA
202/653-1034

Manuel S. Aparicio
ITT A/CD
River Road
Nutley, NJ 07054 USA
201/284-3463

Sanjay K. Asthana
AT&T
101 Crawfords Corner Road
Holmdel, NJ 07733 USA
908/949-1816

Rob Avery
Telecom Solutions
85 West Tasman Drive
San Jose, CA 95134-1703 USA
408/433-0910

Heinz Badura
Ball Corporation
Efratom Division
3 Parker
Irvine, CA 92718 USA
714/770-5000

Alvin L. Bailey
U.S. Army Space Command-CONUS
1003 West 7th Street
Frederick, MD 21701 USA
301/698-2504

Richard G. Bailey
Datum, Incorporated
1363 South State College Boulevard
Anaheim, CA 92806 USA
714/533-6333

Joseph A. Ball
12039 Forbes Glen Drive
Herndon, VA 22070 USA
703/689-2535

James F. Barnaba
Newark Air Force Base
Newark, OH 43057 USA
614/522-7792

Luann Barndt
U.S. Coast Guard
7323 Telegraph Road
Alexandria, VA 22310-3998 USA

James A. Barnes
Austron, Incorporated
3011 Broadway
Boulder, CO 80304

Thomas R. Bartholomew
TASC
1190 Winterson Road
Columbia, MD 21090 USA
410/850-0070

Francoise S. Baumont
Observatoire de la Cote D'Azur
Avenue Copernic
F-06130 Grasse FRANCE
33 93 36 58 49

Ron L. Beard
Naval Research Laboratory
Code 8150
4555 Overlook Avenue, Southwest
Washington, DC 20375-5000 USA
202/767-2595

G. Thomas Becker
Air System Technologies, Incorporated
14232 Marsh Lane
Suite 339
Dallas, TX 75234 USA
214/402-9660

Roger E. Beehler
National Institute of Standards and Technology
325 Broadway
Boulder, CO 80303 USA
303/497-3281

Jacques Beser
3S Navigation
23141 Plaza Pointe Drive
Laguna Hills, CA 92653 USA
714/830-3777

Martin B. Bloch
FEI
55 Charles Lindburgh Boulevard
Uniondale, NY 11553 USA
516/794-4500

Erland Brannstrom
SNT Laboratory
Telia Research
S-136 80 Haninge SWEDEN
46 87 07 51 97

Lee A. Breakiron
U. S. Naval Observatory
Time Service Department
3450 Massachusetts Avenue, Northwest
Washington, DC 20392-5420 USA
202/653-1888

Gerhard Brenninger
ESG Elektroniksystem
Gesellschaft
Vogelweideplatz 9
D-8000 Munchen 80 GERMANY
49 89 9216 2631

James A. Buisson
Naval Research Laboratory
Code 8150
4555 Overlook Avenue, Southwest
Washington, DC 20375-5000 USA
202/404-7062

Edward E. Burkhardt
Burkhardt Monitoring Service
P. O. Box 1411
Glen Allen, VA 23060 USA
804/261-1800

Edgar W. Butterline
AT&T
900 Routes 202 and 206 North
Bedminster, NJ 07921 USA
908/234-4545

Malcolm D. Calhoun
Jet Propulsion Laboratory
California Institute of Technology
4800 Oak Grove Drive
Pasadena, CA 91109 USA
818/354-9763

Harold C. Chadsey
U. S. Naval Observatory
Time Service Department
3450 Massachusetts Avenue, Northwest
Washington, DC 20392-5420 USA
202/653-1888

David N. Chalmers
U.S. Naval Ovservatory
Time Service Department
3450 Massachusetts Avenue, Northwest
Washington, DC 20392-5420 USA
202/653-1412

Mark J. Chandler
BMC Associates
235 Congress Avenue
Lansdowne, PA 19050 USA
215/622-2833

Laura G. Charron
U.S. Naval Ovservatory
Time Service Department
3450 Massachusetts Avenue, Northwest
Washington, DC 20392-5420 USA
202/653-1529

Randolph T. Clarke, III
U.S. Naval Ovservatory
Time Service Department
3450 Massachusetts Avenue, Northwest
Washington, DC 20392-5420 USA
202/653-1034

Franco Cordara
Istituto Elettrotecnico Nazionales
91 Strada Delle Cacce
Torino 10135 ITALY
39 11 348 8933

Lenard S. Cutler
Hewlett Packard
P.O. Box 10350
MS 26M-9
Palo Alto, CA 94303-0867 USA
415/857-5259

William B. Dabney
U.S. Naval Observatory
Time Service Department
3450 Massachusetts Avenue, Northwest
Washington, DC 20392-5420 USA
202/653-1549

James Danaher
3S Navigation
23141 Plaza Pointe Drive
Laguna Hills, CA 92653 USA
714/830-3797

Angela M. Davis
U. S. Naval Observatory
Time Service Department
3450 Massachusetts Avenue, Northwest
Washington, DC 20392-5420 USA
202/653-1528

Gerrit De Jong
NMI-Van Swinden Laboratory
P. O. Box 654
Delft 2600 AR NETHERLANDS
31 13 691 623

James A. DeYoung
U.S. Naval Observatory
Time Service Department
3450 Massachusetts Avenue, Northwest
Washington, DC 20392-5420 USA
202/653-1034

Edoardo Detoma
FIAT CIEI/SEPA
300, Corso Giulio Cesare
Torino 10154 ITALY
39 11 2682523

Wayne P. Dewey
TrueTime Inc.
2467 Westvale Court
Santa Rosa, CA 95403 USA
707/523-2148

Paul B. DiDomenico
U.S. Air Force
GPS Joint Program Office
SMC/CZS
P.O. Box 92960
Los Angeles, CA 92960 USA
310/363-1326

William A. Diener
Jet Propulsion Laboratory
California Institute of Technology
4800 Oak Grove Drive
Pasadena, CA 91109 USA
818/354-4944

R. James Dill
ITT A/CD
492 River Road
Nutley, NJ 07110 USA
201/284-3001

Barbara A. Donaldson
EG&G Frequency Products
35 Congress Street
Salem, MA 01970 USA
508/745-3200

Winfield Donat, III
U. S. Naval Observatory
Time Service Department
3450 Massachusetts Avenue, Northwest
Washington, DC 20392-5420 USA
202/653-1538

Richard A. Dragonette
Johns Hopkins University
Applied Physics Laboratory
Johns Hopkins Road
Laurel, MD 20723 USA
301/953-5000

Lawrence M. Earley
Los Alamos National Laboratory
MS P947
Los Alamos, NM 87545 USA
505/667-5255

James M. Eler
U.S. Naval Observatory
Time Service Department
3450 Massachusetts Avenue, Northwest
Washington, DC 20392-5420 USA
202/653-0350

Robert F. Ellis
FTS/Austron, Inc.
P.O. Box 14766
Austin, TX 78761 USA
512/251-2313

Sheila Faulkner
U. S. Naval Observatory
Time Service Department
3450 Massachusetts Avenue, Northwest
Washington, DC 20392-5420 USA
202/653-1460

Stephen J. Feltham
European Space Agency
Keplerlaan 1
2200 AG Noordwijk HOLLAND
31 1719 83948

Raymond L. Filler
U.S. Army Research Laboratory
AMSEL-EP-ME
Fort Monmouth, NJ 07703-5601 USA
908/544-2467

Henry F. Fliegel
The Aerospace Corporation
2350 East El Segundo Boulevard
El Segundo, CA 93045 USA
310/336-1710

Joe E. Flores
Computer Sciences Corporation
P.O. Box 446
Building 1440
Edwards Air Force Base, CA 93523 USA
805/277-2449

Earl Fossler
TRAK Microwave Corporation
TRAK Systems Division
4726 Eisenhower Boulevard
Tampa, FL 33634 USA
813/884-1411

Roger S. Foster
U.S. Naval Research Laboratory
Code 7210
Washington, DC 20375 USA
202/767-0669

Keith A. Foye
U.S. Army Space Command
Fort Detrick, MD 21702 USA
301/619-7695

Harrison C. Freer
U.S. Air Force
2 SOPS/CC
Stop 82
Falcon Air Force Base, CO 80912-5000 USA
719/550-2400

Dan Friel
Leitch Incorporated
825K Greenbrier Circle
Chesapeake, VA 23320 USA
800/231-9673

Hugo Fruehauf
Ball Corporation
Efratom Division
3 Parker
Irvine, CA 92718 USA
714/770-5000

Robert P. Frueholz
The Aerospace Corporation
P.O. Box 92957
Los Angeles, CA 90009 USA
310/336-6975

Ivan J. Galysh
U. S. Naval Research Laboratory
Code 8152
4555 Overlook Avenue, Southwest
Washington, DC 20375-5000 USA
202/404-7060

Mike Gardner
Leitch, Incorporated
825K Greenbrier Circle
Chesapeake, VA 23320 USA
800/231-9673

Michael Garvey
Frequency and Time Systems, Incorporated
34 Tozer Road
Beverly, MA 01915 USA
508/927-8220

Kurt R. Gibble
Stanford University
Varian Physics
Stanford, CA 94305-4060 USA
415/725-2350

Al Gifford
U. S. Naval Research Laboratory
Code 8151
4555 Overlook Avenue, Southwest
Washington, DC 20375-5000 USA
202/767-2595

Asbjorn Gjelsvik
MITRE Corporation
Burlington Road
Bedford, MA 01730 USA
617/377-9067

William Golding
SFA/NRL
4555 Overlook Avenue
Washington, DC 20375-5354 USA
202/767-2595

Gary M. Graceffo
HRB Systems
800 International Drive
Linthicum, MD USA
202/404-7068

Joe C. M. Green
Allied/Bendix
129 North Hill Avenue
Pasadena, CA 91001 USA
818/584-4472

Charles A. Greenhall
Jet Propulsion Laboratory
California Institute of Technology
4800 Oak Grove Drive
Pasadena, CA 91109 USA
818/393-6944

Fran Groat
Hewlett Packard
MS 52U/14
5301 Stevens Creek Boulevard
Santa Clara, CA 95052-8049 USA
408/553-2307

Pierre J. Grudler
Observatoire de la Cote D'Azur
Avenue Copernic
F-06130 Grasse FRANCE
33 93 36 58 49

D. Michael Haddox
U.S. Naval Observatory
Time Service Department
3450 Massachusetts Avenue, Northwest
Washington, DC 20392-5420 USA
202/653-1212

Mike Haley
Quantic Industries
990 Commercial Street
San Carlos, CA 94070 USA
415/637-3049

Shin'ichi Hama
Communications Research Laboratory
893 Hirai
Kashima Ibaraki 314 JAPAN
81 299 84 6950

Robert L. Hamell
Jet Propulsion Laboratory
California Institute of Technology
4800 Oak Grove Drive
Pasadena, CA 91109 USA
818/354-4944

Walter R. Harding
Naval Electronics Systems Engineering Center
P. O. Box 55
Portsmouth, VA 23705-0055 USA
804/396-0516

Helmut Hellwig
Air Force Office of Scientific Research
ASOSR/CC
Bolling Air Force Base
Washington, DC 20332-6448 USA
202/767-5017

Lisa K. Hubbard
Department of Defense
9800 Savage Road
Fort Meade, MD 20755 USA
410/688-5393

Atsushi Imaoka
NTT Transmission Systems
1-2356 Take
Yokosuka Kanagawa 238-03 JAPAN
81 468 59 3731

Jeffrey S. Ingold
Allied Technical Services Corporation
One Bendix Road
Columbia, MD 21045 USA
301/964-7188

Claude Jacques
National Research Council
M-36 Montreal Road
Ottawa, Ontario K1A 0R6 CANADA
613/993-9330

Nicolette M. Jardine
U. S. Naval Observatory
Time Service Department
3450 Massachusetts Avenue, Northwest
Washington, DC 20392-5420 USA
202/653-1662

Andrew C. Johnson
U.S. Naval Observatory
Time Service Department
3450 Massachusetts Avenue, Northwest
Washington, DC 20392-5420 USA
202/653-1561

Dean R. Johnson
Western Michigan University
Department of Electrical Engineering
Kalamazoo, MI 49008 USA
616/375-4922

Ron Johnson
Odetics, Incorporated
Precision Time Division
1515 South Manchester Avenue
Anaheim, CA 92802-2907 USA
714/758-0400

Todd H. Johnson
U.S. Army Space Command
901-3A Gate Post Lane
Frederick, MD 21701 USA
301/619-2960

Edward C. Jones
Naval Research Laboratory
Code 8150
4555 Overlook Avenue, Southwest
Washington, DC 20375-5000 USA
202/767-2595

Saruna K. Karuza
The Aerospace Corporation
2350 East El Segundo Boulevard
El Segundo, CA 90245-4691 USA
310/366-6837

Shalom Kattan
Guide Technology, Incorporated
920 Saratoga Avenue
Suite 215
San Jose, CA 95129 USA
408/246-9905

Richard E. Keating
U.S. Naval Observatory
Time Service Department
3450 Massachusetts Avenue, Northwest
Washington, DC 20392-5420 USA
202/653-1549

Robert H. Kern
Kernco, Incorporated
28 Harbor Street
Danvers, MA 01923 USA
508/777-1956

Dieter Kirchner
Technische University Graz
12 Inffeldgasse
A-8010 Graz AUSTRIA
3 16 873 7441

Albert Kirk
Jet Propulsion Laboratory
California Institute of Technology
4800 Oak Grove Drive
Pasadena, CA 91109 USA
818/354-3038

William J. Klepczynski
U. S. Naval Observatory
Time Service Department
3450 Massachusetts Avenue, Northwest
Washington, DC 20392-5420 USA
202/653-1521

Curt Knight
Interferometrics, Incorporated
8180 Leesburg Pike, #1400
Vienna, VA 22182 USA
703/790-8500

Greg Kret
TrueTime
3243 Santa Rosa Avenue
Santa Rosa, CA 95407 USA
707/528-1230

Anthony J. Kubik
U.S. Naval Observatory
Time Service Department
3450 Massachusetts Avenue, Northwest
Washington, DC 20392-5420 USA
202/653-1412

Paul F. Kuhnle
Jet Propulsion Laboratory
California Institute of Technology
4800 Oak Grove Drive
Pasadena, CA 91109 USA
818/354-2715

Eugen F. Kunzi
Siemens AG
Department SI E SY 4
Landshuter Strabe 26
D-8044 Unterschleissheim GERMANY
49 89 3179 2297

Paul J. Kushmeider
Allied Technical Services Corporation
M/S VLBI
One Bendix Road
Columbia, MD 21045 USA
410/964-7672

Jack Kusters
Hewlett Packard
5301 Stevens Creek Boulevard
Santa Clara, CA 95052 USA
408/553-2041

Paul Landis
U. S. Naval Research Laboratory
Code 8152
4555 Overlook Avenue, Southwest
Washington, DC 20375-5000 USA
202/404-7061

Richard B. Langley
University of New Brunswick
Department of Surveying Engineering
Frederilton, NB E3B 5A3 CANADA
504/453-5142

Marie M. Largay
U. S. Naval Research Laboratory
Code 8153
4555 Overlook Avenue, Southwest
Washington, DC 20375-5000 USA
202/767-9133

Albert Leong
The Aerospace Corporation
P.O. Box 92957
Los Angeles, CA 90009-2957 USA
310-336-6444

Sigfrido M. Leschiutta
Politecnico-Torino
24 Corso Abruzzi
Torino 10129 ITALY
38 11 564 4035

Judah Levine
National Institute of Standards and Technology
325 Broadway
Boulder, CO 80303 USA
303/492-7785

Wlodzimierz W. Lewandowski
Bureau International des Poids et Mesures
Pavillon de Breteuil
Sevres 92312 FRANCE
33 1 450 77063

Irving Liberman
Westinghouse STC
1310 Beulah Road
Pittsburg, PA 15235 USA
412/256-1571

Chuck P. Little
Hewlett Packard
5301 Stevens Creek Boulevard
Santa Clara, CA 95052-8059 USA
408/553-2506

Patrick E. Lloyd
U.S. Naval Observatory
Time Service Department
3450 Massachusetts Avenue, Northwest
Washington, DC 20392-5420 USA
202/653-1527

Gene E. Long
Odetics, Incorporated
P.O. Box 2727
LaPlata, MD 20646 USA
301/870 3311

Robert J. Lopes
AT&T
NF9308200-14th
Two Gateway Center
Newark, NJ 07102 USA
201/645-5025

Pete Lopez
TRAK Microwave Corporation
TRAK Systems Division
4726 Eisenhower Boulevard
Tampa, FL 33634 USA
813/884-1411

Carl F. Lukac
U.S. Naval Observatory
Time Service Department
3450 Massachusetts Avenue, Northwest
Washington, DC 20392-5420 USA
202/653-1527

Edward M. Lukacs
U.S. Naval Observatory
Richmond Station
11820 Southwest 166th Street
Miami, FL 33177 USA
305/235-0515

George F. Lutes
Jet Propulsion Laboratory
California Institute of Technology
4800 Oak Grove Drive
Pasadena, CA 91109 USA
818/354-6210

George H. Luther
U.S. Naval Observatory
Time Service Department
3450 Massachusetts Avenue, Northwest
Washington, DC 20392-5420 USA
202/653-1549

Phu V. Mai
U.S. Naval Observatory
Time Service Department
3450 Massachusetts Avenue, Northwest
Washington, DC 20392-5420 USA
202/653-0350

Kenneth Martin
Bonneville Power Administration
Division of Labs ELIP
Vancouver, WA 98666 USA
206/690-2694

Demetrios Matsakis
U.S. Naval Observatory
Time Service Department
3450 Massachusetts Avenue, Northwest
Washington, DC 20392-5420 USA
202/653-0585

Edward M. Mattison
Smithsonian Astrophysical Observatory
60 Garden Street
Cambridge, MA 02138 USA
617/495-7265

Keith D. McDonald
SAT TECH Systems
2775 South Quincy Street
Suite 610
Arlington, VA 22206-2204

Teresa D. McGowan
Naval Air Warfare
Center Weapons Division
C2541
China Lake, CA 93555-6001 USA
619/939-2103

Norma G. Meyer
U.S. Naval Observatory
Time Service Department
3450 Massachusetts Avenue, Northwest
Washington, DC 20392-5420 USA
202/653-1525

Thomas E. Meyer
U.S. Air Force
2 SOPS/DOAN
Stop 82
Falcon Air Force Base, CO 80912-5000 USA
719/550-6396

John A. Milford
E-Systems
ECI Division
P.O. Box 12248
MS/45
St. Petersburg, FL 33733 USA
813/381-2000

Mihran Miranian
U.S. Naval Observatory
Time Service Department
3450 Massachusetts Avenue, Northwest
Washington, DC 20392-5420 USA
202/653-1522

Don Mitchell
TrueTime
3243 Santa Rosa Avenue
Santa Rosa, CA 95407 USA
707/528-1230

David D. Morabito
Jet Propulsion Laboratory
California Institute of Technology
4800 Oak Grove Drive
Pasadena, CA 91109 USA
818/354-2424

Forrester Morgan
Odetics, Incorporated
P.O. Box 2727
LaPlata, MD 20646 USA
301/870-3311

Derek Morris
National Research Council
Building M-36
Montreal Road
Ottawa Ontario K1A 0R6 CANADA
613/993-9340

Ruzbeh Mossavati
National Physical Laboratory
Queens Road
Teddington-Middlesex TW11-0lW ENGLAND
81 943 6123

Frank Mullen
Frequency and Time Systems
34 Tozer Road
Beverly, MA 01915 USA
508/927-8220

William J. Murphy, Jr.
Computer Sciences Corporation
P. O. Box 446
Building 1440
Edwards Air Force Base, CA 93523 USA
805/277-2004

James Murray
SFA, Incorporated
6215 Houston, Court
Alexandria, VA 22310 USA
202/404-7057

Robert A. Nelson
W. L. Pritchard and Company, Incorporated
7315 Wisconsin Avenue
Suite 520E
Bethesda, MD 20814 USA
301/654-1144

Gregory A. Norman
Department of Defense
9800 Savage Road
Fort Meade, MD 20755-6000 USA
301/688-5769

Clyde C. Norris
Computer Sciences Corporation
P. O. Box 17
Clearfield, UT 84015 USA
801/773-9271

Jerry R. Norton
Johns Hopkins University
Applied Physics Laboratory
Johns Hopkins Road
Laurel, MD 20723 USA
301/935-6000

Phillip J. Norton
Naval Satellite Operations Center
Building 389
Naval Air Warfare Center
Point Mugu, CA 93042 USA
805/989-4338

Karen F. O'Donoghue
Naval Surface Warfare Center
Code B35 NSWCDD
Dahlgren, VA 22448 USA
703/663-1567

Orville J. Oaks
Naval Research Laboratory
Code 8153
4555 Overlook Avenue, Southwest
Washington, DC 20375-5000 USA
202/767-2595

Rich D. Ochmanowicz
1026 G Spa Road
Annapolis, MD 21403 USA
202/404-7067

Skip Osborne
Allen Osborne Associates
756 Lakefield Road
Building J
Westlake Village, CA 91361-2624 USA
805/495-8420

Terry N. Osterdock
Stellar Navigation, Incorporated
19075 Skyline Boulevard
Los Gatos, CA 95030 USA
408/354-0733

Joseph W. Ouellette
The Aerospace Corporation
P. O. Box 92957, MS M5-681
Los Angeles, CA 90009-2957 USA
310/336-1048

H. Bryan Owings
Sigma Tau Standards Corporation
1711 Holt Road
P.O. Box 1877
Tuscaloosa, AL 35403 USA
205/553-0038

Bob Pagano
Telecom Solutions
85 West Tasman Drive
San Jose, CA 95134-1703 USA
408/433-0910

Yolando C. Page-Rich
U.S. Naval Observatory
Time Service Department
3450 Massachusetts Avenue, Northwest
Washington, DC 20392-5420 USA
202/653-1529

Ralph E. Partridge
Los Alamos National Laboratory
P. O. Box 1663
Los Alamos, NM 87545 USA
505/667-5255

Peter Z. Paulovich
NAVELEXCEN Portsmouth
P. O. Box 55
Portsmouth, VA 23705-0055 USA
804/396-0287

Joseph J. Perkowski
NRAD
Code 322
Warminster, PA 18974 USA
215/441-2951

James C. Perry
NASA/Goddard Space Flight Center
Code 531.3
Greenbelt Road
Greenbelt, MD 20771 USA
301/286-3471

Harry E. Peters
Sigma Tau Standards Corporation
P. O. Box 1877
Tuscaloosa, AL 35403 USA
205/553-0038

Gerard Petit
Bureau International des Poids et Mesures
Pavillon de Breteuil
92312 Sevres FRANCE
33 1 45 07 7067

Peter L. Petrakis
Life Sciences Software
812 Vista Drive
Camano Island, WA 98292 USA
206/387-9788

Tony E. Piotrowski
AT&T
NF9308200-14th
Two Gateway Center
Newark, NJ 07102 USA
201/645-5029

William M. Powell
U. S. Naval Observatory
Time Service Department
3450 Massachusetts Avenue, Northwest
Washington, DC 20392-5420 USA
202/653-1528

Edward D. Powers
Naval Research Laboratory
4555 Overlook Avenue, Southwest
Code 8151
Washington, DC 20375-5000 USA
202/767-7060

Robert E. Price
Allied Technical Services Corporation
One Bendix Road
Columbia, MD 21045 USA
410/964-7437

Harris C. Rawicz
ITT A/CD
549 Lyme Rock Road
Bridgewater, NJ 08807 USA
201/284-2131

Richard A. Rayos
Computer Sciences Raytheon
P. O. Box 4127
CSR 2230
Patrick Air Force Base, FL 32925 USA
407/494-7176

Elza K. Redman
Department of Defense
9800 Savage Road
Fort Meade, MD 20755-6000 USA
301/688-7526

Wilson Reid
U. S. Na al Research Laboratory
Code 8153
4555 Overlook Avenue, Southwest
Washington, DC 20375-5000 USA
202/767-2595

Thomas O. Rieley
HRB Systems
800 International Drive
Linthicum, MD USA
202/404-7068

William J. Riley
EG&G Frequency Products
35 Congress Street
Salem, MA 09170 USA
508/745-3200

Ron Roloff
FTS/Austron, Incorporated
8005 McKenstry Drive
Laurel, MD 20723 USA
301/725-3636

Lauren J. Rueger
Rueger Enterprises
1415 Glenallan Avenue
Silver Spring, MD 20902 USA
301/942-7733

Ernie Ruiz
U.S. Army
STEWS: ID-SD
White Sands, NM 88002 USA
505/678-1545

Rick Sarrica
Hewlett Packard
5301 Stevens Creek Boulevard
MS 23, Building 51U
Santa Clara, CA 95052 USA
408/553-2089

Gary D. Sasaki
Hewlett Packard
5301 Stevens Creek Boulevard
Santa Clara, CA 95052 USA
408/553-2568

Michael C. H. Savvides
Lands and Surveys
Department-Cyprus
Nicosia, Cyprus GREECE

Doug A. Sisk
AT&T
2C526
101 Crawfords Corner Road
Holmdel, NJ 07733-1948 USA
908/949-2486

Andrew G. Snow
Frequency and Time Systems, Incorporated
34 Tozer Road
Beverly, MA 01915 USA
508/927-8220

Dr. James J. Spilker, Jr.
Stanford Telecom
2421 Mission College Boulevard
Santa Clara, CA 95054

Samuel R. Stein
Timing Solutions Corporation
1025 Rosewood Avenue
Suite 200
Boulder, CO 80304 USA
303/443-5152

Edgar L. Stephenson
Overlook Systems Technologies, Incorporated
1950 Old Gallows Road
Suite 400
Vienna, VA 22182 USA
703/893-1411

David A. Stowers
Jet Propulsion Laboratory
California Institute of Technology
4800 Oak Grove Drive
Pasadena, CA 91109 USA
818/354-7055

Joseph J. Suter
Johns Hopkins University
Applied Physics Laboratory
Johns Hopkins Road
Laurel, MD 20723 USA
301/953-6000

Richard L. Sydnor
Jet Propulsion Laboratory
California Institute of Technology
4800 Oak Grove Drive
Pasadena, CA 91109 USA
818/354-2763

Philip E. Talley, Jr.
The Aerospace Corporation
5302 Marina Pacific Drive South
Long Beach, CA 90803 USA
310/431-3226

Patrizia P. Tavella
Istituto Elettrotecnico Nazionales
G. Ferraris
91 Strada Delle Cacce
Torino 10135 ITALY
39 11 348 8933

Murli M. Thirumale
Hewlett Packard
5301 Stevens Creek Boulevard
Santa Clara, CA 95052 USA
408/553-2539

Matthew A. Trippy
U.S. Air Force
GPS Joint Program Office
SMC/CZUD
P.O. Box 92960
Los Angeles, CA 92960 USA
310/363-2023

John L. Van Gross
TrueTime, Incorporated
3243 Santa Rosa Avenue
Santa Rosa, CA 95047 USA
707/520-1230

Marinus J. Van Melle
Rockwell International
5476 Oro Grande Drive
Colorado Springs, CO 80918 USA
719/260-1654

Francine M. Vannicola
U.S. Naval Observatory
Time Service Department
3450 Massachusetts Avenue, Northwest
Washington, DC 20392-5420 USA
202/653-1525

Christian Veillet
Observatoire de La Cote D'Azur
Avenue Copernic
F-06130 Grasse FRANCE
33 93 36 58 49

Frank J. Voit
The Aerospace Corporation
2350 East El Segundo Boulevard
El Segundo, CA 90245-4691 USA
310/366-4691

Todd E. Walter
Stanford University
Gravity Probe B
Via Palou Street
Stanford, CA 94305-4085 USA
415/723-7239

Ben Chun Wang
University of Maryland
Department of Physics
College Park, MD 20742 USA
301/405-6102

S. Clark Wardrip
Allied Technical Services Corporation
726 Foxenwood Drive
Santa Maria, CA 93455 USA
805/937-6448

Marc A. Weiss
National Institute of Standards and Technology
325 Broadway
Boulder, CO 80303 USA
303/497-3261

Paul J. Wheeler
U.S. Naval Observatory
Time Service Department
3450 Massachusetts Avenue, Northwest
Washington, DC 20392-5420 USA
202/653-0516

Joseph D. White
Naval Research Laboratory
Code 8151
4555 Overlook Avenue, Southwest
Washington, DC 20375-5000 USA
202/767-2595

Warren L. Wilson
Lockheed Missiles and Space Company
707 Spindraft Drive
San Jose, CA 95134-1346 USA
408/743-1213

Gernot M. R. Winkler
U. S. Naval Observatory
Time Service Department
3450 Massachusetts Avenue, Northwest
Washington, DC 20392-5420 USA
202/653-1520

Jeffrey A. Wisnia
Kernco, Incorporated
28 Harbor Street
Danvers, MA 01923 USA
508/777-1956

Woody K. Wordsworth
Austron, Incorporated
Signet Bank Building
305 East Main Street
Front Royal, VA 22630 USA
703/636-7777

James L. Wright
Computer Sciences Raytheon
P. O. Box 4127
Patrick Air Force Base, FL 32925 USA
407/494-2014

C. Andy Wu
The Aerospace Corporation
4452 Canoga Drive
Woodland Hills, CA 91364 USA
310/336-0437

C. Eric Youngberg
Hewlett Packard
5301 Stevens Creek Boulevard
Santa Clara, CA 95052 USA
408/553-2308

George Zampetti
Telecom Solutions
85 West Tasman Drive
San Jose, CA 95134-1703

REPORT DOCUMENTATION PAGE

Form Approved
OMB No. 0704-0188

1. AGENCY USE ONLY *(Leave blank)*	2. REPORT DATE	3. REPORT TYPE AND DATES COVERED
	June 1993	Conference Publication

4. TITLE AND SUBTITLE
24th Annual Precise Time and Time Interval (PTTI) Applications and Planning Meeting

5. FUNDING NUMBERS
Code 502
C-NAS5-31000

6. AUTHOR(S)
Dr. Richard Sydnor, Editorial Committee Chairman

7. PERFORMING ORGANIZATION NAME(S) AND ADDRESS(ES)
Goddard Space Flight Center
Greenbelt, Maryland 20771

8. PERFORMING ORGANIZATION REPORT NUMBER
93B00087

9. SPONSORING/MONITORING AGENCY NAME(S) AND ADDRESS(ES)
National Aeronautics and Space Administration
Washington, D.C. 20546-0001

10. SPONSORING/MONITORING AGENCY REPORT NUMBER
CP-3218

11. SUPPLEMENTARY NOTES
Richard Sydnor: Jet Propulsion Laboratory, Pasadena, CA. Other sponsors: U.S. Naval Observatory; Jet Propulsion Laboratory; Space and Naval Warfare Systems Command; Naval Research Laboratory; Army Electronics Technology and Devices Laboratory; Rome Laboratory; and Air Force Office of Scientific Research.

12a. DISTRIBUTION/AVAILABILITY STATEMENT
Unclassified-Unlimited
Subject Category 70
Report available from the NASA Center for AeroSpace Information, 800 Elkridge Landing Road, Linthicum Heights, MD 21090; (301) 621-0390.

12b. DISTRIBUTION CODE

13. ABSTRACT *(Maximum 200 words)*

This document is a compilation of technical papers presented at the 24th Annual PTTI Applications and Planning Meeting, held December 1 through 3, 1992, at the Ritz-Carlton Hotel, McLean, Virginia. Papers are in the following categories:

—Recent developments in rubidium, cesium, and hydrogen-based frequency standards, and in cryogenic and trapped-ion technology.

—International and transnational applications of Precise Time and Time Interval technology with emphasis on satellite laser tracking networks, GLONASS timing, intercomparison of national time scales and international telecommunications.

—Applications of Precise Time and Time Interval technology to the telecommunications, power distribution, platform positioning, and geophysical survey industries.

—Applications of PTTI technology to evolving military communications and navigation systems.

—Dissemination of precise time and frequency by means of GPS, GLONASS, MILSTAR, Loran, and synchronous communications satellites.

14. SUBJECT TERMS
Frequency Standards, Hydrogen Masers, Cesium, Rubidium Trapped Ion, Crystals, Time Synchronization, Precise Time, Time Transfer, GPS, GLONASS, Satellite Clocks, Jitter, Phase Noise

15. NUMBER OF PAGES
496

16. PRICE CODE

17. SECURITY CLASSIFICATION OF REPORT	18. SECURITY CLASSIFICATION OF THIS PAGE	19. SECURITY CLASSIFICATION OF ABSTRACT	20. LIMITATION OF ABSTRACT
Unclassified	Unclassified	Unclassified	Unlimited